OBSERVING, MODELING AND UNDERSTANDING PROCESSES IN NATURAL AND MANAGED PEATLANDS

EDITED BY: Michel Bechtold, Björn Klöve, Annalea Lohila, Massimo Lupascu, Line Rochefort and Hanna Silvennoinen

PUBLISHED IN: Frontiers in Earth Science and Frontiers in Environmental Science

frontiers Research Topics

frontiers

ISSN 1664-8714
ISBN 978-2-88976-052-7
DOI 10.3389/978-2-88976-052-7

About Frontiers

Frontiers is more than just an open-access publisher of scholarly articles: it is a pioneering approach to the world of academia, radically improving the way scholarly research is managed. The grand vision of Frontiers is a world where all people have an equal opportunity to seek, share and generate knowledge. Frontiers provides immediate and permanent online open access to all its publications, but this alone is not enough to realize our grand goals.

Frontiers Journal Series

The Frontiers Journal Series is a multi-tier and interdisciplinary set of open-access, online journals, promising a paradigm shift from the current review, selection and dissemination processes in academic publishing. All Frontiers journals are driven by researchers for researchers; therefore, they constitute a service to the scholarly community. At the same time, the Frontiers Journal Series operates on a revolutionary invention, the tiered publishing system, initially addressing specific communities of scholars, and gradually climbing up to broader public understanding, thus serving the interests of the lay society, too.

Dedication to Quality

Each Frontiers article is a landmark of the highest quality, thanks to genuinely collaborative interactions between authors and review editors, who include some of the world's best academicians. Research must be certified by peers before entering a stream of knowledge that may eventually reach the public - and shape society; therefore, Frontiers only applies the most rigorous and unbiased reviews.
Frontiers revolutionizes research publishing by freely delivering the most outstanding research, evaluated with no bias from both the academic and social point of view. By applying the most advanced information technologies, Frontiers is catapulting scholarly publishing into a new generation.

What are Frontiers Research Topics?

Frontiers Research Topics are very popular trademarks of the Frontiers Journals Series: they are collections of at least ten articles, all centered on a particular subject. With their unique mix of varied contributions from Original Research to Review Articles, Frontiers Research Topics unify the most influential researchers, the latest key findings and historical advances in a hot research area! Find out more on how to host your own Frontiers Research Topic or contribute to one as an author by contacting the Frontiers Editorial Office: frontiersin.org/about/contact

OBSERVING, MODELING AND UNDERSTANDING PROCESSES IN NATURAL AND MANAGED PEATLANDS

Topic Editors:
Michel Bechtold, KU Leuven, Belgium
Björn Klöve, University of Oulu, Finland
Annalea Lohila, University of Helsinki, Finland
Massimo Lupascu, National University of Singapore, Singapore
Line Rochefort, Laval University, Canada
Hanna Silvennoinen, Norwegian Institute of Bioeconomy Research (NIBIO), Norway

Citation: Bechtold, M., Klöve, B., Lohila, A., Lupascu, M., Rochefort, L., Silvennoinen, H., eds. (2022). Observing, Modeling and Understanding Processes in Natural and Managed Peatlands. Lausanne: Frontiers Media SA. doi: 10.3389/978-2-88976-052-7

Table of Contents

frontiers | Frontiers in Earth Science

EDITORIAL
published: 30 June 2022
doi: 10.3389/feart.2022.930834

Editorial: Observing, Modeling and Understanding Processes in Natural and Managed Peatlands

Michel Bechtold[1], Björn Klöve[2], Annalea Lohila[3,4], Massimo Lupascu[5], Line Rochefort[6] and Hanna Silvennoinen[7]*

[1]Department of Earth and Environmental Sciences, KU Leuven, Leuven, Belgium, [2]Water Resources Engineering, University of Oulu, Oulu, Finland, [3]Climate System Research, Finnish Meteorological Institute, Helsinki, Finland, [4]Institute for Atmospheric and Earth System Research/Physics, Faculty of Science, University of Helsinki, Helsinki, Finland, [5]Geography Department, National University of Singapore, Singapore, Singapore, [6]Département de phytologie, Laval University, Quebec, QC, Canada, [7]Norwegian Institute for Nature Research (NINA), Trondheim, Norway

Keywords: greenhouse gas emissions, ecohydrology, peatlands, wetlands, carbon cycle, ecology, restoration, rewetting

Editorial on the Research Topic

Observing, Modeling and Understanding Processes in Natural and Managed Peatlands

INTRODUCTION

Peatlands play a critical role in our climate system. Although they cover only 3% of the global land surface, they store about one third of the world's soil carbon pool. The carbon-rich peat layers accumulated in locations of almost permanently waterlogged conditions over several thousands of years. However, the transition from the Holocene to the Anthropocene exerts a long-lasting change in peatland climatic and nutrient boundary conditions. The global impact of these changes on the stability of peatland ecosystems and their emissions of the greenhouse gases (GHG) carbon dioxide (CO_2), methane (CH_4) and nitrous oxide (N_2O) is currently unknown. In contrast, it is well known that the direct anthropogenic disturbance of peatlands by drainage and land use changes for agriculture, forestry and peat extraction severely alters the GHG budget of peatlands turning them into global hotspots of CO_2 emissions. New land use and management options that effectively mitigate peatland loss and maintain their important related ecosystem services are urgently needed. A deep understanding of peatland processes that can be combined with socio-economic and legal aspects is crucial for human society to explore and manage the future of Earth's pristine, disturbed and used peatlands.

This Research Topic assembles 14 original research papers (+ one corrigendum) and one review paper on various aspects of peatland processes. The Research Topic of papers includes research on peatlands at northern and tropical latitudes and provides new insights into the dynamics of their water, energy, carbon and nitrogen cycles of both natural and managed peatlands. Furthermore, innovative techniques are presented that are important for the upscaling of GHG emissions and their driving factors.

Carbon and Nitrogen Cycle of Natural Peatlands

The water cycle exerts a first order control on peatland processes such as the carbon cycle. The mesocosm study by Kim et al. shows that individual components of the water cycle component can interact with other peatland functions in a complex manner. In their experiments, the change of a specific feature of water level dynamics, i.e., the increase of the frequency of fluctuations, inhibited

OPEN ACCESS

Edited and reviewed by:
Wouter Buytaert,
Imperial College London,
United Kingdom

****Correspondence:***
Michel Bechtold
michel.bechtold@kuleuven.be

Specialty section:
This article was submitted to Hydrosphere, a section of the journal Frontiers in Earth Science

Received: *28 April 2022*
Accepted: *23 May 2022*
Published: *30 June 2022*

Citation:
Bechtold M, Klöve B, Lohila A, Lupascu M, Rochefort L and Silvennoinen H (2022) Editorial: Observing, Modeling and Understanding Processes in Natural and Managed Peatlands. Front. Earth Sci. 10:930834. doi: 10.3389/feart.2022.930834

the growth of *Sphagnum* due to fungal infection and at the same time promoted peat decomposition. This, in turn, may severely destabilize peatland carbon storage. The result also has important implications for the paludiculture practice of *Sphagnum* farming for which biomass production might be maximized by establishing more stable water levels. With another mesocosm experiment, the study of Li et al. shows the fast response of vegetation composition to experimental warming which in turn controlled C fluxes together with water level dynamics. Thus, long-term monitoring of hydrology and vegetation change under climate warming is essential to examine their interactions in determining C fluxes in peatlands. In another study on CH_4 concentrations in ponds in Eastern Siberian peatlands by Rehder et al., the water level in ponds influenced water stratification and the fraction of vascular plants, which in turn mainly controlled CH_4 concentrations for similar pond types. The study, however, also shows that more research is needed to understand drivers that explain CH_4 concentration variability across different pond types.

The possible response of the carbon cycle to global warming was analyzed at a larger scale for the whole Hudson Bay Lowlands in Canada by McLaughlin and Packalen using a Bayesian Belief Network. In their approach, they combined a dataset synthesis on carbon fluxes and its drivers with expert knowledge on causal relationships between system variables. Their modeling results indicate an overall drying of peat under severely warmer climate scenarios that eventually reduces peat carbon sink strength due to increased peat combustion by changing fire activity, among other factors. Any upscaling approach requires best available data on the distribution of peatlands including their types and present carbon stocks. In this context, the study of Bourgeau-Chavez et al. demonstrates that the joint use of multi-temporal synthetic aperture radar (SAR) and optical remote sensing over the Amazonian peatlands improves the mapping accuracy compared to previous approaches. They attribute this improvement to the additional information contained in the strong moisture sensitivity of the SAR data. The strong seasonal hydrological dynamics present in the region generated features in the data that differed across ecotypes.

Compared to the carbon cycle, relatively little research has been conducted on the N cycle in peatlands although the critical interaction between both cycles is well known. Yin et al. provide a systematic review of peatland N cycling and quantified that over northern peatlands the N input through biological N fixation is about 3–4 times higher than by N deposition. However, they emphasize that the uncertainties of the current estimates of the biological N fixation are generally large. This counts in particular for the tropical peatlands for which studies on the N cycle are very limited.

Lateral release of carbon and other substances from peatlands can critically affect ecosystems in the surroundings of peatlands. In this context, Don Racasa et al. provide a detailed analysis of submarine groundwater discharge for a non-tidal coastal peatland located at the Baltic Sea. Using a numerical study, they showed that the release of carbon fluxes and other substances from the peatland through submarine groundwater discharge is probably highest for peatlands with high water levels, large saturated hydraulic conductivities and/or a dune dike or belt.

Peatland Management and Restoration

Several papers in this Research Topic deal with managed and restored peatlands. A detailed understanding of the hydrology of managed and restored peatlands is crucial to efficiently improve their GHG balance. In this regard, Ahmad et al. compared water level fluctuations in a drained and rewetted fen in Germany and showed that differences in the response of water level variation to meteorological conditions can be related to differences in the soil water storage capacity of two peatland sites. The study indicates the difficulty of establishing stable water level conditions given the expected increase in evaporative demands under global warming scenarios once peat properties are altered and thus less capable of buffering water level fluctuations.

Setting land aside from agricultural production has been proposed as a strategy to reduce GHG emissions from drained peatlands, restore natural habitats, and increase C sequestration. By comparing GHG measurements from a set-aside site and a cultivated site in Sweden, the study of Berglund et al. however indicates that the impact is likely limited for the reduction of CO_2 emissions unless drainage is also terminated. In a series of mesocosm experiments of Swedish agricultural peat soils, Norberg et al. examined factors controlling the emission of CH_4 and N_2O emissions. While measured CH_4 emissions were generally low, N_2O emissions were high for low pH and near-saturated conditions. Also biotic factors were found to be important as specific assemblages of nitrogen cycling guilds were detected in soils with low N_2O emissions.

The processes controlling the carbon balance of two drained forested peatlands in Finland with contrasting nutrient content was investigated by Kasimir et al. using a process-oriented model that was calibrated on data of the two sites. They found that the higher fraction of moss vegetation in the nutrient poor site was key for higher carbon accumulation despite lower photosynthesis because the moss added larger litter quantities with a resistant quality and also limited water depletion during dry spells. For tropical peatlands in Kalimantan, Swails et al. assessed changes of the GHG budget associated with peat swamp forest disturbance and conversion to oil palm plantation. The conversion to oil palm plantation implied a large net increase in peat GHG emissions, mainly released as CO_2. Also past land-use change strongly impacted peat net GHG emissions in a secondary peat swamp forest, decades following conversion and without active drainage.

While the direct measurement of GHG emissions is time-consuming and unaffordable for monitoring at many locations, Evans et al. propose a low-cost method that builds upon the link between subsidence and CO_2 emissions that typically control the GHG budget of drained peatlands. The method is image-based and measures peat surface motion and water level using commercially available time-lapse cameras and image processing tools. The proposed method offers the potential to be employed at large scale at multiple sites and is thus suitable for identifying areas of active carbon loss, targeting climate change mitigation interventions, and evaluating intervention outcomes.

Given the strong evidence that only high water levels can substantially mitigate GHG emissions from managed peatlands, economically attractive paludiculture practices need to be

developed. In this context, Nielsen et al. investigated how harvest and fertilization frequency can be optimized to maximize protein yield and extractability of the flood-tolerant grasses tall fescue and reed canary grass in a fen-type peatland of Denmark. They concluded that these grasses have the potential for an enhanced valorization that goes beyond the common utilization for bioenergy. Economically feasible solutions are also urgently needed for peatland restoration projects. Experience in the restoration of peatlands impacted by mineral linear disturbances such as roads is rather limited which is addressed by Pouliot et al. They evaluated the efficiency of burying the mineral material in place below excavated peat in Quebec that was previously underlying the road. The 3-year post-restoration results suggested that the technique meets ecological restoration goals and is thus a cost-effective method in comparison to others that would include the complete removal of the mineral material.

SYNTHESIS

The papers compiled in this Research Topic make important contributions to our capability of observing, modeling and understanding processes in natural and managed peatlands. Several studies illustrated that the biogeochemical links between soil, water and vegetation as well as microbiology are very close and also complex in peatlands and thus require an integrative analysis of peatland functioning. Further advances in observational techniques and more comprehensive lab and field monitoring programs as well as international peatland databases are needed as a basis for integrative analyses that will eventually enable us to improve our predictions of the response of peatland processes to management decisions or climate change.

AUTHOR CONTRIBUTIONS

All authors listed have made a substantial, direct, and intellectual contribution to the work and approved it for publication.

FUNDING

BM acknowledges the support by the Research Foundation Flanders (FWO, G095720N).

ACKNOWLEDGMENTS

We would like to thank all authors and reviewers who have contributed to this Research Topic of papers and acknowledge the funding agencies involved in this research. We thank Klaus-Holger Knorr, Gilles Colinet, and Samuel Abiven for serving as additional handling editors.

Conflict of Interest: The authors declare that the research was conducted in the absence of any commercial or financial relationships that could be construed as a potential conflict of interest.

Publisher's Note: All claims expressed in this article are solely those of the authors and do not necessarily represent those of their affiliated organizations, or those of the publisher, the editors and the reviewers. Any product that may be evaluated in this article, or claim that may be made by its manufacturer, is not guaranteed or endorsed by the publisher.

frontiers in Environmental Science

ORIGINAL RESEARCH
published: 05 March 2021
doi: 10.3389/fenvs.2021.630721

Emissions of CO_2, N_2O and CH_4 From Cultivated and Set Aside Drained Peatland in Central Sweden

Örjan Berglund[1], *Thomas Kätterer*[2] *and Katharina H. E. Meurer*[1]*

[1]Department of Soil and Environment, Swedish University of Agricultural Sciences, Uppsala, Sweden, [2]Department of Ecology, Swedish University of Agricultural Sciences, Uppsala, Sweden

Northern peatlands are important carbon (C) reservoirs, storing about one-third of the global terrestrial soil C pool. Anthropogenic influences, such as drainage for agriculture and forestry, lower the originally high groundwater level, leading to peat aeration and decomposition. This is particularly reflected in significant losses of CO_2, while fluxes of N_2O and CH_4 are generally considered of minor importance for the overall greenhouse gas (GHG) balance of cultivated peatlands in Scandinavia. Setting land aside from agricultural production has been proposed as a strategy to reduce GHG emissions from drained peatland, restore natural habitats, and increase C sequestration. However, the evidence for this is rather scarce unless drainage is terminated. In this study, we measured respiration using dark automatic chambers, and CO_2, N_2O, and CH_4 fluxes using manual static chambers, on: 1) cultivated peatland and 2) adjacent set-aside peatland in Central Sweden. The set-aside site was found to be a greater source of respiration than the cultivated site, while higher N_2O fluxes and lower CH_4 uptake rates were observed for the cultivated site. However, to compare the full GHG balance and assess the abandonment of drained cultivated peatland, additional measures, such as gross primary production (GPP) but also dissolved organic C losses would have to be taken into account.

Keywords: drained cultivated peatlands, setting land aside, greenhouse gas, chamber measurements, mitigation action, data assimilation

OPEN ACCESS

Edited by:
Annalea Lohila,
University of Helsinki, Finland

Reviewed by:
Paavo Ojanen,
University of Helsinki, Finland
Martin Maddison,
University of Tartu, Estonia

***Correspondence:**
Katharina H. E. Meurer
katharina.meurer@slu.se

Specialty section:
This article was submitted to Soil Processes, a section of the journal Frontiers in Environmental Science

Received: *19 November 2020*
Accepted: *21 January 2021*
Published: *05 March 2021*

Citation:
Berglund Ö, Kätterer T and Meurer KHE (2021) Emissions of CO_2, N_2O and CH_4 From Cultivated and Set Aside Drained Peatland in Central Sweden. Front. Environ. Sci. 9:630721. doi: 10.3389/fenvs.2021.630721

INTRODUCTION

During the Holocene, northern peatlands stored large amounts of carbon (C) (Yu et al., 2009). In a global perspective, they now represent about one-third of the total soil carbon pool (Joosten and Clarke, 2002). Under natural conditions, most peatlands still sequester carbon dioxide (CO_2) from the atmosphere (Gorham 1991), but at the same time emit substantial quantities of C as both CO_2 and methane (CH_4) (Moore and Knowles 1987, 1989). Apart from temperature, the water balance of peat soil is generally regulating decomposition, with decomposition occurring faster in the well-aerated part of the peat above the water table (Silvola et al., 1996; Scanlon and Moore 2000). In several studies, a raised water level has been found to reduce CO_2 and nitrous oxide (N_2O) fluxes, but to increase the emissions of CH_4 (Van de Riet et al., 2013; Regina et al., 2015).

Large areas of peatland are subject to anthropogenic influences and, according to Joosten and Clarke (2002), up to 20% of total global peatland area has been drained for agriculture and forestry. Drained peatlands subside due to oxidation of the organic material, but also due to consolidation,

shrinkage, wind and water erosion and compaction (Eggelsman 1972; Heathwaite et al., 1993; Berglund, 1996). Tillage and fertilization can increase decomposition rates caused by higher eration (Glenn et al., 1993; Maljanen et al., 2007). Drainage, in combination with the naturally high organic C concentration in peat soil, leads to increased C losses in the form of CO_2 emissions (e.g., Joosten and Clarke, 2002; Lohila et al., 2004; Joosten 2009; Frolking et al., 2011; Salm et al., 2012; Ballantyne et al., 2014). Moreover, these highly elevated CO_2 emissions persist for decades after drainage of peat soil (e.g., Koizumi et al., 1999; Lohila et al., 2003). The global potential of peatland restoration in reducing GHG emissions is therefore estimated to be very high, 0.31–3.38 Gt CO_2-equivalents according to Leifeld and Menichetti (2018).

In Sweden, peatlands of varying thickness cover approximately 25% of the land area (Fredriksson 1996). Around 8.6% of Swedish agricultural soils are classified as agricultural organic soils (peat and gyttja) (Berglund and Berglund, 2010), which are considered to be 'hotspots' of greenhouse gas (GHG) emissions. Despite comprising a small proportion of total agricultural area, cultivated organic soils in Sweden and Finland are considered to be major sources of CO_2 and N_2O emissions (Kasimir-Klemendtsson et al., 1997; Maljanen et al., 2010). Enhanced nutrient availability through fertilizer application and drainage has been shown to increase N_2O emissions (Alm et al., 2007; Teh et al., 2011; van Beek et al., 2011; Salm et al., 2012). Emissions of CH_4 have been found to decrease due to soil eration and management, suggesting that cultivated peat soils may even act as CH_4 sinks (Kasimir-Klemendtsson et al., 1997; Maljanen et al., 2003; Smith and Conen 2004; Maljanen et al., 2010; Schrier-Uijl et al., 2014; Knox et al., 2015; Wang et al., 2017). Because of their comparatively low fluxes, N_2O and CH_4 are reported to play only a minor role in the overall GHG balance of cultivated peat soils in Northern Europe (e.g., Maljanen et al., 2004; Grönlund et al., 2006; Berglund and Berglund, 2010; Karki et al., 2015). However, most studies agree that conversion of wetlands for agriculture leads to significant net losses of CO_2. Lamb et al. (2016) suggested that land sparing, i.e., setting land aside from agriculture, could have the potential to reduce GHG emissions from agricultural land, through concentrating crop production to intensively managed sites, while restoring natural habitats on the abandoned land and increasing C sequestration. Permanent vegetation on abandoned peatland sites would provide year-round soil cover and enhanced photosynthesis compared with seasonal agricultural crops. This could partially compensate for C losses induced e.g., by the lower water table (Hendriks et al., 2007; Shurpali et al., 2009). However, information about the effects of abandoning or setting aside drained peatlands from agricultural use is scarce. In a study in Newfoundland, Wang et al. (2018) found that an abandoned peatland pasture sequestered more CO_2 from the atmosphere than an adjacent undisturbed bog. On including emissions of N_2O and CH_4, Wang et al. (2020) found that the same abandoned pasture had a cooling effect, primarily resulting from changes in CO_2 and CH_4, while the bog acted as nearly climate-neutral. Based on these findings, the authors reiterated the suggestion that abandoning cultivated peatland sites could mitigate CO_2 emissions. In contrast, Maljanen et al. (2007) found that abandoned organic soils in Finland showed slight net CO_2 uptake during the growing season, but were CO_2 sources outside that period, and that mean annual net CO_2 emissions from those soils were close to those from cultivated cropland. Similarly, Hadden and Grelle (2017) found that a Swedish peatland site under cultivation was a small net C sink, while a previously cultivated site that had been abandoned for 25 years was a C source.

The aim of the present study was to assess the emissions of CO_2, N_2O, and CH_4, from both a cultivated and a set aside organic soil. The study was conducted at two neighboring sites in a peatland area in Central Sweden that was drained in 1878 for agricultural use (Nerman 1898). One of these sites was set aside in the early 1990s, which means that agricultural management has been stopped. However, this did not involve closing the ditches or rising the water table. The other site is still used for agricultural crop production, mainly spring cereals.

MATERIALS AND METHODS

Study Site

Two experimental sites, cultivated (Cult) and set-aside (SA) were established at the margin of a natural peatland area about 30 km north of Uppsala in Central Sweden (**Figure 1**). The climate in this area is cold-temperate (Dfb according to the Köppen-Geiger classification) with mean annual temperature of 5.6°C and mean annual precipitation of 544 mm.

The area underwent large-scale drainage during lowering of Lake Tämnaren in 1878 (Nerman 1898), which also affected the two study sites. The cultivated site (60.0835°N, 17.233°E) was cropped with spring cereals during the study period (2013–2016), to produce standing forage for wild birds. The crop was not harvested, but the site was tilled and re-sown every spring. Prior to the study period, annual crops had been grown in rotation with grass leys (4 out of 10 years) supplying forage for dairy cows. Manure was applied and complemented with small amounts of nitrogen fertilizer during that period. The set-aside site (60.079°N, 17.236°E) was established 0.5 km south of the cultivated site and had been set aside (under permanent grassland) for more than 20 years prior to the start of the study. During the study period, the grass growing at the site was occasionally cut once a year and left on the field.

Soil properties were analyzed at the two sites (**Table 1**). Total nitrogen (N_{tot}) and total carbon (C_{tot}) content were determined by dry combustion on a LECO CN-2000 analyzer (St. Joseph, MI, USA). Soil pH and electrical conductivity (EC) were measured at a soil:solution ratio of 1:5 with deionized water. Four replicate undisturbed soil cores (7.2 cm diameter, 10 cm high) from each soil depth were used for determination of dry bulk density and volumetric water content at suction heads of 0.05, 0.3, 0.6, 1.0 and 6.0 m water column (approximately 0.5, 3.0, 6.0, 10.0, and 60.0 kPa). Physical wilting point (water content at 150 m water column) and particle density were determined on disturbed soil samples. Porosity was calculated from particle and dry bulk densities. Shrinkage was not considered when calculating water content at

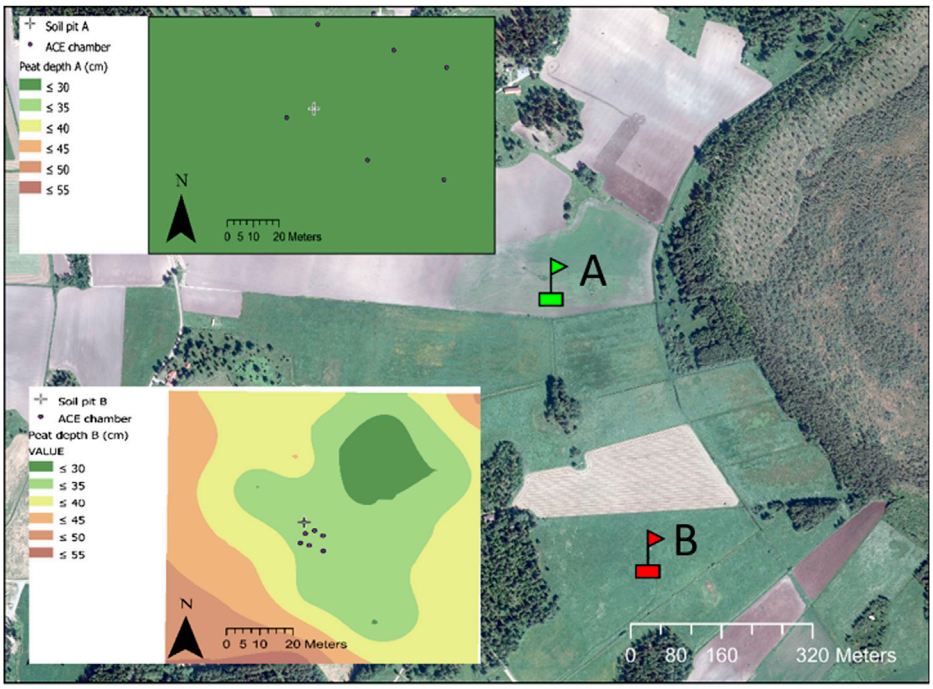

FIGURE 1 | Map showing the location of the cultivated peatland site (soil pit A, green flag) and the set-aside site (soil pit B, red flag) and (inserts) showing peat depth and the positions of the soil pits and automatic chambers (ACE) at each site.

different tensions. Saturated hydraulic conductivity was determined using a constant head method (unit hydraulic gradient) on another set of undisturbed soil cores (4 replicates). Humification degree (H1-H10) of the peat was determined according to von Post (1922). The water table was 0.5 m below the soil surface at both sites at the time of soil sampling in October 2014.

Climate Data

Abiotic variables measured included air temperature, precipitation, and global radiation, which were taken from the nearest official meteorological station (Kerstinbo; 60.270°N, 16.980°E).

Gas Sampling Set-Up

Measurements were performed every year between 2012 and 2016. During that time, gas measurements using dark chambers were taken in 2012, 2013, 2015, and 2016, while CO_2 measurements with automatic chambers were taken in 2013, 2014, and 2015. The duration and intensity of measurements varied between the years.

To estimate root respiration at the set-aside site, the grass sward was removed (SA-bare) and the emissions were compared with those from vegetated plots (SA-veg).

Manual Measurements

Manual measurements were made using the closed chamber method (e.g., Flessa et al., 1995) and following Norberg et al.

TABLE 1 | Soil properties at the set-aside and cultivated study sites. Soil sampling was performed on bare soil at the set-aside site, after removing the grass sward. All values are means (n = 4). H10 = humification degree (von Post, 1922), C_{tot} = total carbon content, N_{tot} = total nitrogen content, soil pH was measured at a soil:solution ratio of 1: 5 with deionized water, EC = electric conductivity, ρ_b = dry bulk density, K_{sat} = saturated hydraulic conductivity, n.a. = no measurements available.

Depth [cm]	Soil type	C_{tot} [%]	N_{tot} [%]	C/N [-]	pH [-]	EC [µS cm^{-1}]	ρ_b [g cm^{-3}]	Porosity [vol%]	K_{sat} [cm h^{-1}]
					Set-aside				
5–15	Fen peat (H10)	33.6	2.03	16.5	5.6	37.2	0.40	78	138
20–30	Fen peat (H10)	33.3	1.97	16.9	5.5	33.4	0.39	78	83
35–45	Gyttja clay	0.90	0.06	15.0	6.3	85.8	0.99	64	3.6
50–60	Clay	0.81	0.06	13.5	6.9	209	n.a	n.a	n.a
					Cultivated				
5–15	Fen peat (H10)	31.7	1.93	16.4	5.7	95.9	0.53	71	2
25–35	Gyttja clay	3.57	0.36	9.9	5.7	48.1	0.89	66	40
40–45	Clay	n.a	0.04	n.a	7.6	270	n.a	n.a	n.a

(2016a, 2016b). In brief, at each site six PVC rings with a base area of 0.07 m^2 were inserted into the soil to approximately 5 cm depth, to act as anchors for the chambers. To measure soil-atmosphere exchange, opaque chambers (V = 0.009 m^3) were set on the rings and sealed with rubber seals. On plots with vegetation, the crop was cut prior to the measurements. Soil and plant (mainly root) respiration was measured in two ways: 1) using a portable infrared analyzer, where measurements were performed every 5 s over a period of 3–5 min (Norberg et al., 2016b); and 2) together with N_2O and CH_4, using vial sampling and gas chromatography. For days when both methods were used, CO_2 fluxes are presented as the mean of both methods. For N_2O and CH_4, the headspace was sampled by circulating the air between the chamber and 22 ml vials for approximately 30 s (Norberg et al., 2016a). Gas samples were taken at 0, 10, 20, and 30 min after closure, and analyzed in the laboratory using gas chromatography (Perkin Elmer Clarus 500, USA). Gas fluxes were calculated using the HMR approach (Pedersen et al., 2010), which is based on the model of Hutchinson and Mosier (1981). Depending on the trend in the concentration data over time, the fluxes were calculated by either a linear or non-linear function. "No flux" is recommended by the algorithm when the concentration data are noisy and do not show a clear trend. In our dataset, this was the case for 25% of the N_2O fluxes and 21% of the CH_4 fluxes, and those were set to zero. In total, 18% and 38% of the fluxes were calculated using the non-linear function for N_2O and CH_4, respectively, while for the remaining fluxes a linear function described the trend best.

Soil moisture (volumetric water content) and soil temperature at 5 cm depth were measured next to each chamber at each measurement event, using a WET sensor (Delta-T) connected to a HH2 moisture meter read-out unit. The air-filled pore space (AFPS) was calculated using the volumetric water content and soil porosity.

Automatic Measurements

Continuous observations of soil and plant respiration (vegetated plots, SA-veg), and of peat oxidation (vegetation cover and roots removed; bare soil, SA-bare), were made using Automatic Soil CO_2 Exchange (ACE) stations (ADC BioScientific Limited, Hertfordshire, United Kingdom). Each station consists of an electronic box and a motorized moveable arm that contains an infrared gas analyzer. Besides measurements of soil respiration, the stations were used to record soil temperature at 5 and 10 cm depth (range: −10° to 50°C), and moisture at 5 cm depth measured as voltage (range 0–2 V), which was converted to volumetric water content. The area of soil analyzed was defined by a stainless steel soil collar (23 cm in diameter) which was inserted into the soil to a depth of 5 cm. To perform CO_2 measurements, the collar was automatically covered by a sealed lid enclosing a volume of 2.6 L. Internal flux was estimated based on the change in CO_2 concentration in the chamber during the closure time, by fitting either a linear or a non-linear function to the concentration data. After measurement, the lid was automatically removed from the collar and the system was left open to the environment. Measurements were performed at hourly intervals. The closure time depended on the change in concentration (maximum 10 μmol m^{-3}), but was never longer than 5 min.

Statistical Analysis

The data were analyzed using the R software (R i386 3.3.1, R Core Team 2016). For data processing, the *openxlsx* package (Schauberger and Walker, 2019) and the ddply function (*plyr* package, Wickham 2011) were used. Gas fluxes were calculated using the *HMR* package (Pedersen 2017). Differences between the sites and years were determined by analysis of variance (ANOVA) (Type-III error, *car* package; Fox and Weisberg 2019) and tested by Honest Significant Difference test (HSD.test in the *agricolae* package; de Mendiburu 2017). Differences were considered significant at $p < 0.05$. Diagrams were created using the *ggplot2* (Wickham 2009) and *cowplot* (Wilke 2017) packages. Pearson correlation coefficient (r) was used to determine linear correlations between manually measured gas fluxes and simultaneously measured soil temperature, and between manually measured gas fluxes and the interaction between soil temperature and water content (calculated as soil temperature [°C] x water content [%]). Outlier analysis was carried out using the *outliers* package (Komsta 2011).

RESULTS AND DISCUSSION

The peat layer (average of nine measurements) was shallower at the cultivated site (25 cm) than at the set-aside site (32 cm). The shallower peat layer at the cultivated site may be due to initial differences in peat depth or cultivation, which may have caused erosion and/or faster decomposition of the peat. It can be assumed that the original peat layer, i.e., before drainage of the area in 1878 (Nerman 1898), was much thicker and that the peat surface was at higher elevation. Subsidence rates due to agricultural drainage of peat soils in Nordic conditions can vary from 0.5 cm yr^{-1} on fields with pasture to 2.5 cm yr^{-1} on fields with row crops (Berglund 1996). Subsidence rates in this range (1–3 cm yr^{-1}) have been reported by e.g., Armentano (1980). The proportion of subsidence attributable to oxidation is estimated to range between 13 and 90% (Armentano and Menges 1986; Joosten and Clarke, 2002). For Swedish conditions, a value of 35% has been used as an average for all cultivated peat soils (Berglund and Berglund, 2010). Varying subsidence rates of fields under different crops have been taken as an indication that GHG emission rates vary due to the crop grown (Kasimir-Klemendtsson et al., 1997). In the present study, this would mean much higher emissions from the cultivated field compared with the set-aside field with permanent grass vegetation.

Manual Measurements

CO_2

The measured CO_2 fluxes varied between sites and years. Median fluxes (2012–2016) were significantly higher from SA-veg and SA-bare (743 and 791 mg m^{-2} h^{-1}, respectively) than from the cultivated site (415 mg m^{-2} h^{-1}) (**Tables 2** and **3**). No significant

TABLE 2 | Ecosystem respiration, nitrous oxide (N_2O) and methane (CH_4) fluxes measured manually at the set-aside and cultivated sites between 2012 and 2016. Values shown are median (Med), minimum (Min), and maximum (Max). n = number of data points. GWP = Global Warming Potential.

Treatment	CO_2 [mg m^{-2} h^{-1}]				N_2O [µg m^{-2} h^{-1}]				CH_4 [µg m^{-2} h^{-1}]				GWP[a] [mg m^{-2} CO_2-eq]
	Med	Min	Max	n	Med	Min	Max	n	Med	Min	Max	N	
Set-aside (SA)													
Vegetated (veg)													
2012	1,192	307	2,547	48									
2013					–9	–458	67	36	0	–778	237	36	
2015	401	144	1,098	58	7	–474	503	129	–37	–221	67	128	
2016	1,018	224	1999	54	0	–295	354	48	–56	–345	69	48	
Average[a]	743	144	2,547	160[b]	0	–474	503	213[b]	–36	–778	237	212[b]	742
Bare soil (bare)													
2012	880	192	4,102	54									
2015	189	98	561	10	0	–81	85	24	–33	–166	11	24	
Average[a]	791	98	4,102	64[b]	0	–81	85	24[b]	–33	–166	11	24[b]	790
Cultivated													
2012	560	69	1,661	72									
2013	543	227	871	30	3	–156	719	36	0	–56	545	36	
2015	226	43	823	84	63	–128	2,447	151	–7	–239	132	153	
2016	645	170	1,285	53	0	–207	303	48	0	–373	84	48	
Average[a]	415	43	1,661	239[b]	30	–207	2,447	235[b]	–5	–373	545	237[b]	424

[a]*Median over the study period.*
[b]*Total number of data points.*
[c]*Calculated using the GWP of N_2O (298) and CH_4 (34) for a 100-year period (Myhre et al., 2013).*

TABLE 3 | Differences in greenhouse gas (GHG) fluxes determined by manual measurements between the set-aside (SA) and cultivated sites and between years, based on analysis of variance (ANOVA) and Honest Significant Difference test. Different letters indicate significant differences between sites/years.

	CO_2 [mg m^{-2} h^{-1}]	N_2O [µg m^{-2} h^{-1}]	CH_4 [µg m^{-2} h^{-1}]
Site	a	a	a
SA-veg	A	B	B
SA-bare	A	B	B
Cultivated	B	A	A
Year	a	n.s	a
2012	A		n.a
2013	B		A
2015	B		B
2016	A		B

[a]*Significant difference (p < 0.05). n. s = no significant difference. n. a. = no data available.*

TABLE 4 | Season-specific average plant-derived carbon dioxide (CO_2) flux [mg m^{-2} h^{-1}] at the set-aside site in seasons covered by manual measurements in 2012 and 2015.

Season	Average CO_2 flux [mg m^{-2} h^{-1}]			
	Vegetated	Bare soil	Plant-derived [%]	n
Spring (until 22 June)	896 b	542 ab	40	2
Summer (until 15 August)	1,118 a	864 a	23	6
Autumn (until 1 November)	398 c	215 b	46	9

n = *number of data points. Different letters after values indicate significant differences between seasons, based on analysis of variance (ANOVA) and Honest Significance Difference test.*

differences between SA-veg and SA-bare were found (**Table 3**). According to the IPCC (2013) emission factors, CO_2 emissions should be much lower from the set-aside site (grassland, drained, boreal: 5.7 t CO_2-C ha^{-1} yr^{-1}) compared with the cultivated site (cropland, drained, boreal: 7.9 t CO_2-C ha^{-1} yr^{-1}), but this was not confirmed by our data.

Plant-derived CO_2, estimated as the difference between CO_2 fluxes from simultaneously measured vegetated plots and bare soil, was 37% (**Table 4**). This is within the range reported by Norberg et al. (2016b) (27%) and Berglund et al. (2011) (27–63%) for different cultivated and non-cultivated organic soils in southern and central Sweden. Berglund et al. (2011) identified seasonal variation in the plant contribution to CO_2 emissions, with the lowest contribution in spring (27%) and the highest in autumn (57%). Based on our limited dataset (17 data points in total), average plant-derived CO_2 fluxes were lower in summer than in spring and autumn (**Table 4**). This can be explained by the significantly higher CO_2 fluxes from both SA-veg and SA-bare during summer ($p < 0.01$).

Soil temperature and soil eration status had a strong impact on formation and release of CO_2, and emissions increased with increasing temperature (**Figure 2**). The correlation with temperature was significant for SA-veg (r = 0.60) and the cultivated site (r = 0.27), but not for SA-bare (r = 0.16). The increase in CO_2 fluxes with increasing air-filled pore space (AFPS) in the soil was significant only for the bare soil (r = 0.45) (data not shown). The relationship between CO_2 emissions and the interaction of soil temperature and water content (soil temperature x water content) was also significant only for SA-bare (r = -0.31).

N_2O

Median fluxes of N_2O from the cultivated site (30 µg m^{-2} h^{-1}) were significantly higher than from the set-aside site (**Table 2**). The fluxes from SA-veg were on average negative in 2013, but were positive in 2015 and zero in 2016. The bare soil (SA-bare)

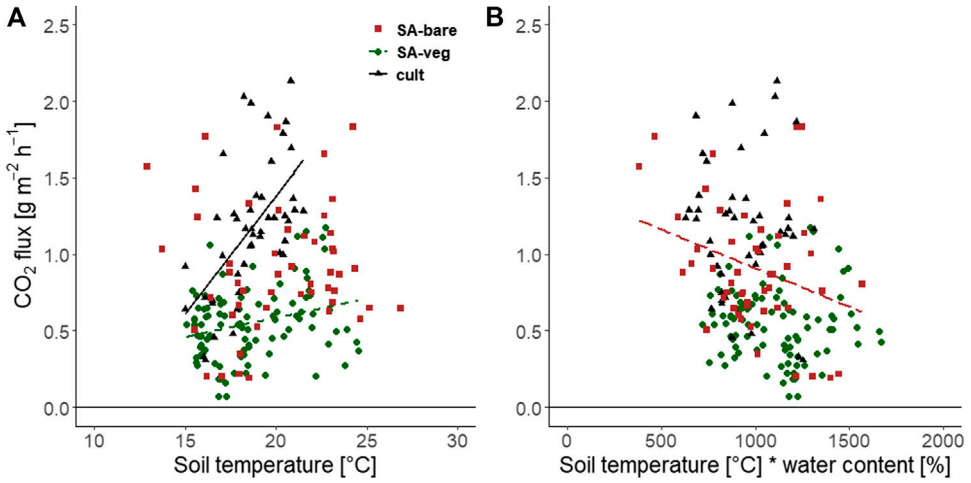

FIGURE 2 | Carbon dioxide (CO_2) flux [g m^{-2} h^{-2}] as a function of (A) soil temperature at 5 cm depth and (B) the interaction between soil temperature and volumetric water content, at the set-aside site (SA-bare (■), SA-veg (○)) and the cultivated site (cult, ▲). Significant correlations ($p < 0.05$) are shown by the respective regression line.

showed zero N_2O fluxes on average. This was mainly due to zero fluxes during summer and autumn, while fluxes were negative during spring (−39 µg m^{-2} h^{-1}; **Table 5**). In SA-veg, the N_2O fluxes were similar in spring and autumn (7 and 5 µg m^{-2} h^{-1}, respectively) and were slightly, but not significantly, higher in summer (14 µg m^{-2} h^{-1}). At the cultivated site, N_2O fluxes were not significantly different during spring and summer (141 and 288 µg m^{-2} h^{-1}, respectively), but were significantly lower ($p < 0.05$) in autumn (27 µg m^{-2} h^{-1}).

In general, N_2O fluxes showed large temporal and spatial variation and both consumption and emission were observed at all sites, irrespective of the vegetation. Absence of plants could be assumed to result in more available nitrogen (N) and, consequently, higher N_2O emissions, due to lack of N uptake by plant roots. However, we found that vegetated plots acted as N_2O sources, while fluxes were on average negative for bare soil plots (**Table 2**). Johansson et al. (2011) found a negative correlation between N_2O consumption and nitrate (NO_3^-) concentration, suggesting that consumption is linked to NO_3^- deficiency (lack of electron acceptors) and that denitrifying bacteria use N_2O as a substitute. Although it can be assumed that denitrification was the main process for N_2O production at all sites in this study, the negative fluxes found for SA-bare indicate reduction of N_2O to molecular nitrogen (N_2) in the final step of the denitrification process. Based on our dataset, decreasing soil moisture, and thus increasing AFPS, significantly decreased N_2O emissions at the cultivated site (r = −0.25). Furthermore, we found no relationship with soil temperature or with the interaction between soil temperature and soil moisture at either SA-veg or the cultivated site, which suggests that other factors influence the formation and emission of N_2O from the soil (**Figure 3**). Although crop management was quite extensive at the cultivated site, its history of manure application and the consequences of tillage in late spring, i.e., before the measurements started, might still be visible in the observed N_2O emissions.

TABLE 5 | Season-specific median nitrous oxide (N_2O) flux [µg m^{-2} h^{-1}] from the set-aside site (SA-bare and SA-veg) and the cultivated site.

Season	Median N_2O flux [µg m^{-2} h^{-1}]			
	Set-aside		Cultivated	n
	Vegetated	Bare soil		
Spring (until 22 June)	7	−39 b	141 a	5
Summer (until 15 August)	14	0 a	288 a	4
Autumn (until 1 November)	5	0 ab	27 b	6

Only measurements taken simultaneously, i.e., on the same day, are shown. n = number of data points. Different letters after values indicate significant differences between seasons, based on analysis of variance (ANOVA) and Honest Significant Difference test.

CH_4

Both the cultivated and the set-aside site were found to be a sink for CH_4 and the latter acted as a sink irrespective of the vegetation (**Table 2**). In 2013, average fluxes were zero from both the set-aside and the cultivated site. In contrast, there was net uptake of CH_4 in 2015 on both sites and in 2016 on the set-aside site. Small and mostly negative fluxes from drained peat soils have been observed in many studies in Sweden (e.g., Kasimir-Klemedtsson et al., 2009; Berglund and Berglund, 2010), Finland (e.g., Nykänen et al., 1995; Maljanen et al., 2003), Canada (Glenn et al., 1993), and Estonia (Salm et al., 2012).

In the present study, CH_4 uptake rates were significantly higher at the set-aside site (36 µg m^{-2} h^{-1}) than at the cultivated site (5 µg m^{-2} h^{-1}). Although CH_4 uptake by SA-bare (33 µg m^{-2} h^{-1}) was on average only slightly lower than that by SA-veg, the latter showed greater variation, with both high emissions (237 µg m^{-2} h^{-1}) and high uptake rates (778 µg m^{-2} h^{-1}). The function of all sites as zero emissions or even a net sink

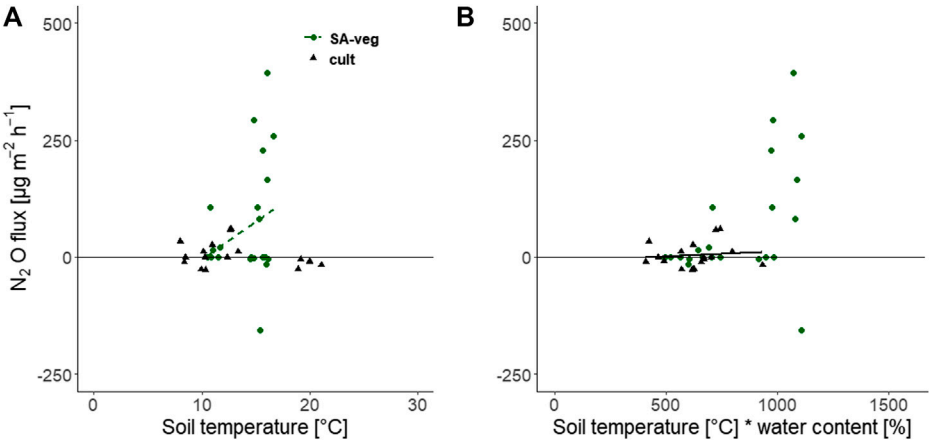

FIGURE 3 | Nitrous oxide (N_2O) flux [µg m^{-2} h^{-1}] as a function of **(A)** soil temperature at 5 cm depth and **(B)** the interaction between soil temperature and volumetric water content, at the set-aside site (SA-veg (○)) and the cultivated site (cult, ▲). No significant relationship was found.

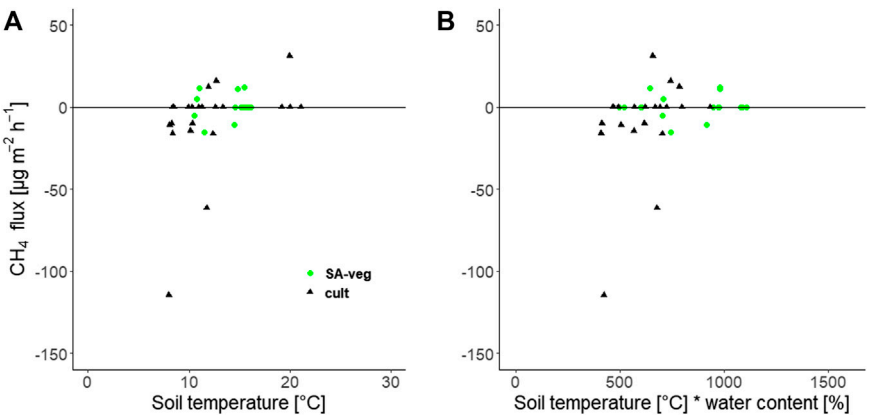

FIGURE 4 | Methane (CH_4) flux [µg m^{-2} h^{-1}] as a function of **(A)** soil temperature at 5 cm depth and **(B)** the interaction between soil temperature and volumetric water content, at the set-aside site (SA-veg (○)) and the cultivated site (▲). No significant relationship was found.

for CH_4 is likely to be related to the shallow peat layer, soil drainage, and the associated lowering of the water table. In the presence of O_2, CH_4 is consumed by methanotrophs for energy production and growth (Lai 2009). Methanotrophic activity in peatland soils is highest at shallower depths and in the boundary between the aerobic and anaerobic zones, where the ratio of CH_4 to O_2 is optimal (Dedysh 2002; Lai 2009). Consequently, rising water levels, e.g., as a consequence of poor drainage, have been found to transform peat soils from a net sink into a net source of CH_4 (e.g., Regina et al., 2007, 2015). The peat soil at the set-aside site was less compacted than that at the cultivated site, with lower dry bulk density and higher porosity and saturated hydraulic conductivity (**Table 1**). This difference in aeration and oxidizing conditions may explain the higher uptake of CH_4 at the set-aside site compared with the cultivated site.

We found no significant correlation between CH_4 flux and soil temperature (**Figure 4A**). However, CH_4 fluxes decreased with increasing AFPS in both SA-bare and the cultivated site (data not shown), but this relationship was not significant at either of the sites. Similarly, Kasimir-Klemedtsson et al. (2009) found positive CH_4 fluxes in wetter areas, and CH_4 uptake in drier areas, of a cultivated Histosol in southern Sweden. In agreement with Kasimir-Klemedtsson et al. (2009), we did not find a significant correlation with soil temperature or with the

TABLE 6 | Season-specific median methane (CH_4) flux [µg m^{-2} h^{-1}] from the set-aside site (bare soil and vegetated) and the cultivated site.

Season	Median CH_4 flux [µg m^{-2} h^{-1}]			
	Set-aside		Cultivated	n
	Vegetated	Bare soil		
Spring (until 22 June)	−29	−35	−11	6
Summer (until 15 August)	−27	−26	−5	7
Autumn (until 1 November)	−44	−48	−9	11

n = number of data points. Fluxes did not differ significantly between the seasons.

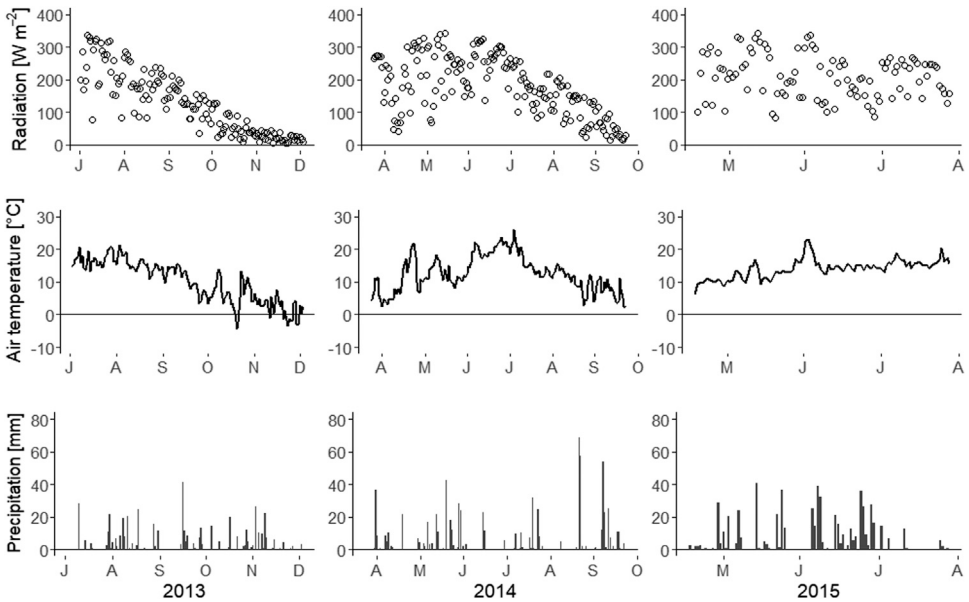

FIGURE 5 | Daily global radiation **(top)**, air temperature **(middle)**, and precipitation **(bottom)** in 2013, 2014, and 2015, measured at the nearest official meteorological station (Kerstinbo) to the study site.

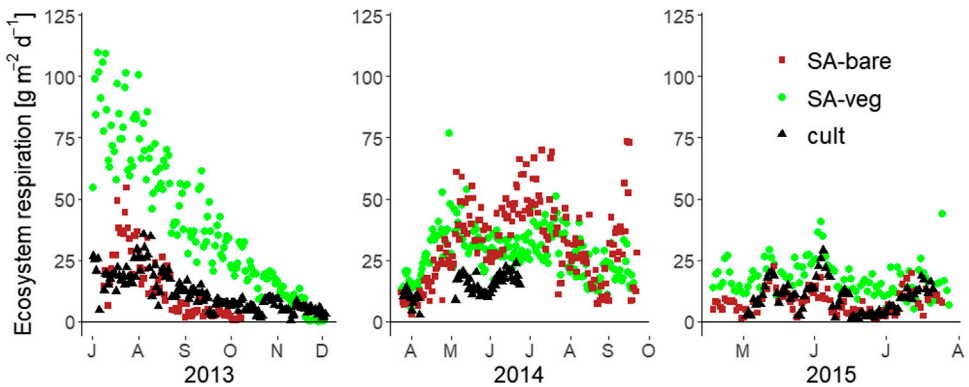

FIGURE 6 | Daily ecosystem respiration [g m^{-2}] measured by automatic chambers at the set-aside site (SA-bare and SA-veg) and the cultivated site (cult) in July-December 2013, April-October 2014, and May-August 2015.

interaction between soil temperature and water content. Lack of correlation between CH_4 flux and soil parameters may be explained by low emissions levels and fluctuations around zero (Kasimir-Klemedtsson et al., 2009).

Using the eddy covariance technique at the set-aside site, Hadden and Grelle (2017) observed higher CH_4 uptake rates during the summer months, while spring and winter usually had small but positive fluxes. In general, those authors found that CH_4 exchange rates were close to zero for air temperatures below freezing, and that higher soil temperatures led to higher uptake rates. On comparing manual measurements made simultaneously in all study plots, we did not find any significant differences between the seasons (**Table 6**). However, uptake rates at the set-aside site were on average highest in autumn (irrespective of vegetation), while uptake rates at the cultivated site were highest in spring and similar in summer and autumn (**Table 6**).

TABLE 7 | Daily ecosystem respiration [mg m^{-2} h^{-1}] in July, determined using automatic chambers, in 2013 (n = 23), 2014 (n = 24), and 2015 (n = 30).

Year	Median CO_2 flux [mg m^{-2} h^{-1}]		
	Set-aside		Cultivated
	Vegetated	Bare soil	
2013	1881 a	1094 a	901 a
2014	1585 b	867 b	908 a
2015	1008 c	632 c	390 b

Flux estimates are based on measurements taken on the same days in July in each year. Values followed by different letters indicate significant differences between years ($p < 0.05$).

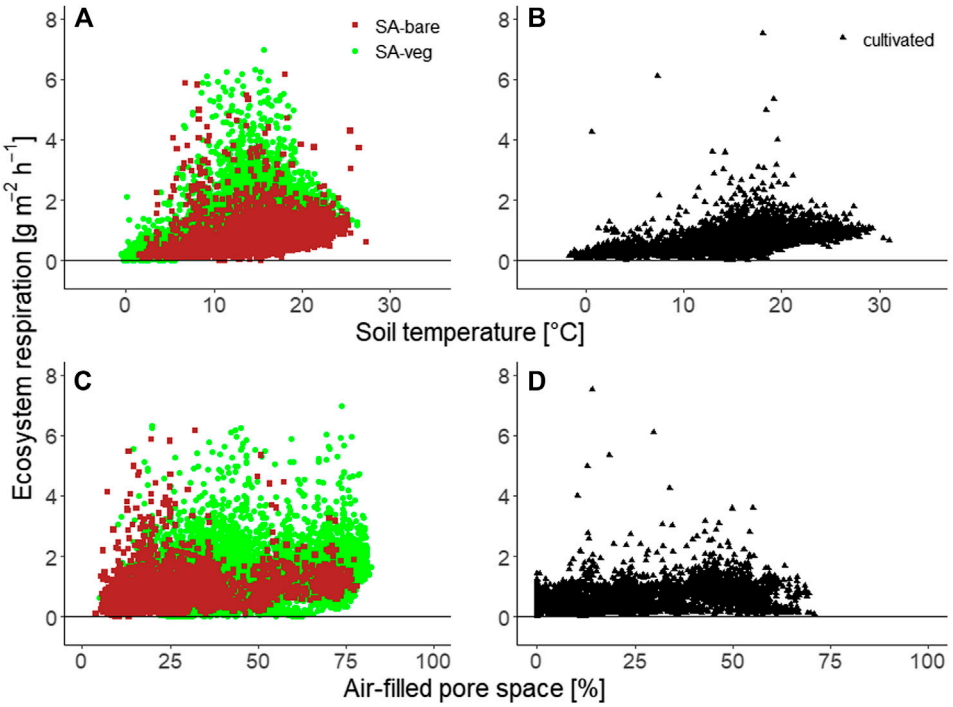

FIGURE 7 | Ecosystem respiration [g m^{-2} h^{-1}] measured by automatic chambers at **(A,C)** the set-aside site and **(B,D)** the cultivated site, as a function of **(A,B)** soil temperature at 5 cm depth and **(C,D)** air-filled pore space.

Automatic Chambers

Respiration measurements using automatic chambers were made between 2013 and 2015. Comparing the three years based on the month of July, which was covered in all three years, the average temperature was higher in 2014 (20°C) than in 2013 (17°C) and 2015 (15°C). However, the summers in 2013 and 2014 were rather dry, with rainfall in July of 25 and 16 mm, respectively. In contrast, 2015 was characterized by a wetter summer, with 105 mm of rain in July (**Figure 5**).

Measured CO_2 followed a seasonal trend, with higher emissions during the summer months and decreasing emissions as winter approached (**Figure 6**).

In July, CO_2 fluxes were higher from the vegetated set-aside plots than from the bare set-aside plots or the cultivated site (**Table 7**). One explanation for this difference might be higher C availability at the set-aside site due to the thicker peat layer, slightly higher soil C content, and greater biomass of vegetation compared with the cultivated site (Hadden and Grelle 2017).

Soil respiration from the bare soil plots (859 mg m^{-2} h^{-1}) was around 55% of ecosystem respiration (vegetated plots, 1,575 mg m^{-2} h^{-1}) when averaged over all three years. In individual years, soil respiration was 45% (2013), 52% (2014), and 37% (2015) of ecosystem respiration. These estimates are lower than the values obtained using the manual chambers, according to which soil respiration accounted for 63% of ecosystem respiration (total CO_2 flux). Similar estimates (62%) were made by Lohila et al. (2003) for a Finnish peat soil in the middle of the summer. Measurements made within controlled lysimeter experiments with ryegrass on a similar peat soil estimated the contribution of soil respiration to total summer-time CO_2 emissions to be 46% (Berglund et al., 2011). Our values are also slightly lower than estimates made in other studies using eddy covariance and chambers, according to which soil respiration accounted for 68–80% of total ecosystem respiration (Goulden et al., 1996; Law et al., 1999; Granier et al., 2000; Davidson et al., 2002). Generally, these rates typically vary throughout the year and can be expected to be lower during the growing season and higher during the non-growing season. For example, Bolstad et al. (2004) found that soil respiration was more than 60% of total ecosystem respiration during the growing season and more than 90% during the non-growing season. However, these estimates relate to forests and forest soils, respectively. The proportion of bare soil respiration estimated in this study (55%) relates to the growing season and the month of July. Moreover, it only relates to the set-aside site, since based on the data available we were unable to make an estimate for the cultivated site. The generally lower respiration observed at the cultivated site might be due to e.g., the shallower peat layer and lower root biomass, leading to less heterotrophic and autotrophic respiration, respectively.

As expected, the variation in ecosystem respiration over single days was rather moderate, but average fluxes increased slightly throughout the morning and decreased toward the evening. In general, measured fluxes were higher at higher

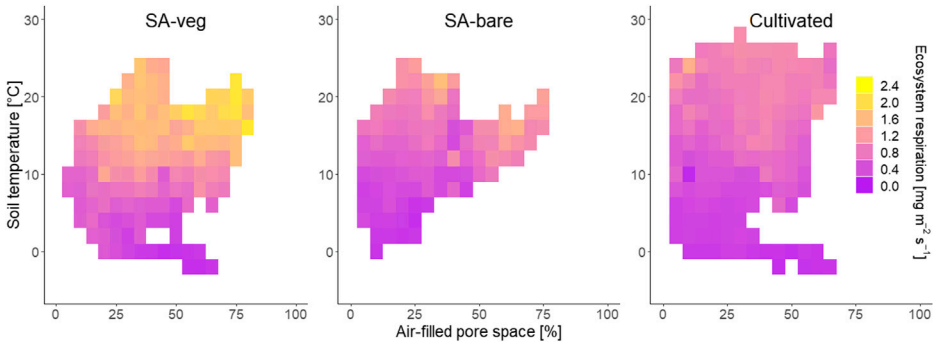

FIGURE 8 | Ecosystem respiration [g m^{-2} h^{-1}] as a function of both soil temperature [°C] and air-filled pore space [AFPS, %]. Individual squares represent increments of 2°C and 5% AFPS, and colors represent the median CO2 fluxes.

soil temperatures (**Figures 7A,B**). No such clear correlation was seen for changes in AFPS (**Figures 7C,D**). The fluxes determined using the automatic chambers are in good agreement with the respective fluxes captured by eddy covariance at the same two sites and over the same period (Hadden and Grelle 2017; data not shown).

Considering both environmental factors simultaneously revealed that higher fluxes generally occurred at higher soil temperatures (**Figure 8**). At all sites, this was also related to higher AFPS but, due to the magnitude of the emissions, this effect was less visible for the cultivated site. The highest average emissions over the respective bins of 2°C soil temperature and 5% APFS were observed at the vegetated set-aside site (SA-veg), for soil temperatures around 20°C and AFPS between 65 and 75%.

Greenhouse Gas Budget

Based on the flux data obtained in this study, we were unable to compare the full GHG budget of the two sites, since our measurements did not include GPP, C losses from water and discharge. In a comprehensive study on an abandoned peat meadow in the The Netherlands, Hendriks et al. (2007) found the area to be a small C sink after rewetting (−86 g CO_2-eq. m^{-2} yr^{-1}). Although we found significant differences for N_2O and CH_4 between the sites, the fluxes were generally low. Despite higher global warming potential (GWP) compared with CO_2, neither N_2O nor CH_4 is expected to change the picture of the set-aside site as a larger source of respiration than the cultivated site. Based on the results obtained using manual chambers, the contribution of N_2O to GWP at the sites (expressed as CO_2-equivalents; **Table 2**) was 0.27% from the bare set-aside soil and 4.33% from the cultivated site, while for CH_4 the contribution was negative for all plots (−0.14, −0.18, and −0.10% from SA-bare, SA-veg, and the cultivated site, respectively). However, N_2O emissions in particular were influenced by the vegetation cover and could be higher when considering the whole year. Our results therefore support the conclusion reached in previous studies that N_2O and CH_4 are of minor importance for the GHG balance of cultivated peat soils.

CONCLUSION

Based on measurements obtained using manual and automatic chambers, ecosystem respiration from drained peat soil was higher at a set-aside site than at a continuously cultivated site. The cultivated site was a greater source of N_2O and a smaller sink for CH_4 compared with the set-aside site, but this had only a small effect on the GHG balance derived in this study. However, in order to compare the full GHG balance, more continuous measurements are needed and GPP, C losses through water and discharge should be taken into account.

DATA AVAILABILITY STATEMENT

The original contributions presented in the study are included in the article/Supplementary Material, further inquiries can be directed to the corresponding author.

AUTHOR CONTRIBUTIONS

ÖB planned and set up the experiment and collected the data. KM analysed the data and provided a first draft of the manuscript. ÖB and TK reviewed and edited the manuscript.

FUNDING

This study was funded by the Swedish Research Council (Formas) under contract no. 214-2010-769 and by the Faculty of Natural Resources and Agricultural Sciences at SLU.

ACKNOWLEDGMENTS

The authors would like to thank Kerstin Berglund for her fundamental help in setting up the experiment and her helpful comments on the manuscript.

REFERENCES

Alm, J., Shurpali, N. J., Minkkinen, K., Aro, L., Hytönen, J., Laurila, T., et al. (2007). Emission factors and their uncertainty for the exchange of CO_2, CH_4 and N_2O in Finnish managed peatlands. *Boreal Environ. Res.* 12, 191–209.

Armentano, T. V. (1980). Drainage of organic soils as a factor in the world carbon cycle. *Bioscience* 30 (12), 825–830. doi:10.2307/1308375

Armentano, T. V., and Menges, E. S. (1986). Patterns of change in the carbon balance of organic soil-wetlands of the temperate zone. *J. Ecol.* 74, 755–774. doi:10.2307/2260396

Ballantyne, D. M., Hribljan, J. A., Pypker, T. G., and Chimner, R. A. (2014). Long-term water table manipulations alter peatland gaseous carbon fluxes in Northern Michigan. *Wetl. Ecol. Manag.* 22, 35–47. doi:10.1007/s11273-013-9320-8

Berglund, K. (1996). Cultivated organic soils in Sweden: properties and amelioration. PhD thesis. Uppsala, Sweden: Sveriges lantbruksuniversitet, 39.

Berglund, Ö., and Berglund, K. (2011). Influence of water table level and soil properties on emissions of greenhouse gases from cultivated peat soil. *Soil Biol. Biochem.* 43, 923–931. doi:10.1016/j.soilbio.2011.01.002

Berglund, Ö., Berglund, K., and Klemedtsson, L. (2011). Plant-derived CO2flux from cultivated peat soils. *Acta Agric. Scand. Sect. B Soil Plant Sci.* 61 (6), 508–513. doi:10.1080/09064710.2010.51021

Bolstad, P. V., Davis, K. J., Martin, J., Cook, B. D., and Wang, W. (2004). Component and whole-system respiration fluxes in northern deciduous forests. *Tree Physiol.* 24, 493–504. doi:10.1093/treephys/24.5.493

Davidson, E. A., Savage, K., Verchot, L. V., and Navarro, R. (2002). Minimizing artifacts and biases in chamber-based measurements of soil respiration. *Agric. For. Meteorol.* 113, 21–37. doi:10.1016/s0168-1923(02)00100-4

de Mendiburu, F. (2017). Agricolae: statistical procedures for agricultural research. R package version 1.2-8. Available at: https://CRAN.R-project.org/package=agricolae.

Dedysh, S. N. (2002). Methanotrophic bacteria of acidic *sphagnum* peat bogs. *Microbiology* 71 (6), 638–650. doi:10.1023/a:1021467520274

Eggelsman, R. (1972). Dränbemessung im Moor nach tiefe, abstand und art. *Telma* 2, 91–108.

Flessa, H., Dörsch, P., and Beese, F. (1995). Seasonal variation of N2O and CH4 fluxes in differently managed arable soils in Southern Germany. *J. Geophys. Res.* 100, 23115–23124.

Fox, J., and Weisberg, S. (2019). *An R companion to applied regression*. 3rd Edn. Thousand Oaks, CA: Sage.

Fredriksson, D. (1996). "Peat resources in Sweden," in *Global peat resources*. Editor E. Lappalainen (London, United Kingdom: International Peat Society), 137–144.

Frolking, S., Talbot, J., Jones, M. C., Treat, C. C., Kauffman, J. B., Tuittila, E.-S., et al. (2011). Peatlands in the Earth's 21st century climate system. *Environ. Rev.* 19, 371–396. doi:10.1139/a11-014

Glenn, S., Heyes, A., and Moore, T. (1993). Carbon dioxide and methane fluxes from drained peat soils, southern Quebec. *Global Biogeochem. Cycles.* 7 (2), 247–257. doi:10.1029/93gb00469

Gorham, E. (1991). Northern peatlands: role in the carbon cycle and probable responses to climatic warming. *Ecol. Appl.* 1 (2), 182–195. doi:10.2307/1941811

Goulden, M. L., Munger, J. W., Fan, S.-M., Daube, B. C., and Wofsy, S. C. (1996). Measurements of carbon sequestration by long-term eddy covariance: methods and a critical evaluation of accuracy. *Global Change Biol.* 2, 169–182. doi:10.1111/j.1365-2486.1996.tb00070.x

Granier, A., Ceschia, E., Damesin, C., Dufrêne, E., Epron, D., Gross, P., et al. (2000). The carbon balance of a young Beech forest. *Funct. Ecol.* 14, 312–325. doi:10.1046/j.1365-2435.2000.00434.x

Grönlund, A., Sveistrup, T. E., Sövik, A. K., Rasse, D. P., and Klöve, B. (2006). Degradation of cultivated peat soils in Northern Norway based on field scale CO_2, N_2O and CH_4 emission measurements. *Arch Acker Pfl Boden.* 52 (2), 149–159. doi:10.1080/03650340600581968

Hadden, D., and Grelle, A. (2017). The impact of cultivation on CO 2 and CH 4 fluxes over organic soils in Sweden. *Agric. For. Meteorol.* 243, 1–8. doi:10.1016/j.agrformet.2017.05.002

Heathwaite, A. L., Eggelsman, R., and Göttlich, K. H. (1993). "Ecohydrology, mire drainage and mire conservation," in *Mires: processes, exploitation and conservation*. Editor A. L. Heathwaite (Chichester, United Kingdom: John Wiley & Sons), 417–484.

Hendriks, D. M. D., van Huissteden, J., Dolman, A. J., and van der Molen, M. K. (2007). The full greenhouse gas balance of an abandoned peat meadow. *Biogeosciences* 4, 411–424. doi:10.5194/bg-4-411-2007

Hutchinson, G. L., and Mosier, A. R. (1981). Improved soil cover method for field measurement of nitrous oxide fluxes. *Soil Sci. Soc. Am. J.* 45, 311–316. doi:10.2135/sssaj1981.03615995004500020017

IPCC (2013). Drained inland organic soils. Available at: https://www.ipcc-nggip.iges.or.jp/public/wetlands/pdf/Wetlands_separate_files/WS_Chp2_Drained_Inland_Organic_Soils.pdf.

Johansson, A. E., Klemedtsson, Å. K., Klemedtsson, L., and Svensson, B. H. (2011). Nitrous oxide exchanges with the atmosphere of a constructed wetland treating wastewater. *Tellus B* 55 (3), 737–750. doi:10.3402/tellusb.v55i3.16363

Joosten, H., and Clarke, D. (2002). *Wise use of mires and peatlands – background and principles including a framework for decision-making*. London, United Kingdom: International Mire Conservation Group and International Peat Society.

Joosten, H. (2009). *The global peatland CO_2 picture: peatland status and drainage related emissions in all countries of the world*. Wageningen, The Netherlands: Report for Wetlands International.

Karki, S., Elsgaard, L., Kandel, T. P., and Lærke, P. E. (2015). Full GHG balance of a drained fen peatland cropped to spring barley and reed canary grass using comparative assessment of CO2 fluxes. *Environ. Monit. Assess.* 187, 62. doi:10.1007/s10661-014-4259-7

Kasimir-Klemedtsson, Å., Klemedtsson, L., Berglund, K., Martikainen, P., Silvola, J., and Oenema, O. (1997). Greenhouse gas emissions from farmed organic soils: a review. *Soil Use Manag.* 13, 245–250. doi:10.1111/j.1475-2743.1997.tb00595.x

Kasimir-Klemedtsson, Å., Weslien, P., and Klemedtsson, L. (2009). Methane and nitrous oxide fluxes from a farmed Swedish Histosol. *Eur. J. Soil Sci.* 60, 321–331. doi:10.1111/j.1365-2389.2009.01124.x

Knox, S. H., Sturtevant, C., Matthes, J. H., Koteen, L., Verfaillie, J., and Baldocchi, D. (2015). Agricultural peatland restoration: effects of land-use change on greenhouse gas (CO2 and CH4) fluxes in the Sacramento-San Joaquin Delta. *Global Change Biol.* 21, 750–765. doi:10.1111/gcb.12745

Koizumi, H., Kontturi, M., Mariko, S., Nakadai, T., Bekku, Y., and Mela, T. (1999). Soil respiration in three soil types in agricultural ecosystems in Finland. *Acta Agric. Scand. Sect. B Soil Plant Sci.* 49, 65–74. doi:10.1080/09064719950135560

Komsta (2011). Outliers: test for outliers. Available at: http://komsta.net.

Lai, D. Y. F. (2009). Methane dynamics in northern peatlands: a review. *Pedosphere* 19 (4), 409–421. doi:10.1016/s1002-0160(09)00003-4

Lamb, A., Green, R., Bateman, I., Broadmeadow, M., Bruce, T., Burney, J., et al. 2016). The potential for land sparing to offset greenhouse gas emissions from agriculture. *Nat. Clim. Change.* 6, 488–492. doi:10.1038/NCLIMATE2910

Law, B. E., Ryan, M. G., and Anthoni, P. M. (1999). Seasonal and annual respiration of a ponderosa pine ecosystem. *Global Change Biol.* 5, 169–182. doi:10.1046/j.1365-2486.1999.00214.x

Leifeld, J., and Menichetti, L. (2018). The underappreciated potential of peatlands in global climate change mitigation strategies. *Nat. Commun.* 9 (1), 1071. doi:10.1038/s41467-018-03406-6

Lohila, A., Aurela, M., Regina, K., and Laurila, T. (2003). Soil and total ecosystem respiration in agricultural fields: effect of soil and crop type. *Plant Soil.* 251, 303–317. doi:10.1023/a:1023004205844

Lohila, A., Aurela, M., Tuovinen, J-P., and Laurila, T. (2004). Annual CO2exchange of a peat field growing spring barley or perennial forage grass. *J. Geophys. Res.* 109, D18116. doi:10.1029/2004JD004715

Maljanen, M., Hyvtönen, J., Mäkiranta, P., Alm, J., Minkkinen, K., Laine, J., et al. (2007). Greenhouse gas emissions from cultivated and abandoned organic croplands in Finland. *Boreal Environ. Res.* 12, 133–140.

Maljanen, M., Komulainen, V.-M., Hytönen, J., Martikainen, P. J., and Laine, J. (2004). Carbon dioxide, nitrous oxide and methane dynamics in boreal organic agricultural soils with different soil characteristics. *Soil Biol. Biochem.* 36, 1801–1808. doi:10.1016/j.soilbio.2004.05.003

Maljanen, M., Liikanen, A., Silvola, J., and Martikainen, P. J. (2003). Methane fluxes on agricultural and forested boreal organic soils. *Soil Use Manag.* 19, 73–79. doi:10.1079/SUM2002171

Maljanen, M., Sigurdsson, B. D., Guðmundsson, J., Óskarsson, H., Huttunen, J. T., and Martikainen, P. J. (2010). Greenhouse gas balances of managed peatlands in the Nordic countries - present knowledge and gaps. *Biogeosciences* 7, 2711–2738. doi:10.5194/bg-7-2711-2010

Moore, T. R., and Knowles, R. (1987). Methane and carbon dioxide evolution from subarctic fens. *Can. J. Soil Sci.* 67, 77–81. doi:10.4141/cjss87-007

Moore, T. R., and Knowles, R. (1989). The influence of water table levels on methane and carbon dioxide emissions from peatland soils. *Can. J. Soil Sci.* 69, 33–38. doi:10.4141/cjss89-004

Myhre, G., Shindell, D., Bréon, F-M., Collins, W., Fuglestvedt, J., Huang, J., et al. (2013). "Anthropogenic and natural radiative forcing," in *Climate change 2013: the physical science basis. Contribution of working group I to the fifth assessment report of the intergovernmental panel on climate change*. Editors T. F. Stocker et al. (Cambridge, MA: Cambridge University Press).

Nerman, G. (1898). Temnarens sänkning. *Svenska Mosskultutföreningens tidskrift.* 2, 61–88.

Norberg, L., Berglund, Ö., and Berglund, K. (2016a). Nitrous oxide and methane fluxes during the growing season from cultivated peat soils, peaty marl and gyttja clay under different cropping systems. *Acta Agric. Scand. Sect. B Soil Plant Sci.* 66 (7), 602–612. doi:10.1080/09064710.2016.1205126

Norberg, L., Berglund, Ö., and Berglund, K. (2016b). Seasonal CO2 emission under different cropping systems on Histosols in southern Sweden. *Geoderma Regional.* 7, 338–345. doi:10.1016/j.geodrs.2016.06.005

Nykänen, H., Alm, J., Lang, K., Silvola, J., and Martikainen, P. J. (1995). Emissions of CH_4, N_2O and CO_2 from a virgin fen and a fen drained for grassland in Finland. *J. Biogeogr.* 22, 351–357. doi:10.2307/2845930

Pedersen, A. R. (2017). HMR: flux estimation with static chamber data. R package version 0.4.2. Available at: https://CRAN.R-project.org/package=HMR.

Pedersen, A. R., Petersen, S. O., and Schelde, K. (2010). A comprehensive approach to soil-atmosphere trace-gas flux estimation with static chambers. *Eur. J. Soil Sci.*, 61, 888. doi:10.1111/j.1365-2389.2010.01291.x

R Core Team (2016). *R: a language and environment for statistical computing*. Vienna, Austria: R Foundation for Statistical Computing.

Regina, K., Pihlatie, M., Esala, M., and Alakukku, L. (2007). Methane fluxes on boreal arable soils. *Agric. Ecosyst. Environ.* 119, 346–352. doi:10.1016/j.agee.2006.08.002

Regina, K., Sheehy, J., and Myllys, M. (2015). Mitigating greenhouse gas fluxes from cultivated organic soils with raised water table. *Mitig. Adapt. Strategies Glob. Change.* 20, 1529–1544. doi:10.1007/s11027-014-9559-2

Salm, J.-O., Maddison, M., Tammik, S., Soosaar, K., Truu, J., and Mander, Ü. (2012). Emissions of CO2, CH4 and N2O from undisturbed, drained and mined peatlands in Estonia. *Hydrobiologia* 692, 41–55. doi:10.1008/s10750-011-0934-7

Scanlon, D., and Moore, T. (2000). Carbon dioxide production from peatland soil profiles: the influence of temperature, oxic/anoxic conditions and substrate. *Soil Sci.* 165 (2), 153–160. doi:10.1097/00010694-200002000-00006

Schauberger, P., and Walker, A. (2019). openxlsx: Read, Write and Edit xlsx Files. R package version 4.1.4. Available at: https://CRAN-R-project.org/package=openxlsx

Schrier-Uijl, A. P., Kroon, P. S., Hendriks, D. M. D., Hensen, A., Van Huissteden, J., Berendse, F., et al. (2014). Agricultural peatlands: towards a greenhouse gas sink - a synthesis of a Dutch landscape study. *Biogeosciences* 11, 4559–4576. doi:10.5194/bg-11-4559-2014

Shurpali, N. J., Hyvönen, N. P., Huttunen, J., Clement, R. J., Reichstein, M., Nykänen, H., et al. (2009). Cultivation of a perennial grass for bioenergy on a boreal organic soil - carbon sink or source? *GCB Bioenergy* 1, 35–50. doi:10.1111/j.1757-1707.2009.01003.x

Silvola, J., Alm, J., Ahlholm, U., Nykänen, H., and Martikainen, P. J. (1996). CO2 fluxes from peat in boreal mires under varying temperature and moisture conditions. *J. Ecol.* 84, 219–228. doi:10.2307/2261357

Smith, K. A., and Conen, F. 2004). Impacts of land management on fluxes of trace greenhouse gases. *Soil Use Manag.* 20, 255–263. doi:10.1079/SUM2004238

Teh, Y. A., Silver, W. L., Sonnentag, O., Detto, M., Kelly, M., and Baldocchi, D. D. (2011). Large greenhouse gas emissions from a temperate peatland pasture. *Ecosystems* 14, 311–325. doi:10.1007/s10021-011-9411-4

van Beek, C. L., Pleijter, M., and Kuikman, P. J. (2011). Nitrous oxide emissions from fertilized and unfertilized grasslands on peat soil. *Nutrient Cycl. Agroecosyst* 89, 453–461. doi:10.1007/s10705-010-9408-y

van de Riet, B. P., Hefting, M. M., and Verhoeven, J. T. A. (2013). Rewetting drained peat meadows: risks and benefits in terms of nutrient release and greenhouse gas exchange. *Water Air Soil Pollut.* 1440, 224–133. doi:10.1007/s11270-013-1140-5

von Post, L. (1922). Sveriges Geologiska Undersöknings torvinventering och några av dess hittills vunna resultat. *Svenska Mosskulturföreningens tidskrift.* 36, 1–27.

Wang, M., Wu, J., Lafleur, P. M., and Luan, J. (2020). Investigation of the climatological impacts of agricultural management and abandonment on a boreal bog in western Newfoundland, Canada. *Sci. Total Environ.* 711, 134632. doi:10.1016/j.scitotenv.2019.134632

Wang, M., Wu, J., Lafleur, P. M., Luan, J., Chen, H., and Zhu, X. (2018). Can abandoned peatland pasture sequestrate more carbon dioxide from the atmosphere than an adjacent pristine bog in Newfoundland, Canada? *Agric. For. Meteorol.* 248, 91–108. doi:10.1016/j.agrformet.2017.09.010

Wang, M., Wu, J., Luan, J., Lafleur, P., Chen, H., and Zhu, X. (2017). Near-zero methane emission from an abandoned boreal peatland pasture based on eddy covariance measurements. *PloS One* 12, e0189692. doi:10.1371/journal.pone.0189692

Wickham, H. (2009). *ggplot2: elegant graphics for data analysis*. New York, NY: Springer-Verlag.

Wickham, H. (2011). The split-apply-combine strategy for data analysis. *J. Stat. Software* 40 (1), 1–29. doi:10.18637/jss.v040.i01

Wilke, C. O. (2017). Cowplot: streamlined plot theme and plot annotations for 'ggplot2'. R package version 0.8.0. Available at: https://CRAN.R-project.org/package=cowplot.

Yu, Z., Beilman, D. W., and Jones, M. C. (2009). Sensitivity of Northern Peatland Carbon Dynamics to Holocene Climate Change. Carbon Cycling in Northern Peatlands. *Geophysical Monograph Series* 184, doi:10.1029/2008GM000822

Conflict of Interest: The authors declare that the research was conducted in the absence of any commercial or financial relationships that could be construed as a potential conflict of interest.

frontiers in Environmental Science

ORIGINAL RESEARCH
published: 18 March 2021
doi: 10.3389/fenvs.2021.617828

Spatio-Temporal Variability of Peat CH_4 and N_2O Fluxes and Their Contribution to Peat GHG Budgets in Indonesian Forests and Oil Palm Plantations

Erin Swails[1], Kristell Hergoualc'h[2], Louis Verchot[3], Nisa Novita[4] and Deborah Lawrence[1]*

[1]Department of Environmental Sciences, University of Virginia, Charlottesville, VA, United States, [2]Center for International Forestry Research, Bogor, Indonesia, [3]International Center for Tropical Agriculture, Cali, Colombia, [4]Yayasan Konservasi Alam Nusantara, Jakarta, Indonesia

Land-use change in tropical peatlands substantially impacts peat emissions of methane (CH_4) and nitrous oxide (N_2O) in addition to emissions of carbon dioxide (CO_2). However, assessments of full peat greenhouse gas (GHG) budgets are scarce and CH_4 and N_2O contributions remain highly uncertain. The objective of our research was to assess changes in peat GHG flux and budget associated with peat swamp forest disturbance and conversion to oil palm plantation and to evaluate drivers of variation in trace gas fluxes. Over a period of one and a half year, we monitored monthly CH_4 and N_2O fluxes together with environmental variables in three undrained peat swamp forests and three oil palm plantations on peat in Central Kalimantan. The forests included two primary forests and one 30-year-old secondary forest. We calculated the peat GHG budget in both ecosystems using soil respiration and litterfall rates measured concurrently with CH_4 and N_2O fluxes, site-specific soil respiration partitioning ratios, and literature-based values of root inputs and dissolved organic carbon export. Peat CH_4 fluxes (kg CH_4 ha^{-1} $year^{-1}$) were insignificant in oil palm (0.3 ± 0.4) while emissions in forest were high (14.0 ± 2.8), and larger in wet than in dry months. N_2O emissions (kg N_2O ha^{-1} $year^{-1}$) were highly variable spatially and temporally and similar across land-uses (5.0 ± 3.9 and 5.2 ± 3.7 in oil palm and forest). Temporal variation of CH_4 was controlled by water table level and soil water-filled pore space in forest and oil palm, respectively. Monthly fluctuations of N_2O were linked to water table level in forest. The peat GHG budget (Mg CO_2 equivalent ha^{-1} $year^{-1}$) in oil palm (31.7 ± 8.6) was nearly eight times the budget in forest (4.0 ± 4.8) owing mainly to decreased peat C inputs and increased peat C outputs. The GHG budget was also ten times higher in the secondary forest (10.2 ± 4.5) than in the primary forests (0.9 ± 3.9) on the account of a larger peat C budget and N_2O emission rate. In oil palm 96% of emissions were released as CO_2 whereas in forest CH_4 and N_2O together contributed 65% to the budget. Our study highlights the disastrous atmospheric impact associated with forest degradation and conversion to oil palm in tropical peatlands and stresses the need to investigate GHG fluxes in disturbed undrained lands.

OPEN ACCESS

Edited by:
Björn Klöve,
University of Oulu, Finland

Reviewed by:
Fumiaki Takakai,
Akita Prefectural University, Japan
Na Li,
Chinese Academy of Science, China

***Correspondence:**
Erin Swails
ees8rg@virginia.edu

Specialty section:
This article was submitted to Soil Processes, a section of the journal Frontiers in Environmental Science

Received: *16 October 2020*
Accepted: *04 February 2021*
Published: *18 March 2021*

Citation:
Swails E, Hergoualc'h K, Verchot L, Novita N and Lawrence D (2021) Spatio-Temporal Variability of Peat CH_4 and N_2O Fluxes and Their Contribution to Peat GHG Budgets in Indonesian Forests and Oil Palm Plantations. Front. Environ. Sci. 9:617828. doi: 10.3389/fenvs.2021.617828

Keywords: GHG emissions, peat swamp forest, oil palm, peatland, methane, nitrous oxide, Indonesia, tropical

INTRODUCTION

Peat swamp forests of Southeast Asia have experienced extensive deforestation and conversion over past decades. In Peninsular Malaysia, Sumatra and Borneo, only 29% of peatlands (or 4.6 Mha) remained covered by forests in 2015 while lands managed by smallholders or industrial groups amounted to 50% of peatlands (7.8 Mha) (Miettinen et al., 2016). Conversion of peat swamp forest, in particular to oil palm, is a large and growing source of greenhouse gas (GHG) emissions to the atmosphere (Koh et al., 2011; Miettinen et al., 2017; Austin et al., 2018). Efforts to characterize the GHG impact of this conversion have largely focused on alterations of soil CO_2 emissions and phytomass C stocks (e.g., Hergoualc'h and Verchot, 2011; Miettinen et al., 2017). Changes in emissions of CH_4 and N_2O from peat can also be significant (Hergoualc'h and Verchot, 2012; Oktarita et al., 2017; Cooper et al., 2020) but have been far less well characterized (Skiba et al., 2020), despite N_2O and CH_4 being potent GHGs, with global warming potentials, respectively 268 and 86 times that of CO_2 over a 20-year time horizon (Myhre et al., 2013). Reliable estimates of N_2O emissions from degraded peatlands are lacking (Tian et al., 2020). Flux studies on peatlands in paired forest-oil palm plantation replicated sites are very scarce, with only one study to our knowledge (Cooper al., 2020). Some of the studies (regardless of sites replication and forest-oil palm pairing) were conducted over very limited periods [e.g., 3 months in Cooper al. (2020)], and many do not stratify the sampling according to microspatial differences affecting the fluxes (e.g., Melling et al., 2007). None measured simultaneously all peat C fluxes for assessing peat net CO_2 and GHG exchanges. Full peat GHG budgets that include net CO_2, CH_4, and N_2O fluxes and concurrent measurements of controlling factors in these ecosystems are thus critically lacking and needed to quantify the impact of forest-to-oil palm conversion on peat GHG emissions and to increase understanding of underlying mechanisms.

Undrained peat soils in the tropics are typically a net source of CH_4, while drained peat soils can act as either a source or a small sink (Hergoualc'h and Verchot, 2012). CH_4 is produced by methanogens through anaerobic digestion of organic matter either by CO_2 reduction or by acetate fermentation (Le Mer and Roger, 2001). Methanotrophs consume CH_4 produced in the soil as well as atmospheric CH_4 for use as a C and energy source (King et al., 1990; Whalen et al., 1990; Jones and Nedwell, 1993). CH_4 production and consumption occur simultaneously in the soil profile. General controls on wetland CH_4 emissions include hydrology, temperature, and vegetation (Wright et al., 2013; Turetsky et al., 2014). The activity of methanotrophs is mainly limited by oxygen availability (Le Mer and Roger 2001) therefore drainage promotes methanotrophy while decreasing methanogenesis (Inubushi et al., 2003). The influence of hydrological factors affecting the fluxes result in strong spatio-temporal variability. In Indonesian peatlands under pristine conditions, soil CH_4 fluxes have been reported to be highest during wet months when the water table level is close to the peat surface (Jauhiainen et al., 2005) but to decrease with flooding above a water table level threshold because of gas diffusion restriction (Ishikura et al., 2019). CH_4 fluxes are also influenced by soil microtopography and were reported to be higher from waterlogged low-lying hollows than drier elevated hummocks in pristine peat forests of Indonesia and Peru (Jauhiainen et al., 2005; Ishikura et al., 2019; Hergoualc'h et al., 2020). Methanogenesis is thought to be more temperature-sensitive than methanotrophy (Turetsky et al., 2014) though in the tropics where temperature fluctuation is small, this factor is considered a less important control on CH_4 fluxes than other variables (Wright et al., 2013). Methanogenesis is often fueled by recent plant photosynthate (Bridgham et al., 2012). Therefore, CH_4 fluxes are altered following land use conversion as the result of vegetation changes and associated substrate supply modifications in addition to drainage. Fires that expose deeper peat layers also alter the substrate supply for methanogenesis (Jauhiainen et al., 2016).

Both undrained and drained peat soils in the tropics function as a source of N_2O (Drösler et al., 2014; Parn et al., 2018). N_2O is generated mainly by soil microbes through nitrification and denitrification. Nitrification is the aerobic oxidation of NH_4^+ or NH_3 to NO_2^- and NO_3^- with N_2O formed as a biproduct (Hynes and Knowles, 1984). Denitrifying bacteria reduce NO_3^- under oxygen (O_2) limited conditions ultimately producing N_2 but also N_2O, with a N_2O:N_2 ratio depending on O_2 availability. Coupling of nitrification and denitrification can occur in soils where oxic and anoxic microenvironments neighbor each other (Arah, 1997). Nitrifier denitrication, distinct from coupled nitrification—denitrification, can also be an important source of N_2O (Wrage et al., 2001; Hergoualc'h et al., 2007). N_2O production in soils depends upon substrate supply from mineralized organic matter, applied N fertilizer, or deposited atmospheric N as well as biotic factors such as plant-microbe interactions and abiotic factors including, e.g., soil moisture and temperature (Skiba and Smith, 2000; Butterbach-Bahl et al., 2013). Soil N_2O emissions often correlate well with the soil water-filled pore space (WFPS), with emission rates in the tropics peaking around a WFPS of 60% and remaining high at 80% WFPS (Van Lent et al., 2015). Nitrous oxide fluxes from peat soils are governed by factors that limit the microbial processes of nitrification and denitrification, especially variations in water table level and soil inorganic N (Martikainen et al., 1993; Melling et al., 2007; Oktarita et al., 2017). Soil-atmosphere exchange of N_2O may be highly spatially variable because of inter-site as well as micro-scale and seasonal variations (Takakai et al., 2006; Jauhiainen et al., 2012) in environmental conditions. Peat N_2O fluxes in the tropics are characterized by the presence of temporal and spatial emission hotspots under natural and drained conditions (Takakai et al., 2006; Jauhiainen et al., 2012; Oktarita et al., 2017; Hergoualc'h et al., 2020) owing to the fine scales over which controlling factors vary. Peat N_2O fluxes in Indonesian peatlands have been found to be higher

during the rainy season than during the dry season (Takakai et al., 2006; Jauhiainen et al., 2012) but seasonal variation in emission is inconsistent across land uses within a peatland area and between peatland areas of Southeast Asia. In oil palm plantation, the response of N_2O emissions to fertilization has been reported to be exponential but restricted to the small area of N application and transient (Sakata et al., 2015; Oktarita et al., 2017). As a result, the impact of fertilized-induced emissions has been observed to be minimal, with annual emissions stemming essentially from peat decomposition (Oktarita et al., 2017).

Peat GHG budgets are estimated from the contribution of individual gases (CH_4, N_2O, CO_2) based on their respective global warming potential. Annual peat CO_2 budgets include on- and off-site CO_2 emissions/removals from soil organic matter mineralization, sequestration processes and leaching (Drösler et al., 2014). They are calculated as the balance between C inputs from above and below ground litter, and outputs via heterotrophic respiration and dissolved organic C export. Total respiration consists of root (autotrophic) and microbial (heterotrophic) respiration, with only the latter contributing actively to soil C stock changes. Degradation and drainage enhance CO_2 production from microbial decomposition (Hergoualc'h and Verchot 2014) and losses of dissolved carbon in water (Rixen et al., 2016). Forest replacement by oil palms decreases aboveground litter production but enhances inputs of fresh organic material from dead roots and root exudates (Hergoualc'h and Verchot, 2014; Harianti et al., 2017). Peat soils are small sinks or sources of CO_2 in pristine swamp forests but strong sources in oil palm plantations, with loss rates varying greatly depending on pre-conversion land-use history and post-conversion plantation age and management practices (Hergoualc'h and Verchot, 2014; Hergoualc'h et al., 2017).

To improve current understanding on GHG dynamics associated with peat swamp forest degradation and conversion to oil palm plantation, we conducted a 19-month study in a peatland in Central Kalimantan, Indonesia. We measured monthly CH_4 and N_2O fluxes from soils along with environmental factors in three undrained forest plots (two primary forests and one secondary forest) and three oil palm plantation plots managed by smallholders. Our measurements covered wet to dry transitions in a year with normal precipitation (2014) and a strong El Niño year (2015). Intra-plot spatial variability was captured by sampling in hummocks and hollows in forest, and near and far from palms in plantations. Total soil respiration and litterfall rates measured concurrently with CH_4 and N_2O fluxes provided for peat CO_2 budgets computation using site-specific soil respiration partitioning ratios and literature-based values for root litter inputs and dissolved organic C losses. Our study addressed five questions: 1) How do peat CH_4 and N_2O emissions differ between and within oil palm plantation and forest? 2) How do they vary on seasonal timescales? 3) How do environmental parameters (moisture, temperature, peat chemistry) control emission rates of these gases? 4) How do peat GHG budgets differ between oil palm plantation and forest and between forest types? And 5) how important is the contribution of CH_4 and N_2O fluxes to peat GHG budgets in these ecosystems?

MATERIALS AND METHODS

Site Description

We conducted our research at permanent plots in a peatland on the southern coast of Indonesian Borneo in Central Kalimantan, approximately 10 km outside the city of Pangkalan Bun (S 02°49,410′, E 111°48.785′). The plots were established in 2012 by the Center for International Forestry Research at three locations in undrained forest inside Tanjung Puting National Park and at three locations in nearby drained smallholder oil palm plantations.

The regional climate is humid tropical. Total annual precipitation is high and average daily temperature remains fairly constant during the year. During 2004–2014 mean annual rainfall in Pangkalan Bun was 2,058 mm and August was, on average, the driest month (105 mm) (National Oceanic and Atmospheric Administration's Climate Data Center). Mean annual temperature over this period was 26.6°C. Mean monthly temperature ranged from 26.1°C in July to 27.2°C in May.

The plots comprised a range of peat depths, land-use history and vegetation age (**Table 1**). The three forest plots were located at different distances from the edge of the main channel of the Sekonyer River. Peat depth varied in forest plots from less than 50 cm at the plot closest to the river to almost 3 m at the plot located farthest from the river. The plot closest to the river (FOR-1) was a 30-year-old secondary forest, managed as an agroforestry garden before Tanjung Puting National Park was established in 1982 and communities were moved across the Sekonyer river (Novita et al., 2020; according to interviews with community members). FOR-1 vegetation was dominated by pioneer species such as *Macaranga motleyana* (*Euophorbiaceae*), *Buchanania sessifolia* (*Anacardiaceae*), *Baccaurea stipulate* (*Phyllanthaceae*), and *Litsea firma* (*Lauraceae*) (Novita et al., 2020). The other two forest plots (FOR-2, FOR-3) were primary forests dominated by *Vatica oblongifolia* (*Dipterocarpaceae*) and *Santiria apiculate* (*Burseraceae*) (Novita et al., 2020). Our oil palm plots were nucleus estate smallholder plantations, an important part of the palm oil industry in Indonesia. Smallholders manage 40% of total oil palm area in Indonesia (DJP, 2015) and accounted for roughly a third of national production in 2011 (Obidzinski et al., 2012). We use the term "plantation" to signify differences in palm age. Oil palm plot locations were selected to represent a range of vegetation ages, as well as peat depth (**Table 1**) and management practices. Our oil palm plots included both young (palm age ≤ 3 years) and mature (palm age > 3 years) palms (Corley and Tinker, 2003). Smallholders started planting their lands with oil palm in the late 2000s following the establishment of a large oil palm plantation adjacent to their properties in the late 1990s. Oil palm was planted in 2007 (OP-2007) and 2009 (OP-2009) on land cleared in 2005. Oil palm was planted in 2011 (OP-2011) on land previously cleared in 1989 and managed for rice and vegetable production.

TABLE 1 | Characteristics of the sampling plots in Central Kalimantan, Indonesia (after Swails et al., 2018).

Plot	Location	Land use	Fires	Distance to river (km)	Peat depth (cm)
FOR-1	S 02° 49.410′ E 111° 48.784′	Forest	Multiple	0.5	27
FOR-2	S 02° 49.341′ E 111° 50.434′	Forest	—	1	155
FOR-3	S 02° 50.852′ E 111° 48.155′	Forest	—	2	290
OP-2011	S 02° 47.379′ E 111° 48.624′	Oil palm	Multiple	3.5	20
OP-2009	S 02° 47.292′ E 111° 48.190′	Oil palm	Multiple	3.5	47
OP-2007	S 02° 47.230′ E 111° 48.089′	Oil palm	Multiple	3.5	47

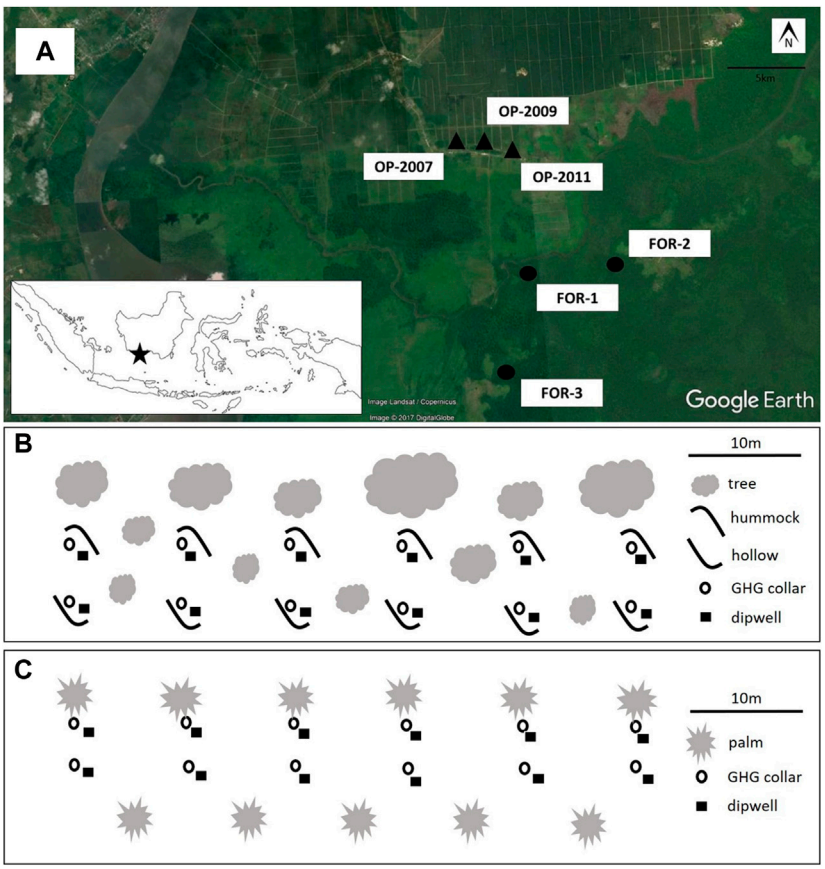

FIGURE 1 | Research site and sampling design. Measurements were collected from a peatland on the island of Kalimantan (inset) in three plots in undrained forest (FOR-1, FOR-2, FOR-3) and three plots in nearby smallholder oil palm plantations (OP-2007, OP-2009, OP-2011) **(A)**. In each plot, GHG collars (circles) and dipwells (squares) were installed at six subplot locations in oil palm **(B)** and forest **(C)**. At each subplot, one collar and dipwell set was installed at the base of a palm and another at a distance of 3 m from the palm in oil palm plots. In forest plots, we installed one set on a hummock and one set in the adjacent hollow (after Swails et al., 2019).

Smallholders applied fertilizers approximately every 3 months. Annual rates of fertilizer application were 150-84-124 kg N-P-K ha^{-1} $year^{-1}$ in the youngest plantation (OP-2011) decreasing to 120-67-100 kg N-P-K ha^{-1} $year^{-1}$ in the oldest plantation (OP-2007). Fertilization rate in OP-2009 was not provided by the smallholder. Information on fertilization dates in the plantations is not available. Land use history and land management practices in smallholder oil palm plantation plots are further described by Swails et al. (2019).

Sampling Regime and Laboratory Analysis

Sampling design is described in **Figure 1**. We designed our sampling approach to capture temporal and spatial heterogeneity in environmental conditions and trace gas fluxes from soils. We put emphasis on characterizing monthly variation which is known to be much larger than diel variation (e.g., Günther et al., 2014). Also, previous work on the research site and elsewhere in Indonesian peatlands found insignificant diel variation in GHG fluxes (Comeau et al., 2016; Novita, 2016). We collected measurements once per month from January 2014 until

June 2015 and once more in September 2015. Plots were sampled on consecutive days between the hours of 08:00 and 12:00. Monthly monitoring over 12–24 months is considered standard to capture the temporal variability of emissions (Inubushi et al., 2003; Furukawa et al., 2005; Jauhiainen et al., 2008; Hergoualc'h et al., 2020). Fluxes were not intensively monitored during post-fertilization periods in the oil palm plantations, thus measured N_2O fluxes represent emissions from peat decomposition. Fertilizer-induced N_2O emissions were found to be minor (9% of total N_2O emissions) in plantations on peat fertilized at 100-200 kg N ha^{-1} $year^{-1}$ (Oktarita et al., 2017).

Rates of CH_4 and N_2O fluxes were determined by the static chamber method (Hutchinson and Livingston, 1993; Verchot et al., 1999). Chambers were PVC collars (inner diameter 25 cm and height approximately 30 cm) permanently installed 16 months before the beginning of this study and equipped with opaque portable PVC hoods. A pair of collars was installed at six subplots for a total of 12 collars per plot (**Figure 1**). In oil palm plots, we installed at each subplot location one collar near the base of a palm under the palm canopy and one collar at mid-distance between two palms. In peat swamp forest, the microtopography was characterized by alternating raised mounds (hummocks) and depressions (hollows). In forest plots, at each subplot location we installed one collar on a hummock and one collar in the adjacent hollow. Samples were taken at 0, 10, 20, and 30 min after closing the chamber with the hood. We collected gas samples in 40 ml pre-evacuated glass vials using a syringe connected to the chamber hood outlet with silicone tubing. Vials were fitted with stopcocks sealed with polycarbonate caps to prevent gas leakage during transportation from the field.

Total soil respiration, soil temperature, air temperature, water table depth, and soil moisture (water-filled pore space) were monitored concurrently with trace gas fluxes, as described by Swails et al. (2019). Total soil respiration was measured by the dynamic closed chamber method (Pumpanen et al., 2009) with a portable infrared gas analyzer/EGM-4 (Environmental Gas Monitor) connected to a Soil Respiration Chamber (SRC-1) (PP System, Amesburry, United States) placed on a permanently installed PVC collar. We measured water table level in dipwells installed permanently next to each collar. The height difference between hummocks and hollows in forest was not measured. We report water table level relative to the soil surface on hummocks and hollows. Soil temperature to 5 cm was recorded using a soil temperature probe (Reotemp Digital TM99-A, United States). We used a pocket humidity/temperature pen (EXTECH 44550) to measure air temperature. Samples for water-filled pore space (WFPS) determination were collected bimonthly from the peat surface using stainless steel rings (height 5 cm and diameter 8 cm). We took six samples per plot, away from collars, three from hummock/near representative conditions and three from hollow/far representative conditions. Soil sampling locations for determination of WFPS were separated by approximately 20 m within plots. Samples were weighed in the field, transported in plastic bags to the laboratory, and oven-dried to constant mass at 60°C (Warren et al., 2012; Farmer et al., 2014). The gas samples were analyzed using a Shimadzu gas chromatograph (GC) equipped with an electron capture detector (ECD) for N_2O, and a flame ionization detector (FID) for CH_4.

Laboratory incubations were carried out to measure the rates of net mineralization and net nitrification. Soil samples were collected to a 5 cm depth in each plot in October 2013 and November 2013, outside of any fertilization event. The samples were collected adjacent to each chamber using a metal ring with a 277 cm^3 internal volume. In October 2013 we took three samples from hummocks/area near palms and three samples from hollows/area mid-distance between palms, and in November 2013 we took six from each spatial position. The November 2013 soil samples were taken 10 m from each other, and the October 2013 soil samples were taken 20 m from each other. Samples were transported to the laboratory and refrigerated at 4 C until incubation. Coarse roots and litter were manually removed from the samples before incubation. We followed the procedure by Hart et al. (1994) to determine net mineralization and net nitrification rates. For each sample a 10 g soil subsample was extracted in 100 ml of 2M KCl to determine inorganic N concentrations. These extracts were shaken for an hour with a rotary shaker and allowed to settle for 24 h. A 20-ml aliquot of the supernatant was filtered (Whatmann filter paper no. 42) and frozen for later analysis. NH_4^+ content was analyzed on an auto analyzer (Bran LuebbeTM) using the colorimetric method with indophenol blue (Solorzano, 1969). Determination of NO_3^- was done on a U-2001 spectrophotometer (Hitachi) using the brucine procedure (EPA, 1971). A second subsample of 10 g was incubated in the dark at room temperature (25–28°C) for 7 days. After 7 days, the incubated sample was extracted according to the procedures described above. The net N mineralization rate was calculated as the change in inorganic N ($NH_4^+ + NO_3^-$) concentration; the net nitrification rate as the change in NO_3^- concentration over 7 days. Initial inorganic N stocks were calculated from the first extraction.

Soil samples for analysis of additional soil properties were collected from the peat surface (0–5 cm) in November 2013 using a metallic ring, air-dried for 72 h and sieved to <2 mm. Samples were taken in triplicate in areas intermediary between hummock and hollow in forests, or between near palm and far from palm positions in plantations. Soil sampling locations in each plot were separated by a distance of approximately 20 m. Exchangeable cations (Ca^{2+}, Mg^{2+}, K^+, Na^+), cation exchange capacity (CEC) and base saturation were determined by displacement from the soil colloids with ammonium acetate adjusted to pH 7 (Pansu et al., 2001). Samples for analysis of soil C and N content were collected in June of 2015 from the peat surface layer (0–5 cm). Analyses of total C and N content were conducted at the University of Virginia by dry combustion using a Thermo Scientific Flash 2000 CHNS/O analyzer after being oven dried at 60°C for 48 h to constant mass. More methodological details are available in the paper by Swails et al. (2019).

Calculations and Statistical Analysis

CH_4 and N_2O fluxes were calculated from the rate of change in concentration of the analyte in the chamber headspace,

determined by linear regression based on the four gas samples (Verchot et al., 1999; Verchot et al., 2000). Whenever a sample had leaked (ambient CH_4 and N_2O concentration except at chamber closure) or the accumulation curve departed from linearity for both GHGs, indicating a chamber effect, the flux was calculated with three samples. Examples of cases where observations were discarded from the regression are provided in SI1. Where there was no trend in the accumulation curve, indicating low gas flux (for instance when uptakes and emissions occur simultaneously), no samples were excluded from the regression. In total, 7% of CH_4 and N_2O flux observations were excluded from analysis.

Trace gas fluxes and physical parameters were calculated per spatial position by land use ($n = 18$ in hummock/hollow and near/far conditions) for micro-spatial comparison. They were also calculated per plot by considering the representativeness of hummock/hollow and near/far conditions at subplot level. These results were used for plot comparison within a land use ($n = 6$ per plot) or for land use comparison ($n = 18$ per land use). Determination of the area ratio representative for each spatial position in oil palm and forest plots is described by Swails et al. (2019). The hummock to hollow area ratios in forest plots were 49:51 (FOR-1), 51:49 (FOR-2), and 57:43 (FOR-3). In oil palm plots, we used the ratio of area within a 2 m radius of palms (near) to the area outside of this radius (far). The 2 m-radius area around palms is where smallholders applied fertilizers and root density is usually highest (Khalid et al., 1999; Comeau et al., 2016). The near to far ratios in oil palm plots were 25:75 (OP-2011), 27:73 (OP-2009), and 37:63 (OP-2007).

Cumulative annual rates of CH_4 and N_2O emissions were estimated per plot using linear interpolation between measurements dates. We summed the average cumulative flux in the first 6 months of the year (January 2014–June 2014 and January 2015–June 2015) with cumulative flux in the last 6 months of 2014 (July–December). There was no monitoring in July and August 2015, so measurements collected during the September 2015 El Niño event were excluded from cumulative annual flux after Swails et al. (2019). We used Kruskal Wallis test to detect differences between average cumulative fluxes in the land-uses ($n = 18$) and among plots within a land-use ($n = 6$).

We used one-way repeated measures ANOVA with planned comparisons to detect differences in trace gas fluxes and physical parameters between spatial positions (hummock/hollow and near/far), among plots within a land use, and between land uses. Data were log transformed to meet normality assumptions. Comparisons were made over the entire study period and during dry and wet months. We treated months with total precipitation ≤100 mm as "dry" months, and months with total precipitation >100 mm as "wet" months after Aini et al. (2015) and Hirano et al. (2007). Relationships among trace gas fluxes and physical parameters were tested with univariate regression using monthly averages either per spatial position or per plot or land use. We additionally used univariate regression to test relationships among annual rates of trace gas fluxes and soil chemical properties using monthly average gas flux per plot. Soil mineral N content and net mineralization and nitrification rates per spatial position among plots within a land-use ($n = 9$), among plots within a land-use ($n = 9$), and between land-uses ($n = 27$) were compared using Kruskal Wallis test. Averages computed by pooling data from the two sampling dates were similar to averages computed separately for each experiment, therefore the data from the two sampling dates were pooled to increase statistical power of the dataset. Soil exchangeable cations, CEC, base saturation, and total C and N were compared for the two land-uses ($n = 9$) and among plots within a land-use ($n = 3$) using Kruskal Wallis test. Repeated measures ANOVA was computed using Statistical Analysis Software (SAS v 9.4). We used R (v 3.2.5) for all other analyses (Kruskal Wallis test and univariate regression). The criteria for significance was $p < 0.05$ for all statistical tests.

Peat CO_2 and GHG Budgets

The peat CO_2 budget was calculated as the sum of on- and off-site C emissions and removals (Hergoualc'h and Verchot, 2014) as:

$$\text{Peat } CO_2 \text{ budget} = (\text{SRh} + \text{DOC}) - (\text{Litterfall} + \text{Roots})$$

Where Peat CO_2 budget: Peat net C uptake or emission; SRh: Soil heterotrophic respiration; DOC: Dissolved organic carbon exported from the soil; Litterfall: above ground C inputs through litterfall; and Roots: below ground C inputs through root mortality and exudation. All components are in Mg C ha^{-1} $year^{-1}$ and a positive budget indicates that the peat is a net source of CO_2.

The peat CO_2 budgets combined site-specific soil heterotrophic respiration and litterfall rates and default values for root inputs and dissolved organic losses from the literature (Hergoualc'h and Verchot, 2014). Heterotrophic respiration rates were estimated from total soil respiration using the partitioning ratios of 55.1 ± 2.8% and 71.8 ± 10.8% in forest and oil palm, respectively, determined previously at the sites considering micro-spatial conditions and, in oil palm plantations, plantation age (Hergoualc'h et al., 2017, SI2). Cumulative annual total soil respiration (SI2) was calculated as for CH_4 and N_2O fluxes (Swails et al., 2019).

Litterfall was collected monthly at the forest plots in one trap (0.3 m^2) per subplot installed 100 cm above the soil. The litter was subsequently oven dried to constant mass at 60°C and weighed. Annual litterfall rate was computed by annualizing the average of monthly rates across plots and its dry mass was converted to carbon using a carbon fraction of 48% (Aalde et al., 2006). Litter input in oil palm plots was calculated from the average number of fronds removed from palms annually, the average dry mass of a frond and the average palm density across plots (162 palms ha^{-1}). Annual frond removal was estimated by counting the number of pruning scars on six palms per plot and dividing by the age of the plantation. The dry mass of fronds was measured from three fronds per plot in June 2015. Fronds were cut, fresh-weighed, and leaflet and stalk subsamples were collected for moisture content determination by oven drying to constant mass at 60°C. Frond dry mass was converted to carbon by applying a carbon fraction of 41.8% (Lamade and Setiyo, 2012).

The peat GHG budget was computed by summing up the peat CO_2 budget expressed in CO_2 units and annual emissions of CH_4

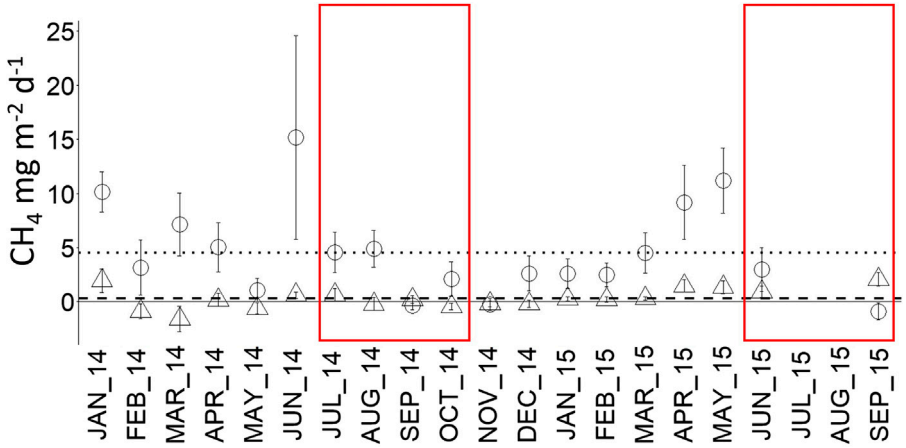

FIGURE 2 | Monthly mean soil CH_4 flux in forest (circle, dotted line) and oil palm (triangle, dashed line) from January 2014 to September 2015. Error bars represent standard error of the mean (n = 18). Dry months are indicated by red boxes. Dotted and dashed lines represent the 19 months averages.

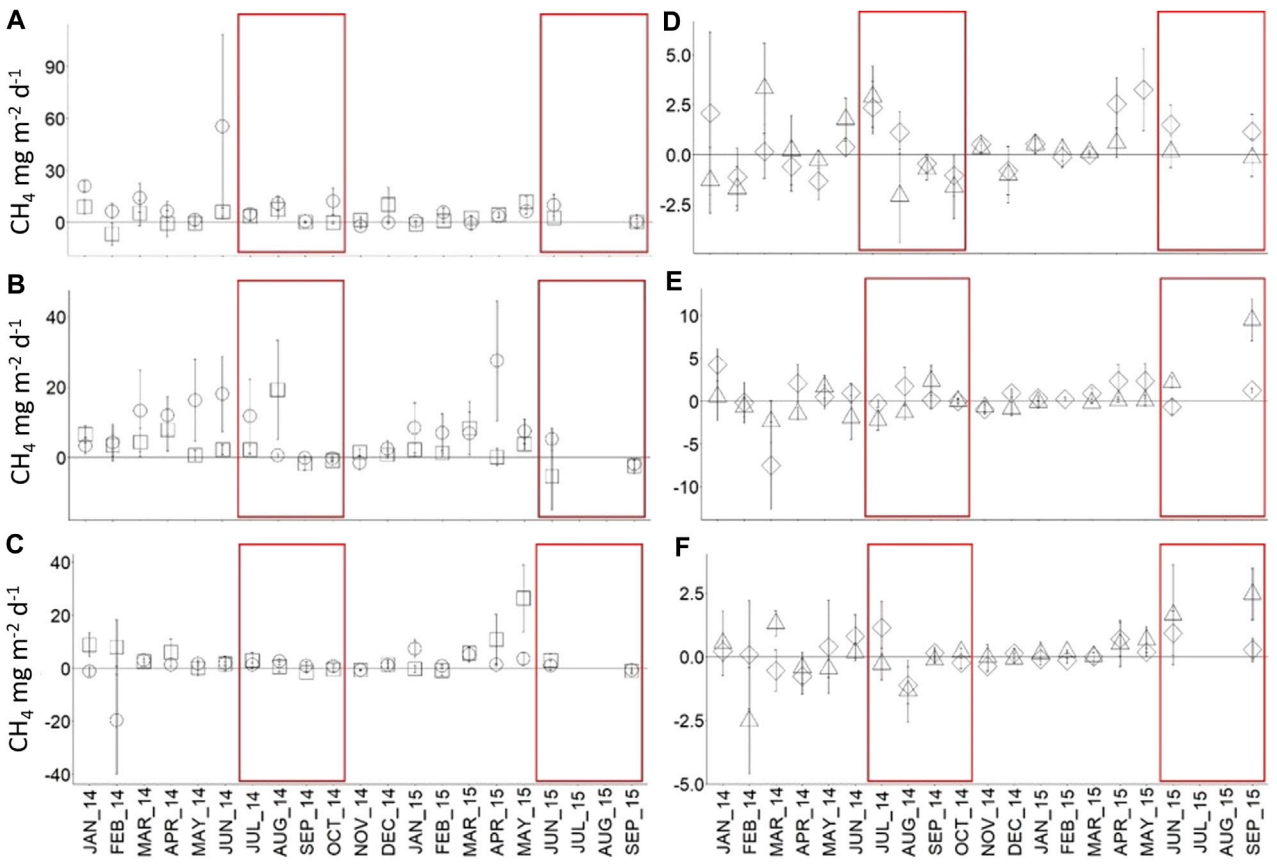

FIGURE 3 | Monthly mean soil CH_4 flux in hummock (square) and hollow (circle) in FOR-1 **(A)**, FOR-2 **(B)**, FOR-3 **(C)** and near (triangle) and far (diamond) positions from palm in OP-2011 **(D)**, OP-2009 **(E)**, and OP-2007 **(F)** from January 2014 to September 2015. Error bars represent standard error of the mean (n = 6). Dry months are indicated by red boxes. Note different scale between panels.

and N_2O expressed in CO_2 equivalent (CO_2e) units. Non-CO_2 gas fluxes were converted to CO_2e considering the global warming potentials of 86 for CH_4 and 268 for N_2O over a 20-year time horizon and with climate-carbon feedbacks (Myhre et al., 2013). Though a 100-year time horizon is the convention for national GHG inventories, a 20-year time horizon is more appropriate for

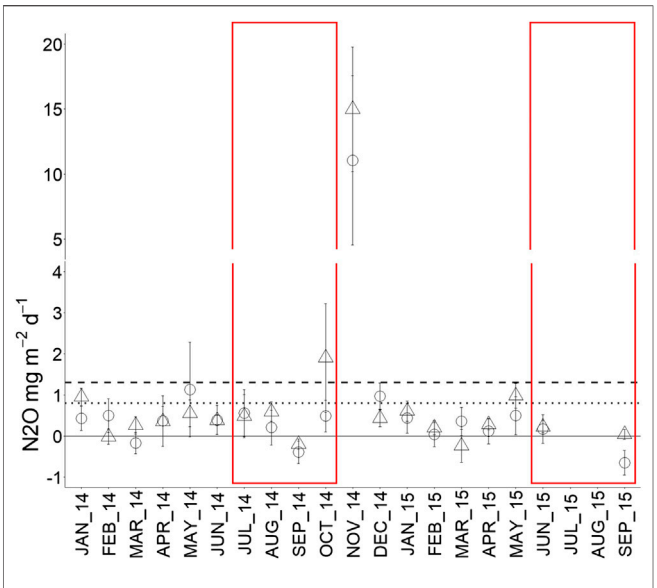

FIGURE 4 | Monthly mean soil N_2O flux in forest (circle, dotted line) and oil palm (triangle, dashed line) from January 2014 to September 2015 (n = 18). Error bars represent standard error of the mean. Dry months are indicated by red boxes. Dotted and dashed lines represent the 19 months averages.

evaluating impacts of land-use conversion that typically occurs over 20–30 years in the tropics.

RESULTS

CH_4 and N_2O Flux Rates

Over the 19 months of the study, mean CH_4 flux rate was roughly fifteen times higher in forest plots (4.5 ± 0.7 mg CH_4 m^{-2} d^{-1}) than in oil palm plots (0.3 ± 0.7 mg CH_4 m^2 d^{-1}, $p < 0.0001$, **Figure 2**), driven by a significant difference during wet months. In wet months CH_4 flux in forest (5.4 ± 0.5 mg CH_4 m^{-2} d^{-1}) was 54 times higher than in oil palm (0.1 ± 0.5 mg CH_4 m^2 d^{-1}, $p < 0.0001$) whereas no difference between the two ecosystems was observed in dry months ($p = 0.3$). Lower CH_4 flux in dry months than in wet months was conspicuous only in forest ($p = 0.002$).

Methane flux in forest ranged from 6.0 ± 1.8 mg CH_4 m^{-2} d^{-1} in the plot nearest the river (FOR-1, **Figure 3A**), to 5.1 ± 1.8 mg CH_4 m^{-2} d^{-1} in plot (FOR-2, **Figure 3B**) to 2.9 ± 1.8 mg CH_4 m^{-2} d^{-1} in the plot furthest from the river (FOR-3, **Figure 3C**). Notwithstanding, the flux was not significantly different among plots ($p = 0.3$) due to high intra-plot spatial variability. In oil palm, CH_4 production ranged from 0.5 ± 0.3 mg CH_4 m^{-2} d^{-1} in OP-2011 (**Figure 3D**) to 0.06 ± 0.25 mg CH_4 m^{-2} d^{-1} in OP-2007 (**Figure 3F**) and was similar among plots ($p = 0.1$).

Hollows (5.5 ± 1.5 mg CH_4 m^{-2} d^{-1}) and hummocks (3.2 ± 1.6 mg CH_4 m^{-2} d^{-1}) exhibited similar CH_4 flux ($p = 0.8$). Nonetheless during dry months, the flux was marginally higher in hollows than hummocks ($p = 0.07$) with a significant difference between spatial positions in FOR-1 ($p = 0.02$, **Figure 3A**) and FOR-3 ($p = 0.02$, **Figure 3C**). In oil palm, CH_4 flux was similar near and far from palm, in wet months, dry months, and overall, at the plot and land-use level.

Mean N_2O fluxes over the monitoring period were alike in oil palm (1.3 ± 0.3 mg N_2O m^{-2} d^{-1}) and forest (0.8 ± 0.3 mg N_2O m^{-2} d^{-1}) ($p = 0.3$), owing to high spatial and temporal variation in both ecosystems (**Figure 4**). The fluxes did not vary seasonally in oil palm ($p = 0.9$) whereas in forest they were marginally higher in wet months (3.3 ± 2.7 mg N_2O m^{-2} d^{-1}) than dry months (0.13 ± 0.44 mg N_2O m^{-2} d^{-1}) ($p = 0.07$).

In November 2014, the first month following the dry season, huge N_2O emissions were recorded in FOR-1 and OP-2011 (**Figures 5A,D**). These were, respectively, 13 and 15 times higher than the ecosystem mean over the monitoring period. Consequently, the range of N_2O flux was large in forest: From 1.8 ± 0.65 mg N_2O m^{-2} d^{-1} in FOR-1 (**Figure 5A**) to 0.5 ± 0.69–0.2 ± 0.67 mg N_2O m^{-2} d^{-1} in FOR-2 and FOR-3 (**Figures 5B,C**). Similarly, oil palm exhibited a wide range of mean N_2O flux: From 3.2 ± 0.4 mg N_2O m^{-2} d^{-1} in OP-2011 (**Figure 5D**) to 0.3 ± 0.4–0.2 ± 0.4 mg N_2O m^{-2} d^{-1} in OP-2009 and OP-2007 (**Figures 5E,F**). However, the mean flux rate was similar among plots in both forest ($p = 0.8$) and oil palm ($p = 0.3$).

N_2O fluxes were not different in hollows (1.1 ± 0.4 mg N_2O m^{-2} d^{-1}) and hummocks (0.8 ± 0.4 mg N_2O m^{-2} d^{-1}) across plots ($p = 0.6$) but greater in hollows than hummocks in FOR-1 (**Figure 5A**, $p = 0.04$) and FOR-2 (**Figure 5B**, $p = 0.004$). In oil palm the soil at near and far from palm positions emitted N_2O at a similar rate at the plot and land-use level.

Environmental Drivers of Trace Gas Fluxes

Inorganic N pools in forest and oil palm were dominated by NH_4^+ (**Table 2**). Soil NH_4^+ content was greater in forest plots than oil palm plots ($p = 0.001$) while the reverse was true for soil NO_3^- content ($p < 0.0001$). Net mineralization was higher in forest than oil palm ($p = 0.008$) but net nitrification was not different between the two land-uses. In forest plots soil NO_3^- content in hollows and net mineralization in hummocks as well as net mineralization at the plot scale was highest in FOR-3 ($p = 0.0009$, $p = 0.0004$, and $p = 0.003$, respectively). In oil palm plots net nitrification was higher far from palms than near palms in OP-2007 ($p = 0.009$). Soil NH_4^+ content was higher near palms than far from palms in OP-2011 ($p = 0.02$).

Soil CEC, base saturation and C and N content were similar in both land uses ($p = 0.3$, 0.4, and 0.5), **Table 3**). In forests, there was a trend towards increasing CEC, base saturation and C content from FOR-1, which was closest to the river and was a secondary forest, to FOR-3, which was furthest from river and was a primary forest.

Results on environmental parameters (water table level, WFPS, and litterfall rates in forest) are presented in SI3. Factors controlling temporal variability of soil non-CO_2 fluxes were primarily hydrological. Fluxes of CH_4 and N_2O were related to water table level in forest, and CH_4 fluxes to WFPS in oil palm. CH_4 flux decreased as water table level dropped in forest plots ($p = 0.02$, **Figure 6A**). On the other hand, CH_4 flux increased when soil WFPS increased in oil palm plots ($p = 0.02$, **Figure 6B**). Soil N_2O flux increased as the water table rose close to the soil surface in forest plots ($p = 0.02$, **Figure 6C**) though the model relatively poorly explained the variation in N_2O flux ($R^2 = 0.28$). In both ecosystems, N_2O flux varied widely when water table was near the

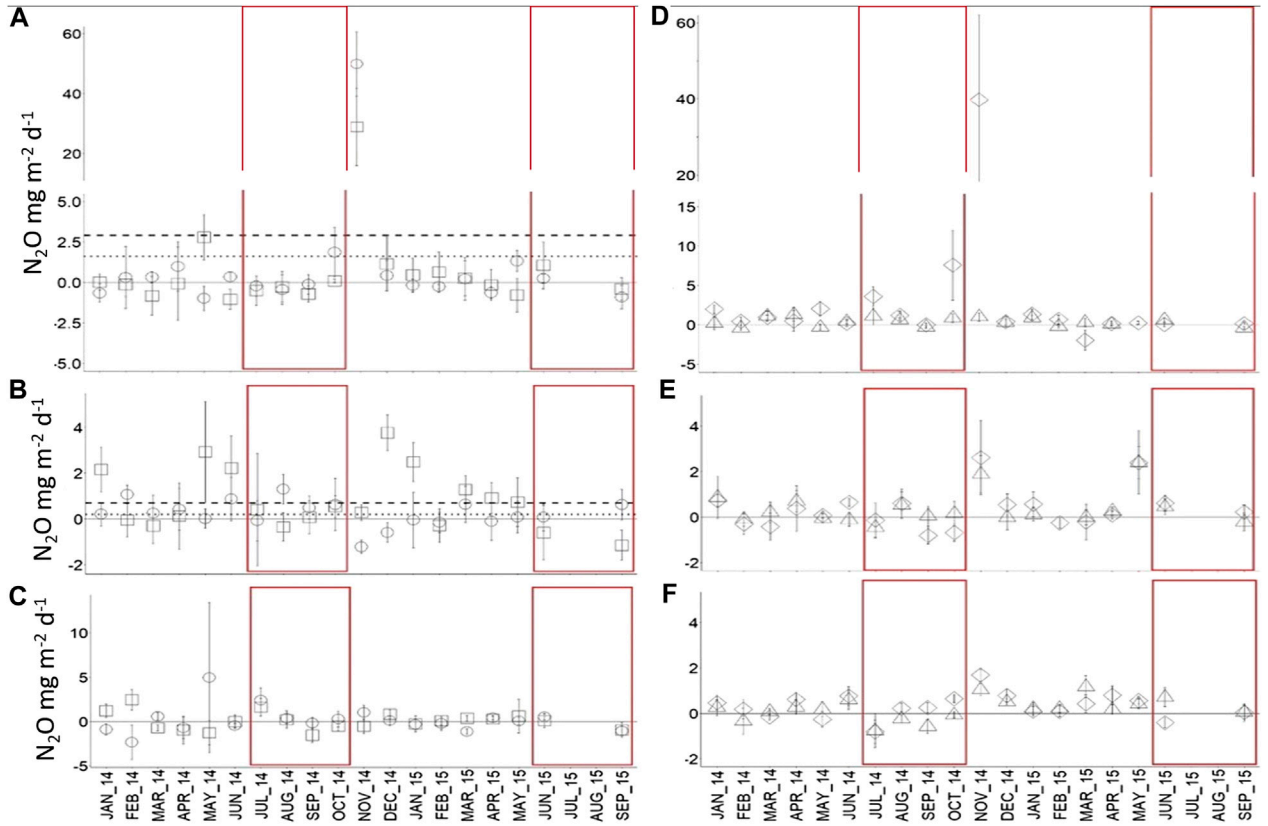

FIGURE 5 | Monthly mean soil N_2O flux in hummock (square, dotted line) and hollow (circle, dashed line) in FOR-1 **(A)**, FOR-2 **(B)**, FOR-3 **(C)** and near (triangle) and far (diamond) positions from palm in OP-2011 **(D)**, OP-2009 **(E)**, and OP-2007 **(F)** from January 2014 to September 2015. Error bars represent standard error of the mean (n = 6). Dry months are indicated by red boxes. Dotted and dashed lines representing the 19 months averages are displayed when significantly different between spatial positions. Note different scale between **(A,D,C)**, and remaining panels.

soil surface, and N_2O consumption occurred occasionally when water table level dropped far below the soil surface. Temporal fluctuations of CH_4 and N_2O fluxes were not related to soil or air temperature in either land use or to litterfall in forest.

Cumulative Annual Fluxes of CH_4 and N_2O

Cumulative CH_4 flux (kg CH_4 ha^{-1} $year^{-1}$) was two orders of magnitude higher in forest (14.0 ± 2.8) than oil palm (0.3 ± 0.4, **Table 4**, $p < 0.0001$). In forest plots there was a trend towards decreased CH_4 flux with distance from river, but cumulative CH_4 flux was not different among forest plots. Cumulative CH_4 fluxes in oil palm plots were very close to each other and not different.

Cumulative N_2O flux (kg N_2O ha^{-1} $year^{-1}$) was similar in the two land-uses (5.2 ± 3.7 in forest and 5.0 ± 3.9 in oil palm, **Table 4**). In forest, it was more than five times higher in secondary forest FOR-1 (12.6 ± 1.1) than in primary forests FOR-2 (2.3 ± 0.4) and FOR-3 (0.6 ± 0.7) (**Table 4**, $p < 0.0001$). In oil palm, N_2O flux was more than 10 times higher in OP-2011 (12.7 ± 3.8) than in OP-2009 (1.1 ± 0.6) and OP-2007 (1.1 ± 0.1) (**Table 4**, $p = 0.048$). Among the six plots, annual N_2O emissions increased with decreasing soil C content with highest emissions in the secondary forest and OP-2011 established on a land cleared 20 years before planting (**Figure 7**).

FOR-1 accounted for 81% of total cumulative N_2O emissions in forest and OP-2011 accounted for 84% of total cumulative N_2O emissions in oil palm. In addition, in OP-2011 three chambers located in the unfertilized zone (far from palm position) contributed 86% of emissions.

Net CO_2 and GHG Emissions From Peat

Forest exhibited higher litterfall C inputs and lower C losses from heterotrophic respiration than oil palm (**Table 5**). During the monitoring period oil palm plantation was a strong net source of CO_2 while forest was neither a source nor a sink. The difference in net CO_2 emissions rate between ecosystems was as high as 28.9 ± 9.7 Mg CO_2 ha^{-1} $year^{-1}$. CH_4 and N_2O contributed importantly to the peat GHG budget in forest whereas in oil palm most emissions were released in the form of CO_2. Forest to oil palm conversion implied large GHG emissions from the peat of about 28 ± 10 Mg CO_2e ha^{-1} $year^{-1}$.

Disaggregation of peat budgets by forest type shows that in the secondary forest the peat was a small net CO_2 source as opposed to net CO_2 neutrality in primary forests. As a result, and also owing to large soil N_2O emissions, secondary forest was an important net GHG source. Regardless of their disturbance

TABLE 2 | Soil ammonium (NH_4^+) and nitrate (NO_3^-) contents and net mineralization and nitrification rates in forest and oil palm plots at site- and plot-scale and according to spatial position. Mean values and standard errors are presented.

Land-use	Plot	Spatial position	NH_4-N (mg N kg d.m.$^{-1}$)	NO_3-N (mg N kg d.m.$^{-1}$)	Net mineralization (mg N kg^{-1} d^{-1})	Net nitrification (mg N kg^{-1} d^{-1})
Forest	All	Site-scale	351.2 ± 64.0$^{\alpha}$	5.0 ± 0.9$^{\alpha}$	25.3 ± 7.6$^{\alpha}$	2.5 ± 0.4
	FOR-1	Plot-scale	233.0 ± 122.6^{AB}	1.7 ± 0.5	−4.5 ± 8.3^{A}	1.9 ± 1.7
		Hum	271.4 ± 107.2	2.1 ± 0.4	−6.9 ± 7.4^{a}	3.0 ± 1.6
		Hol	196.1 ± 59.5	1.4 ± 0.4^{a}	−2.3 ± 3.8	0.9 ± 0.5
	FOR-2	Plot-scale	185.4 ± 53.56^{A}	4.3 1.9	16.5 ± 11.9^{A}	2.2 ± 0.6
		Hum	232.7 ± 49.5	5.7 ± 1.8	23.8 ± 10.3^{a}	2.2 ± 0.6
		Hol	136.3 ± 20.5	2.8 ± 0.7^{a}	8.9 ± 5.9	2.1 ± 0.3
	FOR-3	Plot-scale	546.3 ± 248.9^{B}	7.4 ± 3.2	54.0 ± 29.0^{B}	2.6 ± 1.1
		Hum	608.6 ± 186.1	8.0 ± 3.1	65.0 ± 12.0^{b}	3.0 ± 0.9
		Hol	463.7 ± 165.2	6.7 ± 0.8^{b}	39.4 ± 26.4	2.2 ± 0.6
Oil palm	All	Site-scale	148.0 ± 88.7$^{\beta}$	14.4 ± 9.0$^{\beta}$	3.9 ± 11.2$^{\beta}$	1.6 ± 1.4
	OP-2007	Plot-scale	125.6 ± 40.13	11.6 ± 5.7	1.0 ± 1.8	1.7 ± 0.6^{AB}
		Near	125.3 ± 19.7	10.0 ± 4.6	2.7 ± 1.4	0.6 ± 0.4^{1}
		Far	125.6 ± 34.9	12.1 ± 3.4	0.4 ± 1.2	2.1 ± 0.4^{2a}
	OP-2009	Plot-scale	171.7 ± 64.54	17.2 ± 4.1	1.9 ± 5.4	0.4 ± 0.8^{A}
		Near	204.2 ± 53.2	9.0 ± 2.9	7.0 ± 3.6	0.7 ± 0.5
		Far	159.6 ± 36.5	20.2 ± 2.9	0.0 ± 4.1	0.3 ± 0.6^{ab}
	OP-2011	Plot-scale	146.8 ± 45.68	14.5 ± 5.7	8.8 ± 9.6	2.7 ± 1.1^{B}
		Near	208.2 ± 41.4^{1}	14.2 ± 5.0	6.6 ± 6.2	2.4 ± 0.8
		Far	110.7 ± 19.3^{2}	14.7 ± 2.6	10.0 ± 7.3	2.8 ± 0.8^{b}

Significant differences between land-uses are indicated by α, β. Significant differences among plots are indicated by A, B. Significant differences between spatial positions within a plot are indicated by 1, 2. Significant differences at a spatial position (Hum/Hol or Near/Far) among plots within a land-use are indicated by a, b. Hum: Hummocks, Hol: Hollows, Near: Near to palm, Far: At mid-distance between two palms.

TABLE 3 | Soil cation exchange capacity (CEC), base saturation, C and N content in forest and oil palm plots. Mean values and standard errors are presented.

Land use	Plot	CEC (me/100 g)	Base saturation (%)	C Content (%)	N content (%)
Forest		88.5 ± 4.8	12.5 ± 2.7	40.8 ± 3.2	1.8 ± 0.2
	FOR-1	69.4 ± 0.5^{a}	6.2 ± 0.1^{a}	28.3 ± 0.7^{a}	1.3 ± 0.01^{a}
	FOR-2	98.3 ± 0.4^{b}	7.9 ± 0.1^{ab}	46.1 ± 1.1^{ab}	2.3 ± 0.17^{b}
	FOR-3	97.8 ± 0.5^{b}	23.3 ± 0.3^{b}	48.0 ± 0.5^{b}	1.8 ± 0.06^{ab}
Oil palm		93.5 ± 1.2	7.5 ± 0.5	41.2 ± 2.8	1.5 ± 0.1
	OP-2007	96.0 ± 0.9	6.3 ± 0.1	48.7 ± 1.4	1.6 ± 0.0
	OP-2009	93.7 ± 0.6	6.6 ± 0.4	46.2 ± 1.6	1.6 ± 0.0
	OP-2011	90.8 ± 2.9	9.4 ± 0.3	39.3 ± 2.7	1.3 ± 0.3

Significant differences among plots within a land-use are indicated by a, b.

history, forests' peat net GHG emissions were lower than in oil palm plantations.

DISCUSSION

Spatio-Temporal Variability and Controls of CH_4 Flux

Annual soil CH_4 emission in forest plots (14.0 ± 2.8 kg CH_4 ha^{-1} year^{-1}) was comparable to fluxes measured in undrained peat swamp forest of Kalimantan in Indonesia (Inubushi et al., 2003; Jauhiainen et al., 2005) but under the 38 ± 13 kg CH_4 ha^{-1} year^{-1} average for Southeast Asian peat swamp forests (Hergoualc'h and Verchot, 2014). It was also lower than CH_4 emission in peat swamp forest from eddy covariance studies (e.g., Wong et al., 2018; Deshmukh et al., 2020) which account for peat surface flux as well as vegetation-mediated flux from tree stems and pneumatophores (Pangala et al., 2013; Van Lent et al., 2019).

In forest plots CH_4 flux decreased in dry months when the water table fell further below ground level and oxygenation of peat surface layers promoted methanotrophy over methanogenesis, as observed in previous studies of Southeast Asian peatlands (Jauhiainen et al., 2005; Jauhiainen et al., 2008; Ishikura et al., 2019). In wet months waterlogging of surface layers created anoxic conditions conducive to anaerobic respiration and methanogenesis. Methane emissions increased in magnitude and became more variable as water table level approached the soil surface during wet months, indicating a threshold response to water table level, as observed by Jauhiainen et al. (2008).

Water table level alone only explained 49% of variation in CH_4 flux in forest plots (**Figure 6A**). Soil WFPS may also have played a role in controlling CH_4 flux when sites were not flooded, as suggested by higher soil moisture and CH_4 flux in FOR-1 than in FOR-2 and FOR-3 (**Supplementary Table S3**). Moisture regime could also have controlled flux rates indirectly. For instance, visual inspection of the plots indicated higher density of pneumatophores near the river than further from it, potentially explaining the trend towards decreased CH_4 emission with distance from river as resulting from lower plant-mediated transport. Methane production also often correlates with diverse indexes of soil carbon quality (Le Mer

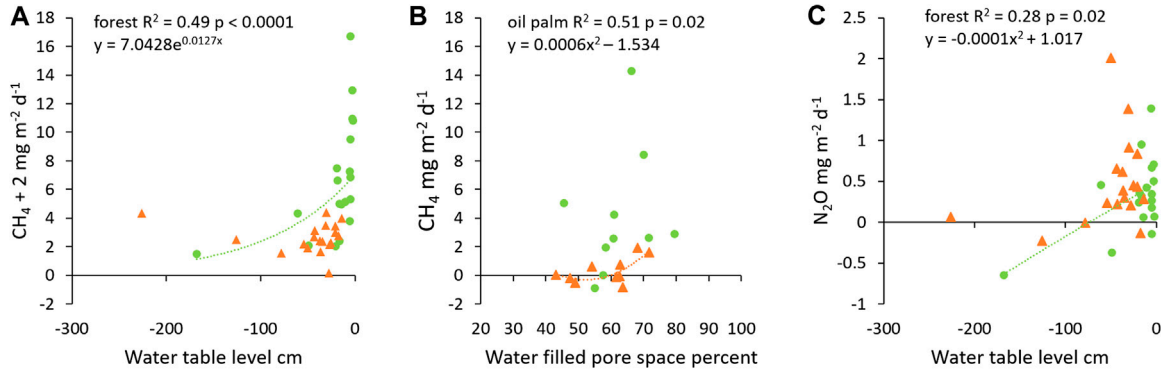

FIGURE 6 | CH_4 flux as a function of water table depth **(A)** and water-filled pore space **(B)** and N_2O flux as a function of water table depth **(C)** in forest (green circle, green dotted line) and oil palm (orange triangle, orange dashed line). Each data point represents the monthly mean in a land use (n = 19 for water table depth and n = 10 for water filled pore space).

TABLE 4 | Cumulative plot-scale soil CH_4 and N_2O flux rates ± standard error at the study sites. Mean values and standard errors are presented.

Land use	Plot	CH_4 (kg ha^{-1} $year^{-1}$)	N_2O (kg ha^{-1} $year^{-1}$)
Forest	Average	14.0 ± 2.8^a	5.2 ± 3.7
	FOR-1	18.7 ± 5.1	12.6 ± 1.1$^\alpha$
	FOR-2	14.3 ± 10.5	2.3 ± 0.4$^\beta$
	FOR-3	9.0 ± 2.6	0.6 ± 0.7$^\beta$
Oil palm	Average	0.3 ± 0.4^b	5.0 ± 3.9
	OP-2011	−0.3 ± 0.4	12.7 ± 3.8$^\alpha$
	OP-2009	0.2 ± 0.9	1.1 ± 0.6$^\beta$
	OP-2007	1.0 ± 0.8	1.1 ± 0.1$^\beta$

a and b indicate significant differences between land-uses. α and β indicate significant differences between plots within a land use.

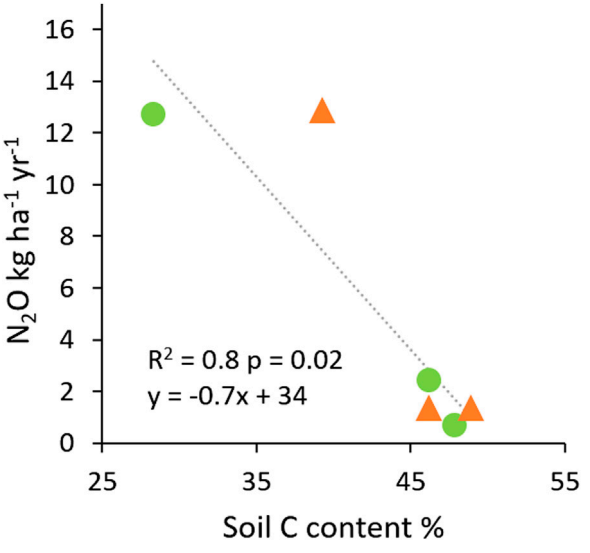

FIGURE 7 | Annual N_2O flux as a function of soil C content in forest and oil palm plantation plots.

and Roger, 2001; Bridgham et al., 2012). The trend toward decreased emission rate with distance from river was associated with increased soil CEC, base saturation and C content (**Table 3**) which suggest changes in organic matter decomposition state (Andriesse, 1988). Also, there was a trend toward rising CH_4 emission with rising total soil respiration (**Supplementary Figure S5**), with FOR-1 the only forest which was secondary and had suffered past burning events (**Table 1**), exhibiting highest emissions of CH_4 and highest total soil respiration.

Though hollows and hummocks displayed a similar CH_4 flux when all forest plots were considered together, the flux was greater in hollows than hummocks in FOR-1 and FOR-2 in dry months, when both microtopographies exhibited similar water table level (Swails et al., 2019). A higher CH_4 flux in hollows than hummocks in pristine peat swamp forest usually coincides with a difference in moisture conditions between microtopographies (Ishikura et al., 2019; Hergoualc'h et al., 2020). As CH_4 production is often fueled by recent plant photosynthate (Bridgham et al., 2012) difference in flux between the microtopographies at our sites may be linked to higher root exudates in hollows than hummocks when soil becomes unsaturated. In drained oil palm plots, CH_4 emissions were negligible as typically found in drained tropical peatlands across various land uses (Hergoualc'h and Verchot, 2012). CH_4 flux did not respond to changes in water levels, contrary to what was measured by Melling et al. (2005). However, as rainfall can briefly create waterlogged layers at the peat surface CH_4 emissions increased with increasing WFPS (**Figure 6B**). There was no tendency toward CH_4 uptake by soil during dry months or overall. Nevertheless, uptake occurred occasionally when the water table level was <50 cm below ground, indicating that water saturation at the soil surface was an important driver of CH_4 emission and uptake. CH_4 emissions did not vary according to spatial position (near and far from palms), though gravimetric soil moisture was higher far from palms than near palms (Swails et al., 2019).

TABLE 5 | Peat CO_2 budget calculated as the difference of mean annual C outputs from heterotrophic soil respiration (SRh) and dissolved organic carbon (DOC) and mean annual C inputs from litterfall and root mortality in forest and oil palm (OP). Peat greenhouse gas (GHG) budget was computed as the sum of emissions of all GHG. Forest budgets are also disaggregated by forest type (secondary: FOR-1, primary: FOR-2 and FOR-3). Mean values ± standard error are expressed in Mg C or CO_2-equivalent ha^{-1} $year^{-1}$. Negative values indicate an emission reduction or removal.

	Secondary forest	Primary forest	Forest	Oil palm	Difference OP-Forest
			(Mg C ha^{-1} $year^{-1}$)		
Litterfall	5.8 ± 0.6	5.3 ± 0.6	5.5 ± 0.8	1.1 ± 0.2	
Roots	*1.5 ± 0.8*	*1.5 ± 0.8*	*1.5 ± 0.8*	*3.6 ± 1.1*	
Total soil C inputs	7.3 ± 1.0	6.8 ± 1.0	7.0 ± 1.1	4.7 ± 1.1	
SRh	8.2 ± 0.7	6.1 ± 0.3	6.8 ± 0.6	12.0 ± 2.0	
DOC	*0.6 ± 0.0*	*0.6 ± 0.0*	*0.6 ± 0.0*	*0.9 ± 0.1*	
Total soil C outputs	8.8 ± 0.7	6.7 ± 0.3	7.4 ± 0.6	12.9 ± 2.0	
Peat C budget	1.4 ± 1.2	−0.1 ± 1.1	0.4 ± 1.3	8.3 ± 2.3	
			(Mg CO_2e ha^{-1} yearr^{-1})		
CO_2 budget	5.2 ± 4.4	−0.5 ± 3.9	1.4 ± 3.9	30.4 ± 8.5	28.9 ± 9.7
CH_4	1.6 ± 0.5	1.0 ± 0.2	1.2 ± 0.2	0.0 ± 0.0	−1.2 ± 0.2
N_2O	3.4 ± 0.8	0.4 ± 0.2	1.4 ± 1.0	1.3 ± 1.0	−0.1 ± 1.4
Peat GHG budget	10.2 ± 4.5	0.9 ± 3.9	4.0 ± 4.8	31.7 ± 8.6	27.7 ± 9.8
(%CO_2, CH_4, N_2O)	(51, 16, 33)	(−51, 109, 42)	(35, 30, 35)	(96, 0, 4)	(104, −4, 0)

Values in italic are from the literature review by Hergoualc'h and Verchot (2014). Values in parenthesis indicate the contribution (%) of CO_2, CH_4 and N_2O to the peat GHG budget.

Spatio-Temporal Variability and Controls of N_2O Flux

Soil annual N_2O emission in forest plots (5.2 ± 3.9 kg N_2O ha^{-1} $year^{-1}$) was within the range of fluxes from undrained peat swamp forests in Indonesia which vary from small net uptakes (−0.5 kg N_2O ha^{-1} $year^{-1}$, Inubushi et al., 2003) to high emissions (21.1 kg N_2O ha^{-1} $year^{-1}$, Hadi et al., 2005). N_2O consumption is not uncommon across the tropics (Chapuis-Lardy et al., 2007) and soils in forest plots also appeared as an occasional sink. N_2O consumption occurred primarily in hummocks, which are better aerated and can remain dry when lower lying hollows are wet (Swails et al., 2019). N_2O uptake has been observed in Southeast Asian peatland (e.g., Takakai et al., 2006; Jauhiainen et al., 2012) and is usually promoted by low nitrate availability, high WFPS and more generally by conditions inhibiting N_2O diffusion in the soil (Chapuis-Lardy et al., 2007). However, in soils with high soil C content, enhanced respiration can create anoxic microenvironments where denitrification takes place, even under well aerated conditions (Chapuis-Lardy et al., 2007), which may explain N_2O uptake by hummocks in our forest plots. N_2O emissions increased as water table rose closer to the soil surface in forest plots, in agreement with findings by Melling et al. (2007) but in disagreement with other studies, e.g., Hergoualc'h et al. (2020), Takakai et al. (2006), Jauhiainen et al. (2012) also observed a control of soil water status over N_2O emissions in undrained forest, with greater flux in wet than dry months. Jauhiainen et al. (2012) attribute the increase in N_2O flux to enhanced decomposition of litter inputs under optimum soil moisture conditions. As for CH_4, the trend of decrease in cumulative N_2O emissions with river distance was associated with a decrease in total soil respiration (**Supplementary Figure S5**) and changes in soil organic matter decomposition state (**Table 3**).

Annual emission in oil palm plots (5.0 ± 3.7 kg N_2O ha^{-1} $year^{-1}$) was above IPCC default value for oil palm plantations on peat (1.2 kg N_2O ha^{-1} $year^{-1}$, Drösler et al., 2014). Assessments of annual N_2O emissions in oil palm plantations on peat (Melling et al., 2007; Sakata et al., 2015; Oktarita et al., 2017; Chaddy et al., 2019; Meijide et al., 2020) indicate much higher rates (32 ± 2 kg N_2O ha^{-1} $year^{-1}$, n = 8) than our result and IPCC default value. They also vary greatly according to site, management practices (tillage/no tillage or use of coated vs. conventional nitrogen fertilizers) (Sakata et al., 2015) and presence of hot spots (Oktarita et al., 2017). Emission rates in OP-2007 and OP-2009 were in the range of flux reported by Melling et al. (2007) while emissions in OP-2011 were closer to but lower than values reported by Sakata et al. (2015), Oktarita et al. (2017), Chaddy et al. (2019) and Meijide et al. (2020). Lower average emission at our site as compared to the literature may arise from low supply of labile carbon as indicated by the ratio of recalcitrant aromatic compounds to labile aliphatic compounds in soil organic matter (Swails et al., 2018) and also potentially from water table levels higher (**Supplementary Table S3**) than on average (65 cm, Hergoualc'h and Verchot, 2014). Water table level was poorly controlled by smallholders, particularly in OP-2011 (**Table 1**), which was flooded in March 2014 and May 2014. High water table can create anaerobic conditions, thereby decreasing N_2O production directly by inhibiting nitrification and indirectly by decreasing the production of NO_3^- substrate for denitrification. Additionally, more anaerobic conditions promote the formation of N_2 over N_2O during denitrification. Emissions could also be slightly under-estimated as our experimental design did not use intensive sampling after fertilization to capture potential transient spikes in emissions from the area of nitrogen application.

OP-2011 included hot spots which contributed 86% of annual emissions. Hot spots have been observed in drained organic soils in the tropics (Oktarita et al., 2017), temperate (Lee et al., 2017) and Arctic zones (Repo et al., 2009; Marushchak et al., 2011). As in the study by Oktarita et al. (2017) hot spots were located far from

palms (**Figure 5D**), where N uptake by roots may be lower (Nelson et al., 2006). Also "*in vitro*" net nitrification rate far from palms was higher in OP-2011 than elsewhere despite similar initial mineral N content across plots at this spatial position (**Table 2**) which suggests that hot spots are driven by microbial or fungal community composition, as proposed by Oktarita et al. (2017).

The strong relationship between annual N_2O emissions and soil C content along the six plots (**Figure 7**) is agreement with findings by Ye et al. (2016) for rice fields on peat in the Sacramento-San Joaquin Delta. This relationship suggests that the highest emission in FOR-1 and OP-2011 may be explained by carbon limitations to microbial growth and linked to past land-use history in these plots. FOR-1 was a 30-year-old secondary forest, managed as an agroforestry garden previously. In OP-2011, forest clearance occurred in 1989 and was followed by successive crop rotations and associated fires while other plots were cleared more recently in 2005. The past history of cultivation in FOR-1 and OP-2011 may have depleted labile carbon supply in soils (Swails et al., 2018) and exposed deeper layers of peat mixed with mineral soil. When facing carbon limitations to growth, microbes break down dissolved organic nitrogen, using carbon to support energy, growth and maintenance requirements and secreting NH_4^+ as a by-product (Chapin et al., 2002). Increased availability of NH_4^+ enhances production of NO_3^- through nitrification under aerobic conditions (Robertson, 1989). Thus, nitrification may have been elevated during dry months in these plots. In FOR-1 as in OP-2011, we observed extremely high N_2O emissions in November 2014. These pulses occurred at the beginning of the wet season, when precipitation increased after four dry months. The sudden change in soil moisture conditions combined with a large supply of NO_3^- could have promoted high rates of denitrification leading to large fluxes of N_2O from soils in FOR-1 and OP-2011 at the beginning of the wet season, similar to observations in an oil palm plantation on tropical peatland by Chaddy et al. (2019).

The Global Warming Impact of Peat Forest Conversion to Oil Palm Plantation

Indonesian peatlands are known as an important and growing source of GHG emissions to the atmosphere but variations in estimates remain large. Our study indicates that forest to oil palm conversion resulted in a massive increase in peat net CO_2 emission rate (29 Mg CO_2e ha^{-1} $year^{-1}$), a small decrease in CH_4 emissions (1 Mg CO_2e ha^{-1} $year^{-1}$) and no alteration in N_2O emissions (**Table 5**). Ensuing GHG loss over a 25-year rotation period typical of oil palm plantation amounts to 693 Mg CO_2e ha^{-1}. This result combined with C stock changes in above ground vegetation (excluding litter) measured at the sites by Novita et al. (2020) (189 and 28 Mg C ha^{-1} in forest and oil palm) leads to emissions of 1,283 Mg CO_2e ha^{-1} over 25 years or 51 Mg CO_2e ha^{-1} $year^{-1}$. This assessment doesn't account for massive emission from peat burning with each land-clearing fire releasing 541 Mg CO_2e ha^{-1} (Drösler et al., 2014). It neither accounts for peat decomposition emissions that occurred during intermediary crop cultivation before conversion to oil palm. The larger share of CO_2 than that of either CH_4 or N_2O to peat GHG emissions from land-use change is consistent with the literature on Southeast Asian peatlands (Hergoualc'h and Verchot, 2014). Drainage resulted in a drastic increase in CO_2 emissions from accelerated soil organic matter decomposition, and vegetation cover change induced substantial reduction in aboveground litter inputs. The latter may be underestimated as branchfall was not monitored in forest.

While in forest, all gases contributed equally to the peat GHG budget, in oil palm CO_2 was the dominant gas but several studies which found high N_2O emissions stemming from peat decomposition highlighted the importance of this gas for GHG accounting (Sakata et al., 2015; Oktarita et al., 2017; Dommain et al., 2018). Forest conversion to croplands and shrublands substantially raises soil emissions of N_2O according to the meta-analysis conducted by Hergoualc'h and Verchot (2014). This was not the case in our study because primary and secondary forests were merged and roughly 80% of the N_2O flux from forest came from FOR-1. Discarding observations from FOR-1 resulted in a four times lower average cumulative N_2O flux (0.4 Mg CO_2e ha^{-1} $year^{-1}$) and peat GHG budget (0.9 Mg CO_2e ha^{-1} $year^{-1}$) (**Table 5**) in primary forest than when all forest types were merged. Current data availability for GHG inventories only allows disaggregating peat GHG emission factors of forest by combined drainage and disturbance (primary/secondary) status, as trace gas measurements in undrained secondary forest have seldom been conducted. Our results indicate that undrained 30-year-old secondary forests still suffer from past land-use history and exhibit soil GHG emissions substantially different from that of primary forest. The lack of distinction between primary and secondary undrained peat forest has implications for national GHG accounting and research is critically needed to support development of more accurate emission factors.

Knowledge on all GHG is required for assessing either climate change impacts on the potential of peat forest to act as a C sink or as a GHG source (Wang et al., 2018), or climate impacts of land-use change in tropical peatlands. Additional assessments across the region are necessary to understand the cumulative impact of simultaneous changes in fluxes of CH_4, N_2O, and CO_2 that occur with conversion and drainage of tropical peatlands.

CONCLUSION

Drainage and conversion of an Indonesian peat swamp forests to oil palm plantation implied a large net increase in peat GHG emissions, mainly released as CO_2. Past land-use change also impacted peat net GHG emissions in a secondary peat swamp forest, decades following conversion. Spatio-temporal variability in peat CH_4 and N_2O flux in forests and oil palm plantations was related to hydrological drivers. Our study highlights the devastating impact of tropical peat swamp forest conversion on peat GHG emissions to the atmosphere, with and without drainage, and for many years following initial conversion.

DATA AVAILABILITY STATEMENT

The datasets presented in this study can be found in online repositories. The names of the repository/repositories and

accession number(s) can be found at: https://doi.org/10.17528/CIFOR/DATA.00201.

AUTHOR CONTRIBUTIONS

ES designed and conducted the study, performed data analysis, and wrote the manuscript. KH, DL, and LV were integrally involved in the study design, data analysis and interpretation, and writing the manuscript. NN selected sites and conducted field and laboratory work in the same area, contributing data on soil mineral N content and rates of net mineralization and net nitrification to this manuscript.

FUNDING

This research was conducted under the Sustainable Wetlands Adaptation and Mitigation Program (SWAMP) and was generously supported by the governments of the United States of America (Grant No. MTO-069018), Norway (Grant Agreement No. QZA-12/0882) and Germany (Grant No. KI II 7—42206-6/75). It was undertaken as part of the CGIAR research program on Climate Change, Agriculture and Food Security (CCAFS).

ACKNOWLEDGMENTS

The authors are grateful to the staff of Tanjung Puting National Park for facilitating the study and providing lodging. We would also like to thank all assistants and villagers for their continuous help in the field, and also Desti Hertanti for her indispensable support to collect data, and Novi Wahyuni for her critical work in analyzing GHG concentrations.

SUPPLEMENTARY MATERIAL

The Supplementary Material for this article can be found online at: https://www.frontiersin.org/articles/10.3389/fenvs.2021.617828/full#supplementary-material.

REFERENCES

Aalde, H., Gonzalez, P., Gytarski, M., Krug, T., Kurz, W. A., Lasco, R. D., et al. (2006). "Chapter 2: generic methodologies applicable to multiple land-use categories," in *2006 IPCC guidelines for national greenhouse gas inventories*. Editors S. Eggleston, L. Buendia, K. Miwa, T. Ngara, and K. Tanabe (Hayama, Japan: IGES).

Aini, F. K., Hergoualc'h, K., Smith, J. U., and Verchot, L. (2015). Nitrous oxide emissions along a gradient of tropical forest disturbance on mineral soils in Sumatra. *Agric. Ecosyst. Environ.* 214, 107–117. doi:10.1016/j.agee.2015.08.022

Andriesse, J. P. (1988). *Nature and management of tropical peat soils. FAO Soils Bull 59*. Rome, Italy: Food and Agriculture Organization (FAO) of United Nations, 165.

Arah, J. R. M. (1997). Apportioning nitrous oxide fluxes between nitrification and denitrification using gas-phase mass spectrometry. *Soil Biol. Biochem.* 29, 1295–1299. doi:10.1016/s0038-0717(97)00027-8

Austin, K. G., Harris, N. L., Wijaya, A., Murdiyarso, D., Harvey, T., Stolle, F., et al. (2018). A review of land-based greenhouse gas flux estimates in Indonesia. *Environ. Res. Lett.* 13, 055003. doi:10.1088/1748-9326/aab531

Bridgham, S., Cadillo-Quiroz, H., Keller, J., and Zhuang, Q. (2012). Methane emissions from wetlands: biogeochemical, microbial, and modeling perspectives from local to global scales. *Glob. Change Biol.* 19, 1325–1346. doi:10.1111/gcb.12131

Butterbach-Bahl, K., Baggs, E. M., Dannenmann, M., Kiese, R., and Zechmeister-Boltenstern, S. (2013). Nitrous oxide emissions from soils: how well do we understand the processes and their controls?. *Philos. Trans. R. Soc. B* 368, 20130122. doi:10.1098/rstb.2013.0122

Chaddy, A., Melling, L., Ishikura, K., and Hatano, R. (2019). Soil N_2O emissions under different N rates in an oil palm plantation on tropical peatland. *Agriculture* 9, 213. doi:10.3390/agriculture9100213

Chapin, F. S., Matson, P. A., and Mooney, H. A. (2002). *Principles of terrestrial ecosystem ecology*. New York, NY: Springer.

Chapuis-Lardy, L., Wrage, N., Metay, A., Chotte, J., and Bernoux, M. (2007). Soil, a sink for N_2O? a review. *Glob. Change Biol.* 13, 1–17. doi:10.1111/j.1365-2486.2006.01280.x

Comeau, L., Hergoualc'h, K., Hartill, J., Smith, J., Verchot, L., Peak, D., et al. (2016). How do the heterotrophic and the total soil respiration of an oil palm plantation on peat respond to nitrogen fertilizer application? *Geoderma* 268, 41–51. doi:10.1016/j.geoderma.2016.01.016

Cooper, H. V., Evers, S., Aplin, P., Crout, N., Dahalan, M. P. B., and Sjogersten, S. (2020). Greenhouse gas emissions resulting from conversion of peat swamp forest to oil palm plantation. *Nat. Commun.* 11, 407. doi:10.1038/s41467-020-14298-w

Corley, R. H. V., and Tinker, P. B. (2003). *The oil palm*. Oxford, United Kingdom: Blackwell Science.

Deshmukh, C. S., Julius, D., Evans, C. D., Susanto, A. P., Page, S. E., Gauci, V., et al. (2020). Impact of forest plantation on methane emissions from tropical peatland. *Glob. Change Biol.* 26, 2477–2495. doi:10.1111/gcb.15019

DJP (2015). *Statistik perkebunan Indonesia; kelapa sawit 2014–2016*. Jakarta, Indonesia: Direktorat Jenderal Perkebunan, 69.

Dommain, R., Frolking, S., Jeltsch-Thömmes, A., Joos, F., Couwenberg, J., and Glaser, P. (2018). A radiative forcing analysis of tropical peatlands before and after their conversion to agricultural plantations. *Glob. Change Biol.* 24, 5518–5533. doi:10.1111/gcb.14400

Drösler, M., Verchot, L. V., Freibauer, A., Pan, G., Evans, C. D., Bourbonniere, R. A., et al. (2014). "Chapter 2: drained inland organic soils," in *Supplement to the 2006 guidelines for national greenhouse gas inventories: wetlands*. Editors T. Hiraishi, T. Krug, K. Tanabe, N. Srivastava, B. Jamsranjav, M. Fukuda, et al. (Geneva, Switzerland: IPCC).

EPA (1971). Analytical method and laboratories. Method 352.1.

Farmer, J., Matthew, R., Smith, P., Langan, C., Hergoualc'h, K., Verchot, L., et al. (2014). Comparison of methods for quantifying soil carbon in tropical peats. *Geoderma* 214-215, 177–183. doi:10.1016/j.geoderma.2013.09.013

Furukawa, Y., Inubushi, K., Ali, M., Itang, A. M., and Tsuruta, H. (2005). Effect of changing groundwater levels caused by land-use changes on greenhouse gas fluxes from tropical peat lands. *Nutr. Cycl. Agroecosyst.* 71, 81–91. doi:10.1007/s10705-004-5286-5

Günther, A. B., Huth, V., Jurasinski, G., and Glatzel, S. (2014). Scale-dependent temporal variation in determining the methane balance of a temperate fen. *Greenh. Gas Meas. Manag.* 4, 41–48. doi:10.1080/20430779.2013.850395

Hadi, A., Inubushi, K., Furukawa, Y., Purnomo, E., Rasmadi, M., and Tsuruta, H. (2005). Greenhouse gas emissions from tropical peatlands of Kalimantan,Indonesia. *Nutr. Cycl. Agroecosyst.* 71, 73–80. doi:10.1007/s10705-004-0380-2

Harianti, M., Sutandi, A., Saraswati, R., Maswarand Sabiham, S. (2017). Organic acids exudates and enzyme activities in the rhizosphere based on distance from the trunk of oil palm in peatland. *Malays. J. Soil Sci.* 21, 73–88.

Hart, S. C., Stark, J. M., Davidson, E. A., and Firestone, M. K. (1994). "Nitrogen mineralization, immobilization and nitrification," in *Methods of soil analysis: part 2 microbial and biochemical properties*. Editors R. W. Weaver, S. Angle,

P. Bottomley, D. Bezdicek, S. Smith, A. Tabatabai, et al. (Madison, WI: Soil Science Society of America), 985–1018.

Hergoualc'h, K., Dezzeo, N., Verchot, L. V., Martius, C., Van Lent, J., Del Aguila-Pasquel, J., et al. (2020). Spatial and temporal variability of soil N_2O and CH_4 fluxes along a degradation gradient in a palm swamp peat forest in the Peruvian Amazon. *Glob. Change Biol.* 26, 7198–7216. doi:10.1111/gcb.15354

Hergoualc'h, K., Hendry, D. T., Murdiyarso, D., and Verchot, L. V. (2017). Total and heterotrophic soil respiration in a swamp forest and oil palm plantations on peat in Central Kalimantan, Indonesia. *Biogeochemistry* 135, 203–220. doi:10.1007/s10533-017-0363-4

Hergoualc'h, K., Skiba, U., Harmand, J. M., and Oliver, R. (2007). Processes responsible for the nitrous oxide emission from a Costa Rican Andosol under a coffee agroforestry plantation. *Biol. Fertil. Soils* 43, 787–795. doi:10.1007/s00374-007-0168-z

Hergoualc'h, K., and Verchot, L. (2012). Changes in soil CH_4 fluxes from the conversion of tropical peat swamp forests: a meta-analysis. *J. Integr. Environ. Sci.* 9, 93–101. doi:10.1080/1943815X.2012.679282

Hergoualc'h, K., and Verchot, L. (2014). Greenhouse gas emission factors for land use and land-use change in Southeast Asian peatlands. *Mitig. Adapt. Strateg. Glob. Change* 19, 789–807. doi:10.1007/s11027-013-9511-x

Hergoualc'h, K., and Verchot, L. (2011). Stocks and fluxes of carbon associated with land use change in Southeast Asian tropical peatlands: a review. *Glob. Biogeochem. Cycles* 25, GB2001. doi:10.1029/2009GB003718

Hirano, T., Segah, H., Harada, T., Limin, S., June, T., Hirata, R., et al. (2007). Carbon dioxide balance of a tropical peat swamp forest in Kalimantan, Indonesia. *Glob. Change Biol.* 13, 412–425. doi:10.1111/j.1365-2486.2006.01301.x

Hutchinson, G. L., and Livingston, G. P. (1993). "Use of chamber systems to measure trace gas fluxes," in Symposium on agroecosystem effects on radiatively important trace gases and global climate change, at the meeting of the American society of agronomy, Denver, CO, October 27–November 1, 1991.

Hynes, R. K., and Knowles, R. (1984). Production of nitrous oxide by *Nitrosomonas europaea*: effects of acetylene, pH, and oxygen. *Can. J. Microbiol.* 30, 1397–1404. doi:10.1139/m84-222

Inubushi, K., Furukawa, Y., Hadi, A., Purnomo, E., and Tsuruta, H. (2003). Seasonal changes of CO_2, CH_4 and N_2O fluxes in relation to land-use change in tropical peatlands located in coastal area of South Kalimantan. *Chemosphere* 52, 603–608. doi:10.1016/s0045-6535(03)00242-x

Ishikura, K., Hirata, R., Hirano, T., Okimoto, Y., Wong, G. X., Melling, L., et al. (2019). Carbon dioxide and methane emissions from peat soil in an undrained tropical peat swamp forest. *Ecosystems* 22, 1852–1868. doi:10.1007/s10021-019-00376-8

Jauhiainen, J., Limin, S., Silvennoinen, H., and Vasander, H. (2008). Carbon dioxide and methane fluxes in drained tropical peat before and after hydrological restoration. *Ecology* 89, 3503–3514. doi:10.1890/07-2038.1

Jauhiainen, J., Silvennoinen, H., Hämäläinen, R., Kusin, K., Limin, S., Raison, R. J., et al. (2012). Nitrous oxide fluxes from tropical peat with different disturbance history and management. *Biogeosciences* 9, 1337–1350. doi:10.5194/bg-9-1337-2012

Jauhiainen, J., Silvennoinen, H., Könönen, M., Limin, S., and Vasander, H. (2016). Management driven changes in carbon mineralization dynamics of tropical peat. *Biogeochemistry* 129, 115–132. doi:10.1007/s10533-016-0222-8

Jauhiainen, J., Takahashi, H., Heikkinen, J. E. P., Martikainen, P. J., and Vasander, H. (2005). Carbon fluxes from a tropical peat swamp forest floor. *Glob. Change Biol.* 11, 1788–1797. doi:10.1111/j.1365-2486.2005.001031.x

Jones, H. A., and Nedwell, D. B. (1993). Methane emission and methane oxidation in land-fill cover soil. *Microb. Ecol.* 102, 185–195. doi:10.1111/j.1574-6968.1993.tb05809.x

Khalid, H., Zin, Z. Z., and Anderson, J. M. (1999). Quantification of oil palm biomass and nutrient value in a mature oil palm plantation: belowground biomass. *J. Oil Palm Res.* 11, 63–71.

King, G. M., Roslev, P., and Skovgaard, H. (1990). Distribution and rate of methane oxidation in sediments of the Florida Everglades. *Appl. Environ. Microbiol.* 56, 2902–2911. doi:10.1128/aem.56.9.2902-2911.1990

Koh, L. P., Miettinen, J., Liew, S. C., and Ghazoul, J. (2011). Remotely sensed evidence of tropical peatland conversion to oil palm. *Proc. Natl. Acad. Sci. U. S. A.* 108, 5127–5132. doi:10.1073/pnas.1018776108

Lamade, E., and Setiyo, I. E. (2012). "Variations of carbon content among oil palm organs in North Sumatra conditions: implications for carbon stock estimation at plantation scale," in International conference on oil palm and environment (ICOPE 2012), Bali, Indonesia, February 22–24, 2012.

Le Mer, J., and Roger, P. (2001). Production, oxidation, emission and consumption of methane by soils: a review. *Eur. J. Soil Biol.* 37, 25–50. doi:10.1016/s1164-5563(01)01067-6

Lee, A., Winther, M., Priemé, A., Blunier, T., and Christensen, S. (2017). Hot spots of N_2O emission move with the seasonally mobile oxic-anoxic interface in drained organic soils. *Soil Biol. Biochem.* 115, 178–186. doi:10.1016/j.soilbio.2017.08.025

Martikainen, P. J., Nykänen, H., Crill, P., and Silvola, J. (1993). Effect of a lowered water table on nitrous oxide fluxes from northern peatlands. *Nature* 366, 51–53. doi:10.1038/366051a0

Marushchak, M. E., Pitkämäki, A., Koponen, H., Biasi, C., Seppälä, M., and Martikainen, P. J. (2011). Hot spots for nitrous oxide emissions found in different types of permafrost peatlands. *Glob. Change Biol.* 17, 2601–2614. doi:10.1111/j.1365-2486.2011.02442.x

Meijide, A., de la Rua, C., Guillaume, T., Roll, A., Hassler, E., Stiegler, C., et al. (2020). Measured greenhouse gas budgets challenge emission savings from palm-oil biodiesel. *Nat. Commun.* 11, 1089. doi:10.1038/s41467-020-14852-6

Melling, L., Hatano, R., and Goh, K. J. (2005). Methane fluxes from three ecosystems in tropical peatland of Sarawak, Malaysia. *Soil Biol. Biochem.* 37, 1445–1453. doi:10.1016/j.soilbio.2005.01.001

Melling, L., Hatano, R., and Goh, K. J. (2007). Nitrous oxide emissions from three ecosystems in tropical peatland of Sarawak, Malaysia. *Soil Sci. Plant Nutr.* 53, 792–805. doi:10.1111/j.1747-0765.2007.00196.x

Miettinen, J., Hooijer, A., Verimmen, R., Liew, S. C., and Page, S. E. (2017). From carbon sink to carbon source: extensive peat oxidation in insular Southeast Asia since 1990. *Environ. Res. Lett.* 12, 024014. doi:10.1088/1748-9326/aa5b6f

Miettinen, J., Shi, C., and Liew, S. C. (2016). Land cover distribution in the peatlands of Peninsular Malaysia, Sumatra and Borneo in 2015 with changes since 1990. *Glob. Ecol. Conserv.* 6, 67–78. doi:10.1016/j.gecco.2016.02.004

Myhre, G., Shindell, D., Bréon, F. M., Collins, W., Fuglestvedt, J., Huang, J., et al. (2013). "Anthropogenic and natural radiative forcing,," in *Climate change 2013: the physical science basis. Contribution of working group I to the fifth assessment report of the intergovernmental panel on climate change*. Editors T. F. Stocker, D. Qin, G. K. Plattner, M. Tignor, S. K. Allen, J. Boschung, et al. (Cambridge, MA and New York, NY: Cambridge University Press).

Nelson, P. N., Banabas, M., Scotter, D. R., and Webb, M. J. (2006). Using soil water depletion to measure spatial distribution of root activity in oil palm (*Elaeis guineensis* Jacq.) plantations. *Plant Soil* 286, 109–121. doi:10.1007/s11104-006-9030-6

Novita, N. (2016). Carbon stocks and soil greenhouse gas emissions associated with forest conversion to oil palm plantations in Tanjung Puting tropical peatlands, Indonesia. PhD dissertation. Corvallis, OR: Oregon State University.

Novita, N., Kauffman, J. B., Hergoualc'h, K., Murdiyarso, D., Tryanto, D. H., and Jupesta, J. (2020). "Carbon stocks from peat swamp forest and oil palm plantation in central kalimantan, Indonesia," in *Climate change research, policy and actions in Indonesia*. Editors R. Djalante, J. Jupesta, and E. Aldrian (Cham, Switzerland: Springer International Publishing).

Obidzinski, K., Andriani, R., Komarudin, H., and Andrianto, A. (2012). Environmental and social impacts of oil palm plantations and their implications for biofuel production in Indonesia. *Ecol. Soc.* 17, 25. doi:10.5751/es-04775-170125

Oktarita, S., Hergoualc'h, K., Anwar, S., and Verchot, L. V. (2017). Substantial N_2O emissions from peat decomposition and N fertilization in an oil palm plantation exacerbated by hotspots. *Environ. Res. Lett.* 12, 104007. doi:10.1088/1748-9326/aa80f1

Pangala, S. R., Moore, S., Hornibrook, E. R., and Gauci, V. (2013). Trees are major conduits for methane gas egress from tropical forested wetlands. *New Phytol.* 197, 524–531. doi:10.1111/nph.12031

Pansu, M., Gautheyrou, J., and Loyer, J. Y. (2001). "Soil analysis," in *Sampling, instrumentation, quality control.* (Lisse, The Netherlands:. A.A. Balkema Publishers).

Parn, J., Verhoeven, J. T. A., Butterbach-Bahl, K., Dise, N. B., Ullah, S., Aaa, A., et al. (2018). Nitrogen-rich organic soils under warm well-drained conditions are

global nitrous oxide emission hotspots. *Nat. Commun.* 9, 1135. doi:10.1038/s41467-018-03540-1

Pumpanen, J., Longdoz, B., and Kutsch, W. L. (2009). "Field measurements of soil respiration: principles and constraints, potentials and limitations of different methods," in *Soil carbon dynamics—an integrated methodology*. Editors A. Heinemeyer, W. L. Kutsch, and M. Bahn (Cambridge, MA: Cambridge University Press), 16–33.

Repo, M., Susiluoto, S., Lind, S., Jokinen, S., Elsakov, V., Biasi, C., et al. (2009). Large N_2O emissions from cryoturbated peat soil in tundra. *Nat. Geosci.* 2, 189–192. doi:10.1038/ngeo434

Rixen, T., Baum, A., Wit, F., and Samiaji, J. (2016). Carbon leaching from tropical peat soils and consequences for carbon balances. *Front. Earth Sci.* 4. doi:10.3389/feart.2016.00074

Robertson, G. P. (1989). "Nitrification and denitrification in humid tropical ecosystems: potential controls on nitrogen retention," in *Mineral nutrients in tropical forest and savanna ecosystems*. Editor J Proctor (Oxford: Blackwell Scientific), 55–69.

Sakata, R., Shimada, S., Arai, H., Yoshioka, N., Yoshioka, R., Aoki, H., et al. (2015). Effects of soil type and nitrogen fertilizer on nitrous oxide and carbon dioxide emissions in oil palm plantations. *Soil Sci. Plant Nutr.* 61, 48–60. doi:10.1080/00380768.2014.960355

Skiba, U., Hergoualc'h, K., Drewer, J., Meijide, A., and Knohl, A. (2020). Oil palm plantations are large sources of nitrous oxide, but where are the data to quantify the impact on global warming?. *Curr. Opin. Environ. Sustain.* 47, 81–88. doi:10.1016/j.cosust.2020.08.019

Skiba, U., and Smith, K. A. (2000). The control of nitrous oxide emissions from agricultural and natural soils. *Chemosphere Glob. Change Sci.* 2, 379–386. doi:10.1016/s1465-9972(00)00016-7

Solorzano, L. (1969). Determination of ammonia in natural water by the phenolhypochlorite method. *Limnol. Oceanogr.* 14, 799–801. doi:10.4319/lo.1969.14.5.0799

Swails, E., Hertanti, D., Hergoualc'h, K., Verchot, L., and Lawrence, D. (2019). The response of soil respiration to climatic drivers in undrained forest and drained oil palm plantations in an Indonesian peatland. *Biogeochemistry* 142, 37–51. doi:10.1007/s10533-018-0519-x

Swails, E., Jaye, D., Verchot, L., Hergoualc'h, K., Schirrmann, M., Borchard, N., et al. (2018). Will CO_2 emissions from drained tropical peatlands decline over time? Links between soil organic matter quality, nutrients, and C mineralization rates. *Ecosystems* 21, 868–885. doi:10.1007/s10021-017-0190-4

Takakai, F., Morishita, T., Hashidoko, Y., Darung, U., Kuramochi, K., Dohong, S., et al. (2006). Effects of agricultural land-use change and forest fire on N_2O emission from tropical peatlands, Central Kalimantan, Indonesia. *Soil Sci. Plant Nutr.* 52, 662–674. doi:10.1111/j.1747-0765.2006.00084.x

Tian, H., Xu, R., Canadell, J. G., Thompson, R. L., Winiwarter, W., Suntharalingam, P., et al. (2020). A comprehensive quantification of global nitrous oxide sources and sinks. *Nature* 586, 248–256. doi:10.1038/s41586-020-2780-0

Turetsky, M. R., Kotowska, A., Bubier, J., Dise, N. B., Crill, P., Hornibrook, E. R. C., et al. (2014). A synthesis of methane emissions from 71 northern, temperate, and subtropical wetlands. *Glob. Change Biol.* 20, 2183–2197. doi:10.1111/gcb.12580

Van Len, J., Hergoualc'h, K., and Verchot, L. V. (2015). Reviews and syntheses: soil N_2O and NO emission from land use and land-use change in the tropics and subtropics: a meta-analysis. *Biogeosciences* 12, 7299–7313. doi:10.5194/bg-12-7299-2015

Van Lent, J., Hergoualc'h, K., Verchot, L., Oenema, O., and van Groenigen, J. W. (2019). Greenhouse gas emissions along a peat swamp forest degradation gradient in the Peruvian Amazon: soil moisture and palm roots effects. *Mitig. Adapt. Strateg. Glob. Change* 24, 625. doi:10.1007/s11027-018-9796-x

Verchot, L. V., Davidson, E. A., Cattânio, H., Ackerman, I. L., Erickson, H. E., and Keller, M. (1999). Land use change and biogeochemical controls of nitrogen oxide emissions from soils in eastern Amazonia. *Glob. Biogeochem. Cycles* 13, 31–46. doi:10.1029/1998gb900019

Verchot, L. V., Davidson, E. A., Cattânio, J. H., and Ackerman, I. L. (2000). Land-use change and biogeochemical controls of methane fluxes in soils of eastern Amazonia. *Ecosystems* 3, 41–56. doi:10.1007/s100210000009

Wang, S., Zhuang, Q., Lähteenoja, O., Draper, F., and Cadillo-Quiroz, H. (2018). Potential shift from a carbon sink to a source in Amazonian peatlands under a changing climate. *Proc. Natl. Acad. Sci. U. S. A.* 115, 12407–12412. doi:10.1073/pnas.1801317115

Warren, M. W., Kauffman, J. B., Murdiyarso, D., Anshari, G., Hergoualc'h, K., Kurnianto, S., et al. (2012). A cost-efficient method to assess carbon stocks in tropical peat soil. *Biogeosciences* 9, 4477–4485. doi:10.5194/bg-9-4477-2012

Whalen, S. C., Reeburgh, W. S., and Sandbeck, K. A. (1990). Rapid methane oxidation in a landfill cover soil. *Appl. Environ. Microbiol.* 56, 3405–3411. doi:10.1128/aem.56.11.3405-3411.1990

Wong, G. X., Hirata, R., Hirano, T., Kiew, F., Aeries, E. B., Musin, K. K., et al. (2018). Micrometeorological measurement of methane flux above a tropical peat swamp forest. *Agric. For. Meteorol.* 256–257, 353–361. doi:10.1016/j.agrformet.2018.03.025

Wrage, N., Velthof, G. L., van Beusichem, M. L., and Oenema, O. (2001). Role of nitrifier denitrification in the production of nitrous oxide. *Soil Biol. Biochem.* 33, 1723–1732. doi:10.1016/s0038-0717(01)00096-7

Wright, E. L., Black, C. R., Turner, B. L., and Sjögersten, S. (2013). Environmental controls of temporal and spatial variability in CO_2 and CH_4 fluxes in a neotropical peatland. *Glob. Chang Biol.* 19, 3775–3789. doi:10.1111/gcb.12330

Ye, R., Espe, M. B., Linquist, B., Parikh, S. J., Doane, T. A., and Horwath, W. R. (2016). A soil carbon proxy to predict CH_4 and N_2O emissions from rewetted agricultural peatlands. *Agric. Ecosyst. Environ.* 220, 64–75. doi:10.1016/j.agee.2016.01.008

Conflict of Interest: The authors declare that the research was conducted in the absence of any commercial or financial relationships that could be construed as a potential conflict of interest.

frontiers in Environmental Science

ORIGINAL RESEARCH
published: 19 March 2021
doi: 10.3389/fenvs.2021.631112

Methane and Nitrous Oxide Production From Agricultural Peat Soils in Relation to Drainage Level and Abiotic and Biotic Factors

Lisbet Norberg[1], Maria Hellman[2], Kerstin Berglund[1], Sara Hallin[2] and Örjan Berglund[1]*

[1] Department of Soil and Environment, Swedish University of Agricultural Sciences, Uppsala, Sweden, [2] Department of Forest Mycology and Plant Pathology, Swedish University of Agricultural Sciences, Uppsala, Sweden

Greenhouse gas emissions from drained agricultural peatlands contribute significantly to global warming. In a laboratory study using intact cores of peat soil from eight different sites in Sweden, factors controlling the emission of the greenhouse gases nitrous oxide (N_2O) and methane (CH_4) were examined. Soil properties, and the abundance of the total microbial community (16S rRNA gene abundance), and genes encoding for functions controlling N_2O emissions (bacterial and archaeal *amoA*, *nirS*, *nirK*, *nosZ*I, and *nosZ*II) were analyzed and compared against measured greenhouse gas emissions. Emissions were measured at different drainage levels, i.e., higher soil water suction values, since drainage is an important factor controlling greenhouse gas emissions from peat soils. The results showed that N_2O and CH_4 emissions were generally low, except for N_2O emissions at near water-saturated conditions, for which three soils displayed high values and large variations in fluxes. Relationships between N_2O emissions and soil properties were mainly linked to soil pH, with higher emissions at lower pH. However, specific assemblages of nitrogen cycling guilds that included *nosZ*II, typically present in non-denitrifying N_2O reducers, were detected in soils with low N_2O emissions. Overall, these results indicate that both pH and biotic controls determine net N_2O fluxes.

Keywords: Histosols, methane, nitrous oxide, functional genes, suction head, ground water level

OPEN ACCESS

Edited by:
Annalea Lohila,
University of Helsinki, Finland

Reviewed by:
Yong Li,
Zhejiang University, China
Stephan Glatzel,
University of Vienna, Austria

****Correspondence:***
Lisbet Norberg
lisbet.norberg@slu.se

Specialty section:
This article was submitted to Soil Processes, a section of the journal Frontiers in Environmental Science

Received: *19 November 2020*
Accepted: *01 March 2021*
Published: *19 March 2021*

Citation:
Norberg L, Hellman M, Berglund K, Hallin S and Berglund Ö (2021) Methane and Nitrous Oxide Production From Agricultural Peat Soils in Relation to Drainage Level and Abiotic and Biotic Factors. Front. Environ. Sci. 9:631112. doi: 10.3389/fenvs.2021.631112

INTRODUCTION

Emissions of the greenhouse gases carbon dioxide (CO_2), nitrous oxide (N_2O), and methane (CH_4) to the atmosphere have resulted in global warming, while N_2O is also involved in destruction of stratospheric ozone (Conrad, 1996). Soils world-wide play an important role in these emissions, with drained agricultural peat soils in particular emitting substantial amounts of CO_2 and N_2O (Taft et al., 2017). In the 19th century, large peatland areas in Sweden were drained for agricultural purposes, in order to produce food for a growing population. Today, many of these drained peat soils have been abandoned or are under forestry, but the remaining agricultural peat soils contribute 6–8% of total annual anthropogenic greenhouse gas emissions in Sweden (Berglund and Berglund, 2010).

The CO_2, CH_4, and N_2O emitted from soils mainly originate from microbial processes. Emissions of CO_2 from drained peat soils occur when the aerated topmost peat layer decomposes,

whereas CH_4 can be produced in the deeper, water-filled layer by methanogens and potentially oxidized in the aerated upper layer by methane-oxidizing bacteria. Nitrous oxide can be produced during the first step of nitrification, oxidation of ammonia (NH_3) to nitrite (NO_2^-), which is performed by ammonia-oxidizing archaea (AOA) or ammonia-oxidizing bacteria (AOB) (**Supplementary Figure 1**). Nitrous oxide is also produced by microbial activity during the denitrification process when conditions in the soil are anoxic. Denitrification reduces nitrate (NO_3^-) to N_2O or dinitrogen (N_2) in a stepwise process, in the latter case with N_2O as an intermediate. There are also non-denitrifying N_2O reducers in soil (Jones et al., 2013). The relationship between N_2O-producing and N_2O-consuming communities regulates net emissions of N_2O from the soil (Philippot et al., 2011; Domeignoz-Horta et al., 2016). Drainage and groundwater level have an impact on relative emissions of CO_2, N_2O, and CH_4. For agricultural peatlands, groundwater level is the most important factor regulating emissions of greenhouse gases (Renger et al., 2002; Beyer and Höper, 2015; Regina et al., 2015). Changes in soil moisture due to drying or wetting can influence the availability of dissolved organic carbon and nitrogen species, and therefore alter the microbial community composition and N_2O emissions (Banerjee et al., 2016). Furthermore, in field conditions N_2O emissions are affected by, e.g., freeze-thaw cycles (Wagner-Riddle et al., 2017), rain events (Kandel et al., 2013), and nitrogen (N) application rates (Bouwman et al., 2002). The presence of living plants can increase both N_2O and CH_4 emissions, as rhizodeposition is an easily available carbon source (Kuzyakov, 2002). The magnitude of these fluxes are controlled by the gas diffusivity in the soil, which is mainly affected by soil bulk density and water-filled pore space (Smith et al., 2018). However, Taft et al. (2018) showed that total greenhouse gas emissions decline when the groundwater level is at the soil surface, but this is not an option in all agricultural fields, where an optimum groundwater level needs to be found to mitigate greenhouse gas emissions while maintaining traditional crop production (Kløve et al., 2017).

The aim of this study was to identify soil factors controlling emissions of N_2O and CH_4 from drained and cultivated peat soils at different groundwater levels, and since N_2O is more important for drained soils further examine the microbial community properties, i.e., abundances if the total bacterial community and genes encoding functions controlling N_2O emissions. To obtain controlled conditions, this was done as a laboratory study using intact cores of peat soil from eight sites in southern Sweden, selected to represent a wide range of drained and cultivated peat soils. Soil properties and gene abundances were analyzed in order to determine general and site-specific responses of N_2O and CH_4 emissions.

MATERIALS AND METHODS

Soil Sampling and Experimental Set-Up

In autumn 2011, soil samples were collected at eight different agricultural sites on drained peat soil in southern Sweden (**Supplementary Figure 2**). Topsoil was sampled at all sites (soils 1–8) and subsoil was sampled at four sites (soils 5–8). All fields except that where soil 8 was sampled were on active farms, with crop production (soils 2 and 4) or combined crop-dairy production (soils 1, 3, 5–7). Soil 8 was taken at a site that was once a dairy farm, but had been abandoned for several years. Three of the farms had vegetables and potatoes in their crop rotation (soils 2, 3, 4). The same eight topsoil and four subsoil samples were used in our previous study Norberg et al. (2018), where they were numbered differently (numbers in brackets); 1–3 (1–3), 4 (5), 5–8 (6–9).

Detailed descriptions of field soil sampling and of the experimental set-up can be found in Norberg et al. (2018). In brief, intact soil cores were sampled in steel cylinders (Ø 7.2 cm, height 10 cm), at approximately 5–15 cm depth for topsoil samples and 20–50 cm depth for subsoil samples. Replicate soil cores to be used in soil analyses and greenhouse gas emissions measurements were taken within a small area (<1 m^2). Upon extraction, the cylinders were sealed at both ends with plastic lids and stored in wooden boxes in a cold store (5°C) until the experiment started.

At the start of the experiment, intact soil cores in their cylinders were assigned to plastic boxes (50 cm × 80 cm). Each box contained one sample from each of the 12 soils, with a total of 84 samples distributed across seven boxes. All boxes were treated similarly and were assumed independent in the statistical analysis. The boxes were brought into the experiment one at a time. Before the start of measurements, the caps on the cylinders were removed and the 12 soil samples in the box were kept at room temperature (20°C) for 2 days and then soaked in tap-water for 3 days, until water-saturated. The 12 samples were then placed on a suction sand bed (Romano et al., 2002) for successive adjustment to one of three soil water suction heads: near water-saturated, 0.5 and 1.0 m water column (∼5 and 10 kPa), corresponding to a groundwater level in field conditions of 0.05, 0.5, and 1.0 m below the soil surface, respectively. At all conditions the soil samples were weighed for water content calculations and then greenhouse gas emissions were measured.

When all gas emissions measurements had been completed, the soil cores in three of the seven boxes were divided into two sub-samples, one frozen at −18°C and one refrigerated at +5°C, to be used for subsequent analyses. Soil cores from the four remaining boxes were dried at 105°C for 72 h and weighed for dry weight-based emissions calculations. The mean dry weight (dw) of soil samples in these boxes was used for the corresponding soil samples in the other boxes.

N_2O and CH_4 Emissions Measurements

Emissions of N_2O and CH_4 were measured using a similar approach to that used for determination of CO_2 emissions in Norberg et al. (2018). Each soil sample cylinder was placed in a polypropylene jar (Ø 11 cm, height 12 cm) with air-tight screw lids equipped with two injection needles (Ø 0.8 mm, 40 mm long). The jars had thick walls (∼1.5 mm) and potential gas leakage was considered negligible. Gas was sampled by connecting plastic tubing to the injection needles in the lid and circulating the air in the closed jar for 30 s in a 22-mL vial sealed with a rubber septum. During this time, the air in the vial was exchanged seven

times, and a representative air sample was thus collected. Fluxes of N_2O and CH_4 were determined by taking samples at time zero when the lid was closed, and then at 40, 80, and 120 min. The gas samples were analyzed using a gas chromatograph equipped with electron capture and flame ionization detectors (Clarus 500 GC, PerkinElmer, United States).

The N_2O and CH_4 emission rates from the soils were calculated from the linear increase in gas concentration in the jar headspace during the closure time, as described in Norberg et al. (2018). All measurements of N_2O and CH_4 were used unless they showed obvious bias upon visual inspection.

Soil Chemical Analysis

Humification degree (H1–H10) of the peat soils was determined according to von Post (1922). The frozen soil samples from the greenhouse gas emissions experiment were used for analysis of mineral nitrogen [nitrate (NO_3^-) and ammonium (NH_4^+)] on a TRAACS 800 AutoAnalyzer (Bran & Luebbe, Germany). The refrigerated soil samples were used for different analyses within 30 days of completion of the gas measurements. Total nitrogen (tot-N), total carbon (tot-C), and carbonate carbon (carb-C) content were determined by dry combustion on a LECO CN-2000 analyzer (St. Joseph, MI, United States). Soil pH was measured at a soil-solution ratio of 1:5 with deionized water. Organic matter content (loss on ignition) was measured by dry combustion at 550°C for 24 h, after pre-drying at 105°C for 24 h. Water-extractable organic carbon (WEOC), here presented as total WEOC, was determined by a modified version of the method of Ghani et al. (2003), as described in detail in Norberg et al. (2018). The results were presented as mg WEOC g^{-1} tot-C in the soil.

Soil Microbiological Sampling and Analysis

Samples for microbiological analyses were taken at a soil water suction head of 0.5 m water column from the soil cylinders in the three boxes used for soil analysis. A small soil drill with inner diameter 3 mm was used to obtain soil cores, with the drill was inserted about 3.5 cm into the soil. The upper 0.5 cm of the core was removed and the remaining 3.0 cm part was placed in a 2 mL microcentrifuge tube and kept frozen until analysis. The drill was disinfected twice between every sample.

DNA was extracted from the soil plug (40–200 mg soil) using the FastDNA Spin kit for Soil (MP Biomedicals, United States) according to the manufacturer's instructions. Extract concentrations were determined with the Qubit system (Thermo Fisher Scientific, United States) and the samples were diluted to 1 ng DNA μL^{-1}. Quantitative PCR (qPCR) was used to determine abundances of specific genes, which in turn were used as proxies for the size of microbial communities harboring those genes. For the abundance of the total bacterial community, the bacterial 16S rRNA gene was quantified (Muyzer et al., 1993). For ammonia oxidizers, the archaeal (Tourna et al., 2008) and bacterial (Rotthauwe et al., 1997) *amoA* genes were quantified, while for denitrifiers, the nitrite reductases encoded by *nirS* (Throbäck et al., 2004) or *nirK* (Henry et al., 2004) genes were quantified. For N_2O reducers, the genes *nosZ*I (Henry et al., 2006) and *nosZ*II (Jones et al., 2013) coding for nitrous oxide reductases were quantified. The quantifications were performed using gene-specific primers as described in Hellman et al. (2019), with bovine serum albumin (BSA) in all reactions and 10 ng of DNA per reaction for *amoA* genes and 2 ng of DNA for *nir* and *nos* genes. Cycling protocols and primer concentrations used are described in **Supplementary Table 1**.

Calculations and Statistics

Normality was tested with a Ryan-Joiner test. Emissions data on N_2O, CH_4, and CO_2 (CO_2 data from Norberg et al., 2018) did not meet the normality requirement and were $\log_{10}$ transformed before statistical analysis. Because of negative data values (consumption of gas), a constant (the smallest possible integer) was added to get a positive value before transformation. Gene abundance data were $\log_{10}$ transformed before statistical analysis to meet the normality requirement. In calculations with gene data per g dw, dry weight data from a soil water suction of 0.5 m were used.

Differences between means of soil properties, greenhouse gas emissions at different suction heads, and gene abundances were tested with one-way ANOVA. When significant effects ($p < 0.05$) were found, Tukey's honest significant difference (HSD) test was used to compare mean values. When only two variables were tested, a students' *t*-test was used. Relationships between soil properties and greenhouse gas emissions were tested with linear and non-linear regression models ($p < 0.05$) for data from boxes I, II, and IV. These statistical analyses were carried out using Minitab (Minitab Inc., version 18.1).

To explore the structure of the nitrogen reducing assemblages, principal component analysis (PCA) was performed using ratios between abundances of each functional gene and the 16S rRNA gene. Soil chemical and physical data were correlated to the ordination using the function *envfit* in the R package *vegan* (Oksanen et al., 2018) and vectors representing significant ($p < 0.05$) factors were included in the ordination. Metadata used for overlaying vectors were the variables in **Table 1** (excluding humification degree), tot-N, air-filled pore space (AFPS) at the three soil water suction heads, pore volume (square root-transformed), and fluxes of N_2O, CH_4, and CO_2 (tot-N, AFPS, pore volume, bulk density, and CO_2 data from Norberg et al., 2018, gas data transformed as described). Permutation MANOVA (PERMANOVA, 999 permutations) on a Bray dissimilarity matrix based on the gene ratios was used to evaluate differences in overall nitrogen cycling assemblages between soils, using the function *adonis* in R package *vegan*. The multivariate analyses were performed in R, version 3.6.1 (R Core Team, 2016).

RESULTS

Soil Characteristics

Topsoil content of tot-C ranged from 26 to 43% and the tot-N content from 1.6 to 3.2%. Soils 3, 4, and 6 had a higher carb-C content (2.9–5.3%) than the other soils (0.2–0.5%). Therefore,

TABLE 1 | Sample depth, description of the soils, and selected soil properties of the eight soils.

Soil no.	Sample depth	Soil description	Humification degree	pH	Org-C %	Carb-C %	WEOC mg g^{-1} tot-C	NH_4^+ mg kg^{-1}	NO_3^- mg kg^{-1}	C/N	ρ_b g cm^{-3}	LOI %
1	5–15 cm	Fen peat	H 9–10	6.0^{e} (0.07)	26^{cd} (5.9)	0.2^{d} (0.27)	1.5^{bc} (0.38)	6^{d} (0.7)	23^{b} (19.6)	16^{b} (0.37)	0.47^{a} (0.012)	56^{bc} (0.7)
2	5–15 cm	Fen peat	H 9–10	5.9^{e} (0.09)	42^{a} (0.2)	0.5^{d} (0.05)	2.1^{abc} (0.09)	9^{d} (1.5)	28^{b} (13.6)	21^{a} (0.08)	0.31^{c} (0.012)	80^{a} (10.1)
3	5–15 cm	Fen peat with lime	H 10	7.1^{ab} (0.13)	28^{bcd} (0.2)	3.4^{b} (0.06)	1.8^{bc} (0.03)	10^{d} (3.7)	15^{b} (7.6)	14^{c} (0.13)	0.47^{a} (0.010)	57^{bc} (0.4)
4	5–15 cm	Fen peat with lime gyttja subsoil	H 10	7.4^{a} (0.07)	33^{abc} (0.2)	2.9^{c} (0.3)	1.5^{bc} (0.09)	10^{d} (0.4)	25^{b} (7.7)	14^{c} (0.17)	0.39^{b} (0.006)	65^{abc} (5.7)
5	5–15 cm	Fen peat with stones	H 9–10	6.7^{cd} (0.20)	37^{ab} (1.0)	0.3^{d} (0.01)	2.9^{a} (0.53)	22^{b} (2.6)	24^{b} (11.7)	11^{e} (0.10)	0.38^{b} (0.044)	73^{ab} (4.0)
5_{sub}	40–50 cm	Fen peat (*Phragmites*) with gyttja intrusion	H 7–8	6.6^{b} (0.20)	43^{a} (1.1)	1.0^{b} (0.05)	3.2^{b} (0.36)	4^{b} (0.9)	28^{b} (28.3)	15^{a} (1.0)	0.19^{b} (0.000)	83^{a} (3.2)
6	5–15 cm	Fen peat with clay intrusion	H 7–8	6.9^{bc} (0.20)	21^{d} (1.1)	5.3^{a} (0.10)	1.4^{c} (0.02)	29^{a} (3.9)	13^{b} (0.8)	11^{f} (0.09)	0.45^{a} (0.015)	48^{c} (8.7)
6_{sub}	20–30 cm	Fen peat (*Phragmites*)	H 3–4	7.2^{a} (0.16)	23^{b} (4.9)	4.4^{a} (0.75)	2.6^{b} (0.12)	20^{a} (3.4)	34^{ab} (4.6)	16^{a} (0.5)	0.24^{a} (0.023)	59^{b} (13.1)
7	5–15 cm	Fen peat	H 9	6.4^{d} (0.11)	37^{ab} (6.9)	0.2^{d} (0.05)	2.5^{ab} (0.53)	17^{bc} (2.7)	3^{b} (1.4)	12^{d} (0.40)	0.29^{c} (0.0123)	80^{a} (8.0)
7_{sub}	20–30 cm	Fen peat (*Phragmites*)	H 8	6.0^{c} (0.15)	42^{a} (5.2)	0.3^{b} (0.04)	4.8^{a} (0.90)	3^{b} (0.4)	10^{b} (6.0)	16^{a} (0.6)	0.17^{b} (0.000)	87^{a} (5.6)
8	5–15 cm	Fen peat	H 9–10	5.9^{e} (0.06)	39^{a} (4.3)	0.5^{d} (0.10)	2.3^{ab} (0.43)	13^{cd} (1.2)	68^{a} (14.0)	14^{c} (0.16)	0.31^{c} (0.017)	81^{a} (11.9)
8_{sub}	30–40 cm	Fen peat	H 8–9	5.8^{c} (0.10)	38^{a} (4.8)	0.8^{b} (0.09)	5.8^{a} (0.66)	8^{b} (2.4)	74^{a} (16.2)	16^{a} (0.8)	0.25^{a} (0.006)	80^{a} (6.4)

Topsoil samples were taken at four sites (soils 1–4) and topsoil and subsoil samples at four sites (soils 5–8). Subsoil samples are marked "sub." Mean values, standard deviation in brackets (n = 3). Different superscript letters denote significantly different values ($p < 0.05$, n = 3) for topsoils and subsoils in separate statistical analysis. WEOC, water-extractable organic carbon; ρ_b, bulk density; LOI, loss on ignition.

these soils also had high pH (6.9–7.4), while pH in the other soils was between 5.9 and 6.7. Soils 5–7 were sampled on the same farm, but soil characteristics showed large variation (**Table 1**). On average, the subsoil differed from the corresponding topsoil, with lower C/N ratio, porosity, and WEOC, but higher bulk density and NH_4^+, while no difference in pH, org-C, carb-C, and NO_3^- was found between topsoil and subsoil ($p < 0.05$).

Greenhouse Gases, Drainage, and Soil Properties

The N_2O emissions from the soil cores were significantly higher ($p < 0.05$) at near water-saturated conditions than at the two drainage steps, which had similar N_2O emissions (**Figures 1A–C**). At near water-saturated conditions, the highest N_2O emissions were recorded from soils 1, 2, and 8, but with a wide range, while for the other soils the N_2O emissions were lower and the range was smaller (**Figure 1A**). At a suction head of 0.5 and 1.0 m water column, the variation between the soils was small and soil 5 displayed the highest N_2O emissions.

Similarly to the N_2O fluxes, the CH_4 fluxes were significantly higher under near water-saturated conditions than at the two drainage steps, which had similar CH_4 fluxes (**Figures 1D–F**). In general, soils 5 and 7 displayed a larger range of CH_4 fluxes, with more high values, and soil 8 showed negative values at all suction heads. The N_2O, CH_4, and CO_2 fluxes (CO_2 data from Norberg et al., 2018) showed no relationship at any of the three soil water suction heads tested ($p > 0.05$).

Subsoil samples had lower N_2O emissions than topsoil samples at a soil water suction head of 0.5 and 1.0 m water column ($p < 0.05$), but no difference at near water-saturated conditions (**Figure 2**). However, subsoil samples had lower emissions of CH_4 than topsoil samples at near water-saturated conditions and at a soil water suction head of 0.5 m, but not at 1.0 m water column (**Figure 2**). At near water-saturated conditions, N_2O fluxes from topsoils correlated positively with NO_3^- and negatively with NH_4^+ ($p < 0.05$) (**Table 2**). Other factors correlating with N_2O fluxes at different soil water suction heads were pH and carb-C, with increasing N_2O emissions with decreasing carb-C and pH ($p < 0.05$) (**Table 2**). Several carbon fractions (org-C, tot-C, C/N ratio, WEOC) showed a significant positive relationship with N_2O emissions ($p < 0.05$) (**Table 2**). Fluxes of CH_4 displayed a negative relationship with NO_3^- and a positive relationship with pH ($p < 0.05$) (**Table 2**).

Abundances of Bacterial Communities and Functional Groups at 0.5 m Water Column

The total bacterial community size, i.e., abundance of 16S rRNA gene copies g^{-1} dw soil, differed between the topsoils ($p < 0.05$) (**Figure 3A**). Soil 3 had a lower abundance than most other soils, while soils 6–8 displayed the highest abundances. The abundance of AOB communities reflected the pattern observed for the total community (**Figure 3B**). In contrast, the AOA could only be properly quantified in soils 2, 4, 5, and 6 and displayed low abundances, 1.7×10^7–5.1×10^8 copies g^{-1} dw soil. Nevertheless, soil 6 had significantly higher AOA abundance

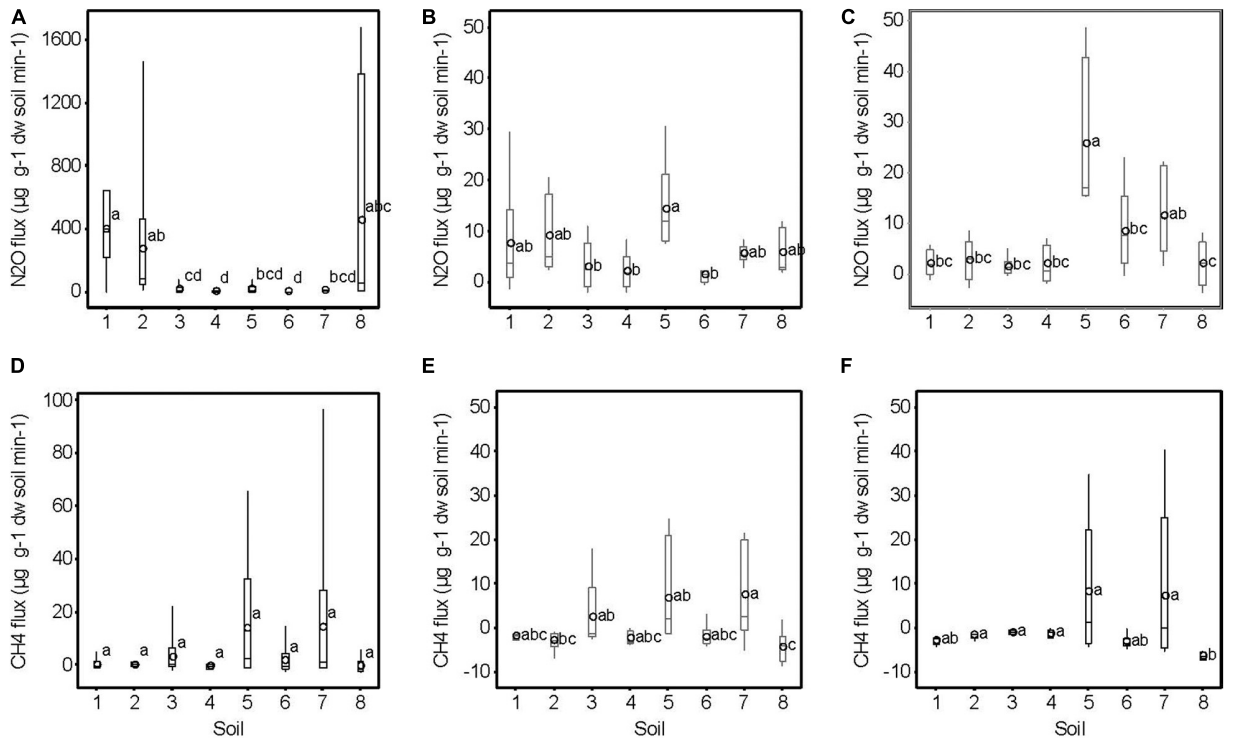

FIGURE 1 | Soil nitrous oxide (N_2O) fluxes (µg g^{-1} dry soil min^{-1}) at **(A)** near water-saturated conditions, **(B)** soil water suction head of 0.5 m water column, and **(C)** soil water suction head of 1.0 m water column; and **(D–F)** methane (CH_4) fluxes (µg g^{-1} dry soil min^{-1}) at the respective soil water suction heads. Different letters denote significantly different values of the mean (open circle, $n = 7$, $p < 0.05$). Note the different scales.

than soils 2, 4, and 5 ($p < 0.05$). Because AOA were not detected in half of the soil samples, they were excluded from other statistical analyses.

Across samples, *nirS* was more abundant than *nirK* ($p < 0.05$) and the variation between soils was higher (**Figures 3C,D**). The abundance of *nosZ*I was higher than that of *nosZ*II across the soils ($p < 0.05$), with the highest in soil 7 and 6, respectively. The abundance was lowest in soils 3 and 4 for *nosZ*I and in soil 3 for *nosZ*II (**Figures 3E,F**). All soils had $\Sigma nos/\Sigma nir$ ratio <1 (range 0.04–0.22), indicating genetic potential for net production of N_2O (**Supplementary Table 2**). The lowest ratio was found in soil 6 and the highest in soil 8 ($p < 0.05$), while for the other soils there were no significant differences. No relationship was found between $\Sigma nos/\Sigma nir$ ratio and N_2O emissions from the eight topsoils at any of the three soil water suction heads tested ($p > 0.05$).

There were differences in gene abundances between topsoil and subsoil at the four sites where this comparison could be made (soils 5–8). AOB and *nosZ*I were more abundant in topsoils than in subsoils, but for the 16S rRNA gene, *nirS*, *nirK*, and *nosZ*II there were no differences ($p > 0.05$, data not shown).

The concatenated functional gene abundances normalized to total bacterial community size, as visualized in the PCA plots, indicated different nitrogen cycling guild assemblages in each of the eight topsoils (PERMANOVA: $R^2 = 0.925$, $p = 0.001$) (**Figure 4**). Soil NH_4^+ content and C/N ratio were the strongest drivers shaping the guild assemblages in the topsoils, but soil pH was also important. The relative abundance of *nirS*-type denitrifiers coincided with AOB and *nosZ*II N_2O reducers, resulting in soils 4 and 6, which were dominated by these assemblages, having lower N_2O emissions than the other soils at near water saturation and at a suction head of 0.5 m water column (**Figures 1**, **4**). The relative abundance of *nirK*-type denitrifiers and *nosZ*I co-varied, with soils 5 and 7 and some of the replicates of soils 1 and 8 having higher emissions (depending on drainage level) (**Figures 1**, **4**). The wide range of soil characteristics exhibited by soils 5–7, which originated from the same farm and were collected within 1 km^2 (**Table 1**), was reflected in the nitrogen cycling guild assemblages (**Figure 4**).

DISCUSSION

Impact of Drainage on N_2O Emissions

Overall, in this laboratory study N_2O emissions from the peat soil samples were higher and more variable at near water-saturated conditions than under more aerated soil conditions, indicating that a fluctuating water level at near saturated soil conditions triggers N_2O emissions. Similarly, a previous field study on agricultural peat soil reported that N_2O emissions increased after several days of rainfall and that a decline in N_2O emissions could be seen after drainage of the topsoil, due to lowering of the groundwater level (Taghizadeh-Toosi et al., 2019). Those authors concluded that a stable groundwater level could potentially

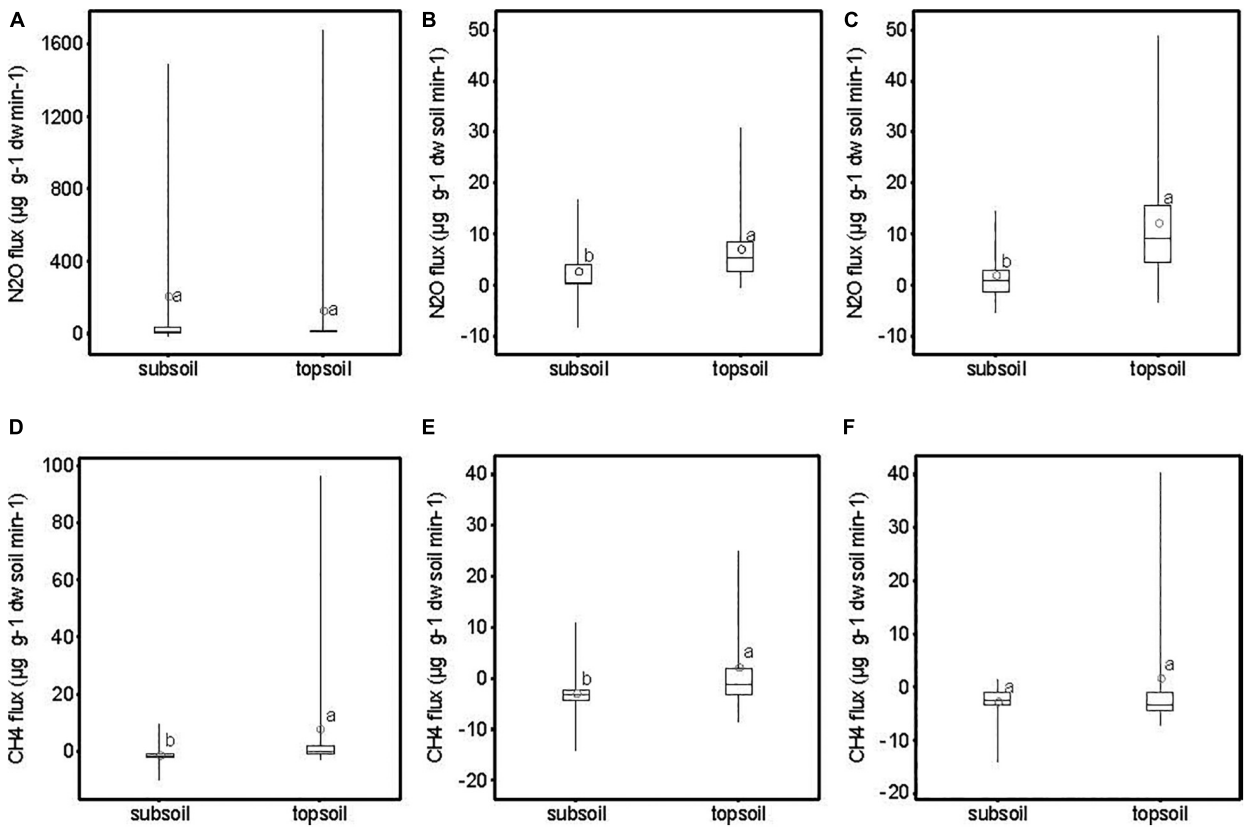

FIGURE 2 | Soil nitrous oxide (N_2O) fluxes ($\mu g\ g^{-1}$ dry soil min^{-1}) from topsoil and subsoil samples of soils 5–8 at **(A)** near water-saturated conditions, **(B)** soil water suction head of 0.5 m water column, and **(C)** soil water suction head of 1.0 m water column; and **(D–F)** methane (CH_4) fluxes ($\mu g\ g^{-1}$ dry soil min^{-1}) at the respective soil water suction heads. Different subscript letters denote significantly different values of the mean (open circle, $n = 28$, $p < 0.05$). Note the different scales.

TABLE 2 | Linear relationships (*p*-values) between nitrous oxide (N_2O) and methane (CH_4) fluxes and soil properties at the three soil water suction heads: −0.05 m (near water-saturated), 0.5 m, and 1.0 m water column.

Soil factor	N_2O			CH_4		
	0.05 m[a]	0.5 m[a]	1.0 m[a]	0.05 m[a]	0.5 m[a]	1.0 m[a]
NH_4	0.016					
NO_3	0.026				<0.001	<0.001
pH	<0.001					0.032
Tot-C		0.016				
Carb-C	<0.001	0.039				
Org-C		0.009				
C/N	0.008					
WEOC			0.042			

Data from box I, II, and IV (n = 21).
[a]*soil water suction head.*

control N_2O emissions from soil. In laboratory studies on peat soil columns, pulses of N_2O emissions have been recorded during draining and wetting events (Dinsmore et al., 2009; Taft et al., 2018). In field studies, episodic N_2O fluxes correlated with rain events have been reported (Maljanen et al., 2004; Elder and Lal, 2008; Kandel et al., 2013). Tiemeyer et al. (2016) suggested that this may be due to N_2O production by nitrification rather than denitrification. This was confirmed by Liimatainen et al. (2018), who concluded that nitrification is the main process for N_2O production in peat soils. However, others have recorded reduced N_2O emissions when the groundwater level is at the soil surface, but elevated emissions when the groundwater level is lowered (Regina et al., 1999; van Beek et al., 2011; Taft et al., 2018). Optimal drainage levels for reduced N_2O emissions have been discussed in several studies and a suction head of 0.1–0.5 m is suggested (Regina et al., 2015; Susilawati et al., 2016; Taft et al., 2018; Wen et al., 2020). However, lowering of the groundwater level as an agricultural mitigation option for N_2O emissions will instead increase soil CO_2 emissions (Norberg et al., 2018). Likely, an optimal drainage level is soil-dependent, due to local abiotic or biotic factors, as is the case in our study. Here, soils 1, 2, and 8 appears to be more likely to emit large amounts of N_2O in near water-saturated conditions while soils 5 and 7 shows higher probability of CH_4 production in more aerated conditions than the other soils. In the present laboratory study, the greenhouse gas emissions measurements probably display higher fluxes than would be the case under field conditions. As was concluded by Norberg et al. (2018), the moisture of the topsoil in the soil cores never reached levels as low as it can be under field conditions and the constant temperature of 20°C in the laboratory was

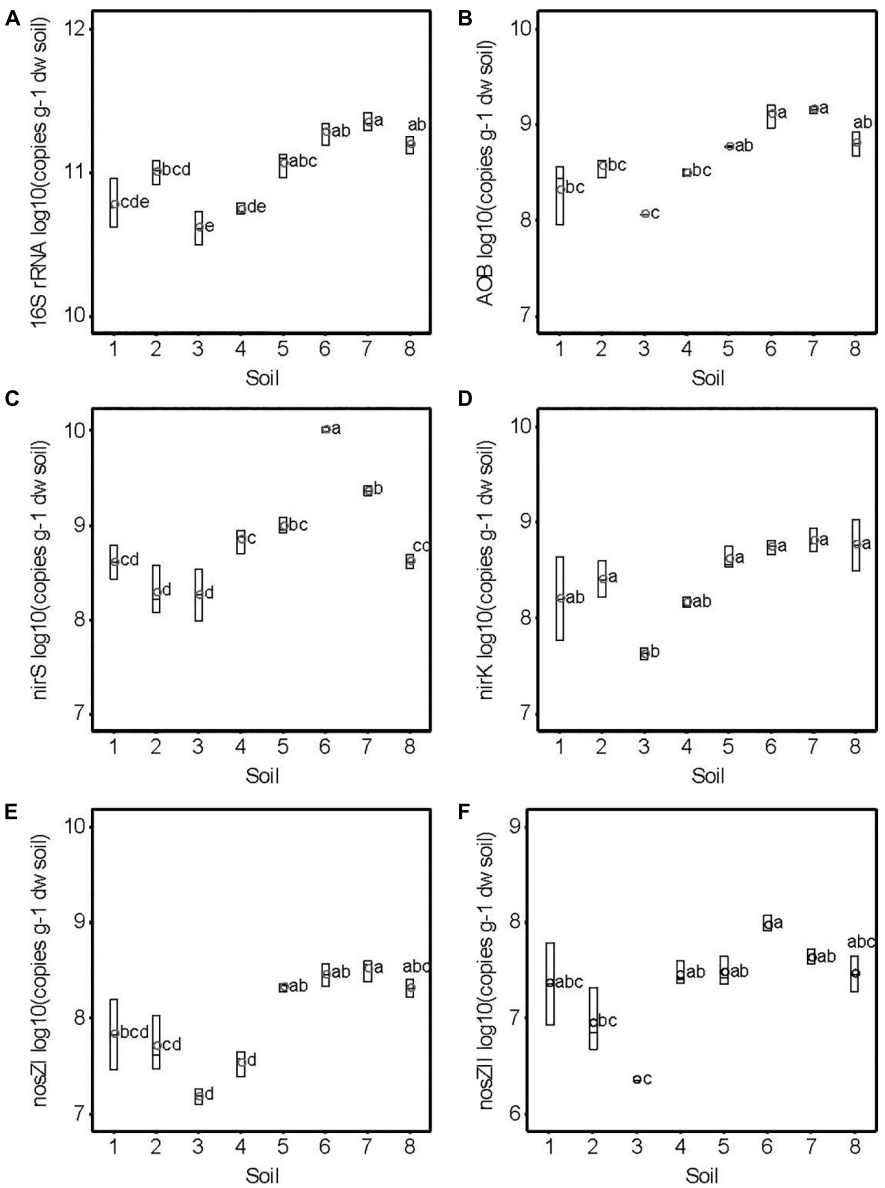

FIGURE 3 | Abundances of **(A)** 16S rRNA gene, **(B)** ammonia-oxidizing bacteria (AOB), **(C)** *nirS*, **(D)** *nirK*, **(E)** *nosZ*I, and **(F)** *nosZ*II (copies g^{-1} dry soil) for the eight topsoils. Different letters denote significantly different values of the mean (open circle, $n = 2–3$, $p < 0.05$). Note the different scales.

much higher than average field temperature during the growing season in Sweden. On the other hand, the absence of living plants probably reduced the N_2O emissions compared to field conditions since rhizodeposition stimulates N_2O production (Ai et al., 2020), although the supply of N may be limited during the growing season due to plant uptake.

Relationship Between Soil Properties, Microbial Abundances, and N_2O Release

There was a correlation between increasing N_2O emissions and decreasing pH of the soil cores tested in this study, as also found in some previous studies (Weslien et al., 2009; Andert et al., 2012; Norberg et al., 2016). However, this is not always the case (Maljanen et al., 2010; Taft et al., 2017). Correlation analysis in the present study showed that N_2O emissions increased with increasing carbon content (tot-C, org-C, WEOC, C/N ratio; $p < 0.05$) at different soil water suction heads. In mineral soils, N_2O emissions have been shown to increase with increasing carbon availability (Petersen et al., 2008), probably due to the limitation in easily available carbon sources, which is not the case in carbon-rich peat soils. Instead, the relationship between N_2O emissions and soil carbon content in peat soils in the present study may be due to the significant correlation between decreasing C content (tot-C, org-C, WEOC, C/N ratio) and increasing carb-C content, i.e., increasing pH. Lower N_2O

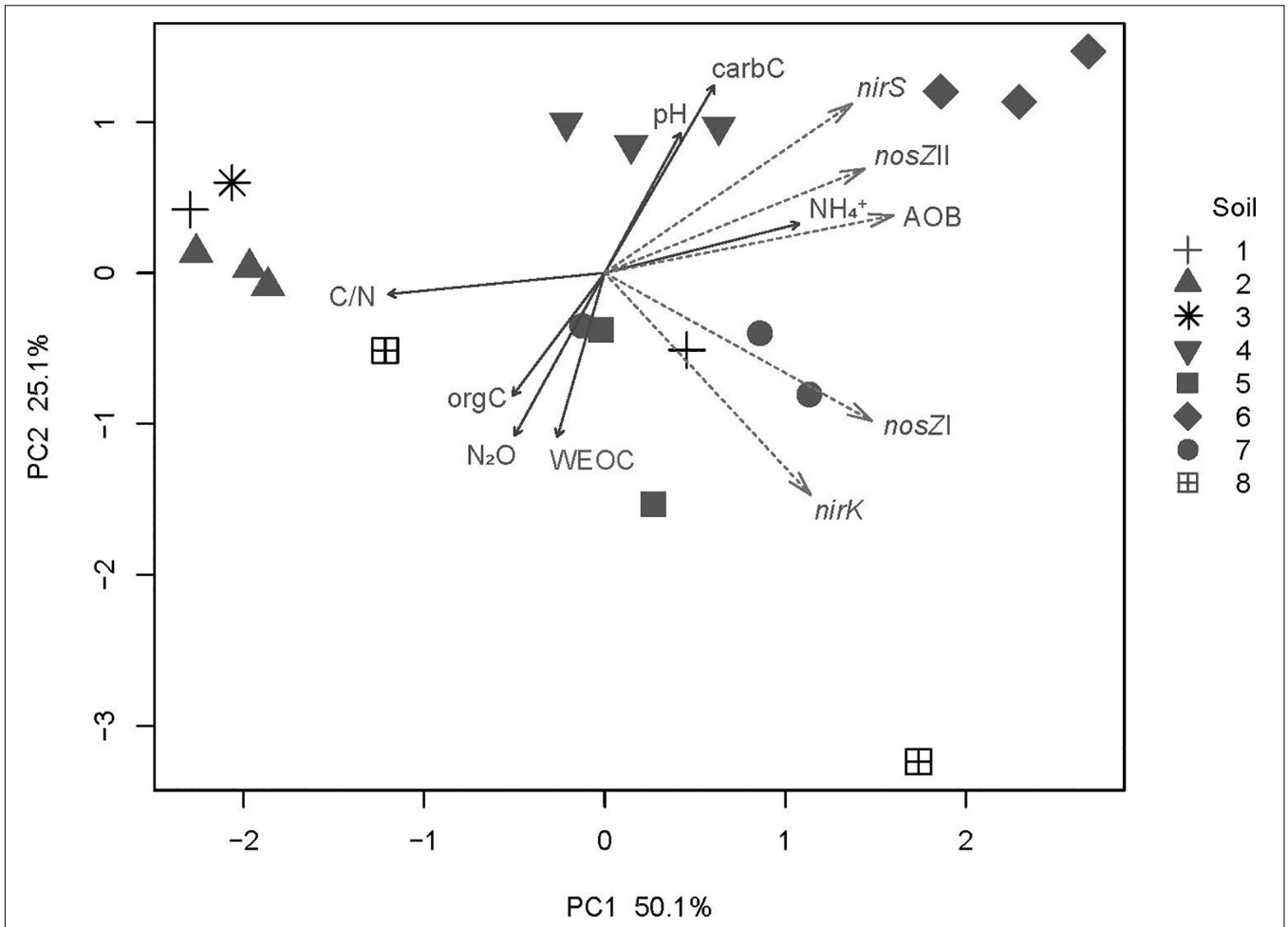

FIGURE 4 | Nitrogen cycling assemblages in topsoils. Principal component analysis of the respective ratios between abundances of *nirS*, *nirK*, *nosZ*I, *nosZ*II, and bacterial *amoA* and 16S rRNA gene abundances in the eight soils at a water suction head of 0.5 m. Solid arrows show direction of soil factors that correlate significantly ($p < 0.05$), with the ordination and arrow length proportional to the strength of correlation. Dashed arrows indicate increasing relative abundance of each functional group in relation to soil sample. The nitrous oxide (N_2O) values represent fluxes at near water-saturated conditions, WEOC, water-extractable organic C; carbC, carbonate carbon; orgC, organic carbon.

emissions at high pH indicate that liming could be an agricultural mitigation option but this will most likely be counteracted by increased CO_2 emissions (Ivarson, 1977).

At near water-saturated conditions, N_2O emissions increased with increasing NO_3^- content and with decreasing NH_4^+ content. Liimatainen et al. (2018) observed a positive correlation between N_2O emissions and NO_3^-, but concluded that increased soil phosphorus and copper concentrations were the most important factor regulating N_2O emissions from peat soils with low C/N ratio (15–27). Copper is an essential part of *nos* activity and lack of copper can prevent the last step in the denitrification process, thus promoting N_2O release, while copper is also essential for the ammonium oxidizers. Findings by Liimatainen et al. (2018) that higher copper content in peat soils gives higher N_2O emissions indicate that nitrification is a more important process than denitrification for N_2O production in peat soils.

The eight soils analyzed had different assemblages of nitrogen cycling guilds, with soil C/N ratio, NH_4^+ content, and pH appearing to be the strongest drivers shaping the different assemblages. Soils 4 and 6, which were dominated by AOB, *nirS*-type denitrifiers, and *nosZ* clade II N_2O reducers, correlated negatively with N_2O emissions. This agrees with findings that *nosZ* clade II microbes, which dominate the non-denitrifying N_2O reducers (Graf et al., 2014), can be important N_2O sinks (Jones et al., 2014; Domeignoz-Horta et al., 2016). Further, *nirS*-type denitrifiers are more often complete denitrifiers, with N_2O reduction capacity, than *nirK* types (Graf et al., 2014). However, the soils with lower N_2O emissions in the present study also had neutral pH. Thus, it is not possible to separate the effects of pH and biotic factors, although both could possibly explain the emissions patterns observed in this study. The abundance ratio of *nir* and *nos* genes was low for all eight soils (0.04–0.22), which indicates higher genetic potential for production of N_2O than for reduction of N_2O to N_2. However, since gene abundance ratios were not related to the emissions patterns observed, this potential was not realized or synchronized during the experiment.

Methane Emissions at Different Drainage Levels

Anoxic conditions, optimal for CH_4 production, probably take a longer time to achieve than the approximately 3 days allowed in this study. Therefore, no high CH_4 emissions were recorded, as also found in other similar studies, where CH_4 emissions are generally low or negligible and CH_4 may instead be consumed (Blodau and Moore, 2003; Karki et al., 2014; Musarika et al., 2017; Taft et al., 2017; Matysek et al., 2019). Nevertheless, CH_4 emissions were higher at near water-saturated conditions than at the two drainage steps, where the CH_4 fluxes were similar. This confirms previous findings in two studies on peat soil monoliths of no difference in fluxes of CH_4 between groundwater levels of 0.15 and 0.55 m depth (Susilawati et al., 2016; Wen et al., 2020). In contrast, Tiemeyer et al. (2016) found a threshold at a groundwater depth of 0.2 m, where CH_4 fluxes increased and showed greater variability than at lower groundwater levels. In the present study, CH_4 fluxes increased with increasing pH, which contradicts findings in Maljanen et al. (2010). The negative relationship between CH_4 fluxes and NO_3^- content was mainly due to the high NO_3^- values in combination with low CH_4 fluxes in soil 8.

Topsoil Compared With Subsoil

Under drained conditions, topsoils emitted more N_2O than subsoil samples, confirming findings by Säurich et al. (2019) and Berglund and Berglund (2011). Possible reasons for the higher N_2O emissions, are higher nutrient availability, higher pH, narrower C/N ratio, and higher bulk density (Säurich et al., 2019). In the present study, there was no difference in pH between topsoil and subsoil samples, while C/N ratio was lower and bulk density and NH_4^+ content were higher for topsoils compared with the corresponding subsoils.

Biotic factors also differed between topsoils and subsoils. The abundance of AOB was significantly lower in subsoils than in topsoils (on average for the four soils for which this comparison could be made). Jia and Conrad (2009) reported a three-fold decrease in AOB from topsoil to subsoil in a mineral soil, while Andert et al. (2011) observed no differences in abundance of ammonia oxidizers between depths in a peat soil. The *nosZI* gene, coding for N_2O reductase as the last step in the denitrification pathway, was also significantly more abundant in the topsoil samples. Koops et al. (1996) showed that the topsoil (0–20 cm) contributes most (over 70%) to total denitrification in drained peat soil, while the subsoil (20–40 cm) contributes up to 30% of the total N losses by denitrification. This indicates that peat soils can have favorable conditions for denitrification in both topsoil and subsoil. Andert et al. (2012) found that the community composition for denitrifiers did not change with soil depth, but that potential denitrification rate decreased rapidly with depth.

Conclusion

Measurements of N_2O emissions from different peat soils revealed wide variations at near water-saturated conditions and lower levels at two experimental drainage intensities (suction head 0.5 and 1.0 m water column). This confirms that high and fluctuating groundwater level can increase N_2O emissions more than deeper drainage with higher air-filled porosity. The N_2O emissions were primarily correlated with peat soil pH and carbonate-carbon content, with increasing N_2O emissions with decreasing pH. No strong correlation between N_2O emissions and individual gene abundances was detected, but specific assemblages of N cycling guilds were indicative of soils with lower emissions. Subsoils emitted less N_2O than topsoils under drained conditions and, as expected, CH_4 fluxes from both topsoil and subsoil were low at all soil water levels. Lower N_2O emissions at high pH and lower groundwater levels indicate that liming and increased drainage intensity could be agricultural mitigation options, but will most likely increase CO_2 emissions. Finding an optimal drainage level to minimize greenhouse gas emissions in agricultural peatlands is a challenge since it is soil-dependent, due to local abiotic and biotic factors.

DATA AVAILABILITY STATEMENT

The raw data supporting the conclusions of this article will be made available by the authors, without undue reservation.

AUTHOR CONTRIBUTIONS

KB, SH, and ÖB designed the research. LN and KB planned the research activities. LN and MH performed the research, collected, and analyzed the data. LN wrote the manuscript. SH, MH, KB, and ÖB adjusted the manuscript. All authors contributed to the article and approved the submitted version.

FUNDING

This work was supported by the Swedish Farmers Foundation for Agricultural Research (grant number H0733481) and the Nordic Joint Committee for Agricultural and Food Research (NKJ) through the Swedish Research Council (Formas) (grant number 220-2010-13).

ACKNOWLEDGMENTS

We wish to thank the farmers at the sampling sites for letting us access their land and the staff in the laboratory at the Department of Soil and Environment for performing all the soil analyses. Special thanks to Christina Öhman for excellent ideas and help with carrying out the experiment.

SUPPLEMENTARY MATERIAL

The Supplementary Material for this article can be found online at: https://www.frontiersin.org/articles/10.3389/fenvs.2021.631112/full#supplementary-material

REFERENCES

Ai, C., Zhang, M., Sun, Y., Zhang, L., Zeng, L., Liu, Y., et al. (2020). Wheat rhizodeposition stimulates soil nitrous oxide emission and denitrifiers harboring the nosZ clade I gene. *Soil Biol. Biochem.* 143:107738. doi: 10.1016/j.soilbio.2020.107738

Andert, J., Börjesson, G., and Hallin, S. (2012). Temporal changes in methane oxidizing and denitrifying communities and their activities in a drained peat soil. *Wetlands* 32, 1047–1055. doi: 10.1007/s13157-012-0335-3

Andert, J., Wessen, E., Börjesson, G., and Hallin, S. (2011). Temporal changes in abundance and composition of ammonia-oxidizing bacterial and archaeal communities in a drained peat soil in relation to N2O emissions. *J. Soils Sediments* 11, 1399–1407. doi: 10.1007/s11368-011-0413-9

Banerjee, S., Helgason, B., Wang, L., Winsley, T., Ferrari, B. C., and Siciliano, S. D. (2016). Legacy effects of soil moisture on microbial community structure and N2O emissions. *Soil Biol. Biochem.* 95, 40–50. doi: 10.1016/j.soilbio.2015.12.004

Berglund, Ö, and Berglund, K. (2010). Distribution and cultivation intensity of agricultural peat and gyttja soils in Sweden and estimation of greenhouse gas emissions from cultivated peat soils. *Geoderma* 154, 173–180. doi: 10.1016/j.geoderma.2008.11.035

Berglund, Ö, and Berglund, K. (2011). Influence of water table level and soil properties on emissions of greenhouse gases from cultivated peat soil. *Soil Biol. Biochem.* 43, 923–931. doi: 10.1016/j.soilbio.2011.01.002

Beyer, C., and Höper, H. (2015). Greenhouse gas exchange of rewetted bog peat extraction sites and a *Sphagnum* cultivation site in northwest Germany. *Biogeosciences* 12, 2101–2117. doi: 10.5194/bg-12-2101-2015

Blodau, C., and Moore, T. R. (2003). Experimental response of peatland carbon dynamics to a water table fluctuation. *Aquat. Sci.* 65, 47–62. doi: 10.1007/s000270300004

Bouwman, A. F., Boumans, L. J. M., and Batjes, N. H. (2002). Emissions of N2O and NO from fertilized fields: summary of available measurement data. *Glob. Biogeochem. Cycles* 16:1058.

Conrad, R. (1996). Soil microorganisms as controllers of atmospheric trace gases (H-2, CO, CH4, OCS, N2O, and NO). *Microbiol. Rev.* 60, 609–640. doi: 10.1128/mr.60.4.609-640.1996

R Core Team (2016). *A Language and Environment for Statistical Computing*. Vienna: R Foundation for Statistical Computing.

Dinsmore, K. J., Skiba, U. M., Billett, M. F., and Rees, R. M. (2009). Effect of water table on greenhouse gas emissions from peatland mesocosms. *Plant Soil* 318, 229–242. doi: 10.1007/s11104-008-9832-9

Domeignoz-Horta, L. A., Putz, M., Spor, A., Bru, D., Breuil, M. C., Hallin, S., et al. (2016). Non-denitrifying nitrous oxide-reducing bacteria – an effective N2O sink in soil. *Soil Biol. Biochem.* 103, 376–379. doi: 10.1016/j.soilbio.2016.09.010

Elder, J. W., and Lal, R. (2008). Tillage effects on gaseous emissions from an intensively farmed organic soil in North Central Ohio. *Soil Tillage Res.* 98, 45–55. doi: 10.1016/j.still.2007.10.003

Ghani, A., Dexter, M., and Perrott, K. W. (2003). Hot-water extractable carbon in soils: a sensitive measurement for determining impacts of fertilisation, grazing and cultivation. *Soil Biol. Biochem.* 35, 1231–1243. doi: 10.1016/s0038-0717(03)00186-x

Graf, D. R. H., Jones, C. M., and Hallin, S. (2014). Intergenomic comparisons highlight modularity of the denitrification pathway and underpin the importance of community structure for N2O emissions. *PLoS One* 9:e114118. doi: 10.1371/journal.pone.0114118

Hellman, M., Bonilla-Rosso, G., Widerlund, A., Juhanson, J., and Hallin, S. (2019). External carbon addition for enhancing denitrification modifies bacterial community composition and affects CH4 and N2O production in sub-arctic mining pond sediments. *Water Res.* 158, 22–33. doi: 10.1016/j.watres.2019.04.007

Henry, S., Baudoin, E., Lopez-Gutierrez, J. C., Martin-Laurent, F., Brauman, A., and Philippot, L. (2004). Quantification of denitrifying bacteria in soils by nirK gene targeted real-time PCR. *J. Microbiol. Methods* 59, 327–335. doi: 10.1016/j.mimet.2004.07.002

Henry, S., Bru, D., Stres, B., Hallet, S., and Philippot, L. (2006). Quantitative detection of the nosZ gene, encoding nitrous oxide reductase, and comparison of the abundances of 16S rRNA, narG, nirK, and nosZ genes in soils. *Appl. Environ. Microbiol.* 72, 5181–5189. doi: 10.1128/aem.00231-06

Ivarson, K. C. (1977). Changes in decomposition rate, microbial population and carbohydrate content of an acid peat bog after liming and reclamation. *Can. J. Soil Sci.* 7, 129–137. doi: 10.4141/cjss77-017

Jia, Z. J., and Conrad, R. (2009). Bacteria rather than Archaea dominate microbial ammonia oxidation in an agricultural soil. *Environ. Microbiol.* 11, 1658–1671.

Jones, C. M., Graf, D. R. H., Bru, D., Philippot, L., and Hallin, S. (2013). The unaccounted yet abundant nitrous oxide-reducing microbial community: a potential nitrous oxide sink. *ISME J* 7, 417–426. doi: 10.1038/ismej.2012.125

Jones, C. M., Spor, A., Brennan, F. P., Breuil, M. C., Bru, D., Lemanceau, P., et al. (2014). Recently identified microbial guild mediates soil N2O sink capacity. *Nat. Clim. Chang.* 4, 801–805. doi: 10.1038/nclimate2301

Kandel, T. P., Elsgaard, L., Karki, S., and Laerke, P. E. (2013). Biomass yield and greenhouse gas emissions from a drained fen peatland cultivated with reed canary grass under different harvest and fertilizer regimes. *Bioenergy Res.* 6, 883–895. doi: 10.1007/s12155-013-9316-5

Karki, S., Elsgaard, L., Audet, J., and Laerke, P. E. (2014). Mitigation of greenhouse gas emissions from reed canary grass in paludiculture: effect of groundwater level. *Plant Soil* 383, 217–230. doi: 10.1007/s11104-014-2164-z

Kløve, B., Berglund, K., Berglund, Ö, Weldon, S., and Maljanen, M. (2017). Future options for cultivated Nordic peat soils: can land management and rewetting control greenhouse gas emissions? *Environ. Sci. Policy* 69, 85–93. doi: 10.1016/j.envsci.2016.12.017

Koops, J. G., Oenema, O., and Van Beusichem, M. L. (1996). Denitrification in the top and sub soil of grassland on peat soils. *Plant Soil* 184, 1–10. doi: 10.1007/bf00029269

Kuzyakov, Y. (2002). Review: factors affecting rhizosphere priming effects. *J. Plant Nutri. Soil* 165, 382–396. doi: 10.1002/1522-2624(200208)165:4<382::aid-jpln382>3.0.co;2-#

Liimatainen, M., Voigt, C., Martikainen, P. J., Hytonen, J., Regina, K., Oskarsson, H., et al. (2018). Factors controlling nitrous oxide emissions from managed northern peat soils with low carbon to nitrogen ratio. *Soil Biol. Biochem.* 122, 186–195. doi: 10.1016/j.soilbio.2018.04.006

Maljanen, M., Komulainen, V. M., Hytönen, J., Martikainen, P., and Laine, J. (2004). Carbon dioxide, nitrous oxide and methane dynamics in boreal organic agricultural soils with different soil characteristics. *Soil Biol. Biochem.* 36, 1801–1808. doi: 10.1016/j.soilbio.2004.05.003

Maljanen, M., Sigurdsson, B. D., Guomundsson, J., Oskarsson, H., Huttunen, J. T., and Martikainen, P. J. (2010). Greenhouse gas balances of managed peatlands in the Nordic countries – present knowledge and gaps. *Biogeosciences* 7, 2711–2738. doi: 10.5194/bg-7-2711-2010

Matysek, M., Leake, J., Banwart, S., Johnson, I., Page, S., Kaduk, J., et al. (2019). Impact of fertiliser, water table, and warming on celery yield and CO2 and CH4 emissions from fenland agricultural peat. *Sci. Total Environ.* 667, 179–190. doi: 10.1016/j.scitotenv.2019.02.360

Musarika, S., Atherton, C. E., Gomersall, T., Wells, M. J., Kaduk, J., Cumming, A. M. J., et al. (2017). Effect of water table management and elevated CO2 on radish productivity and on CH4 and CO2 fluxes from peatlands converted to agriculture. *Sci. Total Environ.* 58, 665–672. doi: 10.1016/j.scitotenv.2017.01.094

Muyzer, G., Dewaal, E. C., and Uitterlinden, A. G. (1993). Profiling of complex microbial-populations by denaturing gradient gel-electrophoresis analysis of polymerase chain reaction-amplified genes-coding for 16s ribosomal-RNA. *Appl. Environm. Microbiol.* 59, 695–700. doi: 10.1128/aem.59.3.695-700.1993

Norberg, L., Berglund, Ö, and Berglund, K. (2016). Nitrous oxide and methane fluxes during the growing season from cultivated peat soils, peaty marl and gyttja clay under different cropping systems. *Acta Agric. Scand. B Soil Plant Sci.* 66, 602–612. doi: 10.1080/09064710.2016.1205126

Norberg, L., Berglund, Ö, and Berglund, K. (2018). Impact of drainage and soil properties on carbon dioxide emissions from intact cores of cultivated peat soils. *Mires Peat* 21, 1–14.

Oksanen, J., Blanchet, F. G., Friendly, M., Kindt, R., Legendre, P., Mcglinn, D., et al. (2018). *vegan: Community Ecology Package*. Available online at: https://CRAN.R-project.org/package=vegan. (accessed April 6, 2020).

Petersen, S. O., Schjonning, P., Thomsen, I. K., and Christensen, B. T. (2008). Nitrous oxide evolution from structurally intact soil as influenced by tillage and soil water content. *Soil Biol. Biochem.* 40, 967–977. doi: 10.1016/j.soilbio.2007.11.017

Philippot, L., Andert, J., Jones, C. M., Bru, D., and Hallin, S. (2011). Importance of denitrifiers lacking the genes encoding the nitrous oxide reductase for N2O emissions from soil. *Glob. Chang. Biol.* 17, 1497–1504. doi: 10.1111/j.1365-2486.2010.02334.x

Regina, K., Sheehy, J., and Myllys, M. (2015). Mitigating greenhouse gas fluxes from cultivated organic soils with raised water table. *Mitig. Adapt. Strateg. Glob. Chang.* 20, 1529–1544. doi: 10.1007/s11027-014-9559-2

Regina, K., Silvola, J., and Martikainen, P. J. (1999). Short-term effects of changing water table on N2O fluxes from peat monoliths from natural and drained boreal peatlands. *Glob. Chang. Biol.* 5, 183–189. doi: 10.1046/j.1365-2486.1999.00217.x

Renger, M., Wessolek, G., Schwarzel, K., Sauerbrey, R., and Siewert, C. (2002). Aspects of peat conservation and water management. *J. Plant Nutr. Soil Sci.* 165, 487–493. doi: 10.1002/1522-2624(200208)165:4<487::aid-jpln487>3.0.co;2-c

Romano, N., Hopmans, J. W., and Dane, J. H. (2002). "Suction table," in *Methods of Soil Analysis, Part 4-Physical Methods*, eds J. H. Dane and C. G. Topp (Madison, WI: Soil Science Society of America), 692–698.

Rotthauwe, J. H., Witzel, K. P., and Liesack, W. (1997). The ammonia monooxygenase structural gene amoA as a functional marker: molecular fine-scale analysis of natural ammonia-oxidizing populations. *Appl. Environ. Microbiol.* 63, 4704–4712. doi: 10.1128/aem.63.12.4704-4712.1997

Säurich, A., Tiemeyer, B., Dettmann, U., and Don, A. (2019). How do sand addition, soil moisture and nutrient status influence greenhouse gas fluxes from drained organic soils? *Soil Biol. Biochem.* 135, 71–84. doi: 10.1016/j.soilbio.2019.04.013

Smith, K. A., Ball, T., Conen, F., Dobbie, K. E., Massheder, J., and Rey, A. (2018). Exchange of greenhouse gases between soil and atmosphere: interactions of soil physical factors and biological processes. *Eur. J. Soil Sci.* 69, 10–20. doi: 10.1111/ejss.12539

Susilawati, H. L., Setyanto, P., Ariani, M., Hervani, A., and Inubushi, K. (2016). Influence of water depth and soil amelioration on greenhouse gas emissions from peat soil columns. *Soil Sci. Plant Nutr.* 62, 57–68. doi: 10.1080/00380768.2015.1107459

Taft, H. E., Cross, P. A., Edwards-Jones, G., Moorhouse, E. R., and Jones, D. L. (2017). Greenhouse gas emissions from intensively managed peat soils in an arable production system. *Agric. Ecosyst. Environ.* 237, 162–172. doi: 10.1016/j.agee.2016.11.015

Taft, H. E., Cross, P. A., and Jones, D. L. (2018). Efficacy of mitigation measures for reducing greenhouse gas emissions from intensively cultivated peatlands. *Soil Biol. Biochem.* 127, 10–21. doi: 10.1016/j.soilbio.2018.08.020

Taghizadeh-Toosi, A., Elsgaard, L., Clough, T. J., Labouriau, R., Ernstsen, V., and Petersen, S. O. (2019). Regulation of N2O emissions from acid organic soil drained for agriculture. *Biogeosciences* 16, 4555–4575. doi: 10.5194/bg-16-4555-2019

Throbäck, I. N., Enwall, K., Jarvis, Å, and Hallin, S. (2004). Reassessing PCR primers targeting nirS, nirK and nosZ genes for community surveys of denitrifying bacteria with DGGE. *FEMS Microbiol. Ecol.* 49, 401–417. doi: 10.1016/j.femsec.2004.04.011

Tiemeyer, B., Albiac Borraz, E., Augustin, J., Bechtold, M., Beetz, S., Beyer, C., et al. (2016). High emissions of greenhouse gases from grasslands on peat and other organic soils. *Glob. Change Biol.* 22, 4134–4149. doi: 10.1111/gcb.13303

Tourna, M., Freitag, T. E., Nicol, G. W., and Prosser, J. I. (2008). Growth, activity and temperature responses of ammonia-oxidizing archaea and bacteria in soil microcosms. *Environ. Microbiol.* 10, 1357–1364. doi: 10.1111/j.1462-2920.2007.01563.x

van Beek, C. L., Pleijter, M., and Kuikman, P. J. (2011). Nitrous oxide emissions from fertilized and unfertilized grasslands on peat soil. *Nutr. Cycl. Agroecosyst.* 89, 453–461. doi: 10.1007/s10705-010-9408-y

von Post, L. (1922). Sveriges geologiska undersöknings torvinventering och några av dess hittills vunna resultat (in swedish). *Sven. Mosskulturföreningens Tidskr.* 36, 1–27.

Wagner-Riddle, C., Congreves, K., Abalos, D., Berg, A. A., Brown, S. E., Ambadan, J. T., et al. (2017). Globally important nitrous oxide emissions from croplands induced by freeze–thaw cycles. *Nat. Geosci.* 10, 279–283. doi: 10.1038/ngeo2907

Wen, Y., Zang, H. D., Ma, Q. X., Freeman, B., Chadwick, D. R., Evans, C. D., et al. (2020). Impact of water table levels and winter cover crops on greenhouse gas emissions from cultivated peat soils. *Sci. Total Environ.* 719:135130. doi: 10.1016/j.scitotenv.2019.135130

Weslien, P., Kasimir Klemedtsson, Å, Börjesson, G., and Klemedtsson, L. (2009). Strong pH influence on N2O and CH4 fluxes from forested organic soils. *Eur. J. Soil Sci.* 60, 311–320. doi: 10.1111/j.1365-2389.2009.01123.x

Conflict of Interest: The authors declare that the research was conducted in the absence of any commercial or financial relationships that could be construed as a potential conflict of interest.

frontiers | Frontiers in Environmental Science

CORRECTION
published: 26 April 2022
doi: 10.3389/fenvs.2022.887952

Corrigendum: Methane and Nitrous Oxide Production From Agricultural Peat Soils in Relation to Drainage Level and Abiotic and Biotic Factors

Lisbet Norberg[1]*, *Maria Hellman*[2], *Kerstin Berglund*[1], *Sara Hallin*[2] and *Örjan Berglund*[1]

[1]Department of Soil and Environment, Swedish University of Agricultural Sciences, Uppsala, Sweden, [2]Department of Forest Mycology and Plant Pathology, Swedish University of Agricultural Sciences, Uppsala, Sweden

OPEN ACCESS

Edited and reviewed by:
Yuncong Li,
University of Florida, United States

***Correspondence:**
Lisbet Norberg
lisbet.norberg@slu.se

Specialty section:
This article was submitted to Soil Processes, a section of the journal Frontiers in Environmental Science

Received: 02 March 2022
Accepted: 16 March 2022
Published: 26 April 2022

Citation:
Norberg L, Hellman M, Berglund K, Hallin S and Berglund Ö (2022) Corrigendum: Methane and Nitrous Oxide Production From Agricultural Peat Soils in Relation to Drainage Level and Abiotic and Biotic Factors. Front. Environ. Sci. 10:887952. doi: 10.3389/fenvs.2022.887952

Keywords: histosols, methane, nitrous oxide, functional genes, suction head, groundwater level

A Corrigendum on

Methane and Nitrous Oxide Production From Agricultural Peat Soils in Relation to Drainage Level and Abiotic and Biotic Factors

by Norberg, L., Hellman, M., Berglund, K., Hallin, S. and Berglund, Ö. (2021). Front. Environ. Sci. 9: 631112. doi: 10.3389/fenvs.2021.631112

In the original article, there was a mistake in **Figures 1**, **2** as published. "The Figures and captions had incorrect units." The corrected figures and captions appear below:

The authors apologize for these errors and state that this does not change the scientific conclusions of the article in any way. The original article has been updated.

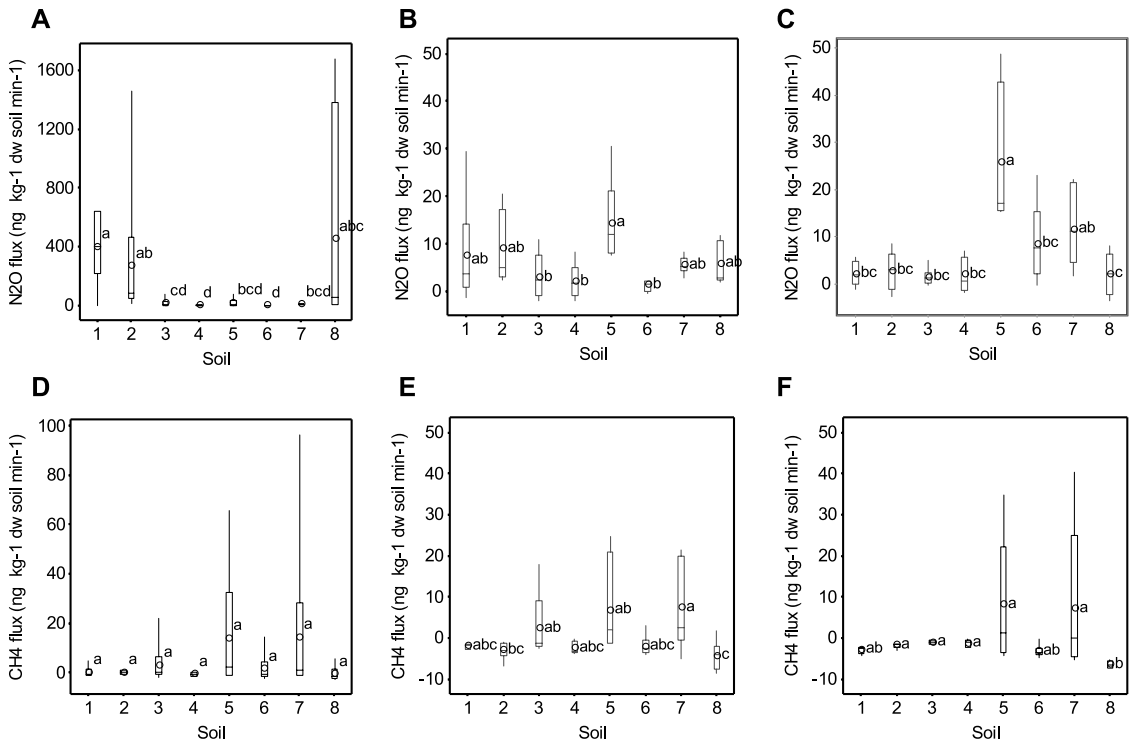

FIGURE 1 | Soil nitrous oxide (N_2O) fluxes (ng kg^{-1} dry soil min^{-1}) at **(A)** near water-saturated conditions, **(B)** 0.5 m water column, and **(C)** 1.0 m water column; and **(D–F)** methane (CH_4) fluxes at the respective soil water suction heads. Different letters denote significantly different values of the mean (open circle, $n = 7$, $p < 0.05$). Note the different scales.

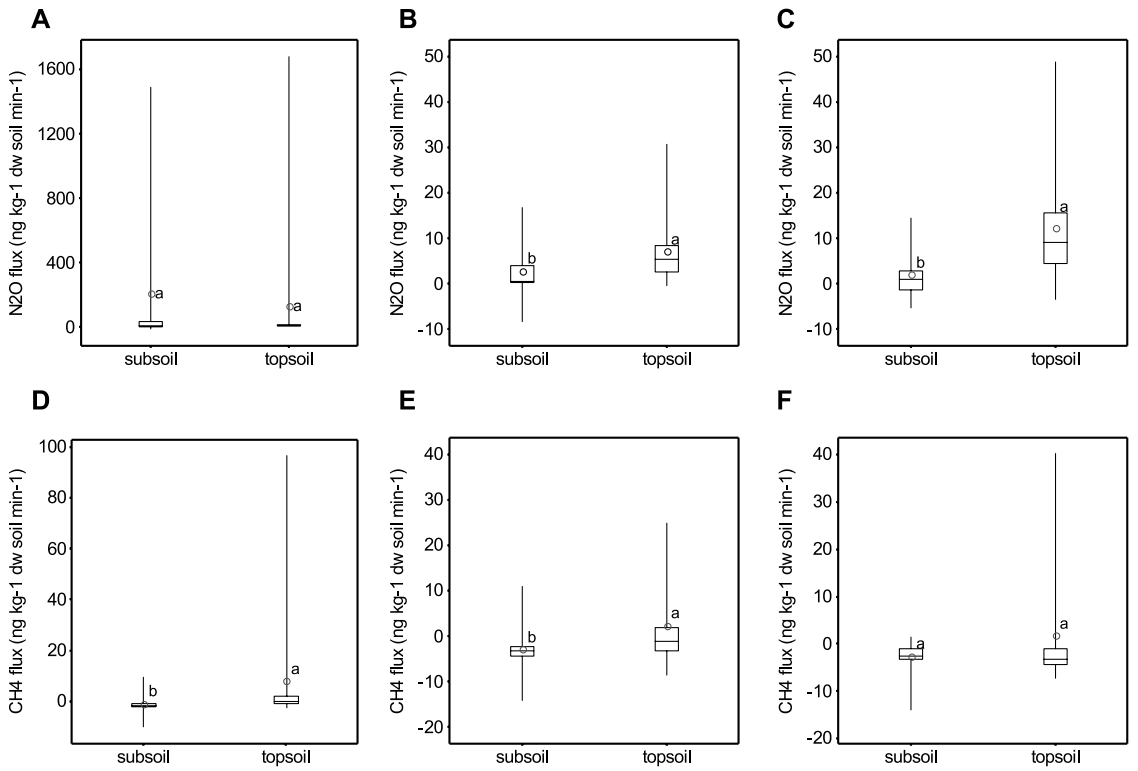

FIGURE 2 | Nitrous oxide (N_2O) fluxes (ng kg^{-1} dry soil min^{-1}) from topsoil and subsoil samples of soils 5–8 at **(A)** near water-saturated conditions, **(B)** 0.5 m water column, and **(C)** 1.0 m water column; and **(D–F)** methane (CH_4) fluxes at the respective soil water suction heads. Different subscript letters denote significantly different values of the mean (open circle, $n = 28$, $p < 0.05$). Note the different scales.

frontiers in Environmental Science

ORIGINAL RESEARCH
published: 22 March 2021
doi: 10.3389/fenvs.2021.630752

A Novel Low-Cost, High-Resolution Camera System for Measuring Peat Subsidence and Water Table Dynamics

Chris D. Evans[1], Nathan Callaghan[1], Adi Jaya[2], Alistair Grinham[3], Sofie Sjogersten[4], Susan E. Page[5], Mark E. Harrison[5,6], Kitso Kusin[7], Lip Khoon Kho[8], Martha Ledger[4], Stephanie Evers[9,10], Zak Mitchell[1], Jennifer Williamson[1], Alan D. Radbourne[1] and A. Jonay Jovani-Sancho[1,4]*

[1]United Kingdom Centre for Ecology and Hydrology, Bangor, United Kingdom, [2]Faculty of Agriculture, University of Palangka Raya, Palangkaraya, Indonesia, [3]School of Civil Engineering, The University of Queensland, Brisbane, QLD, Australia, [4]School of Biosciences, University of Nottingham, Loughborough, United Kingdom, [5]School of Geography, Geology and the Environment, University of Leicester, Leicester, United Kingdom, [6]Centre for Ecology and Conservation, College of Life and Environmental Sciences, University of Exeter, Penryn, United Kingdom, [7]Center for International Cooperation in Sustainable Management of Tropical Peatland (CIMTROP), University of Palangka Raya, Palangkaraya, Indonesia, [8]Peat Ecosystem and Biodiversity Unit, Biology and Sustainability Research Division, Malaysian Palm Oil Board, Kuala Lumpur, Malaysia, [9]School of Biological and Environmental Sciences, Liverpool John Moores University, Liverpool, United Kingdom, [10]School of Environmental and Geographical Sciences, University of Nottingham Malaysia Campus, Selangor, Malaysia

OPEN ACCESS

Edited by:
Massimo Lupascu, National University of Singapore, Singapore

Reviewed by:
Baptiste Dafflon, Lawrence Berkeley National Laboratory, United States
Sudipta Rakshit, Tennessee State University, United States

***Correspondence:**
Chris D. Evans
cev@ceh.ac.uk

Specialty section:
This article was submitted to Soil Processes, a section of the journal Frontiers in Environmental Science

Received: *24 November 2020*
Accepted: *26 January 2021*
Published: *22 March 2021*

Citation:
Evans CD, Callaghan N, Jaya A, Grinham A, Sjogersten S, Page SE, Harrison ME, Kusin K, Kho LK, Ledger M, Evers S, Mitchell Z, Williamson J, Radbourne AD and Jovani-Sancho AJ (2021) A Novel Low-Cost, High-Resolution Camera System for Measuring Peat Subsidence and Water Table Dynamics. Front. Environ. Sci. 9:630752. doi: 10.3389/fenvs.2021.630752

Peatlands are highly dynamic systems, able to accumulate carbon over millennia under natural conditions, but susceptible to rapid subsidence and carbon loss when drained. Short-term, seasonal and long-term peat surface elevation changes are closely linked to key peatland attributes such as water table depth (WTD) and carbon balance, and may be measured remotely using satellite radar and LiDAR methods. However, field measurements of peat elevation change are spatially and temporally sparse, reliant on low-resolution manual subsidence pole measurements, or expensive sensor systems. Here we describe a novel, simple and low-cost image-based method for measuring peat surface motion and WTD using commercially available time-lapse cameras and image processing methods. Based on almost two years' deployment of peat cameras across contrasting forested, burned, agricultural and oil palm plantation sites in Central Kalimantan, Indonesia, we show that the method can capture extremely high resolution (sub-mm) and high-frequency (sub-daily) changes in peat surface elevation over extended periods and under challenging environmental conditions. WTD measurements were of similar quality to commercially available pressure transducers. Results reveal dynamic peat elevation response to individual rain events, consistent with variations in WTD. Over the course of the relatively severe 2019 dry season, cameras in deep-drained peatlands recorded maximum peat shrinkage of over 8 cm, followed by partial rebound, leading to net annual subsidence of up to 5 cm. Sites with higher water tables, and where borehole irrigation was used to maintain soil moisture, had lower subsidence, suggesting potential to reduce subsidence through altered land-management. Given the established link between subsidence and CO_2 emissions, these results have direct implications for the management of peatlands to reduce high

current greenhouse gas (GHG) emissions. Camera-based sensors provide a simple, low-cost alternative to commercial elevation, WTD and GHG flux monitoring systems, suitable for deployment at scale, and in areas where existing approaches are impractical or unaffordable. If ground-based observations of peat motion can be linked to measured GHG fluxes and with satellite-based monitoring tools, this approach offers the potential for a large-scale peatland monitoring tool, suitable for identifying areas of active carbon loss, targeting climate change mitigation interventions, and evaluating intervention outcomes.

Keywords: peatlands, subsidence, water table, carbon, indonesia, oil palm, smallholder farming, peat swamp forest

INTRODUCTION

Peatlands are the most carbon rich terrestrial ecosystems on earth, storing an estimated total of 637 Gt C (Page et al., 2011; Dargie et al., 2017), which is equivalent to three quarters of all the CO_2 currently in the atmosphere (860 Gt C; Friedlingstein et al., 2019). This carbon store is under unprecedented and intensifying pressure from human activities, including land conversion and drainage for agriculture and plantation forestry, grazing, and the use of fire for land clearance or management (Turetsky et al., 2015; Page and Baird, 2016). The oxidation and combustion of peat exposed to oxygen is estimated to generate around 1–2 Gt of CO_2 emissions per year (Smith et al., 2014; Leifeld and Menichetti, 2018), as well as N_2O emissions of 0.36 Gt CO_2-equivalent yr^{-1} (FAOSTAT, 2018, based on a 100 years global warming potential of 298; Smith et al., 2014). Although partly offset by reduced CH_4 emissions as a result of wetland drainage, overall greenhouse gas (GHG) emissions resulting from human utilization of peatlands are estimated to generate in the region of 2–5% of global GHG emissions (Smith et al., 2014). Historically, the most extensive conversion and drainage of peatlands occurred in Northern Europe, with some areas having undergone large-scale change centuries ago. More recently, the tropical peatlands of Southeast Asia have undergone very rapid conversion, with 60% of the original area of peat swamp forest cleared between 1990 and 2010, the majority of which is now under drainage-based cultivation (Wijedasa et al., 2018).

An additional, and closely associated, consequence of peatland drainage is land subsidence. This occurs due to a combination of consolidation and compaction (loss of buoyancy and shrinkage resulting from removal of water from the pore space, often augmented by the use of heavy machinery during agricultural and forestry activities), together with accelerated erobic decomposition of the peat following exposure to oxygen. Initial subsidence of peat due to compaction following drainage may be very rapid (potentially >1 m within 5 years; Hooijer et al., 2012), while subsidence due to ongoing compaction and oxidation can continue for decades to centuries (e.g., Hutchinson, 1980; Stephens et al., 1984). Rates of subsidence depend on drainage depth, time since drainage and climate, with rates of subsidence in high-latitude peatlands subject to long-term drainage typically in the range 1–3 cm yr^{-1}, and those in more recently drained tropical peatlands typically 3–6 cm yr^{-1} (Evans et al., 2019 and references therein). Apart from contributing to CO_2 emissions, the socio-economic consequences of peat subsidence include the need to transition from low-cost gravity drainage to high-cost, energy-intensive pumped drainage; damage to buildings and linear infrastructure such as roads and pipelines; growing flood risk; and loss of agricultural productivity. Many low-lying peat areas subject to long-term drainage are now below sea-level, including parts of the The Netherlands, Eastern England and Northern Germany. In the The Netherlands alone, drainage and subsidence of peatlands has contributed to approximately 2 m of subsidence in coastal areas, most of which are now below sea-level; to an overall loss of 20 km^3 of peat volume; and to CO_2 emissions sufficient to raise atmospheric CO_2 concentrations by 0.39 ppmv (Erkens et al., 2016). Ultimately, peat subsidence may lead to complete loss of the original peat; exposure of underlying mineral substrate, including acid sulfate soils in many coastal peatland areas (Wösten et al., 1997); and salinization through surface water flooding or saline groundwater intrusion (de Louw et al., 2018), resulting in the loss of land for agriculture.

In their natural state, peatlands can accumulate vertically at a rate of around 0.5–2 mm yr^{-1} over millennia (Dommain et al., 2014). They also have the capacity to fluctuate vertically in response to seasonal and short-term climatic variations. This 'bog breathing' confers resilience to the peatland ecosystem by enabling the ground surface to track water table fluctuations, maintaining wet conditions at the peat surface even during dry periods (e.g., Strack and Waddington, 2007; Dise, 2009; Howie and Hebda, 2018). This capacity of the peat to self-regulate in response to hydrological fluctuations is diminished by drainage, due to changes in peat density, water holding capacity, lateral hydraulic conductivity and connectivity to drainage networks (Howie and Hebda, 2018). Consequently the vertical movement of peat over episodic, seasonal, annual and longer time scales is closely related to the combination of climatic and management pressures to which the peat is exposed.

Evidence that peat vertical motion is related to climate and management raises the possibility that it could be used as an effective, and easily measured, proxy for key metrics of peat condition such as water table depth (WTD) and carbon balance, as well as a tool for evaluating restoration outcomes. A number of recent studies have also suggested that this surface motion can be detected remotely using Interferometric Synthetic Aperture Radar (InSAR) data from satellites such as the European Space Agency's Sentinel-1 mission, and the Japan Aerospace Exploration Agency's Advanced Land Observation Satellite-1 (ALOS-1) (Alshammari et al., 2018; Fiaschi et al., 2019;

Marshall et al., 2018; Susanti and Anjasmara, 2019; Zhou et al., 2019; Hoyt et al., 2020). This approach offers clear advantages in terms of the cost, spatial scale and frequency at which information can be obtained, especially for large and remote peatland areas. However, while promising, the use of InSAR as a peatland monitoring tool urgently requires ground validation data, in the form of spatially distributed, high vertical and temporal resolution measurements of peat surface motion.

Despite the societal significance of peat subsidence, and the potential to use vertical peat motion as a proxy for key measures of peat condition and function, records of peat vertical movement are remarkably sparse. Most of the available records are obtained from subsidence poles, which are anchored into the underlying mineral substrate with elevation changes recorded manually, and often infrequently (quarterly or longer). Even these records are sparse in many regions; for example the United Kingdom has a single subsidence pole, the Holme Post, at which a total of 4 m of subsidence has been recorded by periodic measurements made since the original drainage of the site in 1850 (Hutchinson, 1980). Similarly long but isolated records exist for Florida (Stephens et al., 1984) and the San Joaquin delta in California (Deverel and Leighton, 2010). In Southeast Asia, subsidence poles are more widely used, but cover shorter time periods; for example Evans et al. (2019) analyzed subsidence data from over 300 poles deployed across the plantation and forest concessions of one large company, spanning a ten year period. While such records are valuable for determining long-term rates and trajectories of peat subsidence, they reveal little about the short-term (sub-annual) dynamics of peat movement, are labor intensive to maintain, and have a low precision (ca. 1 cm). While it is possible to measure seasonal dynamics of peat surface motion using more frequent measurements of subsidence poles (e.g., Howie and Hebda, 2018; Morton and Heinemeyer, 2019), this approach is labor intensive. As a result, several approaches have been trialled for measuring peat surface elevation change automatically, and with a higher frequency and precision. Zanello et al. (2011) described a system using displacement transducers fixed to a steel tripod, which record movement of aluminum plates resting on the peat surface, with a reported sensitivity of ±0.125 mm and an hourly frequency. Other potential approaches include the use of sonic or laser distance sensors, mechanical 'float and pulley wheel' systems (Strack et al., 2006), or differential elevation changes recorded by pressure transducers deployed below the water table in paired dipwells that are anchored in underlying substrate and free to move within the peat respectively (Fritz et al., 2008). Challenges for these approaches include mechanical breakdown under the extreme climatic conditions typical of many peatlands (e.g., high/low temperatures, high rainfall, humidity); accumulation of debris on reflector plates required for distance sensors; seasonal snow accumulation in high-latitude systems; and human or animal disturbance. Cost may also be a limiting factor for the use of more sophisticated sensors, restricting their use to well-funded research teams, and constraining the spatial coverage of measurements that can be achieved.

Here, we describe a novel, low-cost, high-precision and high-frequency method for monitoring peat surface motion and water table using cheap and commercially available time-lapse cameras. We describe the system design, the derivation of elevation data from photographic images, and the results of a 2-year deployment of multiple cameras to a range of contrasting peatland sites in Indonesia. We evaluate system robustness and accuracy, compare results against manual subsidence pole and commercial water table logger measurements, and examine the temporal dynamics of peat motion as a function of diurnal, hydrological, seasonal and long-term drivers of change. We also examine the extent to which peat behavior is influenced by land-management, and therefore the potential to use remote sensing of peat motion as a proxy for other peatland functions and properties.

METHODS

Peat Camera Design and Operation

We developed a simple, low-cost (around $300 per unit) camera-based system to measure small-scale variations in peat surface elevation, along with changes in WTD. This used a commercially available time-lapse camera (Wingscapes Timelapse Cam Pro WCB-00121, Alabaster, Alabama, United States). Similar cameras have been remotely deployed in similar habitats in the region to monitor wildlife populations with high success (e.g., Cheyne et al., 2016). The camera was fixed to a metal stool within a metal housing (to provide some shelter to the camera and security from theft), facing a horizontal metal strip that acted as a measurement level within the photographs (**Figures 1**, **2**). The stool then was placed over a metal subsidence pole that had previously been inserted vertically through the peat into underlying mineral substrate, which acted as a fixed reference level. Approximately 2 m of the pole was left projecting above the peat surface, and a 1 m metal ruler was attached to this such that the mid-point of the ruler was at the level of the camera lens. The subsidence pole passed through a pre-cut hole in the stool at a distance of 18 cm from the camera lens, behind the metal strip. The stool was then attached to the peat surface using ground screws attached to each leg of the stool, which were adjusted until the stool top and camera were horizontal. The stool and camera thus moved with the peat surface, and took photographs of the meter ruler on the fixed subsidence pole. For flood-prone sites the stool legs were extended to provide greater ground clearance.

To measure changes in WTD, we installed a dipwell comprised of a perforated, 7.5 cm diameter × 2.5 m long plastic pipe with a sealed base into the peat adjacent to the subsidence pole. Water level inside the dipwell was measured by means of a plastic fishing float of slightly smaller diameter than the dipwell, attached to a lightweight aluminum pole with a measurement scale attached, which passed through a second hole at a distance of 10 cm from the subsidence pole, and within the field of view of the camera. After initial trials, the float and pole were found to rotate within the dipwell, making the depth difficult to read. The design was refined by attaching a lightweight flexible PVC fibreglass tape measure to a U-channel aluminum wiggle wire (15 × 25 mm), and passing the U-channel and tape measure through a rectangular hole in a metal plate attached to the stool top. Although the

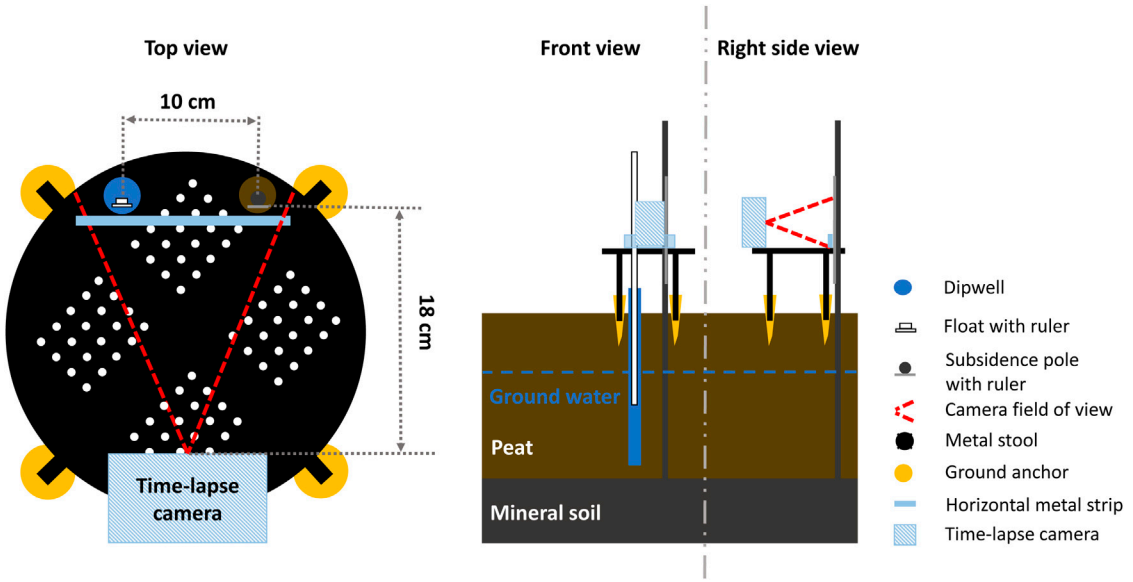

FIGURE 1 | Schematic of peat cameras design.

dipwell was open, to allow the float and the pole to move freely, the stool and the metal plate on top of it acted as a protection against debris and limited rainwater ingress.

The time-lapse camera was programmed to take photographs several times per day, initially at a 3 h frequency. This was changed to an hourly frequency in late February 2020 to enable a detailed assessment of system capability for monitoring change in WTD. To improve night-time imagery, we covered the camera's flash with partially transparent tape to reduce glare from the ruler so that the scale was readable. By taking multiple photographs during each day, we were able to record rapid or diurnal fluctuations in peat elevation and water table, and also ensured that at least one good image was usually obtained during periods of rainfall, when raindrops sometimes caused image blurring.

The cameras were powered by six C-cell alkaline batteries. Camera images were stored to a 32 Gb SD card, which could either be swapped during site visits or downloaded *in situ* via a USB cable. Cameras were typically left to run in the field for a period of one to three months between downloads, to minimize site disturbance, while not risking long periods of undetected equipment malfunction, damage or theft that could occur with less frequent checks.

Study Sites

To date, approximately 50 peat cameras have been installed on tropical peatlands in Central Kalimantan and Sumatra, Indonesia, and in Sarawak and North Selangor, Malaysia; at a range of temperate peatland sites in the United Kingdom; and on a boreal mire in Sweden. Here, we report the first results, spanning two wet and dry seasons, from eight sites in Central Kalimantan (**Table 1**; **Figures 2**, **3**). All cameras were located within established field research sites operated by the University of Palangka Raya as part of the United Kingdom Global Challenges Response Fund SUSTAINPEAT project. All sites are located between the Sebangau and Kahayan Rivers to the north and south of the city of Palangka Raya (from latitude 1.88°–2.35°S, longitude 113.47°–114.10°E). The area south of Palangka Raya was heavily deforested and drained via a network of canals in the 1990s as part of the failed Mega Rice Project, since then it has been subject to severe and repeated fires (Page et al., 2002). The area now comprises fragments of secondary forest, large areas of smallholder agriculture, smallholder and some larger oil palm plantations, and extensive areas of degraded shrubland dominated by ferns, regenerating native trees and non-native *Acacia mangium* (Page et al., 2009). In this area we deployed six cameras: two in smallholder agricultural land, one in a smallholder oil palm plantation, one in secondary forest and two in burned shrubland. The area north of Palangka Raya includes areas of more extensive forest, with some smallholder agriculture and smaller oil palm plantations. This area is in general less drained than the southern area, and fires are less frequent. Here we installed two cameras: one in a smallholder oil palm plantation, and one in secondary forest.

The study region has an average annual temperature of 26°C, with little seasonal variation, and a mean rainfall of 2,500 mm yr^{-1} (Hirano et al., 2012). Rainfall is strongly seasonal with a wet season from November to april and a dry season from around June to September, though this may extend into and beyond October in drought years (**Figure 4**). The severe El Niño related dry season of 2015 led to widespread fires, following which the Indonesian Peat Restoration Agency (Badan Restorasi Gambut, BRG) was created, and instituted a program to restore degraded peatlands and raise water levels through the installation of dams on canals. However another positive El Niño phase in 2019

FIGURE 2 | Peat cameras installed at four sites in Central Kalimantan (clockwise from top left: Forest, oil palm plantation, smallholder agriculture, previously burned scrubland).

TABLE 1 | Locations, properties and management histories of Central Kalimantan study sites.

Name	Latitude	Longitude	Peat depth (cm)	Bulk density (g cm^{-3})	Management history
Oil palm, misik	−2.3001	114.0308	373–392	0.25 ± 0.01	Opened in 2015 after fire, 30 m from main drainage
Oil palm, hampangen	−1.9199	113.578	342–350	0.18 ± 0.01	Affected by fire in 2007, water levels maintained by ditches and dams
Agriculture, kalampangan	−2.28952	114.0134	365–377	0.24 ± 0.01	Opened in 1980s, 35 m from main drainage, irrigated in dry season
Agriculture, misik	−2.3048	114.028	292–300	0.26 ± 0.01	Opened in 2015 (after fire), 220 m from main drainage
Burned Area, RePeat	−2.3370	114.0704	267–277	Not determined	Shrub, severely affected by fire in 2015. Part of 'RePeat' rehabilitation project
Burned Area, south	−2.35411	114.0959	250–300	Not determined	Shrub, affected by fire in 2015
Forest, UPR	−1.8845	113.4733	83–90	0.08 ± 0.01	Secondary forest, affected by fire in 1997
Forest, KHDTK	−2.3527	114.0923	226–284	0.14 ± 0.01	Secondary forest, affected by fire in 1997

resulted in a prolonged dry season, severe water table drawdown in some areas (up to 2 m) and a recurrence of fires in many areas. The 2020 dry season was shorter and wetter than average, and few fires occurred, as La Niña conditions developed.

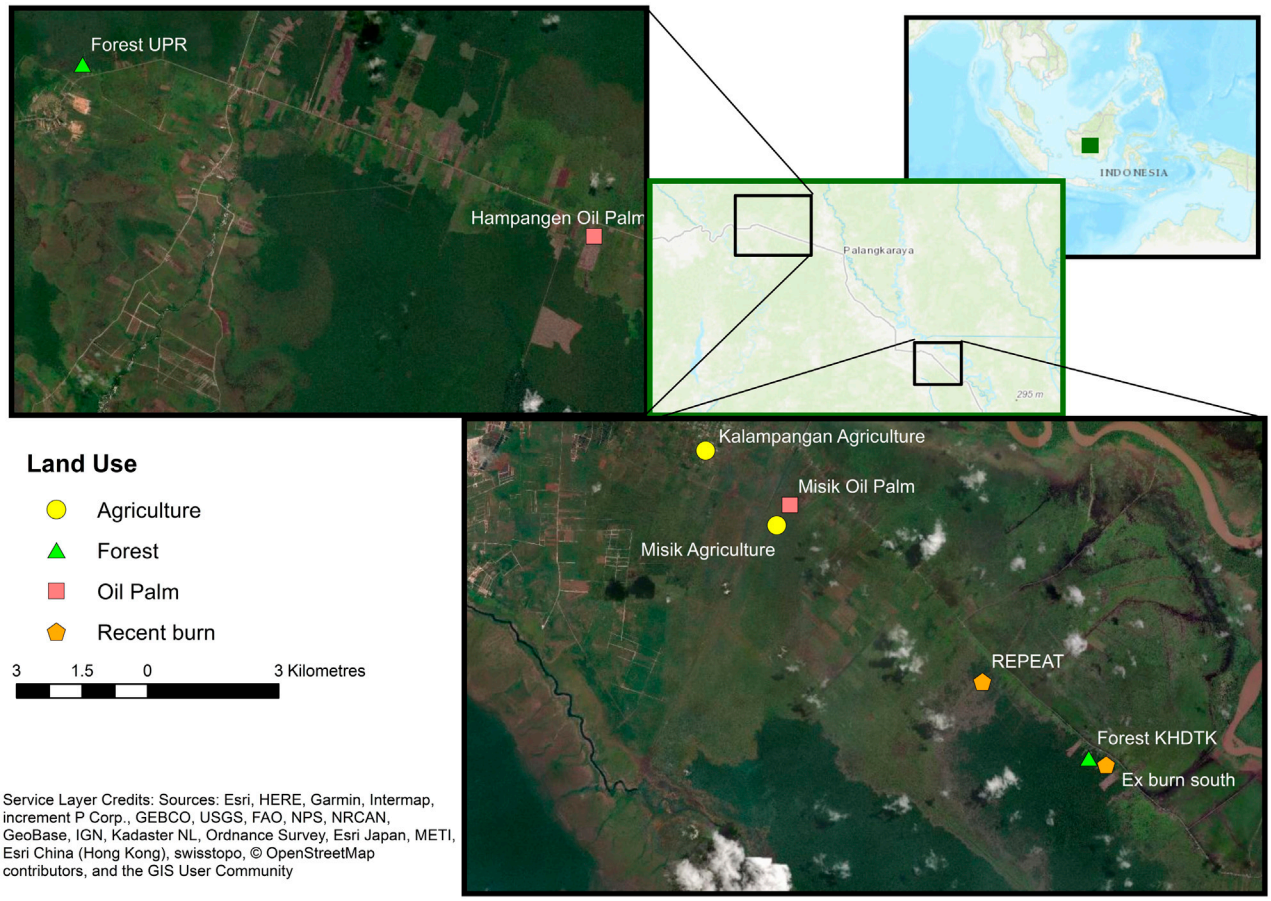

FIGURE 3 | Study site locations, Central Kalimantan.

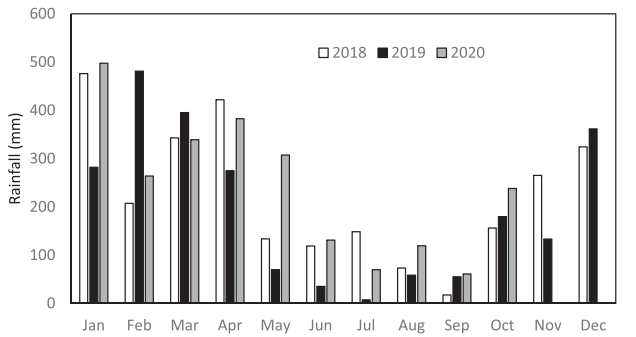

FIGURE 4 | Monthly rainfall for 2018, 2019 and 2020 (to October). Data from Palangka Raya meteorological station, Badan Meteorologi, Klimatologi dan Geofisika.

Test Data Collection

To evaluate instrument performance, a set of 6–10 metal and PVC poles were installed in areas near the camera site, at which subsidence was recorded manually on up to nine occasions during the measurement period, by measuring the distance from the top of the pole to the peat surface (see e.g., Evans et al., 2019). Metal poles were considered likely to be more robust in the actively managed and dynamic landscapes being studied, while PVC poles were installed to check for any sinking of the heavier metal poles into the underlying substrate. As no such sinking was detected during the period of measurement, data from both sets of poles were pooled. To compare camera and manual subsidence data we derived a mean of manual elevation values for each time point, and the mean camera-derived elevation value for the same day. Change in elevation was then calculated relative to a zero datum on the day of the first manual measurement at each location.

Manual subsidence poles were distributed near the camera sites, along transects or grids at a spacing of around 50–100 m, with the intention of measuring variations in subsidence within the surrounding area, rather than specifically for testing camera performance. However in most cases subsidence was found to be fairly consistent at this scale, enabling a comparison to be made. An exception was the Kalampangan agricultural site, where we included poles installed within the farm itself, but excluded four poles located in neighboring scrubland that were affected by fire during the study period. We also excluded manual poles with incomplete data, as well as poles that suffered visible disturbance during the study period as a result of land-management activities.

To test the camera-derived water table measurements we ran cameras at three sites (Misik Oil Palm, RePeat Burned site, UPR Forest) alongside DipperLog Nano pressure transducers (Heron Instruments, Ontario, Canada) installed in adjacent dipwells. Both instruments were set to record at an hourly frequency. The period of parallel measurements ran from February 21st to June 30th, 2020. A DipperLog Nano was also operated at the Hampangen Oil Palm site for the duration of the study. As no water table loggers were operational at any of the southern sites for the first part of 2019 we also obtained water table data collected by the Japanese Science and Technology Agency and Japan International Cooperation Agency "Wild fire and carbon management in peat-forest in Indonesia' project (Takashi Hirano, pers. comm.) located in burned scrubland close to the RePeat Burned site. These data were used to indicate the general pattern of variation in WTD in this area.

Data Analysis

Images were processed using a custom written *Python* script via a graphical user interface (**Figure 5**). Although the script automated the peat height data extraction, it also required some initial parameters that had to be manually provided by the user. After an initial visual assessment of the images to be processed, the most representative image, based on light conditions and the ruler numbers shown on the images, was used as a reference. Images taken at night and during the day, as determined by whether the flash was used, were processed separately, as lighting conditions were too different for processing together. Therefore, the reference image was selected separately for day and night images. Thereafter, an initial height reading (manually read from the ruler in the image) and calibration (line segment drawn on the image and given a measure in centimetres, usually 1 cm) was recorded from the reference images. In addition, a region of interest was manually selected around the ruler. This region of interest defined the area of each image containing the points of interest with distinct features, or keypoints. The defined area was effectively cropped, and compared with the same cropped area from the reference images. Keypoints were characterized by their coordinates, orientation and scale. By positioning the area of interest near the middle of each image, distortion toward the edge of the image was minimized, and selection of keypoints along the ruler both above and below the center meant that any minor distortion within the area of interest was effectively canceled out.

Each cropped image underwent feature matching analysis using the ORB method (Rublee et al., 2011) to locate keypoints. ORB (Oriented FAST and rotated BRIEF) is an open source script which combines two methods, FAST (Features from Accelerated Segment Test) and BRIEF (Binary Robust Independent Elementary Features), where FAST describes the methods of detecting where a feature is and BRIEF is a method for reducing the memory required to store and process all the relevant vectors produced. FAST locates features essentially by detecting corners. For each pixel it evaluates a circular radius of pixels around that pixel and compares their intensity (how light or dark they are) to a threshold intensity difference, starting with opposite orthogonal points around that circle and then continuing round the circle if they are brighter or darker. A feature is detected if there are a significant number of contiguous pixels in that circle that are brighter or darker than the central pixel.

Keypoints in each image (i.e., distinct features identified by ORB as described above) were paired to those found in the

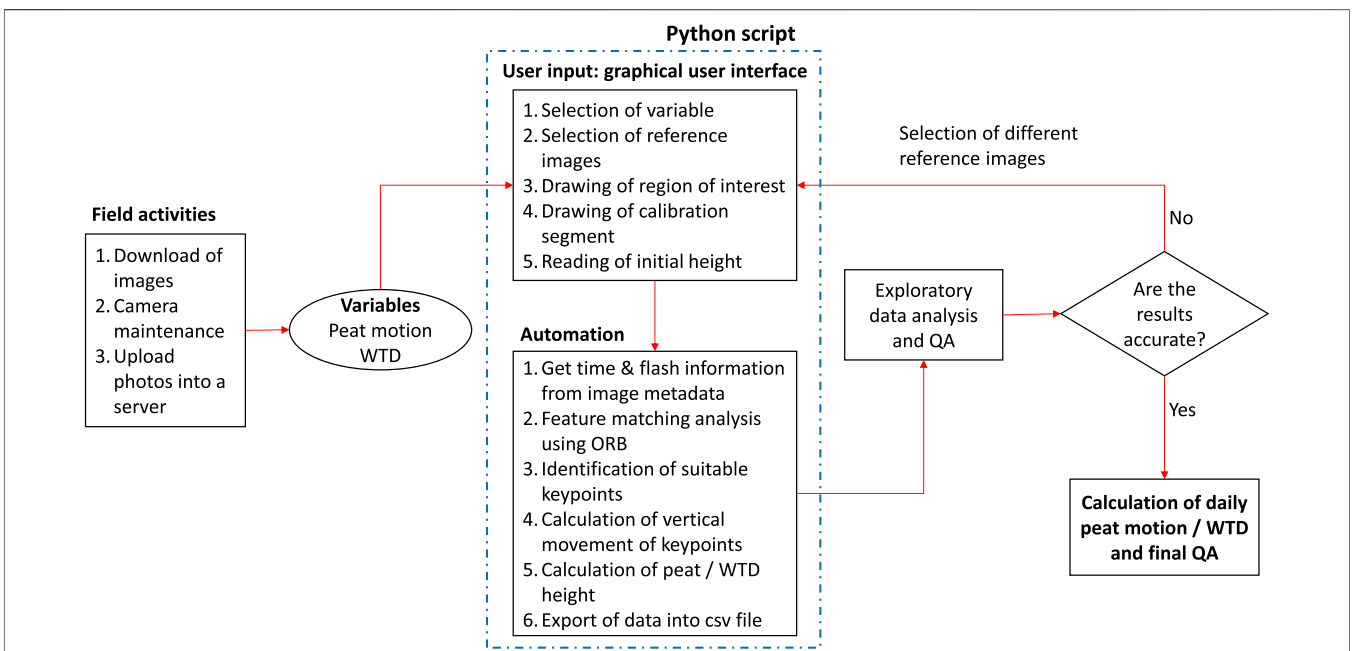

FIGURE 5 | Flow diagram showing procedure for deriving measurements of peat motion and water table depth from image data.

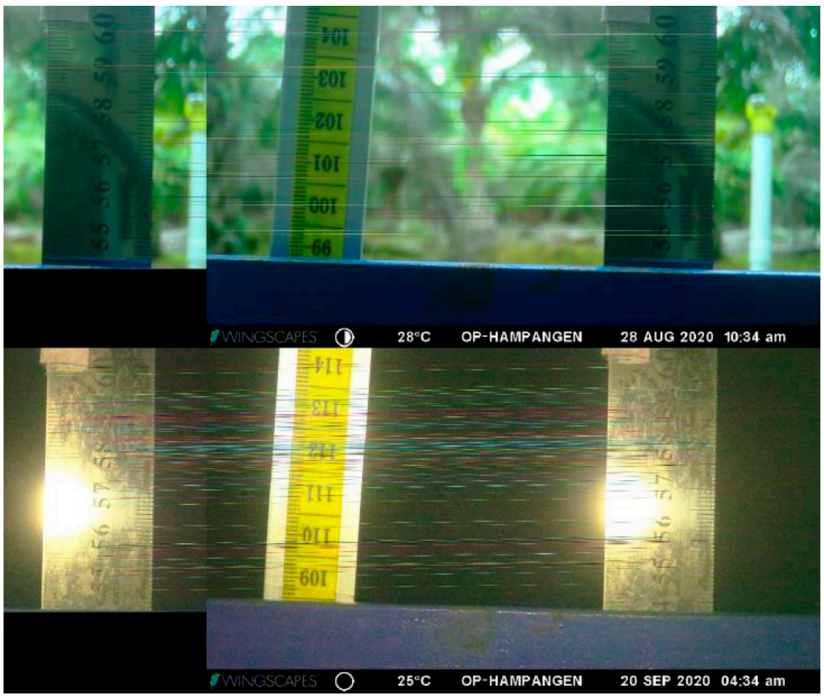

FIGURE 6 | Examples of image processing for daytime and night-time images at the Hampangen Oil Palm site. Ruler in image on right is compared to reference image on left, containing the cropped region of interest with potential keypoints (central scale is the water table gauge). Colored lines represent individual matches between keypoints, which are used to calculate vertical displacement.

reference image using a 'brute force' matcher which compares each keypoint against every keypoint in the reference image to find pairs of keypoints. The pixel locations of each keypoint pair were compared to get a movement vector in pixels. Any pairs that did not have similar vectors (within 1 pixel and 1°) to other pairs from the same image were discarded, and images were required to have at least two matched pairs of keypoints with similar vectors. Only the vertical component of each movement vector was used in analysis as in theory only vertical movements should be possible, however horizontal movements were used to flag anomalous movements. The vertical movement of suitable keypoints from the reference image was converted to movement in cm using a manually provided calibration value based on the number of pixels per cm in the images, and then converted to a height measurement by applying the difference to the manually read measure on the reference image. Images that could not be automatically processed by the script were then manually read by the user, sufficient to obtain at least one elevation value per day. At the end of the automation process, the script exported all the data into a csv file. This file contained the photo id, the date and time, a code identifying if it was a day or a night image, the average vertical movement (in pixels), the average angle change, the number of suitable keypoints, the calculated height (in cm) and a warning message if any horizontal movement was detected. All peat height measurements recorded within each day (either at hourly or 3 hourly intervals) were averaged to obtained daily values. When gaps of no more than 5 days occurred due to system malfunctioning or adverse weather conditions, peat height values were estimated by linear interpolation. Longer gaps were left blank.

The eight Kalimantan monitoring sites provided sufficient data to calculate annual subsidence in 2019. To reduce the effect of short-term hydrologically driven fluctuations we calculated annual net subsidence as the change in peat elevation observed between the first two weeks of January 2019, and the first two weeks of January 2020. At two sites with missing data during one of these time periods, we used the closest available two week period. Although this could introduce an error in the calculation, the December-February period is the wettest part of the year, so relatively little subsidence occurs at this time, and the magnitude of any error is therefore expected to be small.

RESULTS

Image Processing

In general, the image processing method worked well for deriving peat motion data. **Figure 6** shows example of daytime and night-time image matches. Image quality tended to be best at sites with sparse vegetation (fields, plantations and bare ground) where there was little vegetation interference in the field of view, and where humidity was lower. Vegetation interference occurred more often at forest sites, for example due to creeper growth up the instrumentation, which required periodic maintenance. The feature analysis was able to detect keypoints with a modest

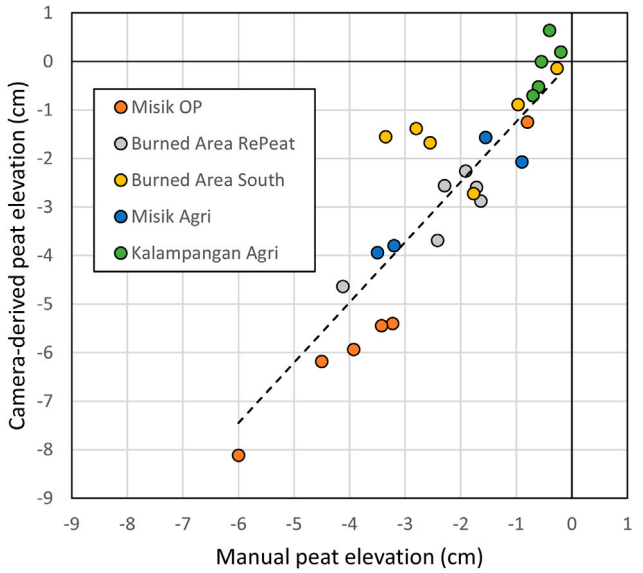

FIGURE 7 | Camera-derived vs. manual elevation data for five sites with near-continuous records, relative to a zero datum value at the time of the first manual measurement.

level of image blurring, but not when blurring was more severe such as during and immediately after rain events. Since these events are typically of short duration in the study area, we were generally able to process at least one image per day. The use of a standard meter ruler provided some non-unique features in the image (e.g., repetition of '3' in the 30, 31 and 32 cm labels) but in a clear image the software was usually able to correctly identify five or more keypoints. Although performance was often similar for daytime and night-time images, at some specific sites, night images showed a better performance (i.e., larger number of identified keypoints, e.g. 100 or more); provided that the opacity of the tape over the flash was sufficient to avoid image burnout and not too dark to negate the effect of the flash. In many cases where the image detection software was unable to identify keypoints, we were able to identify these manually. All images were manually checked for clearly erroneous matches, which were then corrected when numbers were clearly visible. Success rates of image processing using the script varied between 45 and 98% depending on the site and the collection period. Precision of automatically classified measurements was sub-mm (the script was able to detect vertical movements of a single pixel, which was equivalent to 0.03–0.04 mm), while precision of manually processed data, when the value was read directly from the ruler, was around 1 mm (i.e., the smallest subdivision of the ruler).

Processing water level data from the images was in general more problematic, due to the larger range of vertical movement (up to 50 cm in 3 h in response to rainfall at some drained sites). This meant that the entire section of the measurement scale visible in one image could move out of the field of view of the camera by the time of the next image, such that no matching keypoints could be obtained. Image processing through the script resulted in success rates of around 20% and therefore, to extract water level data it was necessary to process the remaining images manually. All images were visually checked to manually correct mismatched keypoints and erroneous extracted water level data. Precision was around 1 mm.

System Performance

Of the eight cameras installed, five provided near-continuous records of surface elevation change over the study period, while the other three provided partial data, sufficient to derive total subsidence over the year. Data loss at the Hampangen Oil Palm site occurred as a result of a programming error with the camera, resulting in only sporadic measurements from april to October 2019. Periods of data loss at the forest sites resulted from camera failure due to moisture ingress (typically leading to the camera to

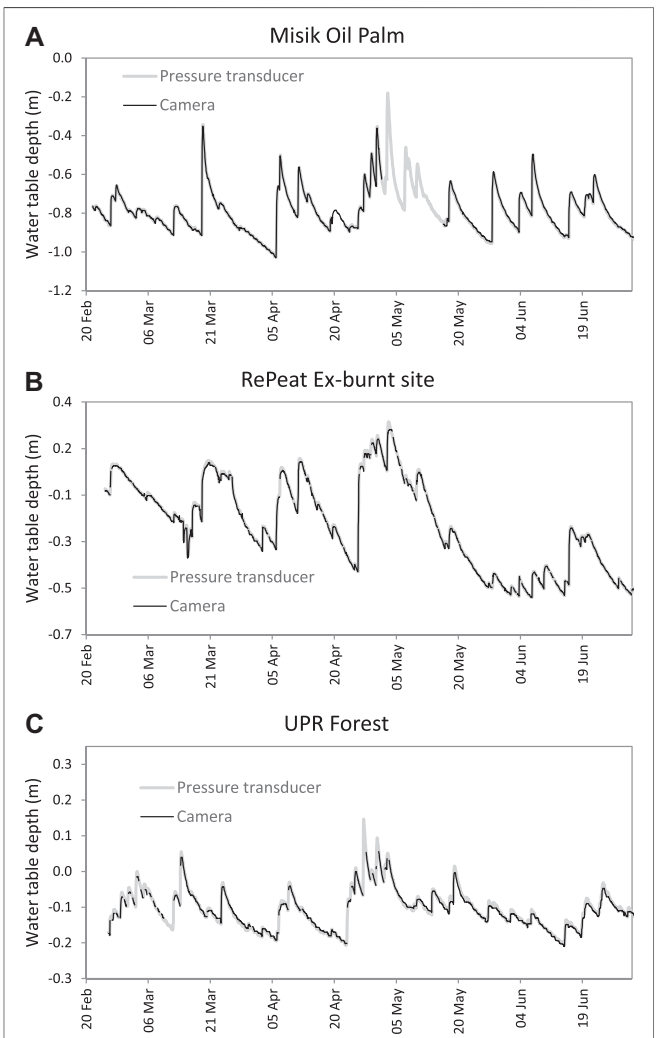

FIGURE 8 | Hourly time series of water table data derived from cameras and pressure transducers over a 4-month period from February to June 2020). Note that *y*-axes vary between panels depending on the observed range of variation at the site, to facilitate comparison of logger and camera performance. **(A–C)** are there as site identifiers to enable specific panels to be referenced from the text.

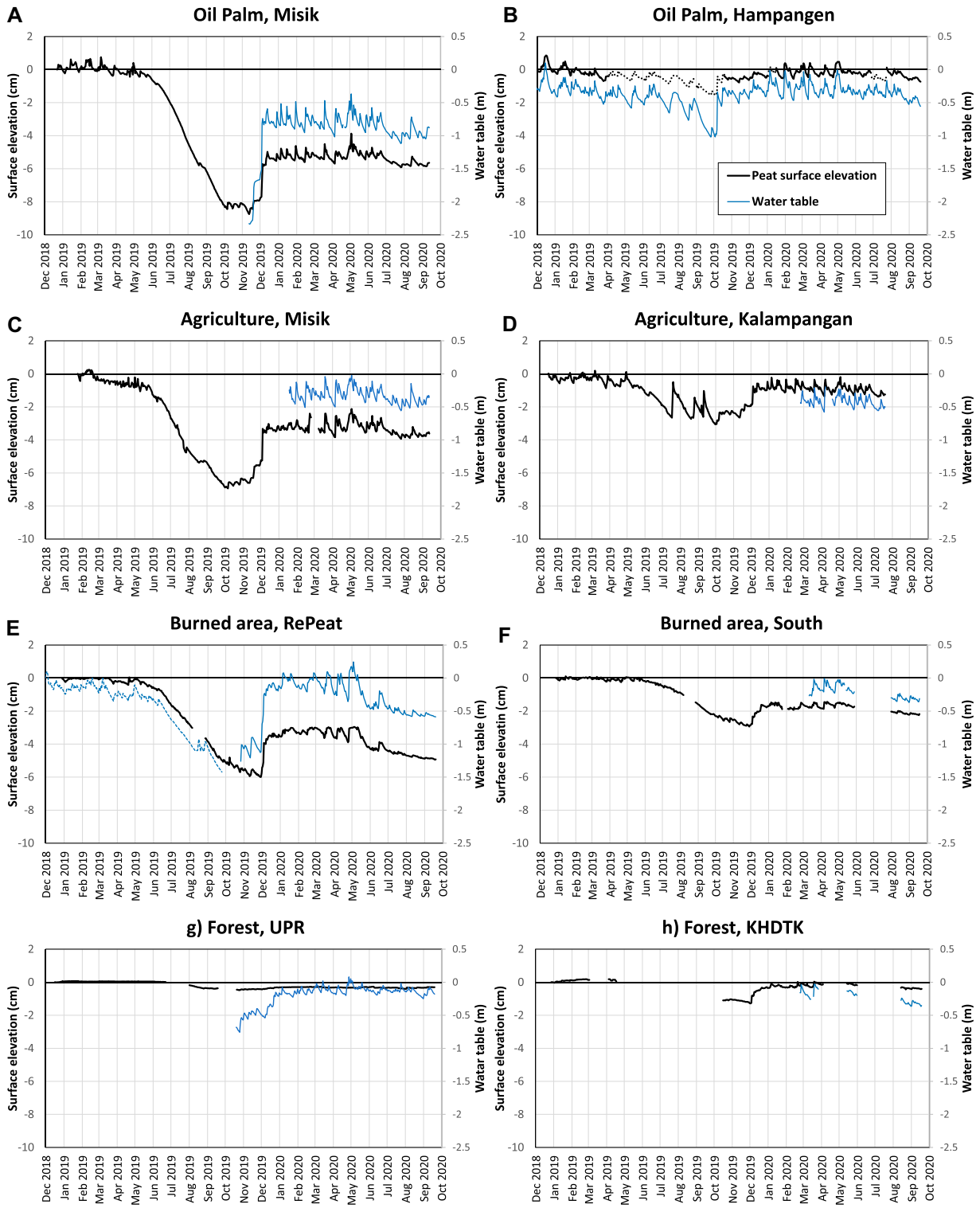

FIGURE 9 | Time series of peat elevation (black, left *y*-axis) and water table depth (blue, right *y*-axis) over the full measurement period. All data are plotted on the same *y*-axis scales to facilitate comparison. The black dashed line at Hampangen Oil Palm indicates data that were gap-filled using WTD data and the blue dashed line at RePeat shows WTD data obtained from a pressure transducer operated nearby (see text for details). **(A–H)** are there as site identifiers to enable specific panels to be referenced from the text.

TABLE 2 | Annual net subsidence for 2019 for the Kalimantan sites.

Type	Location	Subsidence (cm)
Oil palm	Misik	−5.27
Oil palm	Hampangen	−0.36
Agriculture	Misik	−3.21
Agriculture	Kalampangan	−0.40
Burned area	RePeat	−3.17
Burned area	South	−1.50
Forest	UPR	−0.30
Forest	KHDTK	−0.26

taking photos at random intervals, usually every few seconds, or stopping completely, likely due to an electric short-circuit). This problem appears to have been more acute in the forest sites due to extremely high humidity under the forest canopy. Lens fogging also occurred in moisture-affected cameras, while on one occasion, ants were found inside a camera which also resulted in system malfunction. These problems were addressed by taping over the seals on the camera, and by providing protection from rain. Moisture-affected cameras were generally found to recover if removed from the field and dried.

At the two burned sites, we temporarily removed the cameras (poles and platforms were left in place) during August 2019 due to the risk of them being destroyed by fires that were active nearby at the time, although neither site ultimately burned. For the five sites with near-continuous camera data, a comparison of camera-derived and manual elevation change (ΔElevation, i.e., change relative to the site datum value) is shown in **Figure 7**. A linear regression through all measurements (and excluding the 0,0 values for all sites) gave the relationship:

ΔElevation (camera) = 1.295 x ΔElevation (manual) Adjusted $R^2 = 0.916$, $p < 0.001$, $n = 28$.

The coefficient above 1.0 suggests that the cameras might be slightly over-estimating ΔElevation, although this deviation was not observed at all sites. The Misik Oil Palm site exerts a particularly strong influence; without data from this site the regression coefficient would be 1.14. At this site, the camera was located 30 m from a drainage ditch, whereas most manual poles were further away; simultaneous manual measurements of WTD on three occasions suggested that the camera site had considerably deeper drainage (mean WTD -0.75 cm) compared to the subsidence pole locations (mean WTD −0.54 m). Thus, differences between camera and manual ΔElevation values at this site may represent real differences between the sites, rather than measurement artifacts, although clearly the behavior of camera and manual sites was highly correlated ($R^2 = 0.97$, $p < 0.001$).

We compared WTD data obtained from the cameras with those from pressure transducers at three sites, for the period February to June 2020 (**Figure 8**). The Misik Oil Palm logger experienced one extended period of data loss due to a palm frond falling on top of the dipwell. In addition, several shorter periods of data loss occurred at the UPR Forest site when firstly the tape covering the flash was too dark and secondly, when the camera float apparently jammed, notably at very high water levels (>5 cm above the surface) when the float may have jammed against the stool. At this site, it was also often difficult to obtain useable images during rain events, evident in **Figure 8C** as gaps on the rising limb of a number of event hydrographs. For the remainder of the time, however, all three sites showed remarkable correspondence between the two sets of measurements (Misik Oil Palm: $WTD_{camera} = 0.997\ WTD_{pressure\ transducer}$, $R^2 = 0.986$; RePeat Burned: $WTD_{camera} = 0.997\ WTD_{pressure\ transducer}$, $R^2 = 0.999$; UPR Forest: $WTD_{camera} = 0.953\ WTD_{pressure\ transducer}$, $R^2 = 0.994$; all $p < 0.001$). The camera-derived data therefore appear to be of similar quality to the pressure transducer data.

Peat Elevation and Water Table Time Series

Measured elevation changes for all sites are shown in **Figure 9**. The data span two wet seasons and two dry seasons, but the 2019 dry season was notably drier than 2020. As noted above, there were substantial data gaps at the Hampangen Oil Palm site and the two forest sites in 2019. At Hampangen, where a pressure transducer was in operation throughout the study, we observed a strong linear relationship between peat elevation and WTD during periods of camera operation ($R^2 = 0.83$, $p < 0.001$) so this was used to gap-fill the elevation record (dashed line in **Figure 9**). The gap-filled record aligns well with two brief periods of camera operation during this time, providing some support for this approach, however derived peat elevation changes during this gap-filled period are uncertain.

More generally, the elevation data demonstrate high overall coherence among sites. All sites showed stability or slight subsidence during the wet season at the start of 2019, followed by sustained subsidence during the severe dry season, which continued until the end of November 2019. All sites then rebounded rapidly, coincident with a rapid recovery in the water table where this was measured. At some sites, rebound was complete (i.e., peat elevations returned to where they had been in early 2019) but in others it was partial, despite water tables returning to close to the surface in some cases. The less severe 2020 dry season was associated with much less water level drawdown, and at most sites the peat surface remained stable, although there was evidence of renewed subsidence at some sites, including both Misik sites, and the RePeat Burned site. At the RePeat site, a canal was dug close to the camera in around april 2020, which likely accounts for the accelerated subsidence here relative to other locations.

Annual Subsidence and Effects of Land-Use

We were able to estimate annual net subsidence from camera data for the 2019 calendar year at all sites. Observed values (**Table 2**) ranged from −0.3 cm at the two forest sites (where a negative value indicates a decline in the ground surface) to −5.27 cm at the Misik Oil Palm site. Net accumulation did not occur at any site. As is evident from **Figure 9**, peat elevations declined by more than this amount at the peak of the 2019 dry season, then partly recovered. The relative stability of peat elevations during the wet January-April periods in both 2019 and 2020, when hydrological conditions were similar, suggests that the net change between these two periods represented long-term subsidence (i.e., peat oxidation and compaction) rather than a short-term shrink-swell response to drying and re-wetting.

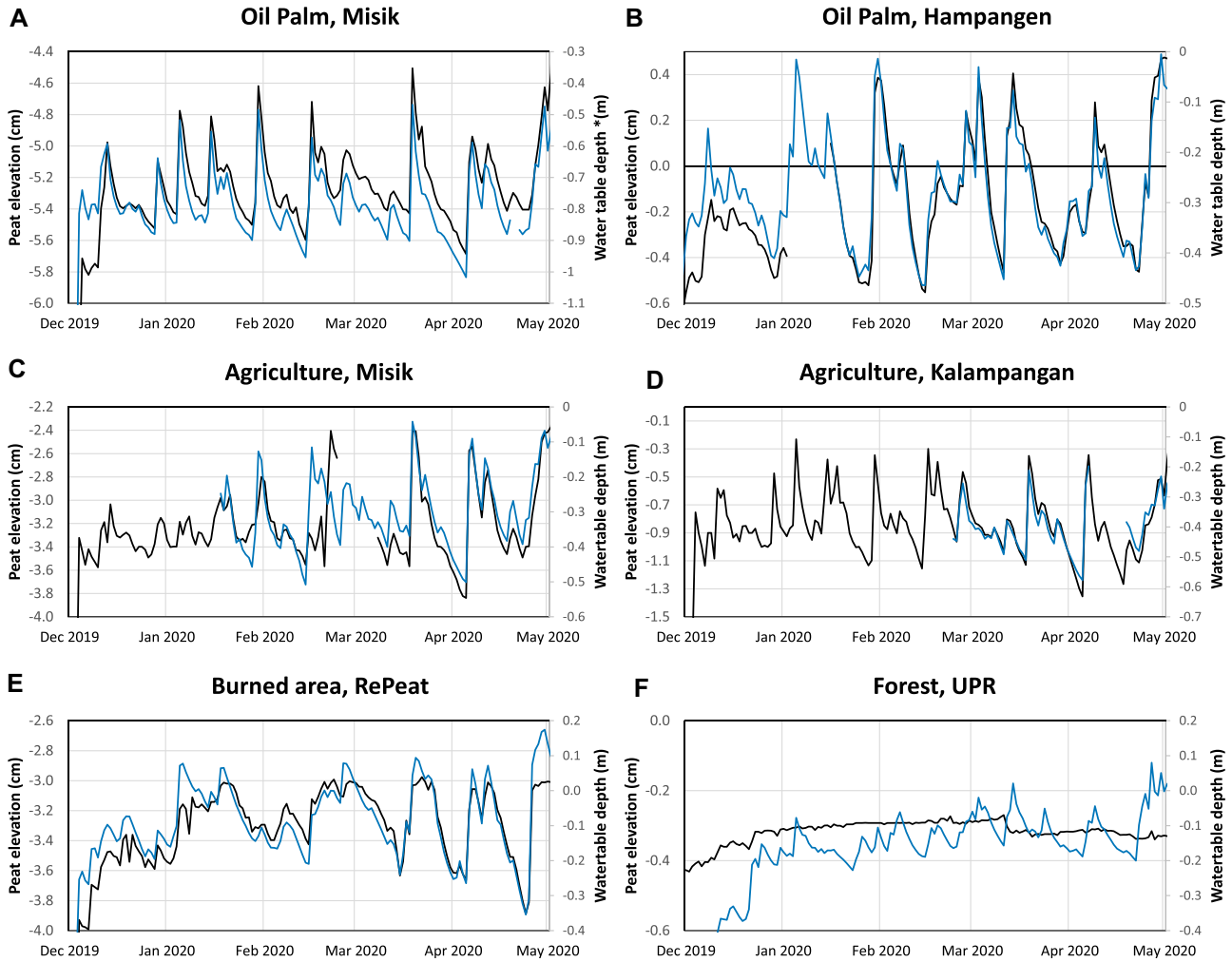

FIGURE 10 | Time series of peat elevation (black, left *y*-axis) and water table depth (blue, right *y*-axis) for six sites with elevation and water table data for the early 2020 wet season. *Y*-axis ranges are adjusted according to the magnitude of observed short-term variation at each site, *y*-axis increments are the same for all sites (thus denser horizontal gridlines indicate sites with greater short-term peat motion). **(A–F)** are there as site identifiers to enable specific panels to be referenced from the text.

At this stage, we do not have sufficient data to estimate annual WTD, which previous studies have shown to be a strong predictor of subsidence rate (e.g., Hooijer et al., 2012; Evans et al., 2019). However from the limited data available it is clear that sites with uncontrolled deep drainage during the dry season (e.g., Misik Oil Palm, where the water table was >2 m below the surface when measurements began in November 2019, and the RePeat Burned site where it was >1 m) experienced relatively high subsidence, whereas sites where water levels remained higher (e.g., UPR Forest, Hampangen Oil Palm) experienced far less subsidence. These relationships partly tracked land-use; the forest sites both showed very limited motion during periods when the cameras were operating, and negligible annual subsidence. The greatest peat shrinkage during the 2019 dry season, and largest annual net subsidence, occurred at the intensively managed and deeply drained Misik Oil Palm and agricultural sites. The two partly drained but unmanaged former burned sites were intermediate between these two extremes, although it is notable that peat elevation at the burned sites (especially RePeat) appears to have decreased again during the less intense 2020 dry season, whereas most other sites remained relatively stable.

Two sites did not behave as expected based on their land-use. The Hampangen Oil Palm plantation showed negligible overall subsidence during the measurement period, despite active plantation management. This site, which is located in the poorly drained area north of Palangka Raya, had much higher water tables than the agricultural sites to the south: apart from a brief period during the peak of the 2019 dry season, water tables were always within 50 cm of the peat surface, and frequently higher. While the camera was not operational during much of the 2019 dry season, gap-filled data based on a correlation with water table (**Figure 9**) suggest that maximum shrinkage may have been less than 2 cm, whereas it exceeded 8 cm at the deep-drained Misik Oil Palm site. The recovery of the peat surface by January 2020, to approximately the same level recorded in January 2019,

suggests that these relatively wet conditions, which are unusual for oil palm cultivation, may have been sufficient to minimize subsidence.

The Kalampangan Agricultural site also diverged strongly from the behavior of the other agricultural site at Misik, despite their close proximity (2.5 km apart) and apparently similar drainage (both sites lie within the same canal network and were observed to have similarly deep water tables during the peak of the 2019 dry season). However, unlike the Misik site, the farm at Kalampangan is periodically surface-irrigated via a borehole that extracts water from the aquifer beneath the peat. The three sharp periods of peat uplift during July-September 2019, which were not associated with rain events, are believed to be due to irrigation of the field containing the camera (A. Jaya, pers. obs.). These irrigation events seem to have played a major role in reducing the degree of peat shrinkage during the dry season (maximum observed shrinkage of 3.0 cm, vs. 7.0 cm at Misik), and in the subsequent wet season the peat recovered almost to its original elevation, whereas it remained 3.2 cm lower at Misik.

Response to Short-Term Hydrological Variation

Figure 10 shows camera-derived peat elevation and water table data for the wet season at the start of 2020, for the six sites with relatively complete data during this period. It is clear that, in almost all cases, peat elevation tracks WTD very closely. This occurs despite marked differences in hydrological conditions at different sites. For example at the Misik Oil Palm site, with efficient drainage, water levels repeatedly rose by around 0.4 m in response to rain events, before rapidly declining until the next rain event. This pattern was replicated in the elevation data, with an amplitude of around 0.8–1 cm. At the Hampangen Oil Palm site, despite much higher water levels, the amplitude of both water level change and peat elevation change between wet and dry periods was the same. The two agricultural sites also had similar amplitudes of short-term variation in response to rain events. The burned site showed a more subdued hydrological response, which was also reflected in the peat motion. The forest site has the smallest water table fluctuations in response to rainfall, typically <0.2 m. Here, in contrast to all other sites, we observed negligible peat elevation variation in response to short-term rain events, although there was some steady upward movement of the peat in December 2019, during the transition from dry to wet season.

At the managed sites, there was very little indication of hysteresis in the response of peat elevation to water table change; i.e. water table and peat elevation rose and fell more or less simultaneously. At the burned site, some peaks in peat elevation were slightly lagged behind peaks in water table, but in other cases no hysteresis was evident.

DISCUSSION

System Performance and Refinement

Given the simplicity and low cost of the camera-based system compared to current commercially available sensors, our results were highly encouraging, and enabled observation of aspects of peat behavior that were not previously detectable, as discussed below. The two main challenges for the camera method are reliability in the field, and data processing.

Field data loss occurred for a number of reasons. One was simply miss-programming of the cameras, for example by setting time intervals to seconds rather than hours. This problem was resolved as instructions were made clearer and operators became more experienced. Adjusting the strength of the camera flash (using semi-opaque tape) reduced issues of image burnout or under-exposure at night, increasing the number of usable images obtained per day. Other causes of data loss were image blurring by raindrops on the lens, incorrect camera focus, water ingress into the camera (particularly in high-humidity forests) and blocking of the camera view by growing or falling vegetation. Refinements to system design made during the study included better waterproofing of the camera, and addition of a roof over the camera, which reduced data loss due to rain and falling debris. Some water ingress to the open dipwell likely still occured, but the near-1:1 correlation with data obtained from pressure transducers in adjacent capped dipwells suggests that this had a negligible impact on results. The lateral hydraulic conductivity of tropical peat is typically high (Evans et al., 2014), which may have limited the extent to which rainwater could accumulation in the dipwell above the water table. In peat with a lower hydraulic conductivity, such as high-latitude bogs, more issues with rain ingress are possible. We plan to reduce this issue in future refinements of the system by adding a PVC cap to the dipwell with a narrow hole through which the float device can move freely.

At another trial site in Malaysia, one camera was damaged by wild boar, but as this problem did not arise elsewhere we did not place the cameras inside enclosures, to avoid ground disturbance. Periodic visits to remove debris and ground vegetation, and to conduct general checks of the equipment and its functioning, generally minimized data loss and are therefore recommended, irrespective of limits imposed by battery life and SD card capacity. However in future we aim to develop a system with telemetry and off-grid power to provide an immediate indication of problems, enabling more efficient operation, and to reduce the need to access the camera to download data and change batteries, thereby minimizing disturbance issues.

The main additional challenge for the water table loggers was jamming of the float system, either within the dipwell or as it passed through the stool. These problems were reduced by using a smaller float relative to the diameter of the dipwell, removing any rough edges inside the dipwell (e.g., those created by drilling holes), and passing the pole and ruler through a metal plate on the stool to minimize friction and ensure that the ruler was correctly oriented toward the camera. The stool itself provided protection against debris ingress into the dipwell, and the addition of a PVC cap in future should further reduce this issue.

Data processing represented a significant challenge. For peat elevation, the image processing software worked well, although some manual error-correction and image matching was generally needed. Processing the water table data was more problematic, because the vertical movements were often too large to allow keypoint pairs to be identified. The use of a standard meter ruler

also presented challenges for identifying unique keypoints, which might partly be overcome through the use of a purpose-built scale, e.g., using unique symbols and colors.

Despite the data processing challenges, the cameras produced water table data that were almost identical to those obtained from commercial pressure transducers, with no evidence of any systematic bias (R^2 and gradient of relationships between the two methods both close to 1; **Figure 8**). The cameras also provided highly precise measurements of change in peat elevation, and could detect movements of less than 1 mm with very little short-term noise. Where small fluctuations were observed during sequential measurements, these were found to be consistent from day to day, and to track diurnal variations in WTD associated with daytime evapotranspiration. While we have not yet been able to precisely quantify measurement error, the method appears to compare well with the dual pressure transducer method of Fritz et al. (2008) (reported standard error ± 2 mm), and is clearly superior to acoustic sensors with a reported precision of ±1 cm (e.g., Campbell SR50A).

The comparison of camera-derived data with manual subsidence pole data (**Figure 7**) indicated that the cameras are able to accurately capture sustained changes in peat surface elevation over time. The subsidence poles were installed to capture local variability rather than with the specific aim of testing camera performance, and were therefore in some cases 100 m or more away from the camera site, which likely contributed to some scatter in the relationship. We also often found weaker coherence in temporal behavior among subsidence poles located in the same area than we did between cameras at different locations, suggesting that measurement errors and disturbance issues may have been greater for the manual pole dataset than for the cameras. In other words, the manual pole dataset does not represent a perfect test dataset for the cameras, and may if anything contain larger errors. As a result, we cannot yet define measurement uncertainty ranges, although the very high precision, absence of short-term noise and consistent fine-scale responses to water level change (**Figure 10**) all suggest that short-team measurement errors are very low.

However, we do identify two potential issues for the camera method. Firstly, if the combined weight of the camera and the stool on which it is mounted could accelerate rates of compaction. While this would have negligible impacts on measured short-term motion, it could lead to an over-estimate of long-term subsidence. While we sought to minimize this issue by limiting the weight of the system and distributing it across four ground anchors, the deviation of camera-derived vs. manual subsidence values below a 1:1 line in **Figure 7** does provide some suggestion that accelerated compaction could be occurring. On the other hand, the gradient of the relationship is strongly influenced by five data points from the strongly subsiding Misik Oil Palm site, where we found that WTD at the camera site was on average 25 cm deeper than at the manual pole sites, which suggests that higher subsidence rates at the camera site may be real. In almost two years of operation we did not find any visual evidence of accelerated subsidence beneath the cameras compared to the area immediately surrounding each stool. A second issue of concern for the camera method is the possibility that, at highly rooted forest sites, the ground screws could anchor into the root network rather than the peat matrix. This could for example have contributed to the very limited peat motion observed at the UPR Forest site, where we unfortunately did not have suitable manual pole data to determine whether this apparent stability was real. However, if as seems likely the surface tree roots are moving vertically along with the peat matrix, then this would not lead to an error in the elevation data. These and other potential methodological issues will be addressed through ongoing operation and testing of the cameras in Kalimantan, as well as increased testing in other climate regions, ecosystems and peat types.

Insights Into Peatland Dynamics

As detailed in the introduction, the concept of 'bog breathing' is well established in the peatland literature, and forms part of the self-regulatory mechanism of natural peatlands. It has also been identified as a potential measure of peat condition, including evaluating the impacts of land-use and restoration as the seasonal amplitude and dynamics of surface oscillation vary as a function of management (e.g., Howie and Hebda, 2018). Due to the reliance of most studies on less frequent manual measurements, however, rather few studies have been able to assess the short-term dynamics of peat motion. Strack et al. (2006) used a mechanical method to measure surface elevation changes in a Canadian fen, and found that water table fluctuations explained 81–99% of surface level variations on shorter timescales (sub-weekly) whereas the accumulation of entrapped gas bubbles, by increasing peat buoyancy, caused the surface level to rise by up to 8 cm over longer periods, followed by rapid deceases when gases were released. For an undrained peatland in New Zealand, Fritz et al. (2008) recorded a mean annual surface oscillation of 15 cm, again driven largely by variations in water level, but with pronounced seasonal variations in behavior. In the wet season, surface oscillation was large and rapid in response to water level variation, and was attributed to floatation of the peat. In the dry season, elevation changes were smaller, and strongly lagged relative to water level changes, which the authors suggested was because elevation changes at these times were the result of compression and shrinkage. This hysteresis of elevation response to water level changes has been observed elsewhere, and over a range of timescales from individual rain events to seasons (e.g., Howie and Hebda, 2018). Zanello et al. (2011) also observed a strong dependency of short-term peat elevation change on WTD in a drained Italian peatland, with both water table and elevation changing rapidly, and with little evidence of hysteresis, in response to individual rain events.

Compared to these previous studies, ours is the first to provide insights into the high-frequency dynamics of multiple sites with contrasting land-use, as well as being the first from a tropical peatland system. Consistent with previous results, we find that WTD exerts a strong seasonal (**Figure 9**) and episodic (**Figure 10**) influence on peat elevation. These effects operate across a management gradient, from forests to drained agricultural land, although they were least evident in the forest sites. In the short-term, we observed the greatest response to

individual rain events in the deep-drained agricultural and plantation sites, where both water table and peat elevation rapidly rose in response to individual rain events, followed by a rapid decline to pre-event levels. This 'spiky' behavior, with little or no hysteresis between water table and peat elevation, resembles that observed for a drained cropland by Zanello et al. (2011), and reflects the efficient drainage of these systems. Similar but smaller-amplitude variations were observed in the less well-drained Hampangen Oil Palm site, while the burned scrubland sites, which lack active drainage, showed a more damped response, and some evidence of hysteresis. The lack of short-term elevation variation at the UPR Forest site contrasts with the more dynamic behavior observed in undisturbed temperate and boreal peatlands (Strack et al., 2006; Fritz et al., 2008; Howie and Hebda 2018). Tropical peat swamp forests differ from high-latitude peatlands in their dense vegetation cover, dense root layers and high lateral hydraulic conductivity, which could lead to differences in their capacity to move vertically in response to hydrological variations, although longer-term subsidence data do suggest that they respond dynamically to climatic variations on a multi-year timescale (Evans et al., in prep.). At this stage, we cannot rule out a possible methodological artifact as an explanation for the lack of measured short-term surface motion at the forest sites.

On longer timescales, we again observed major differences between sites under different management, and also between years, with the severe 2019 dry season leading to much greater peat shrinkage than the much wetter equivalent period in 2020 at all sites. As on episodic timescales, seasonal variations in peat surface elevation were strongly linked to water table and the overall degree of site drainage, with the deep-drained Misik Agriculture and oil palm sites experiencing elevation decreases of over 6 cm at the peak of the 2019 dry season. The burned sites, which are subject to unregulated drainage, also underwent substantial shrinkage at this time, whereas it appears that the poorly drained Hampangen Oil Palm and irrigated Kalampangan Agriculture sites were less affected (see below). The forest sites appeared (subject to the caveat noted above) to show the least vertical oscillation, consistent with apparently smaller water table drawdown. Since both the amplitude and rate of peat elevation change in response to rainfall events were clearly linked to peat hydrological status and management, our results suggest that monitoring of peat motion could provide an effective and low-cost basis for monitoring peat condition, including the outcome of restoration measures. Since peat elevation changes can also be detected using interferometric synthetic aperture radar (Alshammari et al., 2018; Hoyt et al., 2020) this finding opens up the possibility that satellite measurements of peat motion could, by linking with ground observations, provide a basis for the large-scale assessment of peat condition, and associated metrics including carbon balance.

Over the full period of measurements, we found clear evidence of net subsidence at some sites sites, and no evidence of accumulation at any site. Whereas Zanello et al. (2011) used a modeling approach to separate the 'reversible' and 'irreversible' elevation change, here we simply compared to the mean elevations during stable periods of the wet seasons at the start of 2019 and 2020. Nevertheless, it is clear that peat elevation at the deep-drained sites did not rebound in 2020 to the levels observed before the 2019 dry season, suggesting that the severe dry conditions encountered (WTDs of 2 m or more) led to irreversible compaction and peat oxidation. On the other hand, for the wetter 2020 dry season, net subsidence appears to have been minor at most sites, with the exception of the RePeat Burned site (where it remained much smaller than in 2019). Again, it appears subsidence was much lower at the irrigated Kalampangan site, and did not occur at the high water table Hampangen Oil Palm plantation, or at the two forest sites.

Implications for Tropical Peatland Management and Climate Change Mitigation

Given that that the method presented here is new, is still undergoing testing and refinement, and that two years represents a relatively short study period, we recognize that caution is needed when interpreting our results. Nevertheless, both short-term (episodic) and longer-term (seasonal and between-year) measurements of peat elevation change obtained by the camera system appear to provide information relevant to the understanding the effects of land-management on peat condition and function. In particular, the evidence of net subsidence at the more deeply drained sites are likely to be at least partly attributable to peat oxidation, rather than temporary shrink/swell, or longer-term compaction; most studies of tropical peatlands have concluded that over 50% of long-term subsidence in drained systems is due to oxidation (Murayama and Bakar, 1996; Hooijer et al., 2012). As high rates of peat oxidation are in turn associated with high CO_2 emissions, our observations from the Misik sites are consistent with other evidence that deep-drained tropical peatlands under plantation agriculture are major GHG emission sources (e.g., Tonks et al., 2017; Cooper et al., 2020; Jauhiainen et al., 2012; Carlson et al., 2017). Moderate to high subsidence levels at the burned sites suggest that these areas, which have unregulated drainage and are subject to dry season water table drawdown and wet season flooding (**Figure 9**) are also significant CO_2 emission sources. Conversely, low net subsidence at Hampangen and Kalampangan following the severe 2019 dry season suggest that these sites are likely to be much smaller CO_2 sources. At Hampangen this can be attributed to generally high water levels in the peat. While likely to be sub-optimal for productivity, we note that the mean WTD at this site, −0.37 m over the period November 2018 to September 2020, is in line with the Government of Indonesia's '40 cm' regulations for peatland protection (most recently SK.22/PPKL/PKG/PKL.July 0, 2017). At the Kalampangan Agricultural site, this was unlikely to have been the case during the 2019 dry season, when ditch water levels were observed to be below 2 m, yet subsidence (and by inference CO_2 emissions) seem to have been at least partly mitigated by surface irrigation. Although undertaken to support crop production, it is possible that this maintained moisture levels in the upper peat layer at a sufficient level to restrict oxidation. If correct, this has significant implications, as the Indonesian Peat Restoration Agency (BRG) has installed over 10,000 wells in

community-owned peatland areas since 2016 (BRG, 2019). These wells were constructed primarily to provide a source of water for fighting peat fires. However, in areas where water can be sustainably extracted from mineral aquifers below the peat, and used to maintain peat surface moisture levels during dry periods, it is possible that this could generate substantial emissions mitigation (as well as supporting crop production). To our knowledge, surface irrigation has not been considered previously as a form of climate change mitigation in tropical peatlands. While there are clearly risks in extracting water from aquifers below the peat, as well as financial and energy costs, the potential for targeted irrigation to reduce peat subsidence and carbon loss appears to merit further attention.

More generally, for peat under both oil palm and other agricultural cultivation, it is clear from our results that differences in water management between sites led to different rates of subsidence, and therefore likely to different rates of CO_2 emissions. While subsidence rates are less directly connected to methane (CH_4) emissions, these tend to be highest at permanently or seasonally waterlogged sites, where wetland-adapted plant species are present, and negligible when WTD exceeds 20–30 cm (Couwenberg et al., 2011). Information on WTD and peat elevation change obtained from the peat cameras, together with vegetation characteristics may therefore also be of use for inferring rates of CH_4 emission. At present, Intergovernmental Panel on Climate Change Tier 1 emissions inventory reporting methods (IPCC, 2014) provide only a single set of 'emission factors' for tropical peatlands under oil palm plantation, and another set of emission factors for tropical peatlands under all cropland other than paddy rice. In accordance with assessments of CO_2 and CH_4 fluxes from high-latitude peatlands (Couwenberg et al., 2011; Tiemeyer et al., 2020), as well as analyses of long-term subsidence from tropical peatlands (Hooijer et al., 2012; Evans et al., 2019) our analysis suggests that both subsidence and GHG emissions vary greatly within each land-use category, depending on the water management. This is important, as it suggests that measures aimed at raising water levels or increasing near-surface soil moisture levels could–while unlikely to halt emissions entirely–generate substantial climate change mitigation benefits via reduced CO_2 emissions, which cannot currently be captured via IPCC Tier 1 inventory reporting methods. The development of more sophisticated 'Tier 2' reporting methods, describe the effects of improved water management in managed tropical peatland landscapes, would enable the benefits of these mitigation measures to be captured in project level and national level emissions reporting, and might therefore help to reconcile the competing objectives of climate change mitigation and enhancement of livelihoods in these threatened, carbon-rich ecosystems.

CONCLUSION

The 'peat camera' system described in this paper has provided new insights into the behavior of tropical peatlands, revealing a range of highly dynamic peat behaviors on timescales ranging from sub-daily to annual, and linked to management, hydrological and climatic factors. It offers an accurate, reliable and low-maintenance method for simultaneous measurement of peat elevation and water table change, and may also be an effective proxy measure of the peatland carbon balance. The simplicity and low cost of the system (in the region of USD 300) compares favourably to commercial systems for monitoring peat motion and water table, and is orders of magnitude cheaper than eddy covariance systems for CO_2 flux monitoring. At present, the method has only been tested at a small number of sites, and over a limited time period, during which we made a number of modifications to improve reliability and reduce data loss, but the system requires further testing and refinement, and streamlining of the image data processing. Provided that these challenges can be overcome, we believe that the method has widespread potential application, particularly for monitoring of peatlands in remote areas, by groups with limited budgets for research and monitoring, and at a greater number of locations than could be achieved at the same cost using existing technologies. Increasing the spatial coverage of observations could in turn facilitate the implementation of satellite-based monitoring systems by providing robust and representative ground-based calibration and test data. Such large-scale and effective monitoring is urgently required to support the future management, mitigation of GHG emissions and restoration of one of the terrestrial biosphere's most distinctive ecosystems, and largest carbon stores.

DATA AVAILABILITY STATEMENT

The raw data supporting the conclusions of this article will be made available by the authors, without undue reservation.

AUTHOR CONTRIBUTIONS

CE led the study and drafted the manuscript with AJ-S. The peat motion camera concept was conceived by AG in discussion with CE, and the system was designed and tested by NC, with additional refinements by AJ-S and AJ. Image processing scripts were written by ZM with support from AG. AJ and AJ-S led the Central Kalimantan field deployments, and AJ led manual subsidence measurements. LK, ML, KK, and MH contributed to wider system deployment and testing. SS, SP, and SE contributed to the establishment of the field program via the PASSES and SUSTAINPEAT projects, and provided expertize on peatland processes. AJ-S, JW, and AR undertook image processing, quality assurance and data management. All authors read, commented on and contributed to the final manuscript.

FUNDING

The development and operation of the peat motion cameras was undertaken as part of the project PASSES: Peatland Assessment

in Southeast Asia by Satellite, funded by the United Kingdom Space Agency International Partnership Program. Field deployments in Central Kalimantan were undertaken at field sites established by the project SUSTAINPEAT: Overcoming barriers to sustainable livelihoods and environments in smallholder agricultural systems on tropical peatland, funded by United Kingdom Research and Innovation via the Global Challenges Research Fund and the Biotechnology and Biological Sciences Research Council (BBSRC) Grant number BB/P023533/1. CE received additional support from the UK Natural Environment Research Council grant Sustainable Use of Natural Resources to Improve Human Health and Support Economic Development (SUNRISE, Grant No. NE/R000131/1) ML was supported by a Natural Environment Research Council PhD studentship as part of the STARS Doctoral Training Center (Grant number NE/M009106/1). Groundwater level data used at the RePeat Burned site (December 2018 to September 2019) were obtained from the SATREPS: Science and Technology Research Partnership for Sustainable Development project 'Wild fire and carbon management in peat-forest in Indonesia' funded by Japan Science and Technology Agency and Japan International Cooperation Agency.

ACKNOWLEDGMENTS

We are grateful to the Ministry of Research Technology and Higher Education of Indonesia (RISTEKDIKTI) for their support of the SUSTAINPEAT project. We would also like to thank the University of Palangka Raya field staff who supported the measurement program, and the landowners who hosted our field equipment.

REFERENCES

Alshammari, L., Large, D. J., Boyd, D. S., Sowter, A., Anderson, R., Andersen, R., et al. (2018). Long-term peatland condition assessment via surface motion monitoring using the ISBAS DInSAR technique over the Flow Country, Scotland. *Remote Sensing*, 10, 1103. doi:10.3390/rs10071103

BRG (2019). Three years of peat restoration indonesia badan restorasi gambut. Available at: https://brg.go.id/wp-content/uploads/2019/06/3-years-peatland-restoration-inindonesia_eng-pmk_without-track-changes_edit-layout.pdf. (Accessed November 15, 2020)

Carlson, K. M., Gerber, J. S., Mueller, N. D., Herrero, M., MacDonald, G. K., Brauman, K. A., et al. (2017). Greenhouse gas emissions intensity of global croplands. *Nat. Clim. Change* 7, 63–68. doi:10.1038/NCLIMATE3158

Cheyne, S. M., Sastramidjaja, W. J., Muhalir Rayadin, Y., and MacDonald, D. W. (2016). Mammalian communities as indicators of disturbance across Indonesian Borneo. *Glob. Ecol. Conserv.* 7, 157–173. doi:10.1016/j.gecco.2016.06.002

Cooper, H. V., Evers, S., Aplin, P., Crout, N., Bin Dalahan, M. P., and Sjögersten, S. (2020). Greenhouse gas emissions resulting from conversion of peat swamp forest to oil palm plantation. *Nat. Commun.* 11, 407. doi:10.1038/s41467-020-14298-w

Couwenberg, J., Thiele, A., Tanneberger, F., Augustin, J., Bärisch, S., Dubovik, D., et al. (2011). Assessing greenhouse gas emissions from peatlands using vegetation as a proxy. *Hydrobiologia* 674, 67–89. doi:10.1007/s10750-011-0729-x

Dargie, G. C., Lewis, S. L., Lawson, I. T., Mitchard, E. T., Page, S. E., Bocko, Y. E., et al. (2017). Age, extent and carbon storage of the central Congo Basin peatland complex. *Nature* 542, 86–90. doi:10.1038/nature21048

de Louw, P. G., Bootsma, H., Kooi, H., Kramer, M., and Erkens, G. (2018). Land subsidence by peat oxidation leads to enhanced salinization through boils in Dutch polders. *E3S Web Conf.* 54, 00007. doi:10.1051/e3sconf/20185400007

Deverel, S. J., and Leighton, D. A. (2010). Historic, recent, and future subsidence, sacramento-san Joaquin delta, California, USA. *San Francisco Estuary Watershed Sci.* 8, 1–23. doi:10.15447/sfews.2010v8iss2art1

Dise, N. B. (2009). Environmental science peatland response to global change. *Science* 326, 810–811. doi:10.1126/science.1174268

Dommain, R., Couwenberg, J., Glaser, P. H., Joosten, H., and Suryadiputra, I. N. N. (2014). Carbon storage and release in Indonesian peatlands since the last deglaciation. *Quat. Sci. Rev.* 97, 1–32. doi:10.1016/j.quascirev.2014.05.002

Erkens, G., van der Meulen, M. J., and Middelkoop, H. (2016). Double trouble: subsidence and CO_2 respiration due to 1,000 years of Dutch coastal peatlands cultivation. *Hydrogeology J.* 24, 551–568. doi:10.1007/s10040-016-1380-4

Evans, C. D., Page, S. E., Jones, T., Moore, S., Gauci, V., Laiho, R., et al. (2014). Contrasting vulnerability of drained tropical and high-latitude peatlands to fluvial loss of stored carbon. *Glob. Biogeochem. Cycles* 28, 1215–1234. doi:10.1002/2013gb004782

Evans, C. D., Williamson, J. M., Kacaribu, F., Irawan, D., Suardiwerianto, Y., Hidayat, M. F., et al. (2019). Rates and spatial variability of peat subsidence in Acacia plantation and forest landscapes in Sumatra, Indonesia. *Geoderma* 338, 410–421. doi:10.1016/j.geoderma.2018.12.028

FAOSTAT (2018). *Food and agriculture organisation of the united nations.* Rome: FAOSTAT.

Fiaschi, S., Holohan, E. P., Sheehy, M., and Floris, M. (2019). PS-InSAR analysis of Sentinel-1 data for detecting ground motion in temperate oceanic climate zones: a case study in the Republic of Ireland. *Remote Sens.* 11, 348. doi:10.3390/rs11030348

Friedlingstein, P., Jones, M., O'sullivan, M., Andrew, R., Hauck, J., Peters, G., et al. (2019). Global carbon budget 2019. *Earth Syst. Sci. Data* 11, 1783–1838. doi:10.5194/essd-11-1783-2019

Fritz, C., Campbell, D. I., and Schipper, L. A. (2008). Oscillating peat surface levels in a restiad peatland, New Zealand—magnitude and spatiotemporal variability. *Hydrol. Process.* 22, 3264–3274. doi:10.1002/hyp.6912

Hirano, T., Segah, H., Kusin, K., Limin, S., Takahashi, H., and Osaki, M. (2012). Effects of disturbances on the carbon balance of tropical peat swamp forests. *Glob. Change Biol.* 18, 3410–3422. doi:10.1111/j.1365-2486.2012.02793.x

Hooijer, A., Page, S., Jauhiainen, J., Lee, W. A., Lu, X. X., Idris, A., et al. (2012). Subsidence and carbon loss in drained tropical peatlands. *Biogeosciences* 9, 1053–1071. doi:10.5194/bg-9-1053-2012

Howie, S. A., and Hebda, R. J. (2018). Bog surface oscillation (mire breathing): a useful measure in raised bog restoration. *Hydrol. Process.* 32, 1518–1530. doi:10.1002/hyp.11622

Hoyt, A. M., Chaussard, E., Seppalainen, S. S., and Harvey, C. F. (2020). Widespread subsidence and carbon emissions across Southeast Asian peatlands. *Nat. Geosci.* 13, 435–440. doi:10.1038/s41561-020-0575-4

Hutchinson, J. N. (1980). Record of peat wastage in the east-anglian fenlands at Holme Post, 1848–1978 AD. *J. Ecol.* 68, 229–249.

IPCC (2014). *2013 supplement to the 2006 IPCC guidelines for national greenhouse gas inventories: Wetlands*. Switzerland: Intergovernmental Panel on Climate Change.

Jauhiainen, J., Hooijer, A., and Page, S. E. (2012). Carbon dioxide emissions from an *Acacia* plantation on peatland in Sumatra, Indonesia. *Biogeosciences* 9, 617–630. doi:10.5194/bg-9-617-2012

Leifeld, J., and Menichetti, L. (2018). The underappreciated potential of peatlands in global climate change mitigation strategies. *Nat. Commun.* 9, 1071. doi:10.1038/s41467-018-03406-6

Marshall, C., Large, D. J., Athab, A., Evers, S. L., Sowter, A., Marsh, S., et al. (2018). Monitoring tropical peat related settlement using ISBAS InSAR, Kuala Lumpur International Airport (KLIA). *Eng. Geology.* 244, 57–65. doi:10.1016/j.enggeo.2018.07.015

Morton, P. A., and Heinemeyer, A. (2019). Bog breathing: the extent of peat shrinkage and expansion on blanket bogs in relation to water table, heather management and dominant vegetation and its implications for carbon stock assessments. *Wetlands Ecol. Manage.* 27, 467–482. doi:10.1007/s11273-019-09672-5

Murayama, S., and Bakar, Z. A. (1996). Decomposition of tropical peat soils, estimation of *in situ* decomposition by measurement of CO2 flux. *Jarq-jpn. Agr. Res. Q.* 30, 153–158.

Page, S. E., Siegert, F., Rieley, J. O., Boehm, H. D., Jaya, A., and Limin, S. (2002). The amount of carbon released from peat and forest fires in Indonesia during 1997. *Nature* 420, 61–65. doi:10.1038/nature01131

Page, S. E., and Baird, A. J. (2016). Peatlands and global change: response and resilience. *Annu. Rev. Environ. Resour.* 41, 35–57. doi:10.1146/annurev-environ-110615-085520

Page, S. E., Rieley, J. O., and Banks, C. J. (2011). Global and regional importance of the tropical peatland carbon pool. *Glob. Change Biol.* 17, 798–818. doi:10.1111/j.1365-2486.2010.02279.x

Page, S., Hosciło, A., Wösten, H., Jauhiainen, J., Silvius, M., Rieley, J., Ritzema, H., et al. (2009). Restoration ecology of lowland tropical peatlands in Southeast Asia: current knowledge and future research directions. *Ecosystems* 12, 888–905. doi:10.1007/s10021-008-9216-2

Rublee, E., Rabaud, V., Konolige, K., and Bradski, G.(2011). ORB: an efficient alternative to SIFT or SURF. in Proceedings of the IEEE international conference on computer vision (ICCV). Barcelona, Spain.

Smith, P. (2014). "Agriculture, forestry and other land use (AFOLU)," in *Climate change 2014: mitigation of climate change. Contribution of working group III to the fifth assessment report of the intergovernmental panel on climate change.* (Cambridge, United Kingdom and New York, NY: Cambridge University Press).

Stephens, J., Allan, L., and Chen, E. (1984). Organic soil subsidence. *Rev. Eng. Geology.* 6, 107–122.

Strack, M., Kellner, E., and Waddington, J. M. (2006). Effect of entrapped gas on peatland surface level fluctuations. *Hydrol. Process.* 20, 3611–3622. doi:10.1002/hyp.6518

Strack, M., and Waddington, J. M. (2007). Response of peatland carbon dioxide and methane fluxes to a water table drawdown experiment. *Glob. Biogeochem. Cycles* 21, GB1007. doi:10.1029/2006gb002715

Susanti, R. D., and Anjasmara, I. M. (2019). Analysing peatland subsidence in Pelalawan Regency, Riau using DInSAR method. *IPTEK J. Proc. Ser.* 2, 60–64. doi:10.12962/j23546026.y2019i2.5308

Tiemeyer, B., Freibauer, A., Borraz, E. A., Augustin, J., Bechtold, M., Beetz, S., et al. (2020). A new methodology for organic soils in national greenhouse gas inventories: data synthesis, derivation and application. *Ecol. Indicators* 109, 105838. doi:10.1016/j.ecolind.2019.105838

Tonks, A. J., Aplin, P., Beriro, D. J., Cooper, H., Evers, S., Vane, C. H., et al. (2017). Impacts of conversion of tropical peat swamp forest to oil palm plantation on peat organic chemistry, physical properties and carbon stocks. *Geoderma.* 289, 36–45. doi:10.1016/j.geoderma.2016.11.018

Turetsky, M. R., Benscoter, B., Page, S., Rein, G., van der Werf, G. R., and Watts, A. (2015). Global vulnerability of peatlands to fire and carbon loss. *Nat. Geosci.* 8, 11–14. doi:10.1038/ngeo2325

Wösten, J. H. M., Ismail, A. B., and Van Wijk, A. L. M. (1997). Peat subsidence and its practical implications: a case study in Malaysia. *Geoderma.* 78, 25–36.

Wijedasa, L. S., Sloan, S., Page, S. E., Clements, G. R., Lupascu, M., and Evans, T. A. (2018). Carbon emissions from South-East Asian peatlands will increase despite emission-reduction schemes. *Glob. Chang Biol.* 24, 4598–4613. doi:10.1111/gcb.14340

Zanello, F., Teatini, P., Putti, M., and Gambolati, G. (2011). Long term peatland subsidence: experimental study and modeling scenarios in the Venice coastland. *J. Geophys. Res.* 116, F04002. doi:10.1029/2011JF002010

Zhou, Z., Li, Z., Waldron, S., and Tanaka, A. (2019). InSAR time series analysis of L-band data for understanding tropical peatland degradation and restoration. *Remote Sens.* 11, 2592. doi:10.3390/rs11212592

Conflict of Interest: The authors declare that the research was conducted in the absence of any commercial or financial relationships that could be construed as a potential conflict of interest.

frontiers in Earth Science

ORIGINAL RESEARCH
published: 26 March 2021
doi: 10.3389/feart.2021.617662

Identifying Drivers Behind Spatial Variability of Methane Concentrations in East Siberian Ponds

Zoé Rehder[1,2]*, *Anna Zaplavnova*[3,4] *and Lars Kutzbach*[5]

[1] Department of the Land in the Earth System, Max Planck Institute for Meteorology, Hamburg, Germany, [2] International Max Planck Research School on Earth System Modeling, Hamburg, Germany, [3] Department of Geology and Geophysics, Novosibirsk State University, Novosibirsk, Russia, [4] The Trofimuk Institute of Petroleum Geology and Geophysics, Siberian Branch of the Russian Academy of Sciences, Novosibirsk, Russia, [5] Institute of Soil Science, Center for Earth System Research and Sustainability (CEN), Universität Hamburg, Hamburg, Germany

Waterbody methane emissions per area are negatively correlated with the size of the emitting waterbody. Thus, ponds, defined here as having an area smaller than $8 \cdot 10^4$ m^2, contribute out of proportion to the aquatic methane budget compared to the total area they cover and compared to other waterbodies. However, methane concentrations in and methane emissions from ponds show more spatial variability than larger waterbodies. We need to better understand this variability to improve upscaling estimates of freshwater methane emissions. In this regard, the Arctic permafrost landscape is an important region, which, besides carbon-rich soils, features a high pond density and is exposed to above-average climatic warming. We studied 41 polygonal-tundra ponds in the Lena River Delta, northeast Siberia. We collected water samples at different locations and depths in each pond and determined methane concentrations using gas chromatography. Additionally, we collected information on the key properties of the ponds to identify drivers of surface water methane concentrations. The ponds can be categorized into three geomorphological types with distinct differences in drivers of methane concentrations: polygonal-center ponds, ice-wedge ponds and larger merged polygonal ponds. All ponds are supersaturated in methane, but ice-wedge ponds exhibit the highest surface water concentrations. We find that ice-wedge ponds feature a strong stratification due to consistently low bottom temperatures. This causes surface concentrations to mainly depend on wind speed and on the amount of methane that has accumulated in the hypolimnion. In polygonal-center ponds, high methane surface concentrations are mostly determined by a small water depth. Apart from the influence of water depth on mixing speed, water depth controls the overgrown fraction, the fraction of the pond covered by vascular plants. The plants provide labile substrate to the methane-producing microbes. This link can also be seen in merged polygonal ponds, which furthermore show the strongest dependence on area as well as an anticorrelation to energy input indicating that stratification influences the surface

OPEN ACCESS

Edited by:
Annalea Lohila,
University of Helsinki, Finland

Reviewed by:
Ronny Lauerwald,
Université Paris-Saclay, France
Sophia Burke,
University of New Hampshire, United States

***Correspondence:**
Zoé Rehder
zoe.rehder@mpimet.mpg.de

Specialty section:
This article was submitted to Biogeoscience, a section of the journal Frontiers in Earth Science

Received: *15 October 2020*
Accepted: *01 March 2021*
Published: *26 March 2021*

Citation:
Rehder Z, Zaplavnova A and Kutzbach L (2021) Identifying Drivers Behind Spatial Variability of Methane Concentrations in East Siberian Ponds. Front. Earth Sci. 9:617662. doi: 10.3389/feart.2021.617662

water methane concentrations in larger ponds. Overall, our findings underpin the strong variability of methane concentrations in ponds. No single driver could explain a significant part of the variability over all pond types suggesting that more complex upscaling methods such as process-based modeling are needed.

Keywords: ponds, methane, polygonal tundra, permafost, spatial variability, Lena river delta, ice-wedge polygons, waterbodies

1. INTRODUCTION

Ponds are small waterbodies that are often defined by their area with varying thresholds. Here, we follow the Ramsar classification scheme, scheme, which sets a comparably high limit of $8 \cdot 10^4$ m^2 (Ramsar Convention Secretariat, 2016). Notably, ponds are the most common waterbody type in the Arctic (Muster et al., 2017) and emit more methane (CH_4) per area than larger lakes (Juutinen et al., 2009; Downing, 2010; Holgerson and Raymond, 2016; Wik et al., 2016). Thus, they are important contributors to the methane budget of the Arctic. The variability of methane emissions and concentrations is also higher in ponds than it is in lakes (Juutinen et al., 2009; Laurion et al., 2010; Sepulveda-Jauregui et al., 2015; Holgerson and Raymond, 2016) and uncertainty remains as to what causes the variability. In this study, we focus on identifying drivers of local methane concentration variability. A good grasp on the main mechanisms responsible for spatial variability is essential to improve upscaling and modeling of water methane emissions.

Previous upscaling efforts of methane emissions from lakes and ponds differ considerably. Holgerson and Raymond (2016) estimate global waterbody methane emissions of 12 Tg CH_4-C yr^{-1} through diffusion only. Accounting additionally for ebullition Wik et al. (2016) estimates that ponds and lakes north of 50 °N alone emit the same amount. DelSontro et al. (2018), on the other hand, state an estimate for global emissions from lakes and reservoirs of 112 Tg CH_4-C yr^{-1}. This is nearly ten times as high as the estimate from Holgerson and Raymond (2016) who exclude reservoirs but still assume a larger total waterbody area than DelSontro et al. (2018). All three estimates are all based on varying total areas of lakes and ponds, but part of the spread can also be explained by varying upscaling methods. Each study assumes a different main predictor of water methane concentrations: While Holgerson and Raymond (2016) use size classes and Wik et al. (2016) waterbody type as the predictor, DelSontro et al. (2018) use chlorophyll (a proxy for the trophic state of the waterbody and its productivity). This approach is supported by Rinta et al. (2017) who find higher methane emissions from (more productive) central European as opposed to boreal lakes. Contrastingly, Arctic waterbodies tend to still have significant carbon emissions but low primary productivity due to low energy input and due to nutrient deficiencies (Anderson et al., 2001; Hamilton et al., 2001; Ortiz-Llorente and Alvarez-Cobelas, 2012). These waterbodies are very sensitive to changes in allochthonous carbon and nutrient inputs, changes we expect due to climate-change-induced permafrost thaw (Vonk et al., 2015; Burpee et al., 2016). Note, that small absolute changes in inputs have a stronger impact the smaller the waterbody is due to a smaller water volume.

Lake size, with depth being a better predictor than area, is the main predictor in a study of small Finnish lakes (Juutinen et al., 2009). Secondary drivers include the oxygen status and nutrient availability within the lake. Even when considering these drivers, the authors find a large variability in methane concentrations ($r^2_{adj.} < 0.4$ for surface concentrations) with an average summer surface concentration of 0.25 μmol L^{-1}. Higher average concentrations have been found in the Western Siberian Lowlands (0.98 μmol L^{-1} in waterbodies larger than $5 \cdot 10^{-4}$ km^2 and 9 μmol L^{-1} in waterbodies smaller than $5 \cdot 10^{-4}$ km^2). Note that small waterbodies have concentrations one order of magnitude greater than larger lakes. Even though this relation is striking, the spread around it is still broad ($r^2 < 0.3$) (Polishchuk et al., 2018).

Both the study by Polishchuk et al. (2018) and the study by Juutinen et al. (2009) cover a large area. Focusing on a specific region reduces driver variability due to deviating environmental conditions. For the polygonal tundra of northern Canada, Negandhi et al. (2013) found that methane concentration depend on waterbody type (**Figure 1**): In the polygonal tundra, waterbodies can form in the center of a polygon (polygonal-center ponds) or along the edges of a polygon. These edges are underlain by ice wedges, so ice-wedge ponds still have ice at their bottom. According to Negandhi et al. (2013), ice-wedge ponds exhibit significantly higher methane emissions than polygonal-center ponds, which contain a higher number of methane-consuming microbes (methanotrophs) and more dissolved oxygen, while the methane-producing microbes (methanogens) in ice-wedge ponds are more adapted to high substrate availability. But even when separating by pond type, the standard deviation of the surface methane concentrations is still approximately as high as the respective mean, indicating that there is still strong variation in surface methane concentrations within each group which needs an explanation.

Polygonal tundra is prevalent throughout the lowlands of the Arctic, and often peatlands form in these patterned-ground landscapes characterized by a pronounced microrelief (French, 2007; Minayeva et al., 2016). Especially in the centers of the polygons, where the water table is higher than along the rims of the polygons, peat forms. These landscapes feature a high density of small waterbodies and carbon-rich soils. Here, we build on the work by Negandhi et al. (2013) and investigate what drives variability in methane concentrations of ponds in the polygonal tundra of Eastern Siberia. We include a wide range of variables, from wind speed over vegetation cover to

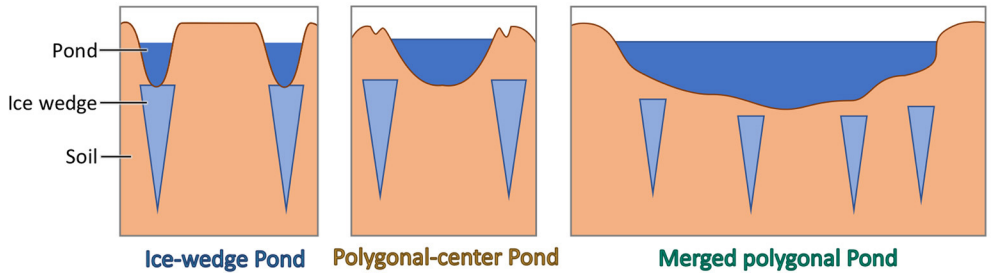

FIGURE 1 | Schematic of the different pond types in the polygonal tundra. Ice-wedge ponds form along the edges of polygons on top of ice wedges, have a frozen bottom and have often an elongated shape and a steep slope. Polygonal-center ponds form in between ice wedges, in the center of the polygons. They tend to be nearly circular. If several polygons subside, merged polygonal ponds form. These ponds are the largest pond type of the three.

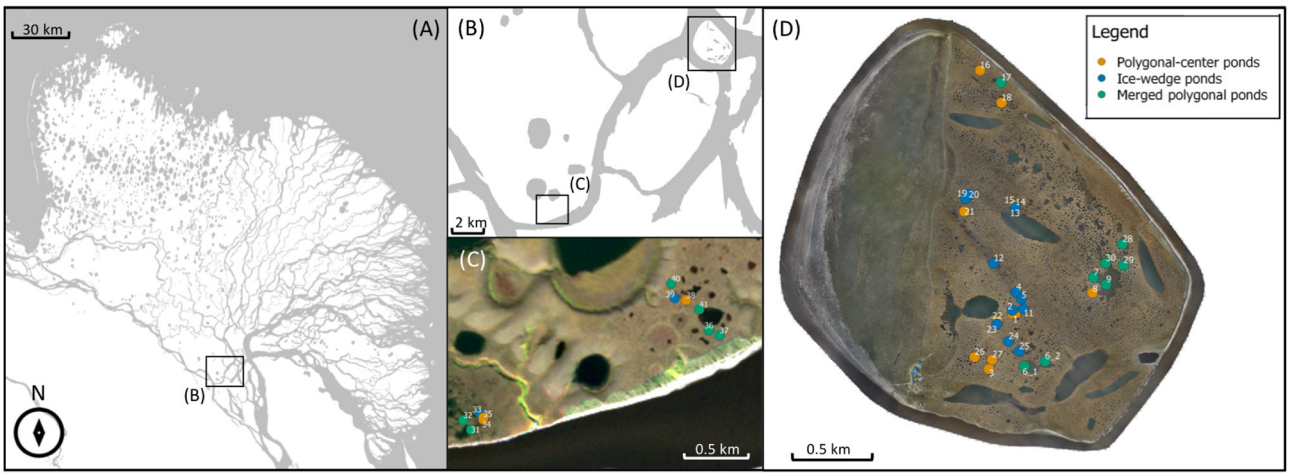

FIGURE 2 | Overview of study region. The Lena River Delta **(A)** is located in Eastern Siberia at the coast of the Laptev Sea. Samoylov and Kurungakh Island are situated in the southern end of the Delta **(B–D)**. Maps in **(A,B)** adapted from OpenStreetMap contributors, under Open Database License. Each dot represents one sampled pond **(C,D)**.

geomorphological pond type. Notably, we also include the effect of submerged mosses on methane-concentration variability. These mosses photosynthesize and create an oxic zone at the bottom of the pond, where methane can be oxidized. This layer is often strongly enriched with methane, and concentrations drop steeply above the moss layer (Liebner et al., 2011; Knoblauch et al., 2015). Though these effects are known, it is unknown how submerged mosses impact methane concentrations on the scale of a whole pond.

2. MATERIALS AND METHODS

2.1. Site Description

We studied 41 ponds on the islands Samoylov and Kurungakh (**Figure 2**). The two islands are located in the Lena River Delta of Eastern Siberia in a zone of continuous permafrost with an annual mean temperature of −12.5 °C (Boike et al., 2013). The delta can be divided into three terraces of different genesis. The first terrace is the youngest, it formed in the Holocene through fluvial deposition. This terrace is the wettest, has the most pronounced microtopography due to active ice-wedge polygon formation and consequently the highest density of small-scale waterbodies (Schwamborn et al., 2002; Schneider et al., 2009; Muster et al., 2012). Both Samoylov and the southern tip of Kurungakh belong to the first terrace, and here we sampled 35 ponds in total. Six additional ponds were measured further north on Kurungnakh on the third terrace. The third terrace consists of sandy deposits overlain by an ice complex which formed in the Pleistocene. This organic-rich ice complex then is often overlain again by Holocene deposits (Schwamborn et al., 2002; Wetterich et al., 2008). The locations we sampled on the third terrace exhibited only weak polygonal structures, and especially smaller waterbodies were more sparse than on the first terrace. Still, overall roughly 20% percent of the delta (excluding the river) are covered by waterbodies—on the first terrace we find most small waterbodies while the third terrace has a higher fraction of large thermokarst lakes (Muster et al., 2012). The second terrace features less ponds and has not been sampled.

We divided the waterbodies into three groups based on their geomorphology (**Figure 1**). Ponds which formed in the center of

a single polygon with intact rims are labeled polygonal-center ponds. These ponds are mostly circular and only seldomly deeper than one meter. Ice-wedge ponds are ponds which formed on top of a thawing ice wedge along the edge of one or several polygons. These ponds tend to have an elongated shape and highly variable water depth with steep margins. Lastly, if several neighboring polygons including their rims are inundated, we call them merged polygonal ponds. These ponds are the largest and differ most in size. They also usually have the gentlest slope. We sampled 15 polygonal-center ponds with areas ranging from 24 to 200 m^2, 13 ice-wedge ponds with areas between 13 and 252 m^2, and 14 merged polygonal ponds (area range 214–24, 301 m^2).

In the shallow parts and along the margins of all pond types, vascular plants species such as Carex aquatilis or Artcophila fulva grow (Knoblauch et al., 2015). On the bottom of many ponds, submerged brown mosses form a thick layer (Liebner et al., 2011; Knoblauch et al., 2015).

2.2. Gas Concentration Measurements

We conducted the field measurements on 22 days between mid-July and the end of August during mid-day to afternoon. In each pond several water samples were taken within an hour. The number of samples was dependent on ground-cover heterogeneity: The ground of a pond was either covered by vegetation like vascular plants or submerged mosses or vegetation free. For each pond, we took at least one sample over each ground-cover type, on average we took two samples. In total, we collected 116 surface water sample, 44 samples over sediment, 37 over moss, and 33 in the overgrown part of ponds. The overgrown fraction got sampled least, as it covers a smaller part of the average pond than mosses. Most samples were taken over sediment, because most of the area of larger ponds has bare ground. To get a better estimate by including more spatial variability, in large ponds surface concentrations over sediment were taken more than once. Water samples were taken through three aluminum tubes which were fixed to a larger 2 m pipe. To this pipe, two floating bodies were attached (see **Supplementary Figure 1**). We carefully placed the pipe in the pond away from the margin with little disturbance of the water. Up to three samples were taken at one spot within the pond: One five centimeters below the water surface through the first aluminum tube; one at the bottom of the pond through a second aluminum tube which end could be lowered; and, if the water was deeper than about half a meter, one additional sample was taken at about 55 cm depth through a third aluminum tube. Water was sucked through the respective tube with 50 mL syringes. After flushing the syringes, a 30 mL water sample was inserted into 50 mL injection bottles, which, beforehand, had been evacuated and then filled with nitrogen. The samples were stored dark between sampling and measuring to avoid photolysis and microbial breakup of dissolved organic carbon. The gas in the headspace of the injection bottles was analyzed within 12 h of sampling using a gas chromatograph (Agilent GC 7890, Agilent Technologies, Germany) with an flame ionization detector (FID). The headspace pressure in the injection bottle was measured with a digital manometer (LEO1, Keller, Switzerland). We estimate a loss of methane due to oxidation between sampling and gas chromatography measurement well below 5%. For this estimate, we use the mean potential methane oxidation rate for Alaskan non-yedoma lakes as determined by Martinez-Cruz et al. (2015) and the approach of the same authors to infer the *in-situ* oxidation rates by a double Monod model.

We computed the methane and carbon dioxide concentrations using the measured partial pressure of the respective gas in the headspace of the injection bottle, the ideal gas law and Henry's law with a temperature-dependent Henry's constant (Sander, 2015). The gas content of each injection bottle was measured at least twice.

2.3. Environmental Sampling

Using the handheld meter WTW Multi 340i (Xylem Analytics, Germany) and, on the last day of measurements, a WTW Multi 350i, equipped with a CellOx325 probe we measured dissolved oxygen in the pond water and water temperature with a SenTix41 probe. After each water sampling, we estimated the thaw depth of the ponds by driving a metal rod into the sediment until it hits the frozen ground. To assess water depth, we submerged a water-level logger Mini-Diver (DI501, Schlumberger Water Services, Netherlands) in the middle of the ponds. This diver measured temperature and hydrostatic pressure. Using a second diver which measured atmospheric pressure and the difference between the hydrostatic and atmospheric pressure, we computed water depth.

In each pond, we collected two subaquatic top-sediment samples near the shore. The sediment sampling was done directly after the water sampling. According to Knoblauch et al. (2015), the top sediment exhibits higher methane production rates than deeper soil layers. We removed large roots from the samples, dried the sample for 24 h at 105°C and measured the sample mass. We then determined the organic fraction of the sample by burning it in a muffle furnace for 4 h at 550°C and remeasuring the mass.

For incoming short-wave radiation, data from a four-component net radiation sensor (NR01, Campell Scientific, UK) was used. Wind speed was measured with a omnidirectional ultrasonic anemometer (R3-50, Gill Instruments, UK). Both of these instruments were stationary installed on Samoylov Island, data was recorded at half-hourly intervals.

2.4. Imagery

We used an orthophoto map of Samoylov and Kurungakh obtained in 2016 (Kartoziia, 2019) to determine the area of each pond, the area covered by moss and the area overgrown by plants. The map has a resolution of 0.05 m px^{-1} thus providing enough detail to differentiate between surface types (see **Figure 3**). The orthophoto map was loaded into the GIS software ArcGIS 10.2.2, in which the ground-cover types were circled manually. The calculations of the enclosed areas were made in automatic mode in the GIS software QGIS. For very small ponds and for quality control, the areas computed through imaginary were compared to measurements of the pond diameter (see **Supplementary Table 1**) and to measurements of the width of the overgrown margin taken during the measurement campaign with a measuring tape. When possible, we also visually estimated

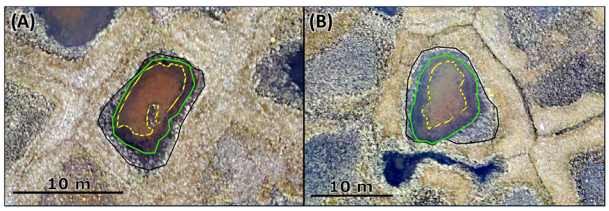

FIGURE 3 | Excerpt of the orthophoto (**Figure 2D**) shows two exemplary polygonal-center ponds, panel **(A)** shows pond 3, panel **(B)** shows pond 21. Both are located on Samoylov Island. The black line marks the edge of the pond, the green line delimits the overgrown area, and the yellow dashed line marks the moss-covered parts of the pond.

the moss-covered fraction, to compare with the orthophoto map. For ponds, where the orthophoto map resolution was insufficient, the area approximated by the tape measurements was used.

2.5. Statistical Analysis

For each time a pond was measured (water and environmental sampling), we averaged all measurements of surface methane concentrations and computed the standard deviation. To assign a standard deviation to those ponds with only one sample, we performed a linear regression between the standard deviation and the mean concentration of the ponds with more than one sample ($R^2 = 0.8$) and used the regression to predict the standard deviation of the ponds with one sample.

As a measure of correlation we applied the Kendall rank correlation index (Knight, 1966). The advantage of this Kendall's tau is that it does not assume a linear relation between the two variables in question. This is achieved by always comparing a pair of two points: If both variables show the same trend (increase or decrease) between two points, it is counted toward the concordant pairs. If one variable shows an increase and the other a decrease, the pair is counted toward the discordant pairs. The index then is computed as the difference between the concordant and the discordant pairs divided by the absolute number of pairs while accounting for ties. Analogously to the more common Pearson correlation, an index of 1 indicates a strong positive correlation, −1 indicates a strong negative correlation, and 0 indicates no correlation.

To investigate the relation between methane concentrations and individual drivers in depth, we used linear regressions based on ordinary least squares, with log-transformed variables when looking at the relation between pond area and surface methane concentrations. To evaluate the goodness of the fit, we utilize the error on the slope parameter and the root mean squared error (RMSE) as well as the predictive R^2. The predictive R^2 gives a measure of how well the regression model predicts new observations. It is determined by removing one measurement from the dataset, redoing the regression and predicting the removed measurement. After repeating this procedure for all measurements in the dataset, the predictive R^2 is computed using the true and the predicted values of the target variable. The predictive R^2 is sensitive to overfitting.

To determine if two distributions are statistically different we used the Kolmogorov–Smirnov test (Hodges, 1958), which is a general, non-parametric test, which is sensitive both to the shape and to the location of a distribution. All analysis was done in python 3.6 using the packages numpy 1.17 (Harris et al., 2020), scipy 1.5 (Virtanen et al., 2020), scikit learn 0.21 (Pedregosa et al., 2011), and matplotlib 3.2 (Hunter, 2007).

2.6. Equilibrium Concentrations

The dissolved gas concentrations of methane and carbon dioxide for equilibrium conditions were computed using the mean measured water temperature, the mean air pressure, the mean atmospheric methane and carbon dioxide concentrations as measured by a nearby eddy-covariance station. Using a temperature-dependent Henry's constant $H(T)$ (Sander, 2015), the concentrations were computed via

$$c = H(T) \cdot p, \tag{1}$$

where c is the equilibrium concentration in water, and p is the partial pressure (atmospheric pressure multiplied by the mole fraction of methane or carbon dioxide).

3. RESULTS

Median concentrations in ice-wedge, polygonal-center and merged polygonal ponds, respectively, are 2.4 μmol L^{-1} (25–75th percentile: 0.9–7.1 μmol L^{-1}), 0.6 μmol L^{-1} (25–75th percentile: 0.4–1.5 μmol L^{-1}) and 0.7 μmol L^{-1} (25–75th percentile: 0.5–1.2 μmol L^{-1}). All these values are far higher than the average methane equilibrium concentration of 0.004 μmol L^{-1}, which was computed using the mean water temperature of 9.7 °C, mean air pressure of 101.144 kPa and mean methane air concentration of 2 ppm. Additionally, all ponds exhibited stratification. When comparing surface concentrations to bottom concentrations over sedimented areas in the ponds, where mixing is not obstructed, bottom concentrations in ice-wedge ponds are on average more than 100 times larger than surface concentrations. For polygonal-center ponds and merged polygonal ponds, bottom concentrations still exceed surface concentrations by a factor of 42 and 38 on average (see **Table 1**).

3.1. Ice-Wedge Ponds

Ice-wedge ponds exhibit by far the highest methane concentrations and the largest spread in the distribution (**Figure 4**). In ice-wedge ponds, the surface concentrations tend to be low when wind speed is below 4 m s^{-1} (**Figure 5**). In this regime, the pond is stratified because bottom temperatures are much lower than in the other two pond types [5.9(2.5) vs. 9.5(2.2)°C (mean with standard deviation)]. With raising wind speeds maximum surface concentrations steeply increase. The strength of this increase mainly correlates with the bottom concentrations. The more methane there is at the bottom, the more gets mixed up (Kendall-tau correlation between bottom and surface methane concentrations for all wind speeds: $p < 0.05$, for wind > 4 m s^{-1} : $p < 0.01$). Both the bottom and the surface methane concentrations significantly correlate

TABLE 1 | Environmental conditions and geomorphological properties of the three pond types during the measurement campaign: dissolved oxygen (O_2), organic content in subaquatic topsoil (C_{org}), mean incoming shortwave radiation in the last 6 h before water sampling (SW_{in}), surface water temperature (T), thaw depth beneath the pond (TD), water depth (WD), area (A), bottom methane concentration (CH_4^{bot}), surface carbon dioxide concentration (CO_2), moss-covered fraction of the pond surface (f_{moss}) fraction of pond overgrown by vascular plants (fveg) and the mean wind speed in the last 1.5 h before water sampling (wind speed).

Pond type		O_2 mg L^{-1}	C_{org} %	SW_{in} W m^{-3}	T C	TD cm	WD cm	A m^2	CH_4^{surf} μmol L^{-1}	CH_4^{bot} μmol L^{-1}	CO_2 μmol L^{-1}	f_{moss} %	f_{veg} %	wind speed m s^{-1}
Ice-	Median	5	10	74	9	22	86	70	2.4	196.2	170	95	72	5
Wedge	Max	11	40	582	12	43	113	252	21.45	815.0	351	100	83	6
Ponds	Min	2	3	35	5	0	21	32	0.4	17.9	26	20	34	1
Polygonal-	Median	8	6	139	11	33	59	94	0.6	66.2	20	100	41	4
Center	Max	10	25	541	17	74	95	188	4.3	445.0	143	100	100	8
Ponds	Min	2	2	31	8	24	17	24	0.2	0.2	11	50	17	1
Merged	Median	11	6	81	10	44	na	1440	0.7	8.6	22	23	22	5
Polygonal	Max	12	17	468	14	81	na	24301	2.7	73.3	118	84	100	7
Pond	Min	5	2	44	8	37	na	214	0.2	0.5	5	0	6	3

solely to each other. The next-strongest correlation of the bottom concentrations is with area ($p = 0.2$). Using area, wind speed and bottom concentrations as regressors in a multiple linear regression, we achieve a predictive R^2 of 0.6.

3.2. Polygonal-Center Ponds

While area was a good predictor for ice-wedge ponds, water depth is more potent for polygonal-center ponds (**Figure 6**). Water depth and area do not significantly correlate for this pond type ($p = 0.3$). Apart from water depth, surface methane concentrations in polygonal-center ponds also significantly correlate with organic content in the top sediment, and these two are slightly correlated with each ($p = 0.07$) and both significantly correlated with the overgrown fraction ($p < 0.05$). Using the first principle component of these three variables as input for a linear regression on the surface concentrations yields a predictive R^2 of 0.6.

3.3. Merged Polygonal Ponds

Polygonal-center and merged polygonal ponds have a similar range of methane surface concentrations, but merged polygonal ponds have the least skewed distribution among the three pond types (**Figure 4**). These ponds also correlate significantly to the largest number of environmental variables, like water temperature and incoming shortwave radiation (**Figure 6**). Using the first two principle components of the pond area, the overgrown fraction, the incoming shortwave radiation, dissolved oxygen and the organic content yields a predictive R^2 of 0.6.

3.4. Pond-Type Independent Results

The relation between surface methane concentration and pond area can be approximated by a log-log relation (**Figure 7**). While the relation between area and methane concentration for merged polygonal ponds is strongest among the three pond types ($R^2_{\text{pred}} = 0.21$), the deviation from the regression model increases for small ponds and no clear trend with area is visible. Compared to the linear regression, ice-wedge ponds have higher-than-expected concentrations, while polygonal-center ponds have lower-than-expected concentrations for a given area.

The fraction covered by mosses has no clear influence on surface methane concentrations. For all three pond types, the error on the slope parameter of a linear regression between surface methane concentrations and moss cover is far larger than the slope parameter (see **Supplementary Figure 2**). This indicated that the sign of the regression can not be determined.

4. DISCUSSION

The surface methane concentrations measured in this study fall in the range of concentrations measured on Samoylov Island before (Abnizova et al., 2012; Knoblauch et al., 2015). The concentrations in the polygonal tundra of the Lena River Delta are lower than the mean concentration of small ponds in the permafrost-affected parts of Western Siberian Lowlands (Polishchuk et al., 2018, 9 μmol L^{-1}). A large fraction of the West Siberian Lowlands is characterized by peatlands and many ponds and lakes formed through thermokarst. Only part of the West Siberian Lowlands is covered by polygonal tundra. A major difference between the two landscapes, which could explain the difference in concentrations, is the water depth of the ponds. The ponds in our study tend to be more than four times deeper (depths of ice-wedge and polygonal-center pond range from 17 to 117 cm) than ponds of the same area in the Western Siberian Lowlands (Polishchuk et al., 2018). When comparing to the more similar landscape of polygonal tundra in Northern Canada, we find that the concentrations and particularly the differences between the two small pond types match very well [Laurion et al., 2010; Negandhi et al., 2013, mean with standard deviation in parenthesis: ice-wedge ponds 4.1(4.7) μmol L^{-1}; polygonal-center ponds 1.3(1.7) μmol L^{-1}]. We can thus assume these concentration ranges hold as well for other regions that contain similar pond types, and that the drivers we identify

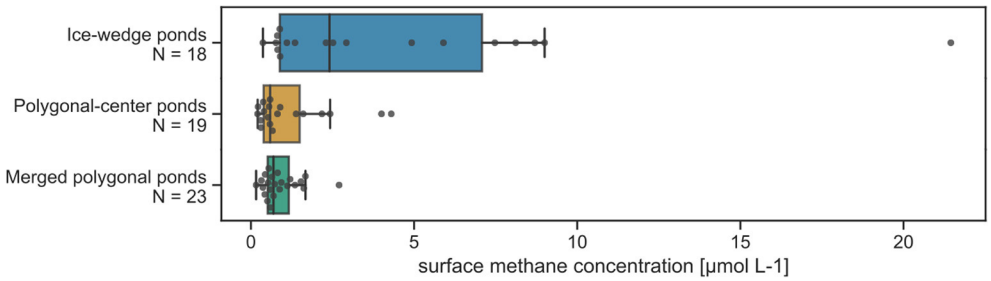

FIGURE 4 | Distribution of surface concentrations separated by pond type. Boxplots with median as well as all data points are displayed. Number of measurements (N) is stated next to each boxplot.

here might apply in other regions, too. We find that the drivers and the distribution of methane concentrations differ between pond types.

4.1. Ice-Wedge Ponds

Surface methane concentrations in ice-wedge ponds can be reasonably well-predicted using area, wind speed and bottom concentrations. However, bottom concentrations in turn do not exhibit a correlation to any of the measured variables. This might be due to stratification, which we observe and has also been observed in ice-wedge ponds by Negandhi et al. (2014). We hypothesize that both bottom and surface concentrations depend on the current and past mixing efficiency, which determines the time methane accumulated in the hypolimnion. Because of this accumulation process, the dependency of bottom concentrations on other drivers, like substrate availability, could be masked. This decoupling between methane production and release has been observed by Sachs et al. (2008) in the polygonal tundra of Samoylov Island. Nevertheless, in Swedish lakes, Juutinen et al. (2009) found that bottom concentrations correlate with nutrient content. We might not capture this dependency in ice-wedge ponds because the organic content in the top sediment might not be representative for the substrate availability in this pond type: Koch et al. (2018) found that especially in newly-formed ice-wedge ponds old carbon leeches into the pond along the edge, which is consistent with results by Negandhi et al. (2013) and Laurion et al. (2010), who find that this pond type emits a larger fraction of old carbon compared to polygonal-center ponds. More of the methanogenesis might be fueled by this leaching of dissolved organic matter, which is a different substrate source than the organic content in the top sediment that was measured in this study. Negandhi et al. (2014) found methane produced from leached organic material to be slightly more abundant in ice-wedge than in polygonal-center ponds. Therefore, the negative dependence of surface methane concentrations in ice-wedge ponds on area could be driven by two mechanisms. First, gas-exchange velocities increase the larger the area of the pond is (Bastviken et al., 2004; Read et al., 2012; Negandhi et al., 2014), and, second, as ice-wedge pond formation is a type of permafrost degradation, the larger the pond, the more advanced is the degradation (Liljedahl et al., 2016). The more degraded the permafrost around the pond is, the less likely is it that labile old permafrost is leached. Reinforcing this, the larger the pond, the smaller the fraction of the pond bottom that is comprised of ice: we found that larger ponds have a deeper than average thaw depth ($p < 0.05$). To sum up, the typical features of ice-wedge ponds tend to be less pronounced the larger the area of an ice-wedge pond, and the ponds become more similar to polygonal-center ponds. The reverse effect can also be observed in **Figure 7**: The smaller the ice-wedge and polygonal center ponds are, the larger is the difference between their methane concentrations.

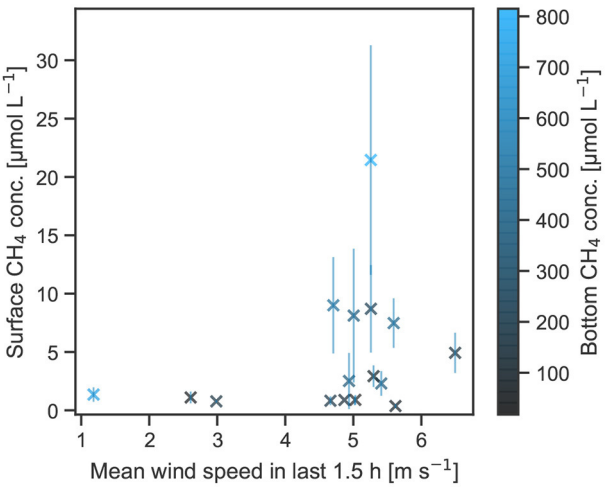

FIGURE 5 | Surface methane concentrations of the ice-wedge ponds in relation to mean wind speed in the last 1.5 h and methane bottom concentrations.

4.2. Polygonal-Center Ponds

Surface area and water depth of waterbodies regulate diffusive gas transport in a similar manner. The larger or the shallower the pond, the better mixed it is: Larger surface areas promote wind-induced mixing and thus a deeper mixed layer as well as a higher gas exchange velocity (Bastviken et al., 2004; Read et al., 2012). The deeper the pond, the longer the distance the gas has to travel from its source in the sediment to the surface. Though depth and area are often correlated (Wik et al., 2016), in our study, we find that water depth and area are hardly correlated for polygonal-center ponds (**Figure 6**). When comparing their

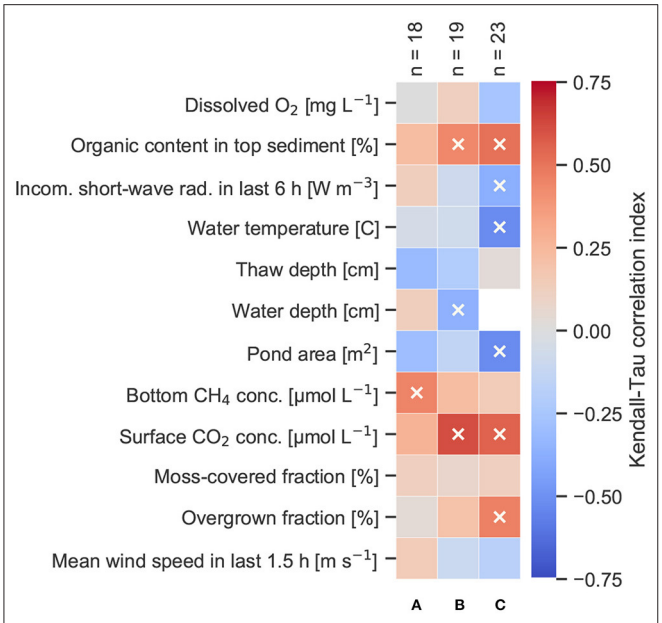

FIGURE 6 | Kendall-Tau correlation index of different variables with surface methane concentrations in **(A)** ice-wedge ponds, **(B)** polygonal-center ponds, **(C)** merged polygonal ponds. Significant correlations ($p < 0.05$) are marked by a white cross. Number of measurements per pond type (n) is indicated at the top of each column.

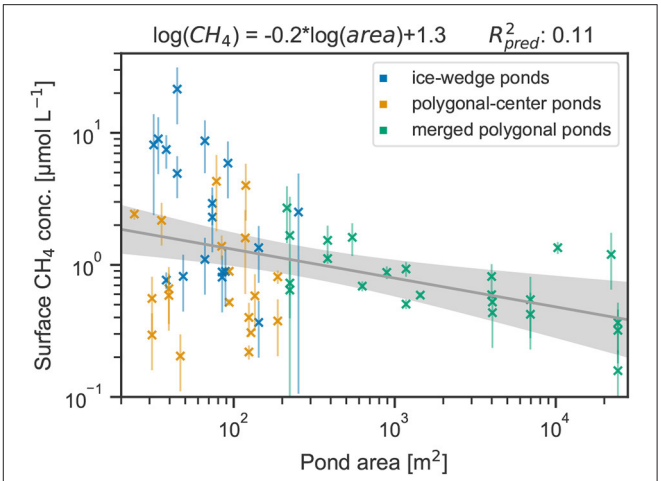

FIGURE 7 | Linear regression between the natural logarithm of methane surface concentrations and the natural logarithm of pond area. Shaded area indicates the 95% confidence band.

relative importance, water depth has a stronger impact than area on surface methane concentrations in polygonal-center ponds. This is in line with Juutinen et al. (2009) and Wik et al. (2016) who found that generally for all waterbody types water depth is a better predictor of methane fluxes than area.

Instead of area, water depth in polygonal-center ponds is highly correlated with the overgrown fraction of the ponds in our study—wherever the water is shallow enough, plants tend to take root. Vascular plants also have a strong impact on the carbon cycling in ponds. For example, vascular plants are known to enhance methane emissions by acting as chimneys through which the methane produced at the sediments can bypass the oxidation zone (Kutzbach et al., 2004; Knoblauch et al., 2015). Further, vascular plants are known to increase substrate quality, consequently enhancing methanogenesis in the sediment (Joabsson and Christensen, 2001; Strom et al., 2003). This second effect might be the reason that ponds with the highest overgrown fraction also are likely to contain high organic fraction in the top sediment. Consequently, shallow polygonal-center ponds are mixed better and have a higher substrate availability as they are overgrown to a greater extent. Since we observe that out of the three drivers, which together well explain the variability of surface methane concentrations, two are connected to substrate availability, we conclude that polygonal-center ponds are substrate-limited. Additionally, the strongest driver of the variability between the ponds is due to variations in topography, primarily water depth.

4.3. Merged Polygonal Ponds

Compared to the other two pond types, merged polygonal ponds are the largest, the deepest and, consequently, the pond type with least moss cover and the smallest overgrown fraction. A larger surface area increases the gas-exchange velocities, and a vegetation-free pond bottom promotes faster upward mixing into the water column. Therefore, we hypothesize that the coupling between the production of methane in the sediment and surface methane concentrations is strongest in merged polygonal ponds among the pond types. The stratification of ice-wedge and polygonal-center ponds might at least partly mask the influence of environmental variables, like water temperature, on surface methane concentrations. Thus, that methane concentrations in merged polygonal ponds significantly correlate with the largest number of variables might be due to their better-mixed state. The negative correlation of methane surface concentrations with incoming solar radiation and water temperature has been observed before in a study by Burger et al. (2016) but stands in contrast to other studies (e.g., Yvon-Durocher et al., 2014; Natchimuthu et al., 2016; Jansen et al., 2020), which find that methane concentrations and fluxes increase with increasing temperatures. We cannot conclusively determine the mechanisms responsible for the negative correlation but offer several arguments. Warmer temperatures strengthen both methanogenesis, which increase surface methane concentrations, and the oxidation of methane in the water column, which decreases methane surface concentrations. Studies come to varying results regarding which of the two processes has a stronger temperature dependency (Duc et al., 2010; Borrel et al., 2011; Lofton et al., 2014; Negandhi et al., 2016). However, in Arctic soils methanogenesis is less temperature-dependent than in warmer regions as the methanogenic communities are adapted to cold temperatures (Tveit et al., 2015). Additionally, the merged polygonal ponds have the lowest overgrown fraction and the lowest fraction of organic content in the top sediment.

The temperature dependence of the methanogenesis might also be dampened because of substrate limitation (Lofton et al., 2014; DelSontro et al., 2016), specifically as methanogenesis in the study area is known to depend on substrate quality (Wagner et al., 2003). At the same time, mainly when the ponds are deeper, the water temperature, which was used in the correlation analysis, can be assumed to be more variable than the sediment temperatures, which more directly affect methane concentrations. The methanotrophs benefit before the methanogens, when water warms. Ensuing temperature differences between water surface and sediment might also enhance stratification: Stratification slows down the transport of methane through the water by inhibiting turbulent mixing, and, if there is still oxygen in the water column, additionally enhances oxidation efficiency.

Rather than water temperature, the incoming radiation in the last 6 h is more likely the root cause of enhanced stratification, as a measure of how much energy got absorbed by the lake in the last 6 h. Supporting this, we find that incoming radiation predicts surface methane concentrations better than the water temperature for predicting surface methane concentrations in merged polygonal pond types together with dissolved oxygen, pond area, organic content in the top sediment and the overgrown fraction. Dissolved oxygen was measured close to the surface making this parameter an indicator of how well the surface layer is mixed and how much oxygen is available for methanotrophs. Both mixing and oxidation decrease methane surface concentrations. Overgrown area can, like for polygonal-center ponds, be seen as a proxy for both the substrate quality and the mean water depth. Especially as the organic content and the overgrown fraction of merged polygonal ponds are smaller than in polygonal-center ponds, we can analogously infer that merged polygonal ponds are substrate-limited and, more than polygonal-center ponds, dependent on those environmental conditions, which influence stratification. Lastly, we note that both stratification and vegetated fraction are at least partly regulated by the topography and mean water depth of the ponds.

4.4. Drivers of Methane Variability Between Pond Types

The three geomorphological pond types have varying drivers of type-internal methane variability, and concurrently, the distributions and mean values of surface methane concentrations of the three pond types differ as well.

Ice-wedge ponds are the most stratified and exhibit other bacterial communities than polygonal-center ponds (Negandhi et al., 2014); merged polygonal ponds are the largest, the best mixed pond type with the highest gas-exchange velocities (Bastviken et al., 2004; Read et al., 2012), and the pond type with the least substrate, the smallest overgrown and moss-covered fraction. Polygonal-center ponds are of the same size as ice-wedge ponds, but for many properties, like dissolved oxygen or thaw depth, fall into the middle of the other two ponds. A reason why the surface methane concentrations of polygonal-center ponds are not as high as would be expected from the log-log regression between methane concentrations and area (see **Figure 7**) might lie with water depth. In polygonal-center ponds, surface methane concentrations strongly depend on water depth, but water depth is not strongly correlated with area. Thus, though polygonal-center ponds have a smaller area than merged polygonal ponds, they might not be shallower.

4.4.1. Area

As previous studies (DelSontro et al., 2018; Zabelina et al., 2020) suggest, we find that pond area alone is not sufficient to explain variability in methane concentrations. Yet, the observed trend is in agreement with prior studies (Juutinen et al., 2009; Wik et al., 2016), and the relation between pond size and methane concentrations is very similar to the estimate by Polishchuk et al. (2018)—their regression line follows $log([CH_4]) = -0.258 \cdot log(\text{area}) + 0.635$. This similarity especially in the slope (our result: -0.2) is astounding since Polishchuk et al. (2018) covered a much larger spatial area, spanning from continuous to sporadic permafrost zones. We conclude that, especially for ponds larger than roughly 10 m^2, an area-based upscaling can be a reasonable choice in permafrost-affected landscapes, but that for smaller ponds additional predictors need to be taken into consideration.

4.4.2. Moss Cover

Most of the subaquatic soils of the ponds in the study area are at least partly covered by submerged mosses (*Scorpidium scorpioides*). This moss photosynthesizes at the bottom of the pond and creates an oxic layer where methane can be oxidized. Additionally, the thick moss captures bubbles and thus suppresses ebullition (Liebner et al., 2011; Knoblauch et al., 2015). Surprisingly, we do not find that moss cover reduces surface methane concentration on the pond scale (**Supplementary Figure 2**). However, we find that moss does inhibit diffusion, if we look at stratification: Bottom methane concentrations in the moss layer are on average (with standard deviation) 1.8(1.2) times higher than in open water. To reconcile these two findings, we hypothesize that moss cover has a counterbalancing effect: If moss also enhances methanogenesis by providing additional organic substrate similar to what has been shown for vascular plants (Joabsson and Christensen, 2001; Strom et al., 2003), then even though moss leads to enhanced oxidation at the bottom of the pond, the higher productivity might balance out the loss through oxidation. Additionally, the accumulation of methane in the moss layer creates a gradient between moss-covered and moss-free areas in the ponds which are not completely covered by moss. Through lateral mixing part of the methane might escape the moss layer and reach the surface.

The mosses in our study area should not be confused with mosses of the genus *Sphagnum*. Kuhn et al. (2018) found that for sphagnum-dominated ponds diffusive methane fluxes are lower than for ponds with open water, but in contrast to the submerged mosses in our study side, *Sphagnum* stays at the water surface, and thus has a direct impact on the gas exchange at the water-air interface.

4.4.3. Carbon Dioxide

All ponds show a positive correlation between surface methane and carbon dioxide concentrations (**Figure 6**). This correlation

was expected, since carbon dioxide is produced during acetoclastic methanogenesis, which is assumed to be the most prominent pathway of methanogenesis in cold lakes and ponds (Borrel et al., 2011; Negandhi et al., 2013; Tveit et al., 2015). Additional carbon dioxide is produced during the oxidation of methane, and the oxidation rates have been found to be coupled to methane production rates (Duc et al., 2010). Thus, at least part of the production of carbon dioxide in the pond is closely coupled to methanogenesis. Additionally, the carbon dioxide produced independently of the methane might follow similar drivers.

5. CONCLUSIONS

The dominant drivers of methane emissions differ depending on the pond type. We consider substrate availability to be an important driver of methane concentrations markedly in polygonal-center and merged polygonal ponds. Smaller, shallower ponds tend to be richer in substrate (more organic content in the sediment and higher overgrown fraction) and thus exhibit higher concentrations. Accordingly, substrate availability is at least partly determined by the topography of the pond. This finding matches results from prior studies (Juutinen et al., 2009; Sepulveda-Jauregui et al., 2015). The easiest-to-measure topographical property of ponds is area, and, for merged polygonal ponds, area is a good predictor of methane concentrations. But for polygonal-center ponds, water depth is a far better predictor. Water depth, overgrown fraction (as both a proxy for mean water depth and for substrate availability) and organic fraction in the top sediment are enough to predict surface methane concentrations reasonably well in polygonal-center ponds. In our study, the incoming short-wave radiation over the past 6 h was the best proxy for stratification, much improving the statistical model for merged polygonal ponds.

Lastly, ice-wedge ponds are the most distinct pond type. Ice-wedge ponds are strongly stratified as they are narrow, steep and feature a large temperature gradient in summer. If bottom waters are mixed up, surface methane concentrations spike. Additionally, these ponds tend to be richer in substrate and have been shown to emit a larger fraction of old carbon than polygonal-center ponds (Laurion et al., 2010; Negandhi et al., 2013). We find that ice-wedge ponds feature the highest concentrations and, thus, likely also the highest diffusive emissions.

We do not find that the moss-covered fraction of a pond controls methane surface concentrations, as moss might enhance local methanogenesis by providing substrate and lateral mixing might reduce the dampening effect of moss on diffusion.

Climate changes at an above-average rate in the Arctic, and there is growing evidence that global warming will enhance methane emissions from ponds (e.g., Tan and Zhuang, 2015; Vonk et al., 2015; Wik et al., 2016; Aben et al., 2017; Yvon-Durocher et al., 2017), especially so from ice-wedge ponds, which are expected to increasingly form (Liljedahl et al., 2016; Martin et al., 2017). When including small waterbodies in large-scale studies, it is import to choose an appropriate representation for the ponds. As it is not possible to approximate the behavior of all pond types in our study with the same drivers, let alone use a single driver to approximate the behavior of all ponds, we conclude that process-based models which ideally capture the different waterbody types will be useful in the improvement of upscaling of pan-Arctic waterbody-methane emissions.

DATA AVAILABILITY STATEMENT

The data has been published at: https://doi.pangaea.de/10.1594/PANGAEA.922399 (Rehder et al., 2020).

AUTHOR CONTRIBUTIONS

ZR: conceptualization (equal), formal analysis (lead), investigation (lead), and writing - original draft. AZ: formal analysis (supporting) and investigation (supporting). LK: conceptualization (equal), formal analysis (supporting), and writing - review and editing. All authors contributed to the article and approved the submitted version.

FUNDING

This study was partly funded by the Deutsche Forschungsgemeinschaft (DFG, German Research Foundation) under Germany's Excellence Strategy—EXC 2037 CLICCS - Climate, Climatic Change, and Society—Project Number: 390683824, contribution to the Center for Earth System Research and Sustainability (CEN) of Universität Hamburg.

ACKNOWLEDGMENTS

The authors thank Norman Rüggen for his tireless support before and remotely during the fieldwork, Andrei Astapov, Waldemar Schneider, and Andrei Kartoziia for their equally tireless support in the field, Victor Brovkin and Thomas Kleinen for the helpful discussions on the analysis, and last but not least David Holl for his valuable suggestions on the manuscript. The authors also thank Sophia Burke and Ronny Lauerwald for their kind and helpful review.

SUPPLEMENTARY MATERIAL

The Supplementary Material for this article can be found online at: https://www.frontiersin.org/articles/10.3389/feart.2021.617662/full#supplementary-material

REFERENCES

Aben, R. C. H., Barros, N., van Donk, E., Frenken, T., Hilt, S., Kazanjian, G., et al. (2017). Cross continental increase in methane ebullition under climate change. *Nat. Commun.* 8, 1–8. doi: 10.1038/s41467-017-01535-y

Abnizova, A., Siemens, J., Langer, M., and Boike, J. (2012). Small ponds with major impact: the relevance of ponds and lakes in permafrost landscapes to carbon dioxide emissions. *Glob. Biogeochem. Cycles* 26, 1–9. doi: 10.1029/2011GB004237

Anderson, N. J., Harriman, R., Ryves, D. B., and Patrick, S. T. (2001). Dominant factors controlling variability in the ionic composition of west greenland

lakes. *Arctic Antarctic Alpine Res*. 33, 418–425. doi: 10.1080/15230430.2001.12003450

Bastviken, D., Cole, J., Pace, M., and Tranvik, L. (2004). Methane emissions from lakes: dependence of lake characteristics, two regional assessments, and a global estimate. *Glob. Biogeochem. Cycles* 18, 1–12. doi: 10.1029/2004GB002238

Boike, J., Kattenstroth, B., Abramova, K., Bornemann, N., Chetverova, A., Fedorova, I., et al. (2013). Baseline characteristics of climate, permafrost and land cover from a new permafrost observatory in the lena river delta, siberia (1998-2011). *Biogeosciences* 10, 2105–2128. doi: 10.5194/bg-10-2105-2013

Borrel, G., Jezequel, D., Biderre-Petit, C., Morel-Desrosiers, N., Morel, J. P., Peyret, P., et al. (2011). Production and consumption of methane in freshwater lake ecosystems. *Res. Microbiol*. 162, 832–847. doi: 10.1016/j.resmic.2011.06.004

Burger, M., Berger, S., Spangenberg, I., and Blodau, C. (2016). Summer fluxes of methane and carbon dioxide from a pond and floating mat in a continental Canadian peatland. *Biogeosciences* 13, 3777–3791. doi: 10.5194/bg-13-3777-2016

Burpee, B., Saros, J. E., Northington, R. M., and Simon, K. S. (2016). Microbial nutrient limitation in arctic lakes in a permafrost landscape of southwest greenland. *Biogeosciences* 13, 365–374. doi: 10.5194/bg-13-365-2016

DelSontro, T., Beaulieu, J. J., and Downing, J. A. (2018). Greenhouse gas emissions from lakes and impoundments: upscaling in the face of global change. *Limnol. Oceanogr. Lett*. 3, 64–75. doi: 10.1002/lol2.10073

DelSontro, T., Boutet, L., St-Pierre, A., del Giorgio, P. A., and Prairie, Y. T. (2016). Methane ebullition and diffusion from northern ponds and lakes regulated by the interaction between temperature and system productivity. *Limnol. Oceanogr*. 61, S62–S77. doi: 10.1002/lno.10335

Downing, J. A. (2010). Emerging global role of small lakes and ponds: little things mean a lot. *Limnetica* 29, 9–23. doi: 10.23818/limn.29.02

Duc, N., Crill, P., and Bastviken, D. (2010). Implications of temperature and sediment characteristics on methane formation and oxidation in lake sediments. *Biogeochemistry* 100, 185–196. doi: 10.1007/s10533-010-9415-8

French, H. M. (2007). *The Periglacial Environment, 3rd Edn*. Chichester: John Wiley Sons, Ltd. doi: 10.1002/9781118684931

Hamilton, P. B., Gajewski, K., Atkinson, D. E., and Lean, D. R. S. (2001). Physical and chemical limnology of 204 lakes from the canadian arctic archipelago. *Hydrobiologia* 457, 133–148. doi: 10.1023/A:1012275316543

Harris, C. R., Millman, K. J., van der Walt, S. J., Gommers, R., Virtanen, P., Cournapeau, D., et al. (2020). Array programming with numpy. *Nature* 585, 357–362. doi: 10.1038/s41586-020-2649-2

Hodges, J. (1958). The significance probability of the smirnov two-sample test. *Arkiv för Matematik* 3, 469–486. doi: 10.1007/BF02589501

Holgerson, M. A., and Raymond, P. A. (2016). Large contribution to inland water co2 and ch4 emissions from very small ponds. *Nat. Geosci*. 9, 222–226. doi: 10.1038/ngeo2654

Hunter, J. D. (2007). Matplotlib: a 2d graphics environment. *Comput. Sci. Eng*. 9, 90–95. doi: 10.1109/MCSE.2007.55

Jansen, J., Thornton, B. F., Cortés, A., Snöälv, J., Wik, M., MacIntyre, S., et al. (2020). Drivers of diffusive ch4 emissions from shallow subarctic lakes on daily to multi-year timescales. *Biogeosciences* 17, 1911–1932. doi: 10.5194/bg-17-1911-2020

Joabsson, A., and Christensen, T. R. (2001). Methane emissions from wetlands and their relationship with vascular plants: an arctic example. *Glob. Change Biol*. 7, 919–932. doi: 10.1046/j.1354-1013.2001.00044.x

Juutinen, S., Rantakari, M., Kortelainen, P., Huttunen, J. T., Larmola, T., Alm, J., et al. (2009). Methane dynamics in different boreal lake types. *Biogeosciences* 6, 209–223. doi: 10.5194/bg-6-209-2009

Kartoziia, A. (2019). Assessment of the ice wedge polygon current state by means of UAV imagery analysis (Samoylov island, the Lena delta). *Remote Sens*. 11:1627. doi: 10.3390/rs11131627

Knight, W. R. (1966). A computer method for calculating Kendall's tau with ungrouped data. *J. Am. Stat. Assoc*. 61, 436–439. doi: 10.1080/01621459.1966.10480879

Knoblauch, C., Spott, O., Evgrafova, S., Kutzbach, L., and Pfeiffer, E. M. (2015). Regulation of methane production, oxidation, and emission by vascular plants and bryophytes in ponds of the northeast siberian polygonal tundra. *J. Geophys. Res. Biogeosci*. 120, 2525–2541. doi: 10.1002/2015JG003053

Koch, J. C., Jorgenson, M. T., Wickland, K. P., Kanevskiy, M., and Striegl, R. (2018). Ice wedge degradation and stabilization impact water budgets and nutrient cycling in arctic trough ponds. *J. Geophys. Res. Biogeosci*. 123, 2604–2616. doi: 10.1029/2018JG004528

Kuhn, M., Lundin, E. J., Giesler, R., Johansson, M., and Karlsson, J. (2018). Emissions from thaw ponds largely offset the carbon sink of northern permafrost wetlands. *Sci. Rep/* 8, 1–7. doi: 10.1038/s41598-018-27770-x

Kutzbach, L., Wagner, D., and Pfeiffer, E. M. (2004). Effect of microrelief and vegetation on methane emission from wet polygonal tundra, Lena delta, northern Siberia. *Biogeochemistry* 69, 341–362. doi: 10.1023/B:BIOG.0000031053.81520.db

Laurion, I., Vincent, W. F., MacIntyre, S., Retamal, L., Dupont, C., Francus, P., et al. (2010). Variability in greenhouse gas emissions from permafrost thaw ponds. *Limnol. Oceanogr*. 55, 115–133. doi: 10.4319/lo.2010.55.1.0115

Liebner, S., Zeyer, J., Wagner, D., Schubert, C., Pfeiffer, E. M., and Knoblauch, C. (2011). Methane oxidation associated with submerged brown mosses reduces methane emissions from siberian polygonal tundra. *J. Ecol*. 99, 914–922. doi: 10.1111/j.1365-2745.2011.01823.x

Liljedahl, A. K., Boike, J., Daanen, R. P., Fedorov, A. N., Frost, G. V., Grosse, G., et al. (2016). Pan-arctic ice-wedge degradation in warming permafrost and its influence on tundra hydrology. *Nat. Geosci*. 9:312. doi: 10.1038/ngeo2674

Lofton, D. D., Whalen, S. C., and Hershey, A. E. (2014). Effect of temperature on methane dynamics and evaluation of methane oxidation kinetics in shallow Arctic Alaskan lakes. *Hydrobiologia* 721, 209–222. doi: 10.1007/s10750-013-1663-x

Martin, A. F., Lantz, T. C., and Humphreys, E. R. (2017). Ice wedge degradation and Co2 and Ch4 emissions in the Tuktoyaktuk coastlands, northwest territories. *Arctic Sci*. 4, 130–145. doi: 10.1139/AS-2016-0011

Martinez-Cruz, K., Sepulveda-Jauregui, A., Walter Anthony, K., and Thalasso, F. (2015). Geographic and seasonal variation of dissolved methane and aerobic methane oxidation in alaskan lakes. *Biogeosciences* 12, 4595–4606. doi: 10.5194/bg-12-4595-2015

Minayeva, T., Sirin, A., Kershaw, P., and Bragg, O. (2016). *Arctic Peatlands*. Dordrecht: Springer. doi: 10.1007/978-94-007-6173-5_109-1

Muster, S., Langer, M., Heim, B., Westermann, S., and Boike, J. (2012). Subpixel heterogeneity of ice-wedge polygonal tundra: a multi-scale analysis of land cover and evapotranspiration in the lena river delta, siberia. *Tellus Ser. B Chem. Phys. Meteorol*. 64. doi: 10.3402/tellusb.v64i0.17301

Muster, S., Roth, K., Langer, M., Lange, S., Aleina, F. C., Bartsch, A., et al. (2017). Perl: a circum-arctic permafrost region pond and lake database. *Earth Syst. Sci. Data* 9, 317–348. doi: 10.5194/essd-9-317-2017

Natchimuthu, S., Sundgren, I., Galfalk, M., Klemedtsson, L., Crill, P., Danielsson, A., et al. (2016). Spatio-temporal variability of lake ch4 fluxes and its influence on annual whole lake emission estimates. *Limnol. Oceanogr*. 61, S13–S26. doi: 10.1002/lno.10222

Negandhi, K., Laurion, I., and Lovejoy, C. (2014). Bacterial communities and greenhouse gas emissions of shallow ponds in the high arctic. *Polar Biol*. 37, 1669–1683. doi: 10.1007/s00300-014-1555-1

Negandhi, K., Laurion, I., and Lovejoy, C. (2016). Temperature effects on net greenhouse gas production and bacterial communities in arctic thaw ponds. *FEMS Microbiol. Ecol*. 92, 1–12. doi: 10.1093/femsec/fiw117

Negandhi, K., Laurion, I., Whiticar, M. J., Galand, P. E., Xu, X. M., and Lovejoy, C. (2013). Small thaw ponds: an unaccounted source of methane in the Canadian high Arctic. *PLoS ONE* 8:e78204. doi: 10.1371/journal.pone.0078204

Ortiz-Llorente, M. J., and Alvarez-Cobelas, M. (2012). Comparison of biogenic methane emissions from unmanaged estuaries, lakes, oceans, rivers and wetlands. *Atmos. Environ*. 59, 328–337. doi: 10.1016/j.atmosenv.2012.05.031

Pedregosa, F., Varoquaux, G., Gramfort, A., Michel, V., Thirion, B., Grisel, O., et al. (2011). Scikit-learn: machine learning in python. *J. Mach. Learn. Res*. 12, 2825–2830.

Polishchuk, Y. M., Bogdanov, A. N., Muratov, I. N., Polishchuk, V. Y., Lim, A., Manasypov, R. M., et al. (2018). Minor contribution of small thaw ponds to the pools of carbon and methane in the inland waters of the permafrost-affected part of the western siberian lowland. *Environ. Res. Lett*. 13:15. doi: 10.1088/1748-9326/aab046

Ramsar Convention Secretariat (2016). *An Introduction to the Ramsar Convention on Wetlands (previously The Ramsar Convention Manual)*. Ramsar Convention Secretariat, Gland.

Read, J. S., Hamilton, D. P., Desai, A. R., Rose, K. C., MacIntyre, S., Lenters, J. D., et al. (2012). Lake-size dependency of wind shear and convection as controls on gas exchange. *Geophys. Res. Lett*. 39, 1–5. doi: 10.1029/2012GL051886

Rehder, Z., Zaplavnova, A., and Kutzbach, L. (2020). *Dissolved-Gas Concentrations, Physical and Chemical Properties of 41 Ponds as well as Key Meteorological Parameters in the Lena River Delta, Siberia*. Pangaea.

Rinta, P., Bastviken, D., Schilder, J., Van Hardenbroek, M., Stotter, T., and Heiri, O. (2017). Higher late summer methane emission from central than northern European lakes. *J. Limnol*. 76, 52–67. doi: 10.4081/jlimnol.2016.1475

Sachs, T., Wille, C., Boike, J., and Kutzbach, L. (2008). Environmental controls on ecosystem-scale Ch4 emission from polygonal tundra in the Lena river delta, Siberia. *J. Geophys. Res. Biogeosci*. 113, 1–12. doi: 10.1029/2007JG000505

Sander, R. (2015). Compilation of Henry's law constants (version 4.0) for water as solvent. *Atmos. Chem. Phys*. 15, 4399–4981. doi: 10.5194/acp-15-4399-2015

Schneider, J., Grosse, G., and Wagner, D. (2009). Land cover classification of tundra environments in the Arctic Lena delta based on landsat 7 etm+ data and its application for upscaling of methane emissions. *Remote Sens. Environ*. 113, 380–391. doi: 10.1016/j.rse.2008.10.013

Schwamborn, G., Rachold, V., and Grigoriev, M. N. (2002). Late quaternary sedimentation history of the lena delta. *Q. Int*. 89, 119–134. doi: 10.1016/S1040-6182(01)00084-2

Sepulveda-Jauregui, A., Anthony, K. M. W., Martinez-Cruz, K., Greene, S., and Thalasso, F. (2015). Methane and carbon dioxide emissions from 40 lakes along a north-south latitudinal transect in Alaska. *Biogeosciences* 12, 3197–3223. doi: 10.5194/bg-12-3197-2015

Strom, L., Ekberg, A., Mastepanov, M., and Christensen, T. R. (2003). The effect of vascular plants on carbon turnover and methane emissions from a tundra wetland. *Glob. Change Biol*. 9, 1185–1192. doi: 10.1046/j.1365-2486.2003.00655.x

Tan, Z. L., and Zhuang, Q. L. (2015). Methane emissions from Pan-Arctic lakes during the 21st century: an analysis with process-based models of lake evolution and biogeochemistry. *J. Geophys. Res. Biogeosci*. 120, 2641–2653. doi: 10.1002/2015JG003184

Tveit, A. T., Urich, T., Frenzel, P., and Svenning, M. M. (2015). Metabolic and trophic interactions modulate methane production by arctic peat microbiota in response to warming. *Proc. Natl. Acad. Sci. U.S.A*. 112, E2507–E2516. doi: 10.1073/pnas.1420797112

Virtanen, P., Gommers, R., Oliphant, T. E., Haberland, M., Reddy, T., Cournapeau, D., et al. (2020). Scipy 1.0: fundamental algorithms for scientific computing in python. *Nat. Methods* 17, 261–272. doi: 10.1038/s41592-019-0686-2

Vonk, J. E., Tank, S. E., Bowden, W. B., Laurion, I., Vincent, W. F., Alekseychik, P., et al. (2015). Reviews and syntheses: effects of permafrost thaw on arctic aquatic ecosystems. *Biogeosciences* 12, 7129–7167. doi: 10.5194/bg-12-7129-2015

Wagner, D., Kobabe, S., Pfeiffer, E. M., and Hubberten, H. W. (2003). Microbial controls on methane fluxes from a polygonal tundra of the Lena delta, Siberia. *Permafrost Periglacial Process*. 14, 173–185. doi: 10.1002/ppp.443

Wetterich, S., Schirrmeister, L., Meyer, H., Viehberg, F. A., and Mackensen, A. (2008). Arctic freshwater ostracods from modern periglacial environments in the Lena river delta (Siberian Arctic, Russia): geochemical applications for palaeoenvironmental reconstructions. *J. Paleolimnol*. 39, 427–449. doi: 10.1007/s10933-007-9122-1

Wik, M., Varner, R. K., Anthony, K. W., MacIntyre, S., and Bastviken, D. (2016). Climate-sensitive northern lakes and ponds are critical components of methane release. *Nat. Geosci*. 9:99. doi: 10.1038/ngeo2578

Yvon-Durocher, G., Allen, A. P., Bastviken, D., Conrad, R., Gudasz, C., St-Pierre, A., et al. (2014). Methane fluxes show consistent temperature dependence across microbial to ecosystem scales. *Nature* 507, 488–491. doi: 10.1038/nature13164

Yvon-Durocher, G., Hulatt, C. J., Woodward, G., and Trimmer, M. (2017). Long-term warming amplifies shifts in the carbon cycle of experimental ponds. *Nat. Clim. Change* 7:209. doi: 10.1038/nclimate3229

Zabelina, S. A., Shirokova, L. S., Klimov, S. I., Chupakov, A. V., Lim, A. G., Polishchuk, Y. M., et al. (2020). Carbon emission from thermokarst lakes in ne european tundra. *Limnol. Oceanogr*. 66, S216–S230. doi: 10.1002/lno.11560

Conflict of Interest: The authors declare that the research was conducted in the absence of any commercial or financial relationships that could be construed as a potential conflict of interest.

The handling editor declared a past co-authorship with one of the authors LK.

frontiers in Earth Science

ORIGINAL RESEARCH
published: 30 March 2021
doi: 10.3389/feart.2021.630469

Meteorological Controls on Water Table Dynamics in Fen Peatlands Depend on Management Regimes

Sate Ahmad[1], Haojie Liu[1], Shajratul Alam[2], Anke Günther[3], Gerald Jurasinski[3] and Bernd Lennartz[1]*

[1] Soil Physics, Faculty of Agricultural and Environmental Sciences, University of Rostock, Rostock, Germany, [2] Statistics, Jack Baskin School of Engineering, University of California, Santa Cruz, Santa Cruz, CA, United States, [3] Landscape Ecology and Site Evaluation, Faculty of Agricultural and Environmental Sciences, University of Rostock, Rostock, Germany

Fens belong to the most threatened ecosystems in Europe. Maintaining a high water table through rewetting is an effective measure to rehabilitate many of their ecosystem functions. However, the impact of meteorological conditions such as vapor pressure deficit (VPD) and precipitation on water tables is still unclear for rewetted fens. Here, we compare the impact of meteorological factors on water table dynamics in a drained and a rewetted fen, using multiple regression with data from continuous high-resolution (temporal) water level monitoring and weather stations. We find that an increase in the daily mean VPD causes a higher drop in the water table at the drained and degraded fen compared to the rewetted fen. Precipitation contributes to recharge, causing the water table to rise higher at the drained site than at the rewetted site. We attribute the differential influence of meteorological conditions on water table dynamics to different soil specific yield values (i.e., water storage capacity) largely driven by lower water table position at the drained site. Our study underlines the importance of understanding how and why water tables in peatlands vary in response to meteorological factors for management decisions (e.g., rewetting). Continuous monitoring of water table and vegetation development in rewetted fen peatlands is advisable to ensure long-term success especially under climate change conditions and associated drought events.

Keywords: peatland hydrology, peatland restoration, evapotranspiration, diurnal groundwater fluctuation, vapor pressure deficit, climate change

OPEN ACCESS

Edited by:
Michel Bechtold, KU Leuven, Belgium

Reviewed by:
Marc-André Bourgault, Laval University, Canada
Daniel Limehouse McLaughlin, Virginia Tech, United States

****Correspondence:***
Sate Ahmad
sate.ahmad@uni-rostock.de

Specialty section:
This article was submitted to Hydrosphere, a section of the journal Frontiers in Earth Science

Received: *17 November 2020*
Accepted: *02 March 2021*
Published: *30 March 2021*

Citation:
Ahmad S, Liu H, Alam S, Günther A, Jurasinski G and Lennartz B (2021) Meteorological Controls on Water Table Dynamics in Fen Peatlands Depend on Management Regimes. Front. Earth Sci. 9:630469. doi: 10.3389/feart.2021.630469

INTRODUCTION

Over the past century, about 90% of minerotrophic peatlands (fens; groundwater-fed peatlands) in Central Europe have been degraded through artificial drainage and deforestation (Joosten and Couwenberg, 2001). As a result, fens have been recognized as one of the most threatened ecosystems in Europe (Schrautzer et al., 2007). Maintenance of water table at or near the peat surface prevents carbon mineralization, allows peat accumulation (Michaelis et al., 2020; Mrotzek et al., 2020), and improves ecosystem functions such as hydrological buffering, water purification, erosion protection, and climate regulation (Kimmel and Mander, 2010; Lennartz and Liu, 2019; Ahmad et al., 2020c; Günther et al., 2020). Therefore, restoration of degraded peatlands is an important climate change mitigation measure, as peatlands store much of the global terrestrial carbon stock.

Although hydrological restoration of peatlands has been implemented throughout Europe and North America (Lamers et al., 2015), rewetted peatlands are under pressure from climate change (Levison et al., 2014). Shifting precipitation patterns and increasing evapotranspiration resulting from global warming may further degrade peatlands (Tarnocai, 2009; Nijp et al., 2015; Helbig et al., 2020). However, the impact of a changing climate on peatland ecohydrology through extreme weather events such as droughts is likely not uniform over different spatial scales and climatic zones. Part of this variability is due to a variation in local meteorological conditions and differences in land management.

Meteorological factors such as temperature, precipitation and relative humidity may affect the water table in peatlands through several processes such as recharge and evapotranspiration (Bridgham et al., 1999; Ferone and Devito, 2004; Menberu et al., 2016; Cooper et al., 2019). The combined effect of air temperature and relative humidity on evapotranspiration and thus on water table fluctuation can be understood by computing the vapor pressure deficit (VPD). VPD is the difference between the amount of moisture in the air and how much of it the air can hold when at saturation at a certain temperature. VPD is considered an accurate indicator of the actual evaporative capacity of the air (Allen et al., 1998).

The effect of such meteorological parameters on water table fluctuation may also be modified by microtopography, vegetation, soil properties, and land management (Dunne et al., 1991; Baldocchi et al., 2004). Peat soils are highly heterogeneous porous media (Rezanezhad et al., 2016; Ahmad et al., 2020b; Liu et al., 2020a) with hydraulic conductivities that may vary over two orders of magnitudes within the same peat horizon (Liu and Lennartz, 2019). The spatial differences in soil properties can cause different responses of the water table to precipitation at different locations within a peatland. Furthermore, peatland rewetting can alter the prevailing vegetation structure and composition (Schrautzer et al., 2013; Malhotra et al., 2016), which can further modify the interactions between meteorological factors and the water table. For example, the relationship between temperature and water loss may be modulated by stands of dominant vegetation, with high evapotranspirative demand (Bridgham et al., 1999).

Water management regimes in peatlands are of key importance and can modify how the water table reacts to meteorological controls by altering peat properties and water table position. In terms of peat properties, specific yield, which is the amount of water that would drain from a unit of soil if the water table would drop by a unit height (Childs, 1969), influence water table response to precipitation (Ahmad et al., 2020c) and evapotranspiration (Ahmad et al., 2020a) as well as controls water table variation (Menberu et al., 2016). Lowering the water table, for example by artificial drainage, exposes the peat to an oxygen-rich environment. As such, aerobic decomposition occurs at a rapid pace, degrading the peat and starting a cascade of different hydrophysical and biogeochemical processes. As aerobic decomposition continues, carbon dioxide and nitrous oxide are released from the system further contributing to global climate forcing (Tiemeyer et al., 2016; Liu et al., 2019, 2020b). The carbon mineralization process and shrinkage cause the peat to become more consolidated and compacted, and as such the hydrophysical properties of peat change (Hooijer et al., 2012; Pronger et al., 2014). With increased effective stress, larger pores in the peat structure are the first to collapse as they are the least supported (Strack et al., 2008) and as such macroporosity decreases. Due to a reduction in macroporosity, saturated hydraulic conductivity decreases (Branham and Strack, 2014; Liu et al., 2016), which further affects the hydrology of peatlands (Whittington and Price, 2006). The reduction in pore size lowers the soil specific yield and thus lowers water storage capacity (Liu and Lennartz, 2019; Liu et al., 2020a). At a given site, following drainage, as the water storage capacity reduces (indicated by a lower peat specific yield), water table fluctuations increase (Whittington and Price, 2006; Menberu et al., 2016). Peatland rewetting raises the water table position and new peat accumulation can occur under saturated conditions (Mrotzek et al., 2020), thereby increasing the peat specific yield (Ahmad et al., 2020c).

The majority of published studies on the link between peatland ecohydrological processes and meteorological conditions so far focus on bogs (ombrotrophic peatlands or rainfed mires; Price, 1996; Ruseckas and Grigaliūnas, 2008; Bourgault et al., 2019; Philippov and Yurchenko, 2019), while similar studies on fens are sparse. Therefore, meteorological effects on water table dynamics in fens, especially with a focus on different management measures (such as rewetting or artificial drainage), are understudied. Establishing such links in fen peatlands is of utmost importance in light of shifting local and global climate regimes. For example, while recent decades are characterized by increasing temperatures worldwide, a resulting exponential increase in vapor pressure deficit has also been observed. Such increases have an impact on terrestrial ecosystems through drought-induced plant mortality (Grossiord et al., 2020), reduced vegetation growth (Yuan et al., 2019), and potentially evapotranspiration associated water table decline. Therefore, rewetting of drained peatlands may become more challenging with increasing VPD, as these ecosystems depend on high water levels as well as plant production to maintain peat accumulation.

To address such shortcomings, we (1) investigate how on-site meteorological conditions (VPD and precipitation) act as controls over water table dynamics (2) unravel the underlying mechanisms involved, and (3) evaluate how these hydrological controls differ over different management regimes (drained versus rewetted). To this end, we characterize water table dynamics, estimate the effect of daily mean VPD and rainfall on the water table and quantify rain-free day actual evapotranspiration at a drained and a rewetted fen in North-east Germany.

MATERIALS AND METHODS

Study Sites

The two study sites (drained fen, PD and rewetted fen, PW) are located in the federal state of Mecklenburg-Vorpommern, Germany (**Figure 1**). They are 8 km apart

and together belong to one of the largest connected fen complexes in northeastern Germany (Jurasinski et al., 2020). According to the hydrogenetic mire classification system (Succow and Joosten, 2001; Joosten et al., 2017), they are "percolation fens" which are minerotrophic peatlands that depend on a large supply of water that is distributed evenly throughout the year. Percolation fens are often located along river valleys which are remains of meltwater channels of the last glaciation, where permanent groundwater flow from adjacent moraines caused paludification (Koch and Jurasinski, 2015). Both sites were drained before 1750. In PW, land drainage was intensified in around 1970 for high-intensity pasture management. In 1997, the site PW was rewetted by ditch blocking, as a part of the state peatland conservation program and the EU-LIFE program, while PD remains drained. PD can be considered to be a fairly homogenous grassland, with a dominance of *Ranunculus repens L.* and *Deschampsia cespitosa* (L.) P. Beauv. with some *Holcus lanatus* L. and *Poa trivialis L.* PW is much more diverse with a mosaic of several dominant stands that established after rewetting. The studied plot in PW is dominated by *Carex acutiformis* Ehrh., with few occurrences of *Epilobium hirsutum* L. In recent times, PW can be considered to feature near-natural percolation fen vegetation and is part of a larger valley mire system (Tiemeyer et al., 2006). Recent studies have found evidence that rewetting of PW has resulted in peat accumulation of around 11 cm, corresponding to 4.5 kg m^{-2} of organic matter (Michaelis et al., 2020; Mrotzek et al., 2020). The relevant site characteristics have been described by Jurasinski et al. (2020) and Ahmad et al. (2020c).

Data Acquisition and Analyses

As part of the WETSCAPES project, described by Jurasinski et al. (2020), one water level logger (SEBA hydrometrie Dipper-PT) was installed for each site, and data was registered every 15 min. Weather stations were also installed at each site, which recorded precipitation (Rain Collector #07852, Davis Instruments), relative humidity and temperature (KPK 1/5-ME, Galltec Mess- und Regeltechnik GmbH and MELA Sensortechnik GmbH) every 10 min using an automated data logger CR300 from Campbell Scientific. Datasets are available on request.

All data were merged and temporal scales were matched to 30-min intervals. All data analyses were carried out using the R version 4.0.3 (R Core Team, 2019). For our analysis, we used data from 22 September 2017 through 19 August 2020 (2.9 years) for both sites. The dataset was aggregated to daily resolution by calculating daily precipitation sums and daily maximum and minimum values of relative humidity and air temperature. Following Allen et al. (1998, Chapter-3) daily mean VPD was calculated as the difference between saturated vapor pressure (*Es*) and actual vapor pressure (*Ea*). *Es* was computed using Eq. 1 and *Ea* was computed using Eq. 2. The graphical representation of daily mean air temperature and VPD for both sites are provided in **Supplementary Material** (**Supplementary Figure 1**).

$$Es = \frac{0.6108exp\left[\frac{17.27T_{max}}{T_{max}+237.3}\right] + 0.6108exp\left[\frac{17.27T_{min}}{T_{min}+237.3}\right]}{2} \quad (1)$$

$$Ea = \frac{\left\{\left(0.6108exp\left[\frac{17.27T_{min}}{T_{min}+237.3}\right]\right) \times \frac{\mathrm{RH_{max}}}{100}\right\} + \left\{\left(0.6108exp\left[\frac{17.27T_{max}}{T_{max}+237.3}\right]\right) \times \frac{\mathrm{RH_{min}}}{100}\right\}}{2} \quad (2)$$

$$VPD = Es - Ea \quad (3)$$

Where, *Es* = the saturation vapor pressure (kPa), *Ea* = actual vapor pressure (kPa), T_{min} = minimum daily temperature (^{0}C), T_{max} = maximum daily temperature (^{0}C), $\mathrm{RH_{min}}$ = minimum relative humidity (%) and $\mathrm{RH_{max}}$ = maximum relative humidity (%) and *VPD* = daily mean vapor pressure deficit (kPa).

Multiple linear regression models were constructed using the "lm" function in R (R Core Team, 2019), by setting the water table as the dependent variable and daily mean VPD and total daily precipitation as the independent variables. Seasonality was statistically adjusted by using dummy/indicator variables of each month (11 months in total) with January as the reference month. This approach is commonly used to control for seasonality or periodicity (Hyndman et al., 2020 – Chapter 5.4; Maki et al., 1978; Hylleberg et al., 1993). Our analysis is based on the assumption that net radiation at the two study sites is the same because of their proximity to each other.

The summary statistics of the key variables are provided in **Table 1**. It should be noted that the purpose of the multiple linear regression analysis is to compare the drained fen with the rewetted fen and not to predict or model the peatland water tables.

Evapotranspiration and Soil Specific Yield Determination

To further investigate the underlying processes of how temperature and humidity impacts water table dynamics through VPD, rain-free day evapotranspiration (ET) from May to October was estimated for both sites using the Hays method (Hays, 2003), which is a modification of the White method (White, 1932). For ecosystems with shallow water tables, groundwater use by vegetation through evapotranspiration (ET) in addition to evaporation of soil moisture can be estimated by analyzing water table fluctuation which is relatively simple to implement (Mould et al., 2010; Mazur et al., 2014; Ahmad et al., 2020a). Water level fluctuation methods can be useful to apply in wetland ecosystems for estimating ET especially because it integrates several factors, including the growth-cycle of plants, the plant types, and moisture availability which are generally missing from micrometeorological methods of ET determination (Lautz, 2008; Mazur et al., 2014). The equation for

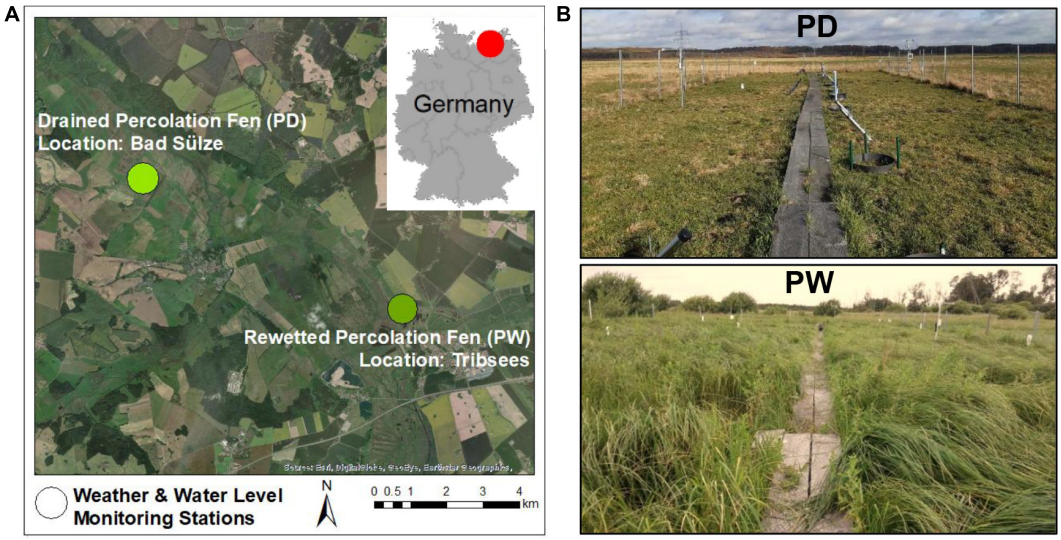

FIGURE 1 | (A) the study sites include a drained fen and a rewetted fen in Mecklenburg-Vorpommern. **(B)** the study plots at PD (upper panel) and PW (lower panel). The weather station at PD appears on the right of the photo. Photo: Haojie Liu (PD) and Michael Franz (PW).

TABLE 1 | Mean values of daily water level and meteorological variables for PD and PW.

Variables	PD	PW
Mean daily water level (mm)	−277.96 [−292.75, −263.18]	2.88 [−3.71, 9.46]
Daily precipitation (mm)	1.28 [1.09, 1.47]	1.54 [1.31, 1.76]
Mean daily vapor pressure deficit (kPa)	0.37 [0.35, 0.39]	0.39 [0.37, 0.42]

The square brackets contain the lower and upper confidence intervals.

ET determination is as follows:

$$\mathbf{E}T = \left[(\mathbf{H_1} - \mathbf{L}) + \frac{(\mathbf{H_2} - \mathbf{L})}{\mathbf{T_1}}\ \mathbf{T_2}\right] \times \mathbf{S_y} \qquad (4)$$

where, ET = evapotranspiration rate (mm/day); H_1 = highest water level (mm) on the observed day (usually early morning), H_2 = highest water level on the day after the observed day (mm), L = lowest water level (mm) on the observed day (usually evening), T_1 = time between L and H_2 (rising period), T_2 = time between H_1 and L (drawdown period), S_y = mean soil specific yield (dimensionless) for the observed diurnal water table fluctuation (see an example of diurnal water table fluctuation in **Figure 2** with respective equation parameters being labeled accordingly). Graphs of days with diurnal groundwater fluctuation for different water table depth stages have been provided as **Supplementary Material** (**Supplementary Figure 2**).

In the first part of Eq. 4, evapotranspiration is calculated as the water level difference between the low L and the high H_1 of the given day. This period of groundwater level fall (T_2) is the "drawdown period" which includes water uptake by plants, soil moisture evaporation, and net groundwater inflow. The second component of the equation is then added, which quantifies the latent water rise caused by inflow during the drawdown period. A key assumption is that ET is zero during this time (Hays, 2003; Mould et al., 2010). Another assumption is that the rate of net groundwater inflow for a given diurnal groundwater fluctuation is constant at H_1 and H_2 as they occur within a 24 h period.

Evapotranspiration was estimated using the dataset with a 30-min resolution. A user-defined function was developed in R to determine evapotranspiration according to Eq. 4, which calculates H_1 as the maximum water level of a given day, L as the minimum water level of the given day, and H_2 as the maximum water level of the following day. If the values of T_1 and T_2 did not add up to 24 h for a given diurnal groundwater fluctuation, the values of ET were corrected to represent 24 h by dividing the ET value by $T_1 + T_2$ and multiplying the result by 24 (hours). The function was applied only to days with diurnal fluctuations in the absence of rainfall in both study sites, evaluated using a graphical method. Diurnal water table fluctuation patterns were not evident for flooded conditions and thus ET was not estimated for such conditions. In total, daily ET could be determined for the same 55 days for PD and PW. The Shapiro-Wilk test showed that the differences of ET between the PD and PW are normally distributed (W = 0.96; p-value = 0.108). Thus, statistical testing was done using paired t-test, pairing the ET values of the sites on the same day.

Soil specific yield, which is the amount of water that would drain from a unit of soil if the water table would drop by a unit height (Childs, 1969), is a required parameter to determine ET when using the diurnal groundwater fluctuation method (see above). To determine soil specific yield we used the following

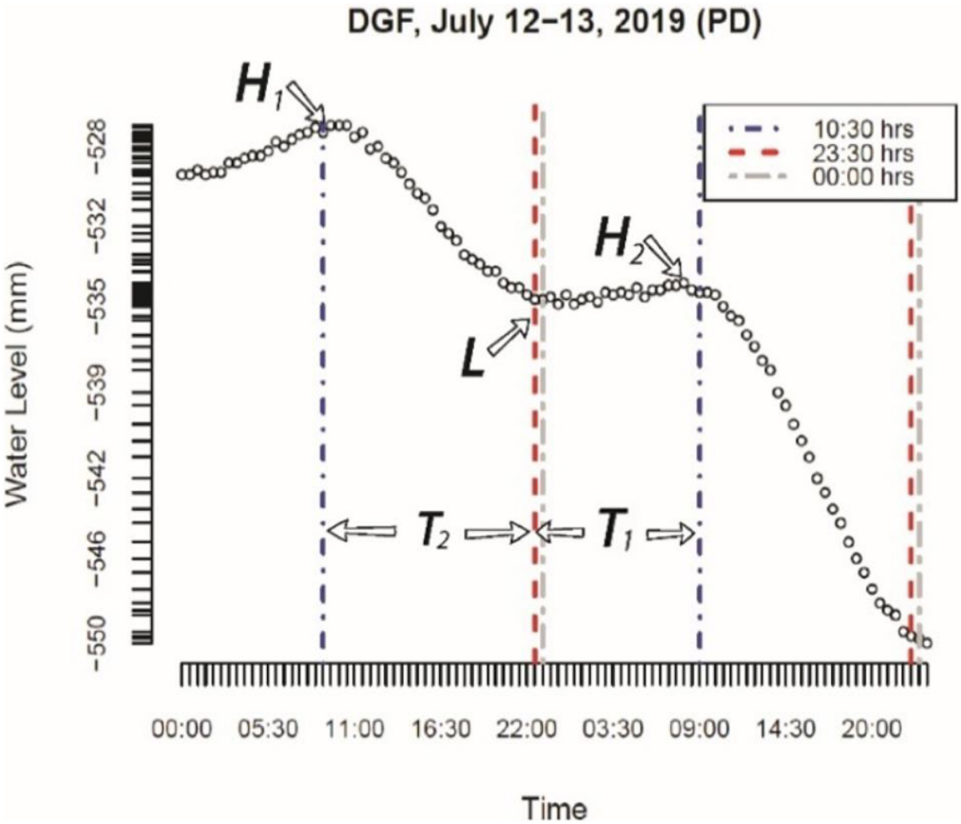

FIGURE 2 | An example of diurnal water table fluctuation (DGF) on a rain-free day at PD. Negative values indicate belowground.

equation according to several authors (Dolan et al., 1984; Dettmann and Bechtold, 2016a; Bourgault et al., 2017; Ahmad et al., 2020a):

$$S_y = \frac{P_{re}}{\Delta GWL} \quad (5)$$

where, S_y = soil specific yield, P_{re} = quantity of precipitation in mm, during the rainfall event, ΔGWL = change in groundwater levels which is the difference between the water levels at the start of the precipitation events and the water levels at the end of the events.

According to Bourgault et al. (2017) this method assumes that the time lag between the end of each precipitation event and the resulting water table position to be sufficiently short for evapotranspiration, net subsurface flow and water table recession following the precipitation events. Additionally, this method assumes that recharge is equal to precipitation (i.e., runoff is negligible), that the static equilibrium water content profile within the unsaturated zone is reached instantaneously following the precipitation event and that any deviation of the $P_{re}/\Delta GWL$ ratio from a theoretical model will be the result of the presence of capillary fringe, air entrapment, peat expansion and shrinkage, net subsurface flow, water table recession following precipitation and antecedent moisture content of the unsaturated zone (Bourgault et al., 2017). As we are interested in finding out difference in soil specific yield with depth, we did not include the calculation of surface specific yield.

P_{re} and ΔGWL were calculated using a user-defined function following Ahmad et al. (2020a) and Ahmad et al. (2020c). The function estimates the quantity of precipitation during precipitation events (in mm) and the respective event duration (in h) using a temporal moving window of 6 h. Summation of precipitation quantity and event duration stopped if precipitation ceased for 30 min. The initial and final water levels were recorded, and the difference (ΔGWL) was calculated for each event. The soil specific yield was plotted against the mean water level (determined as the mean of the initial and the final water level for each precipitation event, **Figure 3**). All events with water levels above the peat surface and all negative values of ΔGWL (indicating declining water levels despite ongoing precipitation) were removed. Specific yield values were constrained to belowground levels as we focus on belowground ET rates. The effect of antecedent soil moisture was assumed to be negligible. A certain rainfall intensity is required for initiating a water table response. We filtered PD to only include rainfall events of at least 0.33 mm h^{-1} intensity. We reduced the threshold for PW to be able to include more events, since PW, being a rewetted site, has water level at the surface for most of the year. Thus, events with intensities of at least 0.1 mm h^{-1} were included for PW. The final number of rainfall events for PD is 73 and for PW is 65.

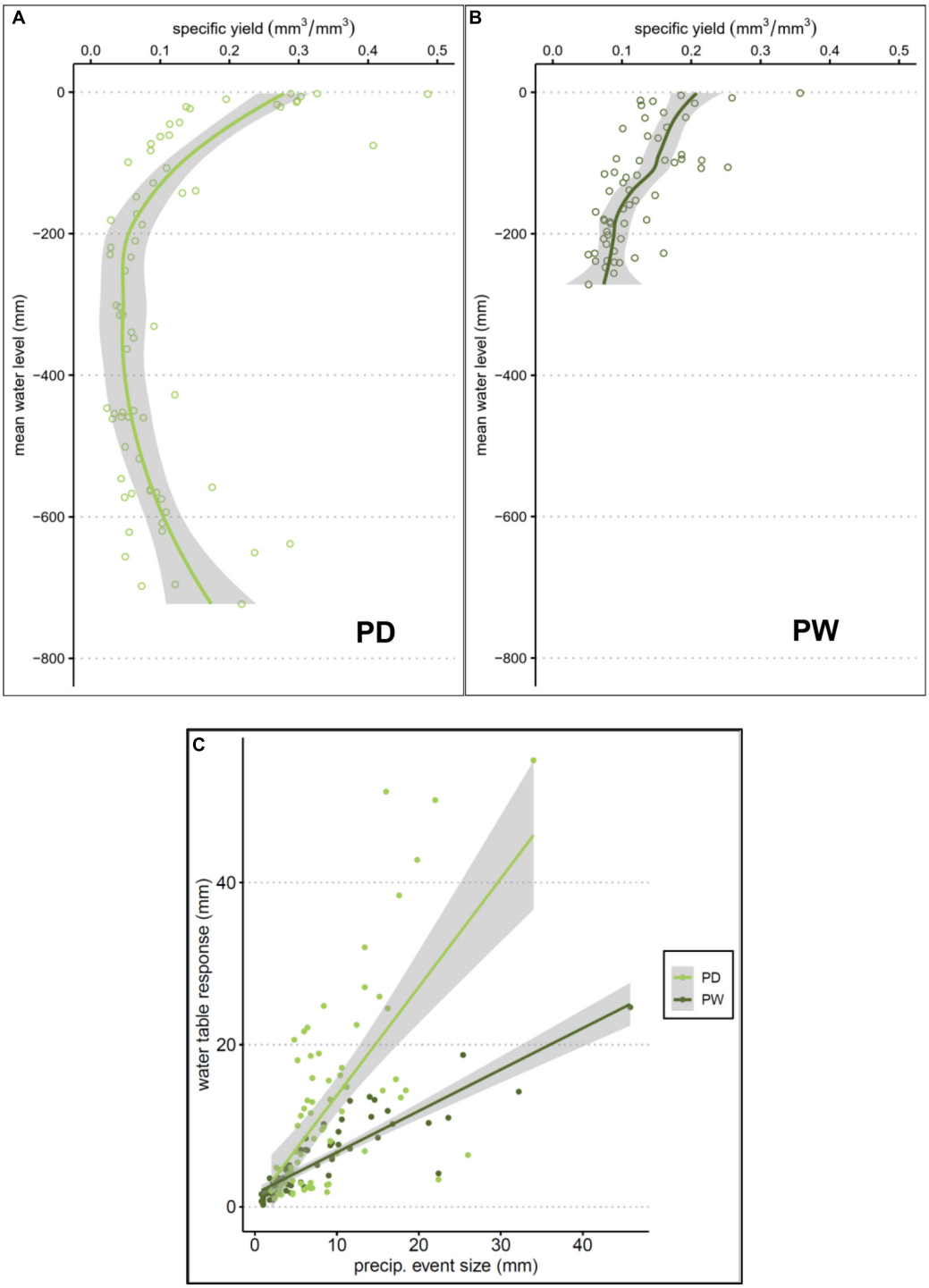

FIGURE 3 | Soil specific yield determined as the precipitation event size (mm) to groundwater table response ratio (P_{re}: ΔGWL) according to mean water level for **(A)** PD and **(B)** PW. The solid lines represent the loess smoothing function and the shaded area represents the 95% confidence interval. **(C)** water table response to precipitation event size for both PD and PW.

The smoothing function "*loess()*" (R Core Team, 2019) was used to determine the soil specific yield for a given mean water level which is indicative of peat depth. The mean soil specific yield for a given diurnal fluctuation was used in the ET Eq. 4 depending on the mean water level for the diurnal fluctuation.

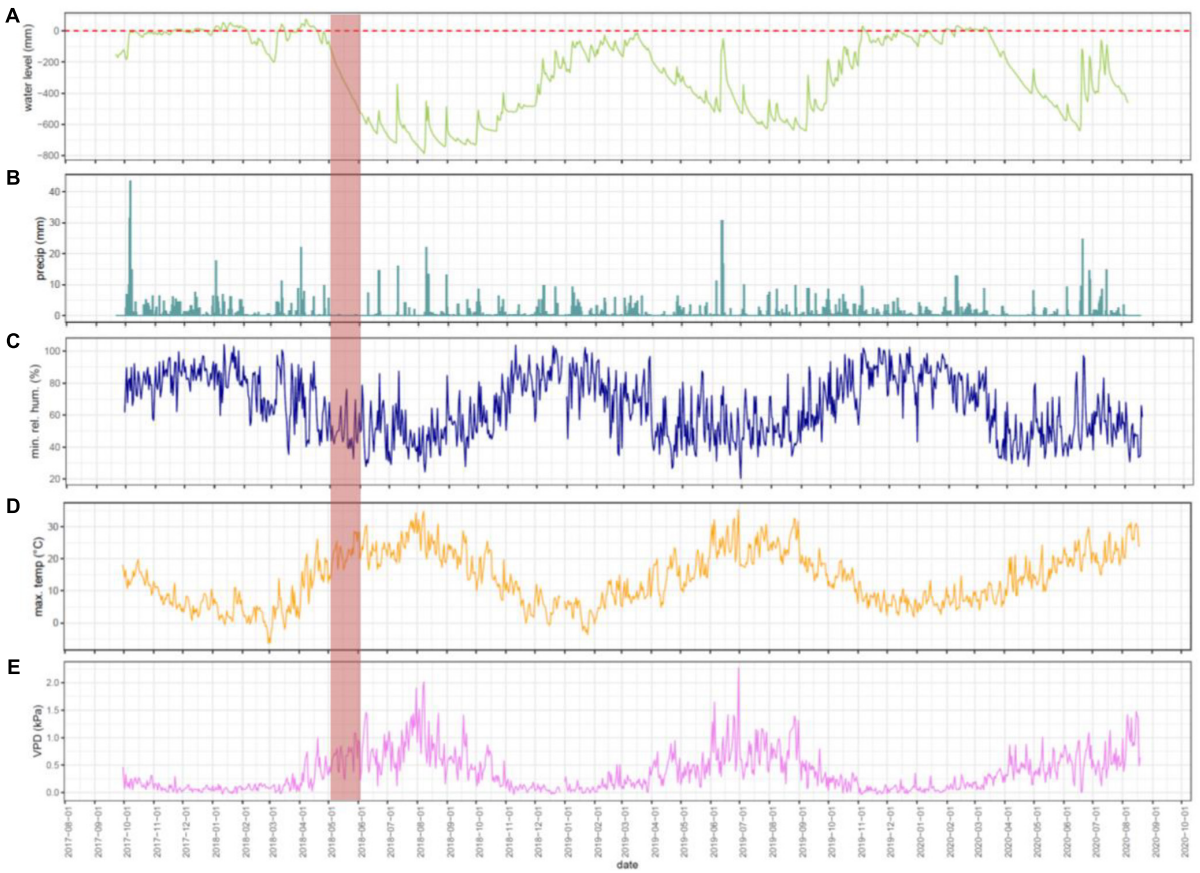

FIGURE 4 | Daily time series of **(A)** water level **(B)** precipitation **(C)** minimum relative humidity **(D)** maximum air temperature **(E)** mean vapor pressure deficit at PD. Dashed lines in panel **(A)** represent the peat surface while positive values indicate aboveground and negative values indicate belowground. An example of rapid water level decline during high maximum daily air temperatures and absence of substantial rainfall is indicated by the translucent pink band.

RESULTS

Water Table Characteristics and Meteorological Conditions

Both sites show a clear seasonality in water tables as well as in meteorological factors (**Figures 4**, **5**). The water level at the drained fen (PD), is below the peat surface for most of the year, with a substantial drop from the middle of spring to the end of summer for all 3 observed years. Even at the rewetted fen (PW), the water table receded substantially to about −300 mm in the summers of 2018 and 2019. Receding water tables at both sites occur at times of rising daily maximum air temperatures and an absence of substantial rainfall (**Figures 4**, **5**; for each site, an example of such a period has been indicated by a translucent pink band). The exceptionally dry late autumn and early winter seasons of 2018 and 2019, caused water levels to stay well below the peat surface at PD. For PD, the maximum daily rainfall (43 mm) occurred in October 2017 and for PW in July 2018 (46 mm). Autumn and winter seasons are characterized by high daily minimum humidity. Daily mean VPD values at both sites show close agreement with daily air temperatures.

The Effect of Meteorological Factors on the Water Table

An increase in daily mean VPD causes the water table to fall much further at PD than at PW. Similarly, an increase in daily precipitation induces the water table to rise more at PD than at PW. The water table at both sites shows an immediate response to rainfall. All meteorological regression terms are significant. Both models (for PD and PW) help to significantly explain more than 59 percent of the variation in the water level. The results of the multiple linear regression for both sites are presented in **Table 2**. A graphical representation of the estimated coefficients for the meteorological factors is provided in the **Supplementary Material** (**Supplementary Figure 3**).

Actual Evapotranspiration and Soil Specific Yield During Rain-Free Days

Daily evapotranspiration (ET) for 55 rain-free days was estimated for PD and PW. Mean ET at PD was 1.96 mm d^{-1} (minimum-maximum: 0.70 mm d^{-1} – 4.11 mm d^{-1}), while at PW mean ET was much higher (4.79 mm d^{-1}, minimum-maximum: 2.16 mm d^{-1} – 8.73 mm d^{-1}). Paired *t*-test reveals that ET at PW

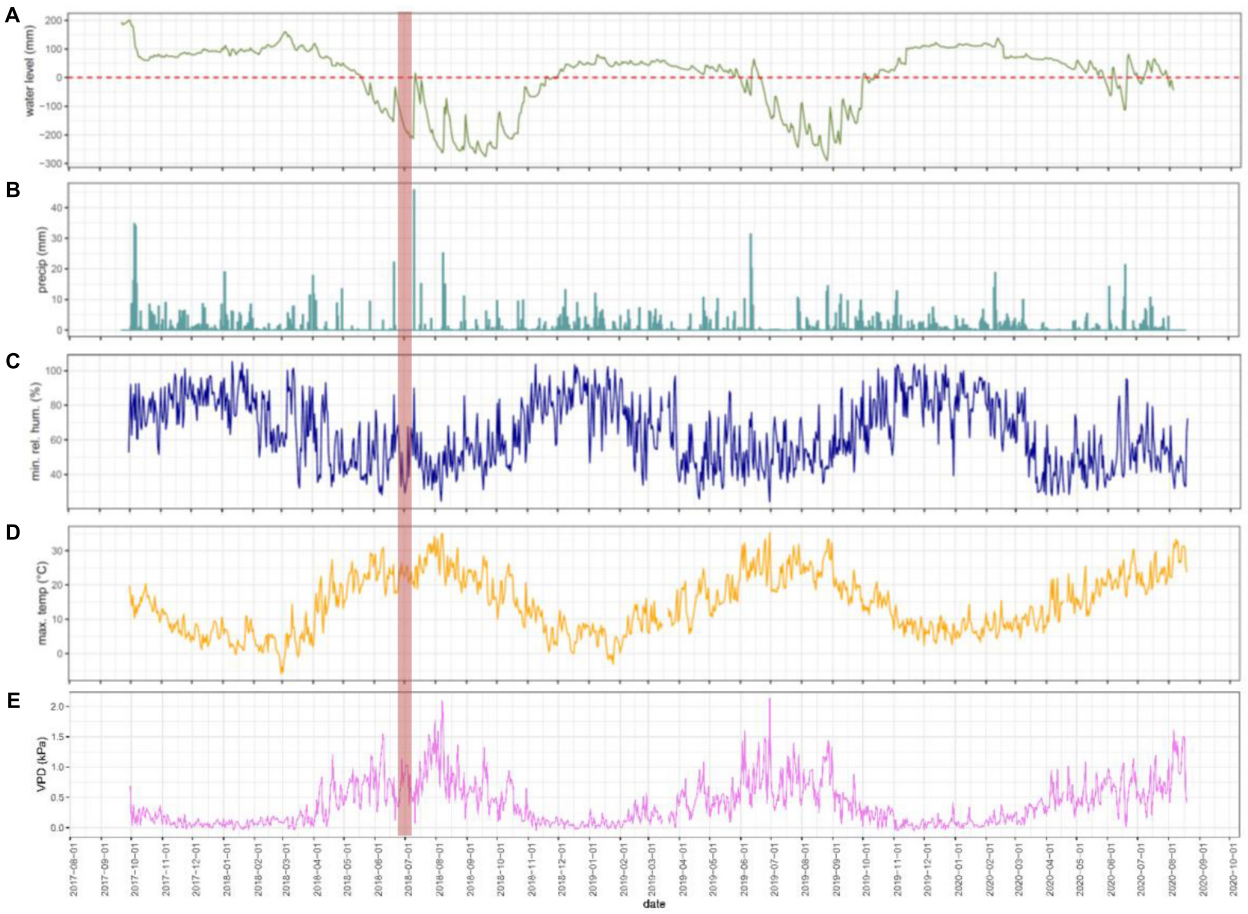

FIGURE 5 | Daily time series of **(A)** water level **(B)** precipitation **(C)** minimum relative humidity **(D)** maximum air temperature **(E)** mean vapor pressure deficit at PW. Dashed lines in panel **(A)** represents the peat surface while positive values indicate aboveground and negative values indicate belowground. An example of rapid water level decline during high maximum daily air temperatures and absence of substantial rainfall is indicated by the translucent pink band.

was significantly higher than at PD for the same days (mean difference = 2.82 mm d^{-1} [95% CI = 2.29 and 3.34], **Figure 6A**). Evapotranspiration at both sites differed over the months, with PW showing higher evapotranspiration compared to PD, for any given month (**Figure 6B**).

The average (median) soil specific yield values with which ET values were estimated were significantly higher at PW (0.284) than at PD (0.229, Wilcoxon rank-sum test with continuity correction, $W = 1074$, p-value = 0.008). Furthermore, the average (median) fluctuation (calculated as the difference between H1 and H2) for these days was significantly higher at PD (10 mm) compared to PW (8.4 mm, Wilcoxon rank-sum test with continuity correction, $W = 1850$, p-value = 0.044).

DISCUSSION

According to our regression analysis, precipitation and VPD affect the water table (significantly) at different magnitudes, depending on the drainage status of the fen, while the direction of the relationship between the meteorological variables and water levels were according to expectations. This was the case even though the local meteorological conditions at both the drained (PD) and rewetted fens (PW) were comparable.

The magnitude of water table response to precipitation at PD is much higher than at PW. The negative effect of daily mean air VPD on the water level can be explained by evapotranspiration as VPD is indicative of the ability of the atmosphere to hold additional water that is evaporated or transpired (evapotranspirative demand, Zipper et al., 2017). Similar to the effect of rainfall, the effect of VPD on the water level was much higher at PD than at PW. However, evapotranspiration for the same dry days was substantially higher at PW than at PD, likely because of differences in vegetation composition and plant biomass (Jiménez-Rodríguez et al., 2019). The vegetation at PD is much shorter (around 20 cm in height) and mostly comprises grasses, while the vegetation at PW is dominated by taller sedges (*Carex acutiformis*), around 1 m in height (see Schwieger et al., 2020). Schwieger et al. (2020) quantified plant production in both these sites and report a much higher plant biomass production at PW (aboveground: 346 g m^{-2} y^{-1}; belowground: 199 g m^{-2} y^{-1}) than at PD (aboveground: 80 g m^{-2} y^{-1}; belowground:

TABLE 2 | Multiple linear regression of water level at **(A)** PD and **(B)** PW.

A						
Sites	**Regression terms**	**Estimated coefficients**	**Std. error**	***t* value**	**Pr(> | t|)**	
PD	Intercept	−54.12	15.22	−3.56	0.00039	***
	January (reference)					
	February	13.98	21.70	0.64	0.51976	
	March	10.96	21.28	0.52	0.60678	
	April	−78.78	22.67	−3.48	0.00053	***
	May	−257.02	22.94	−11.20	$<2\times10^{-16}$	***
	June	−337.67	25.61	−13.18	$<2\times10^{-16}$	***
	July	−351.95	24.99	−14.09	$<2\times10^{-16}$	***
	August	−428.03	27.69	−15.46	$<2\times10^{-16}$	***
	September	−428.82	24.49	17.51	$<2\times10^{-16}$	***
	October	−213.20	21.60	−9.87	$<2\times10^{-16}$	***
	November	−129.83	21.34	−6.08	1.65×10^{-09}	***
	December	−51.65	21.16	−2.44	0.01482	*
	Daily mean VPD (kPa)	**−141.47**	**20.74**	**−6.82**	$\mathbf{1.52\times10^{-11}}$	***
	Daily precipitation (mm)	**7.31**	**1.43**	**5.11**	$\mathbf{3.75\times10^{-7}}$	***
B						
Sites	**Regression terms**	**Estimated coefficients**	**Std. error**	***t* value**	**Pr(> | t|)**	
PW	Intercept	86.96	7.48	11.62	$<2\times10^{-16}$	***
	January (reference)					
	February	2.47	10.66	0.23	0.81700	
	March	−0.83	10.47	−0.08	0.93717	
	April	−16.72	11.24	−1.49	0.13707	
	May	−45.34	11.40	−3.98	7.42×10^{-05}	***
	June	−103.28	12.57	−8.22	6.10×10^{-16}	***
	July	−143.82	12.29	−11.71	$<2\times10^{-16}$	***
	August	−202.35	13.54	−14.94	$<2\times10^{-16}$	***
	September	−206.76	12.14	−17.03	$<2\times10^{-16}$	***
	October	−97.60	10.62	−9.20	$<2\times10^{-16}$	***
	November	−42.66	10.47	−4.07	4.99×10^{-05}	***
	December	−7.33	10.38	−0.71	0.48019	
	Daily mean VPD (kPa)	**−47.23**	**9.82**	**−4.81**	$\mathbf{1.73\times10^{-06}}$	***
	Daily precipitation (mm)	**1.85**	**0.61**	**3.05**	**0.00236**	**

(A) *Residual standard error 144.3 on 1049 degrees of freedom | Multiple R-squared: 0.659 | Adjusted R-squared: 0.655 | F-statistic: 156 on 13 and 1049 DF | p-value:* $<2.2\times10^{-16}$. ***(B)*** *Residual standard error: 70.8 on 1049 degrees of freedom | Multiple R-squared: 0.587 | Adjusted R-squared: 0.582 | F-statistic: 114.6 on 13 and 1049 DF | p-value:* $<2.2\times10^{-16}$. *Signif. codes: <0.001***, <0.01**, <0.05*, <0.1. Meteorological variables and their statistics are in bold.*

43 g m^{-2} y^{-1}). Other than differences in vegetation as a cause for differences in ET, the depth to water table can also provide additional explanation. During the study period, PD had a mean daily water level of around −30 cm while for PW the mean daily water level is nearly 0 cm (at the surface). Several studies show that high ET rates generally occur in sites with shallow water tables, and lower ET rates in sites with deep water tables (Duell, 1988; Nichols, 1994; Cooper et al., 2006; Zhang and Schilling, 2006). Thus, even though PD has lower ET rates than PW, the site demonstrates more water level sensitivity to meteorological forcing.

We attribute the differential influence of meteorological conditions on water table dynamics to different soil-specific yield values (i.e., water storage capacity) largely driven by lower water table position at the drained site. Specific yield relates the change in water storage in a soil to the change in water level (LaRose et al., 1997). Drainage of natural peatlands result in a decline in water level, and thus in absence of water saturated conditions peat accumulation ceases and peat degradation starts. Both, peat degradation as well as shrinkage from lower water table position, causes peat specific yield to decrease. In a recent study by Ahmad et al. (2020c), the rate of water table rise as a response to discrete rainfall events was investigated at the same sites. They found that the water table response at PD was much higher than at PW and attributed the higher response rate to a lower storage capacity of the degraded peat (in the upper horizons) as indicated by a higher bulk density (compared to PW). Mustamo et al. (2016) who studied peat soils

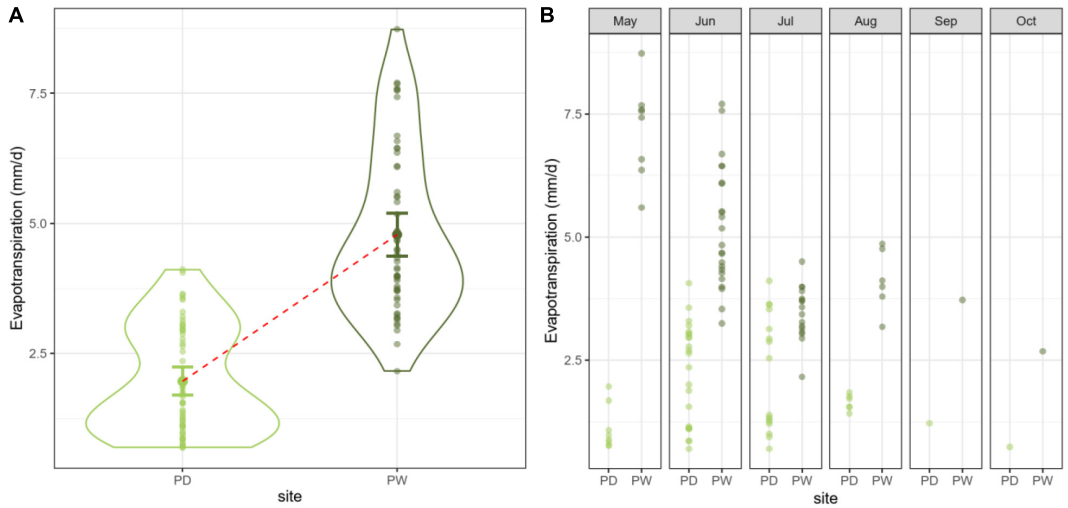

FIGURE 6 | (A) Violin plots of ET with mean and error bars (95% confidence interval). The red dotted line connects the two means (of PD and PW). The violin shapes show the distribution of the data for each site. **(B)** Evapotranspiration for both sites according to months (in panels).

under different land-use options, found drained peat to have low specific yields, causing water tables to increase substantially and rapidly after precipitation events. Similarly, Menberu et al. (2018) found that boreal peatlands had significantly higher water table (WT) rise per rainfall input under drained conditions, due to lower soil specific yield values compared to restored and undisturbed conditions.

The soil specific yield (averaged over the days for which ET was calculated) of peat at PD was significantly lower than that of PW, while the diurnal fluctuation at PD was significantly higher than at PW (although the ET derived at PD was significantly lower than at PW). This means that one unit change in the water-level at PD corresponds to a much lower volume of water than what the same unit drop or rise corresponds to at PW. Therefore, the higher impact of VPD and rainfall on the water table at PD could, in part, be due to the lower water storage capacity of the degraded fen peat (Ahmad et al., 2020c) driven mainly by the difference in water table position. PW, being a rewetted site has a water table near or above the peat surface for most of the study period. According to our analysis, soil specific yield, for PD are lower than for PW at depths below −250 mm, which is not experienced by the water levels at PW. However, according to our calculation of specific yield, the 11 cm peat accumulation over the last 20 years, was not sufficient to increase specific yield for the same depths. Nevertheless, Ahmad et al. (2020c), as mentioned earlier, using a bulk density based pedotransfer function found that the rewetted site has a higher specific yield compared to the drained site.

When the water level is above the soil surface, in the absence of peat as a matrix, the surface specific yield could be assumed to be one (Dettmann and Bechtold, 2016b) and thus showing a lower response to precipitation and VPD. According to Cooper et al. (2019) once water table is near the soil surface, water table response becomes limited. Thus, this difference in water table position between the drained and the rewetted fens, is a major control over how the sites differ in their response to meteorological forcing.

While we were able to evaluate the relationship between meteorological conditions and water table dynamics, several limitations need to be considered. As we had only two monitoring wells at only two sites, care must be taken in generalizing conclusions, particularly for fens with different drainage histories or with a different hydrological regime and/or vegetation. Although the study could have benefitted from a higher number of monitoring wells to capture spatial variability and microtopography, water levels measured in an observation well are representative of an area of at least several tens of square meters (Maréchal et al., 2006). For a better understanding of the effect of rewetting or management regimes, a "before-after-control" approach could be more appropriate (see Menberu et al., 2016). However, such long-term monitoring of hydrometeorological parameters is especially rare for temperate fen peatlands (Bechtold et al., 2014; Ahmad et al., 2020c). We focused on belowground or soil specific yield in an attempt to find out differences in soil properties between the sites with depth. In terms of limitations, this means that we did not include aboveground/surface specific yield; our focus was not the entire landscape or ecosystem, but the locations where water table and meteorological parameters were measured.

Our results underline the importance of meteorological effects, namely vapor pressure deficit on water table dynamics in fens, which in turn are influenced by water management decisions and consequent change to water table position. Our findings have implications for prompt and effective rewetting of drained and degraded peatlands. Degraded fen peatlands, because of their low water storage capacity and water table positions, are likely to be more vulnerable to temperature extremes which can cause water tables to rapidly decline by increasing atmospheric water demand (vapor pressure deficit), thereby further amplifying the process of peat degradation and

carbon mineralization. Therefore, delays in peatland rewetting are likely to result in additional efforts and resources being required to restore ecosystem functions. The longer we wait with rewetting, the more difficult it will be to achieve water levels continuously fluctuating around the peat surface. For rewetted fens, continuous monitoring is advisable to ensure long-term success especially under a changing climate and associated drought events.

DATA AVAILABILITY STATEMENT

The raw data supporting the conclusions of this article will be made available by the authors, without undue reservation.

AUTHOR CONTRIBUTIONS

SAh: conceptualization, methodology, formal analysis and coding, writing – original draft, writing – review and editing, visualization, software, and investigation. HL: conceptualization, supervision, methodology, formal analysis, investigation, writing – review and editing, visualization, and project administration. SAl: formal analysis and coding, writing, review, and editing. AG: data curation, writing – review and editing, and investigation. GJ: formal analysis and coding, funding acquisition, and writing – review and editing. BL: conceptualization, supervision, writing – review and editing, funding acquisition, and project administration. All authors contributed to the article and approved the submitted version.

FUNDING

This work was supported by European Social Fund (ESF) and the Ministry of Education, Science and Culture of Mecklenburg-Western Pomerania funded this work within the project WETSCAPES (ESF/14-BM-A55-0028/16, ESF/14-BM-A55-0030/16, and ESF/14-BM-A55-0035/16). Intellectual support was also received from the Research Training Group "Baltic TRANSCOAST" funded by the Deutsche Forschungsgemeinschaft (DFG, German Research Foundation) under Grant Number DFG-GRK 2000.

ACKNOWLEDGMENTS

We would like to thank Daniel Köhn, Christian Schmidt, and Laurenz Teuber for hydrological and meteorological data transfer/collection. We would also like to express our gratitude to Sarah Schwieger, for providing insights into the vegetation characteristics of the two sites. Finally, we would like to thank the editor and the reviewers.

SUPPLEMENTARY MATERIAL

The Supplementary Material for this article can be found online at: https://www.frontiersin.org/articles/10.3389/feart.2021.630469/full#supplementary-material

REFERENCES

Ahmad, S., Hörmann, G., Zantout, N., and Schrautzer, J. (2020a). Quantifying actual evapotranspiration in fen ecosystems: implications of management and vegetation structure: implications of management and vegetation structure. *Ecohydrol. Hydrobiol.* 20, 381–395. doi: 10.1016/j.ecohyd.2020.04.001

Ahmad, S., Liu, H., Beyer, F., Kløve, B., and Lennartz, B. (2020b). Spatial heterogeneity of soil properties in relation to microtopography in a non-tidal rewetted coastal mire. *Mires Peat* 26, 1–18. doi: 10.19189/MaP.2019.GDC.StA.1779

Ahmad, S., Liu, H., Günther, A., Couwenberg, J., and Lennartz, B. (2020c). Long-term rewetting of degraded peatlands restores hydrological buffer function. *Sci. Total Environ.* 749:141571. doi: 10.1016/j.scitotenv.2020.141571

Allen, R. G., Pereira, L. S., Raes, D., and Smith, M. (1998). *Crop Evapotranspiration-Guidelines for Computing Crop Water Requirements-Fao Irrigation and Drainage Paper 56*. FAO: Rome.

Baldocchi, D. D., Xu, L., and Kiang, N. (2004). How plant functional-type, weather, seasonal drought, and soil physical properties alter water and energy fluxes of an oak–grass savanna and an annual grassland. *Agric. For. Meteorol.* 123, 13–39. doi: 10.1016/j.agrformet.2003.11.006

Bechtold, M., Tiemeyer, B., Laggner, A., Leppelt, T., Frahm, E., and Belting, S. (2014). Large-scale regionalization of water table depth in peatlands optimized for greenhouse gas emission upscaling. *Hydrol. Earth Syst. Sci.* 18, 3319–3339. doi: 10.5194/hess-18-3319-2014

Bourgault, M. A., Larocque, M., and Garneau, M. (2017). Quantification of peatland water storage capacity using the water table fluctuation method. *Hydrol. Process.* 31, 1184–1195. doi: 10.1002/hyp.11116

Bourgault, M. A., Larocque, M., and Garneau, M. (2019). How do hydrogeological setting and meteorological conditions influence water table depth and fluctuations in ombrotrophic peatlands? *J. Hydrol.* 4:100032. doi: 10.1016/j.hydroa.2019.100032

Branham, J. E., and Strack, M. (2014). Saturated hydraulic conductivity in Sphagnum-dominated peatlands: do microforms matter? *Hydrol. Process.* 28, 4352–4362. doi: 10.1002/hyp.10228

Bridgham, S. D., Pastor, J., Updegraff, K., Malterer, T. J., Johnson, K., Harth, C., et al. (1999). Ecosystem control over temperature and energy flux in northern peatlands. *Ecol. Appl.* 9, 1345–1358. doi: 10.1890/1051-0761(1999)009[1345:ecotae]2.0.co;2

Childs, E. C. (1969). *An introduction to the Physical Basis of Soil Water Phenomena*. Hoboken, NJ: John Wiley & Sons, Incorporated.

Cooper, D. J., Sanderson, J. S., Stannard, D. I., and Groeneveld, D. P. (2006). Effects of long-term water table drawdown on evapotranspiration and vegetation in an arid region phreatophyte community. *J. Hydrol.* 325, 21–34. doi: 10.1016/j.jhydrol.2005.09.035

Cooper, D. J., Sueltenfuss, J., Oyague, E., Yager, K., Slayback, D., Caballero, E. M. C., et al. (2019). Drivers of peatland water table dynamics in the central andes, bolivia and peru. *Hydrol. Process.* 33, 1913–1925.

Dettmann, U., and Bechtold, M. (2016a). Deriving effective soil water retention characteristicsfrom shallow water table fluctuations in peatlands. *Vadose Zone J.* 15, 1–13.

Dettmann, U., and Bechtold, M. (2016b). One-dimensional expression to calculate specific yield for shallow groundwater systems with microrelief. *Hydrol. Process.* 30, 334–340. doi: 10.1002/hyp.10637

Dolan, T. J., Hermann, A. J., Bayley, S. E., and Zoltek, J. Jr. (1984). Evapotranspiration of a Florida, USA, freshwater wetland. *J. Hydrol.* 74, 355–371. doi: 10.1016/0022-1694(84)90024-6

Duell, L. F. W. (1988). *Estimates of Evapotranspiration in Alkaline Scrub and Meadow Communities of Owens Valley, California, using the Bowen-ratio, Eddy-Correlation, and Penman-Combination Methods*, Vol. 88. Reston, VA: US Geological Survey.

Dunne, T., Zhang, W., and Aubry, B. F. (1991). Effects of rainfall, vegetation, and microtopography on infiltration and runoff. *Water Resour. Res.* 27, 2271–2285. doi: 10.1029/91wr01585

Ferone, J. M., and Devito, K. J. (2004). Shallow groundwater–surface water interactions in pond–peatland complexes along a Boreal Plains topographic gradient. *J. Hydrol.* 292, 75–95. doi: 10.1016/j.jhydrol.2003.12.032

Grossiord, C., Buckley, T. N., Cernusak, L. A., Novick, K. A., Poulter, B., Siegwolf, R. T. W., et al. (2020). Plant responses to rising vapor pressure deficit. *New Phytol.* 226, 1550–1566. doi: 10.1111/nph.16485

Günther, A., Barthelmes, A., Huth, V., Joosten, H., Jurasinski, G., Koebsch, F., et al. (2020). Prompt rewetting of drained peatlands reduces climate warming despite methane emissions. *Nat. Commun.* 11:1644. doi: 10.1038/s41467-020-15499-z

Hays, K. B. (2003). *Water use by Salt Cedar Saltcedar (Tamarix sp.) and Associated Vegetation on the Canadian, Colorado, and Pecos Rivers in Texas*. Master's Thesis, Texas A&M University, College Station, TX.

Helbig, M., Waddington, J. M., Alekseychik, P., Amiro, B. D., Aurela, M., Barr, A. G., et al. (2020). Increasing contribution of peatlands to boreal evapotranspiration in a warming climate. *Nat. Clim. Change* 10, 555–560. doi: 10.1038/s41558-020-0763-7

Hooijer, A., Page, S., Jauhiainen, J., Lee, W. A., Lu, X. X., Idris, A., et al. (2012). Subsidence and carbon loss in drained tropical peatlands. *Biogeosciences* 9, 1053–1071. doi: 10.5194/bg-9-1053-2012

Hylleberg, S., Jørgensen, C., and Sørensen, N. K. (1993). Seasonality in macroeconomic time series. *Empir. Econ.* 18, 321–335. doi: 10.1007/bf01205406

Hyndman, R. J., Athanasopoulos, G., Bergmeir, C., Caceres, G., Chhay, L., O'Hara-Wild, M., et al. (2020). *Package 'Forecast'*. Available online at: https://cran.r-project.org/web/packages/forecast/forecast.pdf (accessed August 25, 2020).

Jiménez-Rodríguez, C. D., Esquivel-Vargas, C., Coenders-Gerrits, M., and Sasa-Marín, M. (2019). Quantification of the evaporation rates from six types of wetland cover in Palo Verde National Park, Costa Rica. *Water* 11:674. doi: 10.3390/w11040674

Joosten, H., and Couwenberg, J. (2001). "Bilanzen zum moorverlust: das beispiel europa [balance sheet for loss of mires: the example of europe]," in *Landschaftsökologische Moorkunde [Landscape Ecology of Mires]*, 2nd Edn, Vol. 2, eds M. Succow and H. Joosten (Stuttgart: Schweizerbart Science Publishers), 406–409.

Joosten, H., Tanneberger, F., and Moen, A. (Eds.) (2017). *Mires and Peatlands of Europe*. Stuttgart: Schweizerbart'sche Verlagsbuchhandlung.

Jurasinski, G., Ahmad, S., Anadon-Rosell, A., Berendt, J., Beyer, F., Bill, R., et al. (2020). From understanding to sustainable use of peatlands:: the wetscapes approach. *Soil Syst.* 4:14. doi: 10.3390/soilsystems4010014

Kimmel, K., and Mander, Ü (2010). Ecosystem services of peatlands: Implications for restoration. *Progress Phys. Geogr.* 34, 491–514. doi: 10.1177/0309133310365595

Koch, M., and Jurasinski, G. (2015). Four decades of vegetation development in a percolation mire complex following intensive drainage and abandonment. *Plant Ecol. Divers.* 8, 49–60. doi: 10.1080/17550874.2013.862752

Lamers, L. P. M., Vile, M. A., Grootjans, A. P., Acreman, M. C., van Diggelen, R., Evans, M. G., et al. (2015). Ecological restoration of rich fens in Europe and North America: from trial and error to an evidence-based approach. *Biol. Rev. Camb. Philos. Soc.* 90, 182–203. doi: 10.1111/brv.12102

LaRose, S., Price, J., and Rochefort, L. (1997). Rewetting of a cutover peatland: hydrologic assessment. *Wetlands* 17, 416–423. doi: 10.1007/BF03161431

Lautz, L. K. (2008). Estimating groundwater evapotranspiration rates using diurnal water-table fluctuations in a semi-arid riparian zone. *Hydrogeol. J.* 16, 483–497. doi: 10.1007/s10040-007-0239-0

Lennartz, B., and Liu, H. (2019). Hydraulic functions of peat soils and ecosystem service. *Front. Environ. Sci.* 7:92. doi: 10.3389/fenvs.2019.00092

Levison, J., Larocque, M., Fournier, V., Gagné, S., Pellerin, S., and Ouellet, M. A. (2014). Dynamics of a headwater system and peatland under current conditions and with climate change. *Hydrol. Process.* 28, 4808–4822. doi: 10.1002/hyp.9978

Liu, H., Janssen, M., and Lennartz, B. (2016). Changes in flow and transport patterns in fen peat following soil degradation. *Eur. J. Soil Sci.* 67, 763–772. doi: 10.1111/ejss.12380

Liu, H., and Lennartz, B. (2019). Hydraulic properties of peat soils along a bulk density gradient—a meta study. *Hydrol. Process.* 33, 101–114. doi: 10.1002/hyp.13314

Liu, H., Price, J., Rezanezhad, F., and Lennartz, B. (2020a). Centennial-scale shifts in hydrophysical properties of peat induced by drainage. *Water Resour. Res.* 56:141. doi: 10.1029/2020WR027538

Liu, H., Wrage-Mönnig, N., and Lennartz, B. (2020b). Rewetting strategies to reduce nitrous oxide emissions from European peatlands. *Commun. Earth Environ.* 1, 1–7. doi: 10.1038/s43247-020-00017-2

Liu, H., Zak, D., Rezanezhad, F., and Lennartz, B. (2019). Soil degradation determines release of nitrous oxide and dissolved organic carbon from peatlands. *Environ. Res. Lett.* 14:094009. doi: 10.1088/1748-9326/ab3947

Maki, J. E., Hoffman, D. M., and Berk, R. A. (1978). A time series analysis of the impact of a water conservation campaign. *Eval. Q.* 2, 107–118. doi: 10.1177/0193841x8000400106

Malhotra, A., Roulet, N. T., Wilson, P., Giroux-Bougard, X., and Harris, L. I (2016). Ecohydrological feedbacks in peatlands: an empirical test of the relationship among vegetation, microtopography and water table. *Ecohydrology* 9, 1346–1357. doi: 10.1002/eco.1731

Maréchal, J. C., Dewandel, B., Ahmed, S., Galeazzi, L., and Zaidi, F. K. (2006). Combined estimation of specific yield and natural recharge in a semi-arid groundwater basin with irrigated agriculture. *J. Hydrol.* 329, 281–293. doi: 10.1016/j.jhydrol.2006.02.022

Mazur, M. L. C., Wiley, M. J., and Wilcox, D. A. (2014). Estimating evapotranspiration and groundwater flow from water-table fluctuations for a general wetland scenario. *Ecohydrology* 7, 378–390. doi: 10.1002/eco.1356

Menberu, M. W., Haghighi, A. T., Ronkanen, A. K., Marttila, H., and Kløve, B. (2018). Effects of drainage and subsequent restoration on peatland hydrological processes at catchment scale. *Water Resour. Res.* 54, 4479–4497. doi: 10.1029/2017wr022362

Menberu, M. W., Tahvanainen, T., Marttila, H., Irannezhad, M., Ronkanen, A. K., Penttinen, J., et al. (2016). Water-table-dependent hydrological changes following peatland forestry drainage and restoration: analysis of restoration success. *Water Resour. Res.* 52, 3742–3760. doi: 10.1002/2015WR018578

Michaelis, D., Mrotzek, A., and Couwenberg, J. (2020). Roots, tissues, cells and fragments—how to characterize peat from drained and rewetted fens. *Soil Syst.* 4:12. doi: 10.3390/soilsystems4010012

Mould, D. J., Frahm, E., Salzmann, T., Miegel, K., and Acreman, M. C. (2010). Evaluating the use of diurnal groundwater fluctuations for estimating evapotranspiration in wetland environments: case studies in southeast England and northeast Germany. *Ecohydrology* 3, 294–305. doi: 10.1002/eco.108

Mrotzek, A., Michaelis, D., Günther, A., Wrage-Mönnig, N., and Couwenberg, J. (2020). Mass balances of a drained and a rewetted peatland: on former losses and recent gains. *Soil Syst.* 4:16. doi: 10.3390/soilsystems4010016

Mustamo, P., Hyvarinen, M., Ronkanen, A.-K., and Klove, B. (2016). Physical properties of peat soils under different land use options. *Soil Use Manag.* 32, 400–410. doi: 10.1111/sum.12272

Nichols, W. D. (1994). Groundwater discharge by phreatophyte shrubs in the Great Basin as related to depth to groundwater. *Water Resour. Res.* 30, 3265–3274. doi: 10.1029/94wr02274

Nijp, J. J., Limpens, J., Metselaar, K., Peichl, M., Nilsson, M. B., van der Zee, S. E. A. T. M., et al. (2015). Rain events decrease boreal peatland net CO2 uptake through reduced light availability. *Glob. Chang. Biol.* 21, 2309–2320. doi: 10.1111/gcb.12864

Philippov, D. A., and Yurchenko, V. V. (2019). Data on air temperature, relative humidity and dew point in a boreal Sphagnum bog and an upland site (Shichengskoe mire system, North-Western Russia). *Data Brief* 25:104156. doi: 10.1016/j.dib.2019.104156

Price, J. S. (1996). Hydrology and microclimate of a partly restored cutover bog, Quebec. *Hydrol. Process.* 10, 1263–1272. doi: 10.1002/(sici)1099-1085(199610)10:10<1263::aid-hyp458>3.0.co;2-1

Pronger, J., Schipper, L. A., Hill, R. B., Campbell, D. I., and McLeod, M. (2014). Subsidence rates of drained agricultural peatlands in new zealand and the relationship with time since drainage. *J. Environ. Qual.* 43, 1442–1449. doi: 10.2134/jeq2013.12.0505

R Core Team (2019). *R: A Language and Environment for Statistical Computing [Computer software]*. Vienna: R Core Team.

Rezanezhad, F., Price, J. S., Quinton, W. L., Lennartz, B., Milojevic, T., and Van Cappellen, P. (2016). Structure of peat soils and implications for water storage, flow and solute transport: a review update for geochemists. *Chem. Geol.* 429, 75–84. doi: 10.1016/j.chemgeo.2016.03.010

Ruseckas, J., and Grigaliūnas, V. (2008). Effect of drain-blocking and meteorological factors on ground water table fluctuations in kamanos mire. *J. Environ. Eng. Landsc. Manag.* 16, 168–177. doi: 10.3846/1648-6897.2008.16.168-177

Schrautzer, J., Rinker, A., Jensen, K., Mûller, F., Schwartze, P., and Dierßen, K. (2007). "Succession and restoration of drained fens: perspectives from northwestern Europe," in *Springer Series on Environmental Management. Linking Restoration and Ecological Succession*, eds L. R. Walker, J. Walker, and R. J. Hobbs (cham: Springer), 90–120. doi: 10.1007/978-0-387-35303-6_5

Schrautzer, J., Sival, F., Breuer, M., Runhaar, H., and Fichtner, A. (2013). Characterizing and evaluating successional pathways of fen degradation and restoration. *Ecol. Indic.* 25, 108–120. doi: 10.1016/j.ecolind.2012.08.018

Schwieger, S., Kreyling, J., Couwenberg, J., Smiljaniæ, M., Weigel, R., Wilmking, M., et al. (2020). Wetter is better: rewetting of minerotrophic peatlands increases plant production and moves them towards carbon sinks in a dry year. *Ecosystems* 1–17. doi: 10.1007/s10021-020-00570-z

Strack, M., Waddington, J. M., Bourbonniere, R. A., Buckton, E. L., Shaw, K., Whittington, P., et al. (2008). Effect of water table drawdown on peatland dissolved organic carbon export and dynamics. *Hydrol. Process.* 22, 3373–3385. doi: 10.1002/hyp.6931

Succow, M., and Joosten, H. (Eds.) (2001). *Landschaftsökologische Moorkunde [Landscape Ecology of Mires]*, 2nd Edn. Stuttgart: Schweizerbart Science Publishers.

Tarnocai, C. (2009). The impact of climate change on Canadian peatlands. *Can. Water Resour. J.* 34, 453–466. doi: 10.4296/cwrj3404453

Tiemeyer, B., Borraz, E. A., Augustin, J., Bechtold, M., Beetz, S., Beyer, C., et al. (2016). High emissions of greenhouse gases from grasslands on peat and other organic soils. *Glob. Chang. Biol.* 22, 4134–4149. doi: 10.1111/gcb.13303

Tiemeyer, B., Lennartz, B., and Vegelin, K. (2006). Hydrological modelling of a re-wetted peatland on the basis of a limited dataset for water management. *J. Hydrol.* 325, 376–389. doi: 10.1016/j.jhydrol.2005.10.039

White, W. N. (1932). *A Method of Estimating Ground-Water Supplies Based on Discharge by Plants and Evaporation From Soil: Results of Investigations in Escalante Valley, Utah*. (Water Supply Paper 659A). Washington, D.C: U.S. Government Printing Office.

Whittington, P. N., and Price, J. S. (2006). The effects of water table draw-down (as a surrogate for climate change) on the hydrology of a fen peatland, Canada. *Hydrol. Process.* 20, 3589–3600. doi: 10.1002/hyp.6376

Yuan, W., Zheng, Y., Piao, S., Ciais, P., Lombardozzi, D., Wang, Y., et al. (2019). Increased atmospheric vapor pressure deficit reduces global vegetation growth. *Sci. Adv.* 5:eaax1396. doi: 10.1126/sciadv.aax1396

Zhang, Y.-K., and Schilling, K. E. (2006). Effects of land cover on water table, soil moisture, evapotranspiration, and groundwater recharge: a field observation and analysis. *J. Hydrol.* 319, 328–338. doi: 10.1016/j.jhydrol.2005.06.044

Zipper, S. C., Schatz, J., Kucharik, C. J., and Loheide, S. P. II (2017). Urban heat island-induced increases in evapotranspirative demand. *Geophys. Res. Lett.* 44, 873–881. doi: 10.1002/2016GL072190

Conflict of Interest: The authors declare that the research was conducted in the absence of any commercial or financial relationships that could be construed as a potential conflict of interest.

frontiers in Environmental Science

ORIGINAL RESEARCH
published: 21 April 2021
doi: 10.3389/fenvs.2021.619258

Effects of Harvest and Fertilization Frequency on Protein Yield and Extractability From Flood-Tolerant Perennial Grasses Cultivated on a fen Peatland

Claudia Kalla Nielsen[1,2]*, *Lene Stødkilde*[2,3], *Uffe Jørgensen*[1,2] and *Poul Erik Lærke*[1,2]

[1]Department of Agroecology, Aarhus University, Tjele, Denmark, [2]Aarhus University Centre for Circular Bioeconomy, Aarhus University, Tjele, Denmark, [3]Department of Animal Science, Aarhus University, Tjele, Denmark

Paludiculture, and in particular the cultivation of perennial grasses as biomass feedstock for green biorefineries, may be an economic and environmentally sustainable option for agricultural peatlands in temperate regions. However, the optimal biomass quality for protein extraction from flood-tolerant grasses is largely unknown. The aim of this study was to define the combined effect of harvest and fertilization frequency, with one to five annual cuts, on protein yield and extractability for the grasses tall fescue (TF) and reed canary grass (RCG), cultivated on an agricultural fen peatland in Denmark.The content of protein fractions was determined according to the Cornell Net Carbohydrate and Protein System (CNCPS). We assessed protein extractability by lab-scale biorefinery techniques using a screw-press followed by acid precipitation of true protein. The two methods were compared to correlate potential extractable protein yields with actual biorefinery outputs. We found the highest annual biomass and crude protein (CP) yields in the two cut treatments, with 13.4 and 15.6 t dry matter (DM) ha^{-1} $year^{-1}$, containing 2.9–3.4 t CP ha^{-1} $year^{-1}$ for TF and RCG, respectively. The highest neutral-extractable (fractions B_1 and B_2) true protein yields of 1.1 and 1.5 t ha^{-1} $year^{-1}$ were found in the two cut treatments, representing 39% (TF) - 45% (RCG) of total CP. Using biorefining techniques, we were able to precipitate up to 2.2 t DM ha^{-1} $year^{-1}$ of protein concentrate, containing up to 39% CP. Significant correlations between methods were found, with a distinct relationship between CNCPS fractions B_1 + B_2 and CP yield of the protein concentrate, indicating the suitability of the CNCPS as an indicator for extractable protein yields. Biomass and CP yields were not significantly improved beyond two annual cuts. However, timing and harvest frequencies significantly affected plant maturity and consequently extractable CP contents and protein concentrate yields. We conclude that TF and RCG are promising feedstocks for green biorefineries due to high biomass, extractable CP, and protein concentrate yields, and highlight the potential of flood-tolerant grasses, cultivated on wet agricultural peatlands, for an enhanced valorisation beyond the common utilisation for bioenergy.

Keywords: Biorefinery, crude protein, paludiculture, plant fractionation, reed canary grass, tall fescue

OPEN ACCESS

Edited by:
Line Rochefort,
Laval University, Canada

Reviewed by:
Mengyang You,
Northeast Institute of Geography and Agroecology (CAS), China
Yansheng Li,
Chinese Academy of Science, China

****Correspondence:***
Claudia Kalla Nielsen
claudia@agro.au.dk

Specialty section:
This article was submitted to Soil Processes, a section of the journal Frontiers in Environmental Science

Received: *21 October 2020*
Accepted: *04 February 2021*
Published: *21 April 2021*

Citation:
Nielsen CK, Stødkilde L, Jørgensen U and Lærke PE (2021) Effects of Harvest and Fertilization Frequency on Protein Yield and Extractability From Flood-Tolerant Perennial Grasses Cultivated on a fen Peatland. Front. Environ. Sci. 9:619258. doi: 10.3389/fenvs.2021.619258

INTRODUCTION

With an increasing world population, being expected to reach 9.7 billion in 2050 (United Nations, 2019), and the associated escalating demand for food and clean water (Ibarrola-Rivas et al., 2017) the competition for productive land areas is growing (Joosten et al., 2016). At the same time, there is an environmental crisis, with never seen records of ocean temperature and sea level rise, as well as atmospheric greenhouse gas (GHG) concentrations (Kappelle, 2020). Peatlands, being the dominating wetland type globally (Yu et al., 2010) and covering about 3% of the continental surface (Joosten and Clarke, 2002) contribute significantly to GHG emissions. Anthropogenic degradation of peatlands by drainage for agriculture led not only to a substantial loss of global peatlands and the associated ecosystem functions (Wichmann, 2017), but also to emission hotspots releasing 6% of the total anthropogenic emissions in carbon dioxide equivalents (CO_2eq) (Joosten, 2012), contributing up to 37% of the total emissions from the European agricultural sector (Geurts, et al., 2019).

A transition towards more sustainable cultivation practices on peatlands after rewetting may accelerate the extensification of currently drained peatlands. Paludiculture, defined as agriculture on wet or rewetted peatlands, has been proposed as a suitable mitigation strategy (Günther et al., 2014) in order to reverse traditional farming with unsustainable environmental concerns such as land subsidence, nutrient leaching and GHG emissions to the atmosphere (Tanneberger and Wichtmann, 2011; Giannini et al., 2017). In particular, the production of biomass from flood-tolerant perennial grasses for the provision of e.g., fodder and raw materials (Wichtmann and Wichmann, 2011a) or for the purpose of renewable energy (Kandel et al., 2013b) is a well-known option for an economic biomass utilisation. Nevertheless the revenues of the peatland biomass for these purposes have so far been too low to provide a competitive sustainable business plan.

Previous research has shown promising results on the use of perennial grasses as feedstock for protein extraction (Kromus et al., 2006) with subsequent application as a high-quality substitute for soy. Current estimates indicated that up to 47% of the crude protein (CP) fraction present in the biomass can be extracted in a protein concentrate that may substitute the currently used soybean meal in diets for monogastric animals (Santamaría-Fernández et al., 2017; Stødkilde et al., 2018; la Cour et al., 2019). Furthermore, by-products resulting from the biorefining process, such as the fibre fraction and the brown juice, may additionally be used directly as valuable forage for ruminants (Damborg et al., 2018) or can be further refined into value-added products (Ambye-Jensen et al., 2014).

The flood-tolerant perennial grasses reed canary grass (*Phalaris arundinacea*) (RCG) and tall fescue (*Festuca arundinacea*) (TF) can produce high biomass yields on poorly drained peatsoils (Kandel et al., 2013a; Kandel et al., 2016). While there has been extensive research concluding their suitability as efficient energy crops (Kandel et al., 2013b; Tilvikiene et al., 2016), a further assessment of their applicability as biomass feedstock for value-added products from biorefineries has been lacking so far. Assessments of CP contents in RCG and TF cultivated on mineral soils showed yields of up to 3.2 t CP ha^{-1} $year^{-1}$ and 3.1 t CP ha^{-1} $year^{-1}$, respectively, of which about 40% were potentially extractable (Solati et al., 2018b). However, there is a desideratum concerning the CP yield and extractability of these grass species cultivated on wet agricultural peatlands. This also applies to the evaluation of biomass quality for protein extraction as a response to plant maturity and nitrogen (N) uptake, and hence the effect of agricultural management regarding annual harvest and fertilization frequencies.

Until now, there has been research on the content of potential extractable protein fractions in grasses and legumes (e.g., Elizalde et al., 1999; Solati et al., 2017), mainly in order to determine forage quality, following the CNCPS. Further, efforts regarding protein extraction optimisation are at the heart of green biorefinery strategies (Santamaria-Fernandez et al., 2019; Pihlajaniemi et al., 2020) and increasing attention has been paid on the protein extractability and quality using the rather simple method of mechanical screw-press extraction followed by chemical protein precipitation (Stødkilde et al., 2018; Damborg et al., 2020). However, to the authors knowledge, no correlation between the theoretical extractable protein yields as indicated by means of the soluble CNCPS fractions $B_1 + B_2$, respectively acid extractable fractions $B_1 + B_2 + B_3$, and the actual protein yields by precipitation in biorefineries, has yet been conducted. The protein content and allocation in grasses depends on a variety of factors, including environmental conditions, stress factors (e.g., drought; Roy-Macauley et al., 1992) and N availability. Generally, grasses are known to positively respond to N input by fertilization, with reported linear increases of 50–90 g CP kg^{-1} DM per 100 kg N ha^{-1} applied (Peyraud and Astigarraga, 1998) as well as a significant decrease of CP content with N limitation (Dindová et al., 2019). However, the process of lignification in grasses was also found to be positively associated with N fertilisation (Coblentz et al., 2017).

Nevertheless, grass maturity and harvesting time are known to be important factors for biomass quality (Butkutė et al., 2013; Solati et al., 2017). Plant nitrogen is mainly stored as protein in chloroplast (Peoples and Dalling, 1988), and hence located in the form of true proteins within leaves. It has further been shown, that leaf-protein contents decrease with plant maturity as a reaction to senescence and subsequent lignification (Sanderson and Wedin, 1989), contributing to a substantial increase in total plant lignin to about 30% (Butkutė et al., 2013). These constant alterations with increasing plant development facilitate bounding of proteins to cell walls, and hence increases the content of insoluble protein fractions B_3 and C according to the CNCPS method, while the soluble protein fractions B_1 and B_2 decrease.

We hypothesized that high protein yields and extractability can be obtained in flood-tolerant perennial grasses by manipulating the harvest frequency during the growth season under provision of adequate nutrient availability. The aims of this study were to, 1) determine the combined effect of harvest and fertilization frequency on biomass and protein yields of the perennial grasses RCG and TF grown on a wet fen peatland, 2) quantify theoretically and potentially extractable protein

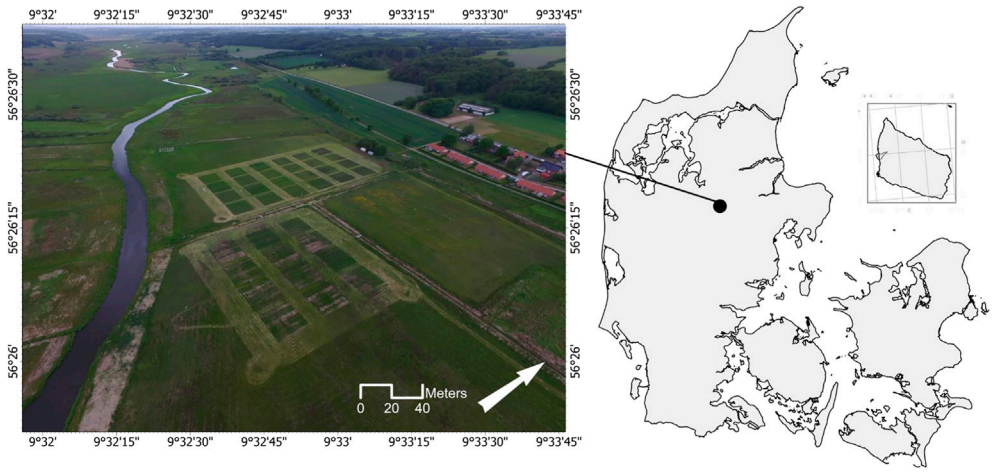

FIGURE 1 | Location of the study site in Denmark including aerial picture, taken in June 2020.

fractions by the CNCPS method, and 3) assess the extractability of soluble plant protein fractions using a screw-press as the initial biorefining separation step followed by protein precipitation.

MATERIALS AND METHODS

Site Description

The field experiment was conducted in 2019 on a riparian fen in Vejrumbro, located in Central Jutland, Denmark (56°26′15.3″N, 9°32′44.1″E; **Figure 1**). Environmental variables were taken from the meteorological station at Foulumgård, Aarhus University, located 6.5 km from the field site. During the study period from May until October 2019, ranged the temperature between 8.7 and 16.8°C, with August as the warmest month. Monthly precipitation ranged between 57 and 122 mm, with May as the driest and October as the wettest month. The site has been shallow drained in the first half of the 20th century and has primarily been used as pasture until the establishment of the present experiment in 2018. Average peat depth at the site is 2 m, overlying a layer of 8 m gyttja. The upper soil layer (0– 20 cm) contains 35.8% total carbon (TC), 2.5% total nitrogen (TN), 0.2% phosphorus (P), 0.2% potassium (K), with a bulk density (BD) of 0.2 g cm^{-3}, and an average pH of 5.1. The lower soil layer (20–100 cm) contains 45.6% TC, 2.6% TN, with 0.1 g cm^{-3} BD, and pH 5.8. The site had in 2019 a mean annual water table depth (WTD) of −0.13 cm, with on average −0.22 cm during the study period.

Experimental Design and Agricultural Management

The effects of species and combined harvest and fertilizer management were tested within a complete split-plot design, with four block replicates, species as main plot and management as sub-plot. The five management sub-plots (3 m × 16 m) were assigned randomly on the established main plot. A total of eight plots (15 m × 16 m) were established in June 2018, with four plots each cultivated with either RCG (*Phalaris arundinacea,* cultivar: Lipaula) or TF (*Festuca arundinacea,* cultivar: Swaj). Soil cultivation and sowing of the seeds occurred in one mechanical process following previous spraying of original vegetation using Round Up (Bayer AG, Leverkusen, Germany). The seeding rates were 25 kg ha^{-1} for both species and all subplots in each plot were fertilized with 40 kg N ha^{-1}, 9 kg P ha^{-1}, and 43 kg K ha^{-1}, using 286 kg ha^{-1} of combined NPK fertilizer with a grade of 14-3-15, after emergence of the seeds. Treatments with TF experienced partial invasion by velvet grass (*Holcus lanatus*). In 2019, subplots were fertilized and harvested according to the treatment plan (**Figure 2**). The one cut treatment was fertilized with 100 kg N ha^{-1} $year^{-1}$ and 100 kg K ha^{-1} $year^{-1}$. Split-fertilizer applications with a total of 200 kg N ha^{-1} $year^{-1}$ and 200 kg K ha^{-1} $year^{-1}$ were applied to two cut, three cut, four cut, and five cut strategies in equal doses for each harvest within each strategy. First fertilization prior to growth onset was performed on April 16, 2019. The remaining split-fertilizer applications were applied the day following the last harvest day for each occurrence. No fertiliser was applied following the last cut. The grass species were harvested up to five times, depending on treatment, in the growth period of May 12 to October 16, 2019, between 15.00 and 18.00 CET. Grass samples were harvested in stripes of between 1.5 and 3.0 m length and 1.18 m width at stubble height of approximately 7 cm within the middle of the sub-plots, using a sickle bar mower (Grillo G107, Grillo SpA, Cesena, Italy). The grass was manually collected and immediately brought to the laboratory for determination of fresh weight and subsequently dry-matter. The dried plant material was milled (Retsch ZM 200, Retsch GmbH, Haan, Germany) and stored for further analysis.

Screw-Pressing and Protein Extraction

A portion of the harvested grass was stored overnight at 2°C and processed the following morning at room temperature in a lab-scale twin-screw-press (Angelia 8500S Angel slow-juicer, Angel

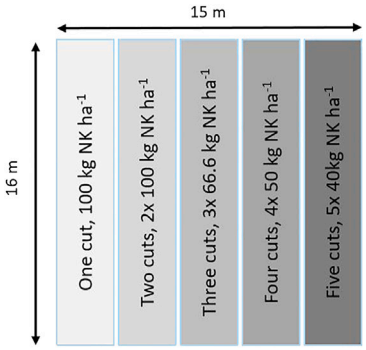

Harvest Dates 2019

Treatment	Week (Dates)				
	12. - 15.05	09. - 12.06	04. - 07.08	01. - 04.09	13. - 16.10
One cut			32		
Two cuts		24		36	
Three cuts	20		32		42
Four cuts	20	24		36	42
Five cuts	20	24	32	36	42

FIGURE 2 | Exemplary split-plot distribution in one main plot, indicating number of annual cuts and corresponding fertilization rates. The distribution of subplots has been randomized on each main plot. Harvest weeks and dates are given for the corresponding treatments and harvest occurrences.

Co. Ltd., Busan, Korea) without prior chopping or discarding of wilted plant fragments or weeds. The resulting pulp and a sample fraction of the juice were frozen at −18°C. The grass protein was isolated from the remaining juice fraction using a two-step procedure as described by Stødkilde et al. (2019). Proteins were precipitated by acidifying the juice to pH 4, using 14.8 mol L^{-1} phosphoric acid. Following overnight-storage at 4°C, the sample was centrifuged for 12 min at 2000×*g* at 4°C for final separation of the acid-precipitated protein from the juice, leading to a protein concentrate and the residual brown juice fraction. All samples were stored frozen at −18°C until drying at 60°C for further analysis. Biomass samples from the one cut treatment could not be processed by the screw-press due to advanced lignification. Total nitrogen (TN) of the screw-pressed fractions were analysed using a Vario MAX CN (Elementar Analysesysteme GmbH, Hanau, Germany), with following conversion to crude protein (CP) by using the conversion factor 6.25 (**Eq. 1**). CP within screw-pressed fractions is referred to as CP content within this text.

Protein Fractionation Following Cornell Net Carbohydrate and Protein System

Fractionation of proteins within the dried whole grass sample was performed following the Cornell Net Carbohydrate and Protein System (CNCPS) as described by Licitra et al. (1996) and as modified by Solati et al. (2018a). Total nitrogen in the plant material was determined using the Kjeldahl method (Kjeltec 8400, FOSS A/S, Hillerød, Denmark) with subsequent conversion to CP by using the conversion factor 6.25 (**Eq. 1**) as described by AOAC (1990), and within the text further referred to as CP content. The fractions A, B_1 and B_2 are soluble in neutral detergent solution, whereas B_3 is soluble in acid detergent solution. Fraction A was determined by subtracting trichloroacetic acid (TCA)-precipitated proteins from TN (**Eq. 2**). Fraction B_1 was determined by subtracting the borate-phosphate buffer insoluble N from the TCA insoluble N (**Eq. 3**). Fraction B_2 was estimated by subtracting the neutral-detergent insoluble N (NDIN) from the borate-phosphate buffer insoluble N (**Eq. 4**). Determination of NDIN was based on a neutral detergent fibre (NDF) assay where 50 µl of heat stable amylase (No. A3306, Sigma-Aldrich, Denmark) was added to the sample, following the procedure described by Van Soest et al. (1991). Both NDF and acid-detergent fibre (ADF) included the residual ash. The insoluble protein fraction B_3 was determined by subtracting the acid-detergent insoluble N (ADIN) from NDIN (**Eq. 5**). Fraction C was equal to ADIN (**Eq. 6**). ADF and NDF analyses were performed on a FOSS Fibertech 2010 (FOSS A/S, Hillerød, Denmark).

$$Crude\ Protein = Total\ N \times 6.25 \quad (1)$$

$$Fraction\ A = Total\ N - TCA\ insoluble\ N \quad (2)$$

$$Fraction\ B_1 = TCA\ insoluble\ N - borate - phosphate\ buffer\ insoluble\ N \quad (3)$$

$$Fraction\ B_2 = Borate - phosphate\ buffer\ insoluble\ N - NDIN \quad (4)$$

$$Fraction\ B_3 = NDIN - ADIN \quad (5)$$

$$Fraction\ C = ADIN \quad (6)$$

Statistical Analysis

Mean yields per cut were summed up to annual yields for treatments with more than one harvest event. Standard deviations are reported to present the distribution of data. Analysis was performed using a linear mixed model with the function *lmer* of the package *lme4* (Bates et al., Version 1.1-23, 2015) in the statistical software R [R Core Team (2020) Version 4.0.2 – "Taking Off Again"], in which the following model was used:

$$Y_{ijk} = \mu + \alpha_i + \eta_{k(i)} + \beta_j + (\alpha\beta)_{ij} + \varepsilon_{k(ij)}$$

Where Y_{ijk} is the observed dependent variable, μ is the population mean, α_i is the fixed combined effect of cut and fertilization treatment, $\eta_{k(i)}$ is the whole plot error, β_j is the fixed effect of species, $(\alpha\beta)_{ij}$ is the fixed interaction between species and management, and $\varepsilon_{k(ij)}$ is the split-plot error. The model residuals were inspected for normality and homoscedasticity, and variables were log-transformed in order to stabilise the variance and normal distribution. When $p < 0.05$ and hence

TABLE 1 | Total annual average biomass yields in dry matter (t DM ha^{-1}) and averaged crude protein (CP) contents (g kg^{-1} DM) per harvest and treatment for reed canary grass and tall fescue. Standard deviation is giving in brackets.

			Reed canary grass		Tall fescue	
Treatment	**Cut**	**Week**	**Yield (t DM ha^{-1})**	**CP (g kg^{-1} DM)**	**Yield (t DM ha–1)**	**CP (g kg^{-1} DM)**
One cut						
	1	32	8.3 (±3.8)	106 (±10)	6.1 (±1.9)	117 (±18)
Annual average			8.3 (±3.8)	106 (±10)	6.1 (±1.9)	117 (±18)
Two cuts						
	1	24	8.8 (±3.3)	230 (±7)	7.9 (±1.9)	231 (±45)
	2	36	6.8 (±4.4)	216 (±43)	5.5 (±2.9)	210 (±48)
Annual average			15.6 (±7.7)	223 (±25)	13.4 (±4.8)	220 (±46)
Three cuts						
	1	20	1.6 (±0.7)	206 (±5)	1.3 (±0.8)	200 (±12)
	2	32	5.5 (±1.4)	153 (±32)	5.1 (±2.7)	163 (±25)
	3	42	3.2 (±0.7)	234 (±10)	2.6 (±1.2)	271 (±28)
Annual average			10.3 (±2.8)	198 (±16)	9.0 (±4.7)	212 (±22)
Four cuts						
	1	20	2.0 (±0.7)	198 (±10)	1.0 (±0.7)	200 (±18)
	2	24	4.0 (±1.3)	271 (±28)	2.7 (±1.6)	276 (±35)
	3	36	8.8 (±4.5)	175 (±36)	4.7 (±0.3)	228 (±26)
	4	42	0.6 (±0.5)	236 (±21)	1.9 (±3.4)	241 (±68)
Annual average			15.4 (±7.0)	220 (±24)	10.3 (±6.0)	236 (±37)
Five cuts						
	1	20	1.7 (±0.6)	187 (±6)	0.9 (±0.5)	184 (±7)
	2	24	3.9 (±1.0)	283 (±47)	2.4 (±1.8)	264 (±31)
	3	32	6.5 (±1.3)	159 (±20)	4.7 (±1.2)	168 (±39)
	4	36	2.4 (±2.1)	242 (±14)	1.1 (±0.1)	283 (±17)
	5	42	0.4 (±0.1)	264 (±24)	0.7 (±0.5)	281 (±17)
Annual average			14.9 (±5.1)	227 (±23)	9.8 (±4.1)	236 (±24)

significant, a Tukey's HSD test at 95% confidence level was performed for pairwise comparison of means. Multiple linear regression using Pearson's correlation was performed to analyse correlation effects between different crude protein and protein fraction yields.

RESULTS

Biomass Yield

Annual average biomass yield across treatments was on average 34% higher in reed canary grass (RCG) than in tall fescue (TF) treatments (**Table 1**). In particular, RCG four and five cut treatments yielded, respectively, 50 and 54% more than TF treatments. The overall highest annual DM yields for both species were found in the two cut treatments, with 15.6 (±7.7) t DM ha^{-1} $year^{-1}$ for RCG and 13.4 (±4.8) t DM ha^{-1} $year^{-1}$ for TF. However, for RCG, there was no difference between the two, four (15.4 (±7.0) t DM ha^{-1} $year^{-1}$) and five cut (14.9 (±5.1) t DM ha^{-1} $year^{-1}$) treatments. In treatments receiving 200 kg NK ha^{-1} $year^{-1}$ of fertilization (two, to five cut), harvest frequencies did not significantly ($p > 0.05$) affect the annual biomass yield. The one cut treatment yielded for both species least biomass and was not significantly different to the three cut treatment ($p > 0.05$).

Crude Protein in Biomass

The CP content (g kg^{-1} DM) of the two grass species was similar, with TF having significantly higher contents as compared to RCG only in weeks 36 (four-, and five cuts) and 42 (three cuts). Further, the content as well as the annual average crude protein yield (in t ha^{-1} $year^{-1}$) were significantly affected by the number of annual cuts [$\chi 2\ (4) = 29.9$, $p < 0.001$] as well as harvest date [$\chi^2\ (4) = 77.9$, $p < 0.001$]. The mean annual CP content of RCG and TF increased from 106 (±10) g kg^{-1} DM and 117 (±18) g kg^{-1} DM for one cut treatments to 227 (±23) g kg^{-1} DM and 236 (±24) g kg^{-1} DM for five cut treatments, respectively (**Table 1**). However, there was no difference between averaged annual CP content for the two to five cut treatments. Further, a general significant decline in CP content was observed in all treatments during summer growth. This applied for stands harvested in late July and August. The highest annual CP yields in biomass for both species were found in the two cut treatments, with 3.4 (±0.9) t ha^{-1} $year^{-1}$ for RCG and 2.9 (±0.4) t ha^{-1} $year^{-1}$ for TF. However, for RCG there was no difference in CP yields for the two, four [3.0 (±0.1) t ha^{-1} $year^{-1}$], and five cut [3.1 (±0.0) t ha^{-1} $year^{-1}$] treatments. The lowest yield was, with 0.7–0.9 t ha^{-1} $year^{-1}$, found in the one cut treatment for TF and RCG, respectively.

CNCPS Fractions in Biomass

Fraction A

The content of fraction A ranged between 28 g kg^{-1} DM (RCG, one cut) and 63 g kg^{-1} DM (TF, two cuts) on an annual average per treatment, and was more affected by harvest date [$\chi^2\ (4) = 36.3$, $p < 0.001$] than number of annual cuts [$\chi^2\ (4) = 18.4$, $p < 0.01$]. However, species did not affect fraction A content. Initial increases in the content of fraction A were observed

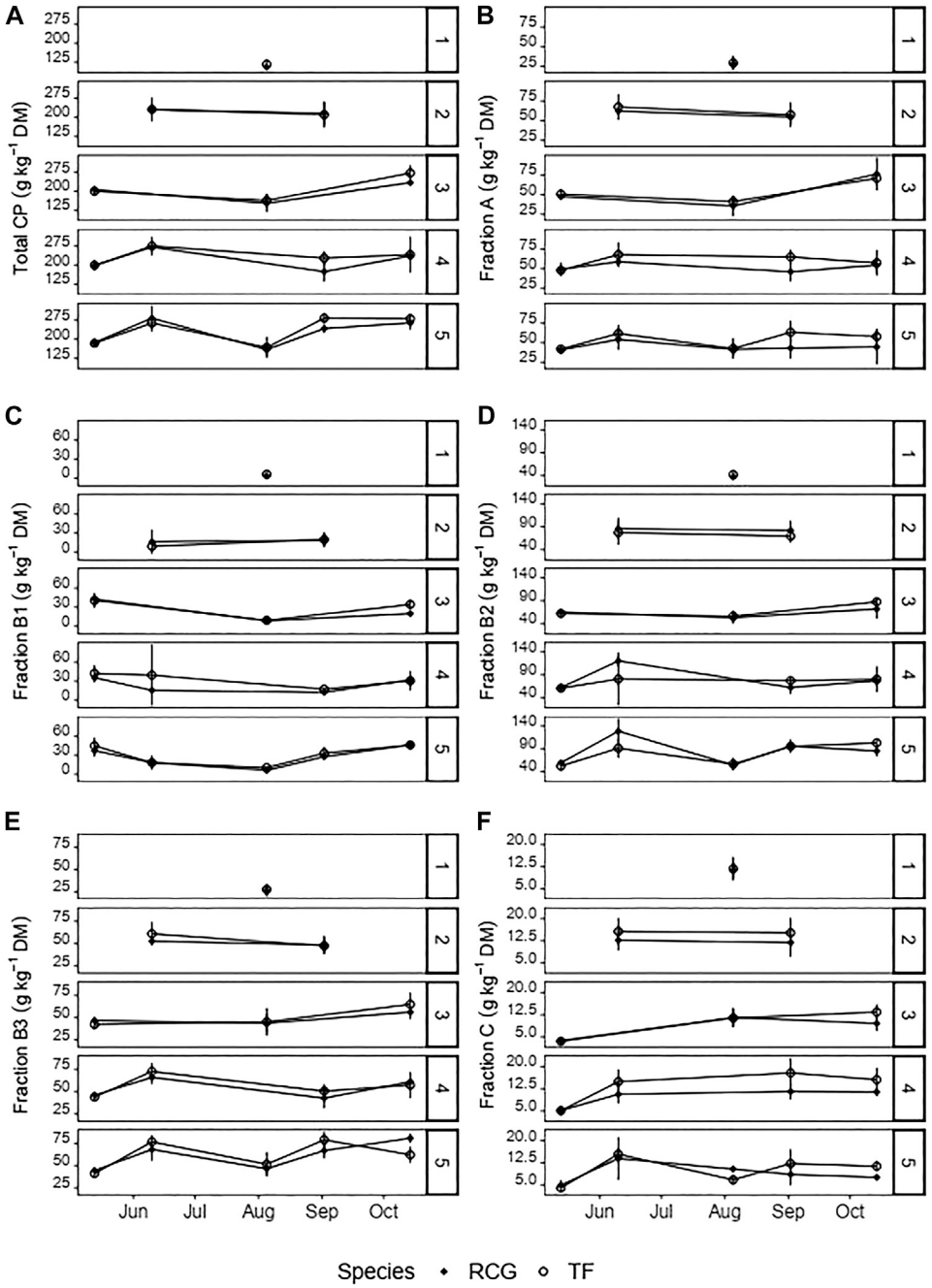

FIGURE 3 | Contents of **(A)** crude protein (CP), and **(B–F)** protein fractions according to the Cornell Net Carbohydrate and Protein System (CNCPS) in the biomass (g kg^{-1} DM) for the various treatments and species on the different harvest dates. Attention should be paid to the different magnitudes of the y-axes. Error-bars show standard deviations.

during spring growth in the period between May and June for the four and five cut treatments of both species (**Figure 3B**). However, this was followed by a decline over summer months. A subsequent significant change ($p < 0.001$) was observed for RCG (three cuts), with a relative increase from 23% (week 20) to 50% (week 42) based on total CP. On an annual average basis, has fraction A only been slightly decreasing with increasing number of harvests (**Supplementary Tables S1, S2**).

Fraction B_1

The biomass content of the neutral buffer soluble protein fraction B_1 ranged between 3 g kg^{-1} DM (RCG, one cut) and 32 g kg^{-1} DM (TF, four cuts) on an annual average per treatment. Based on

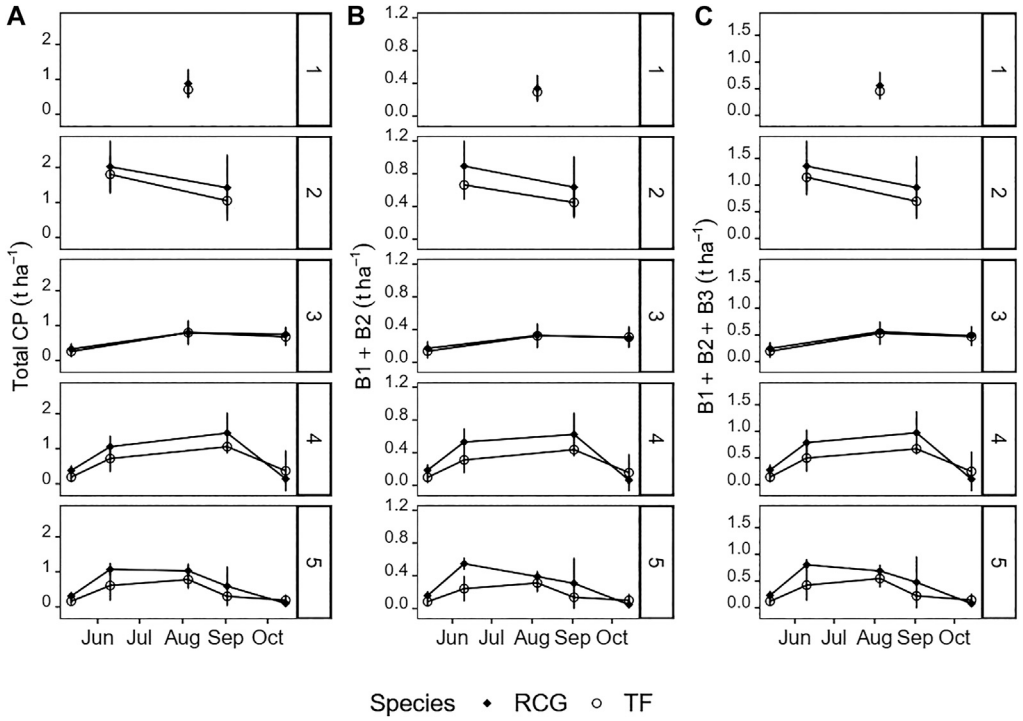

FIGURE 4 | Yields (t DM ha^{-1}) of **(A)** total crude protein (CP), **(B)** protein fractions $B_1 + B_2$, and **(C)** protein fractions $B_1 + B_2 + B_3$ for the various treatments and species on the different harvest dates. Attention should be paid to the different magnitudes of the y-axes. Error-bars show standard deviations.

total CP, this equaled to between 3 and 14% for RCG (one cut) and TF (four cuts), respectively. The three to five cut treatments for both species showed the highest average annual contents with 24–27 g kg^{-1} DM (RCG) and 28–31 g kg^{-1} DM (TF). Harvest week [χ^2 (4) = 100.5, $p < 0.001$] and cut frequency [χ^2 (4) = 22.2, $p < 0.001$] affected the contents of fraction B_1. Fraction B_1 declined in all treatments in dependency of plant maturity, with the lowest average values in week 32 (**Figure 3C**).

Fraction B_2

The neutral detergent soluble protein, fraction B_2, was the largest fraction in relation to CP and was affected by the number of annual cuts [χ^2 (4) = 22.2, $p < 0.001$] In harvests during the spring growth period, RCG had a higher content of fraction B_2 than TF, with a significant difference for the four and five cut treatments. However, spring growth led to a significant increase of fraction B_2 for the four and five cut treatments of both, RCG and TF, showing in week 24 contents of 120 g kg^{-1} DM and 129 g kg^{-1} DM (RCG), and 81 g kg^{-1} DM and 91 g kg^{-1} DM (TF), respectively (**Figure 3D**). Relative to total CP, remained average annual contents of fraction B_2 constant over all treatments within a range of 32–38% for RCG, and 32–36% for TF.

Fraction B_3

The annual average content of the hemicellulose-bound protein fraction B_3 increased with increasing number of annual cuts from 26 g kg^{-1} DM to 61 g kg^{-1} DM (RCG) and 28 g kg^{-1} DM to 62 g kg^{-1} DM (TF). However, the share of B_3 relative to total annual CP remained constant with 23% (RCG, two cuts)–27% (RCG, five cuts) throughout all treatments and species. In line with contents of other fractions, a decline of B_3 during summer cuts was observed (**Figure 3E**). Fraction B_3 content was significantly affected by number of annual cuts [χ^2 (4) = 67.1, $p < 0.001$] and harvest week [χ^2 (4) = 78.2, $p < 0.001$]. There was no effect of species on B_3 content ($p > 0.05$).

Fraction C

The cellulose- and lignin-bound protein fraction C was more affected by harvest date [χ^2 (4) = 128.9, $p < 0.001$] than number of annual cuts ($p > 0.01$) or species ($p > 0.05$). The one cut treatment of both species had the highest share with 11% (11 g kg^{-1} DM) in RCG and 10% (12 g kg^{-1} DM) in TF of total CP. However, a decline in the annual average content of fraction C relative to total CP was observed with increasing number of annual cuts, with 4% each, or 9 g kg^{-1} DM (RCG) and 10 g kg^{-1} DM (TF), for the five cut treatments. Fraction C was lowest in early spring cuts (week 20) with contents between 2% or 3 g kg^{-1} DM (TF, three cuts), to 3% or 5 g kg^{-1} DM, (RCG and TF, four cuts) relative to total biomass CP (**Figure 3F**).

Cumulative Neutral Extractable and Acid Extractable Protein Fractions

The groups of combined neutral extractable fractions B_1 and B_2 (soluble proteins) as well as the acid extractable fractions B_1, B_2 and B_3 (potentially extractable protein) both followed the patterns of biomass CP yield in t DM ha^{-1} (**Figures 4A–C**), as

TABLE 2 | Share of neutral extractable protein fractions B1 + B2, and potentially extractable fractions B1 + B2 + B3 based on total biomass crude protein (CP) for reed canary grass and tall fescue in dry matter (DM).

			Reed canary grass				Tall fescue			
			B1 + B2		B1 + B2 + B3		B1 + B2		B1 + B2 + B3	
Treatment		Week	DM (g kg^{-1} DM)	%	DM (g kg^{-1} DM)	%	DM (g kg^{-1} DM)	%	DM (g kg^{-1} DM)	%
One cut										
	1	32	41 (±3)	38	67 (±6)	63	48 (±4)	41	76 (±8)	65
Annual average			41 (±3)	38	67 (±6)	63	48 (± 4)	41	76 (±8)	65
Two cuts										
	1	24	102 (±5)	44	155 (±8)	67	87 (±24)	38	148 (±34)	64
	2	36	101 (±28)	47	149 (±38)	69	89 (±22)	42	137 (±30)	65
Annual average			101 (±16)	46	152 (±23)	68	88 (±23)	40	142 (±32)	65
Three cuts										
	1	20	108 (±7)	52	155 (±6)	75	155 (±6)	78	146 (±13)	73
	2	32	62 (±10)	40	105 (±18)	69	105 (±18)	64	111 (±22)	68
	3	42	92 (±20)	39	148 (±25)	63	148 (±25)	55	187 (±18)	69
Annual average			97 (±12)	49	136 (±17)	69	104 (± 17)	49	148 (±18)	70
Four cuts										
	1	20	97 (±8)	49	144 (±8)	72	103 (±12)	51	147 (±15)	73
	2	24	136 (±15)	50	202 (±21)	74	120 (±11)	44	193 (±20)	70
	3	36	74 (±15)	43	117 (±26)	67	95 (±8)	42	145 (±13)	64
	4	42	109 (±11)	46	170 (±17)	72	111 (±41)	46	168 (±54)	70
Annual average			104 (±12)	47	158 (±18)	72	107 (±18)	45	163 (±26)	69
Five cuts										
	1	20	97 (±6)	52	141 (±6)	76	97 (±5)	53	138 (±5)	75
	2	24	147 (±31)	52	215 (±39)	76	110 (±17)	42	186 (±23)	71
	3	32	61 (±9)	38	107 (±14)	67	67 (±15)	40	119 (±27)	71
	4	36	123 (±12)	51	190 (±19)	79	129 (±6)	45	208 (±9)	73
	5	42	117 (±10)	50	212 (±10)	80	149 (±5)	53	211 (±12)	75
Annual average			117 (±14)	49	173 (±18)	76	110 (±10)	47	172 (±15)	73

well as annual average CP in t ha^{-1} year^{-1} from biomass harvest, across all treatments. The share of the cumulative fractions B_1 and B_2 ranged from 38% (RCG, one cut) to 49% (RCG, five cuts; and TF, three cuts) relative to total CP (**Table 2**), equivalent to 41 g kg^{-1} DM (RCG, one cut) and 112 g kg^{-1} DM (RCG, five cuts). The lowest neutral extractable protein contents in biomass (61 g kg^{-1} DM, respectively 67 g kg^{-1} DM for RCG and TF, five cuts) was found in summer cuts (week 32). Based on annual average yields of biomass in t DM ha^{-1} year^{-1}, RCG yielded in all treatments more of the cumulative fractions B_1 and B_2 than TF. The two-cut management for both species yielded with 1.5 t DM ha^{-1} year^{-1} (RCG) and 1.1 t DM ha^{-1} year^{-1} (TF) most. There were no significant differences between yields of two, four, and five cut treatments of RCG, as well as two and five cuts of TF (**Figure 5**). The share of neutral extractable protein fractions to total CP yield increased from 39% (one cut) to 47% (five cuts) for RCG, whereas this increase in share was not observed for the TF species.

However, including the potentially acid extractable protein fraction B_3 raised the theoretical extractability to between 63% (RCG, one cut) as well as 76% (RCG, five cuts), equivalent to 67 g kg^{-1} DM and 173 g kg^{-1} DM, respectively. RCG had higher contents of both combined B_1 and B_2, as well as $B_1 + B_2 + B_3$, during spring growth as compared to TF (**Figure 4**). Cumulative fractions of $B_1 + B_2 + B_3$ were only marginally higher in the two cut treatments (2.3 t DM ha^{-1} year^{-1} for RCG, 1.8 t DM ha^{-1} year^{-1} for TF) than in four and five cut treatments (**Figure 5**). On an annual yield basis, the potentially extractable fraction B_3 increased the theoretical protein yield by on average 25% as compared to $B_1 + B_2$ based on total CP (g kg^{-1} DM) for both species across all treatments, with the two and five cut treatments experiencing the highest increase with 27% for RCG and 28% for TF.

Screw-Pressed Fractions

Of the fractions produced during biorefining of biomass, the pulp fraction had the lowest CP content, which was highest in TF treatments with 119 g kg^{-1} DM (two cut)–164 g kg^{-1} DM (five cuts). CP in the residual brown juice ranged between 138 g kg^{-1} DM (RCG, five cuts) and 206 g kg^{-1} DM (TF, four cuts). The precipitated protein fraction had the highest CP content in the five cut treatment for TF with 393 g kg^{-1} DM, and for RCG in the four cut treatment with 383 g kg^{-1} DM. Lowest contents in precipitated protein fractions were observed in three cut treatments for both species (**Tables 3**, **4**). Common for all fractions, had summer cuts the lowest CP contents, whereas late-spring and late-autumn cuts showed the highest values.

Cumulative annual CP yields of precipitated protein concentrate were significantly affected by harvest date [χ^2 (4) = 42.8, $p < 0.001$], indicating plant maturity, as also the number of annual cuts [χ^2 (3) = 25.8, $p < 0.001$]. Between 1.0 t DM ha^{-1} year^{-1} (TF, three cuts) and 2.2 t DM ha^{-1} year^{-1} (RCG, four cuts) of the protein concentrate could be precipitated, resulting in protein concentrate CP yields of 0.4–0.7 t DM ha^{-1} year^{-1}, respectively (**Tables 3**, **4**). Pulp fraction yield (t DM ha^{-1} year^{-1}) was highest in the two cut treatments,

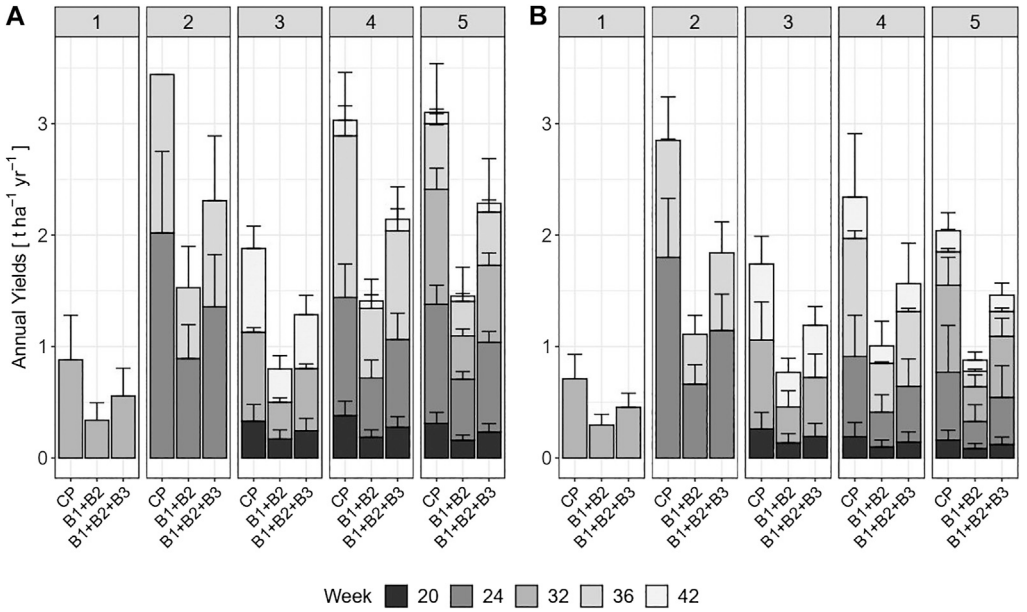

FIGURE 5 | Cumulative annual yields (t ha^{-1} year^{-1}) and yields per cut of crude protein (CP), protein fractions $B_1 + B_2$, and $B_1 + B_2 + B_3$ for the various treatments in **(A)** reed canary grass, and **(B)** tall fescue. Error-bars show standard deviations.

representing 72% (TF) and 73% (RCG) of the total annual biomass input. The CP yield in pulp ranged between 0.7 t DM ha^{-1} year^{-1} (TF, three cuts) and 1.4 t DM ha^{-1} year^{-1} (RCG, two cuts), representing 29% (RCG, five cuts) and 45% (TF, five cuts) on a mass percentage basis. The brown juice fraction yielded least CP in t DM ha^{-1} year^{-1} as well as on a percentage basis. The lowest CP yields in all fractions were observed in early-spring cuts as well as late-autumn cuts in frequent-harvest treatments following an initial increase in yieldable CP during late-summer (**Figures 6A–D**). Losses within the CP balance originate from foaming and related overflow of juice during screw-pressing as well as fibre residues left in the screw-press (**Figure 7**). Composition of DM (g kg^{-1} FW) and CP contents (g kg^{-1} DM) for the different fractions and treatments are provided in the **Supplementary Material**.

Correlation of Crude Protein Yields in Biomass and Precipitated Protein

Results of the Pearson correlation showed a significant positive association between annual cumulative CP yield in the precipitated protein concentrate and the corresponding CP yields in biomass, CNCPS fractions $B_1 + B_2$, as well as CNCPS fractions $B_1 + B_2 + B_3$, across all treatments but depending on species. The highest correlation [r(98) = 0.9, $p < 0.001$] was observed between CP yield in the protein concentrate and CNCPS fractions $B_1 + B_2$ for TF. The correlation decreased with increasing CP yield in the corresponding counterpart ($B_1 + B_2$ > $B_1 + B_2 + B_3$ > Biomass), with TF in all scenarios having a higher correlation coefficient compared to RCG (**Figure 8**).

However, we found distinct differences in correlations for the miscellaneous treatments on a product basis for CP in precipitated protein as compared to CP yields in biomass, and for CNCPS fractions B_1 and B_2, as well as CNCPS fractions $B_1 + B_2 + B_3$. For reed canary grass (**Figures 9A,C,E**), the largest positive association to other CP yields was found for the treatment with four cuts per year [r(98) = 0.98, $p < 0.001$], whereas the highest correlation for tall fescue (**Figures 9B,D,F**) was found in the two cut treatment [r(98) = 0.97, $p < 0.001$]. Generally, tall fescue treatments showed higher positive associations in all correlation tests.

DISCUSSION

Biomass Yield and Crude Protein Content

Prevailing environmental variables and variations in nutrient availability for different sites and years seem to be the driving factors for inconsistencies of biomass yields and CP contents as a response to cut frequency and hence plant maturity (Guretzky et al., 2017; Vitra et al., 2019), making sound comparisons between different study results a vague venture. This is in particular true for yields from paludiculture crops, where we expected to see differences as compared to perennial grass cultivation on mineral soils, due to lower prevailing soil temperatures and requirements for mineral fertilizer application. However, the average annual yield for the two cut treatment of 15.6 t DM ha^{-1} year^{-1} (RCG) was within the range of previously reported yields from the same area and soil type (Kandel et al., 2013b; Karki et al., 2019). For other soil types and management intensities, we found that RCG yields were in

TABLE 3 | Dry matter (DM) and crude protein (CP) yields in plant biomass and screw-pressed fractions for reed canary grass. All yields in t ha^{-1} year^{-1}. Standard deviation (SD) is giving in brackets. Missing SD values due to only one replicate as a consequence of insufficient biomass for processing. NA's due to a lack of sufficient biomass for processing with the screw-press.

		Reed canary grass							
			Plant biomass		Pulp		Protein concentrate		Brownjuice	
Treatment		Week	DM	CP	DM	CP	DM	CP	DM	CP
Two cuts										
	1	24	8.8 (±3.3)	2.0 (±0.7)	6.9 (±2.7)	0.9 (±0.2)	0.8 (±0.2)	0.3 (±0.1)	0.9 (±0.4)	0.2 (±0.1)
	2	36	6.8 (±4.4)	1.4 (±0.9)	4.6 (±3.3)	0.5 (±0.3)	0.9 (±0.4)	0.3 (±0.1)	1.0 (±0.6)	0.2 (±0.1)
Avg. annual yield			15.6 (±7.7)	3.4 (±1.6)	11.5 (±6.0)	1.4 (±0.5)	1.7 (±0.6)	0.6 (±0.2)	1.9 (±1.0)	0.4 (±0.2)
Three cuts										
	1	20	1.6 (±0.7)	0.3 (±0.2)	1.0 (±0.5)	0.2 (±0.1)	0.3 (±0.1)	0.1 (±>0.0)	0.2 (±0.1)	>0.0 (±>0.0)
	2	32	5.5 (±1.4)	0.8 (±>0.0)	4.2 (±1.0)	0.4 (±0.1)	0.4 (±0.1)	0.1 (±>0.0)	0.6 (±0.3)	0.1 (±>0.0)
	3	42	3.2 (±0.7)	0.8 (±0.2)	1.9 (±0.4)	0.2 (±>0.0)	0.5 (±0.1)	0.2 (±0.1)	0.6 (±0.2)	0.1 (±>0.0)
Avg. annual yield			10.3 (±2.8)	1.9 (±0.4)	7.1 (±1.9)	0.8 (±0.2)	1.2 (±0.3)	0.4 (±0.1)	1.4 (±0.6)	0.2 (± >0.0)
Four cuts										
	1	20	2.0 (±0.7)	0.4 (±0.1)	1.3 (±0.5)	0.2 (±0.1)	0.3 (±0.1)	0.1 (±>0.0)	0.3 (±0.1)	>0.0 (±>0.0)
	2	24	4.0 (±1.3)	1.1 (±0.3)	2.9 (±1.0)	0.3 (±0.2)	0.5 (±0.1)	0.2 (±0.1)	0.4 (±0.1)	0.1 (±>0.0)
	3	36	8.8 (±4.5)	1.5 (±0.6)	6.1 (±3.1)	0.5 (±0.2)	1.1 (±0.5)	0.3 (±0.1)	1.3 (±0.7)	0.2 (±0.1)
	4	42	1.3 (±NA)	0.3 (±NA)	0.8 (±NA)	0.1 (±NA)	0.3 (±NA)	0.1 (±NA)	0.2 (±NA)	>0.0 (±NA)
Avg. annual yield			16.1 (±6.5)	3.3 (±1.0)	11.1 (±4.6)	1.1 (±0.5)	2.2 (±0.7)	0.7 (±0.2)	2.2 (±0.9)	0.3 (±0.1)
Five cuts										
	1	20	1.7 (±0.6)	0.3 (±0.1)	1.1 (±0.4)	0.2 (±>0.0)	0.3 (±0.1)	0.1 (±>0.0)	0.2 (±0.1)	>0.0 (±>0.0)
	2	24	3.9 (±1.0)	1.1 (±0.2)	2.8 (±0.8)	0.4 (±>0.0)	0.4 (±0.1)	0.2 (±>0.0)	0.3 (±0.2)	0.1 (±>0.0)
	3	32	6.5 (±1.3)	1.1 (±0.2)	5.0 (±1.3)	0.5 (±0.1)	0.4 (±0.1)	0.1 (±>0.0)	0.7 (±0.1)	0.1 (±>0.0)
	4	36	2.4 (±2.1)	0.6 (±0.6)	1.5 (±1.4)	0.2 (±0.2)	0.4 (±0.3)	0.2 (±0.1)	0.3 (±0.3)	0.1 (±0.1)
	5	42	NA	NA	NA	NA	NA	NA	NA	NA
Avg. annual yield			14.5 (±3.1)	3.1 (±1.1)	10.4 (±3.9)	1.3 (±0.3)	1.5 (±0.6)	0.6 (±0.1)	1.5 (±0.7)	0.3 (±0.1)

the upper range of reported yields (7–13 t DM ha^{-1} year^{-1}) for Europe and North America (Lewandowski et al., 2003; Tahir et al., 2011; Butkute et al., 2014; Tilvikiene et al., 2016). Similar observations were made regarding the yields for TF, where our results meet annual average yields of 8–14 t DM ha^{-1} year^{-1} reported in other studies (Lewandowski et al., 2003; Kandel et al., 2016; Tilvikiene et al., 2016; Manevski et al., 2017). No effect of annual harvest frequency on biomass yield was observed for more than two annual cuts. A sole effect of fertilization on DM yields of RCG as well as TF could not be assessed due to the nested nature of the nitrogen application as a covariate to the number of annual cuts. It was unexpected that intense harvesting frequency on peatsoils provided no additive annual yields, which is in line with the results from Marten and Hovin (1980), but contrary to Guretzky et al. (2017), reporting about 30% more yield when harvesting three times as compared to twice annually.

Our study showed a significant increase by 44% (193–277 g kg^{-1} DM) for RCG and 39% (195–270 g kg^{-1} DM) for TF in biomass CP content in the second as compared to the first cut, for treatments with frequent annual cuts. This is contrary to the results from Buxton and Marten (1989), reporting a decrease of CP in the same magnitude from 282 to 172 g kg^{-1} DM (RCG) and 220 to 131 g kg^{-1} DM (TF). Overall, the results indicated that increased harvest frequencies did not significantly improve average annual CP yields beyond two cuts annually, but that CP contents, and hence grass quality, for the various cuts remained high throughout the year with increased number of cuts. Perotti et al. (2021) found that biomass yields and N contents are higher under lower temperatures, maintaining sufficient soil moisture as an important factor for N cycling and biomass development (Meissner et al., 2019). Further, a decline of CP content with plant maturity (Myhr et al., 1978; Buxton and Marten, 1989; Guretzky et al., 2017; Solati et al., 2018a) caused by lignification and higher stem to leaf ratios are also positively correlated with increased temperatures. The observed increase of CP content in our study was hence potentially favored by adequate soil fertility and moisture (**Supplementary Material**) on the fen peatland, but also by a delayed onset of plant growth due to generally lower soil temperatures in wet peatlands. As highlighted by Huang et al. (2012), root temperature sensitivity is more susceptible to minor increases in soil temperature, affecting not only plant growth but also metabolic processes such as the distribution of N among photosynthetic proteins and thus CP content and allocation (Yin et al., 2018). Wet agricultural peatlands in northern Europe might hence be favorable locations for the cultivation of flood-tolerant perennial grasses for the purpose of green protein biorefinery.

Generally, our results highlight the importance for timing of harvest to match optimal biomass development stages for maximizing biomass and CP yields. This was indicated by differences in annual average biomass and CP yields for the one to three cut treatments of both species. While the one cut treatment was subject to a too late harvest under the experimental climatic conditions relative to the plants developmental stage, resulting in increased plant maturity and lignification, the three cut treatment was subject to a too

TABLE 4 | Dry matter (DM) and crude protein (CP) yields in plant biomass and screw-pressed fractions for tall fescue. All yields in t ha^{-1} $year^{-1}$. Standard deviation (SD) is giving in brackets. Missing SD values due to only one replicate as a consequence of insufficient biomass for processing with the screw-press.

			Tall fescue							
			Plant biomass		Pulp		Protein concentrate		Brownjuice	
Treatment		Week	DM	CP	DM	CP	DM	CP	DM	CP
Two cuts										
	1	24	7.9 (±1.9)	1.8 (±0.5)	6.0 (±1.5)	0.7 (±0.1)	0.7 (±0.2)	0.3 (±0.1)	0.9 (±0.3)	0.1 (±0.1)
	2	36	5.5 (±2.9)	1.1 (±0.4)	3.5 (±1.8)	0.4 (±0.1)	0.5 (±0.3)	0.2 (±0.1)	1.0 (±0.6)	0.1 (±>0.0)
Avg. annual yield			13.4 (±4.8)	2.9 (±0.9)	9.5 (±3.3)	1.1 (±0.2)	1.2 (±0.5)	0.5 (±0.2)	1.9 (±0.9)	0.2 (±0.1)
Three cuts										
	1	20	1.3 (±0.8)	0.3 (±0.2)	0.9 (±0.5)	0.1 (±0.1)	0.2 (±0.1)	0.1 (±0.1)	0.2 (±0.1)	>0.0 (±>0.0)
	2	32	5.1 (±2.7)	0.8 (±0.3)	3.8 (±1.9)	0.4 (±0.2)	0.4 (±0.2)	0.1 (±>0.0)	0.7 (±0.4)	0.1 (±>0.0)
	3	42	2.6 (±1.2)	0.7 (±0.3)	1.5 (±0.7)	0.2 (±0.1)	0.4 (±0.3)	0.2 (±0.1)	0.5 (±0.2)	0.1 (±>0.0)
Avg. annual yield			9.0 (±4.7)	1.8 (±0.8)	6.2 (±3.1)	0.7 (±0.4)	1.0 (±0.6)	0.4 (±0.2)	1.4 (±0.7)	0.2 (±>0.0)
Four cuts										
	1	20	1.0 (±0.7)	0.2 (±0.1)	0.6 (±0.4)	0.1 (±0.1)	0.2 (±0.1)	0.1 (±0.1)	0.1 (±0.1)	>0.0 (±>0.0)
	2	24	2.7 (±1.6)	0.7 (±0.4)	1.9 (±1.1)	0.3 (±0.2)	0.3 (±0.2)	0.2 (±0.1)	0.3 (±0.2)	0.1 (±>0.0)
	3	36	5.5 (±1.7)	1.1 (±0.2)	3.7 (±1.2)	0.4 (±0.1)	0.6 (±0.2)	0.2 (±0.1)	0.9 (±0.4)	0.2 (±>0.0)
	4	42	1.0 (±NA)	0.3 (±NA)	NA	NA	NA	NA	NA	NA
Avg. annual yield			10.2 (±4.0)	2.3 (±0.7)	6.2 (±2.7)	0.8 (±0.4)	1.1 (±0.5)	0.5 (±0.3)	1.3 (±0.7)	0.3 (±>0.0)
Five cuts										
	1	20	0.9 (±0.5)	0.2 (±0.1)	0.6 (±0.3)	0.1 (±0.1)	0.1 (±0.1)	0.1 (±>0.0)	0.1 (±0.1)	>0.0 (±>0.0)
	2	24	2.4 (±1.8)	0.6 (±0.4)	1.7 (±1.2)	0.3 (±0.2)	0.3 (±0.2)	0.1 (±0.1)	0.3 (±0.2)	>0.0 (±>0.0)
	3	32	4.7 (±1.2)	0.8 (±0.2)	3.5 (±0.7)	0.4 (±0.1)	0.4 (±0.1)	0.1 (±>0.0)	0.6 (±0.3)	0.1 (±>0.0)
	4	36	1.1 (±0.1)	0.3 (±>0.0)	0.6 (±0.1)	0.1(± >0.0)	0.1 (±0.1)	0.1 (±>0.0)	0.2 (±>0.0)	>0.0 (±>0.0)
	5	42	1.1 (±0.1)	0.3 (±>0.0)	0.6 (±0.1)	0.1 (± >0.0)	0.3 (±>0.0)	0.1 (±>0.0)	0.2 (±>0.0)	>0.0 (±>0.0)
Avg. annual yield			10.2 (±3.7)	2.2 (±0.7)	7.0 (±2.4)	1.0 (±0.4)	1.2 (±0.5)	0.5 (±0.1)	1.4 (±0.6)	0.1 (±>0.0)

early first cut, preventing optimal plant growth and resulting in unimproved annual yields. Contrary to these observations, the interplay between timing of harvest and climatic conditions seem to have been more favorable for the two, four, and five cut treatments. Our results highlight the need to further elucidate site-specific and climatic drivers for differences in biomass and CP yields.

Cornell Net Carbohydrate and Protein System

As aforementioned and according to Buxton and Marten (1989), environmental factors such as temperature and solar radiation are crucial factors for plant protein allocation within tissue. Considering the enhanced performance of RCG on soils with a water table depth of - 30 cm (Ustak et al., 2019), as in our study, and in years with high rain fall, one should be aware of the theoretical complexity when comparing protein fractions within plants of, though, the same species but in significantly different ecological settings.

In our study, fraction B_1, the smallest of the extractable crude protein partitions, showed to account for up to 20% of total CP in early spring cuts. The ascertained decline of fraction B_1 content during summer months coincided with the observations made by Solati et al. (2018a), likely caused by plant maturity and the associated increase of cell wall and lignin-bound protein fraction C (Solati et al., 2017). The increase of fraction B_1 in our study with increasing number of cuts, and hence prolonged plant adolescence, supports this hypothesis.

Fraction B_2 was the largest CP fraction in perennial grasses, as also stated by other studies (e.g., Elizalde et al., 1999; da Silva et al., 2013; Solati et al., 2017). While our results showed increasing B_2 contents during spring, followed by a minor decline during summer months, Solati et al. (2017) stated a decline of B_2 throughout the growing season. This dependency of fraction B_2 in response to plant maturity and lignification, driven by an interplay of environmental factors and plant developmental stage, is also evident by the constant high contents in the two cut treatments. With averaged annually 84 g kg^{-1} DM for RCG and 73 g kg^{-1} DM for TF, timing of harvest was likely to be optimal for the avoidance of a plant maturity and temperature related decline in fraction B_2. However, B_2 fractions reported in our study were lower than results from other studies (Elizalde et al., 1999; Solati et al., 2018a) which are likely due to plant phenological behavior in relation to soil type and wetness.

The cellulose bound and only theoretically extractable protein fraction B_3 had an average share of 25% on total biomass CP across treatments and species, which was higher than in other studies (e.g., Elizalde et al., 1999; Jardstedt et al., 2017). Generally, the pattern of B_3 development throughout the year in response to harvest frequencies and dates resembled protein fraction B_2 and was caused by an overall increase in total CP. A similar observation was highlighted by Loaiza et al. (2019), stating that management regarding harvest and fertilization affects the content of total biomass CP rather than the relative distribution of protein fractions. On a share basis, fraction B_3 increased with enhanced plant maturity, in

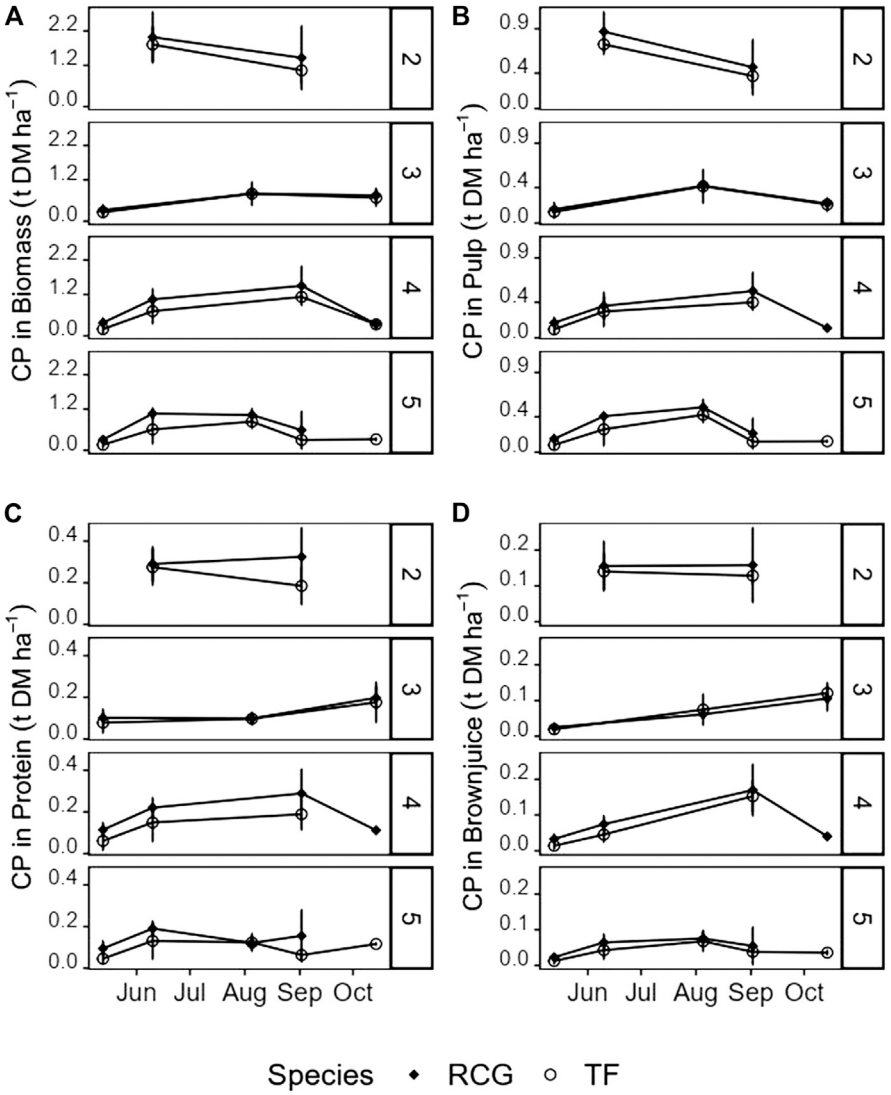

FIGURE 6 | Yields of crude protein (t ha^{-1}) in **(A)** unseparated biomass, and the screw-pressed fractions **(B)** pulp, **(C)** protein precipitate, and **(D)** brownjuice for the various treatments and species on the different harvest dates. Attention should be paid to the different magnitudes of the y-axes. Missing values for late cuts of the four, and five cut treatments due to insufficient biomass for juicing in the screw-press. Error-bars show standard deviations.

particular during summer months, highlighting its characteristic cell-wall bonds.

However, there is a research gap regarding type of plant protein fractions following the CNCPS for perennial grasses grown on wet agricultural peatlands. Not only differences in soil physics and biogeochemical properties, but also the plants response to wetter circumstances should be considered in discussions of results from different ecological settings as well as in future research.

Screw-Pressed Biomass Fractions

The extraction of plant biomass CP by refining techniques for the purpose of potential fodder applications is not a new notion (e.g., Davys and Pirie, 1963), though it only recently gained attention as a tangible future for new pathways in agriculture (Corona et al., 2018). Our results demonstrate that 1.2–2.2 t DM ha^{-1} year^{-1} (RCG) and 1.0–1.2 t DM ha^{-1} year^{-1} (TF) of precipitated protein concentrate were extractable using simple lab-scale biorefining techniques. Average annual CP yields within the protein precipitate ranged between 0.4–0.7 t DM ha^{-1} year^{-1} for RCG, and 0.4–0.5 t DM ha^{-1} year^{-1} for TF. This is similar to the 0.7 t ha^{-1}, reported by Jørgensen et al. (2020) for green triticale, an annual cereal, grown on productive arable land, and to perennial ryegrass, with a reported CP content of 245 g CP kg^{-1} DM (Damborg et al., 2020). Considering that the flood-tolerant perennial grasses in this study were cultivated on a riparian fen peatland, a soil-type being widely considered as an unproductive marginal land area (Wichtmann and Wichmann, 2011b), our results indicated a high efficiency from an ecosystem-perspective.

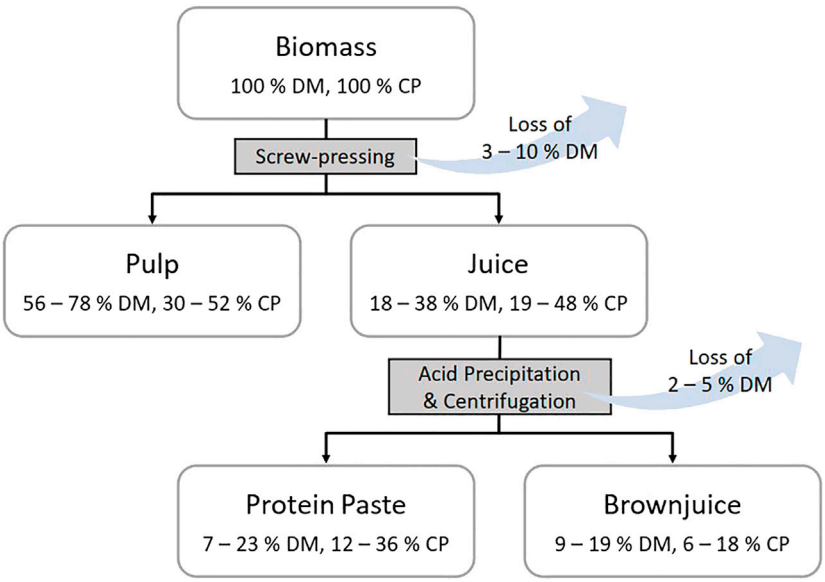

FIGURE 7 | Process flowchart of the biorefinery screw-press technique, indicating dry matter (DM) and crude protein (CP) contents relative to the biomass input. Magnitudes of dry matter losses during processing are given at the two stages. Contents of dry matter (g kg^{-1} fresh weight) and crude protein (g kg^{-1} dry matter) for the various fractions and treatments on different harvest dates are provided in the supplementary material for reed canary grass (**Supplementary Table S3**) and tall fescue (**Supplementary Table S4**).

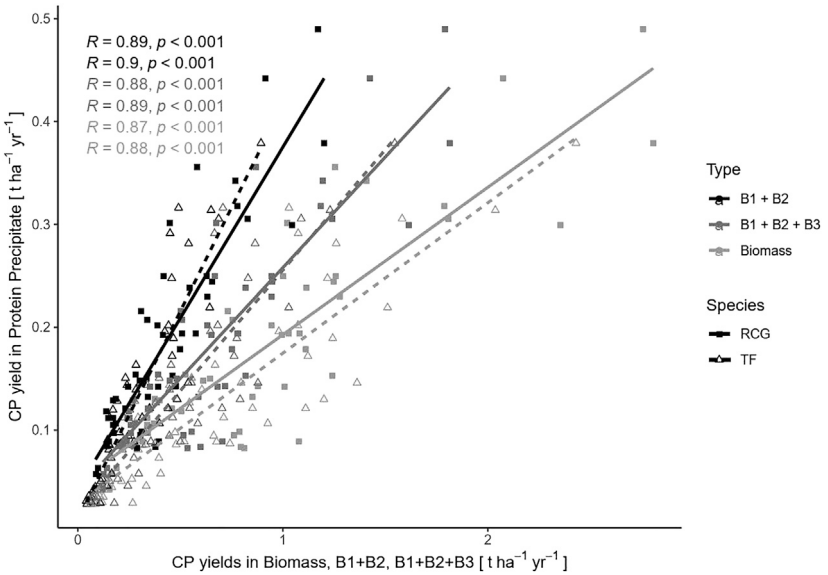

FIGURE 8 | Pearson correlations between yields of crude protein (CP) in precipitated protein and crude protein in biomass (light-grey lines), neutral soluble Cornell Net Carbohydrate and Protein System (CNCPS) fractions B1 + B2 (black lines), and the acid soluble CNCPS fractions B1 + B2 + B3 (grey lines) for the species reed canary grass (RCG, solid lines) and tall fescue (TF, dashed lines), across all treatments and harvest dates.

For the five cut treatments, we were able to extract a protein concentrate with a content of up to between 37% CP (RCG), and 39% (TF), which is lower than the values of up to 40–47% reported for red clover, clover grass blends, alfalfa and oilseed radish concentrates (Santamaría-Fernández et al., 2017; la Cour et al., 2019). However, additional to differences in plant species and families, it should be noticed that, contrary to our study, the fresh biomass input of the reviewed studies was frozen prior to processing, additionally explaining differences in CP content. Freeze-thawing of biomass has the potential to positively

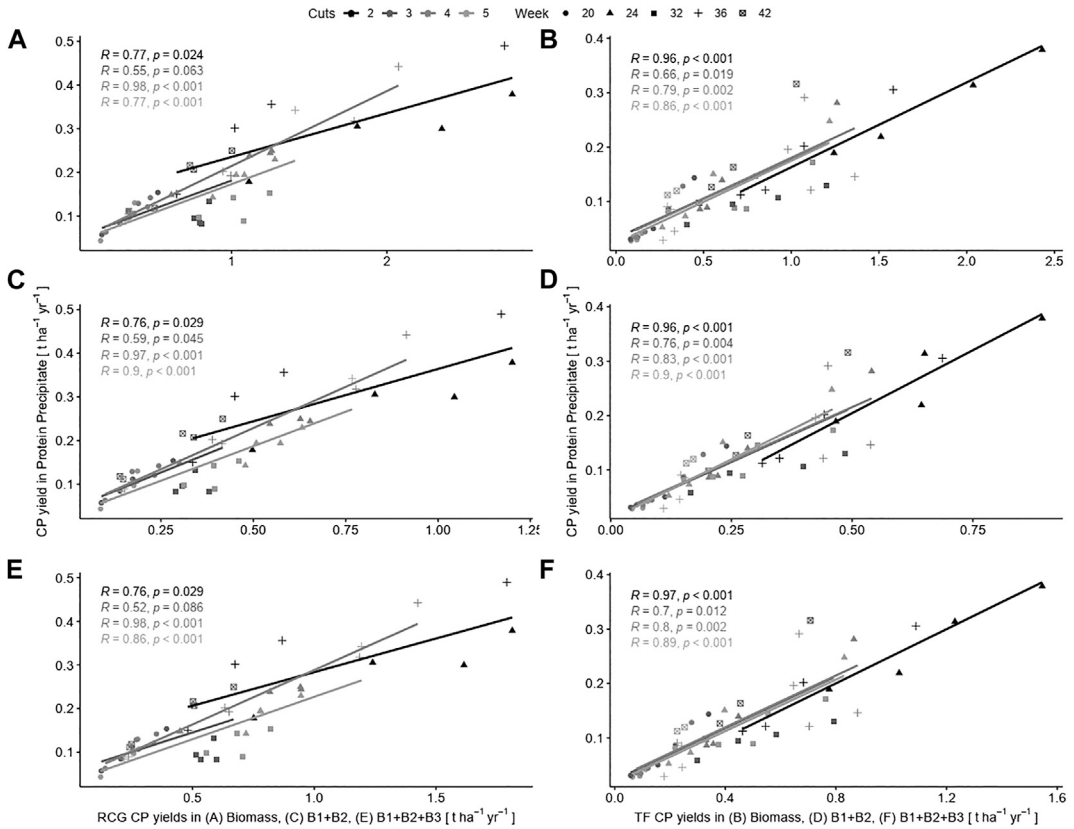

FIGURE 9 | Pearson correlations between crude protein (CP) yields in precipitated protein and crude protein in biomass **(A, B)**, neutral soluble Cornell Net Carbohydrate and Protein System (CNCPS) fractions B1 + B2 **(C, D)**, and acid soluble CNCPS fractions B1 + B2 + B3 **(E, F)** for the species reed canary grass (RCG; **A**, **C**, **D**) and tall fescue (TF; **B**, **D**, **F**). Treatments are indexed by differently shaded correlation lines, and harvest dates by symbols.

contribute to the protein extractability due to tissue denaturation (la Cour et al., 2019), therewith increasing efficiencies. Nonetheless, the difference of only 10% recovered CP in the protein concentrate indicates the potential for perennial grasses grown on peatlands to compete with the more efficient legume species grown on mineral soils. This is also made evident on a product yield basis by a comparison with values published by Santamaría-Fernández et al. (2017), who yielded 6–13 kg of dried protein product per ton of fresh biomass input, having a total CP content of to 46%. In our study, RCG across all treatments yielded between 22–32 kg of dried green protein concentrate per ton of fresh weight input. Though having, with up to 39%, a lower CP content within the green protein product, high protein concentrate yields indicate the potential to offset reduced protein recovery rates as compared to the results from Santamaría-Fernández et al. (2017). However, the quality of the proteins still needs to be defined by an assessment of amino acid composition and digestibility in order to evaluate the appropriateness of paludicrop proteins for animal fodder. The majority of CP within biomass remained in the fibrous pulp fraction (**Figures 10A,B**), with average annual yields of up to 1.4 t DM ha^{-1} $year^{-1}$ (RCG, two cuts) and 1.1 t DM ha^{-1} $year^{-1}$ (TF, two cuts). On a yield basis, this represents approximately 38% of the total biomass CP all treatments. However, the increased valorisation of the fibrous pulp as ruminant forage was highlighted by Damborg et al. (2018).

Future research should hence not only put emphasis on more screw-press fractionation trials regarding flood-tolerant perennial grasses, but in particular of those grown on wet agricultural peatlands in order to further determine their potential for the generation of value-added protein products resulting from biorefining. Further, differences in precipitation efficiencies should be evaluated, as also claimed by Jørgensen et al. (2020). For instance have lactic-acid fermentation (Santamaría-Fernández et al., 2017), microfiltration (Santamaría-Fernández et al., 2020) and lignosulfonates (la Cour et al., 2019), shown to be promising improvements for protein recovery as compared to precipitation by acid precipitation or heat treatment.

Comparison of extractable and potentially extractable proteins indicated by the CNCPS vs. protein precipitated following screw-pressing

Maximising product yield has been highlighted as the most critical optimisation parameter for biorefineries from an enviro-economic perspective (Corona et al., 2018;

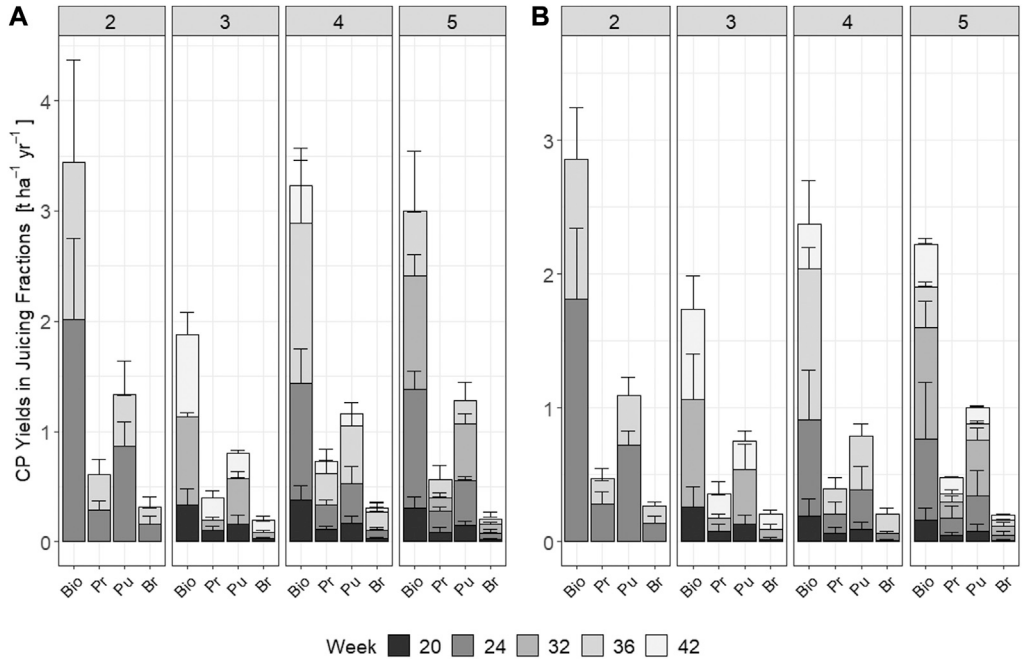

FIGURE 10 | Total annual yields (t ha^{-1} year^{-1}) and yields (t ha^{-1}) for individual harvest weeks of crude protein (CP) in the biomass and in the screw-pressed fractions for the various treatments and species **(A)** reed canary grass (left-hand panel), and **(B)** tall fescue (right-hand panel). Abbreviations: Bio = Biomass, Pr = Protein Paste, Pu = Pulp, Br = Brownjuice. Error-bars show standard deviations.

Santamaría-Fernández et al., 2020). Our results showed maximum yields for fractions B_1 and B_2 of 1.5 t DM ha^{-1} year^{-1} (RCG, two cuts) and 1.1 t DM ha^{-1} year^{-1} (TF, two cuts), representing 45%, respectively 39% of the total biomass CP. However, for these treatments, only 18 and 16% of biomass CP, respectively 40 and 41% of the summed fractions B_1 and B_2, were extracted during the biorefinery process. When also accounting for the potentially extractable protein fraction B_3, the potential for biomass CP recovery by biorefinery increases to 2.3 t DM ha^{-1} year^{-1} and 1.8 t DM ha^{-1} year^{-1}, representing 67 and 64% of total biomass CP. These values for extractable and potentially extractable protein fractions are similar and only marginally higher compared to those reported by Solati et al. (2018b), though cultivated on different soil types and under different environmental conditions.

The strong correlation of methods showed, that using CNCPS fractions B_1 and B_2 as an indicator provides a promising opportunity for prediction of protein extractability, and hence obtainable yields, with current biorefinery techniques. However, there are obstacles regarding the improvement of precipitation efficiencies that need to be overcome in order to make the green biorefinery concept a not only sustainable, but also economically viable enterprise. Adding fraction B_3 to the extraction potential, increasing the potential protein yield by on average 24%, might be a hindering for the near future, when even the easily-soluble protein fractions can not entirely be extracted. However, this should be interpreted as an incentive for more prompt improvements. Additional improvements for the protein precipitation potential, and hence increased protein yields, might be found in cutting of the biomass prior to screw-pressing or multiple pressing of the protein-rich pulp fraction, as indicated by the low DM content of the latter.

CONCLUSION

Paludiculture is a promising option for promoting rewetting of drained agricultural peatlands to mitigate adverse environmental impacts by the provision of critical ecosystem services, while at the same time providing an economic output. However, new opportunities for the generation of value-added products derived from paludicrops have yet to be defined. We found the highest annual biomass and CP yields in the two cut treatments, with 13.4 and 15.6 t DM ha^{-1} year^{-1}, yielding 2.9 and 3.4 t CP ha^{-1} year^{-1} for TF and RCG, respectively. Overall, the results indicated that increased harvest frequencies did not significantly improve average annual biomass and CP yields beyond two cuts annually, but that CP contents, and hence grass quality, for the various cuts remained high throughout the year. Our results showed maximum neutral-extractable (fractions B_1 and B_2) true protein yields of 1.1 and 1.5 t ha^{-1} year^{-1} in the two cut treatments, representing 39% (TF) and 45% (RCG) of total CP. When also accounting for the acid extractable protein fraction B_3, the potential for biomass CP recovery by biorefinery increased to 1.8 t (TF) and 2.3 t (RCG) ha^{-1} year^{-1}. The allocation of plant protein between CNCPS fractions was significantly affected by harvest date, underlining the importance of plant maturity, and frequency of

annual cuts. This also applied for cumulative annual CP yields of precipitated protein concentrate, with a content of up to 39% CP, where 1.0 and 2.2 t DM ha^{-1} $year^{-1}$ were precipitated for TF and RCG, respectively. We found a significant positive correlation between CP yield in the protein concentrate and CNCPS fractions B_1 + B_2, indicating that the CNCPS analysis is suitable for the prediction of protein extractability with current biorefinery techniques. Harvest dates and frequencies should be adjusted to match optimal site-specific climatic conditions and biomass development stages for protein extraction. In conclusion, the results from this study indicated not only high biomass and CP yields, as well as reasonable protein concentrate outputs from biorefining, but also the suitability of paludiculture crops, such as reed canary grass and tall fescue, as promising feedstock candidates for value-added product chains.

DATA AVAILABILITY STATEMENT

The raw data supporting the conclusions of this article will be made available by the authors, without undue reservation.

AUTHOR CONTRIBUTIONS

CN developed and performed the study design and experimental work, the analysis of the data, and the writing of the manuscript. All authors contributed to the study design, the writing and reading of the manuscript, and approved the final manuscript.

FUNDING

This study was financially supported by the PEATWISE project (https://www.eragas.eu/en/eragas/Research-projects/PEATWISE.htm) in the frame of the ERA-NET FACCE ERA-GAS. FACCE ERA-GAS received funding from the European Union's Horizon 2020 research and innovation programme under the grant agreement No. 696356. It further was financially supported by the GrassBot2 project, receiving funding from the European Regional Development Fund (ERDF) and Region Midtjylland, Danmark. In addition, the study was partly supported by the Aarhus University Center for Circular Bioeconomy (CBIO, https://cbio.au.dk/en/).

ACKNOWLEDGMENTS

The authors would like to thank technical and laboratory staff at the Departments of Agroecology and Animal Science, and in particular, the agricultural technologists at Foulumgård, Aarhus University, for excellent guidance as well as assistance with crop management and analyses.

SUPPLEMENTARY MATERIAL

The Supplementary Material for this article can be found online at: https://www.frontiersin.org/articles/10.3389/fenvs.2021.619258/full#supplementary-material.

REFERENCES

Ambye-Jensen, M., Johansen, K. S., Didion, T., Kádár, Z., and Meyer, A. S. (2014). Ensiling and hydrothermal pretreatment of grass: consequences for enzymatic biomass conversion and total monosaccharide yields. *Biotechnol. Biofuels* 7 (1), 95. doi:10.1186/1754-6834-7-95

AOAC (Editor) (1990). *Official methods of analysis*. 15th Edn. Arlington, VA: Association of Official Analytical Chemists).

Bates, D., Mächler, M., Bolker, B., and Walker, S. (2015). Fitting linear mixed-effects models using lme4. *J. Stat. Softw.* 67 (1), 1–48. doi:10.18637/jss.v067.i01

Butkute, B., Lemežiene, N., Kanapeckas, J., Navickas, K., Dabkevičius, Z., and Venslauskas, K. (2014). Cocksfoot, tall fescue and reed canary grass: dry matter yield, chemical composition and biomass convertibility to methane. *Biomass Bioenergy* 66, 1–11. doi:10.1016/j.biombioe.2014.03.014

Butkutė, B., Lemežienė, N., Cesevičienė, J., Liatukas, Ž., and Dabkevičienė, G. (2013). Carbohydrate and lignin partitioning in switchgrass biomass *Panicum virgatum* L. as a bioenergy feedstock. *Zemdirbyste-Agriculture* 100 (3), 251–260. doi:10.13080/z-a.2013.100.032

Buxton, D. R., and Marten, G. C. (1989). Crop quality and utilization: forage quality of plant parts of perennial grasses and relationship to phenology. *Crop Sci.* 29 (2), 429–435. doi:10.2135/cropsci1989.0011183X0029000200039x

Coblentz, W. K., Akins, M. S., Cavadini, J. S., and Jokela, W. E. (2017). Net effects of nitrogen fertilization on the nutritive value and digestibility of oat forages. *J. Dairy Sci.* 100 (3), 1739–1750. doi:10.3168/jds.2016-12027

Corona, A., Ambye-Jensen, M., Vega, G. C., Hauschild, M. Z., and Birkved, M. (2018). Techno-environmental assessment of the green biorefinery concept: combining process simulation and life cycle assessment at an early design stage. *Sci. Total Environ.* 635, 100–111. doi:10.1016/j.scitotenv.2018.03.357

da Silva, M. S., Tremblay, G. F., Bélanger, G., Lajeunesse, J., Papadopoulos, Y. A., Fillmore, S. A. E., et al. (2013). Energy to protein ratio of grass-legume binary mixtures under frequent clipping. *Agron. J.* 105 (2), 482–492. doi:10.2134/agronj2012.0281

Damborg, V. K., Jensen, S. K., Weisbjerg, M. R., Adamsen, A. P., and Stødkilde, L. (2020). Screw-pressed fractions from green forages as animal feed: chemical composition and mass balances. *Anim. Feed Sci. Technol.* 261, 114401. doi:10.1016/j.anifeedsci.2020.114401

Damborg, V. K., Stødkilde, L., Jensen, S. K., and Weisbjerg, M. R. (2018). Protein value and degradation characteristics of pulp fibre fractions from screw pressed grass, clover, and lucerne. *Anim. Feed Sci. Technol.* 244, 93–103. doi:10.1016/j.anifeedsci.2018.08.004

Davys, M., and Pirie, N. (1963). Batch production of protein from leaves. *J. Agric. Eng. Res.* 8 (1), 70–73.

Dindová, A., Hakl, J., Hrevušová, Z., and Nerušil, P. (2019). Relationships between long-term fertilization management and forage nutritive value in grasslands. *Agric. Ecosyst. Environ.* 279, 139–148. doi:10.1016/j.agee.2019.01.011

Elizalde, J. C., Merchen, N. R., and Faulkner, D. B. (1999). Fractionation of fiber and crude protein in fresh forages during the spring growth. *J. Anim. Sci.* 77 (2), 476–484. doi:10.2527/1999.772476x

Geurts, J. J., van Duinen, G.-J. A., van Belle, J., Wichmann, S., Wichtmann, W., and Fritz, C. (2019). Recognize the high potential of paludiculture on rewetted peat soils to mitigate climate change. *J. Sustain. Org. Agric. Syst.* 69 (1), 5–8. doi:10.3220/LBF1576769203000

Giannini, V., Silvestri, N., Dragoni, F., Pistocchi, C., Sabbatini, T., and Bonari, E. (2017). Growth and nutrient uptake of perennial crops in a paludicultural approach in a drained Mediterranean peatland. *Eco. Eng.* 103, 478–487.

Günther, A. B., Huth, V., Jurasinski, G., and Glatzel, S. (2014). Scale-dependent temporal variation in determining the methane balance of a temperate fen. *Greenh. Gas Meas. Manag.* 4 (1), 41–48. doi:10.1080/20430779.2013.850395

Guretzky, J. A., Dunn, C. D., and Bishop, A. (2017). Plant community structure and forage nutritive value of reed canarygrass-invaded wetlands. *Agron. J.* 110 (1), 200–209. doi:10.2134/agronj2017.05.0277

Huang, B., Rachmilevitch, S., and Xu, J. (2012). Root carbon and protein metabolism associated with heat tolerance. *J. Exp. Bot.* 63 (9), 3455–3465. doi:10.1093/jxb/ers003

Ibarrola-Rivas, M. J., Granados-Ramírez, R., and Nonhebel, S. (2017). Is the available cropland and water enough for food demand? a global perspective of the land-water-food nexus. *Adv. Water Resour.* 110, 476–483. doi:10.1016/j.advwatres.2017.09.018

Jardstedt, M., Hessle, A., Nørgaard, P., Richardt, W., and Nadeau, E. (2017). Feed intake and urinary excretion of nitrogen and purine derivatives in pregnant suckler cows fed alternative roughage-based diets. *Livest. Sci.* 202, 82–88. doi:10.1016/j.livsci.2017.05.026

Joosten, H., and Clarke, D. (2002). *Wise use of mires and peatlands – background and Principles, including a Framework for Decision-making*. Jyväskylä, Finland: International Mire Conservation Group and International Peat Society.

Joosten, H., Gaudig, G., Tanneberger, F., Wichmann, S., and Wichtmann, W. (2016). "Paludiculture: sustainable productive use of wet and rewetted peatlands," in *Peatland restoration and ecosystem services: science, policy and practice*. Editor A. Bonn, T. Allott, M. Evans, H. Joosten, and R. Stoneman (Bangkok, Thailand: C. U. Press), 339–357.

Joosten, H. (2012). Status and prospects of global peatlands. *Nat. Landsch.* 87 (2), 50–55. doi:10.17433/2.2012.50153141.50-55

Jørgensen, H., Thomsen, S. T., and Schjoerring, J. K. (2020). The potential for biorefining of triticale to protein and sugar depends on nitrogen supply and harvest time. *Ind. Crops Prod.* 149, 112333. doi:10.1016/j.indcrop.2020.112333

Kandel, T. P., Elsgaard, L., Andersen, M. N., and Lærke, P. E. (2016). Influence of harvest time and frequency on light interception and biomass yield of festulolium and tall fescue cultivated on a peatland. *Eur. J. Agron.* 81, 150–160. doi:10.1016/j.eja.2016.09.010

Kandel, T. P., Elsgaard, L., Karki, S., and Lærke, P. E. (2013a). Biomass yield and greenhouse gas emissions from a drained fen peatland cultivated with reed canary grass under different harvest and fertilizer regimes. *BioEnergy Res.* 6 (3), 883–895. doi:10.1007/s12155-013-9316-5

Kandel, T. P., Sutaryo, S., Møller, H. B., Jørgensen, U., and Lærke, P. E. (2013b). Chemical composition and methane yield of reed canary grass as influenced by harvesting time and harvest frequency. *Bioresour. Technol.* 130, 659–666. doi:10.1016/j.biortech.2012.11.138

Kappelle, M. (2020). *WMO statement on the state of the global climate in 2019*. Geneva, Switzerland: World Meteorological Association. doi:10.13140/RG.2.2.13705.19046

Karki, S., Kandel, T. P., Elsgaard, L., Labouriau, R., and Lærke, P. E. (2019). Annual CO2 fluxes from a cultivated fen with perennial grasses during two initial years of rewetting. *Mires Peat* 25 (01), 01–22. doi:10.19189/MaP.2017.DW.322

Kromus, S., Kamm, B., Kamm, M., Fowler, P., and Narodoslawsky, M. (2006). The green biorefinery concept – fundamentals and potential. *Green Biorefineries* 1, 253–294. doi:10.1002/9783527619849.ch12

la Cour, R., Schjoerring, J. K., and Jørgensen, H. (2019). Enhancing protein recovery in green biorefineries by lignosulfonate-assisted precipitation. *Front. Sustain. Food Syst.* 3, 1–9. doi:10.3389/fsufs.2019.00112

Lewandowski, I., Scurlock, J. M. O., Lindvall, E., and Christou, M. (2003). The development and current status of perennial rhizomatous grasses as energy crops in the US and Europe. *Biomass Bioenergy* 25 (4), 335–361. doi:10.1016/s0961-9534(03)00030-8

Licitra, G., Hernandez, T. M., and Van Soest, P. J. (1996). Standardization of procedures for nitrogen fractionation of ruminant feeds. *Anim. Feed Sci. Technol.* 57 (4), 347–358. doi:10.1016/0377-8401(95)00837-3

Loaiza, P., Balocchi, O., de la Barra, C., and López, I. F. (2019). Perennial ryegrass productivity and nutritive quality as affected by frequency of nitrogen fertilizer addition. *Grassland Sci.* 65 (2), 86–92. doi:10.1111/grs.12227

Manevski, K., Lærke, P. E., Jiao, X., Santhome, S., and Jørgensen, U. (2017). Biomass productivity and radiation utilisation of innovative cropping systems for biorefinery. *Agric. For. Meteorol.* 233, 250–264. doi:10.1016/j.agrformet.2016.11.245

Marten, G. C., and Hovin, A. W. (1980). Harvest schedule, persistence, yield, and quality interactions among four perennial grasses1. *Agron. J.* 72 (2), 378. doi:10.2134/agronj1980.00021962007200020030x

Meisser, M., Vitra, A., Deléglise, C., Dubois, S., Probo, M., Mosimann, E., et al. (2019). Nutrient limitations induced by drought affect forage N and P differently in two permanent grasslands. *Agric. Ecosyst. Environ.* 280, 85–94. doi:10.1016/j.agee.2019.04.027

Myhr, K., Solderg, Y., and Selmer-Olsen, A. R. (1978). The content of minerals, fibre, protein and amino acids in reed canary grass, timothy and meadow fescue. *Acta Agric. Scand.* 28 (3), 269–278. doi:10.1080/00015127809435179

Peoples, M. B., and Dalling, M. J. (1988). "The interplay between proteolysis and amino acid metabolism during senescence and nitrogen reallocation," in *Senescence and Aging in Plants*. Editors L. D. Nooden and A. C. Leopold. San Diego, United States: Academic Press Inc.

Perotti, E., Huguenin-Elie, O., Meisser, M., Dubois, S., Probo, M., and Mariotte, P. (2021). Climatic, soil, and vegetation drivers of forage yield and quality differ across the first three growth cycles of intensively managed permanent grasslands. *Eur. J. Agron.* 122, 126194. doi:10.1016/j.eja.2020.126194

Peyraud, J. L., and Astigarraga, L. (1998). Review of the effect of nitrogen fertilization on the chemical composition, intake, digestion and nutritive value of fresh herbage: consequences on animal nutrition and N balance. *Anim. Feed Sci. Technol.* 72 (3), 235–259. doi:10.1016/S0377-8401(97)00191-0

Pihlajaniemi, V., Ellilä, S., Poikkimäki, S., Nappa, M., Rinne, M., Lantto, R., et al. (2020). Comparison of pretreatments and cost-optimization of enzymatic hydrolysis for production of single cell protein from grass silage fibre. *Bioresour. Technol. Rep.* 9, 100357. doi:10.1016/j.biteb.2019.10035

R Core Team (2020). *R: a language and environment for statistical computing*. Vienna, Austria: R Foundation for Statistical Computing. Available at: https://www.R-project.org/.

Roy-Macauley, H., Zuily-Fodil, Y., Kidric, M., Thi, A. T. P., and Silva, J. V. (1992). Effect of drought stress on proteolytic activities in *Phaseolus* and *Vigna* leaves from sensitive and resistant plants. *Physiol. Plant.* 85 (1), 90–96. doi:10.1111/j.1399-3054.1992.tb05268.x

Sanderson, M. A., and Wedin, W. F. (1989). Nitrogen in the detergent fibre fractions of temperate legumes and grasses. *Grass Forage Sci.* 44 (2), 159–168. doi:10.1111/j.1365-2494.1989.tb01923.x

Santamaria-Fernandez, M., Ambye-Jensen, M., Damborg, V. K., and Lübeck, M. (2019). Demonstration-scale protein recovery by lactic acid fermentation from grass clover – a single case of the production of protein concentrate and press cake silage for animal feeding trials. *Biofuels Bioprod. Biorefin.* 13 (3), 502–513. doi:10.1002/bbb.1957

Santamaría-Fernández, M., Molinuevo-Salces, B., Kiel, P., Steenfeldt, S., Uellendahl, H., and Lübeck, M. (2017). Lactic acid fermentation for refining proteins from green crops and obtaining a high quality feed product for monogastric animals. *J. Clean. Prod.* 162, 875–881. doi:10.1016/j.jclepro.2017.06.115

Santamaría-Fernández, M., Schneider, R., Lübeck, M., and Venus, J. (2020). Combining the production of L-lactic acid with the production of feed protein concentrates from alfalfa. *J. Biotechnol.* 323, 180–188. doi:10.1016/j.jbiotec.2020.08.010

Solati, Z., Jørgensen, U., Eriksen, J., and Søegaard, K. (2017). Dry matter yield, chemical composition and estimated extractable protein of legume and grass species during the spring growth. *J. Sci. Food Agric.* 97, 3958–3966. doi:10.1002/jsfa.8258

Solati, Z., Jørgensen, U., Eriksen, J., and Søegaard, K. (2018a). Estimation of extractable protein in botanical fractions of legume and grass species. *Grass Forage Sci.* 73 (2), 572–581. doi:10.1111/gfs.12325

Solati, Z., Manevski, K., Jørgensen, U., Labouriau, R., Shahbazi, S., and Lærke, P. E. (2018b). Crude protein yield and theoretical extractable true protein of potential biorefinery feedstocks. *Ind. Crops Prod.* 115, 214–226. doi:10.1016/j.indcrop.2018.02.010

Stødkilde, L., Damborg, V. K., Jørgensen, H., Laerke, H. N., and Jensen, S. K. (2018). White clover fractions as protein source for monogastrics: dry matter digestibility and protein digestibility-corrected amino acid scores. *J. Sci. Food Agric.* 98 (7), 2557–2563. doi:10.1002/jsfa.8744

Stødkilde, L., Damborg, V. K., Jørgensen, H., Lærke, H. N., and Jensen, S. K. (2019). Digestibility of fractionated green biomass as protein source for monogastric animals. *Animal* 13 (9), 1817–1825. doi:10.1017/s1751731119000156

Tahir, M. H. N., Casler, M. D., Moore, K. J., and Brummer, E. C. (2011). Biomass yield and quality of reed canarygrass under five harvest management systems for bioenergy production. *BioEnergy Res.* 4 (2), 111–119. doi:10.1007/s12155-010-9105-3

Tanneberger, F., and Wichtmann, W. (2011). *Carbon credits from peatland rewetting: climate – biodiversity – land use*. Stuttgart, Germany: Schweizerbart'sche Verlagsbuchhandlung.

Tilvikiene, V., Kadziuliene, Z., Dabkevicius, Z., Venslauskas, K., and Navickas, K. (2016). Feasibility of tall fescue, cocksfoot and reed canary grass for anaerobic digestion: analysis of productivity and energy potential. *Ind. Crops Prod.* 84, 87–96. doi:10.1016/j.indcrop.2016.01.033

United Nations, Department of Economic and Social Affairs, Population Division (2019). World Population Prospects 2019: Highlights (ST/ESA/SER.A/423).

Ustak, S., Šinko, J., and Muňoz, J. (2019). Reed canary grass (*Phalaris arundinacea* L.) as a promising energy crop. *J. Cent. Eur. Agric.*, 20 (4), 1143–1168. doi:10.5513/JCEA01/20.4.2267

Van Soest, P. J., Robertson, J. B., and Lewis, B. A. (1991). Methods for dietary fiber, neutral detergent fiber, and nonstarch polysaccharides in relation to animal nutrition. *J. Dairy Sci.* 74 (10), 3583–3597. doi:10.3168/jds.s0022-0302(91)78551-2

Vitra, A., Deléglise, C., Meisser, M., Risch, A. C., Signarbieux, C., Lamacque, L., et al. (2019). Responses of plant leaf economic and hydraulic traits mediate the effects of early- and late-season drought on grassland productivity. *AoB Plants* 11 (3), plz023. doi:10.1093/aobpla/plz023

Wichmann, S. (2017). Commercial viability of paludiculture: a comparison of harvesting reeds for biogas production, direct combustion, and thatching. *Ecol. Eng.* 103, 497–505. doi:10.1016/j.ecoleng.2016.03.018

Wichtmann, W., and Wichmann, S. (2011a). Paludikultur: standortgerechte bewirtschaftung wiedervernässter moore. *TELMA - Berichte der Deutschen Gesellschaft für Moor- und Torfkunde, Beiheft* 4, 215–234. doi:10.23689/fidgeo-2979

Wichtmann, W., and Wichmann, S. (2011b). Environmental, social and economic aspects of a sustainable biomass production. *J. Sustain. Energy Environ. Spec. Issue*, 77–81.

Yin, X., Schapendonk, A. H. C. M., and Struik, P. C. (2018). Exploring the optimum nitrogen partitioning to predict the acclimation of C3 leaf photosynthesis to varying growth conditions. *J. Exp. Bot.* 70 (9), 2435–2447. doi:10.1093/jxb/ery277

Yu, Z., Loisel, J., Brosseau, D. P., Beilman, D. W., and Hunt, S. J. (2010). Global peatland dynamics since the last glacial maximum. *Geophys. Res. Lett.* 37 (13), L14302. doi:10.1029/2010gl043584

Conflict of Interest: The authors declare that the research was conducted in the absence of any commercial or financial relationships that could be construed as a potential conflict of interest.

frontiers in Earth Science

ORIGINAL RESEARCH
published: 22 April 2021
doi: 10.3389/feart.2020.579329

Water Table Fluctuation in Peatlands Facilitates Fungal Proliferation, Impedes *Sphagnum* Growth and Accelerates Decomposition

Jinhyun Kim[1], Line Rochefort[2], Sandrine Hogue-Hugron[2], Zuhair Alqulaiti[3], Christian Dunn[3], Remy Pouliot[2], Timothy G. Jones[3], Chris Freeman[3] and Hojeong Kang[1]*

[1]School of Civil and Environmental Engineering, Yonsei University, Seoul, Republic of Korea, [2]Peatland Ecology Research Group (PERG), Centre for Northern Studies, Department of Plant Sciences, Université Laval, Québec, QC, Canada, [3]School of Natural Sciences, Bangor University, Bangor, United Kingdom

Northern peatlands are substantial carbon sinks because organic matter in peat is highly stable due to the low rate of decomposition. Waterlogged anaerobic conditions induce accumulation of *Sphagnum*-derived phenolic compounds that inhibit peat organic matter decomposition, a mechanism referred to as the "enzymic latch". Recent studies have predicted that the water table in northern peatlands may become unstable. We observed that such unstable water table levels can impede the development of *Sphagnum* mosses. In this study, we determined the effects of low and high frequency water table fluctuation regimes on *Sphagnum* growth and peat organic matter decomposition, by conducting a year-long mesocosm experiment. In addition, we conducted a molecular analysis to examine changes in abundance of fungal community which may play a key role in the decomposition of organic matter in peatlands. We found that rapid water table fluctuation inhibited the growth of *Sphagnum* due to fungal infection but stimulated decomposition of organic matter that may dramatically destabilize peatland carbon storage. Increased pH, induced by the fluctuation, may contribute to the enhanced activity of hydrolases in peat. We demonstrated that the water table fluctuation in peatlands impeded *Sphagnum* growth and accelerates decomposition due to fungal proliferation. Thus, we suggested that understanding the microbial community in the northern peatlands is essential for elucidating the possible changes in carbon cycle of peatland under the changing world.

Keywords: peatland, water table fluctuation, sphagnum, fungi, enzymic latch, decomposition

OPEN ACCESS

Edited by:
Klaus-Holger Knorr,
University of Münster, Germany

Reviewed by:
Vincent Jassey,
UMR5245 Laboratoire Ecologie Fonctionnelle et Environnement (ECOLAB), France
Jason Keller,
Chapman University, United States

****Correspondence:***
Line Rochefort
line.rochefort@fsaa.ulaval.ca

Specialty section:
This article was submitted to Biogeoscience, a section of the journal Frontiers in Earth Science

Received: *02 July 2020*
Accepted: *18 December 2020*
Published: *22 April 2021*

Citation:
Kim J, Rochefort L, Hogue-Hugron S, Alqulaiti Z, Dunn C, Pouliot R, Jones TG, Freeman C and Kang H (2021) Water Table Fluctuation in Peatlands Facilitates Fungal Proliferation, Impedes Sphagnum *Growth and Accelerates Decomposition. Front. Earth Sci. 8:579329. doi: 10.3389/feart.2020.579329*

INTRODUCTION

Northern peatlands are characterized by waterlogged, anaerobic, acidic, phenolic-rich, cool conditions, resulting in the low decomposition rate and high accumulation rate (3–80 g C m^{-2} y^{-1}) of organic matter as peat (Gorham, 1991; Aerts et al., 1992; Gallego-Sala et al., 2018). Northern peatlands are recognized to impact the global CO_2 budget as they occupy up to 3% (around 4 millions km^2) of the Earth's terrestrial surface (Yu et al., 2010; Xu et al., 2018), and their peat is a substantial carbon sink where the recently estimated carbon storage was up to 1,055 Pg (Nichols and Peteet, 2019), which is more than a half of global soil organic matter (Scharlemann et al., 2014). This

significant C storage had been considered to continuously increase since last glaciation but now we question its potential changes in stability under changing climate (Zhang et al., 2020).

Northern bogs and muskegs are dominated by *Sphagnum* mosses, whose plant tissues are more recalcitrant than the plant matter of vascular plants or other mosses (Moore and Basiliko, 2006). Water table is a key controlling factor of carbon sequestration in these northern peatlands because it determines oxygen availability (Haraguchi, 1991; Belyea, 1996; Abbott et al., 2013). Waterlogged anaerobic conditions induce accumulation of *Sphagnum*-derived phenolic compounds due to a lack of phenol oxidase activity able to break down phenolic compounds (Abbott et al., 2013; Kim et al., 2014). The abundant phenolic compounds prevent hydrolases activity to degrade organic matter (Freeman et al., 1990; Wetzel, 1992; Freeman et al., 2001). In contrast, if water table is lowered, oxygen becomes available to activate phenol oxidative enzymes, lowering the quantity of phenolic compounds and consequently allowing the decomposition of organic matter. This mechanism is called 'enzymic latch' and it is one of the key mechanisms controlling decomposition of organic matter in peatlands (Freeman et al., 2001; Romanowicz et al., 2015; Kang et al., 2018).

Northern peatlands have the ability to self-regulate their hydrology, keeping water levels relatively stable (Rochefort and Lode, 2006). However in large peatlands (in the order of 1,000 ha or more), some have streams in the watershed. Seasonal fluctuation of water table may occur because of variation of precipitation and temperature (Okland, 1989), but it is not as substantial or as rapid as fluctuations exhibited by riverine wetlands (Junk et al., 1989). We have observed that in the proximity of these streams, *Sphagnum* cover thins out to give rise to a more shrubby vegetation (L. Rochefort pers. obs.). We know that *Sphagnum* species composition and growth is substantially dependent on water table characteristics (Sjors, 1948), and usually grow better when the water tables are stable (Clymo and Duckett, 1986; Holden et al., 2004). In the field, we have observed that frequent inundation appears unfavorable to *Sphagnum* establishment (Brown et al., 2017). In addition, climate changes are expected to be the most pronounced in the high latitudinal region where northern peatlands are distributed (Overland et al., 2014), thus water table levels may become less stable (Taminskas et al., 2018). These observations suggest that the role of the northern peatlands as a carbon sink would be weakened because of water table fluctuation-induced reduction of *Sphagnum* growth and stimulation of decomposition of organic matter by reducing the 'enzymic latch' mechanism (Min et al., 2015). While some studies have attempted to determine the effect of water table level on peatland (Trinder et al., 2008; Kwon et al., 2013; Potvin et al., 2015; Lamit et al., 2017), the effect of fluctuation frequency in a controlled environment has never been tested experimentally and mechanisms driving the responses remain unknown.

Fungi represent a major microbial group playing a fundamental role in the decomposition of phenolic compounds in peatlands (Thormann, 2006; Thormann and Rice, 2007; Sinsabaugh, 2010). *Ascomycetes*, *Deuteromycetes*, and *Basidiomycetes* are the main producer of polyphenol oxidative enzymes called *laccase* (Bourbonnais et al., 1995; Leontievsky et al., 1997; Baldrian, 2006). In addition, fungal *laccases* have higher potential for the decomposition of phenolics than others (e.g., bacterial *laccases*) (Thurston, 1994). Thus, fungal communities may play a critical role in the 'enzymic latch' mechanism in peatlands (Romanowicz et al., 2015). Fungi in peatlands are found in peat soil, roots of vascular plant, and *Sphagnum* tissue. Particularly, *Sphagnum* itself provides habitat for pathogenic and parasitic fungi which alters growth and function of *Sphagnum* (Kostka et al., 2016). Water table, or oxygen availability, is likely to shift microbial community structure, including that of fungi (Freeman et al., 2001; Trinder et al., 2008). Although, previous studies have illustrated the effect of water availability on fungal communities (Jassey et al., 2018), the mechanistic responses of fungal communities and their activity to water table fluctuations are not fully understood.

The objective of this study was to determine the effects of water table fluctuation on the *Sphagnum* growth and decomposition of organic matter in peat. In particular, we hypothesized that 1) fluctuation-induced changes in fungal communities will inhibit the *Sphagnum* growth, 2) decomposition of organic matter in peat will be stimulated by water table fluctuation, and 3) the ability of peat as a carbon sink will be weakened by water table fluctuation. An experiment was carried out in the controlled environment of a greenhouse containing *Sphagnum* peat mesocosms experiencing different water table depths and fluctuation regimes. *Sphagnum* growth as well as peat and *Sphagnum* living layer chemistry, and peat microbial communities were monitored to determine if water table fluctuations affected the establishment of a *Sphagnum* carpet, biomass accumulation and the decomposition of *Sphagnum*, and to uncover the associated microbial mechanisms.

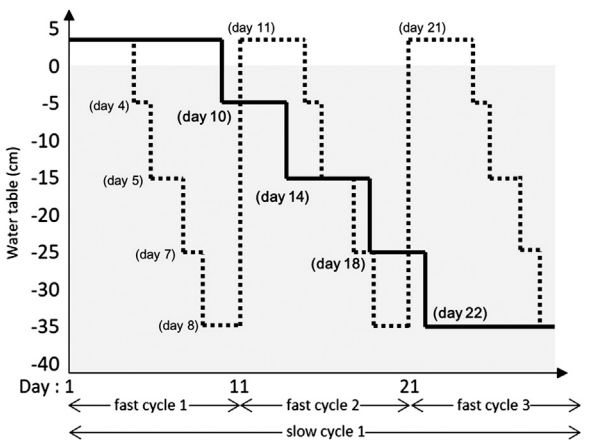

FIGURE 1 | Description of the slow fluctuating (solid line) and the fast fluctuating (dotted line) over 30 days. Positive water table values are levels above the peat surface (i.e., inundations).

MATERIALS AND METHODS

Experimental Design and Implementation

The effect of water table (WT) fluctuation and *Sphagnum* species on biomass accumulation, rate of decomposition, enzymic and microbial activity were tested in a split-plot greenhouse experiment (**Supplementary Figure S1**). Of the three water table regimes (main plots), control involved a stable water table maintained between 0 and −5 cm. The two fluctuating regimes were fast and slowly fluctuating water table cycles between +2 cm (inundation) and −35 cm over 10 and 30 days, respectively (**Figure 1**). In subplots, three *Sphagnum* species from three different subgenera were tested: 1) *S. fallax* (*Cuspidata*), 2) *S. medium* (*Sphagnum*; Hassel et al., 2018) *S. fuscum* (*Acutifolia*). All treatment combinations were replicated four times, in four blocks accounting for possible micro-climatic differences present in the Université Laval greenhouse.

This experiment was carried out in large mesocosms measuring 110 cm (length) × 72 cm (width) × 100 cm (height) (**Supplementary Figure S1**). Each mesocosm was equipped with an individual system of drains and pipes connected to a reservoir that allowed individual control of water table at the desired level. The irrigation system was designed to create groundwater discharge from a 15 cm layer of sand at the base of the mesocosms, which then moved upwards through 35 cm of fibric commercial peat (von post H2-3). Rain water was distributed by hydrostatic pressure from the reservoir to the base of the mesocosm via one perforated inlet pipe coated with nylon. A pipe perforated every 5 cm, connected to the inlet pipe, located outside of each mesocosm allowed manipulation of water table by adding or removing plastic plugs.

Sphagnum plant material was collected by hand in a natural peatland (46°46′N; 71°00′N). Only the first 10 cm of the moss carpet was collected, as this fraction of the moss possesses the highest regeneration capacity (Campeau and Rochefort, 1996). *Sphagnum* was sorted from other plant species and the moss carpet was broken apart into fragments. *Sphagnum* fragments were then spread in a 1 cm thick uniform layer covering 100% of the peat surface. Each mesocosm was divided into three sections (each section measuring 72 cm (length) × 37 cm (width) with clear fiberglass sheets inserted in the top 5 cm of peat, preventing the dispersion of *Sphagnum* beyond its experimental unit, while allowing water circulation. In main plots with fluctuating water tables, the *Sphagnum* layer was covered with a nylon net to prevent displacement of the fragments. After plant spreading, fragments were grown in ideal conditions for 5 weeks: stable water table maintained at −10 cm with watering every two days. Following this acclimatization period, the five different water regimes were implemented over 360 days; i.e., 12 slow fluctuating cycles and 36 fast fluctuating cycles. During the course of the experiment, all mesocosms were abundantly watered with rainwater once every 10 days, at day #1 of each fast fluctuating cycle. Any vascular plant found growing in the experiment was removed. Over the course of the experiment, the growing conditions varied according to the season. Over winter, spring, and fall, daily temperature and relative humidity were maintained at 21°C and 60% respectively while nightly conditions were maintained at 15°C and 70%. Over summer, daily temperatures and RH varied between 23–26°C and 44–59% respectively, while nightly conditions varied between 19–21°C and 68–84%.

Monitoring

Hydrological Parameters

Over the duration of the experiment, the position of the water table in the mesocosm was recorded every 2–3 days, prior to manipulation of the water table. Over a period of 60 days, two (slowly fluctuating) or six (rapidly fluctuating) cycles were imposed, soil moisture was recorded every 2–3 days with a W.E.T Sensor and HH2 Moisture Meter (Delta-T Devices, Cambridge, United Kingdom).

Vegetation

Prior to manipulation of the water table, 15 litter bags (5 per species), were inserted vertically into the upper 5 cm of the peat surface, for a total of 300 bags in the 20 mesocosms. To prepare the litter bags, a small portion of the three *Sphagnum* species harvested was sorted individually and placed in a pre-weighed nylon mesh bags (5 cm × 7.5 cm; mesh gauge of 0.25 mm) and weighed until a constant mass was obtained. Between 0.5 and 2 g of *Sphagnum* fibers were inserted into each bag. The 100 bags containing *S. fallax* were inserted under the *S. fallax* subplots and the same was performed for the two other *Sphagnum* species. At the end of the experiment, the litter bags were retrieved, cleaned and weighed until constant mass. The linear mass loss (k') over the duration of the experiment was calculated following the equation (Reader and Stewart, 1972):

$$k' = \frac{X_0 - X}{X} \times 100 \quad (1)$$

(where X_0 represents the initial dry *Sphagnum* mass (g) and X is the final dry *Sphagnum* mass (g) after incubation in the mesocosms).

At the end of the experiment, all plant material (mostly *Sphagnum*, but also some other bryophytes) was collected down to the commercial peat layer and dried at 70°C until constant mass. A subset of the biomass samples, approximately 25%, was sorted prior to drying to separate *Sphagnum* biomass from the other mosses. The ratio between the known cover of non-*Sphagnum* mosses and its mass was used to adjust the weight of the unsorted samples.

Sphagnum covered-area (%) of each mesocosms were measured, and the reduction of *Sphagnum* covered-area compared to control treatments was determined as response ratio calculated by natural log of values from treatment and control (*ln*(treatment/control)).

Chemical Analyses of *Sphagnum* Living Layer

Sphagnum biomass subsamples from each mesocosm were dried and analyzed for determining the content of total carbon (C), total nitrogen (N), phosphate (PO_4^{3-}), nitrate (NO_3^-), ammonium (NH_4^+), and sulfate (SO_4^{2-}). Analysis of C and N

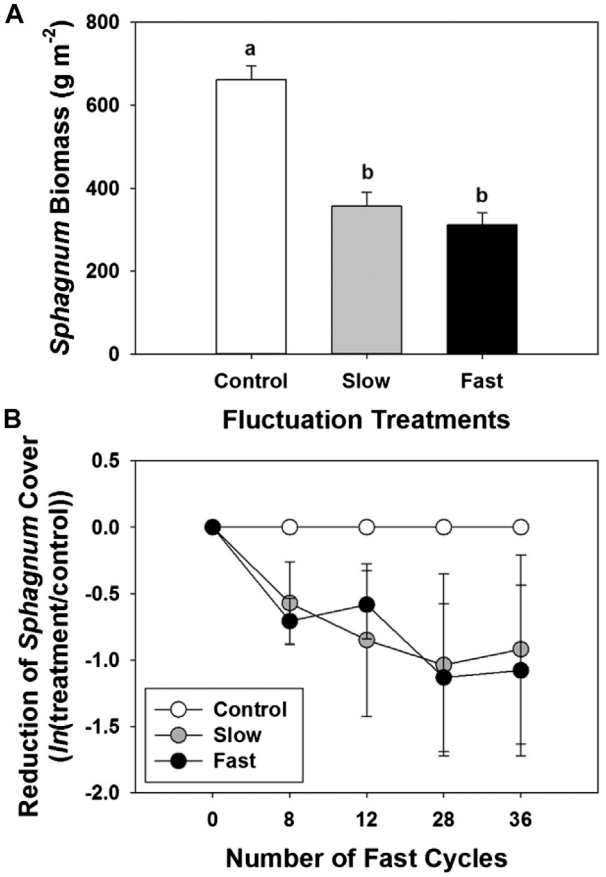

FIGURE 2 | (A) *Sphagnum* biomass, and **(B)** Reduction of *Sphagnum*-covered area during the experiment (response rate, *ln*(treatment/control)). Error bars denote standard errors. Letter denotes statistically significant differences between treatments (n = 12, $p < 0.05$).

were carried out with a Leco TruMac CNS analyser, while PO_4^{3-}, NO_3^-, NH_4^+ and SO_4^{2-} was extracted by 1M KCl and measured by flow injection using a Quikchem 8,500 series 2 FIA system.

Phenolics and Extracellular Enzyme Activity

At the end of the experiment, peat samples were collected per subplots by using peat corer (length 8 cm and diameter 4 cm). The corer and all instruments used to collect the samples were washed in isopropylic alcohol and rinsed with distilled water in between each samples. The samples were placed in a fridge overnight and sent to Bangor University for analyses the following day (in a freezer with icepacks) by express shipment (3 days).

Activities of extracellular enzymes (β-glucosidase, Xylosidase, N-acetyl-glucosaminidase, Arylsulfatase, and Phosphatase) were measured by using methylumbelliferyl (MUF)-substrates (see Freeman et al. (1995) and Kang and Freeman (1999) for detailed method). Extracellular enzymes were extracted from peat samples with acetate buffer (50 mM, pH 5.0). The extracted solution was mixed with MUF-substrates and incubated for 1 h at 25°C. Then the intensities of fluorescence of the solution were measured by fluorometer (Molecular Devices M2e Spectramax plate-reader (wavelength accuracy 2 nm, photometric accuracy 0.006, photometric precision 0.003) at 460 nm emission and 355 nm excitation. The water-soluble phenolics were extracted by distilled water and the concentration was measured by colorimetric method with Folin Ciocalteau phenol reagent (Box, 1983; Dunn et al., 2013).

Molecular Analyses

The peat and *Sphagnum* samples for microbial analysis were collected and stored at −80°C. Microbial DNA was extracted by using DNeasy PowerSoil Kit (Qiagen, Germany) from 400 mg of peat and 200 mg of *Sphagnum* samples. Then, we performed real-time quantitative PCR to quantify the abundance of bacteria, fungi, and fungal *laccase* gene. The primer sets, experimental procedure, and PCR protocol are in the supplementary materials.

Statistical Analyses

The differences in *Sphagnum* biomass, decomposition rates, *Sphagnum* chemistries, extracellular enzyme activities, and abundances of microbes and functional genes among the treatments were analyzed with one-way ANOVA. Spearman method was used to determine the correlations between the measurements. All statistical analyses were conducted by using SPSS 23 (SPSS inc., Chicago, IL, United States) and (R Core Team, 2019).

RESULTS

Sphagnum Biomass and Chemistry

After almost one full year of growth, accumulated *Sphagnum* biomass, including living and dead, was 46–53% lower in the fluctuation treatments than under stable water levels (control) (**Figure 2A**). The area of *Sphagnum*-covered peat was continually reduced by 42–52% during the experiment in the fluctuation treatments compared to the control of more stable water table although it was statistically not significant (**Figure 2B**). Results of biomass and covered area indicated that the growth of *Sphagnum* was reduced if the water table was fluctuating. The near-surface stable water table (0 to -5 cm) resulted in the greatest accumulation of biomass.

Water table fluctuation also altered chemical properties of *Sphagnum* tissue. Especially, PO_4^{3-} (71–78%), NO_3^- (50–51%), and C/N ratio (21–28%) were significantly reduced in the fluctuation WT treatments (**Table 1**).

TABLE 1 | Chemical properties of *Sphagnum* living layer. Letter denotes statistically significant differences between treatments (Mean ± Standard Error, n = 12, $p < 0.05$).

Fluctuation treatments	SO_4^{2-} (ppm)	PO_4^{3-} (ppm)	NH_4^+ (ppm)	NO_3^- (ppm)	C/N ratio
Control	125 ± 18	213 ± 22 **a**	19 ± 0.5 **a**	230 ± 73	66 ± 3 **a**
Slow	143 ± 32	60 ± 7 **b**	16 ± 0.4 **b**	111 ± 20	52 ± 2 **b**
Fast	108 ± 13	45 ± 3 **b**	16 ± 0.3 **b**	113 ± 25	47 ± 1 **b**

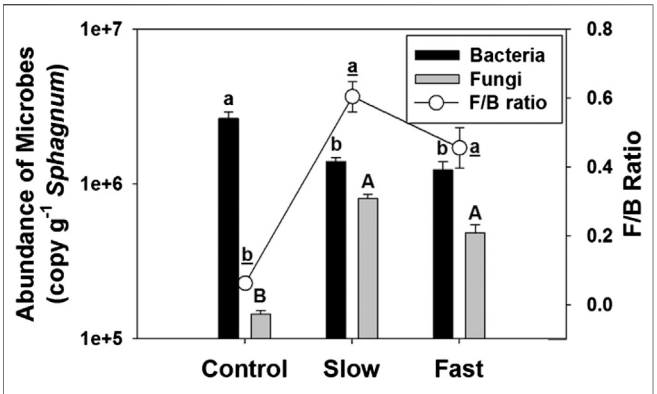

FIGURE 3 | Abundance of fungi (fungal ITS) and bacteria (bacterial 16S rRNA) (bar), and F/B ratio (line) on *Sphagnum* surface. Letter denotes statistically significant differences between treatments (n = 24, $p < 0.05$).

Abundance of Fungi on the *Sphagnum* Surface

The abundance of fungi on the *Sphagnum* surface significantly increased by 236–459% in the fluctuating WT treatments (**Figure 3**), and we have visually observed the fungal invasion in the fluctuation treatments (**Supplementary Figure S2**). In contrast, the abundance of bacteria decreased by 47–54% in the fluctuating WT treatments, which results substantially higher F/B ratio in the fluctuating WT treatments than in controlled stable WT (**Figure 3**). Abundance of fungi (r = −0.425, p = 0.010) and F/B ratio (r = −0.377, p = 0.023) had significant negative correlation with *Sphagnum* biomass, supporting that proliferation of fungi may reduce *Sphagnum* growth (**Supplementary Figure S3**).

Decomposition Rate and Biogeochemistry of Peat

The decomposition rate measured by litter bag method was significantly enhanced by 74–79% in the fluctuating WT treatments (**Figure 4**). Higher decomposition resulted in lower *Sphagnum* biomass and covered-area (**Supplementary Figure S3**).

Among the five extracellular enzymes (β-glucosidase, β-Xylosidase, N-acetyl-β-glucosaminidase, Arylsulfatase, and Phosphatase), the activity of phosphatase significantly increased while the activity of N-acetyl-β-glucosaminidase decreased within the mesocosms of fluctuating WT treatments (**Table 2**). Decomposition rate exhibited a significant positive correlation (r = 0.481, p = 0.003) with the activity of phosphatase (**Supplementary Figure S3**).

Peat pH significantly increased by 1.7–4.6% with higher frequency water table fluctuations, fast fluctuation showing the highest pH value (**Table 3**). Concentrations of phenolics significantly decreased by 18–31% with intensity of water table fluctuation, fast fluctuation showing the lowest concentration of phenolics (**Table 3**). Concentrations of phenolics were negatively correlated with phosphatase (r = −0.929, $p < 0.001$) while pH was positively correlated with phosphatase (r = 0.877, $p < 0.001$) (**Supplementary Figure S3**).

Abundance of Fungi in Peat

The abundance of fungal *laccase* gradually tended to increase with increasing intensity of water table fluctuation, fast fluctuation showed the highest abundance of fungal *laccase* (**Figure 5**). Meanwhile, content of fungal *laccase* to total fungi significantly increased (**Figure 5**).

'Enzymic Latch' Mechanism

The conceptual diagram of 'enzymic latch' mechanism clearly showed that the mechanism was significantly involved in the changes in decomposition rate by water table fluctuation (**Figure 6**). According to **Figure 6**, the increased abundance of fungi by water table fluctuation consequently reduced the concentration of phenolics, which allowed hydrolases to be activated. Then, decomposition was stimulated by the higher activity of hydrolases. *Sphagnum* itself have a significant positive correlation to the concentration of phenolics, which supported that it might regulate its phenolic content and then the antimicrobial effects on hydrolases. Peat pH significantly positively related to the activity of hydrolases, especially phosphatase.

DISCUSSION

Suppressed *Sphagnum* Growth Through Fungal Infection

The results showed that both *Sphagnum* biomass and *Sphagnum*-covered area were substantially reduced by water fluctuation (**Figures 2A,B**), suggesting strongly that the water table fluctuation, regardless of whether fluctuations were slow or fast, impeded growth and development of *Sphagnum*. We had

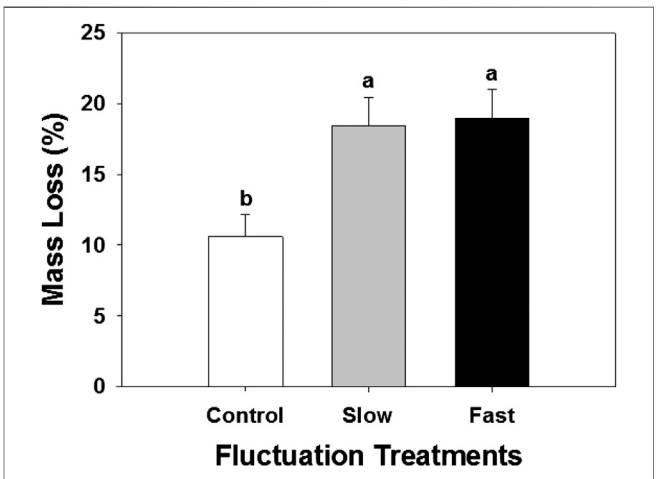

FIGURE 4 | Mass loss determined by decomposition litter bag experiment. Letter denotes statistically significant differences between treatments (n = 60, $p < 0.05$).

TABLE 2 | Activities of extracellular enzymes in peat. Letter denotes statistically significant differences between treatments (n = 12, $p < 0.05$).

Fluctuation treatments	Activities (nmol g^{-1} peat min^{-1})				
	β-glucosidase	β-xylosidase	N-acetyl-β-glucosaminidase	Arylsulfatase	Phosphatase
Control	8.1 ± 0.8	3.4 ± 0.4	1.8 ± 0.1 **a**	0.2 ± 0.04	4.1 ± 0.1 **c**
Slow	7.9 ± 0.4	3.4 ± 0.2	1.6 ± 0.1 **b**	0.3 ± 0.03	6.3 ± 0.3 **b**
Fast	8.3 ± 0.5	3.8 ± 0.3	1.6 ± 0.04 **ab**	0.2 ± 0.04	13.6 ± 1.4 **a**

TABLE 3 | pH and concentration of phenolics in peat. Letter denotes statistically significant differences between treatments (n = 12, 0 < 0.05).

Fluctuation treatments	pH	Phenolics (mg g^{-1} peat)
Control	4.10 ± 0.02 **b**	15.5 ± 0.8 **a**
Slow	4.17 ± 0.02 **b**	12.7 ± 0.7 **b**
Fast	4.29 ± 0.01 **a**	10.6 ± 0.4 **b**

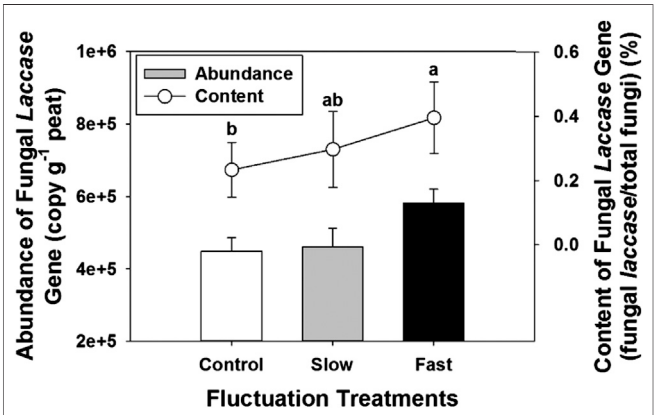

FIGURE 5 | Abundance of fungal *laccase* gene (bar) and content of fungal *laccase* gene to the total fungi (line) in peat. Error bars denote standard errors. Letter denotes statistically significant differences between treatments (n = 24, $p < 0.05$).

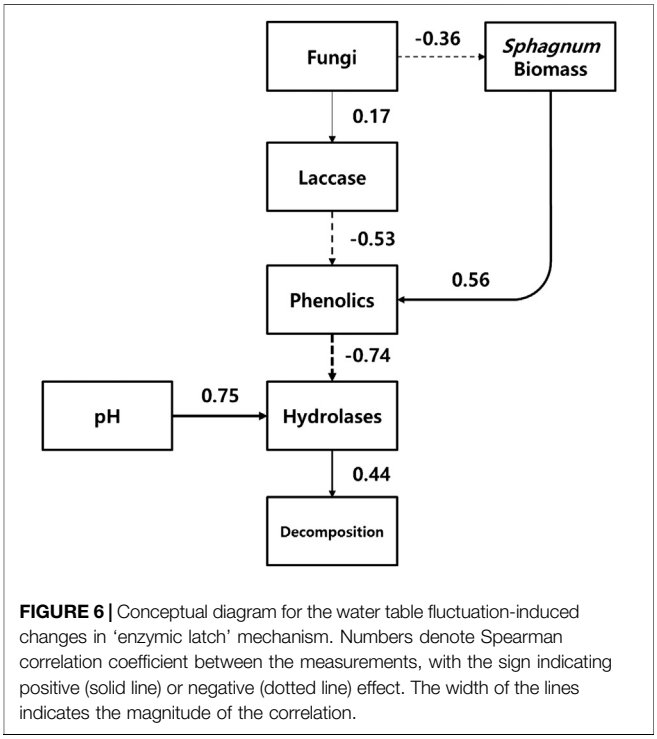

FIGURE 6 | Conceptual diagram for the water table fluctuation-induced changes in 'enzymic latch' mechanism. Numbers denote Spearman correlation coefficient between the measurements, with the sign indicating positive (solid line) or negative (dotted line) effect. The width of the lines indicates the magnitude of the correlation.

hypothesized that fluctuation-induced fungal infection would reduce *Sphagnum* growth which was supported by visual (**Supplementary Figure S2**) and analytical evidences (**Figure 3**). In particular, F/B ratio significantly increased indicating that the fungal community became dominant under the water table fluctuation treatments (**Figure 3**). Many pathogenic fungi (e.g., *Scleroconidioma sphagnicola*, *Acremonium* cf. *curvulum*, and *Oidiodendron maius* for *Sphagnum fuscom*, *Lyophyllum palustre* for *Sphagnum fallax*, and *Discinella schimperi* for *Sphagnum squarrosum* etc.) can invade cell wall, chlorophyllose cells, and cortical cells of leaf and stem of *Sphagnum* (Untiedt and Mller, 1985; Redhead and Spicer, 1981; Tsuneda et al., 2001a; Tsuneda et al., 2001b), resulting in the deformation of cells. The infection of pathogenic fungi generally attacks a specific type of cell and reduces its functioning but does not usually result total destruction of its *Sphagnum* host in pristine peatlands. However, the growth of *Sphagnum* was substantially inhibited by fungal infection in our experimental case.

Water table fluctuation treatments in our experiment were relatively rapid (up to 40 cm 10 $days^{-1}$) so dramatically altered growth of three *Sphagnum* species. Since, *Sphagnum* mosses are sensitive to water availability, insufficient water availability due to rapid water table fluctuation can result in poor growth and even irreversible desiccation (Schipperges and Rydin, 1998; Potvin et al., 2015). The deprived nutrient conditions of *Sphagnum* tissues in the fluctuation treatments (**Table 1**), appears to render *Sphagnum* mosses more vulnerable to fungal infection under the water table fluctuation treatments. In contrast to the *Sphagnum* mosses, the growth of fungi was stimulated in the fluctuation treatments (**Figure 3**). For fungi, low water availability generally promotes more favourable aerobic conditions (Deacon, 1997; Trinder et al., 2008), except extremely dry conditions (Laiho, 2006; Jaatinen et al., 2007). The combined effect of reduced water availability to *Sphagnum* mosses and enhanced fungal infection inhibited growth and development of *Sphagnum* mosses in the both fluctuation treatments. In addition, no substantial impeded *Sphagnum*

growth and fungal proliferation were observed in the lower stable water table treatments (**Supplementary Figures S4,S5**), which supported that the water table fluctuation plays a pivotal role in the proposed responses.

Although the three *Sphagnum* species used in this study grow optimally at different water table levels (0 ~ −5 cm for *S. fallax*, −10 ~ −15 cm for *S. medium*, −20 ~ −25 cm for *S. fuscum*), the responses of all three species were identical in our experiment. We assumed that the intensity of water table fluctuation was too high to separate the responses of different *Sphagnum* species. In future study, subdivided level of water table fluctuation should be applied to differentiate the distinctive responses of different *Sphagnum* species.

Stimulated Decomposition of Organic Matter

Water table fluctuation significantly stimulated decomposition of organic matter (**Figure 4**). Several studies confirm that improved peat aeration can eliminate decomposition-restriction mechanism by phenolics (Freeman et al., 2001), resulting in enhanced hydrolase activity. In this experimental setup, the 'enzymic latch' mechanism is shown to play a key role to the increasing decomposition rate under rapid water table fluctuation (**Figure 6**), supported by the strong negative correlation between the concentration of phenolics and the activity of hydrolases, particularly phosphatase ($r = -0.74$, $p < 0.05$, **Supplementary Figure S3**). Romanowicz et al. (2015) reported that water table level significantly affected phosphatase activity excluding other hydrolases, and Kang and Freeman (1999) reported that phosphatase had the greatest sensitivity for water table condition. The abundance of fungal *laccase* gradually increased with higher frequency of the water table fluctuation (**Figure 5**), which may have contributed to the decomposition of phenolics (Thurston, 1994; Romanowicz et al., 2015). Besides, our experimental water table fluctuations may have directly decreased the concentration of phenolics (as well as other nutrients) by net leaching, potentially contributing to the observed stimulation of phosphatase activity.

In our experiment, pH might also play a critical role in controlling the 'enzymic latch' mechanism under water table fluctuation (**Figure 6**). The activity of total hydrolases was also strongly related to pH (**Figure 6**) because the activity of phosphatase had substantial positive correlation to pH (**Supplementary Figure S3**). Since, acid-phosphatase is dominant in northern peatlands and its optimum pH is near 5 (Kay, 1932), increasing in pH from 4.10 to 4.29 (on a log scale) by water table fluctuation is likely to enhance the activity of phosphatase (**Table 3**). In addition, pH may directly affect microbial community, thus contribute to stimulated decomposition of organic matter (Kang et al., 2018).

Changes in the chemistry of *Sphagnum* living layer might also affected decomposition rates. The C/N ratio of *Sphagnum* living layer is typically high, and peatlands are generally nitrogen-deficient environment (Thormann et al., 2001). In our experiment, rapid water table fluctuation decreased C/N ratio of *Sphagnum* tissue making *Sphagnum* living layer more easily decomposed (Manzoni et al., 2008), while more nitrogen is released, creating a nitrogen source for surrounding decomposers so stimulate their activity. Decreases in C/N ratio (i.e., decreases in carbon content) may be due to changing carbon allocation of *Sphagnum* by water table fluctuation. Since *Sphagnum* with water stress invests more carbon to respiration and essential house-keeping processes rather than secondary processes such as production of phenolics, cell-wall formation, and reproduction, water table fluctuation-induced drier condition may decrease the amount of phenolics released by *Sphagnum* (Jassey et al., 2011). Therefore, water table fluctuation may reduce the inhibitory effect of phenolics and enhance the decomposition rate by decreasing phenolics from *Sphagnum*.

Reduced Carbon Sequestration Ability of Peat by the Water Table Fluctuation

Overall, the water table fluctuation reduced carbon sequestration in peat through two different mechanisms: 1) inhibiting *Sphagnum* growth and 2) stimulating decomposition of organic matter. *Sphagnum* growth was substantially inhibited by lowered water availability and enhanced fungal infection, reducing carbon sequestration through photosynthesis. Decomposition of organic matter in peat was significantly stimulated because the decomposition-restricting 'enzymic latch' mechanism had weakened, thereby reducing carbon sequestration. These two mechanisms may dramatically compromise the capacity of peatlands to act as a carbon sink.

Our original hypothesis, that water table fluctuation would inhibit the growth of *Sphagnum* and accelerate the decomposition rate of organic matter in peat, was confirmed by a manipulation experiment of water table in peat. Particularly, fungal infection plays a key role in the inhibition of *Sphagnum* growth while pH may plays a key role in the controlling of decomposition of organic matter in peat.

Implications

In recent decades, there has been an increasing interest in developing the production of *Sphagnum* biomass as a renewable resource in *Sphagnum* farms (Campeau and Rochefort, 2002; Pouliot et al., 2015; Gaudig et al., 2018). Brown et al., 2017 recently pointed to the importance of maintaining stable moisture peat substrate conditions to support *Sphagnum* growth and CO_2 sink functions. Consequently, if *Sphagnum* biomass production is in future to be significantly enhanced, serious consideration must be given to managing a stable water table levels within the *Sphagnum* farm peat fields. Our study clearly indicates that optimal biomass production will only be achieved under a regime of limited water table fluctuation.

In this mesocosm study, we demonstrated that the water table fluctuation in peatlands impeded *Sphagnum* growth and accelerated decomposition due to fungal proliferation, which consequently compromises the capacity of peatlands to act as a carbon sink. The changes in peatland hydrology and biogeochemistry substantially alter the function of peatland, and microbial activity was deeply involved in the processes. Predicting the effects of global climate change on the carbon cycle of northern peatlands is one of the key objectives of peatland researchers because the global climate change is expected to be

the greatest in the high latitudinal regions (e.g., changes in water table level and stability). However, most current prediction models do not consider microbial processes and microbial community structures as input data, which increases the uncertainty of the model prediction because of the overlooked contribution of microbial activity. Here, we suggested that microbial information should be accounted for in the predictions in order to elucidate the future of the northern peatland in the changing world.

DATA AVAILABILITY STATEMENT

The raw data supporting the conclusions of this article will be made available by the authors, without undue reservation.

AUTHOR CONTRIBUTIONS

JK contributed to the microbial analysis, data curation, preparation of the original draft, revision of the manuscript. The conceptualization of the study, designing and performing the greenhouse experiment, and analysis of *Sphagnum* were conducted by LR and SH-H. ZA, CD, and TJ contributed to soil chemistry and enzyme analysis. RP, CF, and HK contributed to the interpretation of data and critical review of the draft.

FUNDING

The running of this experiment at the Université Laval greenhouse was supported by a NSERC Discovery grant to Line Rochefort (No. 138097-2012) and a Canadian Foundation for Innovation grant. The analyses of samples were supported by funds from the Ministry of Education of Korea (2020R1I1A2072824) and the Ministry of Science and ICT of Korea (2018K2A9A1A01090455, 2019K1A3A1A74107424, 2019K1A3A1A80113041). JK is supported by the funds from the Ministry of Education of Korea (2019R1A6A3A01091184).

ACKNOWLEDGMENTS

JK thanks to the '2019 International Joint Research Grant' funded by Graduate School of Yonsei University. We thank Richard Belanger for providing lab space and resources for microbial analysis, Talal Asif for photos and comments on the final draft, and Jeongeun Yun for the helps in statistical analysis and revision of the manuscript.

SUPPLEMENTARY MATERIAL

The Supplementary Material for this article can be found online at: https://www.frontiersin.org/articles/10.3389/feart.2020.579329/full#supplementary-material.

REFERENCES

Abbott, G. D., Swain, E. Y., Muhammad, A. B., Allton, K., Belyea, L. R., Laing, C. G., et al. (2013). Effect of water-table fluctuations on the degradation of *Sphagnum* phenols in surficial peats. *Geochim. Cosmochim. Acta* 106, 177–191. doi:10.1016/j.gca.2012.12.013

Aerts, R., Wallen, B., and Malmer, N. (1992). Growth-limiting nutrients in *Sphagnum*-dominated bogs subject to low a high atmospheric nitrogen supply. *J. Ecol.* 80, 131–140. doi:10.2307/2261070

Baldrian, P. (2006). Fungal laccases-occurrence and properties. *FEMS Microbiol. Rev.* 30, 215–242. doi:10.1111/j.1574-4976.2005.00010.x

Belyea, L. R. (1996). Separating the effects of litter quality and microenvironment on decomposition rates in a patterned peatland. *Oikos.* 77, 529–539. doi:10.2307/3545942

Bourbonnais, R., Paice, M. G., Reid, I. D., Lanthier, P., and Yaguchi, M. (1995). Lignin oxidation by laccase isozymes from Trametes versicolor and role of the mediator 2,2'-azinobis(3-ethylbenzthiazoline-6-sulfonate) in kraft lignin depolymerization. *Appl. Environ. Microbiol.* 61 (5), 1876–1880. doi:10.1128/AEM.61.5.1876-1880.1995

Box, J. D. (1983). Investigation of the Folin-Ciocalteau phenol reagent for the determination of polyphenolic substances in natural waters. *Water Res.* 17 (5), 511–525. doi:10.1016/0043-1354(83)90111-2

Brown, C., Strack, M., and Price, J. S. (2017). The effects of water management on the CO2 uptake of *Sphagnum* moss in a reclaimed peatland. *Mires Peat.* 20 (5), 1–15. doi:10.19189/MaP.2016.OMB.258

Campeau, S., and Rochefort, L. (2002). "Possibilities and limits to *Sphagnum* farming," in Proceedings of the international peat symposium: peat in horticulture – Quality and environmental challenges. A joint symposium of commission II (Industrial utilization of peat and peatlands) and commission V (After-use of cut-over peatlands) of the international peat society, Pärnu, Estonia, September 3–6, 2002. Editors G. Schmilewski and L. Rochefort (Jyväskylä, Finland: International Peat Society), 264–269.

Campeau, S., and Rochefort, L. (1996). *Sphagnum* regeneration on bare peat surfaces: field and greenhouse experiments. *J. Appl. Ecol.* 33, 599–608. doi:10.2307/2404988

Clymo, R. S., and Duckett, J. G. (1986). "The ecology of *Sphagnum*," in *Bryophyte ecology*. Editor A. J. E. Smith (London: Chapman & Hall), 229–289.

Deacon, J. W. (1997). *Modern mycology*. Oxford: Blackwell Publishing.

Dunn, C., Jones, T. G., Girard, A., and Freeman, C. (2013). Methodologies for extracellular enzyme assays from wetland soils. *Wetlands.* 34, 9–17. doi:10.1007/s13157-013-0475-0

Freeman, C., Liska, G., Ostle, N. J., Jones, S. E., and Lock, M. A. (1995). The use of fluorogenic substrates for measuring enzyme activity in peatlands. *Plant Soil.* 175, 147–152. doi:10.1007/BF02413020

Freeman, C., Lock, M. A., Marxsen, J., and Jones, S. E. (1990). Inhibitory effects of high molecular weight dissolved organic matter upon metabolic processes in biofilms from contrasted rivers and streams. *Freshw. Biol.* 24, 159–166. doi:10.1021/acs.est.9b04105

Freeman, C., Ostie, N., and Kang, H. (2001). An enzymic 'latch' on a global carbon store – a shortage of oxygen locks up carbon in peatlands by restraining a single enzyme. *Nature.* 409, 149. doi:10.1038/35051650

Gallego-Sala, A. V., Charman, D. J., Brewer, S., Page, S. E., Prentice, I. C., Friedlingstein, P., et al. (2018). Latitudinal limits to the predicted increase of the peatland carbon sink with warmin. *Nat. Clim. Change.* 8, 907–913. doi:10.1038/s41558-018-0271-1

Gaudig, G., Krebs, M., Prager, A., Wichmann, S., Barney, M., Caporn, S. J. M., et al. (2018). *Sphagnum* farming from species selection to the production of growing media: a review. *Mires Peat.* 20 (13), 1–30. doi:10.19189s/MaP.2018.OMB.340

Gorham, E. (1991). Northern Peatlands: role in the carbon cycle and probable responses to climatic warming. *Ecol. Appl.* 1, 182–195. doi:10.2307/1941811

Haraguchi, A. (1991). Effects of water-table oscillation on redox property of peat in a floating mat. *J. Ecol.* 79, 1113–1121. doi:10.2307/2261102

Hassel, K., Kyrkjeeide, M. O., Yousefi, N., Prestø, T., Stenøien, H. K., Shaw, J. A., et al. (2018). *Sphagnum divinum* (*sp. nov.*) and *S. medium* Limpr. and their relationship to *S. magellanicum*. *Brid. J. Bryol.* 40, 197–222. doi:10.1080/03736687.2018.1474424

Holden, J., Chapman, P., and Labadz, J. (2004). Artificial drainage of peatlands: hydrological and hydrochemical process and wetland restoration. *Prog. Phys. Geogr.* 28, 95–123. doi:10.1191/0309133304pp403ra

Jaatinen, K., Fritze, H., Laine, J., and Laiho, R. (2007). Effects of short- and long-term water-level drawdown on the populations and activity of aerobic decomposers in a boreal peatland. *Global Change Biol.* 12, 491–510. doi:10.1111/j.1365-2486.2006.01312.x

Jassey, V. E. J., Chiapusio, G., Gilbert, D., Buttler, A., Toussaint, M.-L., and Binet, P. (2011). Experimental climate effect on seasonal variability of polyphenol/

phenoloxidase interplay along a narrow fen-bog ecological gradient in *Sphagnum fallax*. *Global Change Biol.* 17, 2945–2957. doi:10.1111/j.1365-2486.2011.02437.x

Jassey, V. E. J., Reczuga, M. K., Zielinska, M., Stowinska, S., Robroek, B. J. M., Mariotte, P., et al. (2018). Tipping point in plant-fungal interactions under severe drought causes abrupt rise in peatland ecosystem respiration. *Global Change Biol.* 24, 972–986. doi:10.1111/gcb.13928

Junk, W. J., Bayley, P. B., and Sparks, R. E. (1989). "The flood-pulse concept in river-floodplain systems," in Proceedings of the international large river symposium (MARS), Canadian journal of fisheries and aquatic sciences special publications 106. Editor D. P. Dodge (Ottawa: NRC Research Press), 110–127.

Kang, H., and Freeman, C. (1999). Phosphatase and arylsulphatase activities in wetland soils: annual variation and controlling factors. *Soil Biol. Biochem.* 31, 449–454. doi:10.1016/S0038-0717(98)00150-3

Kang, H., Kwon, M. J., Kim, S., Lee, S., Jones, T. G., Johncock, A. C., et al. (2018). Biologically driven DOC release from peatlands during recovery from acidification. *Nat. Commun.* 9, 3807. doi:10.1038/s41467-018-06259-1

Kay, H. D. (1932). Phosphatase in growth and disease of bone. *Physiol. Rev.* 12, 384–422. doi:10.1152/physrev.1932.12.3.384

Kim, S., Kim, Y., Kim, Y., Kim, K., Wang, S., Kang, H., et al. (2014). Effects of planting method and nitrogen addition on *Sphagnum* growth in microcosm wetlands. *Paddy Water Environ.* 12, 185–192. doi:10.1007/s1033-014-0427-1

Kostka, J. E., Weston, D. J., Glass, J. B., Lilleskov, E. A., Shaw, A. J., and Turetsky, M. R. (2016). The *Sphagnum* microbiome: new insights from an ancient plant lineage. *New Phytol.* 211, 57–64. doi:10.1111/nph.13993

Kwon, M. J., Haraguchi, A., and Kang, H. (2013). Long-term water regime differentiates changes in decomposition and microbial properties in tropical peat soils exposed to the short-term drought. *Soil Biol. Bioghem.* 60, 33–44. doi:10.1016/j.soilbio.2013.01.023

Laiho, R. (2006). Decomposition in peatlands: reconciling seemingly contrasting results on the impacts of lowered water tables. *Soil Biol. Biochem.* 38, 2024. doi:10.1016/j.soilbio.2006.02.017

Lamit, L. J., Romanowicz, K. J., Potvin, L. R., Rivers, A. R., Singy, K., Lennon, J. T., et al. (2017). Patterns and drivers of fungal community depth stratification in *Sphagnum* peat. *FEMS Microbiol. Ecol.* 93, fix082. doi:10.1093/femsec/fix082

Leontievsky, A., Myasoedova, N., Pozdnyakova, N., and Golovleva, L. (1997). 'Yellow' laccase of Panus tigrinus oxidizes non-phenolic substrates without electron-transfer mediators. *FEBS Lett.* 413 (3), 446–448. doi:10.1016/S0014-5793(97)00953-8

Manzoni, S., Jackson, R. B., Trofymow, J. A., and Porporato, A. (2008). The global stoichiometry of litter nitrogen mineralization. *Science.* 321, 684–686. doi:10.1126/science.1159792

Min, K., Freeman, C., Kang, H., and Choi, S. U. (2015). The regulation by phenolic compounds of soil organic matter dynamics under a changing environment. *Biomed Res. Int.* 2015, 825098. doi:10.1155/2015/825098

Moore, T., and Basiliko, N. (2006). Decomposition in Boreal Peatlands. In Wieder, R. K., and Vitt, D. H. (eds) *Boreal Peatland Ecosystems. Ecological Studies (Analysis and Synthesis).* Vol 188, Springer, Berlin, Heidelberg. doi:10.1007/978-3-540-31913-9_7

Nichols, J. E., and Peteet, D. M. (2019). Rapid expansion of northern peatlands and doubled estimate of carbon storage. *Nat. Geosci.* 12, 917–921. doi:10.1038/s41561-019-0454-z

Okland, R. H. (1989). A phytoecological study of the mire Northern Kisselbergmosen, SE Norway. I. Introduction, flora, vegetation and ecological conditions. *Sommerfeltia.* 8, 1–172. doi:10.1111/j.1756-1051.1990.tb01755.x

Overland, J. E., Wang, M., Walsh, J. E., and Stroeve, J. C. (2014). Future arctic climate changes: adaptation and mitigation time scales. *Earths Future.* 2, 68–74. doi:10.1002/2013EF000162

Potvin, L. R., Kane, E. S., Chimner, R. A., Kolka, R. K., and Lilleskov, E. A. (2015). Effects of water table position and plant functional group on plant community, aboveground production, and peat properties in a peatland mesocosm experiment (PEATcosm). *Plant Soil.* 387, 277–294. doi:10.1007/s11104-014-2301-8

Pouliot, R., Hugron, S., and Rochefort, L. (2015). *Sphagnum* farming: a long-term study on producing peat moss biomass sustainably. *Ecol. Eng.* 74, 135–147. doi:10.1016/j.ecoleng.2014.10.007

R Core Team (2019). *R: a language and environment for statistical computing*. Vienna, Austria: R Foundation for Statistical Computing.

Reader, R. J., and Stewart, J. M. (1972). The relationship between net primary production and accumulation for a peatland in southeastern Manitoba. *Ecology.* 53 (6), 1024–1037. doi:10.2307/1935415

Redhead, S. A., and Spicer, K. W. (1981). *Discinella schimperi*, a circumpolar parasite of *Sphagnum squarrosum*, and notes on *Bryophytomyces sphagni*. *Mycologia.* 73, 904–913. doi:10.2307/3759801

Rochefort, L., and Lode, E. (2006). "Restoration of degraded boreal peatlands," in *Boreal peatland ecosystems*. Editors R. K. Weider and D. H. Vitt (Berlin: Springer), 381–423.

Romanowicz, K. J., Kane, E. S., Potvin, L. R., Daniels, A. L., Kolka, R. K., and Lilleskov, E. A. (2015). Understanding drivers of peatland extracellular enzyme activity in the PEATcosm experiment: mixed evidence for enzymic latch hypothesis. *Plant Soil.* 397, 371–386. doi:10.1007/s11104-015-2746-4

Scharlemann, J. P. W., Tanner, E. V. J., Hiederer, R., and Kapos, V. (2014). Global soil carbon: understanding and managing the largest terrestrial carbon pool. *Carbon Manag.* 5, 81–91. doi:10.4155/cmt.13.77

Schipperges, B., and Rydin, H. (1998). Response of photosynthesis of *Sphagnum* species from contrasting microhabitats to tissue water content and repeated desiccation. *New Phytol.* 140, 667–684. doi:10.1046/j.1469-8137.1998.00311.x

Sinsabaugh, R. L. (2010). Phenol oxidase, peroxidase and organic matter dynamics of soil. *Soil Biol. Biochem.* 42, 391–404. doi:10.1016/j.soilbio.2009.10.014

Sjors, H. (1948). Myrvegetation i Bergslagen. *Acta Phytogeogr. Suecica.* 21, 1–299.

Taminskas, J., Linkeviciene, R., Simanauskiene, R., Jukna, L., Kibirstis, G., and Tamkeviciute, M. (2018). Climate change and water table fluctuation: implications for raised bog surface variability. *Geomorphology.* 304, 40–49. doi:10.1016/j.geomorph.2017.12.026

Thormann, M. N. (2006). "The role of fungi in boreal Peatlands," in *Boreal Peatland ecosystems*. Editors R. K. Weider and D. H. Vitt (Berlin: Springer), 101–123.

Thormann, M. N., Bayley, S. E., and Currah, R. S. (2001). Comparison of decomposition of belowground and aboveground plant litters in peatlands of boreal Alberta, Canada. *Can. J. Bot.* 79, 9–22. doi:10.1139/b00-138

Thormann, M. N., and Rice, R. V. (2007). Fungi from peatlands. *Fungal Divers* 24, 241–299.

Thurston, C. F. (1994). The structure and function of fungal laccases. *Microbiology.* 140, 19–26. doi:10.1099/13500872-140-1-19

Trinder, C. J., Johnson, D., and Artz, R. R. (2008). Interactions among fungal community structure, litter decomposition and depth of water table in a cutover peatland. *FEMS Microbiol. Ecol.* 64, 433–448. doi:10.1111/j.1574-6941.2008.00487.x

Tsuneda, A., Chen, M. H., and Currah, R. S. (2001b). Characteristics of a disease of *Sphagnum fuscum* caused by *Scleroconidioma sphagnicola*. *Can. J. Bot.* 79, 1217–1224. doi:10.1139/b01-102

Tsuneda, A., Thormann, M. N., and Currah, R. S. (2001a). Modes of cell-wall degradation of *Sphagnum fuscum* by *Acremonium* cf. *curculum* and *Oidiodendron maius*. *Can. J. of Bot.* 79, 93–100. doi:10.1139/b00-149

Untiedt, E., and Mller, K. (1985). Colonization of *Sphagnum* cells by *Lyophyllum palustre*. *Can. J. Bot.* 63, 757–761. doi:10.1139/b85-095

Wetzel, R. G. (1992). Gradient-dominated ecosystems: sources and regulatory functions of dissolved organic matter in freshwater ecosystems. *Hydrologia.* 229, 181–198. doi:10.1007/BF00007000

Xu, J., Morris, P. J., Liu, J., and Holden, J. (2018). PEATMAP: refining estimates of global peatland distribution based on a meta-analysis. *Catena.* 160, 134–140. doi:10.1016/j.catena.2017.09.010

Yu, Z., Loisel, J., Brosseau, P., Beilman, D. W., and Hunt, S. J. (2010). Global peatland dynamics since the last glacial maximum. *Geophys. Res. Lett.* 37, L13402. doi:10.1029/2010GL043584

Zhang, H., Väliranta, M., Piilo, S., Amesbury, M. J., Aquino-López, M. A., Roland, T. P., et al. (2020). Decreased carbon accumulation feedback driven by climate-induced drying of two southern boreal bogs over recent centuries. *Global Change Biol.* 26 (4), 2435–2448. doi:10.1111/gcb.15005

Conflict of Interest: The authors declare that the research was conducted in the absence of any commercial or financial relationships that could be construed as a potential conflict of interest.

frontiers in Earth Science

ORIGINAL RESEARCH
published: 11 June 2021
doi: 10.3389/feart.2021.658470

The Burial Under Peat Technique: An Innovative Method to Restore Sphagnum Peatlands Impacted by Mineral Linear Disturbances

Kathy Pouliot[1], *Line Rochefort*[1]*, *Marie-Claire LeBlanc*[1], *Mélina Guêné-Nanchen*[1] and *Alexandre Beauchemin*[2]

[1]Department of Plant Science, Peatland Ecology Research Group and Centre for Northern Studies, Université Laval, Quebec, QC, Canada, [2]Direction Environnement, Hydro-Québec, Montreal, QC, Canada

Mineral roads in peatlands change the nature of the substrate, influence the water table level of the peatland on either side of the road and the physicochemical characteristics of the water and peat. These changes can in turn affect plant community composition. The efficiency of an innovative and affordable method for the restoration of peatlands impacted by roads was evaluated: the Burial Under Peat Technique. To be considered effective from an ecological point of view, the technique should meet restoration goals by 1) confining the chemical elements and compounds potentially leaching from the mineral material; 2) creating and maintaining a restored surface elevation similar to the adjacent peatland for optimal rewetting; and 3) re-establishing typical peatland vegetation communities. Three years post-restoration, water sampled at various depths and distances to the buried road presented chemical elements and compounds concentrations similar to the means measured in the pristine surrounding peatland for most of the ions analyzed. The different steps of the technique ensured the reestablishment of an elevation similar to the surrounding peatland. The return of peatland plant communities was slow, mainly due to local factors (e.g., presence of drainage ditches). Furthermore, the Burial Under Peat Technique fulfilled the restoration objectives in re-establishing an acid organic soil. Finally, it is a cost-effective method in comparison to completely removing the mineral material and transporting new material to fill the depression left by the excavation of the road.

Keywords: peatland restoration, decommissioning, bog, road, reclamation

OPEN ACCESS

Edited by:
Samuel Abiven,
University of Zurich, Switzerland

Reviewed by:
Rod Chimner,
Michigan Technological University, United States
Steve Pratte,
Zhejiang University, China

***Correspondence:**
Line Rochefort
Line.Rochefort@fsaa.ulaval.ca

Specialty section:
This article was submitted to Biogeoscience, a section of the journal Frontiers in Earth Science

Received: *25 January 2021*
Accepted: *31 May 2021*
Published: *11 June 2021*

Citation:
Pouliot K, Rochefort L, LeBlanc M-C, Guêné-Nanchen M and Beauchemin A (2021) The Burial Under Peat Technique: An Innovative Method to Restore Sphagnum Peatlands Impacted by Mineral Linear Disturbances. Front. Earth Sci. 9:658470. doi: 10.3389/feart.2021.658470

INTRODUCTION

Peatlands cover roughly 4 million km^2 of the Northern Hemisphere (Yu et al., 2010), which represents 25–30% of the circumboreal forest biome (Wieder et al., 2006). It is inevitable that access roads built for industrial activities such as resource extraction, forestry, the deployment or maintenance of electricity transmission networks or the petrol industry cross paths with peatlands in the boreal zone (Pasher et al., 2013). Roads impact various components of peatland ecosystems. In addition to locally stopping the peatland carbon accumulation function, the introduction of the mineral material may restrict the hydrological connectivity across the road and, thus, influence the water table level (Bocking et al., 2017), the physicochemical properties (Plach et al., 2017; Saraswati et al., 2020), the tree and shrub productivity (Saraswati et al., 2020) and the net CO_2 sequestration of

the surrounding peatland (Plach et al., 2017). While road impacts on peatlands have been the subject of several studies in the past decade, there is a need for research regarding restoration techniques (Williams-Mounsay et al., 2021).

Water flows slowly through peat, but linear structures such as roads can create barriers and cause upstream flooding and downstream desiccation problems (Umeda et al., 1985; Miller, 2011; Bocking et al., 2017) which may enhance the overall peatland CH_4 emissions (Saraswati and Strack, 2019). Furthermore, the construction of a road within a peatland also introduces minerals and other nutrients into an oligotrophic acid peaty substrate which have the potential to diffuse laterally. However, the estimation of the distance to which chemical elements and compounds may leach into the adjacent ecosystem is complex, mainly due to the anisotropic characteristic of *Sphagnum* peatlands (i.e., peat hydraulic conductivity is greater horizontally than vertically; Beckwith et al., 2003). Besides, the presence of a gentle slope within a peatland can cause superficial flow, influencing chemical elements and compounds leaching distances.

The modifications in the concentration, ionic form and ratio of the chemical elements within the substrate can modify vegetation composition and diversity, considering that the composition of vegetation communities is closely tied to the hydrological and physicochemical characteristics of the plant species ecological niches (Gignac et al., 1991, 2004). Therefore, the ecosystem can shift from species adapted to poor acidic environments to species preferring richer environments (Kooijman and Bakker, 1995; de Mars et al., 1996; Laiho et al., 2003; Müllerová et al., 2011). When a formerly limiting nutrient is added to a *Sphagnum* peatland, characterized by oligotrophic conditions, graminoid species tend to proliferate whereas bryophytes and other slow-growing species decline (Hogg et al., 1995; Limpens et al., 2011). Consequently, the introduction of a mineral access road in a *Sphagnum* peatland could favor the spread of unwanted or invasive species to the detriment of bog species.

Road mitigation techniques, such as scarification, topsoiling, planting, removal of stream crossing structures and partial or complete decommissioning, have been developed for forest biomes (Cots et al., 1991; Luce, 1997; Bagley, 1998; Switalski et al., 2004; Sosa-Pérez and MacDonald, 2017). Most of these techniques are not adapted to peatlands because the mineral material remains on site, acting as a barrier for hydrological connectivity and a potential source of nutrient enrichment within the peatland. Road decommissioning in peatlands involves removing the mineral material and other materials used (e.g., geotextile, logs) and backfilling with peat, sawdust or woodchips. Backfilling is required to restore an elevation similar to the undisturbed surrounding peatland. In the absence of backfilling, open water bodies may be formed and be colonized by monospecific invasive plant communities (e.g., cattail, common reed, etc.), greatly hindering the establishment of natural pool edges plant communities (Bourgeois et al., 2012) and causing greenhouse gas emissions (Hamilton et al., 1994; Strack and Zuback, 2013).

Prior to this research project, only a few attempts to restore peatlands disturbed by mineral infrastructures have been conducted, particularly in oil sands regions of Alberta (Canada), indicating a study gap between studies on the effects of roads on peatlands and research on the mitigation of these effects. Decommissioning in the known projects involved the removal of the mineral material, either partially (Osko et al., 2014) or completely (Pilon, 2015), and the removal of a well-pad by the burial under a peat layer (Sobze et al., 2012). In Pilon (2015) a slow decompression of the peat was observed following the complete removal of the clay covering it. This meant that the water flow through the disturbance was no longer being obstructed (Pilon, 2015). In Osko (2015), the partial removal of clay did not sufficiently improve water flow. By lowering the surface of the mineral material, depressions were created, where water accumulated instead of flowing toward the adjacent peatland. Osko (2015) recommended filling the excavation with stockpiled peat to restore the hydrological connectivity. Finally, the burial of the well-pad clay, more specifically the vertical inversion of the clay layer and the underlying peat, was an effective technique to reach an elevation similar to what is observed in the surrounding peatland (Sobze et al., 2012). These studies underline the technical knowledge gaps regarding restoration methods adapted to peatlands impacted by roads.

This project aims at developing a restoration technique for peatlands disturbed by linear mineral disturbances based on the burying of the material used for their construction. To favor the hydrological flow through an artificial acrotelm (surface layer of peat where the water table fluctuates), the mineral material must be confined in the catotelm (bottom layer of peat, constantly under anaerobic conditions). The long term lateral diffusion of chemical elements and compounds from the buried mineral should be considered negligible as a result of several unique properties of peat. Firstly, the peat in the catotelm, where the mineral material will be confined, is characterized by a low hydraulic conductivity (Letts et al., 2000). Secondly, peat has a high-buffering capacity that is linked to its high cation exchange capacity (CEC) which increases with peat decomposition (Puustjärvi 1956). Furthermore, the growth of roots and the assimilation of plant nutritive chemical elements are processes that require oxygen (Bates, 2009). Thus, only the species located within or close to the restored strip and that possess specialized structure for oxygen transportation (wetland species; Justin and Armstrong, 1987; Colmer, 2003) could benefit from the mineral material that is buried in the anaerobic zone (catotelm).

The objectives of this study were to (1) confine the chemical elements and compounds potentially released by the mineral material, (2) restore, on the former road, a layer of organic soil of similar elevation to the surrounding peatland, and (3) initiate the revegetation of plant communities characteristic of peatlands and limit the spread of undesired plants. We hypothesized that burying the mineral material should confine the chemical elements and compounds and that the peat substrate on the former road with an elevation similar to the surrounding peatland (water-saturated but not flooded) should favor the establishment of *Sphagnum* peat mosses and other typical peatland species and

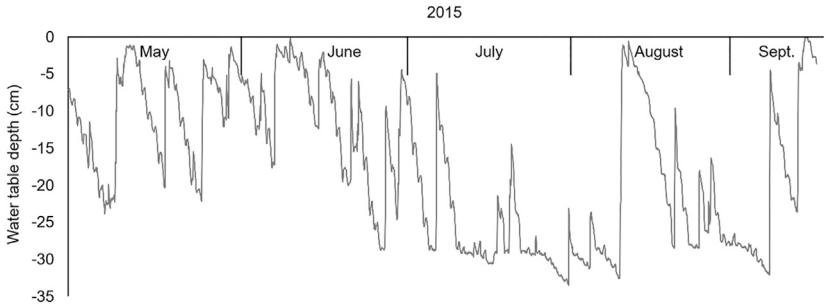

FIGURE 1 | Water table depth at Sainte-Eulalie in 2015.

be an indicator of the restoration of the hydrological connectivity across the former road. The undisturbed right-of-way and the surrounding pristine peatland were used as reference ecosystems (local models or targets derived from multiple sources of information to characterize the state of the ecosystem as it would be if it had not been degraded; McDonald et al., 2016).

MATERIAL AND METHODS

Study Site

In 2012, a temporary access road was built in a 9,000-hectare peatland complex at Sainte-Eulalie (Québec, Canada; 46.098°N, −72.288°W) for the purpose of reconstructing a 60 year-old powerline (**Supplementary Figure S1**). The mean annual temperature and total precipitations are respectively 4.9°C and 968 mm (of which 84% falls as rain), based on 30-years monthly mean values (1981–2010; Government of Canada, 2018). The access road was built in a power-line right-of-way that bisects a peatland complex. Agricultural type ditches are present on both sides of the 30 m right-of-way to maintain relatively dry access to the transmission towers. The effect of the ditches can be seen in the graph of the water table fluctuation (**Figure 1**). Indeed, we can observe that the water level decreases rapidly after rain events, unlike undrained peatlands where water level decreasing is gradual. Nevertheless, since there is no maintenance on the ditches, their effectiveness is limited considering that the lowest level reached by the water table in 2015 is −33 cm. The access road was 3 km long with an average width of 4.5 m. It was composed of basalt gravel placed on a geotextile membrane. The road was reinforced with logs underneath the geotextile in the wetter areas, to prevent machinery from sinking into the peat. Typical open raised bog plant communities as found in the province of Québec (e.g., *Sphagnum* mosses, ericaceous shrubs; Couillard and Grondin, 1986) compose the right-of-way and the surrounding natural peatland vegetation.

Restoration Techniques

The Burial Under Peat Technique (BUPT) was applied on the 3-km road in the fall of 2012, a few months after the construction of the road. Half of the access road is in a treed peatland and the other half is in a *Sphagnum*-peatland, only the latter section is discussed in this paper (**Supplementary Figure S2**). The restoration work was performed with an excavator that operated exclusively over the surface of the access road to avoid additional disturbances and machinery sinking in the adjacent peatland. The following steps (**Figure 2**) were repeated in short segments equivalent to the reach of the excavator's arm (approximately 5 m long in our case): 1) the mineral material, as well as the geotextile membrane and logs when present, were removed from the disturbed area and stockpiled on the road, behind the excavator (after visual evaluation of thickness of the road, in certain areas excessive mineral material has been removed off-site), 2) the underlying peat was excavated and placed beside the road on plywood boards or other types of easily movable platforms, thus creating a pit, 3) the road material stacked behind the excavator was transferred back into the pit, 4) the road material was covered with the excavated peat and the surface peat was flattened to the mean elevation of the surrounding peatland, 5) the peat surface was revegetated with diaspores harvested with the excavator's bucket from the adjacent peatland, shredded with the bucket's teeth to ensure it was spread uniformly, and finally, light pressure was applied to the reintroduced vegetal material with the bucket to favor better contact with the substrate. Once all the steps were completed, the excavator backed up and restarted the process on the next segment of the road.

During the restoration work, we aimed to establish a peat layer of at least 40 cm thick over the mineral material to ensure the construction material was buried in the catotelm under permanent anoxic conditions. The thickness of the acrotelm of the surrounding peatland should be assessed prior to restoration work so the threshold can be adjusted to site conditions. At this experimental site, a mean peat thickness of 52 cm was estimated to recover the foreign material. Furthermore, during restoration, the revegetation step, which is inspired by the Moss Layer Transfer Technique (MLTT; Graf and Rochefort 2016) was done at a ratio varying from 1:5 to 1:10, depending on the diaspores quality and availability in the adjacent peatland. The ratio refers to the area of the collection site to the area of the restoration site. For example, a ratio of 1:10 means that the collection site is ten times smaller than the restoration site. Drainage ditches were not blocked in the study site as they must be maintained for powerline maintenance and vegetation management.

FIGURE 2 | Steps of the Burial Under Peat Technique: 1) excavation and stockpiling of the mineral material, 2) excavation of the underlying peat, 3) filling the pit with the mineral material, 4) covering the mineral material with excavated peat and leveling the soil surface with the adjacent peatland, and 5) revegetating of the peat surface with diaspores from adjacent peatland.

Reference Ecosystems

Since the peatland of the right-of-way has been disturbed by the presence of drainage ditches and vegetation maintenance (tree cutting), it is necessary to consider the right-of-way undisturbed by the road as a target ecosystem, and not the surrounding pristine peatland. Thus, the reference ecosystem for the vegetation and elevation data is the part of the right-of-way undisturbed by the access road and pylons (**Supplementary Figure S1**). However, since we do not know the lateral diffusion distance of the chemical elements from the buried road and that this distance is potentially greater than the width of the right-of-way, it was essential to obtain chemistry data from an ecosystem uninfluenced by the road. For this reason, we consider the natural peatland surrounding the right-of-way as a reference ecosystem for the chemistry data (**Supplementary Figure S2**).

Water Chemistry

Peat pore water was sampled to measure physicochemical conditions within and around the restored strip. Two sampling campaigns took place 3 years post-restoration, in June and September 2015. Water was sampled across four transects, in piezometers collecting surface pore water in the acrotelm (depth of 20 cm) and catotelm pore water (depth of 50 cm) in the middle of the restored strip (0 m) and at different distances from the former edge of the road (0.5, 1, 2, and 10 m; **Supplementary Figure S2**). Water samples were also collected in piezometers in the surrounding pristine peatland outside of the right-of-way, which serves as a reference ecosystem dataset for the physicochemistry.

Water pH and electrical conductivity were measured directly in the field with a handheld device (Hanna instruments 98,129, Woonsocket, RI, United States). Electrical conductivity values were corrected according to pH and water temperature (Sjör, 1950). The concentration of inorganic N, P and S forms (N/NH_4^+, N/NO_3^-, total P, P/PO_4^{3-} and S/SO_4^{2-}), some major metallic cations (K, Mg, Ca, Na, and Al), two trace metals (Fe and Mn) and a major anion (Cl^-) were analyzed in the laboratory. Thereupon, in this paper, we will refer to them using the generic term: chemical elements and components.

Fe, Ca, K, S/SO_4^{2-}, Na, Mg, Mn, Al, and P/PO_4^{3-} were extracted according to the method of Amacher et al. (1990). Total phosphorus was mineralized according to Parkinson and Allen (1975). The extracts were assayed by Inductively Coupled Plasma with optical emission spectrometry (ICP-OES, model 5,110 from Agilent Technologies, Santa Clara, CA, United States). The ammoniacal nitrogen and nitrate nitrogen were extracted according to the method used in Keeney and Nelson (1982) then dosed by continuous flow injection (FIA Quickchem 8500 Serie two from Lachat, Loveland, CO, United States) according to the standard method "Ammonia in surface water, wastewater" (Quikchem method 10-107-06-2-B)

for N/NH_4^+ and according to the standard method "Nitrate in 2M KCl soil extracts" (Quikchem method 12-107-04-1-F) for N/NO_3^-. Finally, the chlorides were extracted according to the method of Buykx et al. (2004) then dosed by continuous flow injection (FIA Quickchem 8500 Serie 2 from Lachat, Loveland, CO, United States) according to the method "Determination of chloride by flow injection analysis colorimetry" (Quikchem method 10-117-07-1-C). Certified reference materials (CRMs) were used to validate analytical measurement methods.

Surface Elevation

To verify if there was compression or decompression of the peat profile following the BUPT, the relative elevation of the restored surface was surveyed at two different times: after 1 year (in September) and 3 years (in August) post-restoration. Elevation was measured on three transects perpendicular to the former road (formerly four but one transect had to be eliminated since the reference stick was lost between the surveys), each covering the restored strip and the adjacent organic soil of the undisturbed right-of-way on both sides (**Supplementary Figure S2**), the latter being the reference ecosystem for elevation. Elevation was measured at 13 locations in the restored strip (every 20 cm) and 22 locations in the right-of-way (every 50 cm). The same sampling points were measured during each survey campaign, allowing data pairing. Relative elevation was measured with a leveling laser (LP410, Sokkia, Mississauga, ON, Canada). The concrete bases of nearby transmission towers were used as benchmarks.

Vegetation

To assess vegetation establishment following the restoration, the cover of each plant species was estimated 3 years post-restoration from their vertical projection on the ground, in 1 m × 1 m quadrats for vascular plants and in 25 cm × 25 cm quadrats for bryophyte species. Quadrats were randomly disposed in the area showed in **Supplementary Figure S3**. Eight quadrats of each type were surveyed over the restored road, as well as four quadrats of each type in the reference ecosystem (the adjacent undisturbed right-of-way).

Analyses

In Canada, from the month of July to September, the variations in concentration of most peatland chemical elements and compounds studied by Vitt et al. (1995) were little and stable, particularly for *Sphagnum* dominated peatlands (bog and poor fen). Consequently, data from water sampled in June, out of the snowmelt period, and in September were combined as one dataset. Descriptive analyses were used to evaluate the efficiency of the BUPT to confine chemical elements and compounds that could potentially be released by the mineral material, and to compare chemical conditions in and around the restored area with the natural reference ecosystem.

Paired *t*-tests were performed to evaluate if the elevations measured at the same location one winter and three years post-restoration were different. The elevation differences were then compared between the restored strip and the reference ecosystem with Welch's *t*-test (independent means with unequal variances).

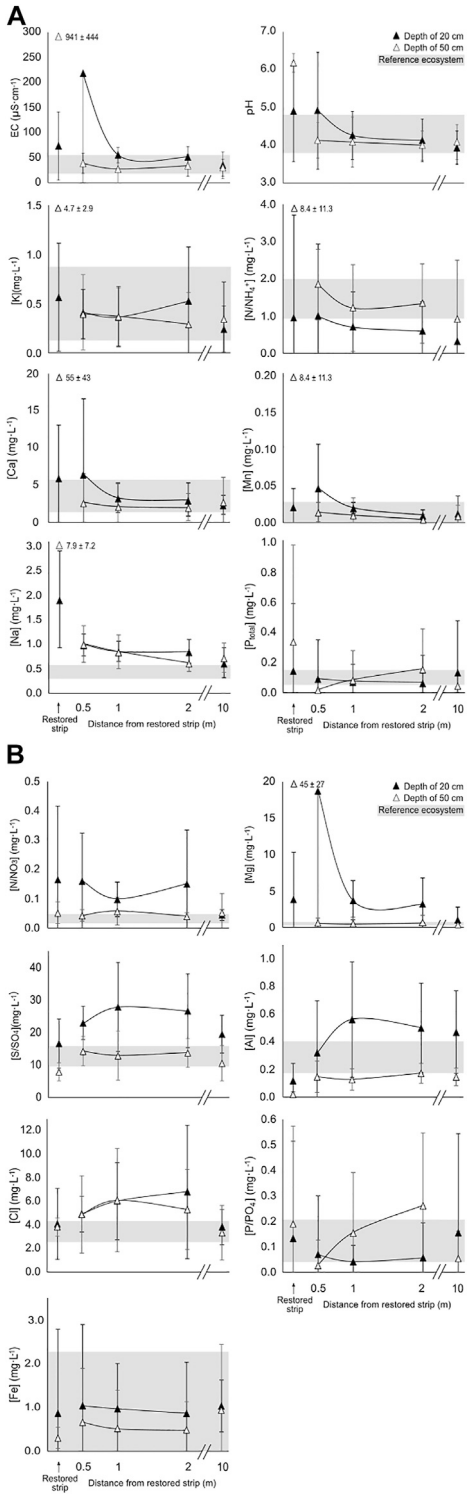

FIGURE 3 | Mean pore water ($\pm Cl_{95\%}$) of corrected electrical conductivity (EC), pH and concentration of K, N/NH4+, Ca, Mn, Na, Ptotal, N/NO_3, Mg, S/SO_4, Al, Cl, P/PO_4 and Fe (n = 4, data combined from two sampling campaigns in June and September 2015) sampled at two depths (20 and 50 cm) in the restored strip and at 0.5, 1, 2, and 10 m from the restored strip. The gray area represents the mean of the reference ecosystem (nearby pristine peatland) values (mean $\pm Cl_{95\%}$, n = 4).

Descriptive analyses were used to assess vegetation recovery on the restored strip in comparison to the reference ecosystem.

RESULTS

Chemical Elements and Compounds

Figure 3 regroup the chemical elements and compounds not by ecological significance but by patterns of response.

EC/pH Pattern of Response

The electrical conductivity (EC), proven to be a practical indicator for the other chemical elemental responses, summarizes the main findings regarding containment by the Burial Under Peat Technique for several elements [see **Figure 3**; the grey band represents the means values (mean ± $CI_{95\%}$) found in the reference ecosystem of the study]. Particularly high values of electrical conductivity (EC), compared to what is observed in the reference ecosystem, were found exclusively in the pore water sampled in the restored strip at a depth of 50 cm. For water pH, the mineral material buried in the peatland had only an alkalizing influence in the restored strip (20 and 50 cm deep) and at the close edge (half a meter) of the buried road for the surface water (20 cm deep). As suggested by the EC/pH patterns of response, K, N/NH_4^+, Ca, Mn, Na and P_{total} (**Figure 3**) showed particularly high concentrations exclusively in the pore water sampled at a depth of 50 cm in the restored strip; although slightly higher Na concentration were found up to 2 m at both depths.

Nitrate Pattern of Response

The NO_3 pattern of response (N/NO_3, Mg, S/SO_4, Al and Cl; **Figure 3**) is characterized by catotelm samples (50 cm depth) with concentrations similar to that of the reference ecosystem over the entire length of the sampled transect, except for the water sampled at a depth of 50 cm in the restored strip which had particularly a high Mg concentration. The chloride (Cl) concentration of the water sampled in the catotelm (50 cm) was rather the same as for the surface samples (20 cm). The NO_3 pattern of response also presented higher concentrations than in the reference ecosystem in surface water sampled up to a distance of 2 m, but back to the mean levels of the reference ecosystem at 10 m. However, the concentration of S/SO_4, Al and Cl in the restored strip were similar to that observed in the reference ecosystem (the natural peatland surrounding the right-of-way).

Phosphate Pattern of Response

P/PO_4 and Fe in the pore water sampled in the restored strip and at up to 10 m away from it (for both depth of 20 and 50 cm) had elemental concentration values similar to the means found in the reference ecosystem. Al and Cl, which were presented in the precedent pattern, could also figure in this pattern since the confidence interval ($CI_{95\%}$) at all distances and both depths are overlapping with the means of the reference ecosystem, suggesting there is no significant differences.

TABLE 1 | *p* value (95%) from paired *t*-test with datasets from 1-year and 3-years post-restoration [subsampling per transect: restored strip, n = 13; reference ecosystem (undisturbed peatland contiguous to the restored strip), n = 22].

	T1	T2	T3
Restored strip	0.00006	0.00002	<0.00001
Reference ecosystem	<0.00001	0.04208	<0.00001

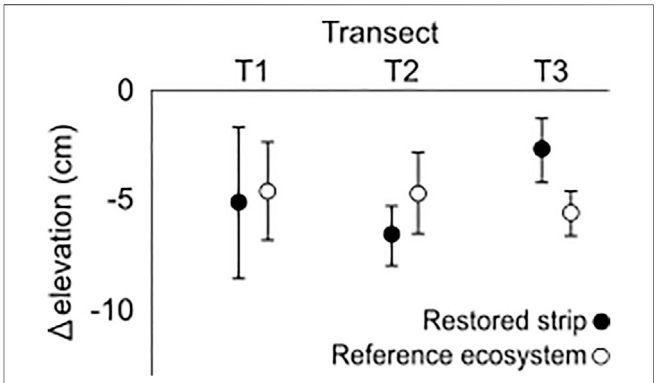

FIGURE 4 | Mean elevation differences (±$CI_{95\%}$) 1 and 3 years post-restoration on the three transects [subsampling per transect: restored strip, n = 13; reference ecosystem (undisturbed peatland contiguous to the restored strip), n = 22].

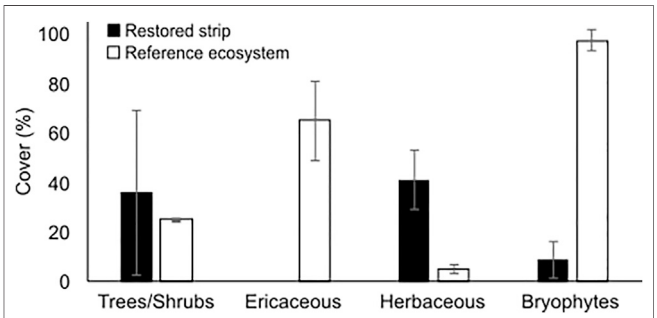

FIGURE 5 | Mean total cover of the main vegetation strata (±$CI_{95\%}$) three years post-restoration in the restored strip (n = 8) and the reference ecosystem (undisturbed peatland contiguous to the restored strip, n = 4).

Elevation

Paired t-tests revealed that the elevation dataset 3-years post-restoration was significantly different than the dataset 1-yr post-restoration both in the restored strip and the reference ecosystem (**Table 1**). However, the differences in elevation (Δ elevation) between one winter following the restoration and 3-years post-restoration were similar between the restored strip and the reference ecosystem (**Figure 4**). However, the Δ elevation on T3 was statistically different (Welch *t*-test, *p*-value = 0.0049) between the restored strip ($CI_{95\%}$ = −4.2 to −1.2 cm) and the adjacent reference ecosystem ($CI_{95\%}$ = −6.5 to −4.5 cm) but not impactful considering the typical microtopography of hummocks and hollows in pristine peatlands (Nungesser, 2003).

Vegetation

Three years post-restoration, the bryophyte cover was low onto the restored strip ($CI_{95\%}$ = 2–17%) in comparison to the reference ecosystem ($CI_{95\%}$ = 94–100%). Nevertheless, the bryophyte cover in the restored strip was dominated by *Sphagnum* (*S. rubellum*, *S. medium*, *S. angustifolium*) species with the presence of three pioneer mosses often found in degraded peatland (*Polytrichum strictum*, *Dicranella cerviculata* and *Pohlia nutans*; Poulin et al., 1999; Poulin et al., 2005; Tuittila et al., 2000). Vegetation cover of the main plant strata found in the peatland differed between the restored strip and the reference ecosystem, except for trees and shrubs other than ericaceous species (**Figure 5**). However, species of this stratum were different between the restored strip (mostly *Rubus hispidus*) and the reference ecosystem (mostly *Larix laricina*, *Betula populifolia* and *Aronia melanocarpa*). The cover of ericaceous shrubs was high in the reference ecosystem ($CI_{95\%}$ = 49–81%) but null in the restored strip. The herbaceous cover was high in the restored strip ($CI_{95\%}$ = 29–53%) in comparison to the reference ecosystem ($CI_{95\%}$ = 3–7%). Indeed, *Scirpus cyperinus* widely colonized entire sections of the restored strip. From the 22 vascular species surveyed in the restored strip, 20 are species found in wetlands [ten are Obligate Wetland (two of them mostly occur in peatland), six are Facultative Wetland, three are Facultative and one is Facultative Upland;.

DISCUSSION

The Burial Under Peat Technique (containment under at least 40 cm of peat) proved to limit the enrichment of the usual chemical signature of peatland from elements that could have diffused from the foreign mineral material brought onto the site for the temporary road construction, which in turn could have caused changes in the vegetation composition. Furthermore, the elevation of the surface of the restored strip was stable over the course of this study and supported the establishment of typical peatland vegetation.

Chemical Elements and Compounds Containment by the BUPT

The Burial Under Peat Technique is an effective method to limit the contamination of the peatland by the chemical elements and compounds released by the mineral material. The concentration of most of the chemical elements and compounds measured in the surface water (20 cm deep) of the restored strip was within or near the reference ecosystem means. This indicates that three years post-restoration, there was no vertical migration of the buried chemical elements and compounds toward the surface with the water table variations. Knowing that the lowest water table depth measured was approximately 30 cm (**Figure 1**), the mineral material buried at 50 cm deep was thus completely comprised in the catotelm, i.e., the bottom layer of peatlands that is permanently below the water table. Therefore, lateral diffusion of chemical elements and compounds from the buried mineral should be negligible in the long term due to the particular properties of the peat (anisotropy, hydraulic conductivity linked to the degree of peat decomposition and the high-buffering capacity due to the cation exchange capacity).

The surface water (depth of 20 cm) had high concentrations of magnesium, nitrates, and sulfates in the restored strip and within at least the first 2 m from it. However, this could also be a residual effect of the presence of the road before the restoration work since the concentrations of chemical elements and compounds within the surface water at a distance of 10 m from the road were the same as in the reference ecosystem. High nitrate and sulfate concentrations may be explained as a side effect of the peat inversion during the BUPT, accentuated by a low water table. Indeed, during the restoration, the peat that was historically in anaerobic conditions, from the long-term peatland development, was suddenly exposed to oxygen. It was then possible for erobic bacteria to oxidize ammoniacal nitrogen into nitrite and then nitrate through the nitrification process (Regina et al., 1996; Limpens et al., 2006). The reoxidation of elemental sulfur and sulfides, that occurs when the water table is low, generates sulfate ions that are dissolved when the water table level rises again (Bayley et al., 1986; Eimers et al., 2003), which might explain the higher concentration of sulphates found. Overall, we consider the physicochemistry of the restored strip and its margins adequate to support and maintain typical bog vegetation. In the longer term, it would be of interest to monitor the efficiency of the BUPT to confine nutrients. However, considering peatland ecology and its resilience, physicochemical conditions are expected to be stable through time.

Substrate Elevation After the BUPT

There was no compression of the peat in the restored strip following the restoration with the BUPT over the course of this study. The elevation differences between year 1 and 3 after the restoration work were similar to that in the restored strip and the reference ecosystem. During the restoration, the leveling of the peat to a similar mean elevation as the reference ecosystem with the excavator's bucket was sufficient to avoid drastic topographic changes in the restored strip. Rigorous daily surveillance of the work may have played a role in achieving satisfying surface elevation. The general lowering of 5 cm between survey on both the restored strip and the reference ecosystem may be an effect of bog surface oscillation (Howie and Hebda, 2018). The goal to restore and maintain a substrate elevation similar to the surrounding peatland was thus achieved.

Revegetation failures in road impacted peatland restoration projects are frequently caused either by extended flooding created by a low surface elevation (Osko, 2015) or by dry substrates caused by high elevations and excessive drainage (Johansen et al., 2017). Since the restored site has already gone through three winters, allowing the substrate to settle under the effect of precipitations and the weight of the snow, no significant changes in the elevation of the restored strip are expected in the future. Although previous studies might have suggested creating a dome-shaped surface over the restored area to compensate for possible substrate compaction, our study shows that there is no need to do so. Doing so could create drier conditions and compromise the survival of the reintroduced

vegetation during the critical period of the first growing seasons (Chirino et al., 2006).

Revegetation

The revegetation method used during BUPT successfully led to the reintroduction of plant species typical of wetlands, as only a few species with low cover were non-wetland species. However, 3 years post-restoration the plant communities of the restored strip did not evolve toward the reference ecosystem. The low establishment of peatland species in the restored strip may be explained by the presence of active drainage ditches maintaining a low water table within the right-of-way and inadequate donor material. A straw application was shown to be a critical step during peatland restoration with the MLTT (Rochefort et al., 2003) to prevent diaspores desiccation and to create favorable microclimatic conditions for plant establishment during the first growing seasons (Price et al., 1998). However, straw application was set aside during the BUPT to minimize costs and circulation over the restored area.

In contrast, results for the revegetation of a peatland impacted by a mineral road in Chénéville, Québec (Canada) where drainage ditches were absent, showed an extremely fast establishment of peatland plant communities only one year following the restoration (*Sphagnum* cover $CI_{95\%}$ = 14–52%; Pouliot, 2018) even without a straw mulch application. The authors believe that the combination of an adequate substrate elevation, a high water table due to the absence of drainage, good diaspores quality and constant work supervision led to this success in this other study (Pouliot, 2018).

Resources

The BUPT is cost-effective compared to the complete removal of the road mineral material because it requires fewer resources as well as fewer workers and heavy machinery, no peat input, and minimal mineral material transport out of the site. The most important expense linked to the complete removal technique is the transportation of the mineral out of the site (the further away the dumping site, the more expensive it is) and to the importation of peat onto the site. Furthermore, the purchase of the peat entails significant costs. The BUPT has minimal needs in machinery, such as a backhoe, and the absence of peat purchase and transportation makes it a technique of choice for the restoration of peatlands impacted by long linear mineral roads, especially in hard-to-access or remote areas. Besides, the time taken to complete both techniques on a 60 m road was estimated to be similar (~3 linear meters per hour) in another project described in Pouliot (2018). At Sainte-Eulalie, the BUPT had a pace of about 4.5 linear meters per hour.

However, the use of the BUPT is limited by the depth of the underlying peat. The minimum peat thickness required to apply the BUPT is approximately 1 m. In peatlands where the peat depth is insufficient, complete or partial removal of the road is recommended, depending on the thickness of the mineral material.

CONCLUSION

The restoration of peatlands impacted by mineral linear disturbances is at an early stage of development, but this study presents a new effective, innovative and affordable technique. Indeed, 3-years post-restoration results suggest that the Burial Under Peat Technique limits the peatland contamination by confining the chemical elements and compounds of the mineral material, and by establishing and maintaining an organic surface of similar elevation than the surrounding peatland without subsequent compaction or decompaction. Applying the principles of the long-proven Moss Layer Transfer Technique, but without the straw mulch application and the fertilization steps, is an indispensable step of the BUPT. The low moss cover observed in our study site three years following the restoration reminds us of the importance to re-establish a high water table and to transfer adequate plant material (Quinty and Rochefort, 2003). Finally, because the BUPT application requires a certain level of meticulousness that makes a difference in the achievement of restoration goals, we stress the capital importance of constant site supervision to adjust the working method and apply corrective measures when needed.

DATA AVAILABILITY STATEMENT

The raw data supporting the conclusions of this article will be made available by the authors, without undue reservation.

AUTHOR CONTRIBUTIONS

LR conceived the experiments. ML, KP, and AB were involved in planning and supervised the work. KP performed the measurements. KP processed the experimental data, performed the analysis, drafted the manuscript and designed the figures. MN aided with the statistics and worked on the manuscript. All authors discussed the results and commented on the manuscript.

FUNDING

Financial support for this study was provided by Hydro-Québec. Financial support to write this paper was provided by the Natural Sciences and Engineering Research Council of Canada (CRDPJ 517951-17) and the Canadian Sphagnum Peat Moss Association. Funds for open access publication fees were provided by Hydro-Québec.

ACKNOWLEDGMENTS

Financial support for this study was provided by Hydro-Québec. We thank Geneviève Corfa, Ghislain St-Laurent, Marie-Ève Pelletier-Marion and Caroline Dubé from Hydro-Québec who made this project possible and the members of the Golder Associates team for onsite supervision. Financial support to write this paper was

provided by the Natural Sciences and Engineering Research Council of Canada and the Canadian Sphagnum Peat Moss Association. Special thanks to Sandrine Hogue-Hugron and Claire Boismenu from the Peatland Ecology Research Group for their help and support.

REFERENCES

Amacher, M. C., Henderson, R. E., Breithaupt, M. P., Seale, C. L., and La Bauve, J. M. (1990). Unbuffered and Buffered Salt Methods for Exchangeable Cations and Effective Cation-Exchange Capacity. *Soil Sci. Soc. Am. J.* 54 (8), 1036–1042. doi:10.2136/sssaj1990.03615995005400040018x

Bagley, S. (1998). *The Road-Ripper's Guide to Wildland Road Removal*. Missoula, MT: Wildlands Center for Preventing Roads.

Bates, J. W. (2009). "Mineral Nutrition and Substratum Ecology," in *Bryophyte Biology*. Editors B. Goffinet and A.J. Shaw. 2nd edition (Cambridge, United Kingdom: Cambridge University Press), 248–311.

Bayley, S. E., Behr, R. S., and Kelly, C. A. (1986). Retention and Release of S from A Freshwater Wetland. *Water Air Soil Pollut.* 31, 101–114. doi:10.1007/bf00630824

Beckwith, C. W., Baird, A. J., and Heathwaite, A. L. (2003). Anisotropy and Depth-Related Heterogeneity of Hydraulic Conductivity in a Bog Peat. I: Laboratory Measurements. *Hydrol. Process.* 17, 89–101. doi:10.1002/hyp.1116

Bocking, E., Cooper, D. J., and Price, J. (2017). Using Tree Ring Analysis to Determine Impacts of a Road on a Boreal Peatland. *For. Ecol. Manag.* 404, 24–30. doi:10.1016/j.foreco.2017.08.007

Bourgeois, B., Hugron, S., and Poulin, M. (2012). Establishing a moss Cover Inhibits the Germination of Typha Latifolia, an Invasive Species, in Restored Peatlands. *Aquat. Bot.* 100, 76–79. doi:10.1016/j.aquabot.2012.03.010

Buykx, S. E. J., van den Hoop, M. A. G. T., and de Joode, P. (2004). Simultaneous Extraction of Bromide, Chloride, Fluoride and Sulfate from Soils, Waste- and Building Materials. *J. Environ. Monitor.* 6, 552–558. doi:10.1039/b400378k

Chirino, C., Campeau, S., and Rochefort, L. (2006). Sphagnum Establishment on Bare Peat: The Importance of Climatic Variability and Sphagnum Species Richness. *Appl. Veg Sci.* 9, 285–294. doi:10.1658/1402-2001(2006)9[285:seobpt]2.0.co;2

Colmer, T. D. (2003). Long-distance Transport of Gases in Plants: A Perspective on Internal Aeration and Radial Oxygen Loss from Roots. *Plant Cel Environ* 26, 17–36. doi:10.1046/j.1365-3040.2003.00846.x

Couillard, L., and Grondin, P. (1986). *La végétation des milieux humides du Québec*. Montreal: Les Publications du Québec, 400.

de Mars, H., Wassen, M. J., and Peeters, W. H. M. (1996). The Effect of Drainage and Management on Peat Chemistry and Nutrient Deficiency in the Former Jegrznia-Floodplain (NE-Poland). *Vegetatio* 126, 59–72.

Eimers, C., Dillon, P. J., Schiff, S. L., and Jeffries, D. S. (2003). The Effects of Drying and Re-wetting and Increased Temperature on Sulphate Release from upland and Wetland Material. *Soil Biol. Biochem.* 13 (12), 1663–1673. doi:10.1016/j.soilbio.2003.08.013

Gignac, L. D., Vitt, D. H., and Bayley, S. E. (1991). Bryophyte Response Surfaces along Ecological and Climatic Gradients. *Vegetatio* 93, 29–45.

Gignac, L. D., Gauthier, R., Rochefort, L., and Bubier, J. (2004). Distribution and Habitat Niches of 37 Peatland Cyperaceae Species across a Broad Geographic Range in Canada. *Can. J. Bot.* 82, 1292–1313. doi:10.1139/b04-081

Government of Canada (2018). Canadian Climate Normals 1981–2010 Station Data. Temperature and Precipitation Graph for 1981 to 2010 Canadian Climate Normals of ST WENCESLAS and Cheneville. Available at: http://climat.meteo.gc.ca/climate_normals/results_1981_2010_f.html?stnID=5586&autofwd=1 http://climat.meteo.gc.ca/climate_normals/results_1981_2010_e.html?stnID=5522&autofwd=1 (Accessed April 16, 2017).

Graf, M. D., and Rochefort, L. (2016). "A Conceptual Framework for Ecosystem Restoration Applied to Industrial Peatlands," in *Peatland Restoration and Ecosystem Services: Science, Policy and Practice*. Editors A. Bonn, T. Allott, M. Evans, H. Joosten, and R. Stoneman (Cambridge: Ecological Reviews of Cambridge University Press), 192–212.

SUPPLEMENTARY MATERIAL

The Supplementary Material for this article can be found online at: https://www.frontiersin.org/articles/10.3389/feart.2021.658470/full#supplementary-material

Hamilton, J. D., Kelly, C. A., Rudd, J. W. M., Hesslein, R. H., and Roulet, N. T. (1994). Flux to the Atmosphere of CH4and CO2from Wetland Ponds on the Hudson Bay Lowlands (HBLs). *J. Geophys. Res.* 99, 1495–1510. doi:10.1029/93jd03020

Hogg, P., Squires, P., and Fitter, A. H. (1995). Acidification, Nitrogen Deposition and Rapid Vegetational Change in a Small valley Mire in Yorkshire. *Biol. Conservation* 71 (2), 143–153. doi:10.1016/0006-3207(94)00040-w

Howie, S. A., and Hebda, R. J. (2018). Bog Surface Oscillation (Mire Breathing): A Useful Measure in Raised Bog Restoration. *Hydrological Process.* 32 (11), 1518–1530. doi:10.1002/hyp.11622

Johansen, M. D., Aker, P., Klanderud, K., Olsen, S. L., and Skrindo, A. B.(2017). Restoration of Peatland by Spontaneous Revegetation after Road Construction. *Appl. Veg. Sci.* 20 (4), 631–640.

Justin, S. H. F. W., and Armstrong, W. (1987). The Anatomical Characteristics of Roots and Plant Response to Soil Flooding. *New Phytol.* 106, 465–495. doi:10.1111/j.1469-8137.1987.tb00153.x

Keeney, D. R., and Nelson, D. W. (1982). "Nitrogen-inorganic Forms," in *Methods of Soil Analysis, Part 2*. Editors A.L. Page, R.H Miller, and D.R. Keeney. 2nd Ed. (Madison, Wisconsin: American Society of Agronomy, Inc., and Soil Science Society of America, Inc.), 643–698.

Kooijman, A. M., and Bakker, C. (1995). Species Replacement in the Bryophyte Layer in Mires: The Role of Water Type, Nutrient Supply and Interspecific Interactions. *J. Ecol.* 83 (1), 1–8. doi:10.2307/2261145

Laiho, R., Vasander, H., Penttilä, T., and Laine, J. (2003). Dynamics of Plant-Mediated Organic Matter and Nutrient Cycling Following Water-Level Drawdown in Boreal Peatlands. *Glob. Biogeochem. Cycles* 17 (2), 111–119. doi:10.1029/2002GB002015

Letts, M. G., Roulet, N. T., Comer, N. T., Skarupa, M. R., and Verseghy, D. L. (2000). Parametrization of Peatland Hydraulic Properties for the Canadian Land Surface Scheme. *Atmosphere-Ocean* 38, 141–160. doi:10.1080/07055900.2000.9649643

Limpens, J., Granath, G., Gunnarsson, U., Aerts, R., Bayley, S., Bragazza, L., et al. (2011). Climatic Modifiers of the Response to Nitrogen Deposition in Peat-forming Sphagnum Mosses: a Meta-analysis. *New Phytol.* 191 (2), 496–507. doi:10.1111/j.1469-8137.2011.03680.x

Limpens, J., Heijmans, M. P. D., and Berendse, F. (2006). "The Nitrogen Cycle in Boreal Peatlands," in *Boreal Peatlands Ecosystems. Ecological Studies, Vol. 188*. Editors K. R Wieder and D.H. Vitt (Berlin, Germany: Springer-Verlag), 195–230.

Luce, C. H. (1997). Effectiveness of Road Ripping in Restoring Infiltration Capacity of forest Roads. *Restor Ecol.* 5 (3), 265–270. doi:10.1046/j.1526-100x.1997.09731.x

McDonald, T., Gann, G. D., Jonson, J., and Dixon, K. W. (2016). *International Standards for the Practice of Ecological Restoration – Including Principles and Key Concepts*. Washington, D.C: Society for Ecological Restoration.

Miller, C. A. (2011). *The Effect of Long-Term Drainage on Plant Community Composition, Biomass, and Productivity in Boreal continental Peatlands*. Guelph, Ontario: MSc thesis, University of Guelph.

Müllerová, J., Vítková, M., and Vítek, O. (2011). The Impacts of Road and Walking Trails upon Adjacent Vegetation: Effects of Road Building Materials on Species Composition in a Nutrient Poor Environment. *Sci. Total Environ.* 409 (19), 3839–3849. doi:10.1016/j.scitotenv.2011.06.056

Nungesser, M. K. (2003). Modelling Microtopography in Boreal Peatlands: Hummocks and Hollows. *Ecol. Model.* 165 (2–3), 175–207. doi:10.1016/s0304-3800(03)00067-x

Osko, T. (2015). *Peatland Road Reclamation: Issues and Considerations Associated with Deep Fill*. Calgary, Alberta: Durvile Publications Ltd.

Osko, T., Vogel, C., Pilon, J., Petrone, R., La Farge, C., Williams, K., et al. (2014). *Natural Restoration of Peat and Re-usability of Fill Material after Road Reclamation on a Fen*. Peace River, Alberta: Durvile Publications Ltd.

Parkinson, J. A., and Allen, S. E. (1975). A Wet Oxidation Procedure Suitable for the Determination of Nitrogen and mineral Nutrients in Biological Material. *Commun. Soil Sci. Plant Anal.* 6 (1), 1–11. doi:10.1080/00103627509366539

Pasher, J., Seed, E., and Duffe, J. (2013). Development of Boreal Ecosystem Anthropogenic Disturbance Layers for Canada Based on 2008 to 2010 Landsat Imagery. *Can. J. Remote Sensing* 39 (1), 42–58. doi:10.5589/m13-007

Pilon, J. (2015). *Characterization of the Physical and Hydraulic Properties of Peat Impacted by a Temporary Access Road*. Ontario: MSc thesis, University of Waterloo.

Plach, J. M., Wood, M. E., Macrae, M. L., Osko, T. J., and Petrone, R. M. (2017). Effect of a Semi-permanent Road on N, P, and CO2 Dynamics in a Poor Fen on the Western Boreal Plain, Canada. *Ecohydrol* 10 (7), e1874. doi:10.1002/eco.1874

Poulin, M., Rochefort, L., and Desrochers, A. (1999). Conservation of Bog Plant Species Assemblages: Assessing the Role of Natural Remnants in Mined Sites. *Appl. Veg. Sci.* 2, 169–180. doi:10.2307/1478980

Poulin, M., Rochefort, L., Quinty, F., and Lavoie, C. (2005). Spontaneous Revegetation of Mined Peatlands in Eastern Canada. *Can. J. Bot.* 83, 539–557. doi:10.1139/b05-025

Pouliot, K. (2018). *Les routes minérales en tourbières à sphaignes : restauration par enfouissement*. Québec: Mémoire M.Sc., Université Laval, 68.

Price, J., Rochefort, L., and Quinty, F. (1998). Energy and Moisture Considerations on Cutover Peatlands: Surface Microtopography, Mulch Cover and Sphagnum Regeneration. *Ecol. Eng.* 10, 293–312. doi:10.1016/s0925-8574(98)00046-9

Puustjärvi, V. (1956). On the Cation Exchange Capacity of Peats and on the Factors of Influence upon its Formation. *Acta Agriculturae Scand.* 6 (4), 410–449. doi:10.1080/00015125609438024

Quinty, F., and Rochefort, L. (2003). *Peatland Restoration Guide*. Second Edition. Québec, Canada: Canadian Sphagnum Peat Moss Association and New Brunswick Department of Natural Resources and Energy.

Regina, K., Nykänen, H., Silvola, J., and Martikainen, P. J. (1996). Fluxes of Nitrous Oxide from Boreal Peatlands as Affected by Peatland Type, Water Table Level and Nitrification Capacity. *Biogeochemistry* 35, 401–418. doi:10.1007/bf02183033

Rochefort, L., Quinty, F., Campeau, S., Johnson, K., and Malterer, T. (2003). North American Approach to the Restoration of Sphagnum Dominated Peatlands. *Wetl. Ecol. Manag.* 11 (1–2), 3–20. doi:10.1023/a:1022011027946

Saraswati, S., Bhusal, Y., Trant, A. J., and Strack, M. (2020). Roads Impact Tree and Shrub Productivity in Adjacent Boreal Peatlands. *Forests* 11 (5), 594. doi:10.3390/f11050594

Saraswati, S., and Strack, M. (2019). Road Crossings Increase Methane Emissions from Adjacent Peatland. *J. Geophys. Res. Biogeosci.* 124 (11), 3588–3599. doi:10.1029/2019jg005246

Sjörs, H., and Sjors, H. (1950). On the Relation between Vegetation and Electrolytes in north Swedish Mire Waters. *Oikos* 2, 241–257. doi:10.2307/3564795

Sobze, J.-M., Rochefort, L., and Schoonmaker, A. (2012). Wellsite clay Pad Removal and Inversion Peatland Restoration. *Can. Reclamation* 12 (1), 10–13. doi:10.3368/er.34.3.225

Sosa-Pérez, G., and MacDonald, L. H. (2017). Reductions in Road Sediment Production and Road-Stream Connectivity from Two Decommissioning Treatments. *For. Ecol. Manag.* 398 (8), 116–129. doi:10.1016/J.FORECO.2017.04.031

Strack, M., and Zuback, Y. C. A. (2013). Annual Carbon Balance of a Peatland 10 Yr Following Restoration. *Biogeosciences* 10, 2885–2896. doi:10.5194/bg-10-2885-2013

Switalski, T., Bissonette, J., DeLuca, T., Luce, C., and Madej, M. (2004). Benefits and Impacts of Road Removal. *Front. Ecol. Environ.* 2 (1), 21–28. doi:10.1890/1540-9295(2004)002[0021:baiorr]2.0.co;2

Tuittila, E.-S., Rita, H., Vasander, H., and Laine, J. (2000). Vegetation Patterns Around *Eriophorum Vaginatum* L. Tussocks in a Cut-Away Peatland in Southern Finland. *Can. J. Bot.* 78 (1), 47–58. doi:10.1139/b99-159

Umeda, Y., Tsujii, T., and Inoue, T. (1985). Influence of Banking on Groundwater Hydrology in Peatland. *J. Fac. Agric. Hokkaido Univ.* 62 (3), 222–235.

Vitt, D. H., Bayley, S. E., and Jin, T.-L. (1995). Seasonal Variation in Water Chemistry over a Bog-Rich Fen Gradient in continental Western Canada. *Can. J. Fish. Aquat. Sci.* 52 (3), 587–606. doi:10.1139/f95-059

Wieder, R. K., Vitt, D. H., and Benscoter, B. W. (2006). "Peatlands and the Boreal forest," in *Boreal Peatland Ecosystems* (Berlin, Heidelberg: Springer), 1–8.

Williams-Mounsey, J., Grayson, R., Crowle, A., and Holden, J. (2021). A Review of the Effects of Vehicular Access Roads on Peatland Ecohydrological Processes. *Earth-Science Rev.* 214, 103528. doi:10.1016/j.earscirev.2021.103528

Yu, Z., Loisel, J., Brosseau, D. P., Beilman, D. W., and Hunt, S. J. (2010). Global Peatland Dynamics since the Last Glacial Maximum. *Geophys. Res. Lett.* 37 (13), 134–141. doi:10.1029/2010gl043584

Conflict of Interest: The authors declare that the research was conducted in the absence of any commercial or financial relationships that could be construed as a potential conflict of interest.

frontiers in Earth Science

ORIGINAL RESEARCH
published: 18 June 2021
doi: 10.3389/feart.2021.631368

Response of Peatland CO_2 and CH_4 Fluxes to Experimental Warming and the Carbon Balance

Qian Li[1], Sébastien Gogo[1], Fabien Leroy[1], Christophe Guimbaud[2] and Fatima Laggoun-Défarge[1]*

[1]Université d'Orléans, Institut des Sciences de La Terre d'Orléans, CNRS, BRGM, UMR 7327, Orléans, France, [2]Université d'Orléans, Le Laboratoire de Physique et de Chimie de l'Environnement et de l'Espace (LPC2E), CNRS, UMR 7328, Orléans, France

The function of peatlands as a large carbon (C) reservoir results from the net C uptake under cold, wet, and acid environments. However, in the context of global warming, the balance between C input and release is expected to change, which may further alter the C sink of peatlands. To examine the response to climate warming of a temperate *Sphagnum* peatland which has been invaded by vascular plants, a mesocosm experiment was conducted with open top chambers (OTCs) to simulate a moderate temperature increase. Gross primary production (GPP), ecosystem respiration (ER), and methane (CH_4) emissions were monitored for 2 years. The CO_2 and CH_4 fluxes were modeled by relating to abiotic and biotic factors, including temperature, water table depth (WTD), and vegetation, in order to calculate the annual C budget. Results showed that the annual cumulated GPP was significantly enhanced by the simulated warming (–602 compared to –501 gC m^{-2} yr^{-1} in OTC and control plots, respectively), mainly due to the increase of graminoid biomass by warming, while experimental warming had no significant effect on the annual ER and CH_4 emissions (an output of 615 and 500 gC m^{-2} yr^{-1} for ER; 21 and 16 gC m^{-2} yr^{-1} for CH_4 emissions in OTC and control plots, respectively). The annual NEE and C budget were not affected by the short-term experimental warming. The mesocosms under both treatments acted as a gaseous C source with 34 and 14 gC m^{-2} yr^{-1} output under OTC and control treatment, respectively. This C source was driven by the strong net carbon dioxide (CO_2) release during a low WTD period in summer, as CH_4 emissions only accounted for 0.9–2.2% of the total C fluxes. Our study identified the effect of moderate warming on the C fluxes, even on a short-term basis. Also, our findings highlighted that the response of C fluxes to warming largely depends on the WTD and vegetation composition. Thus, long-term monitoring of hydrology and vegetation change under climate warming is essential to examine their interactions in determining the C fluxes in peatlands.

Keywords: CO_2 fluxes, methane emissions, carbon budget, climate warming, peatland

OPEN ACCESS

Edited by:
Annalea Lohila,
University of Helsinki, Finland

Reviewed by:
Maria Strack,
University of Waterloo, Canada
Wei-Li Hong,
Stockholm University, Sweden

****Correspondence:***
Qian Li
qian.li@univ-orleans.fr

Specialty section:
This article was submitted to Biogeoscience, a section of the journal Frontiers in Earth Science

Received: *19 November 2020*
Accepted: *28 May 2021*
Published: *18 June 2021*

Citation:
Li Q, Gogo S, Leroy F, Guimbaud C and Laggoun-Défarge F (2021) Response of Peatland CO_2 and CH_4 Fluxes to Experimental Warming and the Carbon Balance. Front. Earth Sci. 9:631368. doi: 10.3389/feart.2021.631368

INTRODUCTION

Peatlands are important carbon (C) storage terrestrial ecosystems in the world as they accumulate about 30% of the world's soil C in only 3% of the land area (Gorham, 1991; Yu et al., 2010; Jackson et al., 2017). Their C sink function results from the positive small but long-lasting imbalance between the C input from photosynthesis and the C output from decomposition of soil organic matters (OMs) (Bragazza et al., 2009). The specific abiotic and biotic conditions in peatlands, such as low temperature, waterlogging, acidity, and litter intrinsically recalcitrance to decay (*Sphagnum* litters) limit the microbial decomposition, thus leading to the accumulation of OMs. Nevertheless, due to the large amount of anthropogenic greenhouse gas (GHG) emissions into the atmosphere, the earth surface temperature has been observed to be increasing since the last century, and it is expected to increase 1–3.7°C by the end of the 21st century (Intergovernmental Panel on Climate Change, 2014). As elevated temperature can stimulate the soil decomposition (Dieleman et al., 2016), the projected warmer climate may shift the C sink of peatlands to a C source. Furthermore, due to the large C stocks in peatlands, small disturbances in the C cycle processes may lead to marked C release, which will in turn exacerbate the global warming. Therefore, understanding the C balance of peatlands in response to climate warming is of great importance and is a subject of considerable concern.

Temperature controls numerous metabolic processes related to photosynthesis as well as autotrophic and heterotrophic respiration (e.g., Lloyd and Taylor, 1994; Medlyn et al., 2002). Generally, higher temperature could induce more carbon dioxide (CO_2) release by ecosystem respiration (ER; e.g., Chivers et al., 2009; Flanagan and Syed, 2011). For example, Dorrepaal et al. (2009) observed an increase of over 50% in ER from peat soil induced by a temperature rise of approximately 1°C. However, the response of photosynthesis to temperature change varies with vegetation types and environmental conditions (Medlyn et al., 2002; Voigt et al., 2017). Methane (CH_4) emissions from peatlands to the atmosphere depend on the balance of CH_4 production, oxidation, and transportation rate. Both CH_4 production by methanogens and oxidation by methanotrophs are strongly correlated with temperature (Segers, 1998). Nevertheless, CH_4 production was reported to be more sensitive to temperature change than CH_4 consumption (Dunfield et al., 1993). Thus, a warmer climate is expected to increase CH_4 release into the atmosphere. Due to the different responses of these processes, estimating the net response of C in peatlands to climate warming is still challenging.

In addition, climate warming can affect the peatland C cycle indirectly *via* modifying the vegetation structure. It has been demonstrated that warming could promote the growth of vascular plants, especially ericaceous shrubs and graminoids, to the detriment of *Sphagnum* species (Bragazza et al., 2013; Buttler et al., 2015; Dieleman et al., 2015). *Sphagnum* litter is resistant to decay, which is beneficial for the C sequestration in peatlands (AminiTabrizi et al., 2020). However, the presence of vascular plants alters the litter quality in peatlands with an increase of its degradability, which enhances the decomposition (Straková et al., 2011; Leroy et al., 2019). Furthermore, the root exudates from vascular plants are a source of labile C input, which on the one hand provide substrate for microbial degradation and on the other hand lead to the priming effect, thus stimulating the decomposition of "old" and the so-called recalcitrant OMs (Gavazov et al., 2018; Girkin et al., 2018). Nevertheless, this vegetation shift also increases the C input to peatlands because of the higher primary productivity of vascular plants (Gavazov et al., 2018; Leroy et al., 2019).

To date, numerous studies have tried to understand the response of peatlands to global warming. However, most of them focused on northern peatlands in subarctic regions (e.g., Aurela et al., 2004; Chivers et al., 2009; Dieleman et al., 2015; Munir et al., 2015; Voigt et al., 2017; Laine et al., 2019), where the majority of peatlands are located (Strack, 2008). Previous results showed that the effect of warming on the C sequestration of peatlands varied from strengthening to diminishing (e.g., Waddington et al., 1998; Chivers et al., 2009; Ward et al., 2013; Munir et al., 2015; Hanson et al., 2020). Therefore, it is still difficult to draw a conclusion on the precise feedback of peatlands to climate warming. More importantly, there is still a large gap in the understanding of how temperate peatlands will respond to the warming climate. Temperate low-latitude peatlands are already below the temperature which is the projected level of subarctic regions in the future. Furthermore, they have suffered high anthropogenic pressures (e.g., hydrological disturbance, peat cutting, or nutrient amendment), and a vegetation shift has occurred (Berendse et al., 2001; Bubier et al., 2007). These disturbances have diminished their C storage (Dorrepaal et al., 2005; Gogo et al., 2016). Thus, they have significant potential to act as a C source in the future (Leifeld et al., 2019). Especially under the projected climate warming, it is important to assess how these temperate peatlands will respond to both anthropogenic and climatic disturbances.

In order to understand the response to climate warming of a temperate *Sphagnum* peatland which has been invaded by vascular plants (especially *Molinia caerulea*), we conducted a mesocosm experiment. The mesocosms were submitted to two temperature treatments: 1) ambient (control) and 2) moderate experimental warming by open top chambers (OTCs). The CO_2 and CH_4 fluxes were monitored for two years. Then, they were modeled by relating to abiotic and biotic factors in order to estimate the annual C budget. We hypothesized that the warming treatment would 1) promote both the C input to peatland through photosynthesis and the C release to the atmosphere through respiration and CH_4 emissions and 2) diminish the C sink function of this ecosystem.

MATERIALS AND METHODS

Mesocosm Experiment

Sample Preparation and Monitored Variables

Twelve mesocosms (intact cylindrical peat monoliths, 30 cm in diameter, and 40 cm in depth; **Supplementary Figure S1A**) were collected from La Guette peatland (France) in June 2018. This site is a transitional acid fen with typical species including *Sphagnum* mosses (*Sphagnum cuspidatum* and *Sphagnum rubellum*) and ericaceous shrubs (*Erica tetralix* and *Calluna vulgaris*). However, this site has been invaded by vascular plants (mainly *Molinia caerulea* and *Betula* spp.) for 30 years, and the invasion was accelerated in recent decades due to the hydrological disturbance (Gogo et al., 2011). The sampling

locations were selected to ensure that all the mesocosms contained a representative species assemblage, including mosses, vascular plants, and ericaceous shrubs. The mesocosms were sealed at the bottom and placed in the holes dug into the ground outside the Institut des Sciences de la Terre d'Orléans (ISTO) laboratory in July 2018 (**Supplementary Figure S1B**). They were separated into two treatments: six for warming treatment equipped with passive warming OTCs (called "OTC" plots) designed following the International Tundra Experiment (ITEX) protocol (Marion et al., 1997; Aronson and McNulty, 2009; **Supplementary Figure S1C**), and another six without OTCs were used as control (called "control" plots).

The air temperature at 10 cm above the soil surface, and the soil temperature at 5, 15, and 30 cm depths of the mesocosms were monitored with temperature probes (Campbell Scientific T107, United States). The water content of surface *Sphagnum* peat at 5 cm depth was monitored with soil moisture probes inserted vertically into the soil (Decagon EC-5, METER group United States). The temperature and relative humidity of the ambient air were monitored by temperature and relative humidity probes (Campbell Scientific CS215, United States), the solar radiation of the ambient environment was monitored by a SP-LITE pyranometer (Campbell Scientific, United States), the precipitation was monitored by a tipping bucket rain gauge (Campbell Scientific AGR100), the wind speed and direction of the ambient environment were monitored by a wind monitor (Campbell Scientific 05103, United States), and the atmospheric pressure of the ambient environment was monitored by a barometric pressure sensor (Campbell Scientific CS100, United States). These probes were connected to dataloggers (Campbell Scientific CR800, United States) in the weather stations installed near the study site (**Supplementary Figure S1D**), and the data were recorded every 5 min.

The water supply of mesocosms was mainly from natural precipitation. However, in order to maintain a similar WTD in all the mesocosms during the summer drought period, water collected from the drainage ditch near La Guette peatland was added to mesocosms when necessary. The WTD was measured manually by piezometers installed in mesocosms.

The vegetation communities in mesocosms were separated into three groups: bryophytes (*Sphagnum* spp.), graminoids (*Molinia caerulea* and *Eriophorum angustifolium*), and ericaceous shrubs (*Erica tetralix* and *Calluna vulgaris*). Each group was regarded as a distinct plant stratum, and the percentage cover of each stratum could reach 100%. The percentage cover of each species in their stratum and the number of graminoid leaves were measured after gas flux measurement. A vegetation index (VI), representing the amount of vegetation present, was calculated by summing the percentage cover of the three groups and dividing it by the total potential maximum cover (**Eq. 1**; D'Angelo et al., 2021):

$$\mathrm{VI} = \frac{\mathrm{BS} + \mathrm{GS} + \mathrm{SS}}{\mathrm{TC}}, \quad (1)$$

where BS, GS, and SS represent the percentage cover of bryophytes, graminoids, and ericaceous shrubs, respectively. TC is the total potential maximum cover calculated as $n \times 100\%$, in which n is the number of plant strata.

CO_2 and CH_4 Fluxes Measurements

The measurements of CO_2 and CH_4 fluxes were carried out by the static chamber method (e.g., Leroy et al., 2019) from August 2018 to July 2020. The transparent PVC chamber was equipped with a low-speed battery-operated fan to circulate the air inside the chamber during measurements. Between measurements, the chamber was air-flushed to equilibrate the headspace concentration with that of the ambient air. The CO_2 measurements were performed using a CO_2 sensor (Vaisala Carbocap GMP343, Finland) inserted into the chamber. The transparent chamber was used to measure the net ecosystem exchange (NEE), which is the difference between ecosystem respiration (ER) and gross primary production (GPP). ER was measured by covering the chamber with an opaque cover to prevent the photosynthesis. The NEE was measured under different light conditions which were artificially modulated by adding different numbers of plastic nets above the mesocosms. In this case, the light response of GPP was assessed, and it was used to calculate the GPP modeling parameters (see *Gross primary production*). During the measurement, CO_2 concentration (ppm) was recorded every 5 s. The measurements always lasted until a clear linear slope of CO_2 concentration vs. time was obtained, but for a maximum of 5 min. During the CO_2 measurements, the air temperature and humidity inside the chamber were also measured with a temperature and humidity meter (Vaisala Humicap HM70, Finland) inserted into the chamber. Photosynthetically active radiation (PAR; mol m^{-2} s^{-1}), which is measured as the photosynthetic photon flux density (PPFD), was measured by placing a PAR sensor (SDEC JYP 1000, France) on the top of chamber. PAR was measured at the beginning and at the end of each CO_2 measurement, and their mean was used to represent PAR during this measurement. CH_4 emissions were measured using a LGR Ultraportable Greenhouse Gas Analyzer (Los Gatos Research, United States) connected to the transparent chamber. The measurement of CH_4 concentration (ppm) also lasted until a clear linear slope of CH_4 concentration vs. time was obtained, but for a maximum of 5 min. The CO_2 and CH_4 concentrations measured during the first 30 s of measurement were always excluded to remove the fluctuation caused by the placement of the chamber (e.g., ebullition). If saturation occurred at the end of the measurement, the data were also excluded to keep only the linear slope. If ebullition occurred during the CH_4 measurement, the measurement was repeated to include only the diffusive emissions of CH_4. Atmosphere was regarded as the reference for C fluxes. Thus, positive values of CO_2/CH_4 fluxes indicated an emission into atmosphere and negative values indicated an uptake by the ecosystem.

The flux of CO_2/CH_4 (μmol m^{-2} s^{-1}) was calculated by **Eq. 2**

$$F_{\mathrm{CO_2/CH_4}} = \frac{(V/A) \times (d_c/d_t) \times \mathrm{Pat_m}}{R \times (T + 273.15)}, \quad (2)$$

where R is the gas constant at 273.15 K (8.314 m^3 Pa K^{-1} mol^{-1}), T is the temperature inside the chamber (°C), V is the volume of the chamber (m^3), A is the surface area of the chamber (m^2), $\mathrm{Pat_m}$ is the atmospheric pressure (Pa), and d_c/d_t is the CO_2/CH_4

concentration change against time (ppm s^{-1}) calculated using linear regression.

Modeling of CO_2 and CH_4 Fluxes

Gross Primary Production

The relationship between GPP and PPFD was often described by a rectangular hyperbolic saturation curve (Thornley and Johnson, 1990):

$$\mathrm{GPP} = \frac{\mathrm{GPP_{max}} \times \mathrm{PAR}}{k + \mathrm{PAR}}, \tag{3}$$

where $\mathrm{GPP_{max}}$ (μmol m^{-2} s^{-1}) is the asymptotic maximum GPP at light saturation and k (μmol photon m^{-2} s^{-1}) is the half-saturation value. These two variables were calculated by the Michaelis–Menten equation (Johnson and Goody, 2011) based on the light response curve of GPP (methods described above). PAR (mol m^{-2} s^{-1}) is the photosynthetically active radiation.

This approach was modified by Kandel et al. (2013) who introduced the effect of temperature and vegetation into the light response model. Here, we modeled GPP following their equation, while a simple VI (**Eq. 1**) was used instead of the ratio vegetation index (RVI) in their equation. The model performance was improved when the number of graminoid leaves and WTD were incorporated with the linear function:

$$\mathrm{GPP} = \frac{\mathrm{GPP_{max}} \times \mathrm{PAR}}{k + \mathrm{PAR}} \times \left(a \times \mathrm{Graminoid_{leaves}} + b \times \mathrm{VI} + c \times \frac{\mathrm{WTD}}{\mathrm{WTD_{ref}}} \right) \times T_{\mathrm{scale}}, \tag{4}$$

where $\mathrm{Graminoid_{leaves}}$ is the number of graminoid leaves, VI is the vegetation index (**Eq. 1**), and WTD is the water table depth (cm), and its reference value, $\mathrm{WTD_{ref}}$, was set at −25 cm, which was the lowest value we observed in the mesocosms. The coefficients a, b, and c are fitted empirical parameters. T_{scale} represents the temperature sensitivity of photosynthesis (Raich et al., 1991; Mahadevan et al., 2008):

$$T_{\mathrm{scale}} = \frac{(T - T_{\mathrm{min}})(T - T_{\mathrm{max}})}{(T - T_{\mathrm{min}})(T - T_{\mathrm{max}}) - \left(T - T_{\mathrm{opt}}\right)^2}, \tag{5}$$

where T is the measured air temperature (°C). T_{min}, T_{max}, and T_{opt} are the minimum, maximum, and optimum air temperatures (°C) for photosynthesis, respectively. Following Leroy et al. (2019), they were set as 0, 20, and 40°C, respectively.

Ecosystem Respiration

ER was modeled based on the equation of Bortoluzzi et al. (2006) and Leroy et al. (2019). The measured ER data were fitted with temperature using nonlinear power regression. Then, the residuals of this power regression were related to other abiotic and biotic variables. WTD and the number of graminoid leaves were linearly correlated to the residuals of the power regression. Thus, they were included in the model by a linear function:

$$\mathrm{ER} = \left(d \times \frac{\mathrm{WTD}}{\mathrm{WTD_{ref}}} + e \times \mathrm{Graminoid_{leaves}} \right) \times \left(\frac{T - T_{\mathrm{min}}}{T_{\mathrm{ref}} - T_{\mathrm{min}}} \right)^f, \tag{6}$$

where the reference of water table depth, $\mathrm{WTD_{ref}}$, was also set at −25 cm as mentioned above. T_{min} is the minimum temperature (°C) for positive respiration and T_{ref} is the reference temperature (°C). They were set as −5 and 15°C, respectively, following the study of Bortoluzzi et al. (2006). T is the measured temperature (°C). The model was fitted with air temperature and soil temperature at 5, 15, and 30 cm depths. The best fit was found when using the soil temperature at 5 cm. Thus, it was used as T here. The coefficients d, e, and f are fitted empirical parameters.

CH_4 Emissions

In accordance with Laine et al. (2007), data of CH_4 emissions were fitted with soil temperature using nonlinear regression, and then the residuals of the nonlinear regression were related to other variables. WTD was linearly correlated to the residuals when values were above 9 cm, and the number of graminoid leaves was also linearly correlated to the residuals. Thus, they were included in the model as follows:

$$\mathrm{CH_4} = \left(g \times \frac{\mathrm{WTD}}{\mathrm{WTD_{ref}}} + h \times \mathrm{Graminoid_{leaves}} \right) \times \left(\frac{T_s - T_{\mathrm{min}}}{T_{\mathrm{ref}} - T_{\mathrm{min}}} \right)^i (\mathrm{WTD} > -9\,cm). \tag{7}$$

where T_{min} is the minimum temperature (°C) for CH_4 emissions; it was set as 1°C, which was the minimum soil temperature observed at 5 cm depth. T_{ref} is the reference temperature (°C); it was set as 20°C which was the median value of annual soil temperature at 5 cm depth. T_s is the measured soil temperature (°C). The model was fitted with soil temperature at 5, 15, and 30 cm depths. The best fit was found when using the soil temperature at 5 cm. Thus, it was used as T_s here. The coefficients g, h, and i are fitted empirical parameters.

There were 74 WTD data points measured below WTD of −9 cm, that is, 28.6% of the total of 259 measured data. When WTD was below 9 cm, CH_4 emissions were independent of temperature and WTD. Thus, the CH_4 emissions were not modeled by **Eq. 7**, but they were linearly interpolated in this case.

Calibration and Evaluation of Models

Two-thirds (randomly selected) of the available data from each treatment were used to calibrate the model, and another one-third of the data were used to evaluate the model. The quality of model was evaluated by the adjusted determination coefficient R^2_{adj} and the normalized root-mean-square error (NRMSE; %) of the linear relationship between measured and modeled data:

$$R^2_{\mathrm{adj}} = 1 - \left(1 - \frac{(1 - R^2)(n - 1)}{n - k - 1} \right), \tag{8}$$

where R^2 is the coefficient of determination, n represents the number of data, and k is the number of independent regressors.

$$\mathrm{NRMSE} = 100 * \frac{\sqrt{\left(\frac{\sum (y-\hat{y})}{n}\right)}}{\overline{y}}, \quad (9)$$

where y is the measured value, $\hat{y}$ is the modeled value, $\overline{y}$ is the mean of measured values, and n is the number of data.

The fitted parameters of the GPP model (a, b, and c), ER model (d, e, and f), and the CH_4 emission model (g, h, and i) were calibrated by minimizing the NRMSE using the "SANN" method of the optimum function in *R* (version 3.6.3, R Core Team, 2020).

Calculation of Annual C Fluxes and C Budget

After calibration and evaluation of the C flux models, the models were parameterized for each mesocosm under both treatments individually. All the variables used in the models were interpolated to set a 1-h dataset. To do so, PAR, air, and soil temperature at 3 depths, which were monitored with a high frequency (5 min), were averaged over a 1-h time step. The other variables which were measured with a low frequency (WTD, number of graminoid leaves, and VI) were linearly interpolated between the punctual measurements to set a 1-h dataset. Then, the GPP, ER, and CH_4 emissions were calculated at a 1-h time step using the relationships between C fluxes and environmental variables constructed above (**Eq. 6**, **Eq. 7**, and **Eq. 8**). Due to the technical problems in August 2018 and the lockdown because of COVID-19 from March 2020, the environmental variable data recorded by weather stations were not complete during these periods. Thus, the modeled GPP, ER, and CH_4 emissions at a 1-h time step were only calculated from September 2018 to September 2019. Then, the annual cumulated GPP, ER, and CH_4 emissions ($gC\,m^{-2}\,yr^{-1}$) during this period were calculated as the sum of values at a 1-h time step.

The annual greenhouse gas C budget (GGCB; $gC\,m^{-2}\,yr^{-1}$) indicates the net gaseous C accumulation/release rate of the ecosystem. It was calculated for each mesocosm under both treatments as follows:

$$\mathrm{GGCB} = -\mathrm{GPP} + \mathrm{ER} + F_{CH_4}. \quad (10)$$

where GPP is the annual cumulated gross primary production ($gC\,m^{-2}\,yr^{-1}$), ER is the annual cumulated ecosystem respiration ($gC\,m^{-2}\,yr^{-1}$), and FCH_4 is the annual cumulated emission of CH_4 ($gC\,m^{-2}\,yr^{-1}$).

Statistics

The significant differences in the annual mean of air temperature (T_a) and soil temperature (T_s) at 5, 15, and 30 cm depths, and the WTD and water content of surface *Sphagnum* peat between control and OTC treatment were assessed by one-way ANOVA. The effects of experimental warming and time on the percentage cover of vegetation species, number of graminoid leaves, and vegetation index (VI) were analyzed by two-way repeated measure ANOVA using time as the repeated-measure factor and treatment as the between-group factor. The differences of the measured GPP, ER, NEE, and CH_4 emissions between control and OTC plots at different periods of the growing season [early growing season (EG; April–May), middle growing season (MG: June–August), late growing season (LG: September), and the whole growing season (WG: April–September)] were analyzed by two-way repeated measure ANOVA using time as the repeated-measure factor and treatment as the between-group factor. The differences of the calculated GPP_{max} between the two treatments at different dates were analyzed by one-way ANOVA. The significant differences in the modeled annual cumulated GPP, ER, CH_4 emission, NEE, and GGCB between the two treatments were assessed by one-way ANOVA. Before statistical analysis, the normality of distribution and the homogeneity of variance of the data were tested. All the statistics were performed in OriginPro 2019 (OriginLab, United States).

TABLE 1 | Mean value of air temperature (T_a) and soil temperature (T_s) at 5, 15, and 30 cm depths of mesocosms, water table depth (WTD), and water content of *Sphagnum* at 5 cm depth from August 2018 to July 2020. Significant differences of ANOVA are expressed as $^*p < 0.05$, $^{**}p < 0.01$, and $^{***}p < 0.001$. Data are presented as mean ± SD, $n = 6$.

	Mean		Significance
	Control	OTCs	
T_a (°C)	14.01 ± 0.07	14.91 ± 0.14	***
T_s at 5 cm (°C)	13.85 ± 0.42	15.20 ± 0.32	**
T_s at 15 cm (°C)	14.38 ± 0.17	15.30 ± 0.33	**
T_s at 30 cm (°C)	14.77 ± 0.10	14.94 ± 0.32	
WTD (cm)	−6.80 ± 0.47	−6.68 ± 1.08	
Water content (%)	65.87 ± 3.53	70.71 ± 7.51	

RESULTS

Environmental Variables

The air temperature and soil temperature at 5 and 15 cm depths increased significantly under OTC treatment. The mean air temperature was 0.9°C higher in OTC plots than in control during the 2 years of monitoring (**Table 1**). The mean soil temperature at 5 cm depth was increased by 1.35°C, and at 15 cm depth, it was increased by 0.92°C with OTC treatment. However, the mean soil temperature at 30 cm was not significantly affected by OTC treatment (**Table 1**). The mean WTD and water content of surface peat throughout the monitoring were similar between the two treatments (**Table 1**). During the 2 years of monitoring, the WTD ranged from −0.4 to −23.5 cm for control plots and from −0.5 to −18 cm for OTC plots (**Supplementary Figure S2A**), with higher levels in winter and lower levels in summer. The water content of surface *Sphagnum* peat showed similar seasonal variations to the WTD. However, significant differences between the two treatments were found during July–September 2019 and April–May 2020, with higher values in OTC plots than in control plots (**Supplementary Figure S2B**). The percentage cover of *Sphagnum* increased significantly with time ($p < 0.05$; **Figure 1A**), while that of graminoids and shrubs remained constant (**Figures 1B,C**),

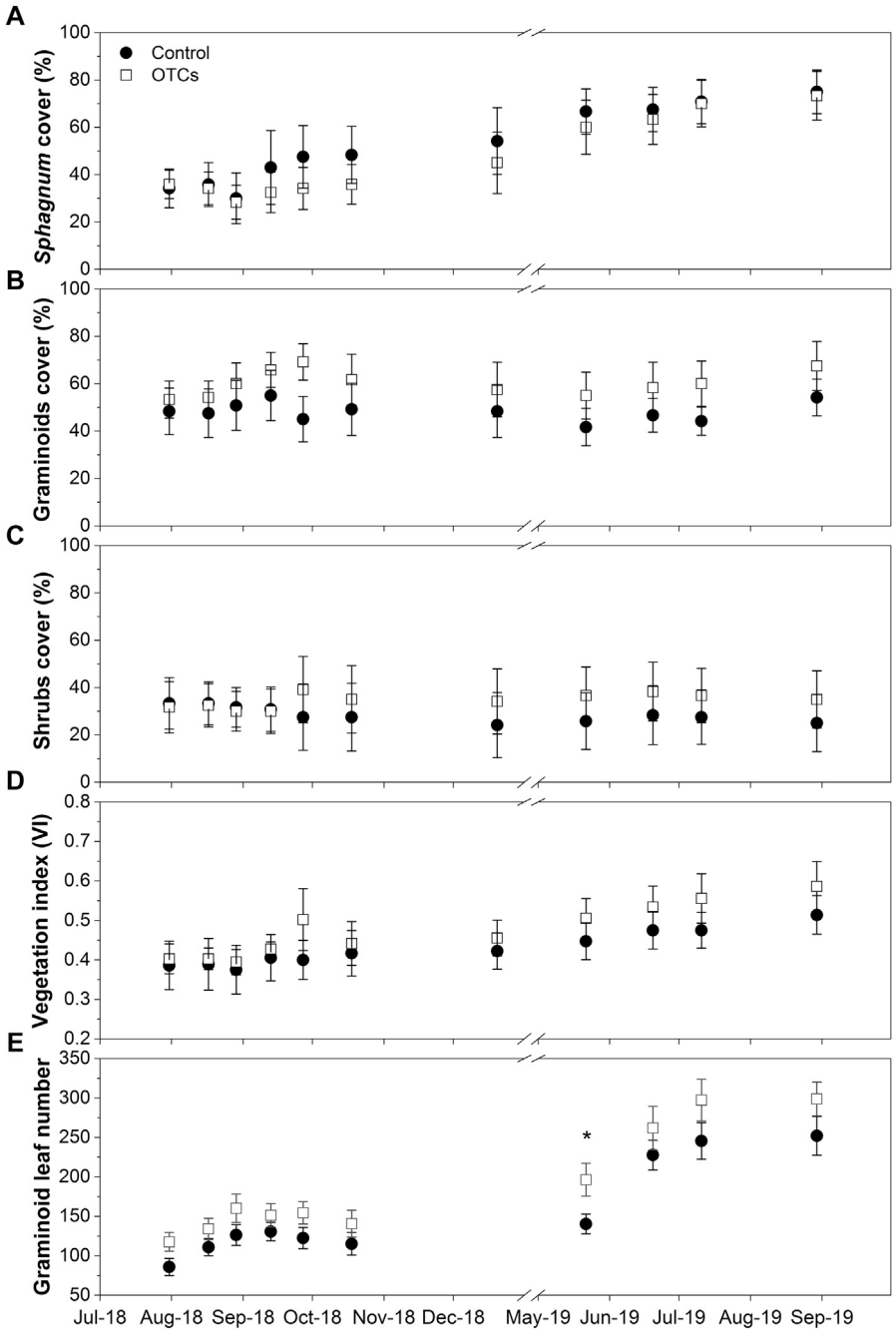

FIGURE 1 | Percentage cover (%) of **(A)** bryophytes (*Sphagnum*), **(B)** graminoids (*Molinia caerulea* and *Eriophorum angustifolium*), and **(C)** ericaceous shrubs (*Erica tetralix* and *Calluna vulgaris* and **(D)** vegetation index (VI) and **(E)** the number of graminoid leaves from August 2018 to September 2019. Significant differences are expressed as $^{*}p < 0.05$, $^{**}p < 0.01$, and $^{***}p < 0.001$.

resulting in an increase of the vegetation index (VI) with time ($p < 0.05$; **Figure 1D**). However, the differences between the two treatments were not significant. The number of graminoid leaves increased significantly with time ($p < 0.05$), and it was significantly higher in OTC plots than in control plots in May 2019 ($p < 0.05$; **Figure 1E**).

Measured CO_2 and CH_4 Fluxes

The GPP, ER, and NEE showed clear seasonal variations with high absolute values during summer and low absolute values during winter (**Figures 2A–C**). Comparing the two treatments, GPP was increased by OTC treatment during EG ($p < 0.001$) and LG ($p < 0.05$) in 2019, while no significant differences were

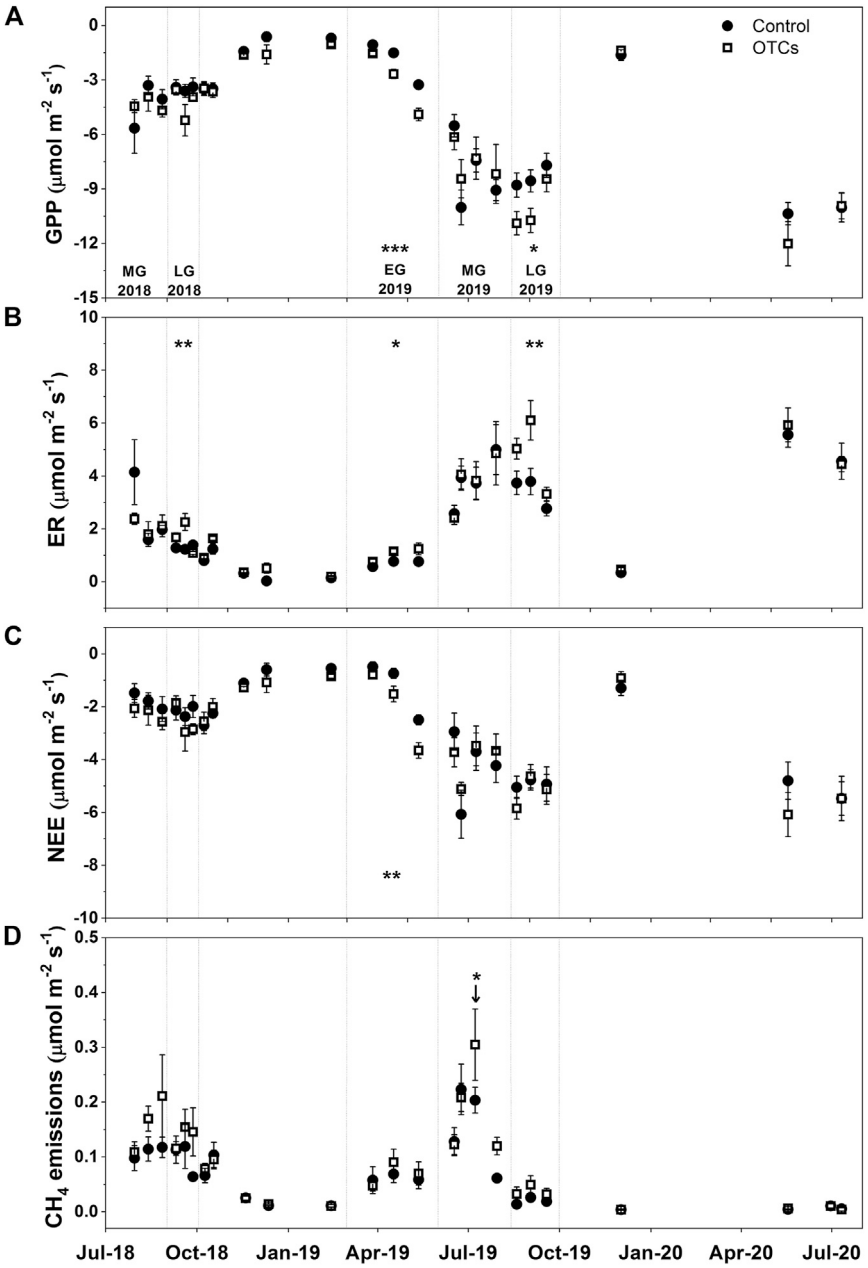

FIGURE 2 | Measured **(A)** GPP (μmol m^{-2} s^{-1}), **(B)** ER (μmol m^{-2} s^{-1}), **(C)** NEE (μmol m^{-2} s^{-}), and **(D)** CH_4 emissions (μmol m^{-2} s^{-1}) from August 2018 to July 2020 in control and OTC plots. Significant differences are expressed as *$p < 0.05$, **$p < 0.01$, and ***$p < 0.001$. Letters indicate different periods of growing season (EG = early growing season, MG = middle growing season, and LG = late growing season).

observed in 2018 ($p = 0.41$), and during MG ($p = 0.60$) and WG in 2019 ($p = 0.21$; **Figure 2A**). ER was increased during LG in 2018 ($p < 0.01$), and EG ($p < 0.05$) and LG in 2019 ($p < 0.01$; **Figure 2B**). NEE was enhanced only during EG in 2019 ($p < 0.01$; **Figure 2C**). CH_4 emissions also showed high values in summer and low values in winter (**Figure 2D**). Nevertheless, low values were also observed during August–September 2019 and May–July 2020 corresponding to the low WTD (below −10 cm; **Supplementary Figure S2A**) in these periods. CH_4 emissions were not significantly affected by warming treatment during any period of growing season (**Figure 2D**), while a significant difference between the two treatments was found when the WTD initially reached to the lowest level, with higher values under OTC treatment than in control ($p < 0.05$; **Figure 2D**).

Modeled CO_2 and CH_4 Fluxes

The GPP, ER, and CH_4 models were calibrated and evaluated for the two treatments separately. Calibration of the models showed

TABLE 2 | Modeled annual cumulated gross primary production (GPP; gC m^{-2} yr^{-1}), ecosystem respiration (ER; gC m^{-2} yr^{-1}), CH_4 emissions (CH_4; gC m^{-2} yr^{-1}), net ecosystem exchange (NEE; gC m^{-2} yr^{-1}), and greenhouse gases carbon budget (GGCB; gC m^{-2} yr^{-1}) from September 2018 to September 2019 in control and OTC plots. Data are presented as mean ± SD, n = 6.

	GPP	ER	CH_4	NEE	GGCB
Control	−501 ± 70	500 ± 102	16 ± 5	−2 ± 83	14 ± 82
OTCs	−602 ± 73	615 ± 171	21 ± 9	13 ± 136	34 ± 137

that the modeled data were in good agreement with the measured data, with high R^2_{adj} (>0.5) and low NRMSE (<70%). Meanwhile, the evaluation results also suggested the good representative of the models to the measured data, with R^2_{adj} higher than 0.8 and NRMSE lower than 42% (except for the CH_4 model which showed an R^2_{adj} < 0.4 and an NRMSE >70%; **Supplementary Table S1**).

Modeled Gross Primary Production

The GPP_{max}, which was calculated using the Michaelis–Menten equation based on the photosynthesis-irradiation curve, exhibited obvious seasonal trends. It ranged from −1.60 to −15.61 μmol m^{-2} s^{-1} for control plots and from −1.96 to −20.26 μmol m^{-2} s^{-1} for OTC plots, with higher photosynthetic capacity during summer and lower during winter (**Supplementary Figure S3A**). GPP_{max} was enhanced

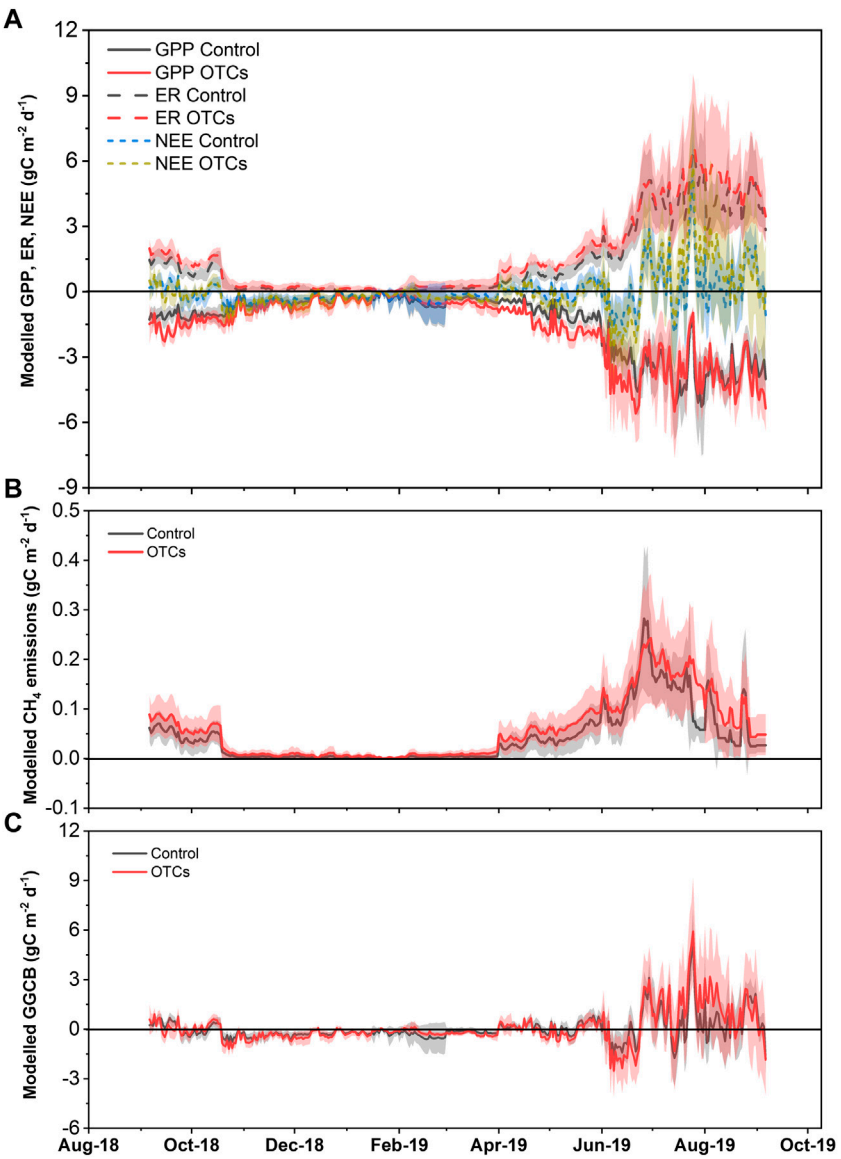

FIGURE 3 | Modeled daily cumulated **(A)** GPP (gC m^{-2} d^{-1}; solid lines), ER (gC m^{-2} d^{-1}; dash lines), NEE (gC m^{-2} d^{-1}; short dash lines), **(B)** CH_4 emissions (gC m^{-2} d^{-1}), and **(C)** greenhouse gas carbon budget (GGCB; gC m^{-2} d^{-1}) from September 2018 to September 2019 in control and OTC plots. Lines indicate the mean values of replicates, and colored shading indicates the error bars of standard deviation.

by OTC treatment in September 2018 and September 2019 (**Supplementary Figure S3A**). A linear relationship between GPP_{max} and the number of graminoid leaves was observed for both treatments (**Supplementary Figure S3B**).

The GPP model was parameterized for each replicate under the two treatments individually. The results showed that the R^2_{adj} of mesocosms ranged from 0.81 to 0.99, and the NRMSE values ranged from 6.0 to 45.3% (**Supplementary Table S2**). Therefore, this model represented the measured GPP well (**Supplementary Figures S4A,B**). The model parameters a and b which represent the sensitivity to vegetation change, and the parameter c which represents the sensitivity to WTD change, all showed similar values between the two treatments (**Supplementary Table S2**). The annual cumulated GPP during September 2018 to September 2019 ranged from −449 to −640 gC m^{-2} yr^{-1} for control plots and from −523 to −719 gC m^{-2} yr^{-1} for OTC plots (**Supplementary Table S2**). Comparing the two treatments, it was significantly higher in OTC plots than in control plots (602 ± 73 vs. 501 ± 70 gC m^{-2} yr^{-1}; p = 0.036; **Table 2**). This result suggested that experimental warming increased the CO_2 input through photosynthesis. In particular, the enhancement of warming on the GPP mainly occurred during April–May 2019 (**Figure 3A**), corresponding to the higher graminoid leaf number under OTC treatment in this period (**Figure 1E**).

Modeled Ecosystem Respiration

The results of parameterizing the ER model for each mesocosm showed that the R^2_{adj} values ranged from 0.58 to 0.95, with the exception of R6 under OTC treatment (R^2_{adj} = 0.06). The NRMSE values ranged from 23.8 to 70.2%, except for R6 under OTC treatment (NRMSE = 104.1%; **Supplementary Table S2**). These results suggested the good agreements between modeled and measured ER values (**Supplementary Figures S4C, D**). The model parameters d, e, and f (represent the sensitivity to WTD, vegetation, and temperature change, respectively) were similar between the two treatments (**Supplementary Table S2**). The annual cumulated ER from September 2018 to September 2019 was 500 ± 102 gC m^{-2} yr^{-1} in control plots (ranging from 354 to 641 gC m^{-2} yr^{-1}) and 615 ± 171 gC m^{-2} yr^{-1} in OTC plots (ranging from 382 to 840 gC m^{-2} yr^{-1}; **Table 2** and **Supplementary Table S2**), but the difference was not significant (p = 0.19; **Figure 3A**).

Modeled CH_4 Emissions

After parameterizing the CH_4 model for each replicate, we found that the R^2_{adj} ranged from 0.82 to 0.97, except R3 under OTCs (R^2_{adj} = 0.44). The NRMSE values ranged between 18.3 and 41.7%, with the exception of R3 under OTCs (NRMSE = 66.7%; **Supplementary Table S2**). Thus, this model represented the measured CH_4 emissions well (**Supplementary Figures S4E, F**). The model parameters g, h, and i (represent the sensitivity to WTD, vegetation, and temperature, respectively) were similar between the two treatments (**Supplementary Table S2**). The modeled annual CH_4 emission ranged from 11 to 22 gC m^{-2} yr^{-1} under control and from 11 to 33 gC m^{-2} yr^{-1} under OTC treatment (**Supplementary Table S2**), with an average of 16 ± 5 and 21 ± 9 gC m^{-2} yr^{-1} in control and OTC plots, respectively (**Table 2**). However, the warming treatment had no significant effect on the annual CH_4 emission (p = 0.83; **Figure 3B**).

Modeled Net Ecosystem Exchange and Greenhouse Gas C Budget

The annual NEE of the control plots showed a slight input of CO_2 (−2 ± 83 gC m^{-2} yr^{-1}) but that of OTC plots exhibited a slight output of CO_2 (13 ± 136 gC m^{-2} yr^{-1}; **Table 2**); however, no significant difference between the two treatments was found (p = 0.83). The annual GGCB showed a release of 14 ± 82 and 34 ± 137 gC m^{-2} yr^{-1} for control and OTC treatment, respectively (**Table 2**). However, the difference was not significant (p = 0.77). Thus, mesocosms under both treatments acted as a C source. Particularly, a strong net C source was found during July–August 2019 for both treatments (**Figure 3C**), corresponding to the low WTD in this period (**Supplementary Figure S2A**). This strong net C source mainly resulted from the net CO_2 source, as NEE showed similar values as GGCB during this period (**Figure 3A**), while CH_4 emissions only accounted for 0.9–2.2% in the total C fluxes.

DISCUSSION

Climate Regime and Vegetation Control on the CO_2 Fluxes

On the whole, the annual GPP (~450–720 gC m^{-2} yr^{-1}) and ER (~350–840 gC m^{-2} yr^{-1}; **Supplementary Table S2**) in the present study were higher than those from boreal peatlands, which showed the GPP and ER fluxes between 100 and 500 gC m^{-2} yr^{-1} (e.g., Cliche Trudeau et al., 2014; Peichl et al., 2014). This may be caused by the differences in climate regime, particularly by the higher annual temperature in our study site than in sites at higher latitudes. While when compared to studies conducted under the same climatic condition, our values were lower. In the same site (La Guette peatland) where our mesocosms were collected, D'Angelo et al. (2021) reported the GPP and ER were all above 1,000 gC m^{-2} yr^{-1} with *in situ* measurements. In addition, Leroy et al. (2019) estimated an annual GPP of 1,300 gC m^{-2} yr^{-1} and ER of 1,000 gC m^{-2} yr^{-1} in mesocosms dominated by *Molinia caerulea* collected from La Guette peatland. This could be attributed to the differences in vegetation. La Guette peatland was almost entirely invaded by *Molinia caerulea* (Gogo et al., 2011). Thus, the percentage cover of *Molinia* in both field and *Molinia*-dominated mesocosms was higher than that of our mesocosms. The GPP of graminoids was higher than that of shrubs and bryophytes, and the GPP of graminoid-dominated peatlands was similar with those of temperate grasslands (Rydin and Jeglum, 2013; Leroy et al., 2019). Therefore, compared with the results of D'Angelo et al. (2021) and Leroy et al. (2019), the lower GPP observed in our study could be attributed to the lower abundance of graminoids. This was supported by the fact that mesocosms with only *Sphagnum* had a lower GPP and ER (400 and 380 gC m^{-2} yr^{-1}, respectively, Leroy et al., 2019) than those in our study. In addition, the positive relationship between GPP_{max} and the number of graminoid leaves also confirmed the strong effect of graminoid abundance on GPP (**Supplementary Figure S3B**). The lower ER observed in our study can also be attributed to the

lower abundance of graminoids. *Molinia caerulea* has an extensive root system, which is larger than that of other species. Thus, the lower abundance of this species compared with previous studies could induce lower root and leaf respiration in our mesocosms.

Stimulation of Experimental Warming on the Gross Primary Production

In previous studies, the effect of temperature rise on GPP varied from increasing (e.g., Chivers et al., 2009) to decreasing (e.g., Voigt et al., 2017) or no effect (e.g., Johnson et al., 2013; Laine et al., 2019), depending on the peatland type and initial vegetation composition. In our research, the warming treatment significantly increased the annual cumulated GPP of mesocosms from 500 to 615 $gC\,m^{-2}\,yr^{-1}$ (**Table 2**). The enhancement mainly occurred during April–May 2019 (**Figure 3A**), when the number of graminoid leaves was higher under warming treatment than that in control (**Figure 1E**). Experimental warming facilitated the growth of graminoids, thus increasing the plant biomass (evidenced by the higher leaf number). The increase of plant biomass in turn increased the capacity of vegetation to withdraw CO_2 from the atmosphere (higher GPP). Our result of a significant correlation between GPP_{max} and graminoid leaf number (**Supplementary Figure S3B**) confirmed this statement. In addition, Tuittila et al. (2004) found that the GPP of *Sphagnum* increased with the water content. In our study, the *Sphagnum* at 5 cm depth was wetter under OTC treatment than that under control during summer (**Supplementary Figure S2B**), probably caused by the lower wind presence and speed in OTCs than in ambient environment, which reduced the evapotranspiration. Thus, the higher water content of *Sphagnum* in OTC plots may also have contributed to the higher GPP under warming treatment.

Water Table Depth Modulates the Ecosystem Respiration Response to Warming

The warming treatment had no significant effect on the annual cumulated ER in our research. This result was inconsistent with previous studies which reported an increase of ER with temperature (e.g., Updegraff et al., 2001; Chivers et al., 2009; Voigt et al., 2017; Samson et al., 2018). Laine et al. (2019) found a low temperature sensitivity of ER under the wet condition. In their study, warming had no significant effect on ER under the ambient wet condition, while ER was significantly increased by moderate warming under the dry condition. The low temperature sensitivity of ER under the wet condition may be attributed to the low temperature sensitivity of soil respiration as it was reported to be less sensitive to temperature change under the anaerobic than aerobic condition (Szafranek-Nakonieczna and Stepniewska, 2014). Meanwhile, Chen et al. (2018) found a positive relationship between the temperature sensitivity (Q_{10}) of soil respiration and the soil redox potential, which confirmed this result. In our study, the mean WTD throughout the monitoring was −6.80 and −6.68 cm for control and OTC treatment, respectively (**Table 1**). The WTD was mostly above −5 cm except during summer (**Supplementary Figure S2A**), suggesting a dominant anaerobic condition in our mesocosms. Therefore, the water saturated condition may lead to a low temperature sensitivity of soil respiration and thus a similar ER under both treatments.

Water Table Depth Dependence of CH_4 Emissions

The annual cumulated CH_4 emission in our results was lower than 33 $gC\,m^{-2}\,yr^{-1}$ found by Leroy et al. (2019), with mesocosms collected from the same peatland. This was caused by the lower WTD in our mesocosms (**Supplementary Figure S2A**) than in their experiment. During our monitoring, WTD reached to a level below −15 cm during July–September 2019, while it remained above −10 cm most of the time in their experiment (data in Leroy et al., 2017). WTD has been reported to be a stronger regulator on CH_4 emissions than temperature (Roulet et al., 1992; Turetsky et al., 2008). When the WTD decreased, the amount of water-saturated (i.e., anaerobic) peat decreased and the aerobic layer increased. Thus, the oxidation of CH_4 was promoted. In our study, the correlation between CH_4 emissions and temperature was only found when WTD ranged between 0 and −9 cm. However, when WTD dropped below −9 cm, CH_4 emissions were independent of temperature (**Figure 2D**). This result confirmed the controlling of WTD on CH_4 emissions. In our results of the measured CH_4 emissions, the enhancement of CH_4 emission by warming treatment was only found when WTD initially reached the lowest level (**Figure 2D**). Thus, warming alone may have only a slight effect on the CH_4 emissions, while if warming interacted with WTD dropdown, their interaction could have a significant effect on the CH_4 emissions (Munir and Strack, 2014).

Temperature and Water Table Depth Modulate the Peatland Functioning

Previous research showed that the peatlands varied from C sink (e.g., Koehler et al., 2011; Nilsson et al., 2008; Roulet et al., 2007) to C source (e.g., Waddington and Roulet, 2000; Voigt et al., 2017). In our study, the C balance of individual mesocosm showed large variations ranging from gaseous C sink to the source, with an average of 14 and 34 $gC\,m^{-2}\,yr^{-1}$ output of C under control and OTC treatment, respectively (**Table 2**). The La Guette peatland also acted as a C source with an output of 220 $gC\,m^{-2}\,yr^{-1}$ between 2013 and 2014. The stronger C source in the field than our mesocosms was linked to the repeated droughts in the previous years (D'Angelo et al., 2021). However, in the study of Leroy et al. (2019), both *Sphagnum* and *Molinia caerulea* dominated mesocosms collected from this peatland acted as gaseous C sink. This difference may be caused by the low WTD in our mesocosms during summer (**Supplementary Figure S2A**). We found that the mesocosms under both treatments showed high positive NEE

values during July–September 2019 (**Figure 3A**), suggesting a strong CO_2 source. This strong CO_2 source corresponded to the low WTD in this period (**Supplementary Figure S2A**). The low WTD induced a higher respiration under the aerobic condition. Thus, the ER exceeded GPP and led to a net CO_2 release. The CH_4 emissions decreased following the decline of WTD, while it only accounted for 0.9–2.2% of the total C fluxes. Therefore, the net C losses in our study were mainly driven by the net CO_2 output. The controlling of WTD on the CO_2 exchange was in accordance with the findings of Laine et al. (2019), who observed a decreasing CO_2 uptake with low WTD due to the increase of CO_2 release as a result of the increased OM decomposition.

Hanson et al. (2020) have found that an air temperature increase of 2.25–9°C enhanced the net C source of peatland during 3 years of monitoring. Bridgham et al. (2008) conducted a 7-year monitoring, and the results showed that a soil warming of 1.6–4.1°C significantly reduced the C accumulation of peatland. Bragazza et al. (2016) also observed a reduction of peatland C accumulation with 5°C air temperature increase during 3 years. Compared with our study, these studies which found an impact of warming on the C budget of peatlands always have a stronger temperature increase than our study (0.9°C increase in air temperature; 1.35 and 0.95°C increase in soil temperature at 5 and 15 cm depths, respectively) or longer time warming treatment. With moderate warming (+0.7°C soil warming at 2 cm depth) for 2 years like in our study, Chivers et al. (2009) found that warming did not modify the C balance of peatland. In addition, there was another research that found the C sink of peatland can be enhanced by manipulated warming (about 1°C air temperature increase; Munir et al., 2015). This was caused by the enhanced growth of shrubs by warming in their treed bog. It has been demonstrated that the response of GHG emissions to warming largely depended on the vegetation composition and environmental conditions of the study site, as well as the warming methods, the warming rate, and the duration of the experiment (Gong et al., 2020). Any difference in these factors could lead to contrasting results. In our study, we found that a temperate peatland which has suffered a vegetation shift from *Sphagnum* to vascular plants dominance remained stable in response to short-term moderate warming. However, as the vascular plants could benefit more from warming than *Sphagnum* (Bragazza et al., 2013; Buttler et al., 2015; Dieleman et al., 2015), a vegetation structure change under long-term warming is expected, which may lead to a modification of C balance in the future.

CONCLUSION

In our study, the CO_2 and CH_4 fluxes of mesocosms collected from a temperate peatland were monitored and modeled using abiotic and biotic factors, including temperature, WTD, and vegetation. Models based on these variables described the measured data well. The modeled results showed that the experimental warming significantly enhanced the annual CO_2 uptake through photosynthesis but had no effect on the ER and CH_4 emissions. The increase of photosynthesis was attributed to the faster growth of graminoids under warming treatment during the early growing season. The mesocosms under both treatments acted as a gaseous C source, and it was caused by the net CO_2 release during a low WTD period in summer. The gaseous C balance remained stable under the 2 years of moderate warming. Our study demonstrated the strong effect of moderate warming on the gaseous C fluxes of temperate peatlands. Moreover, we emphasized the necessity of integrating the WTD and vegetation change along with warming to determine the effect of their interactions on the peatland C fluxes. Further studies of long-term monitoring with a consideration of climate induced both abiotic and biotic factors will be needed to better estimate the feedback of peatlands to global changes as well as its magnitude.

DATA AVAILABILITY STATEMENT

The raw data supporting the conclusion of this article will be made available by the authors, without undue reservation.

AUTHOR CONTRIBUTIONS

QL, SG, and FL-D designed and prepared the experiment. QL collected data. CG helped on the CH_4 measurements. QL, SG, and FL performed the data treatment and modeling. QL wrote the article with the help of all coauthors.

FUNDING

This article is a contribution to the research conducted in the Labex VOLTAIRE (ANR-10-LABX-100-01). This work was funded as part of the CAREX project supported by the Loire Valley Center Region and the FEDER. The study was undertaken in the framework of the French Peatland Observatory, SNO Tourbières, accredited by CNRS-INSU.

ACKNOWLEDGMENTS

The authors would like to thank J-B. Paroissien for help on the R script for data treatment, E. Salmon and L. Jourdain for their suggestions on the modeling of CH_4 fluxes, A-J. Francez from ECOBIO Université de Rennes1 for the help of sampling mesocosms, L. Perdereau for his help in programming the dataloggers, and E. Mochado and X-L. Liu for their help in setting up the mesocosms. We also thank Elizabeth Rowley-Jolivet for English language editing.

SUPPLEMENTARY MATERIAL

The Supplementary Material for this article can be found online at: https://www.frontiersin.org/articles/10.3389/feart.2021.631368/full#supplementary-material

REFERENCES

AminiTabrizi, R., Wilson, R. M., Fudyma, J. D., Hodgkins, S. B., Heyman, H. M., Rich, V. I., et al. (2020). Controls on Soil Organic Matter Degradation and Subsequent Greenhouse Gas Emissions across a Permafrost Thaw Gradient in Northern Sweden. *Front. Earth Sci.* 8, 381. doi:10.3389/feart.2020.557961

Aronson, E. L., and McNulty, S. G. (2009). Appropriate Experimental Ecosystem Warming Methods by Ecosystem, Objective, and Practicality. *Agric. For. Meteorology* 149, 1791–1799. doi:10.1016/j.agrformet.2009.06.007

Aurela, M., Laurila, T., and Tuovinen, J.-P. (2004). The Timing of Snow Melt Controls the Annual CO2balance in a Subarctic Fen. *Geophys. Res. Lett.* 31, L16119. doi:10.1029/2004GL020315

Berendse, F., Van Breemen, N., Rydin, H., Buttler, A., Heijmans, M., Hoosbeek, M. R., et al. (2001). Raised Atmospheric CO2 Levels and Increased N Deposition Cause Shifts in Plant Species Composition and Production in Sphagnum Bogs. *Glob. Change Biol.* 7, 591–598. doi:10.1046/j.1365-2486.2001.00433.x

Bortoluzzi, E., Epron, D., Siegenthaler, A., Gilbert, D., and Buttler, A. (2006). Carbon Balance of a European Mountain Bog at Contrasting Stages of Regeneration. *New Phytol.* 172, 708–718. doi:10.1111/j.1469-8137.2006.01859.x

Bragazza, L., Buttler, A., Robroek, B. J. M., Albrecht, R., Zaccone, C., Jassey, V. E. J., et al. (2016). Persistent High Temperature and Low Precipitation Reduce Peat Carbon Accumulation. *Glob. Change Biol.* 22, 4114–4123. doi:10.1111/gcb.13319

Bragazza, L., Buttler, A., Siegenthaler, A., and Mitchell, E. A. D. (2009). Plant Litter Decomposition and Nutrient Release in Peatlands. *GMS* 184, 99–110. doi:10.1029/2008GM000815

Bragazza, L., Parisod, J., Buttler, A., and Bardgett, R. D. (2013). Biogeochemical Plant-Soil Microbe Feedback in Response to Climate Warming in Peatlands. *Nat. Clim Change* 3, 273–277. doi:10.1038/nclimate1781

Bridgham, S. D., Pastor, J., Dewey, B., Weltzin, J. F., and Updegraff, K. (2008). Rapid Carbon Response of Peatlands to Climate Change. *Ecology* 89, 3041–3048. doi:10.1890/08-0279.1

Bubier, J. L., Moore, T. R., and Bledzki, L. A. (2007). Effects of Nutrient Addition on Vegetation and Carbon Cycling in an Ombrotrophic Bog. *Glob. Change Biol.* 13, 1168–1186. doi:10.1111/j.1365-2486.2007.01346.x

Buttler, A., Robroek, B. J. M., Laggoun-Défarge, F., Jassey, V. E. J., Pochelon, C., Bernard, G., et al. (2015). Experimental Warming Interacts with Soil Moisture to Discriminate Plant Responses in an Ombrotrophic Peatland. *J. Veg. Sci.* 26, 964–974. doi:10.1111/jvs.12296

Chen, H., Zou, J., Cui, J., Nie, M., and Fang, C. (2018). Wetland Drying Increases the Temperature Sensitivity of Soil Respiration. *Soil Biol. Biochem.* 120, 24–27. doi:10.1016/j.soilbio.2018.01.035

Chivers, M. R., Turetsky, M. R., Waddington, J. M., Harden, J. W., and McGuire, A. D. (2009). Effects of Experimental Water Table and Temperature Manipulations on Ecosystem CO2 Fluxes in an Alaskan Rich Fen. *Ecosystems* 12, 1329–1342. doi:10.1007/s10021-009-9292-y

Cliche Trudeau, N., Garneau, M., and Pelletier, L. (2014). Interannual Variability in the CO2 Balance of a Boreal Patterned Fen, James Bay, Canada. *Biogeochemistry* 118, 371–387. doi:10.1007/s10533-013-9939-9

D'Angelo, B., Leroy, F., Guimbaud, C., Jacotot, A., Zocatelli, R., Gogo, S., et al. (2021). Carbon Balance and Spatial Variability of CO_2 and CH_4 Fluxes in a *Sphagnum*-Dominated Peatland in a Temperate Climate. *Wetlands* 41, 5. doi:10.1007/s13157-021-01411-y

Dieleman, C. M., Branfireun, B. A., McLaughlin, J. W., and Lindo, Z. (2015). Climate Change Drives a Shift in Peatland Ecosystem Plant Community: Implications for Ecosystem Function and Stability. *Glob. Change Biol.* 21, 388–395. doi:10.1111/gcb.12643

Dieleman, C. M., Lindo, Z., McLaughlin, J. W., Craig, A. E., and Branfireun, B. A. (2016). Climate Change Effects on Peatland Decomposition and Porewater Dissolved Organic Carbon Biogeochemistry. *Biogeochemistry* 128, 385–396. doi:10.1007/s10533-016-0214-8

Dorrepaal, E., Cornelissen, J. H. C., Aerts, R., Wallén, B., and Van Logtestijn, R. S. P. (2005). Are Growth Forms Consistent Predictors of Leaf Litter Quality and Decomposability across Peatlands along a Latitudinal Gradient?. *J. Ecol.* 93, 817–828. doi:10.1111/j.1365-2745.2005.01024.x

Dorrepaal, E., Toet, S., van Logtestijn, R. S. P., Swart, E., van de Weg, M. J., Callaghan, T. V., et al. (2009). Carbon Respiration from Subsurface Peat Accelerated by Climate Warming in the Subarctic. *Nature* 460, 616–619. doi:10.1038/nature08216

Dunfield, P., Knowles, R., Dumont, R., and Moore, T. (1993). Methane Production and Consumption in Temperate and Subarctic Peat Soils: Response to Temperature and pH. *Soil Biol. Biochem.* 25, 321–326. doi:10.1016/0038-0717(93)90130-4

Flanagan, L. B., and Syed, K. H. (2011). Stimulation of Both Photosynthesis and Respiration in Response to Warmer and Drier Conditions in a Boreal Peatland Ecosystem. *Glob. Change Biol.* 17, 2271–2287. doi:10.1111/j.1365-2486.2010.02378.x

Gavazov, K., Albrecht, R., Buttler, A., Dorrepaal, E., Garnett, M. H., Gogo, S., et al. (2018). Vascular Plant-Mediated Controls on Atmospheric Carbon Assimilation and Peat Carbon Decomposition under Climate Change. *Glob. Change Biol.* 24, 3911–3921. doi:10.1111/gcb.14140

Girkin, N. T., Turner, B. L., Ostle, N., Craigon, J., and Sjögersten, S. (2018). Root Exudate Analogues Accelerate CO2 and CH4 Production in Tropical Peat. *Soil Biol. Biochem.* 117, 48–55. doi:10.1016/j.soilbio.2017.11.008

Gogo, S., Laggoun-Défarge, F., Delarue, F., and Lottier, N. (2011). Invasion of a *Sphagnum*-Peatland by *Betula Spp* and *Molinia Caerulea* Impacts Organic Matter Biochemistry. Implications for Carbon and Nutrient Cycling. *Biogeochemistry* 106, 53–69. doi:10.1007/s10533-010-9433-6

Gogo, S., Laggoun-Défarge, F., Merzouki, F., Mounier, S., Guirimand-Dufour, A., Jozja, N., et al. (2016). *In Situ* and Laboratory Non-additive Litter Mixture Effect on C Dynamics of *Sphagnum Rubellum* and *Molinia Caerulea* Litters. *J. Soils Sediments* 16, 13–27. doi:10.1007/s11368-015-1178-3

Gong, Y., Wu, J., Vogt, J., and Ma, W. (2020). Greenhouse Gas Emissions from Peatlands under Manipulated Warming, Nitrogen Addition, and Vegetation Composition Change: a Review and Data Synthesis. *Environ. Rev.* 28, 428–437. doi:10.1139/er-2019-0064

Gorham, E. (1991). Northern Peatlands: Role in the Carbon Cycle and Probable Responses to Climatic Warming. *Ecol. Appl.* 1, 182–195. doi:10.2307/1941811

Hanson, P. J., Griffiths, N. A., Iversen, C. M., Norby, R. J., Sebestyen, S. D., Phillips, J. R., et al. (2020). Rapid Net Carbon Loss from a Whole-Ecosystem Warmed Peatland. *AGU Adv.* 1, e2020AV000163. doi:10.1029/2020AV000163

Intergovernmental Panel on Climate Change (2014). *Climate Change 2014: The Physical Science Basis: Working Group I Contribution to the Fifth Assessment Report of the Intergovernmental Panel on Climate Change*. Cambridge: Cambridge University Press.

Jackson, R. B., Lajtha, K., Crow, S. E., Hugelius, G., Kramer, M. G., and Piñeiro, G. (2017). The Ecology of Soil Carbon: Pools, Vulnerabilities, and Biotic and Abiotic Controls. *Annu. Rev. Ecol. Evol. Syst.* 48, 419–445. doi:10.1146/annurev-ecolsys-112414-054234

Johnson, C. P., Pypker, T. G., Hribljan, J. A., and Chimner, R. A. (2013). Open Top Chambers and Infrared Lamps: A Comparison of Heating Efficacy and CO2/CH4 Dynamics in a Northern Michigan Peatland. *Ecosystems* 16, 736–748. doi:10.1007/s10021-013-9646-3

Johnson, K. A., and Goody, R. S. (2011). The Original Michaelis Constant: Translation of the 1913 Michaelis-Menten Paper. *Biochemistry* 50, 8264–8269. doi:10.1021/bi201284u

Kandel, T. P., Elsgaard, L., and Laerke, P. E. (2013). Measurement and Modelling of CO2flux from a Drained Fen Peatland Cultivated with Reed Canary Grass and spring Barley. *GCB Bioenergy* 5, 548–561. doi:10.1111/gcbb.12020

Koehler, A.-K., Sottocornola, M., and Kiely, G. (2011). How strong Is the Current Carbon Sequestration of an Atlantic Blanket Bog?. *Glob. Change Biol.* 17, 309–319. doi:10.1111/j.1365-2486.2010.02180.x

Laine, A., Wilson, D., Kiely, G., and Byrne, K. A. (2007). Methane Flux Dynamics in an Irish lowland Blanket Bog. *Plant Soil* 299, 181–193. doi:10.1007/s11104-007-9374-6

Laine, A. M., Mäkiranta, P., Laiho, R., Mehtätalo, L., Penttilä, T., Korrensalo, A., et al. (2019). Warming Impacts on Boreal Fen CO 2 Exchange under Wet and Dry Conditions. *Glob. Change Biol.* 25, 1995–2008. doi:10.1111/gcb.14617

Leifeld, J., Wüst-Galley, C., and Page, S. (2019). Intact and Managed Peatland Soils as a Source and Sink of GHGs from 1850 to 2100. *Nat. Clim. Change* 9, 945–947. doi:10.1038/s41558-019-0615-5

Leroy, F., Gogo, S., Guimbaud, C., Bernard-Jannin, L., Hu, Z., and Laggoun-Défarge, F. (2017). Vegetation Composition Controls Temperature Sensitivity

of CO2 and CH4 Emissions and DOC Concentration in Peatlands. *Soil Biol. Biochem.* 107, 164–167. doi:10.1016/j.soilbio.2017.01.005

Leroy, F., Gogo, S., Guimbaud, C., Bernard-Jannin, L., Yin, X., Belot, G., et al. (2019). CO2 and CH4 Budgets and Global Warming Potential Modifications in Sphagnum-Dominated Peat Mesocosms Invaded by Molinia Caerulea. *Biogeosciences* 16, 4085–4095. doi:10.5194/bg-16-4085-2019

Lloyd, J., and Taylor, J. A. (1994). On the Temperature Dependence of Soil Respiration. *Funct. Ecol.* 8, 315–323. doi:10.2307/2389824

Mahadevan, P., Wofsy, S. C., Matross, D. M., Xiao, X., Dunn, A. L., Lin, J. C., et al. (2008). A Satellite-Based Biosphere Parameterization for Net Ecosystem CO2exchange: Vegetation Photosynthesis and Respiration Model (VPRM). *Glob. Biogeochem. Cycles* 22, GB2005. doi:10.1029/2006GB002735

Marion, G. M., Henry, G. H. R., Freckman, D. W., Johnstone, J., Jones, G., Jones, M. H., et al. (1997). Open-top Designs for Manipulating Field Temperature in High-Latitude Ecosystems. *Glob. Change Biol.* 3, 20–32. doi:10.1111/j.1365-2486.1997.gcb136.x

Medlyn, B. E., Dreyer, E., Ellsworth, D., Forstreuter, M., Harley, P. C., Kirschbaum, M. U. F., et al. (2002). Temperature Response of Parameters of a Biochemically Based Model of Photosynthesis. II. A Review of Experimental Data. *Plant Cell Environ* 25, 1167–1179. doi:10.1046/j.1365-3040.2002.00891.x

Munir, T. M., Perkins, M., Kaing, E., and Strack, M. (2015). Carbon Dioxide Flux and Net Primary Production of a Boreal Treed Bog: Responses to Warming and Water-Table-Lowering Simulations of Climate Change. *Biogeosciences* 12, 1091–1111. doi:10.5194/bg-12-1091-2015

Munir, T. M., and Strack, M. (2014). Methane Flux Influenced by Experimental Water Table Drawdown and Soil Warming in a Dry Boreal continental Bog. *Ecosystems* 17, 1271–1285. doi:10.1007/s10021-014-9795-z

Nilsson, M., Sagerfors, J., Buffam, I., Laudon, H., Eriksson, T., Grelle, A., et al. (2008). Contemporary Carbon Accumulation in a Boreal Oligotrophic Minerogenic Mire - a Significant Sink after Accounting for All C-Fluxes. *Glob. Change Biol.* 14, 2317–2332. doi:10.1111/j.1365-2486.2008.01654.x

Peichl, M., Öquist, M., Ottosson Löfvenius, M., Ilstedt, U., Sagerfors, J., Grelle, A., et al. (2014). A 12-year Record Reveals Pre-growing Season Temperature and Water Table Level Threshold Effects on the Net Carbon Dioxide Exchange in a Boreal Fen. *Environ. Res. Lett.* 9, 055006. doi:10.1088/1748-9326/9/5/055006

Raich, J. W., Rastetter, E. B., Melillo, J. M., Kicklighter, D. W., Steudler, P. A., Peterson, B. J., et al. (1991). Potential Net Primary Productivity in South America: Application of a Global Model. *Ecol. Appl. Publ. Ecol. Soc. Am.* 1, 399–429. doi:10.2307/1941899

Roulet, N., Moore, T., Bubier, J., and Lafleur, P. (1992). Northern Fens: Methane Flux and Climatic Change. *Tellus B* 44, 100–105. doi:10.1034/j.1600-0889.1992.t01-1-00002.x

Roulet, N. T., Lafleur, P. M., Richard, P. J. H., Moore, T. R., Humphreys, E. R., and Bubier, J. (2007). Contemporary Carbon Balance and Late Holocene Carbon Accumulation in a Northern Peatland. *Glob. Change Biol.* 13, 397–411. doi:10.1111/j.1365-2486.2006.01292.x

R Core Team (2020). *A Language and Environment for Statistical Computing*. Vienna, Austria: R Foundation for Statistical Computing.

Rydin, H., and Jeglum, J. K. (2013). *The Biology of Peatlands*. 2e. Oxford: Oxford University Press.

Samson, M., Słowińska, S., Słowiński, M., Lamentowicz, M., Barabach, J., Harenda, K., et al. (2018). The Impact of Experimental Temperature and Water Level Manipulation on Carbon Dioxide Release in a Poor Fen in Northern Poland. *Wetlands* 38, 551–563. doi:10.1007/s13157-018-0999-4

Segers, R. (1998). Methane Production and Methane Consumption: a Review of Processes Underlying Wetland Methane Fluxes. *Biogeochemistry* 41, 23–51. doi:10.1023/A:1005929032764

Strack, M. (2008). *Peatlands and Climate Change*. Saarijärvi, Finland: International Peat Society, Saarijärven Offset Oy.

Straková, P., Niemi, R. M., Freeman, C., Peltoniemi, K., Toberman, H., Heiskanen, I., et al. (2011). Litter Type Affects the Activity of Aerobic Decomposers in a Boreal Peatland More Than Site Nutrient and Water Table Regimes. Available at: https://jukuri.luke.fi/handle/10024/516544 ((Accessed July 23, 2020).

Szafranek-Nakonieczna, A., and Stepniewska, Z. (2014). Aerobic and Anaerobic Respiration in Profiles of Polesie Lubelskie Peatlands. Int. Agrophysics 28. , 2014 Available at: http://yadda.icm.edu.pl/yadda/element/bwmeta1.element.agro-9a68ce86-a247-40f5-ae04-41017c4101d4 (Accessed May 31, 2020).

Thornley, J. H. M., and Johnson, I. R. (1990). Plant and Crop Modelling: a Mathematical Approach to Plant and Crop Physiology. Available at: https://agris.fao.org/agris-search/search.do?recordID=XF2016001523 (Accessed August 3, 2020).

Tuittila, E.-S., Vasander, H., and Laine, J. (2004). Sensitivity of C Sequestration in Reintroduced *Sphagnum* to Water-Level Variation in a Cutaway Peatland. *Restor Ecol.* 12, 483–493. doi:10.1111/j.1061-2971.2004.00280.x

Turetsky, M. R., Treat, C. C., Waldrop, M. P., Waddington, J. M., Harden, J. W., and McGuire, A. D. (2008). Short-term Response of Methane Fluxes and Methanogen Activity to Water Table and Soil Warming Manipulations in an Alaskan Peatland. *J. Geophys. Res.* 113, G00A10. doi:10.1029/2007JG000496

Updegraff, K., Bridgham, S. D., Pastor, J., Weishampel, P., and Harth, C. (2001). Response of CO 2 and CH 4 Emissions from Peatlands to Warming and Water Table Manipulation. *Ecol. Appl.* 11, 311–326. doi:10.2307/3060891

Voigt, C., Lamprecht, R. E., Marushchak, M. E., Lind, S. E., Novakovskiy, A., Aurela, M., et al. (2017). Warming of Subarctic Tundra Increases Emissions of All Three Important Greenhouse Gases - Carbon Dioxide, Methane, and Nitrous Oxide. *Glob. Change Biol.* 23, 3121–3138. doi:10.1111/gcb.13563

Waddington, J. M., Griffis, T. J., and Rouse, W. R. (1998). Northern Canadian Wetlands: Net Ecosystem CO_2 Exchange and Climatic Change. *Clim. Change* 40, 267–275. doi:10.1023/A:1005468920206

Waddington, J. M., and Roulet, N. T. (2000). Carbon Balance of a Boreal Patterned Peatland. *Glob. Change Biol.* 6, 87–97. doi:10.1046/j.1365-2486.2000.00283.x

Ward, S. E., Ostle, N. J., Oakley, S., Quirk, H., Henrys, P. A., and Bardgett, R. D. (2013). Warming Effects on Greenhouse Gas Fluxes in Peatlands Are Modulated by Vegetation Composition. *Ecol. Lett.* 16, 1285–1293. doi:10.1111/ele.12167

Yu, Z., Loisel, J., Brosseau, D. P., Beilman, D. W., and Hunt, S. J. (2010). Global Peatland Dynamics since the Last Glacial Maximum. *Geophys. Res. Lett.* 37, L13402. doi:10.1029/2010GL043584

Conflict of Interest: The authors declare that the research was conducted in the absence of any commercial or financial relationships that could be construed as a potential conflict of interest.

frontiers in Earth Science

ORIGINAL RESEARCH
published: 21 July 2021
doi: 10.3389/feart.2021.650662

Peat Carbon Vulnerability to Projected Climate Warming in the Hudson Bay Lowlands, Canada: A Decision Support Tool for Land Use Planning in Peatland Dominated Landscapes

James W. McLaughlin and Maara S. Packalen*

Ontario Forest Research Institute, Science and Research Branch, Ontario Ministry of Natural Resources and Forestry, Sault Ste Marie, ON, Canada

Peatlands help regulate climate by sequestering (net removal) carbon from the atmosphere and storing it in plants and soils. However, as mean annual air temperature (MAAT) increases, peat carbon stocks may decrease. We conducted an in-depth synthesis of current knowledge about ecosystem controls on peatland carbon storage and fluxes to constrain the most influential parameters in probabilistic modelling of peat carbon sinks, such as Bayesian belief networks. Evaluated parameters included climate, carbon flux and mass, land cover, landscape position (defined here as elevation), fire records, and current and future climate scenarios for a 74,300 km^2 landscape in the Hudson Bay Lowlands, Canada. The Bayesian belief network was constructed with four tiers: 1) exposure, expressed as MAAT, and the state variables of elevation and land cover; 2) sensitivity, expressed as ecosystem conditions relevant to peat carbon mass and its quality for decomposition, peat wetness, and fire; 3) carbon dioxide and methane fluxes and peat combustion; and 4) vulnerability of peat carbon sink strength under warmer MAAT. Simulations were conducted using current (–3.0 to 0.0°C), moderately warmer (0.1–4.0°C), and severely warmer (4.1–9.0°C) climate scenarios. Results from the severely warmer climate scenario projected an overall drying of peat, with approximately 20% reduction in the strong sink categories of net ecosystem exchange and peat carbon sink strength for the severely and, to a lesser degree, the moderately warmer climate scenarios relative to current MAAT. In the warmest temperature simulation, probability of methane emission decreased slightly and the probability of the strong peat carbon sink strength was 27% lower due to peat combustion. Our Bayesian belief network can assist land planners in decision-making for peatland-dominated landscapes, such as identifying high carbon storage areas and those projected to be at greatest risk of carbon loss due to climate change. Such areas may be designated, for example, as protected or reduced management intensity. The Bayesian belief network presented here is built on an in-depth knowledge synthesis to construct conditional probability tables, so is expected to apply to other peatland-dense jurisdictions by changing only elevation, peatland types, and MAAT.

Keywords: hudson bay lowlands, moisture index, climate warming, peat carbon vulnerability, probabilistic modelling, land use planning

OPEN ACCESS

Edited by:
Line Rochefort,
Laval University, Canada

Reviewed by:
Julie Loisel,
Texas A&M University, United States
Hongjun Wang,
Duke University, United States

****Correspondence:***
James W. McLaughlin
jim.mclaughlin@ontario.ca

Specialty section:
This article was submitted to Biogeoscience, a section of the journal Frontiers in Earth Science

Received: *07 January 2021*
Accepted: *05 July 2021*
Published: *21 July 2021*

Citation:
McLaughlin JW and Packalen MS (2021) Peat Carbon Vulnerability to Projected Climate Warming in the Hudson Bay Lowlands, Canada: A Decision Support Tool for Land Use Planning in Peatland Dominated Landscapes. Front. Earth Sci. 9:650662. doi: 10.3389/feart.2021.650662

INTRODUCTION

Peatlands (40 cm or more of peat accumulation) supply many ecosystem functions that maintain values or provide services beneficial to people, such as climate regulation (Bonn et al., 2016). Many beneficial services in the boreal and subarctic regions center around the accumulation, storage, and decomposition of peat. For example, climate regulation by peatlands is partly a consequence of carbon (C) accumulation in peat over the millennia resulting from cold temperatures and wet soils (Gorham, 1991), herein referred to as peat C sink strength, and is the focus of this paper.

Conserving peat C sink strength is a relatively new concept in land use and climate adaptation planning and complicates both the development of planning tools and plan implementation. For example, McLaughlin and Webster (2014) showed peat depth, inception, and age represented long-term factors that influence total amount of peat C at a site, while long term rates of C accumulation (LORCA) represented peat C sink strength over millennia. Longer-term indicators were less likely to change in response to climate change than those with shorter (annual to decadal) C exchange timeframes (e.g., greenhouse gases; GHGs).

Greenhouse gas [i.e., carbon dioxide (CO_2) and methane (CH_4)] fluxes are commonly used indicators in peatland C reporting and monitoring programs (IPCC et al., 2014). Of the C indicators tested, however, GHG fluxes were the least useful for detecting changes in ecosystem conditions, primarily due to small sample sizes and highly variable data (McLaughlin and Webster, 2014). For example, in a synthesis of published research, Frolking et al. (2011) reported uncertainties up to 100% in GHG estimates for peatlands that varied by more than an order of magnitude. Also, the Canadian Model for Peatlands (CaMP) is being considered for peat C inventories to meet Canada's commitments to the United Nations Framework on Climate Change (Bona et al., 2020). However, CaMP overestimated net ecosystem exchange (NEE) of fens by more than 100% relative to site measurements, which was attributed to poorly calibrated decomposition and net primary production coefficients (Bona et al., 2020). In contrast, Roulet et al. (2007) reported contemporary C balance (NEE + CH_4 emission + DOC leaching) collected over 6 years was comparable to LORCA estimates at the Me Bleu Bog, Canada.

Peatland fires may contribute up to 23% of the direct C emissions in Canada (Zoltai et al., 1998; Turquety et al., 2007). While peat ignites at less than 30% moisture (water) content by weight, combustion and vertical or lateral burn expansion can be maintained at moisture contents ranging from 160 to nearly 500% (Chistjakov et al., 1983; Huang and Rein, 2015; Prat-Guitart et al., 2016). Critical thresholds to maintain future background peat moisture content were estimated to be about 25% more precipitation input when air temperatures were 3–4°C warmer than current conditions (Rouse, 1998).

Hydro-climate data, such as mean annual air temperature (MAAT), mean annual precipitation (MAP), and potential evapotranspiration (PET), have effectively explained peatland C sinks and sources at landscape (Beilman et al., 2009; Packalen et al., 2016) and site (Webster et al., 2013; Wu and Roulet, 2014) scales in boreal and sub-arctic regions. Webster et al. (2013) developed a regression equation using hydro-climate data to predict water table level (WTL) in open (i.e., rich and moderately rich) and treed (i.e., poor) fens. In that study, PET was a particularly important influence on WTL, with the latter linked to plant functional types.

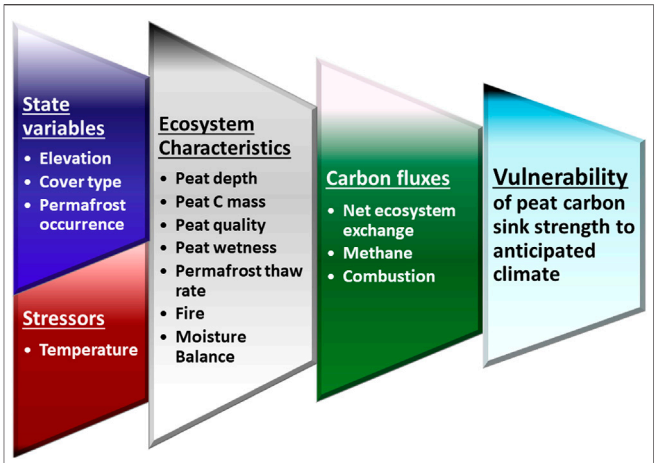

FIGURE 1 | Conceptual framework used in this study to assess vulnerability of peatland carbon to climate change.

Globally, land use planners are considering peat C sinks in large (thousands km^{-2}) tracts of land, and frequently in combination with other ecological and human values (Bonn et al., 2016). Therefore, effective and efficient planning tools need to be scientifically credible, robust, easily applied to landscapes, and amenable to integration with other values of interest by planning teams. A Bayesian belief network (BBN) is a method that simplifies complex ecological processes into basic probabilities of occurrence that can support land use planning to minimize perceived risks to soils in the short and long term (Webster and McLaughlin, 2014). Bayesian belief networks are also amenable to different types of learning, for example, Indigenous social and cultural values, as well as technical based indicators for clean air, soil, and water.

The vulnerability assessment reported here was based on sensitivity and direction of change in peat C sink strength by way of alterations in net CO_2 exchange between peatlands and the atmosphere (defined here as NEE), CH_4 emission, and peat C combustion due to fire using future climate scenarios of the International Panel on Climate Change (IPCC et al., 2014). To construct conditional probability tables that informed the BBN, previously published data were synthesized and new data were analyzed pertaining to C flux and mass, land cover, elevation, fire records, and current and future climate scenarios.

METHODS

Conceptual Framework and Vision

Our conceptual model says geology has been the key driver of peat C sink strength in the Hudson Bay Lowlands throughout the

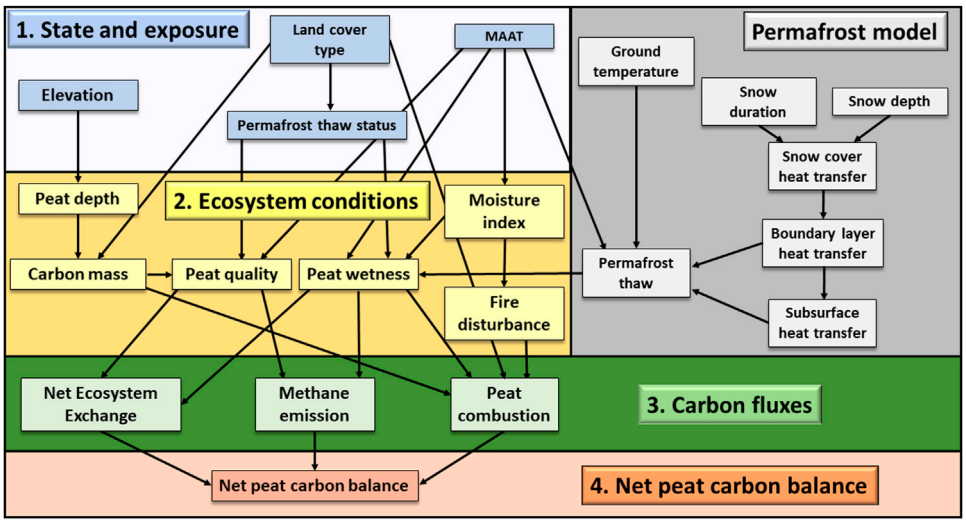

FIGURE 2 | General structure of influence diagram of Bayesian belief network framework for the study area in the southern Hudson Bay Lowlands under current climate. Arrows connect parent nodes to child nodes and black bars indicate state (terminal parent nodes) or probability of influence based on conditional probabilities (child nodes).

Holocene (Packalen et al., 2014; Packalen et al., 2016). However, many poorly documented variables interactively affect peat C sink strength, impeding its use in land planning and policymaking. We grouped interactive variables into a hierarchical framework to conduct a landscape assessment of peat C sink strength (**Figures 1**,**2**). In the Hudson Bay Lowlands, glacial isostatic adjustment of the land during the last 6,000–8,000 years (Mid-Holocene) created elevational gradients that restricted water movement (Andrews and Peltier, 1976; Glaser et al., 2004). Resulting water inundation created anaerobic soils that favored peat initiation, development, and expansion throughout the Mid-Holocene (Hargan et al., 2015). Although a net CO_2 sink during this timeframe, peatlands in the Hudson Bay Lowlands were net CH_4 sources to the atmosphere, the effect of which has been an overall net C sink (Packalen and Finkelstein, 2014; Davies et al., 2021).

During the Late Holocene MAAT warmed, but changes in MAP were marginal. Increasing MAAT and stable MAP contributes to drying conditions (i.e., lower moisture index; MAP/PET) as water demand of plants increases under warmer temperatures (Roulet et al., 1992; Rouse, 1998). Peat drying appears to be occurring faster in bogs than fens (Bunbury et al., 2012; O'Reilly et al., 2014). Furthermore, drier peat is released from anaerobic controls on litter and peat decomposition and replaced by mostly aerobic controls (Laiho, 2006). Elevated decomposition produces more CO_2 that is released to the atmosphere (Preston et al., 2012), with the net balance dependent on ecosystem conditions (**Figures 1**,**2**). Furthermore, the amount and severity of fire may increase CO_2 fluxes, while CH_4 emissions will likely decrease as peat dries (Webster et al., 2018). Combined, higher C fluxes may weaken landscape scale peat C sink strength.

We expect glacial isostatic adjustment to remain the key control of peat C sink strength in future, with bogs drying more rapidly than fens (Bunbury et al., 2012; O'Reilly et al., 2014). Permafrost occurrence has also affected peat C sink strength, with NEE rates near neutrality (**Table 1**). Permafrost occurrence in the study area results primarily from presence of a combination of high elevation and forested or treed bogs (Ou et al., 2016B; Pironkova, 2017). However, collapsing peat and subsequent water inundation create anaerobic soil, enhancing both CH_4 emissions and CO_2 uptake in wetter and warmer peat in thermokarst in future years relative to non-thawed peat (**Table 1**).

To test the conceptual model, we categorized a 74,300 km^2 landscape in the southern Hudson Bay Lowlands (**Figures 3A,B**) by: 1) state variables of elevation, land cover and permafrost occurrence, and stressor variable of MAAT; 2) ecosystem condition was defined by peat depth, C mass, susceptibility to decomposition, wetness, moisture index, permafrost thaw, and fire, all of which depend on their respective state or stressor variables (**Figures 1**,**2**); 3) carbon fluxes defined by CO_2 fluxes from NEE and peat combustion by fires, and CH_4 emissions, all of which depend on ecosystem conditions; and 4) peat C sink strength, which depends on C fluxes. Data sources included climate scenarios, satellite imagery, field sampling, and literature syntheses to inform a probabilistic model known as a BBN to simulate probabilities of change in peat C sink strength for future years as a result of climate change. The power of the BBN lies in user-defined conditional probability tables. To construct these tables, previously published data were synthesized and analyzed pertaining to the state, stressors, ecosystem condition, and C fluxes (**Figures 1**,**2**) in peatlands. Simulations were conducted for three common land cover types in the Hudson Bay Lowlands—bog, fen, permafrost (defined here as palsa, peat plateau, internal lawn, or collapse scar) — to describe baseline and project future conditions using current (−3.0° to 0.0°C), moderately (0.1° to 4.0°C), and severely (4.1° to 9.0°C) warmer scenarios.

TABLE 1 | Range in data for net ecosystem exchange and methane (CH_4) emissions for peatlands north of 45° latitude.

Peatland type	Location	Range in net ecosystem exchange (g C m^{-2} d^{-1})	Range in CH_4 emission (mg C m^{-2} d^{-1})	References
Palsa and plateau	Saskatchewan	—	<0.1	Turetsky et al. (2002)
—	Northwest Territories	0.4 to 0.5	—	Chasmer et al. (2012)
—	Alberta	−0.38	—	Wilson et al. (2017)
—	Alaska	−0.81 to 1.0	−1.6 to 24	Wickland et al. (2006), Myers-Smith et al. (2007), Euskirchen et al. (2014), Mauritz et al. (2014)
—	Finland	—	1.0 to 2.1	Nykanen et al. (2003)
—	Sweden	−0.7 to 0.7	0.5	Bäckstrand et al. (2010), Jackowicz-Korczy ski et al. (2010), Christensen et al. (2012)
—	Siberia	—	−1.1 to 15	Christensen et al. (1995), Flessa et al. (2008)
Bog	Ontario	−2.2 to 0.4	−0.4 to 156	Bubier et al. (1993), Klinger et al. (1994), Moore et al. (1994), Neumann et al. (1994), Bubier, (1995); Lafleur et al. (2003), Roulet et al. (2007), Strilesky and Humphreys (2012), Lai et al. (2014)
—	Québec	−0.9 to 0.3	30 to 65	Trudeau et al. (2013)
—	Saskatchewan	—	<0.1 to 0.1	Turetsky et al. (2002)
—	Alberta	−0.7 to −0.5	—	Munir et al. (2015)
—	Northwest Territories	—	-1 to 160	Liblik et al. (1997)
—	Sweden	−1.22 to 0.73	—	Sagerfors et al. (2008), Bäckstrand et al. (2010)
—	Finland	−2.56 to 20.4	1 to 256	Alm et al. (1999), Nykanen et al. (2003)
—	Siberia	—	150 to 450	Bohn et al. (2007)
—	Estonia	—	12 to 43	Salm et al. (2012)
Fen	Ontario	—	−3 to 128	Roulet et al. (1992), (Bubier et al., 1993), Moore et al. (1994), Bubier (1995)
—	Quebec	—	6 to 190	Strack et al. (2004), Strack et al. (2007)
—	Manitoba	−1.7 to 0.5	6 to 210	Bubier et al. (1995), Schreader et al. (1998)
—	Saskatchewan	−2.6 to 0.7	—	Suyker et al. (1997)
—	Alberta	−2.3 to 0.7	—	Syed et al. (2006), Adkinson et al. (2011)
—	Northwest Territories		1 to 221	Liblik et al. (1997)
—	Alaska	−3.3 to −0.5	18 to 136	Turetsky et al. (2007), Olefeldt et al. (2017)
—	Finland	−4.6 to 1.8	2.0 to 113	Heikkinen et al. (2002), Aurela et al. (2007), Riutta et al. (2007), Leppälä et al. (2011), Peichl et al. (2014), Järveoja et al. (2018)
—	Sweden	−2.1 to 8.1	79 to 118	Ström and Christensen (2007), Erikkson et al. (2010)
Thermokarst	Manitoba	−0.54	9.5 to 50	Bubier et al. (1999), Bellisario et al. (1999)
—	Northwest Territories	—	29 to 160	Liblick et al. (1997), Helbig et al. (2019)
—	Yukon	—	2 to 65	Cooper et al. (2017)
—	Alaska	−21.7 to −0.7	84 to 298	Wickland et al. (2006), Myers-Smith et al. (2007), Euskirchen et al. (2014), Neumann et al. (2019)
—	Finland	−1.1	80 to 234	Nykanen et al. (2003)
—	Sweden	−0.5 to 0.3	87 to 137	Bäkstrand et al. (2010), Jackowicz-Korczyski et al. (2010), Christensen et al. (2012)
—	Siberia	—	0 to 290	Christensen et al. (1995), Nakano et al. (2000)

Bayesian Belief Network Design

The vulnerability assessment was created using Netica (ver 5.18, Norsys Software Corp, 2014). Netica is a user-friendly software program that provides a framework to create probabilistic expert systems, known as BBN. The first tier contained the exposure and state variables. Tier 1 was parent node for the ecosystem conditions, which defined the sensitivity to changing MAAT in Tier 2. Ecosystem conditions were the parent nodes for C fluxes of NEE, CH_4, and peat combustion (Tier 3), which in turn were parent nodes for peat C sink strength (Tier 4). Response of peat C sink strength was considered to reflect the peatlands' vulnerability in the future. A previously published BBN for permafrost thaw in the Hudson Bay Lowlands (Webster and McLaughlin 2014) was adapted and linked to MAAT and peat wetness; all other nodes were retained as presented by Webster and McLaughlin (2014). Simulations also included a permafrost thaw effects node, which indirectly affected fens, but had no effect on bogs because they were considered to occur at high elevation when permafrost was present. Adding permafrost effects was necessary to constrain peat wetness in the absence of permafrost.

In the study area, permafrost features may span across bog, forest, or swamp land categories, and thermokarst features, such as internal lawns, may span across fen categories (Ontario Ministry of Natural Resources and Forestry, 2014). Additionally, small pools may cover much of peatland landscapes in the Hudson Bay Lowlands (McLaughlin and

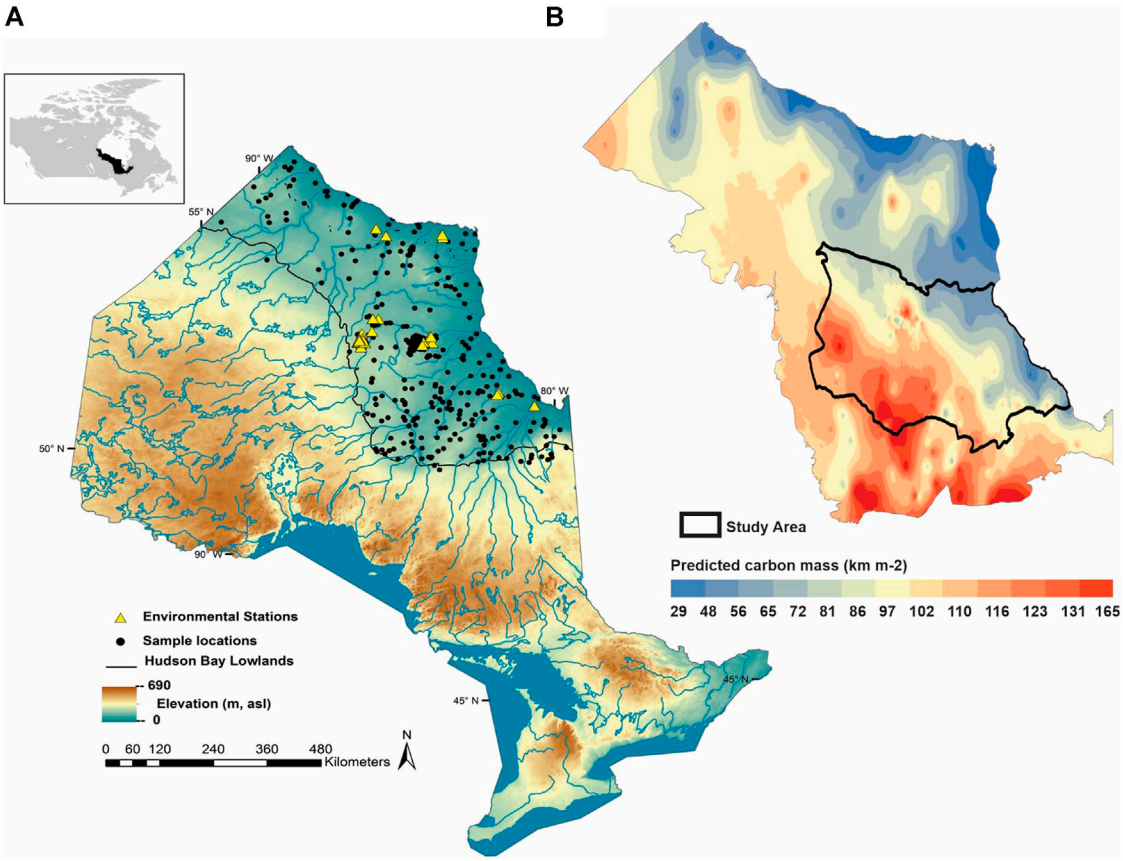

FIGURE 3 | Location of study site in northern Ontario, Canada, and maps of **(A)** elevation and peat sampling points and **(B)** predicted peat carbon mass for Ontario's portion of the Hudson Bay Lowlands (location indicated in insert) and the study area (outlined in black).

Webster, 2013 [1]). Pools may be derived from different processes, such as rapid elevational changes in peat surfaces caused by permafrost thawing or by gradual changes over thousands of years of peatland development.

We chose not to pursue detailed separation of bog/permafrost or fen/thermokarst because of the difficulties in separating those features in 30 m pixels. Furthermore, a goal is to provide land planners a peat C vulnerability assessment for large landscapes using currently available tools and data sets for large tracts of land in the Hudson Bay Lowlands. Therefore, and for the purpose of the current study, we assumed that thermokarst covered 6% of the fen area. Permafrost features in the study area occur on ombrotrophic peat deposits about 150–350 cm thick (Ou et al., 2016A) so we assigned a conservative estimate of 6% of the bogs to contain permafrost, although some palsas/peat plateaus are also classified as forests or swamps, which we assumed to be approximately 3% of those cover types. We recognize the importance of separating bog/permafrost and fen/thermokarst features from non-permafrost features, particularly when large tracts of land containing permafrost are considered in land use planning decisions. For example, and from a peat C perspective, NEE and CH_4 emission may differ significantly between permafrost/thermokarst and non-permafrost features (**Table 1**).

Conditional probability tables have one probability for every possible combination of the parent nodes. To constrain the range of possible responses in a given child node, the number of parent nodes was restricted to four and the maximum number of conditions was generally restricted to three or four. In some cases, four conditions and four parent nodes were used to describe the probability distribution of a child node; however, resulting combinations that were not possible in nature were suppressed in the conditional probability tables (Webster and McLaughlin, 2014).

Data produced from the analyses described below were used to inform the range in conditions for MAAT, elevation, and land cover associated with each of the ecosystem conditions using the conditional probability tables. The number of responses ranged from a minimum of nine (three states and two parent nodes) to a maximum of 81 (three states and four parent nodes), with exceptions as noted above. Most conditional probability tables were symmetrical, meaning that when the responses of parent nodes were maximized, the probability value of the largest

[1]http://www.climateontario.ca/scripts/MNR_Pub/publication_summary.php?pubId=25

(strongest) condition was also maximized. For example, when C loss from NEE, CH_4 emission, and peat C combustion is low, the probability of a strong peat C sink (child node) is maximized; the conditional probability table is symmetrical in that when the loss of C from each potential parent node is high, the probability of the child node being a peat C source is maximized.

We used the Shannon entropy [H(X)] (**Equation 1**) to calculate uncertainty in the BBN. Shannon entropy indicates the average information conveyed by data sources used to develop a BBN and H(X) values vary between 0 and 1, with high values indicating variables in the BBN requiring additional information to improve projections (Uusiitalo et al., 2015; Thomsen et al., 2016; Pagano et al., 2018).

$$H(X) = -\sum_{i=1}^{n} P(Xi) * logP(Xi) \quad (1)$$

We calculated H(X) for ecosystem conditions, C fluxes, and peat C sink strength to identify key variables requiring additional information. For example, the conditional probability table for C fluxes consisted of 27 combinations of NEE (strong sink, weak sink, source), C combustion (high, moderate, low), and CH_4 emissions (high, moderate, low). Using knowledge obtained (as per methods described in subsequent sections below), we assigned probabilities of occurrence as 90, 7, and 3% for the conditions of NEE source, high peat combustion, and CH_4 emission using **Eq. 2**. We then calculated the mean H(X) for C fluxes across the 27 combinations of NEE and CH_4 emission, which resulted in a 29.1% uncertainty in the probability distribution of peat C sink strength, with minimum and maximum uncertainties of 26.3 and 72.5% across the 27 combinations of the C flux conditional probability tables. Mean H(X) values, as well as those for ecosystem conditions were ranked, with values > 30% uncertainty identified as the most uncertain. The H(X) values were then standardized relative to overall peat C sink strength to evaluate the cumulative uncertainty of ecosystem conditions and C fluxes relative to peat C sink strength.

$$\begin{aligned} H(X) &= -(0.90 * log_{10}(0.9) + 0.07 * log_{10}(0.07) \\ &\quad + 0.03 * log_{10}(03) \\ &= 0.263, \text{ or } 26.3\% \end{aligned} \quad (2)$$

uncertainty in the peat C sink strength.

State and Stressor Variables

Hydro-Climate Data and Simulations

Gridded contemporary climate data (Price et al., 2011) were used to examine the role of climate (**Figures 3A,B**) on ecosystem conditions, C fluxes, and peat C sink strength. Gridded climate data sets were generated in the ANUSPLINE climate model, which helps to interpolate verified North American hydro-climate station data using thin-plate smoothing splines to generate a continuous climate estimate (Price et al., 2011). Hydro-climate variables considered to describe baseline and future C processes and functions in this analysis were MAAT, MAP, and PET. Monthly PET values were provided by the Canadian Forest Service Natural Resources Canada and were based on incoming solar radiation calculated using a modified form of the Priestley and Taylor equation (Bonan, 1989). The method assumes soil heat flux is equal to zero when averaged over several days and that net radiant flux is proportional to solar irradiance (Rs) and air temperature (Ta) and is calculated as $E_p = a*(T_a + b)$: R_s where E_p is mean monthly PET (cal cm^{-2} day^{-1}), T_a mean is the monthly air temperature (°C), R_s mean monthly solar radiation (cal cm^{-2} day^{-1}), and a and *b* are empirically derived site constants defined by elevation (m) and saturation vapor pressures (mbar) at the mean maximum and mean minimum daily temperatures, respectively, of the warmest month of the year. A gridded moisture index was calculated as the ratio of MAP to PET (MAP:PET) across the study area. High MAP:PET values represent wet conditions while low MAP:PET values indicate dry conditions. Additional details were documented by Packalen et al. (2016).

Climate scenarios used in the IPCC's Fifth Assessment Report (AR5)[2] were denoted by representative concentration pathways (RCP); RCP4.5 and RCP8.5 were used in this study, representing lower and higher atmospheric CO_2 concentrations, respectively (IPCC et al., 2014). Projections of future climate for the study area were produced for 2041–2070 and 2071–2,100, referred to as 2050s and 2080s, respectively. Climate data sets were obtained using the AR5 composite model adapted from Price et al. (2011). Current and projected gridded climate data for the study area were evaluated in ArcGIS (ESRI, 2011) and descriptive statistics (mean, standard deviation, minimum, maximum, and range) calculated for all available hydro-climate parameters.

Land Cover and Elevation

The Ontario land cover classification (Ontario Ministry of Natural Resources and Forestry, 2014[3]) involving satellite imagery of 1:50,000 to 1:100,000 images was used to classify wetlands in this study. Landsat 5-TM satellite imagery captured at 30 m pixel resolution was extracted from Land Information Ontario[4] and land cover interpretations were consistent with data specifications for classification used by the Ontario Ministry of Natural Resources and Forestry, (2014).

Elevation in the study area the was extracted from the Ontario Digital Elevation Model (**Figure 4A**) obtained from Land Information Ontario (Ontario Ministry of Natural Resources and Forestry 2016). Coverage was sourced from 1 arc-second space-borne C-band Interferometric radar data, which was used to create the Ontario radar digital surface model data product, providing a 30 m resolution. Further details are provided by Ontario Ministry of Natural Resources and Forestry, (2016).

Ecosystem Conditions

Peat Depth and Carbon Mass

Estimating C storage at landscape scale requires calculating peat C mass per unit area of dry peat (e.g., kg C m^{-2}) as per **Eq. 3**. In

[2]https://www.ipcc.ch/site/assets/uploads/2018/05/SYR_AR5_FINAL_full_wcover.pdf

[3]https://www.sse.gov.on.ca/sites/MNR-PublicDocs/EN/CMID/Far%20North%20Land%20Cover%20-%20Data%20Specification.pdf

[4]https://geohub.lio.gov.on.ca

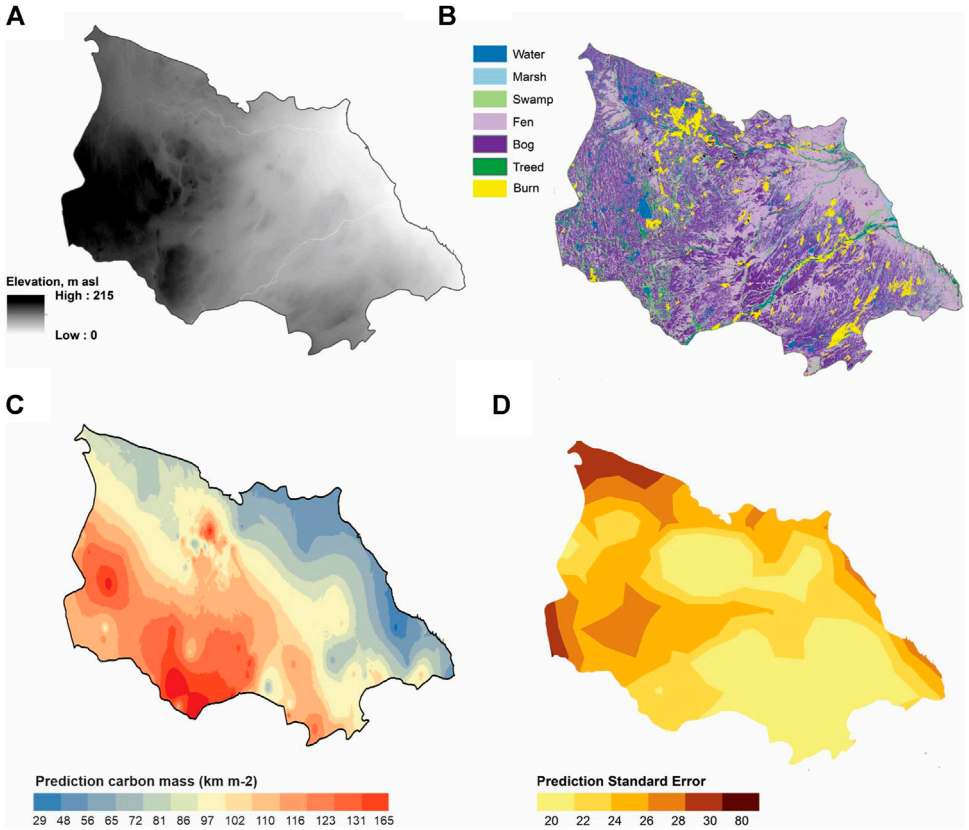

FIGURE 4 | Selected characteristics in the 74,300 km^2 study area in the southern Hudson Bay Lowlands: **(A)** elevation, **(B)** land cover, **(C)** peat carbon mass, and **(D)** uncertainty of peat carbon mass; expressed as standard error of carbon mass measurements.

this study, peat C storage was defined as the product of C mass and area of peatland in a landscape estimated using remote sensing, modelling, or geospatial statistical methods.

$$Carbon\ mass\ (kg\ m^{-2}) = Carbon\ concentration\ (kg\ kg^{-1}) \times bulk\ density\ (kg\ m^{-3}) \times peat\ depth\ (m) \quad (3)$$

Previously published data sets containing 364 peat depths, 100 peat ages, and 42 profiles of peat chemical and physical properties were assembled for the Hudson Bay Lowlands (Packalen and Finkelstein, 2014; Packalen et al., 2014, 2016). To estimate peat C mass from peat depth, a regression equation was produced (**Eq. 4**). Spatial patterns of peat C mass calculated from **Eq. 1**, **Eq. 2** were interpolated using empirical Bayesian kriging (EBK) implemented in ArcGIS geostatistical analyst (ESRI 2011). The EBK was informed by an updated version of the data set used by Packalen et al. (2016) that included 525 peat depth measurements from the Hudson Bay Lowlands, from which 237 depth measurements were specific to the current study area (**Figure 3A**); herein referred to as the Packalen et al. (2016) equation. This approach was considered a top-down estimation of peat C mass because it was calculated for the entire Hudson Bay Lowlands (approximately 372,000 km^2). Even though data from the 74,300 km^2 study area were included in the amalgamation for the Hudson Bay Lowlands, it is uncertain if the Packalen et al. (2016) equation calculated C mass adequately in smaller landscapes.

$$Carbon\ mass\ (kg\ m^{-2}) = 0.4\,X\ peat\ depth\ (m) + 17; R^2 = 0.82\,(Packalen\text{et al.}, 2016) \quad (4)$$

The top-down equation (e.g., Packalen et al., 2016) was tested against a linear and a power estimation of peat C mass produced by fitting Equation 1 to 44 measurements of peat C concentration, bulk density, and depth collected in the 74,300 km^2 studied landscape and designated as calibration peat, or bottom-up equations (e.g., specific information) to assess net changes in peat C mass in response to changing climate. Following calibration, 22 independent measurements of peat C, bulk density, and depth in the study area previously reported (Packalen et al., 2016) were designated as test peat. The three equations were tested for their applicability in predicting C mass from 177 peat depth measurements in the study area (**Figures 3A,B**). Evaluations included testing slopes of the regression lines, residual (observed–predicted C mass) plots, Kruskal-Wallis tests of no difference among equations, and Mann-Whitney U test of no difference in calculated C mass between peat types.

Peat Carbon Susceptibility

Quality of surface peat (upper 50 cm; the most biologically active region) for microbial decomposition was used to indicate peat susceptibility to changes in climate. We used peat C to N ratio (C:N) as the indicator of surface peat C susceptibility. The C:N ratio reflects mass loss of organic matter and changes in its functional composition in response to the microbial and plant communities present (Turetsky et al., 2015). Peat from six study sites that represented a range in C:N values of 17–73 was incubated to measure potential peat respiration at known C:N values; analyses were conducted using consistent methods across studies (Godin et al., 2012; Myers et al., 2012; Preston et al., 2012; Haynes et al., 2015).

Carbon Fluxes

Net Ecosystem Exchange and Methane

Data from McLaughlin and Webster (2014) were updated, with 36 published studies selected for further analyses in this study (**Table 1**). Compiled from the publications were data sets of 215 measurements of NEE, peat temperature, and WTL and 188 measurements of CH_4 emission, peat temperature, and WTL. Temperature measurements selected were restricted to the surface peat (i.e., 0–30 cm) to represent the approximate range in depth of the long-term acrotelm in peatlands in the study area (Bunbury et al., 2012; O'Reilly et al., 2014). Mean CH_4 emissions were compared against those from independent published studies from the Hudson Bay Lowlands (Turetsky et al., 2014; Webster et al., 2018) and CO_2 fluxes were compared with those measured at two eddy covariance flux towers in the north-central part of the study area operated by the Ontario Ministry of Environment, Conservation, and Parks (Humphreys et al., 2014; Helbig et al., 2019).

In addition to descriptive statistics (e.g., mean, standard deviation, and coefficient of variation), peat temperature, WTL, and NEE or CH_4 emission, the Man Whitney test was used to test hypotheses of no differences in NEE or CH_4 fluxes between bogs and fens. Numbers and percentages of positive, negative, and no significant correlations of each GHG with peat temperature and WTL were calculated for each published study to represent possible spatial patterns for baseline conditions of the two GHGs.

Peat Combustion

Fire patterns in the study area were inferred using the Ontario satellite-derived disturbance mapping product (1:50,000–1:100,000) to evaluate vegetation change for three time periods: before 1990, 1990–2000, and 2000–2009 (Ontario Ministry of Natural Resources and Forestry, 2014). Interpretation of fire events before 1990 were based on an historical time series of aerial photography dating to the mid-1980s that were classified alongside three Landsat 5-TM images (30 m pixel resolution) on which features as small as 0.5 ha were identified. Additional details are provided by Ontario Ministry of Natural Resources and Forestry, (2014).

Data describing fire and its regulation of peatland C fluxes in the Hudson Bay Lowlands are limited, but about 25 and 5% of the above- and belowground C fractions, respectively, may be susceptible to combustion (Balshi et al., 2009). These fractions were assumed to represent peatlands in the study area, with potentially available peat fuel calculated as the product of peat depth or C mass multiplied by 0.05 fraction of belowground peat potentially susceptible to fire since the 1980s. Estimates of consumed peat for bogs (10–14 cm) and fens (7–10 cm) were consistent with the estimated 5–20 cm of peat consumed during wildfires in western Canada and Alaska (Zoltai et al., 1998; Turetsky et al., 2011). The amount per unit area of potentially consumable C (t ha^{-1}) was then calculated from **Eq. 5** using 0.45 and 0.05 fractions of burned area for bogs and fens, respectively, since the 1980s and total consumable C (Mt) was calculated from **Eq. 6**.

$$\begin{aligned} &Potentially\ consumable\ C\ (t\ ha^{-1}) \\ &\quad = Peat\ fuel\ C\ X\ \%\ bog\ or\ fen\ burned\ X\ \%\ total\ area\ burned \end{aligned} \tag{5}$$

$$\begin{aligned} &Total\ consumable\ C\ (Mt) = \\ &\quad [Potentially\ consumable\ peat\ C\ X\ areas\ of\ bogs\ or\ fens \\ &\qquad (ha^{-1})] \div 10^6\ t\ Mt^{-1} \end{aligned} \tag{6}$$

RESULTS

Exposure and State Variables

Hydro-Climate

Baseline MAAT (1971–2000) in the study area was −1.7 ± 0.6°C (mean ± standard deviation) and was projected to increase to 2.0 to 7.6°C by the 2080s (**Supplementary Table 1.1** and **Supplementary Table 1.2**). Baseline MAP in the study area was 590 ± 39 mm and was projected to increase to 610–665 mm for all timeframes simulated (**Supplementary Table 1.2**). Baseline moisture index was lowest (i.e., driest) along much of the James Bay coast and progressively increased to the west, north, and south (**Figures 5A,B**). Both warming scenarios projected drying (i.e., lower moisture index) would occur across the study area.

Based on previous work, moisture index values between 1.4 and 2.0 were deemed optimal for C storage and sequestration (Webster et al., 2013; McLaughlin and Webster, 2014; Packalen et al., 2016). As the moisture index decreases to between 1.4 and 1.2, peatland C sink strength is expected to decrease but peatlands frequently remain net C sinks. A moisture index of 1.2 was assigned as the threshold value below which net C uptake from the atmosphere and its storage in peat are endangered through lower net primary production and more widespread fires that burn deeper into the peat. Only the severely warmer scenario projected moisture index conditions near the 1.2 threshold for the 2080s (**Supplementary Table 1.2**), primarily in the southern and eastern parts of the study area, although drying near the James Bay coast was apparent for the moderately warmer scenario in the 2080s (**Figures 6**, **7**).

Land Cover and Elevation

Fens (41%) and bogs (35%) dominated the land cover, with treed fens the most prevalent and open fens the least prevalent peatland types by area. However, based on verification by field sampling, misclassification of open vs. treed fen was more than 50%, whereas more than 80% of open and treed bogs were correctly

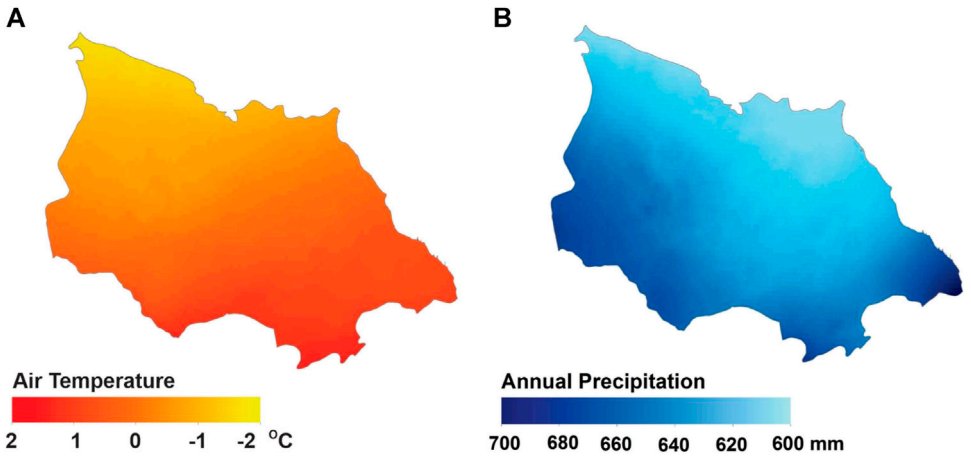

FIGURE 5 | Mean annual air temperature **(A)** and mean annual precipitation **(B)** for the 74,300 km^2 study area in the southern Hudson Bay Lowlands, Canada, for the period 1971–2000.

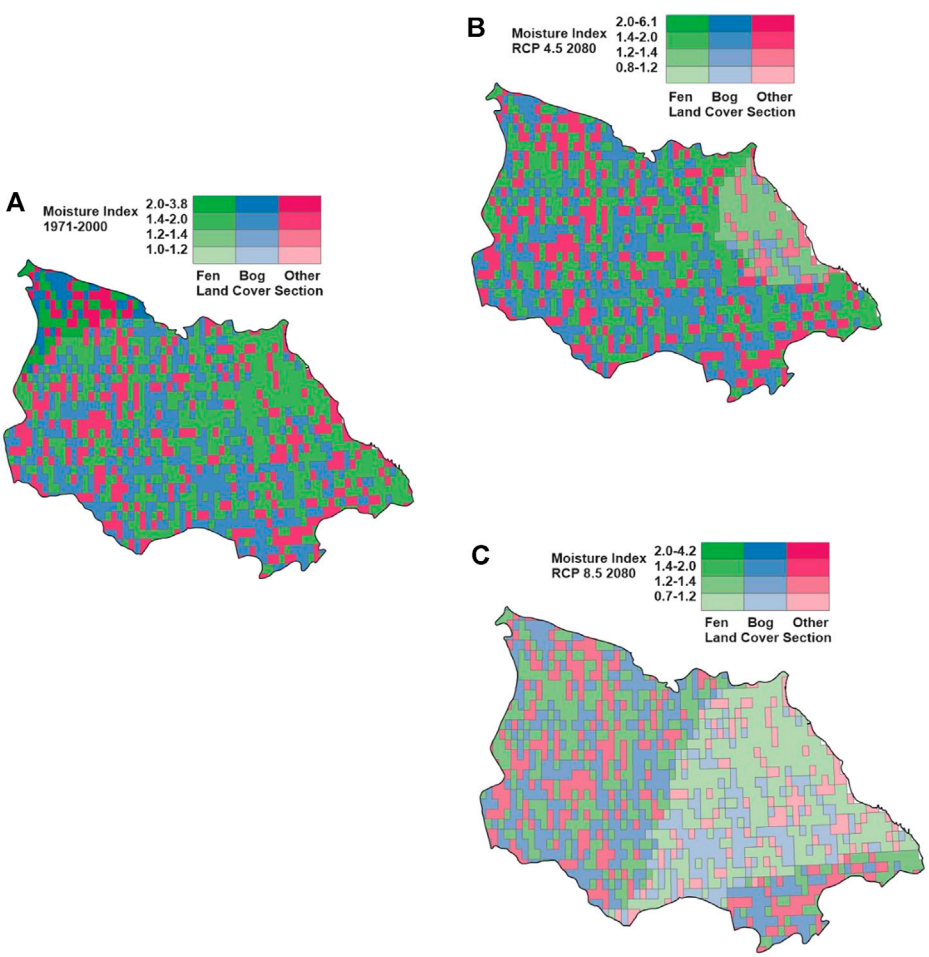

FIGURE 6 | Bivariate maps for the 74,300 km^2 study area for land cover baseline **(A)**, the 2080s for RCP4.5 **(B)**, and RCP8.5 **(C)**.

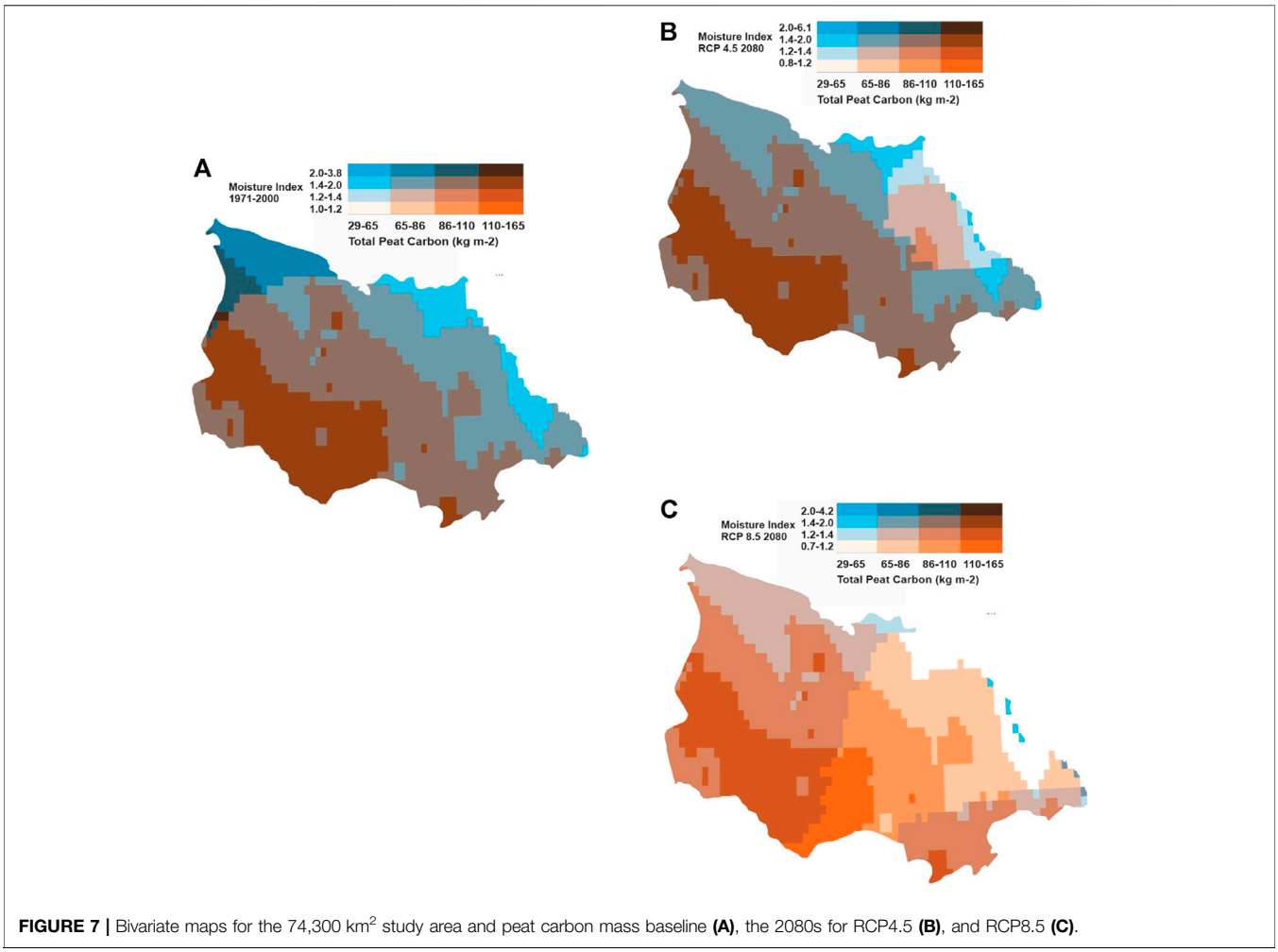

FIGURE 7 | Bivariate maps for the 74,300 km^2 study area and peat carbon mass baseline **(A)**, the 2080s for RCP4.5 **(B)**, and RCP8.5 **(C)**.

classified (Akumu and McLaughlin, 2014; Ou et al., 2016; Pironkova, 2017). Therefore, data are presented for bogs and fens, both of which include treed and open peatlands.

Fens are common throughout the study area, but are most abundant within about 100 km of the James Bay coast, which is at the lowest elevation in the study area (**Figures 4A,B**). Bogs are most prevalent in interior portions of the study area; they occur primarily at high elevation and are often inter-mixed with fens resulting in the patterned nature of the peatlands in the region. Elevation of the study area ranges between 0 and 215 m above sea level and is highest in the western part, decreasing in a north-easterly direction. About 40% of the peatland area was projected to be at or below the 1.2 moisture index threshold for current peat accumulation rates to be maintained in the 2080s under the severely warmer scenario (**Figure 6**). More fens than bogs were present, with nearly 50% of fens compared to about 30% of bogs occurring where projected moisture index was 1.2 or less.

Ecosystem Conditions

Peat Depth, Carbon Mass, and Spatial Arrangement

At the calibration peatlands (N = 44), neither mean peat C concentration (48 ± 3%, p = 0.27) nor bulk density (0.097 ± 0.054 g cm^{-3}, p = 0.35) differed between bogs and fens. However, bogs had the deepest peat; hence they had the highest C mass (**Table 2**). All three regression equations were consistent in predicting peat C mass (R^2 = 0.64–0.73, p < 0.0001) based on residual plots (**Figures 8A–D**). Nevertheless, the highest C mass was predicted with the linear equation when peat depth was less than about 150 cm and lowest C mass was predicted for the deepest peat. Also, the power equation produced more positive residuals (e.g., underpredicting), and the Packalen et al. (2016) equation (e.g., top-down) produced more negative residuals (overpredicting) than did the linear equation. In spite of these differences, and across bogs and fens, the slopes of the three equations did not differ (p = 0.66–0.93) and mean C mass (p = 0.10) predicted by all equations was similar and within 10% of the C mass measured in the calibration cores (**Table 2**).

At the test peatlands (N = 22), measured peat C concentration (50 ± 4%, p = 0.15) and bulk density (0.087 ± 0.010 g cm^{-3}, p = 0.57) were similar for bogs and fens. In contrast to the calibration peat, measured peat depth (p = 0.09) and C mass (p = 0.74) were similar for the two peat types (**Table 2**). Across bogs and fens, the three equations produced similar mean C mass (p = 0.08) and predicted values within 11% of mean C

TABLE 2 | Mean (±standard deviation) peat depth and carbon mass for 45 calibration, 22 test, and 117 application sites sampled in the 74,300 km^2 study area in the southern Hudson Bay Lowlands, Canada.

Characteristic	Overall	Bog	Fen	Bog vs. fen p- value
Calibration sites				
Measured peat thickness (m)	2.2 (0.7)	2.4 (0.7)	1.9 (0.6)	0.01
Carbon mass (kg m^{-2}) (measured)	97 (27)	102 (25)	86 (27)	0.04
Carbon mass (kg m^{-2}) (predicted, linear equation)	96 (19)	101 (16)	86 (18)	0.02
Carbon mass (kg m^{-2}) (predicted, power equation)	96 (27)	102 (26)	84 (24)	0.02
Carbon mass (kg m^{-2}) predicted, linear equation; Packalen et al. (2016)	106 (28)	113 (28)	94 (25)	0.03
N	44	29	15	
Test sites				
Measured peat thickness (m)	2.3 (4.8)	2.4 (5.2)	2.1 (3.8)	0.09
Carbon mass (kg m^{-2}) (measured)	97 (48)	100 (52	94 (38)	0.74
Carbon mass (kg m^{-2}) (predicted, linear equation)	97 (14)	102 (16)	92 (11)	0.10
Carbon mass (kg m^{-2}) (predicted, power equation)	98 (18)	103 (19)	92 (14)	0.09
Carbon mass (kg m^{-2}) predicted, linear equation; Packalen et al. (2016)	108 (19)	114 (21)	102 (15)	0.09
N	22	12	10	
Application sites				
Measured peat thickness (m)	2.1 (0.8)	2.5 (0.7)	1.9 (0.7)	<0.0001
Carbon mass (kg m^{-2}) (predicted, linear equation)	93 (20)	100 (18)	85 (19)	<0.0001
Carbon mass (kg m^{-2}) (predicted, power equation)	93 (25)	102 (23)	85 (24)	<0.0001
Carbon mass (kg m^{-2}) predicted, linear equation; Packalen et al. (2016)	102 (27)	112 (24)	91 (25)	<0.0001
N	173	91	82	

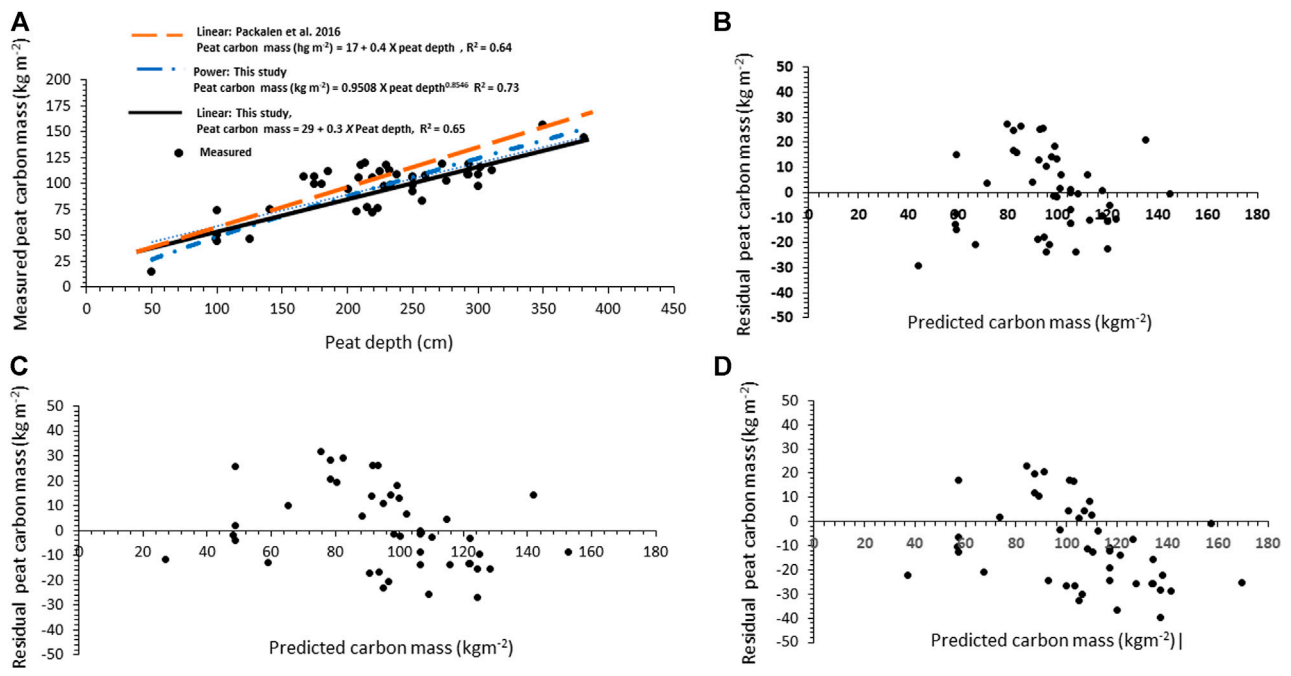

FIGURE 8 | Peat carbon mass calculations based on 44 peat profiles sampled in the 74,300 km^2 study area in the southern Hudson Bay Lowlands, Canada, for **(A)** peat depth vs. measured carbon mass for three regression equations, **(B)** measured–predicted residual carbon mass for **(B)** linear, **(C)** power, and **(D)** Packalen et al. (2016) regression equations.

mass measured at test sites (**Table 2**). Again, the top-down equation (e.g., Packalen et al., 2016) seemed to overpredict peat C mass relative to the two bottom-up equations (**Figures 8A–D**). At the application peatlands (N = 173 peat depth measurements), peat depth and estimated C mass differed between peat types and among equations (p = 0.001), with the top-down equation predicting higher mean C mass than the bottom–up linear (p = 0.001) or power (p = 0.001) equations; the latter two equations predicted similar mean C mass (p = 0.87) (**Table 2**).

Peat depth measurements were most common in the southeastern part of the study area, producing low uncertainty (measured as standard error) in peat C mass estimates (**Figure 1A**, **Figure 4C,D**). In contrast, depth measurements in western parts were underrepresented relative to the rest of the studied landscape, producing higher uncertainty in peat C mass estimates. Peat C mass generally was highest in the southwestern portion of study area; consistent with high elevation, a moisture index between 1.4 and 2.0, and bog-dominated (**Figure 4C,D**; **Figure 6C,D**). Similar to peatland area, nearly 40% of the peat C in the study area was projected to occur in areas at, or below, the 1.2 threshold moisture index in the 2080s when simulated with the severely warmer scenario (**Figure 7C**), representing 0.3–0.4 Gt and 1.8–2.4 Gt of C in fen and bog peat, respectively.

Carbon Fluxes

Net Ecosystem Exchange

The literature synthesis indicated bogs and fens, combined, were net CO_2 sinks of 0.54 ± 1.07 g CO_2–C m^2 d^{-1} and NEE was similar (p = 0.69) between peatland types, and neither peat temperature or WTL explained significant variation in NEE for bogs and fens, combined (**Supplementary Figure 1A**). However, peat temperature and NEE were negatively correlated (r = −0.70, p = 0.03) in bogs but not fens (r = −0.19, r = 0.76). Furthermore, NEE was correlated negatively with peat temperature more often in bogs than fens, when calculated for individual studies, whereas NEE and WTL were positively correlated more frequently in bogs than fens (decreasing CO_2 sink as WTL increased) (**Table 3**). For the entire data set, NEE and peat temperature of bogs was best explained by a quadratic equation, with peat temperature explaining 64% (p < 0.001) of the variation in NEE (**Supplementary Figure 2A**). In contrast, WTL failed to explain significant variation in NEE of bogs.

Methane Emissions

Peatlands in the current study were net CH_4 sources of 48 ± 67 mg CH_4-C m^{-2} d^{-1}, a finding that was similar between bogs and fens. Correlations between CH_4 and WTL of fens were 34% more likely be positive (increasing CH_4 emission with increasing WTL) than those of bogs, whereas less than 10% of peatlands had negative (i.e., increasing CH_4 emissions at lower WTL) correlations (**Table 3**).

For the entire data set (i.e., across published studies, N = 188), CH_4 emission and peat temperature were significantly correlated in bogs only (r = 0.50, p = 0.04), but regression analyses showed neither peat temperature nor WTL explained significant amounts of variation in CH_4 emission (**Supplementary Figure 1B**). However, bogs and fens combined had low CH_4 emission when WTL was less than −35 cm, at which point both CH_4 emission rate and its variability increased as WTL increased, and peak CH_4 emissions occurred between WTL of about −25 to 5 cm below the peat surface (**Supplementary Figure 2B**). Most of the variation was due to microtopography, with wet features (i.e., lawns, carpets, hollows, and pools) emitting more CH_4 than dry features (i.e., hummocks) when WTL favors high CH_4 emissions (**Supplementary Figure 2C**).

Peat Combustion

Peat available for consumption by fire in bogs during baseline conditions ranged from 10 to 14 cm (25th–75th percentiles) that contained 48–63 t C ha^{-1} (25th–75th percentiles). Assuming 90% of the peat fires (45% of total burned area) occurred in bogs and 10% of the landscape burned (**Figure 4B**), since the 1980s 5.6–7.4 Mt (10^6 tons or 10^{12} g) C may have been released to the atmosphere from the study area by fires. An estimated 1.8–2.4 Mt C (25th–75th percentiles) in bog peat may be exposed to a moisture index of 1.2 or less in the 2080s under the severely warmer scenario. In fens, peat available for consumption by fire during baseline conditions ranged from 7 to 10 cm (25th–75th percentiles) that contained 39–55 t C ha^{-1} (25th–75th percentiles). Assuming 10% of the peat fires (5% total burn area) occurred in fens and 10% of the landscape burned, 0.6–0.8 Mt C (25th–75th percentiles) of fen peat C may have been combusted in the study area since the 1980s, with 0.3–0.4 Mt C (25th–75th percentiles) potentially exposed to a future moisture index of 1.2 or less under the severely warmer scenario.

Bayesian Belief Network

Applying the BBN to the proportion of total peat area occurring as bog (43%), fen (51%), and permafrost (6%) in the study area produced similar probabilities for their distributions for peat C mass across MAAT regimes. Peat C mass was more susceptible to decomposition based on increased probabilities of high and moderate susceptibility classes when MAAT exceeded current conditions. Fire disturbance was under the influence of the net moisture index, and transitioned from less than 20% to almost 50% high fire occurrence in the 1.4 to 2.0 moisture index category (range for optimal C storage and sequestration) under the most severe MAAT scenario. (See **Supplementary Tables 2.1–2.9** for conditional probability tables).

All 3 C fluxes responded to warmer temperature (**Figures 9A–C**). The strong sink category for CO_2 was 27% lower and was offset by more sources in the severely and, to a lesser degree, in the moderately warmer scenario relative to current MAAT (**Figure 9A**). Methane had slightly higher probabilities of low emission, offset by lower probabilities of moderate and

TABLE 3 | Percentages of net ecosystem exchange or methane correlations with peat temperature in the upper 0.3 m and water table level for overall peatlands, bogs, and fens calculated from 20 peatlands in the boreal and subarctic regions analyzed from the literature.

Regression type	Overall	Bog	Fen
Percentage of net ecosystem exchange and peat temperature correlations (*N* = 20)			
Positive	20	14	23
Negative	35	43	31
Not correlated	45	43	46
Percentage of net ecosystem exchange and water table level correlations (*N* = 20)			
Positive	30	57	15
Negative	30	29	31
Not correlated	40	14	54
Percentage of methane emission and peat temperature correlations (*N* = 20)			
Positive	40	42	38
Negative	10	8	12
Not correlated	50	50	50
Percentage of methane emission and water table level correlations (*N* = 20)			
Positive	70	58	82
Negative	4	8	0
Not correlated	26	34	18

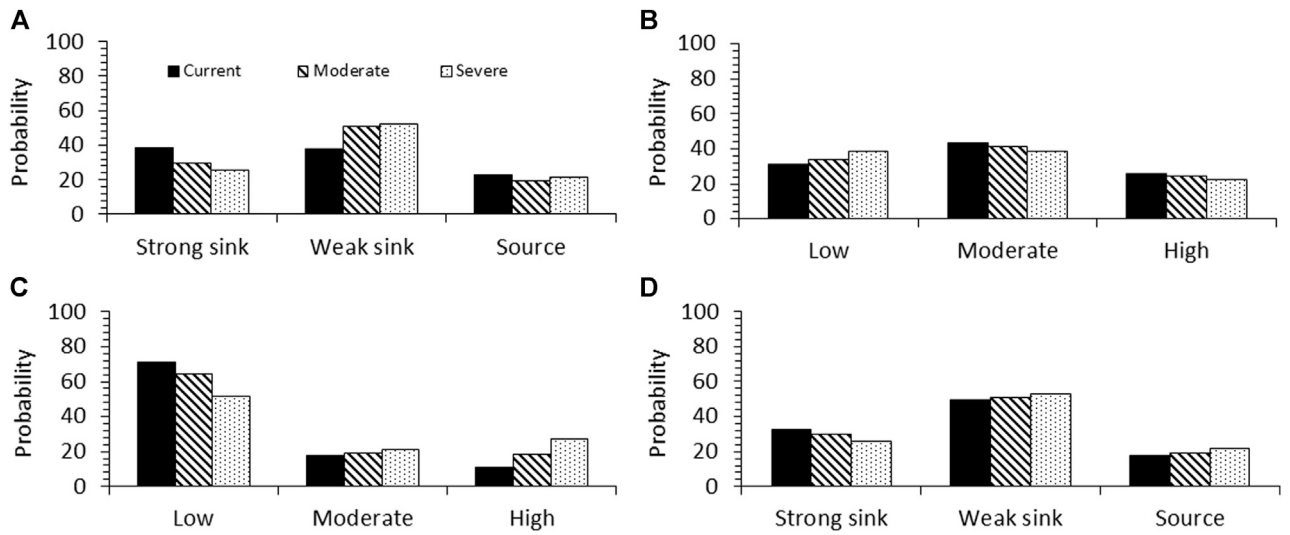

FIGURE 9 | In consideration of current, moderate, and severely warmer scenarios of a landscape containing 43% bogs, 51% fens, and 6% permafrost, probabilities of **(A)** strong sink, weak sink, and source of carbon dioxide; **(B)** low, moderate, and high methane emissions, **(C)** low, moderate, and high peat combustion, and **(D)** a strong sink, weak sink, and source of peat C.

high CH_4 emission categories (**Figure 9B**). Probability of peat C combustion increased with warmer MAAT, as suggested by smaller probabilities for the low category of combustion offset by larger probabilities for the high combustion class (**Figure 9C**). Combined, changes in NEE, CH_4, and peat C combustion contributed to a 21% lower probability of a strong C sink under severe MAAT (**Figure 9A**).

Sensitivity analyses revealed all 3 C fluxes responded to peat wetness, with NEE and CH_4 emission being most responsive to peat wetness, and peat C combustion most responsive to fire disturbance and the peat C sink strength was mostly a function of NEE (**Figure 10**). Net ecosystem exchange (27%) was the only variable (i.e., node) to contribute more than 1% of the influence on peat C sink strength (**Supplementary Tables 3.1–3.4**), which in turn had an H(X) value of 29% (**Figure 11A**), with the cumulative percent uncertainty shown in **Figure 11B**.

DISCUSSION

Exposure and State Variables

Hydroclimate Data

Baseline MAAT was –1.7±-0.6°C and was predicted to increase to 2.7–3.6°C in the 2050s and 2080s, respectively, when simulated with the moderately warmer scenario (**Supplementary Table 1.2**). The severely warmer simulation projected MAAT of 3.6 and 7.6°C for the 2050s and 2080s, respectively. Simulated warming was consistent with other lines of evidence for warming

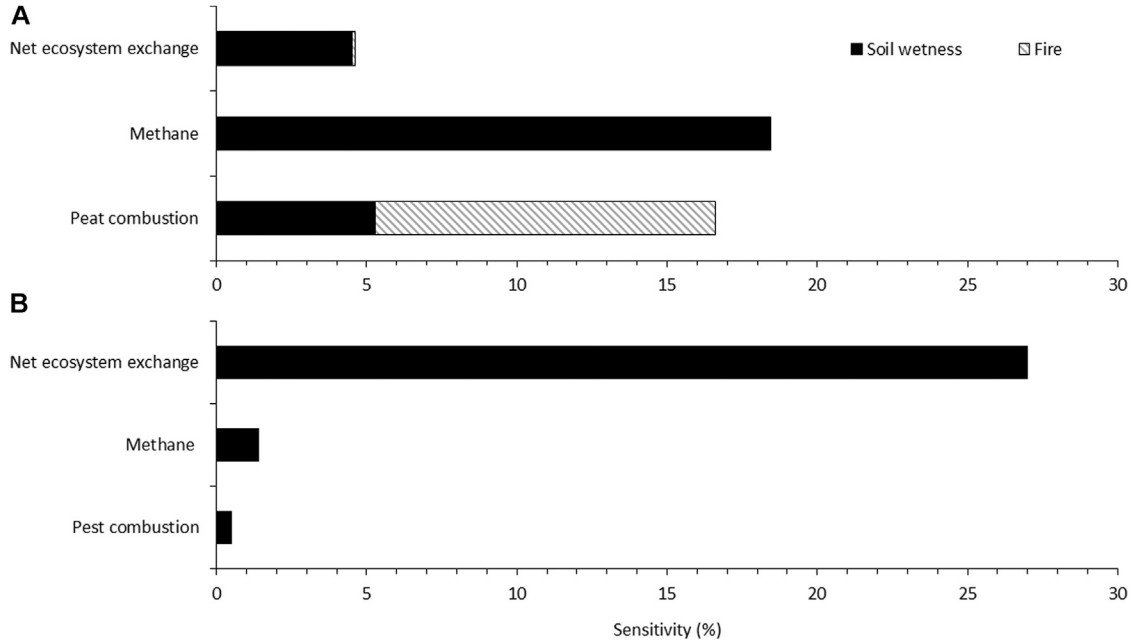

FIGURE 10 | In consideration of current, moderate, and severely warmer scenarios of a landscape containing 43% bogs, 51% fens, and 6% permafrost, **(A)** sensitivities of net ecosystem exchange, methane emissions, and peat combustion to soil wetness and fire and **(B)** sensitivity of the net peat carbon balance to net ecosystem exchange, methane emissions, and peat combustion.

temperature in the region. For example, using the Northern Ecosystem Soil Temperature (NEST) model, MAAT was projected to have increased by 1.8–2.0°C between 1961–1970 and 2000–2010 in a 7,480 km^2 landscape in the north-central part of the study area (Ou et al., 2016A). Also, the Canada Regional Climate Model (CRCM) projected MAAT increases of 3°C during 2041–2070 relative to 1961–1990 (Sushama et al., 2006). Paleoclimate records for the study area and surrounding Hudson Bay Lowlands also indicate warming and drying occurred during the last 600 years (Bunbury et al., 2012; Hargan et al., 2015).

Mean annual precipitation increased by 8 and 11% for the moderately and severely warmer simulations, respectively, compared with baseline MAP. Those values are well below the 25% precipitation increase threshold needed to maintain baseline soil moisture levels. For example, warming by 4.0°C resulted in more intensive soil moisture deficits during spring when precipitation did not change, caused primarily by higher PET rates compared with baseline conditions (Rouse, 1998). However, a 23% increase in precipitation was enough to maintain background PET and soil moisture levels. Additionally, warming fens by 3.5°C and increasing precipitation by 1 mm per month resulted in projected summer soil moisture deficits in excess of 100% in several northern fens (Roulet et al., 1992), further supporting likelihood of drying conditions and subsequently longer, more intensive soil moisture deficits in future.

Land Cover and Elevation

Peatlands contributed 76% to the total land area, with bogs (41%) and fens (35%) contributing similarly to the total land cover in the 74,300 km^2 landscape. This finding was consistent with other studies conducted in the Hudson Bay Lowlands (Glaser et al., 2004; Riley, 2011). About 30 and 50% of bog and fen area, respectively, was exposed to moisture index values that were less than 1.2, mostly occurring in the eastern part of the study area (**Figure 6**). Thus, on an area basis, fens are differentially exposed to severely warmer temperatures than bogs. Treed fens were the most common peatland type (Akumu and McLaughlin, 2014) but NEE results in treed fens varied and misclassification of open vs. treed fen was about 50% (Akumu and McLaughlin, 2014; Ou et al., 2016; Pironkova, 2017). Open fens may sequester more C from the atmosphere when MAAT is warmer and drier than current conditions (Fan et al., 2013; Webster et al., 2013). However, results have been inconsistent for treed fens, where they may be weaker (Gong et al., 2013; Webster et al., 2013; Wu and Roulet, 2014) or stronger (Flanagan and Syed, 2011) C sinks when MAAT is warmer and peat is drier. Thus, additional research is needed to improve the separation of open and treed fens using satellite techniques, such as Landsat 5-TM that was used in this study, as well as understanding work on NEE fluxes in open and treed fens.

Ecosystem Conditions

Peat Depth and Carbon Mass

At the calibration peatlands, bogs had deeper peat that contained more C mass than fens, but that was not the case at the test sites (**Table 2**). This discrepancy may be due to sample size differences between calibration (N = 44) and test (N = 22) peatlands. For example, previous work showed that across boreal and subarctic peatlands, a sample size of 55 was needed to detect a 20% difference in mean peat depth and C mass using statistical

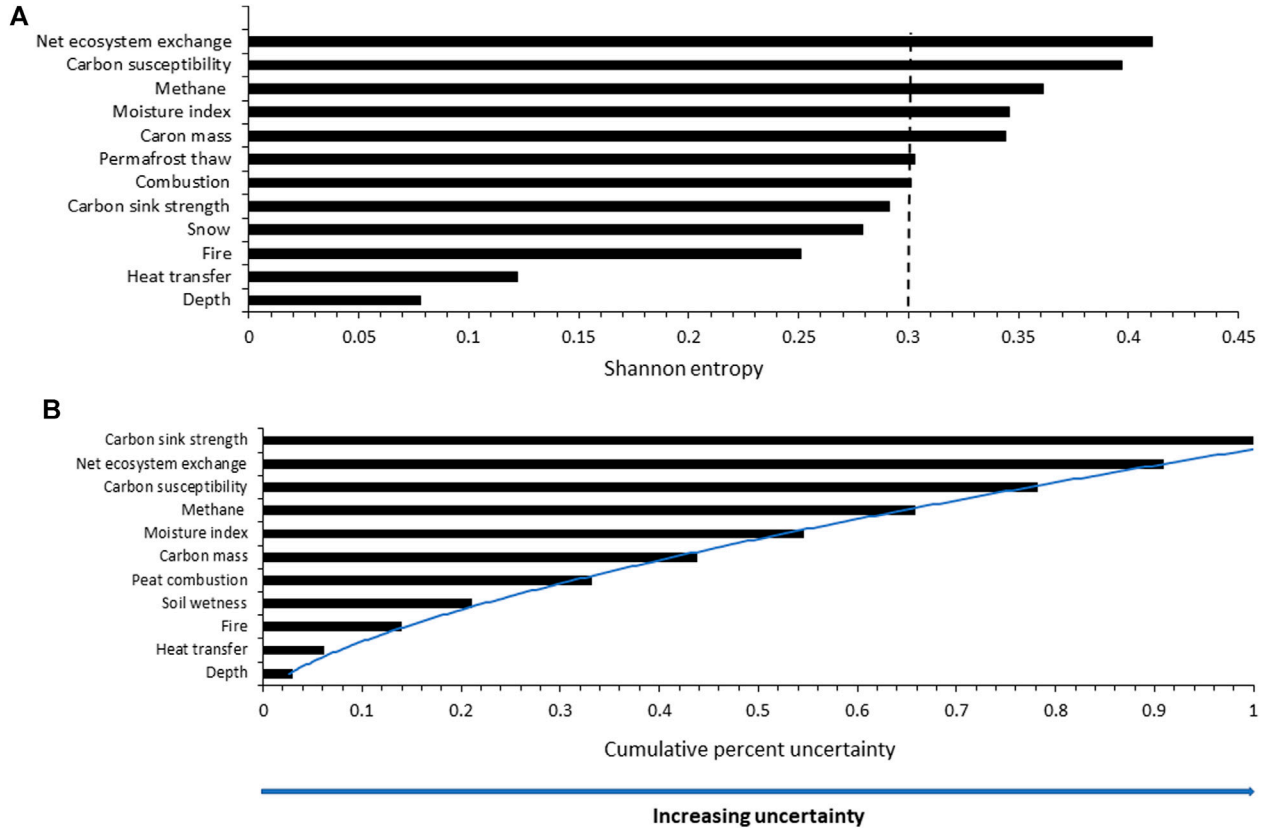

FIGURE 11 | Uncertainty of results for selected variables describing **(A)** posterior probability dispersion (Shannon entropy) and **(B)** cumulative probability in the standardized $(x_i - \bar{x})$ Shannon entropy in a 74,300 km^2 study area in the Hudson Bay Lowlands, Canada.

power of 70 and 5% level of significance (McLaughlin and Webster, 2014). In the current study, a sample size of 44 was adequate to detect differences in depth and C mass between bogs and fens at the calibration plots. However, a *p*-value of 0.09 produced from the Mann-Whitney test for differences in peat depth indicated the possibility of a Type II error occurring at the test sites because of the smaller sample size.

For the application peatlands, estimates of mean C mass in peat were similar from a top-down and two bottom-up equations; values were within 10% of that measured for the calibration and test peat samples (**Table 2**). However, in the shallowest peat situated closer to James Bay coast a power equation poorly predicted peat C mass relative to the two linear equations (Packalen et al., 2014). Residual plots indicated that, in addition to increased sample size, all equations would benefit from more independent variables, such as peat age or acrotelm-to-catotelm boundary, given they also differ across the studied landscape. For example, peat was deeper in a bog than a fen though they were of similar age (~6,700 cal y BP) (Bunbury et al., 2012; O'Reilly et al., 2014). Furthermore, bogs and fens had similar C mass in the interior of the study area, but fens were most common closer to James Bay coast and contained about 40 g C m^{-2} compared with 99 kg m^{-2} in the interior (Packalen et al., 2014).

Although reduced, when simulated with moderately warmer temperature the moisture index was higher than the threshold value of 1.2 near the James Bay coast. However, drying was evident near James Bay, suggesting this region may account for the projected 10% reduction in the strong peat C sink category compared to baseline conditions projected by the BBN. This result is consistent with other evidence. For example, simulations using the Terrestrial Ecosystem Model (TEM) showed soil organic C increased between 2012 and 2061 for a rich fen in Alaska because of more NPP relative to decomposition (Fan et al., 2013). After 2061, the soil organic C sink weakened, potentially functioning as a soil C source as decomposition rates increased relative to NPP.

Paleoclimate records from a bog in the study area revealed most rapid peat C accumulation occurred before 5,500 cal y BP, followed by relatively steady LORCA values until 1,000–600 cal y BP when LORCA decreased, and continued to about 100 cal y BP, when LORCA again increased (Bunbury et al., 2012). In contrast, based on LORCA, an adjacent fen continued to lose C during the past 100 years. Differences may be due to development of acrotelm:catotelm boundary at 33 cm (520 cal y BP) in the bog that was not present in the fen. Acrotelm peat is composed primarily of Sphagnum remains, having lower bulk density that is less humified than the catotelm peat (Glaser et al., 2004). As such, more C accumulated in the bog than the adjacent fen (O'Reilly et al., 2014). Although LORCA may be overestimated in acrotelm relative to catotelm peat (Bunbury et al., 2012), ^{210}Pb calculations indicate that, over the last 200 years, recent rates of C

accumulation in acrotelm peat are as much as 40–126 g C m^{-2}-yr^{-1}, depending on wetness and depth of measurements (McLaughlin and Webster, 2014). A caveat is that the higher C accumulation rates measured with ^{210}Pb may be important for conserving legacy C, but accumulation rates do not equal LORCA values of catotelm peat. For example, less than 10% of Sphagnum litter added to the acrotelm is deposited to the catotelm for long-term storage of recalcitrant peat (Laiho, 2006).

When simulated with the severely warmer scenario, moisture index in much of the eastern half of the study area was at or below the threshold value of 1.2 for the 2080s, exposing about one-third of the bogs and one-half of the fens to the driest future conditions. Bogs and fens containing the most C mass (Packalen et al., 2014) occurred in the southcentral part of the study area. This region may be most sensitive to peat C combustion, which may account for much of the 27–60% shift from low to high probability of fire occurrence projected in response to severely warmer temperatures from the BBN. In the rest of the study area, moisture index was projected to decrease to 1.2 to 1.4, indicating C mass reductions may arise from lower NPP relative to peat decomposition, as shown in other regions (Gong et al., 2013; Wu and Roulet, 2014). In contrast, using output from the Hadley Global Environment Model 2, simulations conducted with the LPJ-GUESS (Lund–Postdam–Jena General Ecosystem Simulator) showed possible LORCA increases up to 10 g C m^{-2}- yr^{-1} in the Hudson Bay Lowlands during the 2080s when simulated with RCP8.5 (Chaudhary et al., 2017).

Carbon Susceptibility

The quality of surface peat for microbial decomposition has often been identified as a key control on peat decomposition (Turetsky et al., 2011; Preston et al., 2012). In the current study, peat potential respiration was best explained by the natural log of the C:N ratio and potential peat decomposition rate was best explained by a power function, with rapid decreases in respiration occurring between C:N ratios of 20–40, after which respiration decreased at higher C:N values. The C:N gradient was consistent with a rich to moderately rich-- > poor fen-- > bog sequence, and to reduced alkalinity from smallest to largest C:N (McLaughlin and Webster, 2010, 2014; Webster and McLaughlin, 2010).

Decomposition proxies, such as C:N, reflect mass loss of organic matter and changes in its functional composition in response to the microbial and plant communities present (Turetsky et al., 2015). This change in organic matter contributes to fen peat commonly having lower C:N than bogs (Biester et al., 2014). However, alkalinity (favoring microbial activity) is generally higher, and combined with lower C:N, fen peat often has higher initial decomposability compared to bog peat. Conversely, based on Q_{10} values, bog peat was more sensitive to warmer temperature than fen peat (Preston et al., 2012). Lower WTL in bogs promotes oxygen penetration deeper into the peat, stimulating its decomposition. In contrast, shallow WTL in fens inhibits peat decomposition due to lack of oxygen but enhances methanogen activity and subsequent CH_4 production (Godin et al., 2012). Similar to bogs, deepening WTL in fens promotes oxygen diffusion into the peat, enhancing its decomposition. Also, plant shifts from mosses to graminoids are known to reduce C use efficiency of microbial communities when peat is warm and dry (Dieleman et al., 2016). Thus, it is likely C use efficiency will continue to decrease in future years as more easily degradable graminoid litter is added to surface peat. As well, rooting depth of graminoids can exceed 2 m, contributing easily degradable C from root turnover, potentially functioning as a 'primer' for decomposition of deeper, more recalcitrant peat (Haynes et al., 2015; Kettridge et al., 2019).

Carbon Fluxes

Net Ecosystem Exchange

Peatlands were net CO_2 sinks of 58 ± 1.07 g CO_2-C m^{-2} d^{-1}, a result that did not differ between bogs and fens. Additionally, mean NEE was on the high end (smaller sink) of the range in annual NEE (−1.62 to −0.48 g CO_2-C m^{-2} d^{-1}) measured for a bog and fen at eddy covariance towers in the north-central part of the study area (Humphreys et al., 2014; Helbig et al., 2019). In the current study, and for baseline conditions, bogs and fens were net CO_2 sources (positive correlations) about 14–23% of the time, respectively (**Table 3**). This finding is consistent with a 23% probability of bogs and fens, combined, being net CO_2 sources projected using the BBN (**Figure 9A**). As well, about 30% of bogs and fens were net CO_2 sources in boreal and subarctic peatlands (McLaughlin and Webster, 2014). Negative correlations between NEE and peat temperature indicate bogs were more likely than fens to be net CO_2 sinks at warmer temperature (**Table 3**). This finding is broadly consistent with a 70 days longer CO_2 sink period for the bog compared to the fen measured at the eddy covariance towers (Helbig et al., 2019). Bogs were also more likely to be net CO_2 sinks when WTL deepened. However, differences between bog and fen responses to temperature and WTL were not reflected in annual or seasonal (May–October) NEE fluxes in the current study or at the eddy covariance towers (Helbig et al., 2019).

When simulated with the moderately warmer scenario, the probability of a strong CO_2 sink decreased by 23% and was offset by a concomitant increase of the weak CO_2 sink category in the BBN; consistent with previous results (Gong et al., 2013; Webster et al., 2013; Wu and Roulet, 2014). Simulations with severely warmer temperature produced minor changes in probabilities of strong and weak CO_2 sink strengths relative to moderate warming. However, differences among type of bogs and fens should be considered in future work. For example, CO_2 sink increased at warmer temperatures in an open rich fen when simulated with the Terrestrial Ecosystem Model (Fan et al., 2013), Wetland DNDC model (Webster et al., 2013), and measured (Euskirchen et al., 2014). In contrast, CO_2 sink remained unchanged in a forested fen (Flanagan and Syed, 2011) or decreased but remained a sink (Webster et al., 2013), while a forested peat plateau and collapsed scar switched from CO_2 sink to source (Euskirchen et al., 2014).

Methane

Peatlands in the current study were net CH_4 sources of 48 ± 67 mg CH_4-C m^{-2} d^{-1}, which was similar between bogs and

fens. Mean CH_4 emission calculated in this study was the same order of magnitude as the 17–32 mg CH_4-C m^{-2} d^{-1} previously reported in the Hudson Bay Lowlands (Webster et al., 2018) and the 26–51 mg CH_4-C m^{-2} d^{-1} for boreal and subarctic regions (Turetsky et al., 2014). Positive correlations (CH_4 source) between CH_4 and temperature indicated bogs and fens were equally likely to be sources as temperature warms (**Table 3**). Positive correlations between CH_4 and WTL indicated both peatland types were likely to be CH_4 sources, with fens having a higher probability.

Neither peat temperature nor WTL explained significant amounts of variation in CH_4 emission, likely attributable to variability in the data. For example, McLaughlin and Webster (2014) showed low statistical power for CH_4 emissions that reduced the likelihood of detecting statistical relationships. However, in this study, peak emissions occurred when WTL was between −25 and 5 cm (**Supplementary Figure 2B**). Peatlands occurring in that WTL range largely consisted of lawn, carpet, and pool microtopographic features that emit large amounts of CH_4 (McLaughlin and Webster, 2014). In contrast, hummock-hollow microtopography is common in bogs. While hollows emit relatively large amounts of CH_4 to the atmosphere, hummocks release small amounts (Bubier et al., 1993). Therefore, the combined effect of hummocks and hollows to CH_4 emission depends on the hummock:hollow ratio, with high ratios favoring low CH_4 emission and low ratios favoring high CH_4 emissions (McLaughlin and Webster, 2014). Thus, microtopography warrants consideration in landscape-scale assessments of CH_4 emissions.

When simulated with the moderately warming scenario, the BBN showed bogs and fens, combined, had minor increases in the probability of low CH_4 emission that was mostly offset by changes in the moderate emission category. Simulations with severely warmer MAAT showed the same trend as that for moderately warmer temperature, but differences were double (**Figure 9B**), a finding consistent with previous work (Webster et al., 2013; Wu and Roulet, 2014).

Peat Combustion

Data describing fire and its regulation of peatland C cycles and fluxes in the Hudson Bay Lowlands are limited, but the area is thought to have the lowest organic matter combusting rate in Canada (Balshi et al., 2009). Additionally, small peatlands bordering forested uplands may be most sensitive to fire, with smouldering fires being the most important in peatlands (Turetsky et al., 2015; Ingram et al., 2019). In small peatlands, moderate deepening of WTL can convert net C accumulating bogs to a shrub- and grass-dominated ecosystem, and thus a net C source (Kettridge et al., 2019; Dieleman et al., 2015, 2017). Furthermore, wildfires are more common in drained and mined peatlands than in undisturbed and large peatlands such as those in the Hudson Bay Lowlands, which may currently be resistant to large-scale fire disturbance.

In the current study, 48–63 t C ha^{-1} C was estimated to be available for consumption. Of this, since the 1980s, 5.6–7.4 Mt C may have been released to the atmosphere from the study area due to fires. Similarly, using the 5% organic layer consumed and 1.43 kg C ha m^{-2} per fire emission reported for the Hudson Bay Lowlands (Balshi et al., 2009), 48 Mt C was estimated to be available for combustion, of which 6.7 Mt were estimated to be combusted to the atmosphere (bog = 6.1 Mt C and fen = 0.6 Mt C) since the 1980s. Thus, both methods appear to be adequate representations of peat C combustion caused by fire. Of the total amount of peat available for consumption, about 2.4–2.7 Mt C were exposed to a moisture index of 1.2 or less in the 2080s under the RCP8.5, of which about 90% occurred in bogs.

Bayesian Belief Network

Application and Examining Scenarios

In this study, a BBN projected severely warming MAAT (>4.0 C) reduced the probability of peat being a strong C sink by 21% that was mostly offset by a higher probability of peat being a weak C sink in the 2080s. Reduction in peat C sink strength was mostly due to lower probabilities of strong sinks for NEE and peat combustion (**Figure 9D**). The projections in this study were consistent with current knowledge of peat C cycling and fluxes. For example, and as discussed earlier, compared to baseline conditions drier peat enhances microbial decomposition rates (Godin et al., 2012; Preston et al., 2012) and fire frequency and depth of burning (Turetsky et al., 2011, 2015; Granath et al., 2016). Both conditions can increase net CO_2 losses from peat, desite CH_4 sink increases. That amount of change in the strong peat C sink strength is frequently on the threshold to detect differences using statistical hypothesis testing because of wide variation in climatic, ecosystem, and carbon conditions (McLaughlin and Webster, 2014). Thus, under the most severe MAAT increases, the peat C sink strength in the 74,300 km^2 study area will likely remain an overall C sink and sequestration rates will decrease slightly, thereby displaying moderate vulnerability in response to warmer MAAT.

All 3 C fluxes responded to peat wetness, with NEE and CH_4 emission being most responsive to peat wetness and peat combustion most responsive to fire disturbance, similar to other studies in northern peatlands (Webster et al., 2013; Turetsky et al., 2014; Webster and McLaughlin, 2014). Low (less than 20%) sensitivity values likely resulted from at least four causes: 1) wide variation in NEE and CH_4 emission values within and among peatland types; 2) soils in the study area are frequently wetter than those in similar landcover types in other areas, such as western Canada and Alaska; 3) uncertainty in current and future peatland fire severity, frequency, longevity, and size; and 4) relatively similar MAAT across much of the study area (**Figure 5A**). Peat C sink strength was most sensitive to changes in NEE (**Figures 10A,B**), indicating field research and monitoring to obtain the data needed to constrain conditional probability tables for NEE in future versions of the BBN is a priority. Data from field research can also inform ecosystem conditions in numerical, semi-distributed, and process modelling of the net peat C balance.

Limitations to the Bayesian Belief Network

The BBN approach relies on expert knowledge rather than explicit links to physical processes, as is the case in process-based models. The BBN approach simplifies the model and

produces results that may be accurate, but not necessarily precise (Webster and McLaughlin, 2014). The extensive research presented here describing ecosystem controls on peatland C mass and GHG fluxes likely contributed adequate precision in projections based on the conditional probability tables. The BBN's power lies in the conditional probability tables, and improving their accuracy provides more certain results. Based on the sensitivity analysis, as knowledge about the system improves, efforts are needed to refine the conditional probability tables relative to peat wetness, fire disturbance, and NEE.

A second limitation to the BBN includes inability to factor in how plant and microbial communities will change over time as peat becomes wetter or drier, for example in response to natural succession following fire. However, this limitation also applies to process-based models of peat C budgets (St.-Hilaire et al., 2010; Mezbahuddin et al., 2017). Another limitation of the BBN is the lack of linkages between C and other nutrient cycles, and that it does not include surface energy budgets.

Many of the processes captured in the framework of the BBN decision tool are fundamental to northern peatland dynamics; however, the Hudson Bay Lowlands is further characterized at the regional to landscape scale by a nearly continuous low relief surface driven by geophysical controls that unify the space and support consideration of other factors across a large geography. For example, the ratio of MAP:PET captures the influence of marine and continental climate regimes in the Hudson Bay Lowlands. The decision tool parameters used here are specified with regional current and future climate conditions, land cover, fire history, and empirically derived relationships for peat properties specific to the region, including permafrost. How these controls translate to other peatland geographies requires additional inquiry. Understanding the vulnerability of peatlands to climate change in the context of strategic land use decisions should be informed by a portfolio of approaches including integrative semi-quantitative decision tools, such as the BBN approach presented here.

CONCLUSION

Based on a combination of literature syntheses, field sampling, spatial analyses, and probabilistic modelling, about 40% of the peat C in the 74,300 km^2 study area in northern Ontario, Canada, may be subjected to moisture index values below the 1.2 threshold needed to maintain the current C sink strengths. Using a BBN, severely warmer MAAT reduced, by about 20%, the probability that the peat C would be a strong sink would be a strong sink, a finding that was most persistent in the eastern half of the study area. Because of variation in climate, ecosystem, and C conditions, this value is on the threshold to detect statistical differences in hypothesis testing. Therefore, in this study area the peat C sink strength is expected to be moderately vulnerable to increasing MAAT. Sensitivity analyses revealed that NEE is the most uncertain C flux affecting the peat C sink strength, and peat wetness was the most uncertain ecosystem condition affecting NEE. As such, recommended research and monitoring projects are those that obtain data on NEE to improve projections of vulnerability in the net peat C balance when exposed to warmer MAAT. These include 1) obtaining additional data to constrain conditional probability tables for NEE, test the BBN in other peatland-dominated geographies, and apply a spatial BBN in landscapes; 2) additional field sampling of peat depth and C mass in areas with the most uncertain peat C mass estimates and measurements of fire patterns and their effects on peat C combustion; and 3) modelling studies to test numerical, semi-distributed, and process-based simulations of the peat C sink strength of large, intermediate, and small landscapes.

DATA AVAILABILITY STATEMENT

The raw data supporting the conclusions of this article will be made available by the authors, without undue reservation.

AUTHOR CONTRIBUTIONS

JM and MP: Conceptualization; data curation; formal analysis; methodology; investigation; visualization; writing.

ACKNOWLEDGMENTS

We thank D. McKenny for providing climate projections; B. Hamel, M. Crofts, J. Ralston for their dedication to field work; and S.0. Bowman of the Ontario Forest Research Institute Laboratory Services' for providing chemical analyses of samples, and Lisa Buse for editing previous versions of the manuscript. This research was funded by Ontario Ministry of Natural Resources and Forestry to JM and MP. Partial contents of this manuscript have previously appeared online (McLaughlin and Webster, 2013; McLaughlin et al., 2018).

SUPPLEMENTARY MATERIAL

The Supplementary Material for this article can be found online at: https://www.frontiersin.org/articles/10.3389/feart.2021.650662/full#supplementary-material

REFERENCES

Adkinson, A. C., Syed, K. H., and Flanagan, L. B. (2011). Contrasting Responses of Growing Season Ecosystem CO2exchange to Variation in Temperature and Water Table Depth in Two Peatlands in Northern Alberta, Canada. *J. Geophys. Res.* 116, G01004. doi:10.1029/2010JG00151510.1029/2010jg001512

Akumu, C. E., and McLaughlin, J. W. (2014). Modeling Peatland Carbon Stock in a Delineated Portion of the Nayshkootayaow River Watershed in Far North, Ontario Using an Integrated GIS and Remote Sensing Approach. *Catena* 121, 297–306. doi:10.1016/j.catena.2014.05.025

Alm, J., Schulman, L., Walden, J., Nykänen, H., Martikainen, P. J., and Silvola, J. (1999). Carbon Balance of a Boreal Bog during a Year with an Exceptionally Dry Summer. *Ecology* 80, 161–174. doi:10.1890/0012-9658(1999)080[0161:cboabb]2.0.co;2

Andrews, J. T., and Peltier, W. R. (1976). Collapse of the Hudson Bay Ice center and Glacio-Isostatic Rebound. *Geol* 4, 73–75. doi:10.1130/0091-7613(1976)4<73:cothbi>2.0.co;2

Aurela, M., Riutta, T., Laurila, T., Tuovinen, J. P., Vesala, T., Tuittila, E.-S., et al. (2007). CO2 Exchange of a Sedge Fen in Southern Finland-the Impact of a Drought Period. *Tellus B: Chem. Phys. Meteorology* 59, 826–837. doi:10.1111/j.1600-0889.2007.00309.x

Bäckstrand, K., Crill, P. M., Jackowicz-Korczyñski, M., Mastepanov, M., Christensen, T. R., and Bastviken, D. (2010). Annual Carbon Gas Budget for a Subarctic Peatland, Northern Sweden. *Biogeosciences* 7, 95–108. doi:10.5194/bg-7-95-2010

Balshi, M. S., McGuire, A. D., Duffy, P., FlanniganKicklighter, M. D. W., Kicklighter, D. W., and Melillo, J. (2009). Vulnerability of Carbon Storage in North American Boreal Forests to Wildfires during the 21st century. *Glob. Change Biol* 15, 1491–1510. doi:10.1111/j.1365-2486.2009.01877.x

Beilman, D. W., MacDonald, G. M., Smith, L. C., and Reimer, P. J. (2009). Carbon Accumulation in Peatlands of West Siberia over the Last 2000 Years. *Glob. Biogeochem. CyclesCycles* 23, a–n. doi:10.1029/2007GB003112

Biester, H., Knorr, K.-H., Schellekens, J., Basler, A., and Hermanns, Y.-M. (2014). Comparison of Different Methods to Determine the Degree of Peat Decomposition in Peat Bogs. *Biogeosciences* 11, 2691–2707. doi:10.5194/bg-11-2691-2014

Bohn, T. J., Lettenmaier, D. P., Sathulur, K., Bowling, L. C., Podest, E., McDonald, K. C., et al. (2007). Methane Emissions from Western Siberian Wetlands: Heterogeneity and Sensitivity to Climate Change. *Environ. Res. Lett.* 2, 045015. doi:10.1088/1748-9326/2/4/045015

Bonan, G. B. (1989). A Computer Model of the Solar Radiation, Soil Moisture, and Soil thermal Regimes in Boreal Forests. *Ecol. Model.* 45, 275–306. doi:10.1016/0304-3800(89)90076-8

Bonn, A., Allott, T., Evans, M., Jooston, H., and Stoneman, R. (2016). "Peatland Restoration and Ecosystem Services: an Introduction," in *Peatland Restoration and Ecosystem Services: Science, Policy and Practice*. Editors A. Bonn, T. Allott, M. Evans, H. Joosten, and R. R. Stoneman (Cambridge University Press), 1–16.

Bubier, J., Costello, A., Moore, T. R., Roulet, N. T., and Savage, K. (1993). Microtopography and Methane Flux in Boreal Peatlands, Northern Ontario, Canada. *Can. J. Bot.* 71, 1056–1063. doi:10.1139/b93-122

Bubier, J. L., Frolking, S., Crill, P. M., and Linder, E. (1999). Net Ecosystem Productivity and its Uncertainty in a Diverse Boreal Peatland. *J. Geophys. Res.* 104, 27683–27692. doi:10.1029/1999jd900219

Bubier, J. L., Moore, T. R., Bellisario, L., Comer, N. T., and Crill, P. M. (1995). Ecological Controls on Methane Emissions from a Northern Peatland Complex in the Zone of Discontinuous Permafrost, Manitoba, Canada. *Glob. Biogeochem. Cycles* 9, 455–470 doi:10.1029/95gb02379

Bubier, J. L. (1995). The Relationship of Vegetation to Methane Emission and Hydrochemical Gradients in Northern Peatlands. *J. Ecol.* 83, 403–420. doi:10.2307/2261594

Bunbury, J., Finkelstein, S. A., and Bollmann, J. (2012). Holocene Hydro-Climatic Change and Effects on Carbon Accumulation Inferred from a Peat Bog in the Attawapiskat River Watershed, Hudson Bay Lowlands, Canada. *Quat. Res.* 78, 275–284. doi:10.1016/j.yqres.2012.05.013

Chasmer, L., Kenward, A., Quinton, W., and Petrone, R. (2012). CO2 Exchanges within Zones of Rapid Conversion from Permafrost Plateau to Bog and Fen Land Cover Types. *Arctic, Antarctic, Alpine Res.* 44, 399–411. doi:10.1657/1938-4246-44.4.399

Chaudhary, N., Miller, P. A., and Smith, B. (2017). Modelling Past, Present and Future Peatland Carbon Accumulation across the Pan-Arctic Region. *Biogeosciences* 14, 4023–4044. doi:10.5194/bg-14-4023-2017

Chistjakov, V. I., Kuprijanov, A. I., Gohrskov, V. V., and Artsybashe, E. S. (1983). "Measures for Fire protection on Peat Deposits," in *The Role of Fire in Circumpolar Ecosystems*. Editors R. W. Wein and D. A. MacLean (New York, NY: John Wiley), 259–271.

Christensen, T. R., Jackowicz-Korczyński, M., Aurela, M., Crill, P., Heliasz, M., Mastepanov, M., et al. (2012). Monitoring the Multi-Year Carbon Balance of a Subarctic Palsa Mire with Micrometeorological Techniques. *Ambio* 41 (Suppl. 3), 207–217. doi:10.1007/s13280-012-0302-5

Christensen, T. R., Jonasson, S., Callaghan, T. V., and Havström, M. (1995). Spatial Variation in High-Latitude Methane Flux along a Transect across Siberian and European Tundra Environments. *J. Geophys. Res.* 100, 21035–21045. doi:10.1029/95jd02145

Cooper, M. D. A., Estop-Aragonés, C., Fisher, J. P., Thierry, A., Garnett, M. H., Charman, D. J., et al. (2017). Limited Contribution of Permafrost Carbon to Methane Release from Thawing Peatlands. *Nat. Clim Change* 7, 507–511. doi:10.1038/nclimate3328

Davies, M. A., McLaughlin, J. W., Packalen, M. S., and Finkelstein, S. A. (2021). Using water table depths inferred from testate amoebae to estimate Holocene methane emissions from the Hudson Bay Lowlands, Canada. *J. Geophys. Res.* 126, doi:10.1029/2020JG005969

Dieleman, C. M., Branfireun, B. A., and Lindo, Z. (2017). Northern Peatland Carbon Dynamics Driven by Plant Growth Form - the Role of Graminoids. *Plant Soil* 415, 25–35. doi:10.1007/s11104-016-3099-3

Dieleman, C. M., Branfireun, B. A., McLaughlin, J. W., and Lindo, Z. (2015). Climate Change Drives a Shift in Peatland Ecosystem Plant Community: Implications for Ecosystem Function and Stability. *Glob. Change Biol.* 21, 388–395. doi:10.1111/gcb.12643

Dieleman, C. M., Branfireun, B. A., McLaughlin, J. W., and Lindo, Z. (2016). Enhanced Carbon Release under Future Climate Conditions in a Peatland Mesocosm experiment: the Role of Phenolic Compounds. *Plant Soil* 400, 81–91. doi:10.1007/s11104-015-2713-0

Erikkson, Y., Öquist, M. G., and Nilsson, M. B. (2010). Effects of Decadal Deposition of Nitrogen and Sulfur, and Increased Temperature, on Methane Emissions from a Boreal Peatland. *J. Geophys. Res.* 115, G04036. doi:10.1029/2010JG001285

ESRI (2011). *ArcGIS Desktop: Release 10*. Redlands, CA: Environmental Systems Research Institute.

Euskirchen, E. S., Bret-Harte, M. S., Scott, G. J., Edgar, C., and Shaver, G. R. (2012). Seasonal Patterns of Carbon Dioxide and Water Fluxes in Three Representative Tundra Ecosystems in Northern Alaska. *Ecosphere* 3, art4. doi:10.1890/ES11-00202.1

Euskirchen, E. S., Edgar, C. W., Turetsky, M. R., Waldrop, M. P., and Harden, J. W. (2014). Differential Response of Carbon Fluxes to Climate in Three Peatland Ecosystems that Vary in the Presence and Stability of Permafrost. *J. Geophys. Res. Biogeosci.* 119, 1576–1595. doi:10.1002/2014jg002683

Fan, Z., David McGuire, A., Turetsky, M. R., Harden, J. W., Michael Waddington, J., and Kane, E. S. (2013). The Response of Soil Organic Carbon of a Rich Fen Peatland in interior Alaska to Projected Climate Change. *Glob. Change Biol.* 19, 604–620. doi:10.1111/gcb.12041

Flanagan, L. B., and Syed, K. H. (2011). Stimulation of Both Photosynthesis and Respiration in Response to Warmer and Drier Conditions in a Boreal Peatland Ecosystem. *Glob. Change Biol* 17, 2271–2287. doi:10.1111/j.1365-2486.2010.02378.x

Flessa, H., Rodionoc, A., Guggenberger, G., Fuchs, H., Magdon, P., Shibistova, et al. (2008). Landscape controls of CH4 fluxes in a catchment of the forest tundra ecotone in northern Siberia. *Glob. Change Biol.* 14, 2040–2056.

Frolking, S., Talbot, J., Jones, M. C., Treat, C. C., Kauffman, J. B., Tuittila, E. S., et al. (2011). Peatlands in the Earth's 21st century Climate System. *Environ. Rev.* 19, 371–396. doi:10.1139/a11-014

Glaser, P. H., Hansen, B. C. S., Siegel, D. I., Reeve, A. S., and Morin, P. J. (2004). Rates, Pathways and Drivers for Peatland Development in the Hudson Bay Lowlands, Northern Ontario, Canada. *J. Ecol.* 92, 1036–1053. doi:10.1111/j.0022-0477.2004.00931.x

Godin, A., McLaughlin, J. W., Webster, K. L., Packalen, M., and Basiliko, N. (2012). Methane and Methanogen Community Dynamics across a Boreal Peatland Nutrient Gradient. *Soil Biol. Biochem.* 48, 96–105. doi:10.1016/j.soilbio.2012.01.018

Gong, J., Kellomäki, S., Wang, K., Zhang, C., Shurpali, N., and Martikainen, P. J. (2013). Modeling CO2 and CH4 Flux Changes in Pristine Peatlands of Finland under Changing Climate Conditions. *Ecol. Model.* 263, 64–80. doi:10.1016/j.ecolmodel.2013.04.018

Gorham, E. (1991). Northern Peatlands: Role in the Carbon Cycle and Probable Responses to Climatic Warming. *Ecol. Appl.* 1, 182–195. doi:10.2307/1941811

Granath, G., Moore, P. A., Lukenbach, M. C., and Waddington, J. M. (2016). Mitigating Wildfire Carbon Loss in Managed Northern Peatlands through Restoration. *Sci. Rep.* 6, 28498. doi:10.1038/srep28498

Hargan, K. E., Rühland, K. M., Paterson, A. M., Holmquist, J., MacDonald, G. M., Bunbury, J., et al. (2015). Long-term Successional Changes in Peatlands of the Hudson Bay Lowlands, Canada Inferred from the Ecological Dynamics of Multiple Proxies. *The Holocene* 25, 92–107. doi:10.1177/0959683614556384

Haynes, K. H., Preston, M. D., McLaughlin, J. W., Webster, K., and Basiliko, N. (2015). Dissimilar Bacterial and Fungal Decomposer Communities across Rich to Poor Fen Peatlands Exhibit Functional Redundancy. *Can. J. Soil Sci.* 95, 19–30. doi:10.4141/cjss-2014-062

Heikkinen, J. E. P., Maljanen, M., Aurela, M., Hargreaves, K. J., and Martikainen, P. J. (2002). Carbon Dioxide and Methane Dynamics in a Sub-arctic Peatland in Northern Finland. *Polar Res.* 21, 49–62. doi:10.3402/polar.v21i1.6473

Helbig, M., Humphreys, E. R., and Todd, A. (2019). Contrasting Temperature Sensitivity of CO_2 Exchange in Peatlands of the Hudson Bay Lowlands, Canada. *J. Geophys. Res. Biogeosci.* 124, 2126–2143. doi:10.1029/2019jg005090

Huang, X., and Rein, G. (2015). Computational Study of Critical Moisture and Depth of Burn in Peat Fires. *Int. J. Wildland Fire* 24, 798–808. doi:10.1071/wf14178

Humphreys, E. R., Charron, C., Brown, M., and Jones, R. (2014). Two Bogs in the Canadian Hudson Bay Lowlands and a Temperate Bog Reveal Similar Annual Net Ecosystem Exchange of CO2. *Arctic, Antarctic, Alpine Res.* 46, 103–113. doi:10.1657/1938-4246.46.1.103

Ingram, R. C., Moore, P. A., Wilkinson, S., Petrone, R. M., and Waddington, J. M. (2019). Postfire Soil Carbon Accumulation Does Not Recover Boreal Peatland Combustion Loss in Some Hydrogeological Settings. *J. Geophys. Res. Biogeosci.* 124, 775–788. doi:10.1029/2018jg004716

Jackowicz-Korczyski, M., Christensen, T. R., Bäckstrand, K., Crill, P., Friborg, T., Mastepanov, M., et al. (2010). Annual Cycle of Methane Emission from a Subarctic Peatland. *J. Geophys. Res.* 115, G03009. doi:10.1029/2008JG000913

Järveoja, J., Nilsson, M. B., Gažovič, M., Crill, P. M., and Peichl, M. (2018). Partitioning of the Net CO2 Exchange Using an Automated Chamber System Reveals Plant Phenology as Key Control of Production and Respiration Fluxes in a Boreal Peatland. *Glob. Change Biol.* 24, 3436–3451. doi:10.1111/gcb.14292

Kettles, L. M., Garneau, M., and Jette, H. (2000). *Macrofossil, Pollen, and Geochemical Records of Peatlands in the Kinosheo Lake and Detour Lake Areas, Northern Ontario*. Bulletin 545. 24p. Ottawa, ON: Geological Survey of Canada. Available at:. https://geoscan.nrcan.gc.ca/starweb/geoscan/servlet.starweb. (Accessed October 19, 2019). doi:10.4095/211326

Kettridge, N., Lukenbach, M. C., Hokanson, K. J., Devito, K. l., Petrone, R. M., Mendoza, C. A., et al. (2019). Severe Wildfire Exposes Remnant Peat Carbon Stocks to Increased post-fire Drying. *Sci. Rep.* 9, 3727. doi:10.1038/s41598-019-40033-7

Klinger, L. F., Zimmerman, P. R., Greenberg, J. P., Heidt, L. E., and Guenther, A. B. (1994). Carbon Trace Gas Fluxes along a Successional Gradient in the Hudson Bay Lowland. *J. Geophys. Res.* 99, 1469–1494. doi:10.1029/93jd00312

Lafleur, P. M., Roulet, N. T., Bubier, J. L., Frolking, S., and Moore, T. R. (2003). Interannual Variability in the Peatland-Atmosphere Carbon Dioxide Exchange at an Ombrotrophic Bog. *Glob. Biogeochem. Cycles* 17, a–n. doi:10.1029/2002GB001983

Lai, D. Y. F., Roulet, N. T., and Moore, T. R. (2014). The Spatial and Temporal Relationships between CO2 and CH4 Exchange in a Temperate Ombrotrophic Bog. *Atmos. Environ.* 89, 249–259. doi:10.1016/j.atmosenv.2014.02.034

Laiho, R. (2006). Decomposition in Peatlands: Reconciling Seemingly Contrasting Results on the Impacts of Lowered Water Levels. *Soil Biol. Biochem.* 38, 2011–2024. doi:10.1016/j.soilbio.2006.02.017

Leppälä, M., Laine, A. M., Seväkivi, M. L., and Tuittila, E. S. (2011). Differences in CO2 Dynamics between Successional Mire Plant Communities during Wet and Dry Summers. *J. Veg. Sci.* 22, 357–366. doi:10.1111/j.1654-1103.2011.01259.x

Libilik, L. K., Moore, T. R., Bubier, J. L., and Robinson, S. D. (1997). Methane Emissions from Wetlands in the Zone of Discontinuous Permafrost: Fort Simpson, Northwest Territories, Canada. *Glob. Biogeochem. Cycles* 11, 485–494. doi:10.1029/97GB01935

Mauritz, M., Bracho, R., Celis, G., Hutchings, J., Natali, S. M., Pegoraro, E., et al. (2014). Nonlinear CO2 Flux Response to 7 years of Experimentally Induced Permafrost Thaw. *Glob. Chang. Biol.* 23, 3646–3666. doi:10.1111/gcb.13661

McLaughlin, J., and Webster, K. (2014). Effects of Climate Change on Peatlands in the Far North of Ontario, Canada: A Synthesis. *Arctic, Antarctic, Alpine Res.* 46, 84–102. doi:10.1657/1938-4246-46.1.84

McLaughlin, J. W., Packalen, M. S., and Shrestha, B. (2018). *Assessment of the Vulnerability if Peatland Carbon in the Albany Ecodistrict of the Hudson Bay Lowlands, Ontario, Canada to Climate Change*. Climate Change Research Report 34. 151p. Ontario Ministry of Natural Resources, Applied Research and Development Branch. Sault Ste. Marie, ON, Canada. Available at: http://www.climateontario.ca/scripts/MNR_Pub/publication_summary.php?pubId=67 (Accessed January 4, 2019).

McLaughlin, J. W., and Webster, K. L. (2010). Alkalinity and Acidity Cycling and Fluxes in an Intermediate Fen Peatland in Northern Ontario. *Biogeochemistry* 99, 143–155. doi:10.1007/s10533-009-9398-5

McLaughlin, J. W., and Webster, K. L. (2013). *Effects of a Changing Climate on Peatlands in Permafrost Zones: A Literature Review and Application to Ontario's Far North*. Climate Change Research Report 34. 151p. Ontario Ministry of Natural Resources, Applied Research and Development Branch. Sault Ste. Marie, ON, Canada. Available at: http://www.climateontario.ca/scripts/MNR_Pub/publication_summary.php?pubId=25 (Accessed June 20, 2014).

Mezbahuddin, M., Grant, R. F., and Flanagan, L. B. (2017). Coupled Eco-Hydrology and Biogeochemistry Algorithms Enable the Simulation of Water Table Depth Effects on Boreal Peatland Net CO2 Exchange. *Biogeosciences* 14, 5507–5531. doi:10.5194/bg-14-5507-2017

Moore, T. R., Heyes, A., and Roulet, N. T. (1994). Methane Emissions from Wetlands, Southern Hudson Bay Lowland. *J. Geophys. Res.* 99, 1455–1467. doi:10.1029/93jd02457

Munir, T. M., Perkins, M., Kaing, E., and Strack, M. (2015). Carbon Dioxide Flux and Net Primary Production of a Boreal Treed Bog: Responses to Warming and Water-Table-Lowering Simulations of Climate Change. *Biogeosciences* 12, 1091–1111. doi:10.5194/bg-12-1091-2015

Myers, B., Webster, K. L., McLaughlin, J. W., and Basiliko, N. (2012). Microbial Activity across a Boreal Peatland Nutrient Gradient: the Role of Fungi and Bacteria. *Wetlands Ecol. Manage.* 20, 77–88. doi:10.1007/s11273-011-9242-2

Myers-Smith, I. H., McGuire, A., Harden, J., and Chapin, F. (2007). Influence of disturbance on carbon exchange in a permafrost collapse and adjacent burned forest. *J. Geophys. Res.* 112, G04017. doi:10.1029/2007JG000423

Nakano, T., Kuniyoshi, S., and Fukuda, M. (2000). Temporal Variation in Methane Emission from Tundra Wetlands in a Permafrost Area, Northeastern Siberia. *Atmos. Environ.* 34, 1205–1213. doi:10.1016/s1352-2310(99)00373-8

Neumann, H. H., den Hartog, G., King, K. M., and Chipanshi, A. C. (1994). Carbon Dioxide Fluxes over a Raised Open Bog at the Kinosheo Lake tower Site during the Northern Wetlands Study (NOWES). *J. Geophys. Res.* 99, 1529–1538. doi:10.1029/93jd01360

Neumann, R. B., Moorberg, C. J., Lundquist, J. D., Turner, J. C., Waldrop, M. P., McFarland, J. W., et al. (2019). Warming Effects of spring Rainfall Increase Methane Emissions from Thawing Permafrost. *Geophys. Res. Lett.* 46, 1393–1401. doi:10.1029/2018gl081274

Nykänen, H., Heikkinen, J. E. P., Pirinen, L., Tiilikainen, K., and Martikainen, P. J. (2003). Annual CO2exchange and CH4fluxes on a Subarctic Palsa Mire during Climatically Different Years. *Glob. Biogeochem. Cycles* 17, 1018. doi:10.1029/2002GB001861

O'Reilly, B. C., Finkelstein, S. A., and Bunbury, B. (2014). Pollen-derived Paleovegetation Reconstruction and Long-Term Carbon Accumulation at a Fen Site in the Attawapiskat River Watershed, Hudson Bay Lowlands, Canada. *Arct. Antarct. Alp. Res.* 46, 6–18. doi:10.1657/1938-4246-46.1.6

Olefeldt, D., Euskirchen, E. S., Harden, J., Kane, E., McGuire, A. D., Waldrop, M. P., et al. (2017). A Decade of Boreal Rich Fen Greenhouse Gas Fluxes in Response to Natural and Experimental Water Table Variability. *Glob. Change Biol.* 23, 2428–2440. doi:10.1111/gcb.13612

Ontario Ministry of Natural Resource and Forestry (2016). *Provincial Digital Elevation Model Technical Specification*. Peterborough, ON, Canada. Available at: https://www.sse.gov.onca/sites/MNR-PublicDocs/EN/CMID/ProvDigitalElevationModelTechSpec.pdf (Accessed January 5, 2019).

Ontario Ministry of Natural Resources and Forestry (2014). *Far North Land Cover Data Specifications Version 1.4*. Peterborough, ON, Canada. Available at: https://www.sse.gov.on.ca/sites/MNR-PublicDocs/EN/CMID/Far%20North%20Land%20Cover%20-%20Data%20Specification.pdf (Accessed January 5, 2019).

Ou, C., Leblon, B., Zhang, Y., LaRocque, A., Webster, K., and McLaughlin, J. (2016). Modelling and Mapping Permafrost at High Spatial Resolution Using Landsat and Radarsat Images in Northern Ontario, Canada: Part 1 - Model Calibration. *Int. J. Remote Sensing* 37, 2727–2750. doi:10.1080/01431161.2016.1157642

Packalen, M. S., Finkelstein, S. A., and McLaughlin, J. W. (2016). Climate and Peat Type in Relation to the Spatial Distribution of the Peat Carbon Mass in the Hudson Bay Lowland, Canada. *J. Geophys. Res. Biogeosci.* 121, 1104–1117. doi:10.1002/2015JG002938

Packalen, M. S., Finkelstein, S. A., and McLaughlin, J. W. (2014). Holocene Peat Initiation, Carbon Storage and Potential Methane Production in the Hudson Bay Lowlands, Canada. *Nat. Commun.* 5, 4078. doi:10.1038/ncomms5078

Packalen, M. S., and Finkelstein, S. A. (2014). Quantifying Holocene Variability in Carbon Uptake and Release since Peat Initiation in the Hudson Bay Lowlands, Canada. *The Holocene* 24, 1063–1074. doi:10.1177/0959683614540728

Pagano, A., Pluchinotta, I., Giordano, R., Petrangeli, A. B., Fratino, U., and Vurro, M. (2018). Dealing with Uncertainty in Decision-Making for Drinking Water Supply Systems Exposed to Extreme Events. *Water Resour. Manage.* 32, 2131–2145. doi:10.1007/s11269-018-1922-8

Peichl, M., Öquist, M., Löfvenius, M. O., Ilstedt, U., Sagerfors, J., Grelle, A., et al. (2014). A 12-year Record Reveals Pre-growing Season Temperature and Water Table Level Threshold Effects on the Net Carbon Dioxide Exchange in a Boreal Fen. *Environ. Res. Lett.* 9, 05500. doi:10.1088/1748-9326/9/5/055006

Pironkova, Z. (2017). Mapping Palsa and Peat Plateau Changes in the Hudson Bay Lowlands, Canada, Using Historical Aerial Photography and High-Resolution Satellite Imagery. *Can. J. Remote Sensing* 43, 455–467. doi:10.1080/07038992.2017.1370366

Prat-Guitart, N., Rein, G., Hadden, R. M., Belcher, C. M., and Yearsley, J. M. (2016). Effects of Spatial Heterogeneity in Moisture Content on the Horizontal Spread of Peat Fires. *Sci. Total Environ.* 572, 1422–1430. doi:10.1016/j.scitotenv.2016.02.145

Preston, M. D., Smemo, K. A., McLaughlin, J. W., and Basiliko, N. (2012). Peatland Microbial Communities and Decomposition Processes in the James Bay Lowlands, Canada. *Front. Microbio.* 3, 70. doi:10.3389/fmicb.2012.00070

Price, D. T., McKenney, D. W., Joyce, L. A., Siltanen, R. M., Papadopol, P., and Lawrence, K. (2011). *High-resolution Interpolation of Climate Scenarios for Canada Derived from General Circulation Model Simulations. Natural Resources Canada, Canadian Forest Service, Northern Forestry Centre, Edmonton, AB.* Information Report NOR-X-421.Riley, J.L. 2011. Toronto, ON: Nature Conservancy of Canada, 156. Wetlands of the Ontario Hudson Bay Lowland: A Regional Overview.

Riley, J. L. (2011). *Wetlands of the Ontario Hudson Bay Lowland: A Regional Overview*. Toronto, ON: Nature Conservancy of Canada, 156.

Riutta, T., Laine, J., Aurela, M., Rinne, J., Vesala, T., Laurila, T., et al. (2007). Spatial Variation in Plant Community Functions Regulates Carbon Gas Dynamics in a Boreal Fen Ecosystem. *Tellus B Chem. Phys. Meteorol.* 59 (5), 838–852. doi:10.1111/j.1600-0889.2007.00302.x

IPCC (2014). in *Synthesis Report. Contribution of Working Groups I, II and III to the Fifth Assessment Report of the Intergovernmental Panel on Climate Change [Core Writing Team*. Editors R. K. Pachauri and L. A. Meyer (Geneva, Switzerland: IPCC), 151. Available at: https://www.ipcc.ch/site/assets/uploads/2018/05/SYR_AR5_FINAL_full_wcover.pdf (Accessed June 19, 2019)., Editors].

Roulet, N., Moore, T., Bubier, J., and Lafleur, P. (1992). Northern Fens: Methane Flux and Climatic Change. *Tellus B: Chem. Phys. Meteorology* 44, 100–105. doi:10.3402/tellusb.v44i2.15429

Rouse, W. R. (1998). A Water Balance Model for a Subarctic Sedge Fen and its Application to Climatic Change. *Clim. Change* 38, 207–234. doi:10.1023/a:1005358017894

Sagerfors, J., Lindroth, A., Grelle, A., Klemedtsson, L., Weslien, P., and Nilsson, M. (2008). Annual CO2 exchange between a Nutrient-Poor, Minerotrophic, Boreal Mire and the Atmosphere. *J. Geophys. Res.* 113, a–n. doi:10.1029/2006JG000306

Salm, J. O., Maddison, M., Tammik, S., Soosaar, K., Truu, J., and Mander, Ü. (2012). Emissions of CO2, CH4 and N2O from Undisturbed, Drained and Mined Peatlands in Estonia. *Hydrobiologia* 692, 41–55. doi:10.1007/s10750-011-0934-7

Schreader, C. P., Rouse, W. R., Griffis, T. J., Boudreau, L. D., and Blanken, P. D. (1998). Carbon Dioxide Fluxes in a Northern Fen during a Hot, Dry Summer. *Glob. Biogeochem. Cycles* 12, 729–740. doi:10.1029/98GB02738

St.-Hilaire, F., Wu, J., Roulet, N. T., Frolking, S., Lafleur, P. M., Humphreys, E. R., et al. (2010). McGill Wetland Model: Evaluation of a Peatland Carbon Simulator Developed for Global Assessments. *Biogeosciences* 7, 351. doi:10.5194/bg-7-3517-2010

Strack, M., Waddington, J. M., and Tuittila, E. S. (2004). Effect of Water Table Drawdown on Northern Peatland Methane Dynamics: Implications for Climate Change. *Glob. Biogeochem. Cycles* 8, GB4003. doi:10.1029/2003GB002209

Strack, M., and Waddinton, J. M. (2007). Response of Peatland Carbon Dioxide and Methane Fluxes to a Water Table Drawdown experiment. *Glob. Biogeochem. Cycles* 21, GB1007. doi:10.1029/2006GB002715.200.Strack

Strilesky, S. L., and Humphreys, E. R. (2012). A Comparison of the Net Ecosystem Exchange of Carbon Dioxide and Evapotranspiration for Treed and Open Portions of a Temperate Peatland. *Agric. For. Meteorology* 153, 45–53. doi:10.1016/j.agrformet.2011.06.006

Ström, L., and Christensen, T. R. (2007). Below Ground Carbon Turnover and Greenhouse Gas Exchanges in a Sub-arctic Wetland. *Soil Biol. Biochem.* 39, 1689–1698. doi:10.1016/j.soilbio.2007.01.019

Sushama, L., Laprise, R., and Allard, M. (2006). Modeled Current and Future Soil thermal Regime for Northeast Canada. *J. Geophys. Res.* 111, D18111. doi:10.1029/2005JD007027

Suyker, A. E., Verma, S. B., and Arkebauer, T. J. (1997). Season-long Measurement of Carbon Dioxide Exchange in a Boreal Fen. *J. Geophys. Res.* 102, 29021–29028. doi:10.1029/96jd03877

Syed, K. H., Flanagan, L. B., Carlson, P. J., Glenn, A. J., and Van Gaalen, K. E. (2006). Environmental Control of Net Ecosystem CO2 Exchange in a Treed, Moderately Rich Fen in Northern Alberta. *Agric. For. Meteorology* 140, 97–114. doi:10.1016/j.agrformet.2006.03.022

Thomsen, N. I., Binning, P. J., McKnight, U. S., Tuxen, N., Bjerg, P. L., and Troldborg, M. (2016). A Bayesian Belief Network Approach for Assessing Uncertainty in Conceptual Site Models at Contaminated Sites. *J. Contaminant Hydrol.* 188, 12–28. doi:10.1016/j.jconhyd.2016.02.003

Trudeau, N. C., Garneau, M., and Pelletier, L. (2013). Methane Fluxes from a Patterned Fen of the Northeastern Part of the La Grande River Watershed, James Bay, Canada. *Biogeochemistry* 113, 409–422. doi:10.1007/s10533-012-9767-3

Turetsky, M. R., Benscoter, B., Page, S., Rein, G., van der Werf, G. R., and Watts, A. (2015). Global Vulnerability of Peatlands to Fire and Carbon Loss. *Nat. Geosci* 8, 11–14. doi:10.1038/ngeo2325

Turetsky, M. R., Kane, E. S., Harden, J. W., Ottmar, R. D., Manies, K. L., Hoy, E., et al. (2011). Recent Acceleration of Biomass Burning and Carbon Losses in Alaskan Forests and Peatlands. *Nat. Geosci* 4, 27–31. doi:10.1038/ngeo1027

Turetsky, M. R., Kotowska, A., Bubier, J., Dise, N. B., Crill, P., Hornibrook, E. R. C., et al. (2014). A Synthesis of Methane Emissions from 71 Northern, Temperate, and Subtropical Wetlands. *Glob. Change Biol.* 20, 2183–2197. doi:10.1111/gcb.12580

Turetsky, M. R., Wieder, R. K., Vitt, D. H., Evans, R., and Scott, K. D. (2002). Boreal Peatland C Fluxes under Varying Permafrost Regimes. *Soil Biol. Biochem.* 34, 907–912. doi:10.1016/s0038-0717(02)00022-6

Turetsky, M. R., Wieder, R. K., Vitt, D. H., Evans, R., and Scott, K. D. (2007). The Disappearance of Relict Permafrost in Boreal North America: Effects on Peatland Carbon Storage and Fluxes. *Glob. Change Biol.* 13, 1922–1934. doi:10.1111/j.1365-2486.2007.01381.x

Turquety, S., Logan, J. A., Jacob, D. J., Hudman, R. C., Leung, F. Y., Heald, C. L., et al. (2007). Inventory of Boreal Fire Emissions for North America in 2004: Importance of Peat Burning and Pyroconvective Injection. *J. Geophys. Res.* 112, D12S03. doi:10.1029/2006JD007281

Uusiitalo, L., Lehikonen, A., Helle, I., and Myberg, K. (2015). An Overview of Methods to Evaluate Uncertainty of Deterministic Models in Decision Support. *Environ. Model. Softw.* 63, 24–31. doi:10.1016/j.envsoft.2014.09.017

Webster, K. L., Bhatti, J. S., Thompson, D. K., Nelson, S. A., Shaw, C. H., Bona, K. A., et al. (2018). Spatially-integrated Estimates of Net Ecosystem Exchange and Methane Fluxes from Canadian Peatlands. *Carbon Balance Manage* 13, 16. doi:10.1186/s13021-018-0105-5

Webster, K. L., and McLaughlin, J. W. (2014). Application of a Bayesian Belief Network for Assessing the Vulnerability of Permafrost to Thaw and Implications for Greenhouse Gas Production and Climate Feedback. *Environ. Sci. Pol.* 38, 28–44. doi:10.1016/j.envsci.2013.10.008

Webster, K. L., and McLaughlin, J. W. (2010). Importance of the Water Table in Controlling Dissolved Carbon along a Fen Nutrient Gradient. *Soil Sci. Soc. Am. J.* 74, 2254–2266. doi:10.2136/sssaj2009.0111

Webster, K. L., McLaughlin, J. W., Kim, Y., Packalen, M. S., and Li, C. S. (2013). Modelling Carbon Dynamics and Response to Environmental Change along a Boreal Fen Nutrient Gradient. *Ecol. Model.* 248, 148–164. doi:10.1016/j.ecolmodel.2012.10.004

Wickland, K., Striegl, R., Neff, J., and Sachs, T. (2006). Effects of permafrost melting on CO2 and CH4 exchange of a poorly drained black spruce lowland. *J. Geophys. Res.* 111, G02011. doi:10.1029/2005JG000099

Wilson, R. M., Fitzhugh, L., Whiting, G. J., Frolking, S., Harrison, M. D., Dimova, N., et al. (2017). Greenhouse Gas Balance over Thaw-freeze Cycles in Discontinuous Zone Permafrost. *J. Geophys. Res. Biogeosci.* 122, 387–404. doi:10.1002/2016jg003600

Wu, J., and Roulet, N. T. (2014). Climate Change Reduces the Capacity of Northern Peatlands to Absorb the Atmospheric Carbon Dioxide: The Different Responses of Bogs and Fens. *Glob. Biogeochem. Cycles* 28, 1005–1024. doi:10.1002/2014gb004845

Zoltai, S. C., Morrissey, L. A., Livingston, G. P., and Groot, W. J. (1998). Effects of Fires on Carbon Cycling in North American Boreal Peatlands. *Environ. Rev.* 6, 13–24. doi:10.1139/a98-002

Conflict of Interest: The authors declare that the research was conducted in the absence of any commercial or financial relationships that could be construed as a potential conflict of interest.

frontiers in Earth Science

ORIGINAL RESEARCH
published: 29 July 2021
doi: 10.3389/feart.2021.665802

Submarine Groundwater Discharge From Non-Tidal Coastal Peatlands Along the Baltic Sea

Erwin Don Racasa[1]*, *Bernd Lennartz*[1], *Miriam Toro*[1,2] and *Manon Janssen*[1]

[1]Soil Physics, Faculty of Agricultural and Environmental Sciences, University of Rostock, Rostock, Germany, [2]Landesamt für Landwirtschaft, Umwelt und ländliche Räume, Flintbek, Germany

Submarine groundwater discharge (SGD) is an important pathway for water and materials within the land-ocean transition zone that can impact coastal environments and marine life. Although research from sandy shorelines has rapidly advanced in recent years, there is very little understanding of coastal areas characterized by a low hydraulic conductivity, such as carbon-rich coastal peatlands. The objective of this study was to determine the magnitude and location of terrestrial SGD to be expected from a non-tidal low-lying coastal peatland located along the Baltic Sea and to understand the controlling factors using numerical modeling. We employed the HYDRUS-2D modeling package to simulate water movement under steady-state conditions in a transect that extends from the dune dike-separated rewetted fen to the shallow sea. Soil physical properties, hydraulic gradients, geological stratifications, and topography were varied to depict the range of properties encountered in coastal peatlands. Our results show that terrestrial SGD occurs at the study site at a flux of 0.080 $m^2\,d^{-1}$, with seepage rates of 1.05 $cm\,d^{-1}$ (upper discharge region) and 0.16 $cm\,d^{-1}$ (lower discharge region above submerged peat layer). These calculated seepage rates compare to observations from other wetland environments and SGD sites in the Baltic Sea. The groundwater originates mainly from the dune dike—recharged by precipitation and infiltration from ponded peatland surface water—and to a lesser extent from the sand aquifer. The scenario simulations yielded a range of potential SGD fluxes of 0.008–0.293 $m^2\,d^{-1}$. They revealed that the location of terrestrial SGD is determined by the barrier function of the peat layer extending under the sea. However, it has little impact on volume flux as most SGD occurs near the shoreline. Magnitude of SGD is mainly driven by hydraulic gradient and the hydraulic conductivity of peat and beach/dune sands. Anisotropy in the horizontal direction, aquifer and peat thickness, and peatland elevation have little impacts on SGD. We conclude that SGD is most probable from coastal peatlands with high water levels, large K_s and/or a dune dike or belt, which could be an essential source for carbon and other materials via the SGD pathway.

Keywords: coastal wetlands, HYDRUS-2D, terrestrial SGD, hydraulic conductivity (K), non-tidal shorelines, dune dike, rewetted peatlands

OPEN ACCESS

Edited by:
Michel Bechtold,
KU Leuven, Belgium

Reviewed by:
Ullrich Dettmann,
Thuenen Institut Braunschweig, Germany
Joseph James Tamborski,
Old Dominion University, United States

***Correspondence:**
Erwin Don Racasa
erwin.racasa@uni-rostock.de

Specialty section:
This article was submitted to Hydrosphere, a section of the journal Frontiers in Earth Science

Received: *09 February 2021*
Accepted: *08 July 2021*
Published: *29 July 2021*

Citation:
Racasa ED, Lennartz B, Toro M and Janssen M (2021) Submarine Groundwater Discharge From Non-Tidal Coastal Peatlands Along the Baltic Sea. Front. Earth Sci. 9:665802. doi: 10.3389/feart.2021.665802

INTRODUCTION

Submarine groundwater discharge has been recognized as an important land-ocean route for water and materials (Burnett et al., 2003; Burnett et al., 2006; Moore, 2010; Taniguchi et al., 2019) and often has higher concentrations of carbon, nutrients, and metals than river waters (Moore, 2010). Along the German coast of the southern Baltic Sea, low-lying coastal areas with peatlands (<1 masl elevation) have been abundantly documented (Jurasinski et al., 2018), some with submerged peat extending beyond the coastline (Kreuzburg et al., 2018). The vast majority of these coastal peatlands are degraded due to a long history of drainage for agricultural usage (Baird, 1997) and bordered by coastal protection measures (Bollmann et al., 2010). They are thus characterized by a low hydraulic conductivity (K_s) and low hydraulic gradients. In organic-rich subterranean estuaries, high concentrations of remineralized forms of organic matter have been reported (Taniguchi et al., 2019). Coastal peatlands with their large stores of carbon, organic matter, and nutrients from decaying plants could thus be a potentially overlooked source of water and materials for the Baltic Sea via the SGD pathway.

The occurrence of SGD—sourced from terrestrial groundwater or recirculated seawater and usually a mixture of both—depends on several factors. Soil hydrological properties, such as hydraulic conductivity, anisotropy, and preferential flow pathways, can affect the magnitude and location of terrestrial SGD. Real-world complexities such as geological heterogeneities, non-uniform and evolving alongshore and cross-shore morphology (Robinson et al., 2018), topographic differences, and anthropogenic structures can also be important factors. Global coastal groundwater discharge is predominantly controlled by the flow capacity of aquifers–a product of permeability, topographic gradient, and thickness of coastal aquifers (Luijendijk et al., 2020). In contrast, SGD from recirculated seawater or "recirculated SGD" is driven by currents, waves, tides, and density differences (Taniguchi et al., 2019). In this research, we focus only on terrestrial SGD.

Although SGD studies have rapidly advanced in recent years, most information was generated from sandy shorelines. Very little research has been conducted on muddy shorelines such as salt marshes, mangroves (Taniguchi et al., 2019), and even coastal peatlands. Previous SGD studies in the Baltic Sea have focused on known and expected groundwater discharge areas (Szymczycha et al., 2014; Szymczycha et al., 2016; Szymczycha and Pempkowiak, 2016; Szymczycha et al., 2020) but new sources, such as submarine terraces (Jakobsson et al., 2020) and pockmarks (Idczak et al., 2020), have also been proposed. Total groundwater discharge in the Baltic Sea was estimated at 1% of total river runoff but phosphorus and carbon SGD fluxes were calculated to be 86 and 30%, respectively, of rivers (Szymczycha and Pempkowiak, 2016). The measured annual average concentrations of dissolved organic carbon (DOC) in the Bay of Puck is 5.8 mg C L^{-1} (Szymczycha et al., 2014). However, in coastal peatlands, DOC and other materials concentrations can be much more relevant.

Our study seeks to address the lack of data for SGD from coastal peatlands using numerical simulations. The main objectives are to 1) quantify magnitude and location (distance from coast) of terrestrial SGD flux from a coastal peatland located along the Baltic Sea and 2) determine the factors that govern terrestrial SGD from peatlands in low-lying coastal environments by assessing the impact of soil hydraulic properties, sea and groundwater levels, and geological stratification and topography. With the current trend on restoring extensively modified coastal peatlands to mitigate greenhouse gas emissions, understanding how groundwater flows and how materials are transported is ever more imperative.

MATERIALS AND METHODS

Study Site

The reference peatland for simulating groundwater flow and discharge in this study is based on a coastal peatland near the city of Rostock, northeast Germany, the Hütelmoor Nature Reserve ("Naturschutzgebiet Heiligensee und Hütelmoor"; 54.2139 N 12.1725 E) (**Figure 1**). This coastal peatland borders the Baltic Sea along a 3-km long shoreline, but is physically separated by a 40-m wide dune dike that thins out in its northern part. The area was shaped by the Weichselian ice age. The glacial till is covered by glacio-fluvial sands with 2.5–15 m thickness, which now form a shallow aquifer (Ibenthal, 2020 and references therein). During the Littorina transgression 8,000–1,200 BP, the rising groundwater level resulted in the development of a paludification fen from 7,000 BP onwards (Kreuzburg et al., 2018). Peat thickness is up to 3 m in the central peatland and near the coast, while it thins out towards the forest. A special feature is the outcropping of the peat at the coastline and in the shallow Baltic Sea. Strongly decomposed sedges and reed make up the peat. Elevation of the peatland is −0.15–0.75 masl (meters above sea level) with a total area of 350 ha (Ibenthal, 2020). Annual precipitation, annual evapotranspiration, and average daily temperature are 693 mm, 604 mm (1951–2010; Miegel et al., 2016), and 9.7°C (at Warnemünde, ~7 km away, 1990–2019; DWD(Deustcher Wetterdienst), 2020), respectively.

The Hütelmoor, similar to many coastal peatlands in the southern Baltic Sea region, has been artificially drained, diked, and utilized as pasture. Initial drainage started in the 18th century and extensive pumping from 1976 to 1991 led to degradation and compaction of the peat's upper decimeters (Jurasinski et al., 2018). In December 2009, the construction of a ground sill with an elevation of 0.4 masl at the outlet of the peatland's ditch system enabled rewetting and renaturation of the peatland. Since then, most of the peatland is flooded with surface waters. The ditches still drain the peatland when the water level exceeds the groundsill, they affect local groundwater flow fields and divert water inflow from the forest (Ibenthal, 2020). The peatland is still separated from the Baltic Sea by a dune dike, that is not maintained anymore. The electrical conductivity (EC) in ground- and surface water in the peatland ranged from 4–13 mS/cm and thus revealed brackish waters, originating from earlier inundations and occasional seawater inflow via the dike system during storms (Ibenthal, 2020). In comparison, several EC measurements from the nearshore waters in front of the

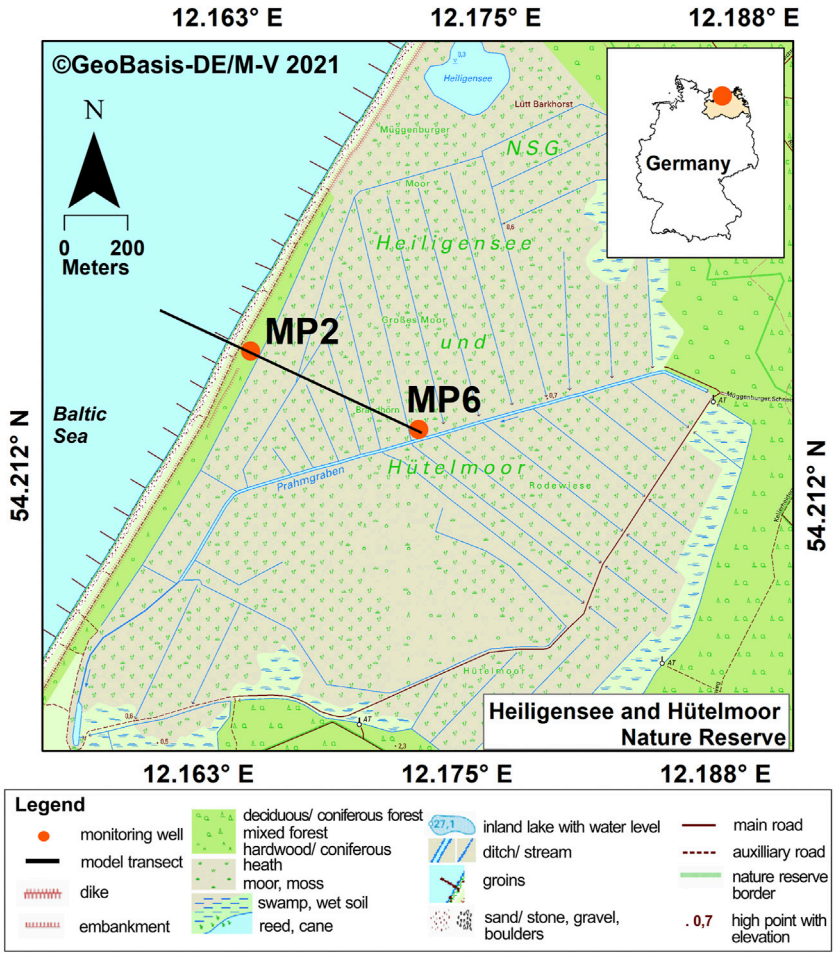

FIGURE 1 | The nature reserve "Heiligensee und Hütelmoor," in Mecklenburg-Western Pomerania, Germany. The black line indicates the transect for the 2D groundwater model. MP2 and MP6 are groundwater observation wells. A groundsill was installed at the outlet of the ditch system in December 2009, restricting the drainage function of the ditches to high water levels. The background topographical map was taken from https://www.laiv-mv.de/Geoinformation/Karten/Topographische-Karten/.

Hütelmoor ranged from 18 to 27 mS/cm, corresponding to a salinity of 11–15 psu. Due to the brackish nature of groundwater in the peatland, we name the submarine groundwater discharging from land "terrestrial" (and not fresh) SGD in this study.

Approach for Modelling Terrestrial SGD

We simulated terrestrial submarine groundwater discharge in the Hütelmoor using the HYDRUS-2D modeling package. HYDRUS simulates water movement in variably saturated media by solving the Richards equation for Darcian water flow:

$$\frac{\partial \theta}{\partial t} = \frac{\partial}{\partial x_i}\left[K\left(K_{ij}^{A}\frac{\partial h}{\partial x_j} + K_{iz}^{A}\right)\right] - s \qquad (1)$$

where θ is the volumetric water content, h is pressure head, x_i are spatial coordinates, t is time, S is the sink term, K_{iz}^{A} are components of anisotropy tensor K_{ij}^{A}, and K is unsaturated hydraulic conductivity (Šimůnek et al., 2018). The equations are solved using the Galerkin-type linear finite elements method which can be discretized spatially and temporally. An iterative process is used to solve the equations due to the non-linear nature of the Richards equation (Šimůnek et al., 2018).

HYDRUS can simulate the flow of water both in the unsaturated dune dike and the fully saturated peatland. The reference scenario comprises a 2D cross-section reaching from the central part of the Hütelmoor Nature Reserve peatland into the shallow Baltic sea (**Figures 1**, **2**). The topography, geological stratification, material properties, and boundary conditions were based on measured data, and steady-state groundwater fluxes were simulated to yield a long-term average of terrestrial SGD. Fluxes originating from aquifer, peat, and dune were quantified separately. In subsequent model runs, these factors were changed one by one based on actual and realistic predicted conditions, to determine their respective impacts on SGD.

Water inflows (**Figure 2**–blue arrows) into the coastal peatland system come from 1) the ponded surface waters above the peat, 2) precipitation at dune dike and beach, 3) recharge from recirculated SGD at the seafloor (corresponding

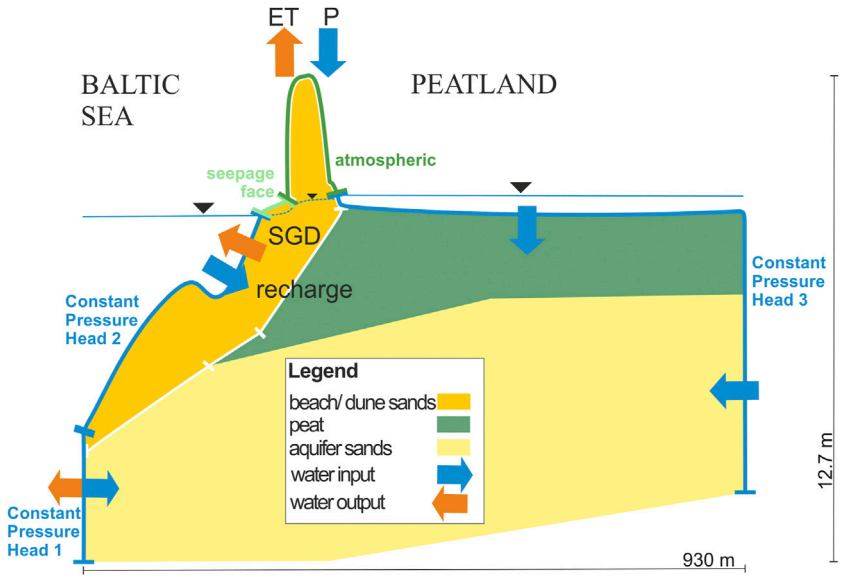

FIGURE 2 | Coastal peatland system with water in- and outflows and model boundary conditions. White lines at the boundary of the beach/dune sands are mesh lines used to calculate water fluxes. The peat extension layer is also depicted here. Note the vertical exaggeration of the cross-section.

to Constant Pressure Head 2), and 4) lateral groundwater inflow from the landside. Outflows (orange arrows) from the system occur as evapotranspiration in the dune and the total SGD from the seafloor. Uncertainty in water flow from the sea-submerged aquifer sands (left boundary) makes it either an inflow or outflow region. Infiltration from ponded peatland surface waters is also expected into the dune dike.

Modeling Domain

We established the modeling domain (**Supplementary Figure 1**) using published and available data. It extends from the shallow Baltic Sea to the central peatland (**Figure 1**). Elevation measurements at the groundwater observation wells (Ibenthal, 2020) and seawater level were used as reference points of the domain, while ground heights in between these reference points were obtained from a Digital Elevation Map (provided by Landesamt für innere Verwaltung Mecklenburg-Vorpommern, Schwerin, Germany) using the 3D Analyst Toolbox of ARCMap. The materials were distributed following the geological profile constructed based on sediment cores (Jurasinski et al., 2018; Ibenthal, 2020). Bathymetric data from marine surveys (Kreuzburg et al., 2018) completed the model geometry, taking note of the longshore bar mound 100 m from the coast. The modeling domain's total length is 930 m, of which 245 m extend into the sea. In the vertical direction, it extends from 3.7 masl at the top of the dune dike to −9 masl at the aquifer bottom. The bottom boundary follows the surface of the glacial till.

The modeling domain's discretization was carefully scrutinized and yielded a final target size of 1.0 m, *x*-direction stretching factor of 25, and a smoothing factor of 1.8. To account for the highly non-linear water flow in the unsaturated zone of the dune dike, a surface mesh refinement of 0.05 m was applied in the upper beach/dune sands. Surface refinements of 0.2 and 0.5 m were also applied at the lower beach/dune sands and peat materials, respectively. A total of 3,454 nodes resulted from this configuration with 351 nodes and 351 elements on the domain boundary.

Model Runtime

The maximum model runtime was set at 360 days. All simulations achieved steady-state in the given runtime except for the minimum beach/dune K_s scenario, where runtime was increased to 720 days. Initial, minimum, and maximum time steps were set at 0.01, 0.001, and 5 days, respectively.

Soil Hydraulic Parameters

We applied the single-porosity van Genuchten-Mualem model. Soil hydraulic properties of the reference scenario (**Table 1**) were derived from soil data gathered previously at the study site. For soil texture of the aquifer sands and beach/dune sands, average particle size distributions were calculated from 34 to 6 soil samples, respectively. The resulting composition of aquifer sands was 89.4% sand, 7.5% silt and 3.1% clay. The beach/dune sands were sandier with 98.3% sand, 0.9% silt and 0.8% clay. Soil hydraulic parameters were then generated using the neural network prediction "Rosetta" incorporated into the Hydrus software (Schaap et al., 2001). Peat hydraulic parameters were calculated with the pedotransfer functions for sedge bulk density of ≤0.2 g cm^{-3} proposed by Liu and Lennartz (2019), based on measured bulk density ranging from 0.12 to 0.15 g cm^{-3} in the peatland (L. Gosch, personal communication, August 23, 2019) and 0.17 g cm^{-3} in the peat exposed at the coastline (Gosch et al., 2019). The residual water content for peat was assigned a value of 0.2. For the tortuosity and pore-connectivity parameter (L), a value of 0.5 is acceptable for degraded fen peat under wet or saturation conditions

TABLE 1 | Soil hydraulic parameters used in the standard scenario.

Name	Q_r ($m^3\ m^{-3}$)	Q_s ($m^3\ m^{-3}$)	α (m^{-1})	n	K_s ($m\ d^{-1}$)	l
Beach/Dune sands	0.05150	0.37662	3.39265	4.04174	11.8100	0.5
Peat	0.20000	0.88000	2.90000	1.22000	0.00864	0.5
Aquifer sands	0.04644	0.38180	3.72309	2.52943	1.73000	0.5

Q_r = residual water content; Q_s = saturated water content; α and n = parameters in the soil water retention function; K_s = saturated hydraulic conductivity; l = tortuosity parameter in the conductivity function.

(Dettmann et al., 2014; Liu and Lennartz, 2019) as well as for sands, as this is the average value for most soils based on calculations by Mualem (1976) (Simunek et al., 2018). For the peat and aquifer sands, saturated hydraulic conductivities (K_s), values determined with slug tests at the study site were used (Ibenthal, 2020); the resulting K_s values (geometric means) are 8.64×10^{-3} m d^{-1} for the peat (n = 4) and 1.73 m d^{-1} for the aquifer sands (n = 4). Dune K_s of 11.8 m d^{-1} (n = 8) was laboratory-determined on samples taken in the northern part of the dune and was adapted from a previous study (Mohawesh et al., 2017).

Boundary and Initial Conditions

The model boundary conditions (BC) were set as follows (see also **Figure 2**): Atmospheric BC was applied to the dune surface wherein long-term averages of meteorological variables were used (average precipitation: 1.90 mm d^{-1}; average evapotranspiration: 1.65 mm d^{-1}) (Rostock-Warnemünde 1951–2010; Miegel et al., 2016). At the beach, a seepage face BC was applied which switches to atmospheric BC in the absence of seepage. However, no seepage was observed across the seepage face in any of the simulations. In HYDRUS, "seepage face" refers to the boundary condition applied in surfaces where water leaves the saturated part of the flow domain. Constant head BCs in hydrostatic equilibrium were set on the left side (Constant Pressure Head 1) and at the seafloor (Constant Pressure Head 2), the pressure head corresponds to the average sea water level at Warnemünde, Rostock (2005–2015) of 0.091 masl (WSV(Wasserstraßen und Schiffahrtsverwaltung des Bundes), 2020). Likewise, the right-side boundary (Constant Pressure Head 3), which continues to the peatland surface, was assigned a constant BC in hydrostatic equilibrium, corresponding to the average peatland water level of 0.357 masl (September 2016 to October 2018; derived from 73,735 individual 15-min interval measurements; converted to equivalent freshwater heads). No flux was assumed at the bottom as the glacial till was considered impermeable.

Initial pressure heads were set to correspond with the constant head boundary conditions. As such, the initial bottom pressure head amounted to 9.357 m. A slight slope (0.05, x-direction) from the sea up to behind the dike was added because of pressure head differences. The peatland's ponded conditions have a higher pressure head compared to the seawater on the left side. The angular slope was not applied in sea level scenarios as the hydraulic gradient's difference was only 0.001 m.

Uncertainty Analysis

Most groundwater bodies are heterogeneous with hydraulic conductivity variability influencing groundwater transport (Peña-Haro et al., 2011). In peat soils, it has been shown that a heterogeneous hydraulic conductivity distribution can lead to complex groundwater flow patterns (Beckwith et al., 2003). Since our simulations are based on homogenous hydraulic conductivities in the three materials considered, uncertainty of the model outcome resulting from the variability of K_s cannot be assessed. To address this, we performed 100 extra simulation runs with random K_s values (**Supplementary Table 1**). The number of replicates of the K_s measurements was too small to derive distributions (aquifer, peat), or samples were only taken from a single site (beach/dune K_s). We therefore additionally analyzed K_s values calculated from particle size distributions following Beyer (1964) both for the aquifer (n = 34) and the beach/dune sands (n = 6). The geometric means were close to the ones of the measured K_s values. All K_s values were then $\log_{10}$-transformed. Random numbers were drawn from normal distributions with means based on the measured values, and the standard deviations of the Beyer-derived values.

For the peat K_s, the coefficient of variation reported by Baird (1997) for a degraded peat was used to calculate the SD. Other published datasets for fen peat (Liu et al., 2016; Wang et al., 2021) were not considered because of much higher K_s values. The $\log_{10}$ mean and SD were then used to generate the random K_s values. In **Supplementary Table 1**, a descriptive statistics summary of the random K_s values is listed.

Scenarios

To investigate the factors that affect the magnitude and location of terrestrial SGD from coastal peatlands, three clusters of scenarios were analyzed: 1) soil physical properties, 2) hydraulic gradients and, 3) geological stratification and topography (**Table 2**). The parameters were changed one at a time to better determine their individual impacts on SGD.

Soil Physical Properties

We investigated the effects of different magnitudes of material K_s and peat anisotropy. The peat K_s in the reference scenario is similar to mesic-humic peat in a peatland-pond system (Ferone and Devito, 2004) but lower than the average K_s for peatland sedges compiled in a meta-study (2.24×10^{-1} m d^{-1}; Liu and Lennartz, 2019). To picture a realistic range of potential peat K_s in coastal peatlands, the minimum, maximum and geometric mean of sedge peat K_s reported by Liu and Lennartz (2019) was used as well as mean ± one standard deviation of the log-transformed K_s. For the aquifer and beach/dune sands, K_s values were estimated from particle size distributions described previously. For the beach/dune sands, though, the aquifer

TABLE 2 | Steady-state scenarios used in the modeling.

Scenario cluster	Specific scenario	Values used
Soil physical properties	Peat hydraulic conductivity (K_s) (m d^{-1})	**0.00864** (0.000408, 0.0339, 0.224, 1.48, 17.4)
	Aquifer sands K_s (m d^{-1})	**1.73** (0.429, 2.20, 3.94, 7.06, 10.7)
	Beach/Dune sands K_s (m d^{-1})	**11.8** (1.73, 6.90, 19.8, 56.5, 66.1)
	Anisotropy of K_s (K_{sh}/K_{sv})[a]	**1.00** (3.00, 5.75, 8.50, 11.2, 14.0)
	Anisotropy of K_s (K_{sv}/K_{sh})	**1.00** (3.00, 5.75, 8.50, 11.2, 14.0)
Hydraulic gradients	Peatland water level (masl)	**0.36** (-0.40, 0.09, 0.12, 0.59, 0.82)
	Sea level (masl)	**0.09** (0.23, 0.37, 0.51, 0.65, 0.79)
Geological stratification and topography	Thickness of peat layer and aquifer sands (m; mid-peatland)	**2.2** + **6.0** (0.3 + 7.9, 1.0 + 7.2, 3.0 + 5.2, 4.0 + 4.2, 5.0 + 3.2)
	Thickness of aquifer sands[b] (m; mid-peatland)	**6.0** (1.0, 2.0, 3.0, 4.0, 5.0)
	Seafloor depth (masl)	**-5.5** (0.0, −1.4, −2.7, −4.1, −5.5 (without longshore bar))
	Seaward peat extension (m)	**90** (0, 45, 135, 180, 245)
	Peatland surface elevation (masl; mid-peatland)	**0.0** (0.1, 0.2, 0.3, 0.4, 0.5)
	Dike height (masl)	**3.7** (3.0, 2.3, 1.5, 0.8, 0.1)

[a]K_{sv} = *hydraulic conductivity in the vertical direction,* K_{sh} = *hydraulic conductivity in the horizontal direction.*
[b]*Changed by raising the lower boundary of the aquifer, while the boundary to the peat remained constant.*

sand K_s value of the reference scenario (1.73 m d^{-1}) was used as the minimum value.

Anisotropy of K_s has been reported repeatedly in peat (Beckwith et al., 2003; Wang et al., 2020), with fen peats showing a higher K_s either in vertical or horizontal direction depending on peat type (Liu et al., 2016). Wang et al. (2020) reported anisotropy in two fens with K_s in the vertical direction being larger than the horizontal direction ($K_{sv} > K_{sh}$) by a factor of six. Liu et al. (2016) described anisotropy with the higher flow in the horizontal direction by factors of up to seven. However, vertical flow was higher by a factor of 14 in one sample. Therefore, we examined the anisotropy's effect in both the vertical and horizontal direction, with factors ranging from three to fourteen.

Hydraulic Gradients

To analyse the effect of changing water levels in peatlands on terrestrial SGD, we used the minimum and maximum values measured during a three-year well monitoring period. The mean ± one standard deviation was also used to depict intermediate peat water levels. Furthermore, a 0.090 masl peat water level, similar to sea level, was simulated.

Investigated seawater levels were based on sea-level rise scenarios (BACC II Author Team, 2015; Grinsted et al., 2015). A global mean sea level rise mid-range estimate of +0.70 m is expected. We took this as the maximum value and divided it into five equal increments. We assumed that the peatland water level will rise in response to rising sea levels, so that the peatland water level was set equal to the sea level (hydraulic head = 0.001 m).

Geological Stratification and Topography

Geological stratifications, changing profiles, and the topography could also influence the magnitude and location of groundwater across the seafloor. Changing the thickness of the peat and aquifer sands layers plays a major role in water transport due to their relation to hydraulic conductivity. Here, the original peat thickness of 2.2 m was varied from 0.3 m up to 5 m–from the minimum peat depth for soils to be considered a mire based on the German soil classification system (Trepel et al., 2017), to thick fen peats. On average, peat layers are often assumed to be between 1.5–2 m (Zauft et al., 2010). As a response to the changing peat thickness, the upper limit of the aquifer sands also changed, while the lower limit was kept constant. However, to determine the impact of the aquifer sands thickness alone, simulations of 1–5 m thick aquifer sands with a constant peat thickness were also performed.

In the Hütelmoor and other coastal peatlands, it has been observed that the peat layer extends below the dune dike and beyond the shoreline, sometimes with outcropping peat in shallow waters. To examine the impact of varying seaward peat extension, the peat layer ended under the shoreline in the minimum scenario and was extended until the left border of the modeling domain in the maximum scenario. We also simulated scenarios of various seafloor depths ranging from −4.1 to 0.0 masl to represent coastal areas with broader and shallower nearshore zones. An additional scenario of the same seafloor geometry as the reference scenario without the longshore bar at 100 m from the shore was also simulated.

Scenarios for changing the topography of the study area were conducted by altering the man-made dike height and the peat elevation. The dike height was incrementally decreased by 0.7 m from 3.7 m up to 0.8 masl. Concurrently, peat elevation was raised from its current height of 0.0 masl in the middle of the peatland to 0.5 masl, which is a realistic value for more natural peatlands. The 0.357 masl peat water level was kept constant in this set of simulations to determine the effect of the topography alone.

Quantification of Terrestrial SGD

HYDRUS calculates flow velocities for each of the nodes and reports integrated fluxes across boundaries. Terrestrial SGD was assumed to be equal to the flux across the Constant Pressure Head two boundary, which extends across the entire seafloor (**Figure 2**). The net flux of recirculated seawater across this boundary is zero under steady-state conditions. The terrestrial SGD comprises all the water from the peat, aquifer sands, and beach/dune sands that come out as submarine groundwater discharge. Water fluxes from each of the different materials were determined using mesh lines in the material boundaries

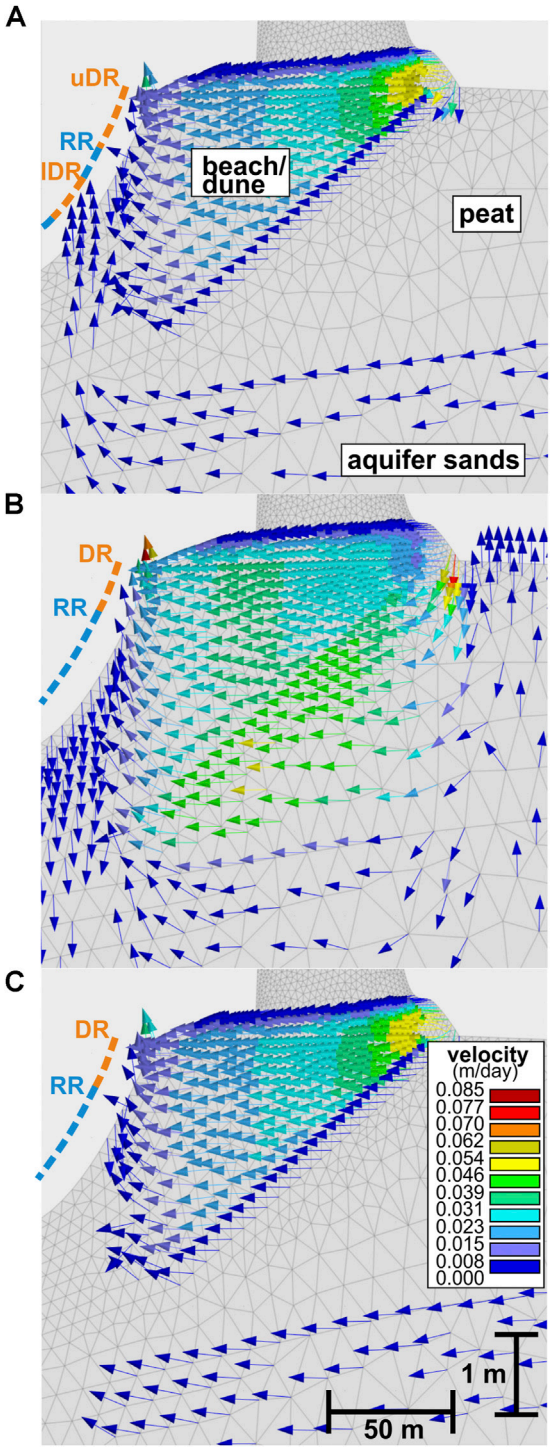

FIGURE 3 | Groundwater flow paths of the reference and selected scenarios illustrated using velocity vectors, in subset of the modelling domain. From top to bottom: **(A)** reference **(B)** peat K_s max, **(C)** peat extension max. Discharge (DR) and recharge regions (RR) are indicated with orange and blue dashed lines, respectively. The upper (uDR) and lower (lDR) discharge regions are shown in panel 3A.

(**Figure 2**); fluxes across mesh lines are calculated by HYDRUS in the same way as those across the boundary conditions.

Discharge and recharge regions in the seafloor were identified by looking at velocity vectors and streamlines, both of which are outcomes of HYDRUS graphic user interface post-processes. After identification of discharge and recharge regions, we added meshlines to these regions to quantify water fluxes separately. Discharge determined from these regions can be defined as "total SGD", since it includes both terrestrial and recirculated SGD. However, caution should be taken when interpreting total and recirculated SGD as the model does not consider marine forcings such as waves. The calculated fluxes across boundaries or mesh lines are reported in $m^2\,d^{-1}$. To determine the seepage rate from the seafloor ($m\,d^{-1}$), the fluxes were divided by the total length of the respective boundary or mesh line.

RESULTS

Flow Patterns and Location of SGD in Coastal Peatlands

Reference Peatland

Submarine groundwater discharge has been observed in two separate areas of the seafloor in the reference simulation (**Figure 3A**). Firstly, SGD is released in the upper 0.6 m water depth over a distance of 10 m from the shoreline into the sea (upper discharge region). Here, water originates from 1) atmospheric input to the dune and the beach and 2) peatland surface water that infiltrated into the dune base, as deduced from velocity vectors. Water flows from the dune base into the beach sands and towards the Baltic sea, following the hydraulic gradient. The underlying peat acts as an aquitard due to its low hydraulic conductivity, limiting the infiltration of surface water and groundwater flow.

The lower discharge region is located at 1.4–1.7 m depth (length ~15 m), with water coming from the sand aquifer. Flowing particles (user-defined particles showing trajectory and position through time) were observed to cross from the aquifer sands through the thinly buried peat layer and to the beach/dune sands (**Supplementary Figure 2A**). In between the two described discharge regions, areas with seawater recharge are found, contributing to the overall SGD flux. No seepage from the beach occurred.

Scenarios

Among all scenario simulations, two different patterns of SGD were observed with either two discharge regions (as in the reference peatland) or one discharge region (**Figures 3B,C**). However, most submarine groundwater appears to discharge in the upper 0.6 m of the seafloor based on velocity vectors.

The two-discharge-region pattern seems to form when there is considerable water flow from the aquifer (due to higher aquifer K_s than minimum value, increased aquifer thickness) or when the

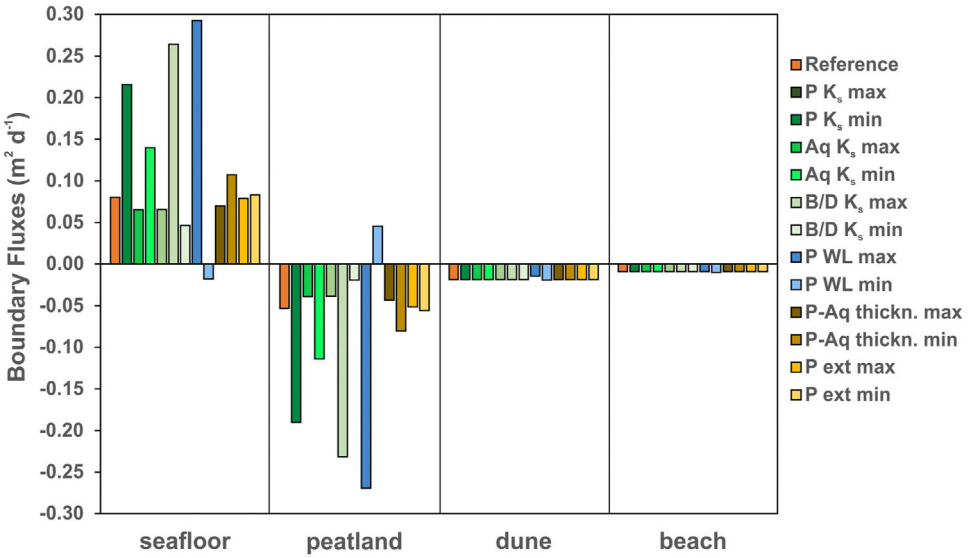

FIGURE 4 | Net boundary fluxes of the reference scenario (orange) and selected scenarios of soil physical properties (green shades), hydraulic gradients (blue shades), and geological stratifications (yellow shades). For location of boundaries, see **Figure 2** (seafloor ≙ Constant Pressure Head two; peatland ≙ Constant Pressure Head three; dune ≙ atmospheric; beach ≙ seepage face). Fluxes from the left boundary (Constant Pressure Head 1) were not included due to low values (10^{-4} to 10^{-6} m^2 d^{-1}). Notations: P, peat; Aq, aquifer; B/D, beach/dune; WL, water level; ext, extension.

hydraulic gradient is large. The pattern is maintained when beach/dune K_s, peat K_{sh}/K_{sv} ratio, seafloor depth, peat elevation, and dike height are varied. In all those scenarios, the general groundwater discharge pattern remains similar to the reference peatland mainly due to the strong impact of the peat layer extending towards the sea. However, the lengths of the discharge regions may differ between the simulations. For example, the upper discharge region is smallest for the shallowest seafloor scenario, where SGD is limited to a few meters near the shore.

The single discharge region, located in the upper seafloor, occurs whenever the influence of the peat layer extending to the sea to act as a barrier is either diminished (upper and lower discharge regions merge) or amplified (development of lower discharge region is impeded). For instance, larger peat K_s than the reference (**Figure 3B**) or peat K_{sv}/K_{sh} ratios >3 reduce the barrier effect of the peat extension layer. Thus, both the dune and aquifer flow pathways merge in the beach sands to a one-discharge area. In contrast, increasing peat thickness and continuing the peat layer (**Figure 3C**) farther under the Baltic Sea magnify the barrier effect of the peat layer, and upflow of water from the aquifer to the seafloor is prevented. Furthermore, a decrease in aquifer flow due to a decrease in aquifer thickness leads to a single discharge-region flow pattern.

SGD Fluxes From Coastal Peatlands

Reference Peatland

Water inputs into the modelling domain mainly originate from infiltration at the dune dike base and peat surface and the lateral groundwater inflow (these latter two cannot be distinguished), while atmospheric input at dune and beach is less important (**Figure 4**). Outputs are terrestrial SGD across the seafloor and a minimal groundwater outflow through the sea-submerged aquifer sands on the left boundary of the modeling domain.

Looking at the simulated terrestrial SGD flux across the seafloor, our long-term average SGD is 0.080 m^2 d^{-1} (0.056 L min^{-1} m^{-1}) (**Figure 5**). Upscaled total terrestrial SGD for the entire 3-km coastline of the Hütelmoor is estimated to be 240 m^3 d^{-1}, or 168 L min^{-1}. We evaluated the uncertainty of the reference scenario's SGD based on the combination of random K_s for the three materials, due to its high variability in nature. The boxplot in **Figure 5** presents the uncertainty analysis results (see also **Supplementary Table 1**). The median SGD of the 100 simulation runs is 0.083 m^2 d^{-1} and thus close to the value of the reference scenario. The lower and upper bounds are 0.038 m^2 d^{-1} and 0.195 m^2 d^{-1}.

The seepage rate calculated separately for both observed discharge regions revealed that discharge is distinctly higher near the shore. Most SGD flows out in the upper discharge region with a flux of 0.106 m^2 d^{-1} and a corresponding seepage rate of 0.0105 m d^{-1} (**Table 3**). An additional but vitally lower flux of 0.023 m^2 d^{-1} (seepage rate: 0.0016 m d^{-1}) is found in the lower discharge region. The seafloor's average seepage rate is 0.0033 m d^{-1} based on the terrestrial SGD flux of the whole seafloor and the lengths of the discharge regions. Average discharge flux (0.128 m^2 d^{-1}) and seepage rate (0.0052 m d^{-1}) calculated from the two discharge regions are slightly higher than the terrestrial SGD flux across the seafloor, which is due to the additional input of recirculated SGD from the recharge regions. Still, we are able to show here that most terrestrial SGD occurs in the upper seafloor with minor flux arising from the thin section of the peat extension.

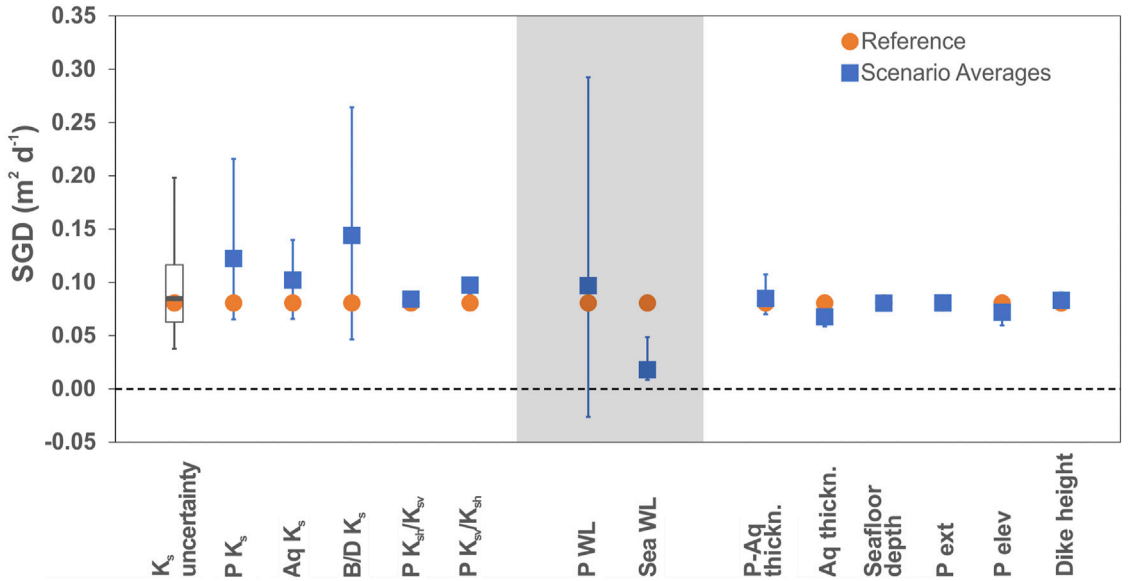

FIGURE 5 | Range of submarine groundwater discharge in different scenarios with results of K_s uncertainty analysis (boxplot). Blue boxes are averages of the scenario simulations and the error bars represent the range. Error bars of uncertainty analysis represent the upper and lower bounds based on ±1.5* Interquartile Range. The reference scenario flux is represented here in orange dots. The shaded area separates the three groups of properties. Notations: P, peat; Aq, aquifer; B/D, beach/dune; WL, water level; ext, extension.

TABLE 3 | Fluxes across specific discharge and recharge regions of the reference peatland. Total discharge/recharge flux, length, and seepage rate are highlighted in bold.

	Flux ($m^2\ d^{-1}$)	Length (m)	Seepage rate ($m\ d^{-1}$)
Upper discharge region	0.106	10.0	0.0105
Lower discharge region	0.023	14.6	0.0016
Total discharge	**0.128**	**24.6**	**0.0052**[a]
			0.0033[b]
Upper recharge region	−0.036	12.0	−0.0030
Lower recharge region	−0.017	208.5	−0.0001
Total recharge	**−0.053**	**220.5**	**−0.0002**

[a]*Based on SGD flux of discharge regions.*
[b]*Based on terrestrial SGD flux of total seafloor.*

Range of SGD Expected From Coastal Peatlands

In nearly all scenarios, the majority of the water inputs come from the peatland with only minor atmospheric inputs from the dune and beach (**Figure 4**). The water input through the peatland increases with large hydraulic conductivity or gradient, while the atmospheric input remains constant.

The SGD fluxes simulated in the various scenarios range from 0.008 to 0.293 $m^2\ d^{-1}$, corresponding to 10–360% of the reference scenario's flux (**Figure 5**). In one scenario—with low peatland water level—a flow reversal was observed, i.e., seawater intrudes with a flux of −0.019 $m^2\ d^{-1}$. The largest SGD flux is observed in the maximum water level scenario, and also the maximum K_s for peat and beach/dune sands yield large fluxes (270 and 330% of reference, respectively). The effect of the aquifer sand K_s is less pronounced, with SGD fluxes amounting to 80–170% of the reference, but still considerably more than that of the other factors. All sea level rise simulations recorded minimal SGD fluxes (0.008–0.048 $m^2\ d^{-1}$; 10–60%). Peat anisotropy (0.081–0.104 $m^2\ d^{-1}$; 101–130%), peat-aquifer thickness (0.070–0.107 $m^2\ d^{-1}$; 87–134%), aquifer thickness (0.059–0.075 $m^2\ d^{-1}$; 73–94%), seafloor depth (0.079–0.081 $m^2\ d^{-1}$; 98–101%), peat extension (0.079–0.083 $m^2\ d^{-1}$; 98–104%), and dike height (0.081–0.091 $m^2\ d^{-1}$; 100–113%) have little impact on the SGD flux. Most of the simulated SGD fluxes fall within the range of values obtained from the K_s-based uncertainty analysis, where a minimum and maximum SGD flux of 0.038 $m^2\ d^{-1}$ and 0.493 $m^2\ d^{-1}$ were determined, respectively. The beach/dune sands K_s is highly linearly correlated with SGD (R^2 = 0.9837) in the uncertainty analysis, while peat K_s (R^2 = 0.016) and aquifer sands K_s (R^2 = 0.0356) are not (**Figure 7**).

Origin of SGD Flux

To better understand the SGD flow and magnitude patterns in a coastal peatland system, we determined the source of terrestrial SGD (**Figure 6**). For this purpose, fluxes from different subsections of the materials (dune, beach, main peat body, thin peat extension, aquifer) to the beach sands were quantified in selected scenarios

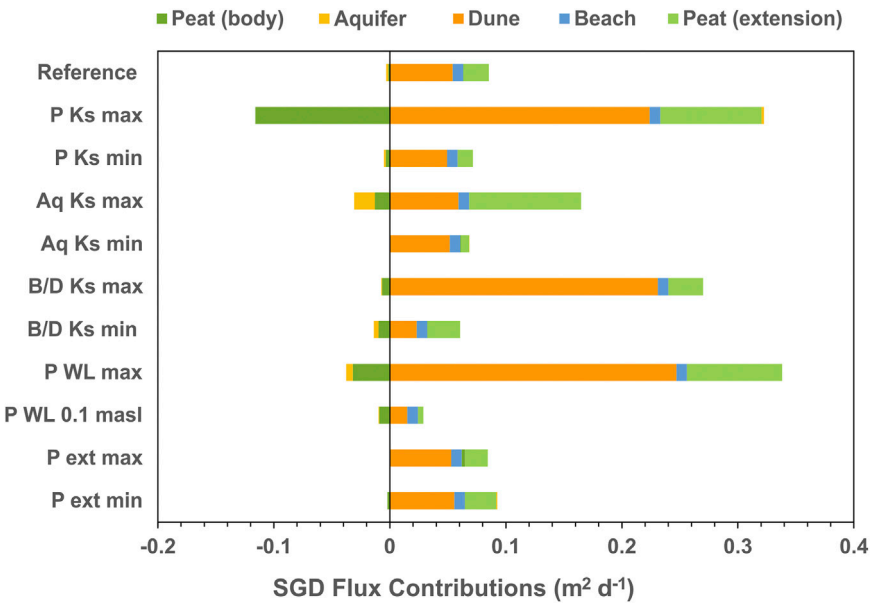

FIGURE 6 | Contributions from the dune, beach, peat body, peat extension, and aquifer sands to submarine groundwater discharge for selected scenarios. Positive fluxes are inputs while negative fluxes represent output of water from the beach sands. In P K_s max scenario, a large volume of water infiltrated the dune dike and then, water flowed down to the peat body.

using meshlines (**Figure 2**). Positive fluxes are inputs and contributors to the beach sands while negative fluxes represent outflow of water (**Figure 6**). The sum of these fluxes should be equal to the terrestrial SGD determined at the seafloor boundary. The reference peatland has a 2.4% accuracy. However, we observed deviations ranging from −13 to 9% in other scenarios. This can be attributed to the fact that nodes at the edges of meeting meshlines are considered for flux calculations across both meshlines.

In the reference peatland, most of the terrestrial SGD comes from the dune dike (0.054 $m^2\ d^{-1}$; 63%), recharged by precipitation (1/3) and infiltrating peatland surface waters (2/3), and the beach (0.0092 $m^2\ d^{-1}$; 11%). The remaining part of the SGD originates from the aquifer, but flows upward through the thin, buried peat extension layer under the seafloor (0.022 $m^2\ d^{-1}$; 26%). No discharge was observed from the main peat body, or directly from the aquifer into the marine sediments.

In the scenarios, the relative contributions of dune, beach, and aquifer to the terrestrial SGD vary as a function of soil properties and hydraulic gradient: With a high aquifer K_s, the aquifer (via the peat extension) gains in importance, while a low peatland water level or low K_s of peat or aquifer enhance the contribution from the dune. The relative contributions only increased/decreased by 3% for the peat extension scenarios compared to the reference scenario. The share of the dune and beach varies from 41 to 89%.

DISCUSSION

SGD Flux From Coastal Peatland

The upscaled total terrestrial SGD for the entire 3-km coastline of the Hütelmoor is 240 $m^3\ d^{-1}$. Lower and upper limits of estimates based on K_s uncertainty are 114 and 596 $m^3\ d^{-1}$, respectively. The results are slightly higher than previous terrestrial SGD estimates from the same study site with 15–164 $m^3\ d^{-1}$ (Miegel et al., 2016) and 180 $m^3\ d^{-1}$ (Ibenthal, 2020), which were calculated using water balance equations of the contribution of peat and aquifer sands (Miegel et al., 2016) and MODFLOW 3D numerical simulations including the dune sands (Ibenthal, 2020).

Comparing with other wetland environments, our average seepage rate of 0.33 cm d^{-1} is comparable in magnitude to a mudflat in China (Qu et al., 2017) and lower estimates of a tide-dominated coastal wetland in Taiwan (Hsu et al., 2020) (**Table 4**). However, it is expectedly lower than seepage rates from crab burrows-influenced tropical mangrove systems in Australia due to preferential flow pathways (Tait et al., 2017) and from a subtropical estuarine creek adjacent to a dune-wetland system (Sadat-Noori et al., 2015). The seepage rate near the shore (1.05 cm d^{-1}) is comparable to rates observed in sandy beaches (Kotwicki et al., 2014; Qu et al., 2017) and a sandy pockmark (Virtasalo et al., 2019) in the Baltic Sea. This result may be explained by the fact that terrestrial SGD could also be generated from small dune dike systems with additional inputs from infiltrating peatland surface waters. However, it should be noted that our average seepage rate represents terrestrial SGD only while seepage rate near the shore has contributions from recirculated SGD. Fresh SGD contributes 0.01–10% of surface water runoff (Church, 1996), with recent global estimates of 0.6% (Luijendijk et al., 2020). In tide-dominated systems, a conservative estimate of fresh SGD contribution is ~5% of the total flux (Li et al., 2009; Santos et al., 2009:; Hsu et al., 2020). Total SGD flux estimates could thus be larger with possible large inputs from recirculated SGD.

TABLE 4 | Seepage rates of SGD studies from wetland environments and different locations in the Baltic Sea.

Environment	Seepage rate (cm d^{-1})	Time period	Remarks	Location	Method used	Reference
Fen peatland	0.330 (0.154–0.807) 1.053	Long-term average	Terrestrial SGD only; discharge regions 0.6 m depth incl. recirc. SGD	Rostock, Germany, Baltic Sea	HYDRUS 2D simulation	This study
Sandy beach	7.600	Short-term		Jiaozhou Bay, China	Darcy's law	Qu et al. (2017)
Mud flat	0.710					
Estuarine intertidal zone	0.058					
Tidal marsh	0.004					
Tide-dominated coastal wetland	0.200–25.000	Dry season		Gaomei Wetland, Western Taiwan	Ra, rn, H, O isotopes	Hsu et al. (2020)
	0.100–47.000	Wet season				
Mangrove creeks	1.500–30.900	Short-term	From temperate to tropics	Australia (several)	Ra tracer	Tait et al. (2017)
Estuarine creek adjacent to a dune-wetland	18 ± 5, 20 ± 6	Dry season	Subtropical	New South Wales, Australia	Ra tracers	Sadat-Noori et al. (2015)
	65 ± 18, 84 ± 48	Wet season				
Muddy sediments, subseafloor aquifers	0.054	Long-term average	Maximal discharge	Eckernförde Bay, Germany, Baltic Sea	Cl^- tracer	Schlüter et al. (2004)
	>0.900					
Sandy beach	1.000–4.000	Winter/spring		Puck Bay, Poland, Baltic Sea	Lee-type seepage meters	Kotwicki et al. (2014)
	5.000–15.000	Summer/ autumn				
Sandy pockmark	0.400–1.200	Short-term	SGD concentrated in active pockmarks	Hanko peninsula, Finland	Rn tracer	Virtasalo et al. (2019)

Factors Controlling SGD From Coastal Peatlands

Importance of Peat Extension Layer to SGD Flow

The prevailing two-discharge region flow pattern in the reference peatland is due to the strong impact of the peat layer extending underneath the beach. In sandy lakeshores (McBride and Pfannkuch, 1975; Fukuo and Kaihotsu, 1988) and coastal areas (Bokuniewicz, 1992), the concentration of terrestrial SGD at the interface of land and water body is expected with groundwater discharge rapidly decreasing as the distance from the shore increases. The distribution is affected, though, by aquifer heterogeneity and sediment hydraulic conductivity, which may vary over several orders of magnitude (Taniguchi et al., 2003). In this study, the occurrence of a lower SGD region is due to the barrier function of the peat extension layer, interrupting the flow field because of its hydraulic properties. This parallels offshore SGD originating from aquifers that have been confined by a low permeability material (Kooi and Groen, 2001; Post et al., 2013), which can extend several kilometers into the sea. In Sweden and Finland, groundwater has been observed to discharge from submarine terraces in siltier, more permeable portions of glacial clay at water depths of ~12 m (Jakobsson et al., 2020).

The barrier function of the peat layer interplays with its K_s, K_s anisotropy, and geological stratifications. It diminishes with larger peat K_s and K_{sv}/K_{sh} anisotropy values but is magnified with increasing peat thickness and longer extension of the peat into the sea. In a similar way that the peat extension and the main peat body restrict groundwater discharge to the sea, our model shows that the low-conductivity peat layer also hinders seawater intrusion towards the peatland. Scenarios with higher sea level did not result in the formation of a seawater wedge but rather in landward discharge behind the dune dike (**Supplementary Figure 2B**). This pattern may be unique to ponded coastal peatlands and muddy shorelines. Thus, the peat may serve as a barrier for both groundwater discharge and seawater intrusion.

In terms of SGD magnitude, however, the peat extension layer is not important. Compared to the reference peatland, the SGD flux only decreased by 2% when the peat was extended to the left border of the modelling domain and only increased by 3% when it ended under the shoreline. Nonetheless, more peat material extending into the sea in the groundwater-seawater mixing zone may still be significant for material transport and biogeochemical processes (see below).

K_s and Hydraulic Gradient

While the peat extension layer determines the discharge patterns, the hydraulic conductivity and hydraulic gradient are the main controls of the magnitude of SGD from coastal peatlands. The peat K_s influences the infiltration of surface waters into the peat and subsequent SGD generation. A low peat K_s reduces the infiltration of surface water into the peat and limits the contribution of peat and underlying aquifer to SGD. However, it might prolong ponding under transient conditions, enabling infiltration into the dune dike base that eventually flows out as terrestrial SGD. For the aquifer sands K_s, a low K_s restricts discharge from the aquifer, resulting in a single SGD region related to the dune. Meanwhile, the beach/dune sands K_s only affects the SGD flux magnitude and not the location. The high

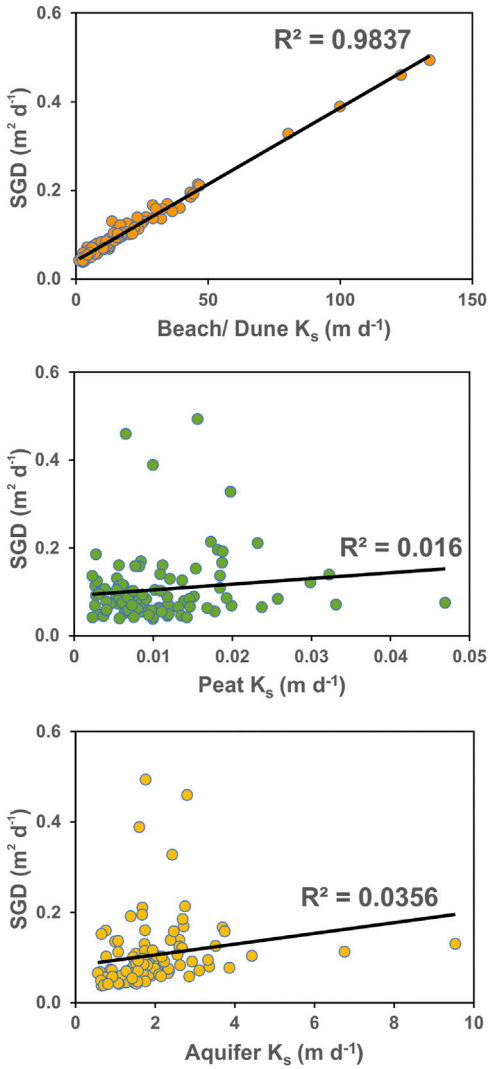

FIGURE 7 | Linear regressions of SGD and material K_s, K_s data generated for uncertainty analysis. Beach/dune sands K_s is highly correlated with SGD.

positive correlation of the beach/dune Ks with SGD (**Figure 7**) emphasizes the role of the coastal sediments for SGD generation in coastal peatlands.

The peat and the underlying aquifer sands' properties thus affect not only groundwater flow in the peatland (Quillet et al., 2017), but also SGD magnitude and location. Large hydraulic conductivities are typically found in pristine peat, while lower values are characteristic of degraded peatlands (Lennartz and Liu, 2019) and are related to a decrease in macroporosity due to disintegration of plant materials (Liu et al., 2016). Peat can have macropores; a single-large pore space may take up 94–99% (Rezanezhad et al., 2016), which may dominate water and solute transport (Baird and Gaffney, 2000). In marine sediments, bioturbator bivalves such as *Mya arenaria,* found in most of the Baltic Sea (Forster and Zettler, 2004), may distinctly increase K_s. A direct correlation between hydraulic conductivity and SGD rates has been observed in a study of four different types of wetlands in China (Qu et al., 2017). Moreover, it has been shown that the bottleneck for coastal groundwater discharge is the flow capacity, which is a function of permeability, thickness of permeable units, and topographic gradient (Luijendijk et al., 2020).

The peatland's water level is the most sensitive factor determining the magnitude of terrestrial SGD (**Figure 5**). While Luijendijk et al. (2020) assumed the topographic gradient as the maximum possible hydraulic gradient, the average hydraulic gradient is larger than the topographic one at our study site. This is due to the ponded peatland surface waters maintained after rewetting by a groundsill, combined with the low peat K_s and the dune dike. We can assume that the resulting hydraulic gradient is similar to pristine conditions since subsidence and peat degradation after drainage lowered surface elevation of up to 1 m at the study site. However, it is expected that sea level rise will reduce the hydraulic gradient in the future. According scenarios have shown that the water flow direction even reverses and is directed towards the peatland inside the dune body if the sea level rises above the average peatland water level, while simultaneously SGD occurs underneath (**Supplementary Figure 2B**). This results in a decreased SGD as a function of reduced hydraulic gradients.

The data presented here is from steady-state conditions depicting long-term averages, neglecting temporal dynamics of the hydraulic gradient. In reality, both seasonal and short-term variations occur (Ibenthal 2020). For example, larger gradients in winter due to rising ground- and surface water levels will induce higher SGD rates than in summer when evaporation is high (Miegel et al., 2016). In the short term, storms and changing seawater levels cause a high variability of hydraulic gradients. These variations will not affect the average SGD but will have an important impact on solute transport in the transition zone between land and sea.

Other Factors

The remaining factors studied in this work have little impact on SGD flow and magnitude. Anisotropy of K_s, peat and aquifer thickness, and peat elevation have a relatively small impact compared to K_s and hydraulic gradient. Large peat K_{sh}/K_{sv} may only slightly enhance water flow into the peat extension but not strong enough to cancel its barrier function. Our findings are consistent with Beckwith et al. (2003), who showed that anisotropy has a smaller influence on groundwater flow patterns in peat than geological heterogeneity. Anisotropy also appeared to have a minor effect on phosphate transport than peat soil heterogeneity (Wang et al., 2020). The anisotropic angle was shown to be highly significant for determining the landward extent of seawater in a high hydraulic conductivity homogenous aquifer (Costall et al., 2020). However, such saltwater wedge has not been observed at the study site neither in drillings nor in our simulations. Material thickness can - depending on its inherent K_s—impact SGD positively or negatively (Smith and Nield, 2003).

The impact of peat and aquifer thickness on flow and magnitude in our system is small compared to K_s and hydraulic gradient. However, we only simulated peat and

aquifer sands thickness of 0.3—5.0 m and 1.0—5.0 m, respectively, typical of German coastal peatlands. In other peatlands, peat (Habicht et al., 2017) and aquifer sands (Vilumaa et al., 2017) might be thicker and may have a higher impact on SGD. Scenarios of higher peat elevation, expected in less degraded peatlands, resulted in slightly decreasing SGD because less surface water is available that can freely infiltrate into the dune dike base. However, it is also expected that less degraded peatlands will have larger K_s and thus will allow a larger volume of groundwater flow. To illustrate, a simulation of 0.4 masl peat elevation and K_s of 17.4 m d^{-1} resulted in 0.215 m^2 d^{-1} SGD flux, similar to the flux calculated from the scenario with the same peat K_s value.

Dike height and the seafloor depth do not have any distinct impact on neither SGD magnitude nor location. With a shallower seafloor, only the water depth at which SGD occurs decreases, with implications for the mixing into the water column. These results may be explained by the fact that the source of terrestrial SGD remains unaffected by the changes.

Model Limitations

This is the first time that HYDRUS-2D was used to determine SGD from a coastal peatland system, and it was able to address our objectives. The model has performed reasonably well—all scenarios have less than 1% relative mass balance error, the prescribed rate for water flow simulations. The lowest and highest relative errors were 0.01 and 0.89%, respectively.

A drawback of the model for applications at the coast is that it does not account for density-driven flow. We assume, however, that density effects can be neglected at our study site due to small density difference between the Baltic Sea and the peatland's groundwater. While the salinity of the Baltic Sea is comparably low near the study site with 11.4 psu (IOW(Leibniz Institute for Baltic Sea Research Warnemünde), 2020), high electrical conductivities and chloride concentrations have been recorded in the groundwater of the peatland (Ibenthal, 2020). They are rather homogeneously distributed in the peat and the underlying aquifer and are attributed to former floodings of the peatland with seawater, as has been proven with sulfur isotopes (Koebsch et al., 2019). The groundwater in the aquifer of the considered transect is decades old, as has been revealed by tritium-helium dating (Ibenthal, 2020). The densities of water samples collected between 2019 and 2020 from the groundwater peatland (n = 32) and dune (n = 3), from surface water (n = 15) and Baltic Sea (n = 5) were calculated for the long-term average temperature of 9.7°C, following Millero and Poisson (1981). Likewise, density from salinity measurements by IOW (n = 169; 1996–2018) was also calculated (**Supplementary Table 2**). A density difference of 0.006 g cm^{-3} between Baltic Sea waters (IOW(Leibniz Institute for Baltic Sea Research Warnemünde), 2020) and groundwater in the Hütelmoor is more than four times lower than the value used by Robinson et al. (2007) to simulate variable-density flow experiments. As such, less convective mixing is expected due to the lower density difference of groundwater and seawater.

The effect of density on the sea level pressure head and SGD was tested by calculating the equivalent freshwater head for a water depth of 1.0 m, where most of the SGD comes out. The calculated head difference between the reference scenario and the density-corrected head is 0.01 m, with discharge flux decreasing by only 0.002 m^2 d^{-1} (2%). We, therefore, assume that the model results are reliable despite neglecting density effects.

Furthermore, tides were not accounted for by the model, as they are assumed to be minimal at the study site. The Baltic Sea is an enclosed basin with a maximal tidal height of 23 cm (100-year period estimate) for the whole region and 6 cm in the nearby Danish straight (Medvedev et al., 2016).

Proposed Mechanisms for SGD Occurrence

Based on our simulations, it can be suggested that terrestrial SGD occurs more in peatlands that are 1) rewetted and diked with low peat K_s and 2) lowly-degraded peatlands with higher K_s and elevation. Future investigations on matter fluxes are thus recommended to focus on these environments.

Most coastal peatlands along the Baltic Sea are assumed to have low peat hydraulic conductivity as a result of draining and diking activities arising from agricultural use and coastal protection measures. Many of these peatlands may be rewetted in the future like the Hütelmoor since the restoration of peatlands by increasing the height of the water table is a cost-effective measure to cut down on greenhouse gas emissions (Leifeld and Menichetti, 2018). Low K_s and diking result in less infiltration of surface waters and ponding in the peatland. This water infiltrates the dune and eventually flows out as SGD. One interesting finding of this study is that most waters that come out as SGD are from the ponded surface waters.

Conversely, we can also expect SGD in peatlands that have higher elevation and are less degraded. In this setting, the peatlands have higher K_s allowing more water to infiltrate the ground, flowing into the dune and out of the seafloor as SGD. The peat extension, likely compacted due to pressure, may still hinder upflow from the aquifer sands. However, the upper peat layer will allow more groundwater to flow to the beach. Less degraded peat will also have a higher percentage of macroporosity, leading to preferential flow pathways. These observations point out the importance of land use in the past and land management activities in the future.

In both mechanisms, we have demonstrated that even a narrow dune can be important for groundwater recharge and subsequent SGD generation, as reported earlier for larger dune belts (Stieglitz, 2005; Röper et al., 2012). These results have consequences not only for the quantity but also for the quality of the discharged water, emphasizing the role of the dune and beach in total SGD flux. Taken together, our findings suggest that the dune is important for recharge and infiltration of peatland surface waters.

Implications for Carbon and Material Transport

It is now well-known that groundwater often has higher concentrations of carbon and materials (Moore, 2010) than its receiving body of water where it discharges. Over the last few years, organic-rich subterranean estuaries have been shown to

have higher concentrations of remineralized components of organic matter, including nutrients, DOC, DIC, DOM, trace elements, reduced species such as ammonium and iron (II), and lower pH (Taniguchi et al., 2019). At our study site, DOC concentrations measured in groundwater in peat and aquifer amount to 48–490 mg C L^{-1} and 12–99 mg C L^{-1}, respectively, and to 38–380 mg C L^{-1} in the peatland's surface water. Our values are much higher than the previously mentioned DOC average from SGD (Szymczycha et al., 2014). While DOC may undergo several biogeochemical transformations before it is discharged to the sea, the high concentrations in peatland surface and groundwaters offer a glimpse of potential large DOC inputs via SGD. In addition, the absence of large rivers in the southern Baltic Sea could increase the importance of SGD as pathways for water and material transport.

Our study showed that a peat layer extending to the sea, and potentially cropping out, hardly influences the quantity of water fluxes. However, the peat could still be important biogeochemically. Peat from the study site has been shown to release DOC in contact with saline water (Gosch et al., 2018) and low-saline groundwater (Kreuzburg et al., 2020). Exposure of peat to water with changing salinity can promote the release of DOC and remineralized components such as CO_2 and DIC (Kreuzburg et al., 2020). As such, peat deposits along coastal zones could be potential hot spots of increased release of these materials and may be important to the release of climate-relevant gases (Kreuzburg et al., 2020). Moreover, additional geological complexities such as marine sediment bulldozing by bivalves and other groups in marine environments (Santos et al., 2012) and peat degradation and preferential solute transport on land (Liu et al., 2017) can enhance material export from coastal peatlands. Given the knowledge gaps in material transport and its abundance in the Baltic Sea, coastal peatlands warrant further scientific investigation to address their potential as an overlooked source of water and materials for the Baltic Sea via the SGD pathway, characterized by low hydraulic conductivity and low hydraulic gradient.

CONCLUSION

Coastal peatlands are widespread along the German Baltic Sea coast. They have often been drained and diked but are increasingly rewetted. This study aimed at assessing whether terrestrial submarine groundwater discharge is likely to occur from such a low-lying, low hydraulic conductivity coastal peatland using 2D numerical modelling of water flow, and at evaluating the factors that determine the magnitude and pattern of SGD from coastal peatlands presuming a range of realistic properties. Our simulations show that terrestrial SGD can originate from a low K_s and low gradient coastal peatland, although the SGD flux at our study site is in the lower range of other wetland environments and Baltic Sea SGD sites. The terrestrial SGD is sourced primarily from the dune dike, recharged from the ponded peatland surface waters and precipitation, and to a lesser extent from the shallow aquifer underlying the peat. As the peatland's surface and groundwater are typically enriched in remineralized organic matter, SGD is a potential source of these materials with consequences for marine geochemical budgets and ecosystems, and matter fluxes need to be quantified.

A specific feature of coastal peatlands is that the peat layer may continue underneath the sea. Scenario simulations reveal that this extending peat layer has a barrier function and mainly determines the location of SGD in interplay with K_s and geological stratification. It is thus assumed to play a crucial role in how the marine ecosystem is affected locally. However, it has little effect on the SGD magnitude, which is mainly controlled by the hydraulic gradient and Ks, especially of beach/dune and peat. The high positive correlation between beach/dune Ks and SGD underlines the importance of even a small dune belt for SGD generation.

We conclude that SGD is most probable from those coastal peatlands with 1) high water levels, 2) large Ks and/or 3) a dune dike or belt, irrespective of the specific geologic setup or topography. This is assumed to be the case for rare, lowly-degraded peatlands, typically characterized by high permeability and water level, and for rewetted (formerly drained) peatlands, where the K_s of the degraded peat is small, but a high water level is maintained artificially and ponded water constitutes a unique water source for SGD. While current efforts of rewetting coastal peatlands are thus expected to increase their contribution to SGD, the expected sea level rise will counteract this development in the future.

DATA AVAILABILITY STATEMENT

The raw data supporting the conclusions of this article will be made available by the authors, without undue reservation.

AUTHOR CONTRIBUTIONS

ER gathered data, conducted the numerical modeling, analyzed the data, wrote and revised the article. BL conceived the topic and reviewed the article. MI gathered data and reviewed the article. MJ conceived the topic, gathered data, contributed to development of the model set up and data analysis, wrote and revised the article.

FUNDING

This study was conducted within the framework of the Research Training Group "Baltic TRANSCOAST" funded by the DFG (Deutsche Forschungsgemeinschaft) under grant number GRK 2000 (www.baltic-transcoast.uni-rostock.de/). This is Baltic TRANSCOAST publication no. GRK 2000/0048. We acknowledge financial support by the DFG and the University of Rostock within the funding programme Open Access Publishing.

ACKNOWLEDGMENTS

We thank the Stadtforstamt Rostock for their support in the conduct of this research in the Naturschutzgebiet

Heiligensee und Hütelmoor. We also thank editor and the reviewers for their valuable inputs which greatly improved this article. The authors would also like to thank Haojie Liu for his help in identifying the hydraulic properties of the peat soils.

REFERENCES

BACC II Author Team (2015). "Second Assessment of Climate Change for the Baltic Sea Basin. Regional Climate Studies," in *Second Assessment of Climate Change for the Baltic Sea Basin. Regional Climate Studies* Geesthacht, Germany: Springer, Cham. doi:10.1007/978-3-319-16006-1

Baird, A. J. (1997). Field Estimation of Macropore Functioning and Surface Hydraulic Conductivity in a Fen Peat. *Hydrol. Process.* 11, 287–295. doi:10.1002/(sici)1099-1085(19970315)11:3<287::aid-hyp443>3.0.co;2-l

Baird, A. J., and Gaffney, S. W. (2000). Solute Movement in Drained Fen Peat: A Field Tracer Study in a Somerset (UK) Wetland. *Hydrol. Process.* 14 (14), 2489–2503. doi:10.1002/1099-1085(20001015)14:14<2489::aid-hyp110>3.0.co;2-q

Beckwith, C. W., Baird, A. J., and Heathwaite, A. L. (2003). Anisotropy and Depth-Related Heterogeneity of Hydraulic Conductivity in a Bog Peat. II: Modelling the Effects on Groundwater Flow. *Hydrol. Process.* 17, 103–113. doi:10.1002/hyp.1117

Beyer, W. (1964). Zur Bestimmung der Wasserdurchlassigkeit von Kieson und Sanduen aus der Kornverteilung, Wasserwirt. *Wassertech* 14, 165–169.

Bokuniewicz, H. J. (1992). Analytical Descriptions of Subaqueous Groundwater Seepage. *Estuaries* 15 (4), 458–464. doi:10.2307/1352390

Bollmann, M., Bosch, T., Colijn, F., Ebinghaus, R., Froese, R., Güssow, K., et al. (2010). *World Ocean Review: Living with the Oceans*. Hamburg: Maribus GmbH.

Burnett, W. C., Aggarwal, P. K., Aureli, A., Bokuniewicz, H., Cable, J. E., Charette, M. A., et al. (2006). Quantifying Submarine Groundwater Discharge in the Coastal Zone via Multiple Methods. *Sci. Total Environ.* 367, 498–543. doi:10.1016/j.scitotenv.2006.05.009

Burnett, W. C., Bokuniewicz, H., Huettel, M., Moore, W. S., and Taniguchi, M. (2003). Groundwater and Pore Water Inputs to the Coastal Zone. *Biogeochemistry* 66, 3–33. doi:10.1023/b:biog.0000006066.21240.53

Church, T. M. (1996). An Underground Route for the Water Cycle. *Nature* 380 (6575), 579–580. doi:10.1038/380579a0

Costall, A. R., Harris, B. D., Teo, B., Schaa, R., Wagner, F. M., and Pigois, J. P. (2020). Groundwater Throughflow and Seawater Intrusion in High Quality Coastal Aquifers. *Sci. Rep.* 10 (1), 1–33. doi:10.1038/s41598-020-75736-9

Dettmann, U., Bechtold, M., Frahm, E., and Tiemeyer, B. (2014). On the Applicability of Unimodal and Bimodal Van Genuchten-Mualem Based Models to Peat and Other Organic Soils under Evaporation Conditions. *J. Hydrol.* 515, 103–115. doi:10.1016/j.jhydrol.2014.04.047

DWD(Deustcher Wetterdienst) (2020). *Warnemünde*. Available at: https://cdc.dwd.de/portal/201912031600/mapview (Accessed July 20, 2020)

Ferone, J. M., and Devito, K. J. (2004). Shallow Groundwater-Surface Water Interactions in Pond-Peatland Complexes along a Boreal Plains Topographic Gradient. *J. Hydrol.* 292 (1–4), 75–95. doi:10.1016/j.jhydrol.2003.12.032

Forster, S., and Zettler, M. L. (2004). The Capacity of the Filter-Feeding Bivalve *Mya Arenaria* L. To Affect Water Transport in sandy Beds. *Mar. Biol.* 144 (6), 1183–1189. doi:10.1007/s00227-003-1278-2

Fukuo, Y., and Kaihotsu, I. (1988). A Theoretical Analysis of Seepage Flow of the Confined Groundwater into the lake Bottom with a Gentle Slope. *Water Resour. Res.* 24 (11), 1949–1953. doi:10.1029/wr024i011p01949

Gosch, L., Janssen, M., and Lennartz, B. (2018). Impact of the Water Salinity on the Hydraulic Conductivity of Fen Peat. *Hydrological Process.* 32, 1214–1222. doi:10.1002/hyp.11478

Gosch, L., Townsend, H., Kreuzburg, M., Janssen, M., Rezanezhad, F., and Lennartz, B. (2019). Sulfate Mobility in Fen Peat and its Impact on the Release of Solutes. *Front. Environ. Sci.* 7, 189. doi:10.3389/fenvs.2019.00189

SUPPLEMENTARY MATERIAL

The Supplementary Material for this article can be found online at: https://www.frontiersin.org/articles/10.3389/feart.2021.665802/full#supplementary-material.

Grinsted, A., Jevrejeva, S., Riva, R., and Dahl-Jensen, D. (2015). Sea Level Rise Projections for Northern Europe under RCP8.5. *Clim. Res.* 64 (1), 15–23. doi:10.3354/cr01309

Habicht, H.-L., Rosentau, A., Jõeleht, A., Heinsalu, A., Kriiska, A., Kohv, M., et al. (2017). GIS-based Multiproxy Coastline Reconstruction of the Eastern Gulf of Riga, Baltic Sea, during the Stone Age. *Boreas* 46, 83–99. doi:10.1111/bor.12157

Hsu, F.-H., Su, C.-C., Wang, P.-L., and Lin, I.-T. (2020). Temporal Variations of Submarine Groundwater Discharge into a Tide-Dominated Coastal Wetland (Gaomei Wetland, Western Taiwan) Indicated by Radon and Radium Isotopes. *Water* 12, 1806. doi:10.3390/w12061806

Ibenthal, M. (2020). Marine and Terrestrial Influence on Submarine Groundwater Discharge in Coastal Waters Connected to a Peatland. E dissertation. Göttingen, Germany: Georg-August-Universität Göttingen. Avaialble at: https://ediss.uni-goettingen.de/handle/21.11130/00-1735-0000-0005-13C2-A.

Idczak, J., Brodecka-Goluch, A., Łukawska-Matuszewska, K., Graca, B., Gorska, N., Klusek, Z., et al. (2020). A Geophysical, Geochemical and Microbiological Study of a Newly Discovered Pockmark with Active Gas Seepage and Submarine Groundwater Discharge (MET1-BH, central Gulf of Gdańsk, Southern Baltic Sea). *Sci. Total Environ.* 742, 140306. doi:10.1016/j.scitotenv.2020.140306

IOW(Leibniz Institute for Baltic Sea Research Warnemünde) (2020). Environmental Long-Term Data Programme, Station TFO5 - Oceanographic Database Search with Interactive Navigation - ODIN2. Avaialble at: https://odin2.io-warnemuende.de/#/(Accessed December 12, 2020).

Jakobsson, M., O'Regan, M., Mörth, C.-M., Stranne, C., Weidner, E., Hansson, J., et al. (2020). Potential Links between Baltic Sea Submarine Terraces and Groundwater Seeping. *Earth Surf. Dynam.* 8, 1–15. doi:10.5194/esurf-8-1-2020

Jurasinski, G., Janssen, M., Voss, M., Böttcher, M. E., Brede, M., Burchard, H., et al. (2018). Understanding the Coastal Ecocline: Assessing Sea-Land Interactions at Non-tidal, Low-Lying Coasts through Interdisciplinary Research. *Front. Mar. Sci.* 5, 342. doi:10.3389/fmars.2018.00342

Koebsch, F., Winkel, M., Liebner, S., Liu, B., Westphal, J., Schmiedinger, I., et al. (2019). Sulfate Deprivation Triggers High Methane Production in a Disturbed and Rewetted Coastal Peatland. *Biogeosciences* 16, 1937–1953. doi:10.5194/bg-16-1937-2019

Kooi, H., and Groen, J. (2001). Offshore Continuation of Coastal Groundwater Systems; Predictions Using Sharp-Interface Approximations and Variable-Density Flow Modelling. *J. Hydrol.* 246, 19–35. doi:10.1016/s0022-1694(01)00354-7

Kotwicki, L., Grzelak, K., Czub, M., Dellwig, O., Gentz, T., Szymczycha, B., et al. (2014). Submarine Groundwater Discharge to the Baltic Coastal Zone: Impacts on the Meiofaunal Community. *J. Mar. Syst.* 129, 118–126. doi:10.1016/j.jmarsys.2013.06.009

Kreuzburg, M., Ibenthal, M., Janssen, M., Rehder, G., Voss, M., Naumann, M., et al. (2018). Sub-marine Continuation of Peat Deposits from a Coastal Peatland in the Southern Baltic Sea and its Holocene Development. *Front. Earth Sci.* 6, 103. doi:10.3389/feart.2018.00103

Kreuzburg, M., Rezanezhad, F., Milojevic, T., Voss, M., Gosch, L., Liebner, S., et al. (2020). Carbon Release and Transformation from Coastal Peat Deposits Controlled by Submarine Groundwater Discharge: a Column experiment Study. *Limnol. Oceanogr.* 65 (5), 1116–1135. doi:10.1002/lno.11438

Leifeld, J., and Menichetti, L. (2018). The Underappreciated Potential of Peatlands in Global Climate Change Mitigation Strategies. *Nat. Commun.* 9, 1071. doi:10.1038/s41467-018-03406-6

Lennartz, B., and Liu, H. (2019). Hydraulic Functions of Peat Soils and Ecosystem Service. *Front. Environ. Sci.* 7, 92. doi:10.3389/fenvs.2019.00092

Li, X., Hu, B. X., Burnett, W. C., Santos, I. R., and Chanton, J. P. (2009). Submarine Ground Water Discharge Driven by Tidal Pumping in a Heterogeneous Aquifer. *Ground Water.* 47 (4), 558–568. doi:10.1111/j.1745-6584.2009.00563.x

Liu, H., Forsmann, D. M., Kjaergaard, C., Saki, H., and Lennartz, B. (2017). Solute Transport Properties of Fen Peat Differing in Organic Matter Content. *J. Environ. Qual.* 46 (5), 1106–1113. doi:10.2134/jeq2017.01.0031

Liu, H., Janssen, M., and Lennartz, B. (2016). Changes in Flow and Transport Patterns in Fen Peat Following Soil Degradation. *Eur. J. Soil Sci.* 67 (6), 763–772. doi:10.1111/ejss.12380

Liu, H., and Lennartz, B. (2019). Hydraulic Properties of Peat Soils along a Bulk Density Gradient-A Meta Study. *Hydrological Process.* 33, 101–114. doi:10.1002/hyp.13314

Luijendijk, E., Gleeson, T., and Moosdorf, N. (2020). Fresh Groundwater Discharge Insignificant for the World's Oceans but Important for Coastal Ecosystems. *Nat. Commun.* 11, 126. doi:10.1038/s41467-020-15064-8

McBride, M. S., and Pfannkuch, H. O. (1975). The Distribution of Seepage within Lakebeds. *J. Res. US Geol. Surv.* 3 (5), 505–512.

Medvedev, I. P., Rabinovich, A. B., and Kulikov, E. A. (2016). Tides in Three Enclosed Basins: The Baltic, Black, and Caspian Seas. *Front. Mar. Sci.* 3, 46. doi:10.3389/fmars.2016.00046

Miegel, K., Graeff, T., Selle, B., Salzmann, T., Franck, C., and Bronstert, A. (2016). Investigation of a Renatured Fen on the Baltic Sea Coast of Mecklenburg - Part I: System Description and Basic Hydrological Characterisation. *Hydrol. Wasserbewirtscahftung.* 60 (4), 242–258.

Millero, F. J., and Poisson, A. (1981). International One-Atmosphere Equation of State of Seawater. *Deep Sea Res. A. Oceanographic Res. Pap.* 28 (6), 625–629. doi:10.1016/0198-0149(81)90122-9

Mohawesh, O., Janssen, M., Maaitah, O., and Lennartz, B. (2017). Assessment the Effect of Homogenized Soil on Soil Hydraulic Properties and Soil Water Transport. *Eurasian Soil Sci.* 50 (9), 1077–1085. doi:10.1134/s1064229317090046

Moore, W. S. (2010). The Effect of Submarine Groundwater Discharge on the Ocean. *Annu. Rev. Mar. Sci.* 2, 59–88. doi:10.1146/annurev-marine-120308-081019

Peña-Haro, S., Pulido-Velazquez, M., and Llopis-Albert, C. (2011). Stochastic Hydro-Economic Modeling for Optimal Management of Agricultural Groundwater Nitrate Pollution under Hydraulic Conductivity Uncertainty. *Environ. Model. Softw.* 26, 999–1008. doi:10.1016/j.envsoft.2011.02.010

Post, V. E. A., Groen, J., Kooi, H., Person, M., Ge, S., and Edmunds, W. M. (2013). Offshore Fresh Groundwater Reserves as a Global Phenomenon. *Nature* 504, 71–78. doi:10.1038/nature12858

Qu, W., Li, H., Huang, H., Zheng, C., Wang, C., Wang, X., et al. (2017). Seawater-groundwater Exchange and Nutrients Carried by Submarine Groundwater Discharge in Different Types of Wetlands at Jiaozhou Bay, China. *J. Hydrol.* 555, 185–197. doi:10.1016/j.jhydrol.2017.10.014

Quillet, A., Larocque, M., Pellerin, S., Cloutier, V., Ferlatte, M., Paniconi, C., et al. (2017). The Role of Hydrogeological Setting in Two Canadian Peatlands Investigated through 2D Steady-State Groundwater Flow Modelling. *Hydrological Sci. J.* 62 (15), 2541–2557. doi:10.1080/02626667.2017.1391387

Rezanezhad, F., Price, J. S., Quinton, W. L., Lennartz, B., Milojevic, T., and Van Cappellen, P. (2016). Structure of Peat Soils and Implications for Water Storage, Flow and Solute Transport: A Review Update for Geochemists. *Chem. Geology.* 429, 75–84. doi:10.1016/j.chemgeo.2016.03.010

Robinson, C. E., Xin, P., Santos, I. R., Charette, M. A., Li, L., and Barry, D. A. (2018). Groundwater Dynamics in Subterranean Estuaries of Coastal Unconfined Aquifers: Controls on Submarine Groundwater Discharge and Chemical Inputs to the Ocean. *Adv. Water Resour.* 115, 315–331. doi:10.1016/j.advwatres.2017.10.041

Robinson, C., Li, L., and Barry, D. A. (2007). Effect of Tidal Forcing on a Subterranean Estuary. *Adv. Water Resour.* 30, 851–865. doi:10.1016/j.advwatres.2006.07.006

Röper, T., Kröger, K. F., Meyer, H., Sültenfuss, J., Greskowiak, J., and Massmann, G. (2012). Groundwater Ages, Recharge Conditions and Hydrochemical Evolution of a Barrier Island Freshwater Lens (Spiekeroog, Northern Germany). *J. Hydrol.* 454-455, 173–186. doi:10.1016/j.jhydrol.2012.06.011

Sadat-Noori, M., Santos, I. R., Sanders, C. J., Sanders, L. M., and Maher, D. T. (2015). Groundwater Discharge into an Estuary Using Spatially Distributed Radon Time Series and Radium Isotopes. *J. Hydrol.* 528, 703–719. doi:10.1016/j.jhydrol.2015.06.056

Santos, I. R., Burnett, W. C., Chanton, J., Dimova, N., and Peterson, R. N. (2009). Land or Ocean?: Assessing the Driving Forces of Submarine Groundwater Discharge at a Coastal Site in the Gulf of Mexico. *J. Geophys. Res.* 114, C04012. doi:10.1029/2008JC005038

Santos, I. R., Eyre, B. D., and Huettel, M. (2012). The Driving Forces of Porewater and Groundwater Flow in Permeable Coastal Sediments: A Review. *Estuarine, Coastal Shelf Sci.* 98, 1–15. doi:10.1016/j.ecss.2011.10.024

Schaap, M. G., Leij, F. J., and van Genuchten, M. T. (2001). Rosetta : a Computer Program for Estimating Soil Hydraulic Parameters with Hierarchical Pedotransfer Functions. *J. Hydrol.* 251, 163–176. doi:10.1016/s0022-1694(01)00466-8

Schlüter, M., Sauter, E. J., Andersen, C. E., Dahlgaard, H., and Dando, P. R. (2004). Spatial Distribution and Budget for Submarine Groundwater Discharge in Eckernförde Bay (Western Baltic Sea). *Limnol. Oceanogr.* 49 (1), 157–167. doi:10.4319/lo.2004.49.1.0157

Šimůnek, J., M., van Genuchten, T., and Šejna, M. (2018). The HYDRUS Software Package for Simulating Two- and Three Dimensional Movement of Water, Heat, and Multiple Solutes in Variably- Saturated Porous Media, Technical Manual (Version 3). Prague, Czech Republic: PC Progress.

Smith, A. J., and Nield, S. P. (2003). Groundwater Discharge from the Superficial Aquifer into Cockburn Sound Western Australia: Estimation by Inshore Water Balance *Biogeochemistry* 66, 125–144.

Stieglitz, T. (2005). Submarine Groundwater Discharge into the Near-Shore Zone of the Great Barrier Reef, Australia. *Mar. Pollut. Bull.* 51 (1–4), 51–59. doi:10.1016/j.marpolbul.2004.10.055

Szymczycha, B., Borecka, M., Białk-Bielińska, A., Siedlewicz, G., and Pazdro, K. (2020). Submarine Groundwater Discharge as a Source of Pharmaceutical and Caffeine Residues in Coastal Ecosystem: Bay of Puck, Southern Baltic Sea Case Study. *Sci. Total Environ.* 713, 136522. doi:10.1016/j.scitotenv.2020.136522

Szymczycha, B., Kroeger, K. D., and Pempkowiak, J. (2016). Significance of Groundwater Discharge along the Coast of Poland as a Source of Dissolved Metals to the Southern Baltic Sea. *Mar. Pollut. Bull.* 109, 151–162. doi:10.1016/j.marpolbul.2016.06.008

Szymczycha, B., Maciejewska, A., Winogradow, A., and Pempkowiak, J. (2014). Could Submarine Groundwater Discharge Be a Significant Carbon Source to the Southern Baltic Sea?. *Oceanologia* 56 (2), 327–347. doi:10.5697/oc.56-2.327

Szymczycha, B., and Pempkowiak, J. (2016). *The Role of Submarine Groundwater Discharge as Material Source to the Baltic Sea*. Switzerland: Springer International Publishing. doi:10.1007/978-3-319-25960-4

Tait, D. R., Maher, D. T., Sanders, C. J., and Santos, I. R. (2017). Radium-derived Porewater Exchange and Dissolved N and P Fluxes in Mangroves. *Geochimica et Cosmochimica Acta.* 200, 295–309. doi:10.1016/j.gca.2016.12.024

Taniguchi, M., Burnett, W. C., Smith, C. F., Paulsen, R. J., O'Rourke, D., Krupa, S. L., et al. (2003). Spatial and Temporal Distributions of Submarine Groundwater Discharge Rates Obtained from Various Types of Seepage Meters at a Site in the Northeastern Gulf of Mexico. *Biogeochemistry* 66, 35–53. doi:10.1023/b:biog.0000006090.25949.8d

Taniguchi, M., Dulai, H., Burnett, K. M., Santos, I. R., Sugimoto, R., Stieglitz, T., et al. (2019). Submarine Groundwater Discharge: Updates on its Measurement Techniques, Geophysical Drivers, Magnitudes, and Effects. *Front. Environ. Sci.* 7, 141. doi:10.3389/fenvs.2019.00141

Trepel, M., Pfadenhauer, J., Zeitz, J., and Jeschke, L. (2017). *Mires and Peatlands of Europe: Status, Distribution, and Conservation*. Editors H. Joosten, F. Tanneberger, and A. Moen (Stuttgart, Germany: Schweizerbart Science Publishers).

Vilumaa, K., Ratas, U., Tõnisson, H., Kont, A., and Pajula, R. (2017). Multidisciplinary Approach to Studying the Formation and Development of beach-ridge Systems on Non-tidal Uplifting Coasts in Estonia. *Boreal Env. Res.* 22, 67–81.

Virtasalo, J. J., Schröder, J. F., Luoma, S., Majaniemi, J., Mursu, J., and Scholten, J. (2019). Submarine Groundwater Discharge Site in the First Salpausselkä Ice-Marginal Formation, South Finland. *Solid Earth.* 10, 405–423. doi:10.5194/se-10-405-2019

Wang, M., Liu, H., and Lennartz, B. (2021). Small-scale Spatial Variability of Hydro-Physical Properties of Natural and Degraded Peat Soils. *Geoderma* 399, 115123. doi:10.1016/j.geoderma.2021.115123

Wang, M., Liu, H., Zak, D., and Lennartz, B. (2020). Effect of Anisotropy on Solute Transport in Degraded Fen Peat Soils. *Hydrological Process.* 34, 2128–2138. doi:10.1002/hyp.13717

WSV(Wasserstraßen- und Schiffahrtsverwaltung des Bundes) (2020). Stammdaten–Warnemünde. Available at: https://www.pegelonline.wsv.de/gast/stammdaten?pegelnr=9640015 (Accessed April 5, 2020)

Zauft, M., Fell, H., Glasser, F., Rosskopf, N., and Zeitz, J. (2010). Carbon Storage in the Peatlands of Mecklenburg-Western Pomerania , north-east Germany. *Mires Peat.* 6 (4), 1–12.

Conflict of Interest: The authors declare that the research was conducted in the absence of any commercial or financial relationships that could be construed as a potential conflict of interest.

Publisher's Note: All claims expressed in this article are solely those of the authors and do not necessarily represent those of their affiliated organizations, or those of the publisher, the editors and the reviewers. Any product that may be evaluated in this article, or claim that may be made by its manufacturer, is not guaranteed or endorsed by the publisher.

frontiers in Environmental Science

ORIGINAL RESEARCH
published: 29 September 2021
doi: 10.3389/fenvs.2021.680430

Mosses are Important for Soil Carbon Sequestration in Forested Peatlands

Å. Kasimir[1], H. He[2], P.-E. Jansson[3], A. Lohila[4,5] and K. Minkkinen[6]*

[1]Department of Earth Sciences, University of Gothenburg, Gothenburg, Sweden, [2]Department of Geography, McGill University, Montreal, QC, Canada, [3]Department of Land and Water Resources Engineering, Royal Institute of Technology (KTH), Stockholm, Sweden, [4]Finnish Meteorological Institute, Helsinki, Finland, [5]INAR Institute for Atmospheric and Earth System Research/Physics, Faculty of Science, University of Helsinki, Helsinki, Finland, [6]Department of Forest Sciences, University of Helsinki, Helsinki, Finland

Nutrient-rich peat soils have previously been demonstrated to lose carbon despite higher photosynthesis and litter production compared to nutrient-poor soils, where instead carbon accumulates. To understand this phenomenon, we used a process-oriented model (CoupModel) calibrated on data from two closely located drained peat soil sites in boreal forests in Finland, Kalevansuo and Lettosuo, with different soil C/N ratios. Uncertainty-based calibrations were made using eddy-covariance data (hourly values of net ecosystem exchange) and tree growth data. The model design used two forest scenarios on drained peat soil, one nutrient-poor with dense moss cover and another with lower soil C/N ratio with sparse moss cover. Three vegetation layers were assumed: conifer trees, other vascular plants, and a bottom layer with mosses. Adding a moss layer was a new approach, because moss has a modified physiology compared to vascular plants. The soil was described by three separate soil organic carbon (SOC) pools consisting of vascular plants and moss litter origin and decomposed organic matter. Over 10 years, the model demonstrated a similar photosynthesis rate for the two scenarios, 903 and 1,034 g C m^{-2} yr^{-1}, for the poor and rich site respectively, despite the different vegetation distribution. For the nutrient-rich scenario more of the photosynthesis produce accumulated as plant biomass due to more trees, while the poor site had abundant moss biomass which did not increase living aboveground biomass to the same degree. Instead, the poor site showed higher litter inputs, which compared with litter from vascular plants had low turnover rates. The model calibration showed that decomposition rate coefficients for the three SOC pools were similar for the two scenarios, but the high quantity of moss litter input with low decomposability for the nutrient poor scenario explained the major difference in the soil carbon balance. Vascular plant litter declined with time, while SOC pools originating from mosses accumulated with time. Large differences between the scenarios were obtained during dry spells where soil heterotrophic respiration doubled for the nutrient-rich scenario, where vascular plants dominated, owing to a larger water depletion by roots. Where moss vegetation dominated, the heterotrophic respiration increased by only 50% during this dry period. We suggest moss vegetation is key for carbon accumulation in the poor soil, adding large litter quantities with a resistant quality and less water depletion than vascular plants during dry conditions.

Keywords: drained peat soils, vascular plants, mosses, coupmodel, boreal forest, litter, drought

OPEN ACCESS

Edited by:
Gilles Colinet,
University of Liège, Belgium

Reviewed by:
Na Li,
Northeast Institute of Geography and Agroecology, Chinese Academy of Science, China
Jeroen Meersmans,
University of Liège, Belgium

****Correspondence:***
Å. Kasimir
asa.kasimir@gu.se

Specialty section:
This article was submitted to Soil Processes, a section of the journal Frontiers in Environmental Science

Received: *17 March 2021*
Accepted: *23 August 2021*
Published: *29 September 2021*

Citation:
Kasimir Å, He H, Jansson P-E, Lohila A and Minkkinen K (2021) Mosses are Important for Soil Carbon Sequestration in Forested Peatlands. Front. Environ. Sci. 9:680430. doi: 10.3389/fenvs.2021.680430

INTRODUCTION

Worldwide, natural peatlands and other organic soils cover only 3% of the land area but contain 30% of the soil carbon (Gorham, 1991; FAO, 2014). The peat have accumulated after the last glaciation period where the northern peatlands carbon stock have been estimated to contain 500 ± 100 Gtonnes C (Yu, 2012). The peat soil is formed by a litter production slightly larger than its decomposition (Frolking et al., 2001), and many factors influence the balance of soil accumulation and decomposition, mainly climate and water conditions, alongside soil fertility forming the plant community (Waddington and Roulet, 1996; Alm et al., 1997; Laiho et al., 2003). Climate warming and soil drain operations dry out the peat causing decomposition and large increase in greenhouse gas emissions, why there is an urgent need to manage the peatlands in a way that preserve the carbon (Huang et al., 2021), where the main tool is to raise the soil water table (Evans et al., 2021). The photosynthesis is an important part of the carbon budget, where mosses and lichens should not to be neglected besides vascular plants in model studies of cool climate and nutrient limiting conditions (Chadburn et al., 2017). When restoring disturbed peatlands, mosses have been shown to be important to regain carbon accumulation, thus peat mosses need to be preserved or introduced by moss fragments (Huth et al., 2021).

Rewetting is expected to result in reduced CO_2 emission but increased methane (CH_4) emission, where climate warming by CO_2 have been shown the most important to mitigate (Günther et al., 2020). However, the resulting soil carbon (C) balance is not easy to predict owing to the complexity of soil processes and influencing factors, where systems that look similar at first have been demonstrated to act differently, as either a large carbon dioxide (CO_2) source or a small sink (Ojanen et al., 2013). High losses have been displayed for fertile peat soil ecosystems, for example in Skogaryd Sweden, where the combined Net Ecosystem Exchange (NEE) measured by Eddy Covariance (EC), and measured forest growth, revealed a net carbon soil loss of 630 g C m^{-2} yr^{-1} despite high spruce tree growth of 830 g C m^{-2} yr^{-1} including fine roots (Meyer et al., 2013). Similarly, the loss from a fertile peatland forest soil in southern Finland averaged 200 g C m^{-2} yr^{-1} (Korkiakoski, 2020), whereas a nutrient-poor peatland forest soil nearby was a sink of 60 g C m^{-2} yr^{-1} (Minkkinen et al., 2018). Other poor peat soil sites in Finland were also revealed to be small CO_2 sinks, while fertile peat soils were sources (Ojanen et al., 2013; Ojanen and Minkkinen, 2019). Since fertile peat soil sites have larger plant production than poor soil sites, it is counter-intuitive that the poor sites accumulate C rather than the fertile sites. The higher emissions from fertile soils have earlier been hypothesized to be caused by more nutrients for plants and decomposers or a higher topsoil bulk density in fertile soils where more carbon are available for decomposition (Minkkinen and Laine, 1998; Ojanen et al., 2013). Besides the soil properties, the plant composition and function have also been demonstrated to have influence on the soil water table where a forest vegetation keeps the soil drained even in wet years (Leppä et al., 2020), with more oxygen in the soil increasing soil processes. Plant composition is important for how the photosynthesis fixed C is stored, as a living biomass or litter. Vascular plants, having roots, adds litter both on top of the soil and as root litter, while mosses only adds litter in the top soil below the living moss. Nutrient-poor conditions favor mosses over vascular plants, which could be fundamental for the ecosystem function (Van Breemen, 1995; Pedrotti et al., 2014). In fertile sites with deciduous trees like birch, moss growth could be hindered by a thick leaf litter layer (Laine and Vanhamajamaa, 1992), preventing the formation of a new peat layer.

It is a need to investigate why nutrient-poor and rich peat soils show different soil decomposition rate. By combining field NEE data with process-based models, linking ecological theory and data, we can examine and identify the processes most important for gain and losses of carbon. An earlier model study suggested the quantity of litter input from vascular and nonvascular plants, together with decomposability and input location, at the soil surface or deeper layers by roots, to be decisive for peat accumulation (Frolking et al., 2001). Litter input results in a mixture of different organic substances in continuous transition into decomposed organic materials, simplified by assuming all organic matter as a litter decomposing by time (Frolking et al., 2001; St-Hilaire et al., 2010). The soil organic carbon (SOC) have also been separated into two organic matter pools, one with a fast decomposition which C partly ends up into a slow pool, with rates overall faster for nutrient-rich peat soils than poor soils (Metzger et al., 2015).

In this investigation we use the Coupled Heat and Mass Transfer Model for Soil–Plant-Atmosphere Systems (CoupModel, www.coupmodel.com), which been used previously for peat soil greenhouse gas flux investigations (Metzger et al., 2015; He et al., 2016a; Metzger et al., 2016; Kasimir et al., 2018) and is designed to include a wide range of ecosystems and soils. The model was first presented by (Jansson and Halldin, 1979) for forest soils and later developed for agricultural soils by (Johnsson et al., 1987). A recent development of the model have been to include phosphorous (He et al., 2021). Model development and applications is provided in (Jansson, 2012). The model can provide simplified views and conceptualize our understanding of the system function. However, the degree of simplification and conceptualization of the system is a challenge. In earlier use of the model, peatland vegetation has been modeled either as one simplified explicit big leaf, including grass and mosses (Metzger et al., 2015; Metzger et al., 2016) or by assuming two canopies with two "simple big leaves", one for the trees and another for smaller vascular plants like grass (He et al., 2016a; He et al., 2016b). The specific role of mosses has not been the focus (Metzger et al., 2016), although it has been described and included as part of the system when calibrating the model. In this study, we explore the importance of mosses and their influence on the ecosystem by explicitly modeling their particular morphology and physiology and compare two systems having either large or small quantities of moss cover. We also in the CoupModel separate the litter pool into two pools, generated by vascular and moss plants. We based the present study on empirical studies that have demonstrated vascular leaf litter to decompose faster than moss litter (Dorrepaal et al., 2005;

Lang et al., 2009; Strakova et al., 2011). The approach used these new concepts describing the systems to calibrate the CoupModel on measured data from two forested drained peatlands, having contrasting soil fertility (**Supplementary Table S1**).

We aim to answer the question: how a sparser tree canopy with a more developed moss layer and low soil fertility can result in a higher soil carbon sequestration than a forest with a dense tree canopy and a sparse moss layer on fertile peat soil?

The specific purposes of the study were:

1) To present a new model explicitly including moss litter production and decomposition.
2) To develop a common model set-up and design valid for both nutrient-rich and nutrient-poor peatland forest soils.
3) To discuss the role of vascular plants versus mosses on C soil balance.

MATERIALS AND METHODS

Site Description

We used data from two forest sites located 80 km northwest of Helsinki, and approximately 20 km from each other in Southern Finland, Kalevansuo and Lettosuo, to set up the model. Both sites are on drained peat soil but have contrasting soil fertility expressed as C/N, where the nutrient-poor site, Kalevansuo, (60°38′ N, 24°21′ E, elevation 123 m a.s.l.), have C/N = 40 in the top 50 cm soil, and the nutrient-rich site, Lettosuo (60°38′ N, 23°57′ E; 111 m a.s.l), have C/N = 27. Both sites have the same long term annual mean precipitation of 722 mm and annual mean air temperature of 5°C. The first draining took place during the 1930s by manually dug, widely spaced ditches. Then, Lettosuo in 1969 and Kalevansuo in 1971 were drained by 1 m deep ditches spaced 45 m apart and fertilized with phosphorus and potassium. No cleaning of ditches has taken place at Kalevansuo; conversely, various ditches were cleaned at Lettosuo during the 1990s. Ditches at both sites are still functional but are now partly overgrown with *Sphagnum* mosses. At Kalevansuo, the trees have grown bigger, and mire species coverage has decreased while common forest species have taken over in the field and bottom layers. Scots pine (*Pinus sylvestris*), on average 120 years old in 2008, dominates the tree stand (forming 98% of the stand volume), and small pubescent birch (*Betula pubescent*) trees grow alongside ditches (Lohila et al., 2011). The basal area of the tree stand is 18.4 $m^2\ ha^{-1}$, with a tree stand C stock of 4,600 g C m^{-2}, and tree stand C sequestration of 170 g C $m^{-2}\ yr^{-1}$ (above and below ground, excluding roots <1 cm) (Minkkinen et al., 2018). The field layer is dominated by *Ledum palustre*, Vaccinium uliginosum, and others (**Supplementary Table S1**). The bottom layer covers approximately 90% of the land surface and is dominated by forest mosses with several *Sphagnum* mosses on the wetter spots. At Lettosuo, Scots pine and pubescent birch dominated the canopy, with an understory of small-sized Norway spruce and pubescent birch. The trees' total basal area was 27.5 $m^2\ ha^{-1}$, with a tree stand C stock of 8,000 g C m^{-2}, and a C sequestration rate of 270 g C m-2 $years^{-1}$ (above and below ground, excluding roots <1 cm; unpublished data). Because the tree stand is larger than in Kalevansuo, the forest floor is more shaded and has patchy vegetation. The field layer consists of *Dryopteris carthusiana* and *Vaccinium myrtillus*. In the patchy bottom layer, forest mosses can be found alongside *Sphagnum* in moist patches (Bhuiyan et al., 2017).

The topsoil at Kalevansuo is *Sphagnum*-dominated peat with a mixture of *Eriophorum vaginatum* and shrub constituents, while fen peat (i.e., sedges and herbs) is present in the deep layers (Mathijssen et al., 2017). Remains of earlier forest fires (charcoal particles) can be found, especially at a depth of 30–50 cm. After drainage, the oxic peat layer to a depth of approximately 10–30 cm below the surface has decomposed to a high degree. In the topmost 10 cm of the soil, remnants of forest mosses and woody roots can be observed. The peat soil at Lettosuo is sedge-peat with a mixture of *Sphagnum* and wood, namely, typical peat for a treed fen. The peat in the topsoil is more decomposed than at Kalevansuo.

Data Used for the Current Study

The turbulent fluxes of CO_2 (net ecosystem exchange NEE), water vapor (H_2O), and sensible/latent heat were measured with the eddy covariance technique on top of 21.5-m telescopic masts. Supporting meteorological measurements included wind speed, relative humidity, incoming short-wave radiation, total net radiation, air and soil temperatures, precipitation, soil moisture, and water table (WT) depth. The eddy covariance system, footprint calculation, and flux data handling for Kalevansuo were described in detail by Lohila et al. (2011) and Minkkinen et al. (2018). For Kalevansuo, the data covers 2005–2008, and for Lettosuo, 2009–2012. The daily mean was estimated upon data measured hourly, with no gap-filling. When measured data had gaps, the simulation also had the same gaps to make sure that we had no bias because of the different temporal resolution. For the partition of NEE, into gross primary production (GPP) and ecosystem respiration (Reco), tree growth data was used. In this paper, we use the convention that a positive value of NEE indicates a flux from the ecosystem to the atmosphere, while a negative value means uptake of CO_2 by the ecosystem.

The WT depth was continuously recorded close to the EC mast. In Kalevansuo, WT data were recorded daily from 2005 to 2008 and hourly from 2010 to 2016. In Lettosuo, hourly WT data were obtained from 2010 to 2016. Soil temperatures were recorded from four plots in 16 points with temperature loggers from the depths of 5 cm, 15 cm, and 30 cm below the soil surface at intervals of 30 min. Peat C stock was estimated based on average peat layer thickness (Lohila et al., 2011) and average carbon density in peat (Mathijssen et al., 2017). Tree diameter at breast height was measured in spring 2005 and fall 2008 for Kalevansuo, and in fall 2003 and 2008 for Lettosuo to estimate the biomass growth (Ojanen et al., 2012). Most of the publications cited here describe the measurements at Kalevansuo (Minkkinen et al., 2018), and the same methods were applied at Lettosuo, making data from both sites comparable.

Modeling Approach

The CoupModel is an ecosystem model platform designed to simulate water and heat fluxes alongside C and nitrogen (N) cycles in terrestrial soil-plant ecosystems based on well-established equations to represent all major processes and components (Jansson, 2012). The main model structure is a one-dimensional layered soil profile including plants, containing all main flows of water, heat, C, and N dynamics between the atmosphere, plants, and soil, based on detailed descriptions of soil and plant physical and biogeochemical processes. A general description of the model and how the components are linked to each other can be found in Jansson (2012); Metzger et al. (2015) and He et al. (2016a). The model main equations used in this study are described in the **Supplementary Table S2**.

Two systems named K and L were thus modeled based on Kalevansuo and Lettosuo data, describing a poor scenario with a large moss cover and a nutrient-rich scenario with low moss cover, respectively (**Figure 1**). In the model, vascular plants are represented by three components: root, stem, and leaf. Photosynthetic assimilates (mobile C and N pools) are transformed to the biomass of the three components based on tissue partitioning and nutrient demand and availability. Nutrient partitioning is defined with the highest priority for the roots, followed by the leaf, and finally, the remaining for the stem. Optimal C/N ratios are defined by parameters governing together with the C allocation the N demand from the soil. Thus, roots are a relatively large fraction of the normal growth for vascular plants. Vascular plants feed the soil with litter from above ground components to the soil surface and from root litter to different horizons. Vascular plants extract water and nutrients through roots, exponentially distributed by depth. In contrast, mosses have no roots, only the leaf and stem act as primary targets for the photosynthesis products. Here we introduce an explicit description of mosses, new for the model, where mosses are defined as plants without roots, a living component located partly inside the topsoil layer where uptake of water and nutrients occurs. When mosses grow, the old parts are covered by new parts from above, and the old parts of the moss die. Moss litter from the stem and leaf takes place as a continuous flux directly to a position inside the soil and not to the soil surface. For this application, we assumed that mosses die in the modeled soil layer 2, 5–15 cm soil depth. Moreover, N fixation was assumed for moss plants only.

Three vegetation layers were constructed for the model to represent the major differences in light, water, and N availability: Vegetation1 consisted of the coniferous tree canopy, Vegetation2 of deciduous trees of all sizes, and smaller evergreen vascular plants, and Vegetation3 the bottom layer with moss plants. The vegetation can be understood by the model as three big leaves allowing the competition of light, water, and nutrients. A big leaf can intercept light from a certain height down to the soil surface. The interception of light follows the exponential Beers law as a function of the Leaf Area Index (LAI) and a corresponding uniform distribution of leaf with height. The light extinction coefficients were assumed to be the same for the vascular plants, 0.5, but for the mosses, the coefficient of two was used, a number often used for field layer plants. The vegetation of each height segment share light, regulated both by the degree of cover and LAI. The LAI, maximal height, and degree of soil cover estimated for K and L scenarios based on the two sites Kalevansuo and Lettosuo (**Supplementary Table S3**). The model calculates photosynthesis to be proportional to the global radiation absorbed by the canopy; however, it is limited by unfavorable temperature, water conditions, and lack of N in the leaf. On

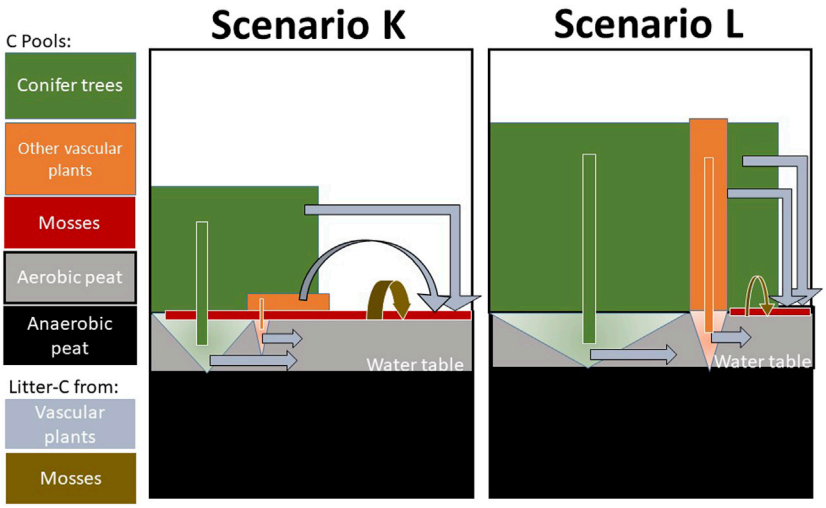

FIGURE 1 | Overview of the two simulated systems K and L, where K is nutrient-poor. Vascular plants, Vegetation1 (conifers) dominate at L, both in height and coverage. Vegetation2 consists also of vascular plants, mainly of small shrubs but also tall birch trees at L. Mosses are incorporated in the soil surface and cover the soil at K but are sparse at L. Note that mosses have no roots and add litter only to the soil layer just below the mosses. The soil column is divided into 10 layers to 2.5 m depth, each with three soil organic carbon components with different decomposition rates. The surface soil is oxic, in average to a depth of 0.3 m, where most roots can be found.

average, 92% of the total incoming global radiation was intercepted by vegetation at K and 93% at L. The conifers (Vegetation1) of the poor scenario intercepted only 53% of the light, while 88% was intercepted at L. At K, the Vegetation2 plant type was composed mainly of dwarf shrubs, while at L deciduous trees dominated. The mosses (Vegetation3) differed most, intercepting 35% of the light at K but only 2% at L (**Supplementary Table S3**).

Vascular plants access water through roots in the uppermost 50 cm of the soil, with most roots in the surface 20 cm according to the measured root biomass data (Bhuiyan et al., 2017). Besides larger access to water, vascular plants are able to keep the cell water potential quite stable by stomata regulation. Conversely, mosses access only water in the soil surface and have no leaf stomata why they lose water by evaporation from the leaf surface, regulated by the resistance between the soil and atmosphere. Mosses are thus unable to control tissue water as vascular plants, which have stomata, why mosses need to cope periods of low tissue water content (Proctor et al., 2007). The model approach for moss water evaporation was a resistance based on leaf moisture only and no stomata control as used in vascular plants.

The model set-up assumes a soil structure with three soil organic matter components and 10 soil layers to describe the differences down to 2.5 m depth focusing on the uppermost 50 cm of the soil profile (**Supplementary Table S4**). The soil of the top 5 cm was assumed composed of both SOC and living mosses. The SOC component design was: two litter pools SOC1 and SOC2, originating from vascular plants and mosses, respectively. The third pool, SOC3, was produced from decomposed SOC1 and SOC2. The initial soil organic C of each layer was divided into SOC1, SOC2, and SOC3, assuming a C/N of 45 for SOC1, 65 for SOC2 (Kuhry and Vitt, 1996), and 20 for SOC3 (Svensson et al., 2008). The distribution of each layer of SOC1, SOC2, and SOC3 is presented in the **Supplementary Table S4**. This pool separation mainly aimed to link the soil processes to the plant functional roles. Soil physical properties are presented in **Supplementary Table S5**. All water was assumed to be added through precipitation only.

Decomposition was simulated as a first-order equation, controlled by the decomposition rate coefficient *RateCoefSOC,* combined with response functions for soil temperature and moisture around an optimal range with the assumption of zero decomposition at full saturation. The decrease from an optimal to zero decomposition rate was assumed to follow a simple expression accounting only for the air-filled pore space described by the parameters *ThetaUpperRange,* describing the percentage of air-filled soil pores when decomposition starts to slow down, together with *ThetaPowerCoef* describing unlinearity. These parameters demonstrate the range of air-filled pores where decomposition is negatively impacted by air-filled soil pores and the rate of decrease. In general, a higher value of *ThetaUpperRange* and *ThetaPowerCoef* means a smaller moisture response, thus a lower simulated soil decomposition. Temperature functions were not calibrated since they were assumed to be well described by scenario-independent parameters.

Calibration and Sensitivity

Measured data from the two sites represent two different periods in time and could therefore not be compared directly due to the between-year variability. However, the data could be used for calibration and extended to cover the same period and weather conditions. A common climate forcing dataset covering 10 years was used for calibration and simulation. We used measured characteristics as independent inputs and assumed that the vegetation cover characteristics and the soil properties displayed relatively slow changes during this period. In contrast, the EC flux data displays high variability within a day, between seasons, and between years depending on the specific climate variability. The approach was only to use measured, hourly quality checked data (Vesala et al., 2008) to find the best possible parameter representation of the model when fitting to the NEE data. The calibration protocol was using a Monte-Carlo based approach using a stepwise design of a selection of parameters, with appropriate uncertainty ranges, to make sure that we generated a high amount of more than 10,000 candidates that was used for selection of posterior parameter distributions.

To make sure we did not obtain a systematic bias between our two systems, especially in the dynamics of the WT, we used many parameters values based on previous applications of the model and to a common value for both systems (**Supplementary Table S6**), and we initially calibrated the model to represent good enough abiotic conditions and seasonal variability in WT, and atmospheric fluxes of latent and sensible heat flows. The first step of calibration used subjective criteria and literature values for most parameters and calibrated a few parameters (hydraulic conductivity function, the spacing between the ditches, and approximate drainage depths). The resulting model outputs were compared with measured WT dynamics and latent and sensible heat flux. After this, the model was constrained to represent the carbon flux dynamics. First, we tested using only NEE flux data but found it was necessary to include and fit the model with measured data on tree growth. In principle, we wanted to investigate all different parameters possibly influencing the dynamics of NEE in forest ecosystems. However, a parameter-rich model has many problems with possible overparameterizations and equifinality in the results. Calibrated parameters were thus selected to have an expected strong impact on the NEE fluxes. Initially, we tried to include details on the N cycle, to calibrate N mineralization, N uptake, internal N allocation within the plants, and N fixation. However, because of the many uncertainties, especially for within-year dynamics, we decided to keep only one parameter representing N of the leaf, *N_PhotoFactor*. This single parameter represents the N control on photosynthesis rate for fixed light adsorption of a vegetation layer, meaning the N supply needed to fit a reasonable photosynthesis level. To clarify, N processes are still included and modeled. Moreover, radiation efficiency, meaning the CO_2 fixed per quantum light, was assumed to be similar for both sites and for each of the vegetation layers concerning plant function type, namely, vascular plants or mosses (**Supplementary Table S6**).

Another choice of simplification was that vascular plants of layer one and two were assumed to have a similar N control; thus vascular plants were assigned a common *N_PhotoFactor*, and moss plants a separate *N_PhotoFactor*. Transpiration/evaporation regulation was

calibrated on the parameter *CriticalThresholdDry*, which describes at which soil water potential, expressed in cm water column (hekto Pascal), photosynthesis starts to be negatively impacted by drought. Again, we assumed the moss layer would have a different sensitivity compared with vascular plants. Acclimation of photosynthesis from winter conditions into spring is necessary for a forest in the boreal region, reflected by the parameter *TF SUM Start,* which was included in the calibration scheme, undifferentiated by vegetation type.

Decomposition of the three soil organic pools (SOC1, SOC2, and SOC3) was assumed controlled by the decomposition rate coefficient, *RateCoefSOC,* assigned an assumed fixed range of sensitivity with decreasing sensitivity from SOC1 to SOC3. The decomposition rate of vascular plant litter (SOC1) was assumed to be much higher than that of mosses (SOC2) (Hobbie et al., 2000). Moreover, decomposition is controlled by oxygen availability which decreases when the soil water content becomes high. This was included by the two parameters, *ThetaUpperRange* and *ThetaPowerCoef*.

In the calibration, each of the selected parameters was allowed to randomly vary within a range according to **Table 1** and **Supplementary Table S7**. To avoid the noise from the high resolution of the 30 min measured flux data, hourly mean values were cumulated each year. A prior representation of the two sites was made by 15,000 simulations, out of which the best acceptable ensemble of 100 candidates was selected using several criteria (**Supplementary Table S11A**). The least-square criteria was applied since it focused on the seasonal dynamic of the carbon fluxes. It also reduced the bias between simulated and measured values to a low level. A full set of statistical performance indicators was estimated both on untransformed and on transformed cumulative data. Details of those are presented in the **Supplementary Table S8**.

TABLE 1 | Parameter setting, prior range. Plant growth parameters 1–3 refer to the three vegetation layers. SOC pool one and two refer to litter pools originating from vascular and moss plants respectively, and the decomposed organic matter SOC3.

Module	Parameter name	Unit	Min and Max	
Plant growth				
	TF SUM Start(1)+ (2)+(3)	—	0.01	1
	N_PhotoFactor (1)+(2)	—	0.3	0.6
	N_PhotoFactor(3)	—	0.3	0.6
	CriticalThresholdDry(1)+(2)	cm water	200	2000
	CriticalThresholdDry(3)	cm water	200	2000
Soil organic matter decomposition				
	RateCoefSOC1	day^{-1}	5.E-4	0.004
	RateCoefSOC2	day^{-1}	5E-5	2.E-4
	RateCoefSOC3	day^{-1}	1.E-5	2.E-4
	ThetaUpperRange	vol%	3	20
	ThetaPowerCoef	—	0.2	2.2

RESULTS

Calibrated Model Parameters and Performance

Vegetation

The calibrated rate coefficients controlling photosynthesis, *N_PhotoFactor,* revealed no major differences for vascular plants and mosses at K (**Figure 2**). The *N_PhotoFactor* could not be constrained for mosses at L owing to an exceedingly low proportion of this vegetation. Thus, the calibration resulted in similar and narrower parameter ranges compared to the prior min and max values of **Table 1**, for both K and L alongside the vegetation types. Besides light and N control on photosynthesis, plant water availability was also important as regulated by the parameter *CriticalThresholdDry*; although this displayed minor changes following calibration, vascular plants at K were somewhat more sensitive to dry conditions than at L. Mosses displayed the same sensitivity as vascular plants. The *TF SUM Start*, which describes the seasonality of photosynthesis, namely, the transition to full photosynthesis after the dormant winter conditions, resulted in a lower value for K but not for L. This low value suggested a need for a long start-up period for the plants at K.

Soil

Calibrated rate coefficients for SOC decomposition were similar for both systems, but all three *RateCoefSOC* were constrained to higher values than the prior values. The threshold for the lowest posterior values shifted to higher values, especially for the L scenario, however, comparing mean or median values indicated no differences. Both scenarios also displayed similar sensitivity to soil anaerobicity, *ThetaUpperRange*, alongside the nonlinearity of this parameter, *ThetaPowerCoeff* (**Figure 3**).

Overall, the calibration showed that the parameters for both scenarios were quite similar concerning photosynthesis and soil decomposition. The largest change compared to the prior setting was found for the *N_PhotoFactor* and *TF SUM Start* parameters.

Performance

The Kalevansuo measured NEE data was on average $-0.74\ g\ C\ m^{-2}\ day^{-1}$ between September 2004 and March 2009 (n = 28,862), whereas the mean of the K simulated ensemble was $-0.77\ g\ C\ m^{-2}\ day^{-1}$ with a simulated range from −0.88 to $-0.53\ g\ C\ m^{-2}\ day^{-1}$. Measurements at Lettosuo were conducted later, from September 2009 to December 2012, with an average NEE of $-0.17\ g\ C\ m^{-2}\ day^{-1}$ (n = 22,145), whereas the L simulated ensemble was -0.19 $g\ C\ m^{-2}\ day^{-1}$ with a range from −0.21 to −0.08. In the growing season, both the modeled and measured NEE data fluctuated, with the model displaying a good performance overall (**Figure 4**). The simulated and measured winter NEE fluxes were small and demonstrated good agreement. One systematic deviation with overestimations of NEE appeared in the late summer and autumn of 2006 at K. Similar overestimation tendencies for NEE appeared in late summer during 2010 and 2011 at L. Measurements displayed high, meteorology-driven day-to-day variability at both sites, but this short-term variability was difficult for the model to fully capture. The scatter plot representation (**Figure 5**) of the daily mean values displays similar patterns for the two systems/sites, without systematic data noise patterns.

The time series of simulated WT for K demonstrates frequent occasions with a higher (wetter) water saturation level than the

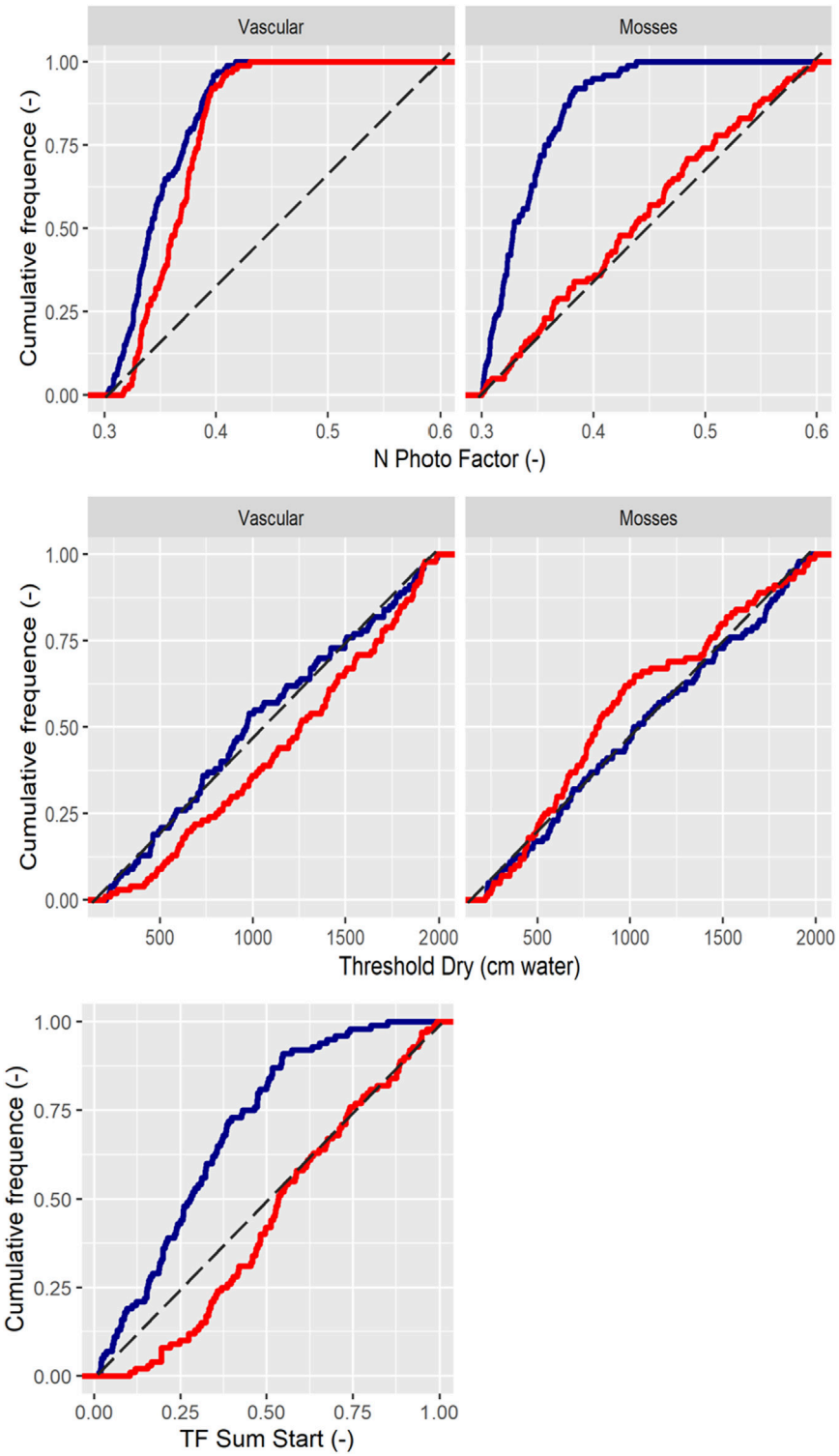

FIGURE 2 | The cumulative frequency distribution of accepted parameter values associated with plant growth. K = blue and L = red.

measured data. Besides this, the dry summer of 2006 was revealed to be a key period for K, where modeled WT drop followed measured Kalevansuo data. Unfortunately, WT measurements were not done deep enough to allow a comparison for the deeper levels. The model was able to reflect the normal seasonal variability and between-year variability. No deviating

systematic patterns could be seen between measured and simulated WT for the two systems/sites. The mean measured and simulated WT levels were similar (**Figure 5**). However, one similar systematic pattern was apparent for shallow WT. The simulated values were lacking representation of values around −0.2 m depth, which was similar for both systems. This reflects a problem with a continuous representation of the WT when a discrete representation of the compartment is used in the numerical representation of the model. Additionally, the model demonstrated higher WT in 2008 for the K site and 2011 for the L site (**Figure 4**).

Modeled 10-years Balance

The modeled 10-years balance of NEE demonstrated the nutrient-poor K to be a sink, $-232\ g\ C\ m^{-2}\ yr^{-1}$, and L to be a source, $+7\ g\ C\ m^{-2}\ yr^{-1}$. On many occasions, both K and L had the same NEE, but the L scenario also had many occasions with overall C-loss when K demonstrated uptake (**Figure 6**). In early summer, net uptake dominated for both K and L, while in late summer and autumn, many days with losses occurred, most pronounced for the fertile L which displayed the largest flux variability. During winter, NEE was small overall with low variability for both.

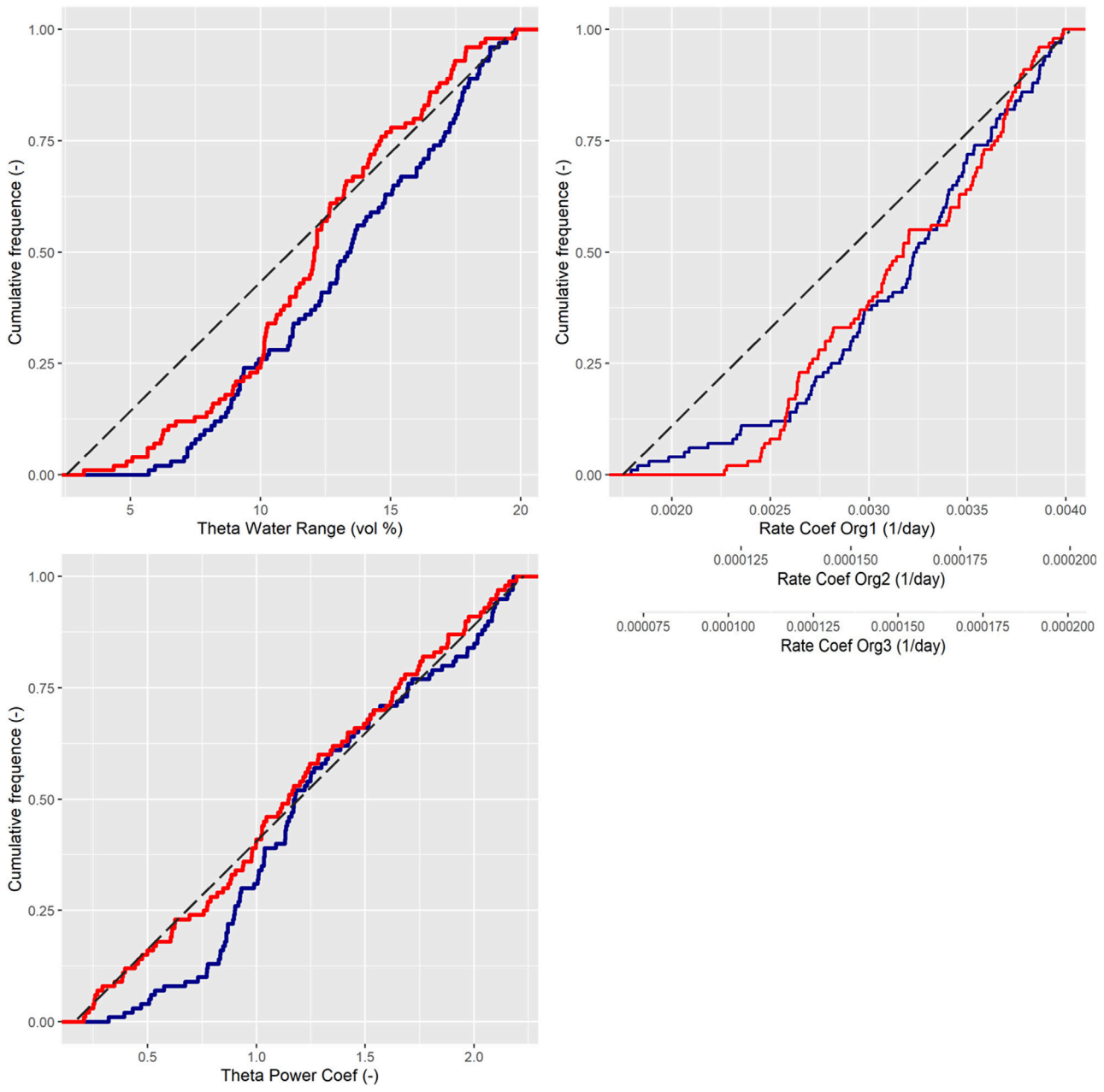

FIGURE 3 | The cumulative frequency distribution of the accepted parameter values associated with soil processes. K = blue and L = red.

FIGURE 4 | Daily measured and simulated average NEE, g C m^{-2} day^{-1} and WT, m, expressed over the measurement period. On the left measured Kalevansuo data (red) together with simulated K (blue-green). On the right the same for Lettosuo and L data.

Net ecosystem exchange is composed of two large terms, photosynthesis and ecosystem respiration (Reco), where **Supplementary Table S9-a** presents selected carbon flux outputs with uncertainty range of the two systems. Neither can be measured directly but it is possible to disentangle them from various models. The seasonal pattern of GPP follows that of light and temperature, being large in summer and almost zero in winter (**Figure 6**). On most occasions, both systems had quite similar GPP for the total vegetation. The average GPP was −920 g C m^{-2} yr^{-1} for the K scenario, slightly lower than the L-scenario, −1,060 g C m^{-2} yr^{-1}. The largest difference between the scenarios was the Vegetation3, mosses, which were responsible for a large part of the GPP at K while the moss GPP was barely visible for L. However, at L, Vegetation2 (tall birch trees and vascular plants in the field layer) displayed a certain importance while it was very small at K. The carbon fixed in the GPP is either lost in autotrophic respiration or stored in living and dead biomass (litter). The average litter production was the largest for K, 474 g C m^{-2} yr^{-1} compared to 330 g C m^{-2} yr^{-1} at L, despite a smaller GPP at K. Of the total litter production, mosses contributed 54% at K while only 7% at L. This is fundamental for the next term, Reco, since litter quality differs between vascular plants and mosses. The Reco over the 10 years on average was 688 for K and 1,068 g C m^{-2} yr^{-1} for L. Every year the Reco was larger for L than for K, and this was most pronounced during dry years (**Figure 6**).

Over the 10 years, plant growth accumulated more C at L than at K (**Figure 7**). Owing to competition for light and nutrients, the vegetation layers two and three did not grow much during this time, which is also inherent in their life-form as shrubs and moss. Only the birches grew in Vegetation2 at L. Despite, or because of, the lack of biomass growth, mosses at K were almost as essential as the trees adding litter carbon to the system. More C accumulated as biomass at L than K, but for the soil accumulation, the opposite was found, with a loss for the L scenario and a gain for K (**Figure 8**). The modeled overall soil C-loss at L was from all three soil components. In K, net losses were from SOC1, while the C-pool increased for SOC2 and SOC3.

All data on fluxes and carbon stock changes above were displayed as the average of the 100 accepted simulation runs. The accepted 100 model runs demonstrated a narrow distribution range for the C stock change of both for vegetation and soil and for K and L (**Figure 9**). No overlap for the scenarios was found, indicating a significant difference. While the L vegetation gained carbon, this did not compensate for the high soil C-loss For K, both the plants and the soil gained C for all the accepted simulations, where the soil accumulated C in the range from 0 to 130 g C m^{-2} yr^{-1} (**Figure 9**).

Simulated Impact of Drought

During the 10 simulated years, three dry years occurred: 2006, 2010, and 2013. These explained most of the difference between K and L (**Figures 6**, **8**). In 2007, the WT depth was approximately 0.3 m, similar for both sites, but in the dry year 2006, the WT drop was larger for L, reaching below 0.9 m, while for K, the WT dropped to 0.75 m (**Figure 10**). The model predicted that the especially dry year 2006 impacted L the most, with a NEE of +137 g C m^{-2} yr^{-1} for K and +599 g C m^{-2} yr^{-1} for L. In contrast, in a more "normal" year represented by 2007, the NEE demonstrated an overall uptake for both scenarios, −226 C m^{-2} yr^{-1} for K and −45 g C m^{-2} yr^{-1} for L.

The photosynthesis rate for the L-scenario was relatively unaffected despite dry conditions in 2006, while that for K

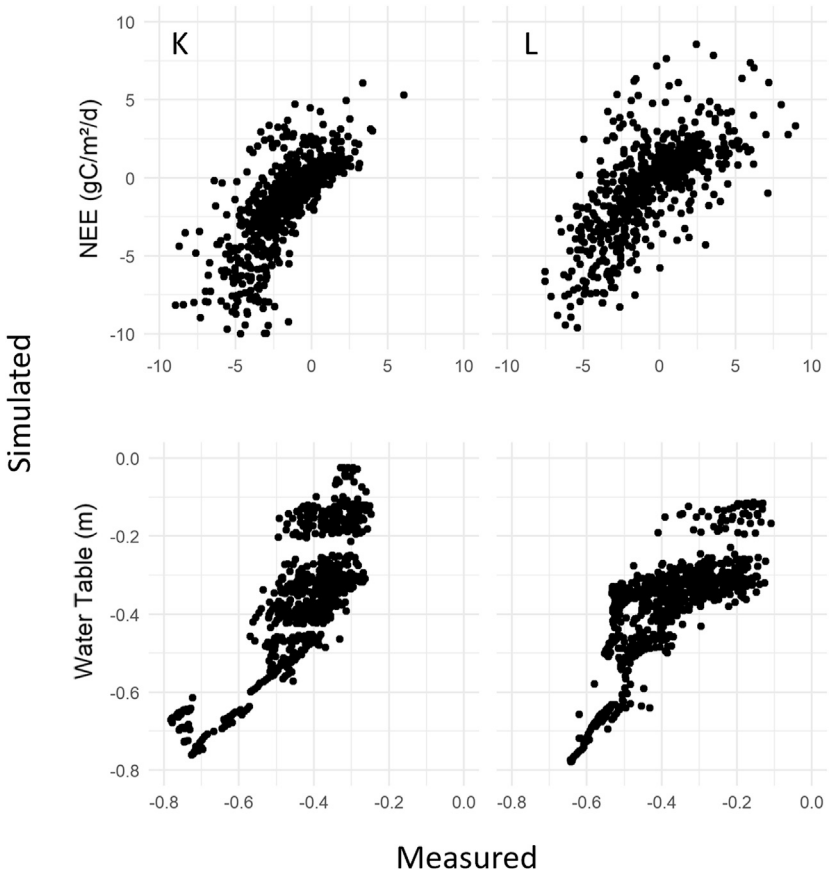

FIGURE 5 | 1:1 plots of daily measured vs. simulated average NEE, g C m^{-2} day^{-1} and WT, m. On the left measured Kalevansuo data together with simulated K. On the right Lettosuo and L data.

photosynthesis became smaller (**Figure 11**). At K, the Vegetation1 (conifers) photosynthesis rate in 2006 was 95% compared of that in 2007. This was the least affected vegetation compared to Vegetation2 (birch and field layer), 79%, and Vegetation3 (mosses), which reached only 44% of the photosynthesis rate compared a more normal year. One explanation is that vascular plants with deep roots are less negatively impacted due to access to water resources deeper down compared to mosses living in the soil surface with no roots. Mosses at L had lower photosynthesis rate in 2006, 86% of the normal rate; however, mosses at L generally had a lower coverage and lived in a more shaded environment than at K. It was also possible to see a transpiration increase for Vegetation1 by 8 and 15% for K and L, respectively, in 2006, while evaporation from mosses decreased for K and L by 48 and 14% of a normal year evaporation. Thus, vascular plants mediated a lowered WT, whereby the soil in the L scenario with more vascular plants dried out more than in the K site. An effect of the lowered WT was a larger aerobic soil volume and consequently increased heterotrophic respiration: 50 and 140% for the K and L scenario, respectively (**Figure 11**), displayed by the red line, and adding the autotrophic respiration gives the total respiration delineated by the top brown line.

The simulation shows that K and L had different drought vulnerabilities: photosynthesis was the most sensitive at the K scenario because of a dominant moss layer, while at L, it increased the decomposition owing to a larger soil aerobic volume, which caused the soil to lose carbon. The soil C loss was the most decisive concerning C balance.

DISCUSSION

This study aimed to examine how a sparsely forested nutrient-poor site could sequester more carbon than a fertile and dense forest, as observed previously by flux measurements. We hypothesized this could be explained by differences in the moss layer coverage, litter production, and decomposition. In many studies, the focus has been on vascular plants like trees, while the importance of mosses as a vital part of the ecosystem has not been recognized. Moreover, investigations of carbon balances with micrometeorological methods are complicated since many components interact with uncertain storage terms and are not easy to separate. Data coverage is never 100%, thus measured field data must be complemented with a modeling approach to fill data gaps and close the carbon balance,

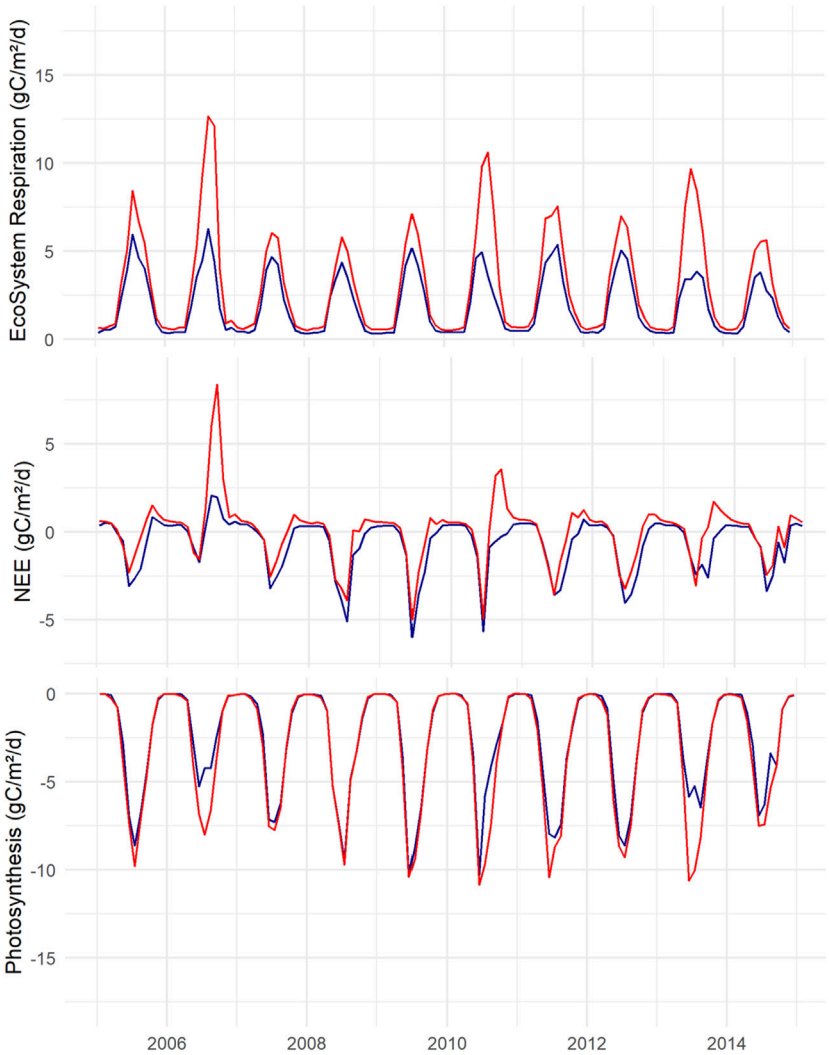

FIGURE 6 | Top, modelled ecosystem respiration (Reco) for K (blue) and L (red). **Middle,** net ecosystem exchange (NEE). **Bottom,** gross primary production (GPP). Negative numbers show uptake, monthly averages expressed as g C m^{-2} day^{-1}.

namely, the GPP and Re partitioning by using NEE data. Since the micrometeorological technique measures the net CO_2 flux of the whole ecosystem, it is not possible to understand the role of separate vegetation layers without additional biomass growth measurements. In this study, we attempted to disentangle the importance of the many ecosystem components by using the CoupModel constrained with the best available measured field data. Our model keeps track of all major carbon fluxes and is based on the law of mass conservation, although there can still be uncertainties in partitioning. Thus, it is important to have a realistic model structure where the major components are identified. This was the background to why we developed the model also to describe the special morphology and physiology of mosses which in previous peat soil studies utilizing the COUP-model were not separated from vascular plants (Metzger et al., 2015; He et al., 2016a; He et al., 2016b; Metzger et al., 2016). The model was conceptualized with three vegetation layers to include and separate conifer trees, other vascular plants, and mosses. The soil description separated moss plant litter from vascular plant litter, both of which decomposed into a common third pool of decomposed soil organic matter. With these descriptions, the aim was to obtain a fitted model for drained peat soil, which could be used as a tool to investigate differences in carbon fluxes at different peatland ecosystems. In the following sections, we discuss the major findings and remaining challenges to explicitly describe the different vegetation functional roles.

Model Calibration and Uncertainties

Of the 15,000 calibration simulations, 100 were selected, and many different criteria were tested to obtain the reduced uncertainty for the simulation. The specific choice was made to produce the same type of error for both sites and to reduce errors for general impacts

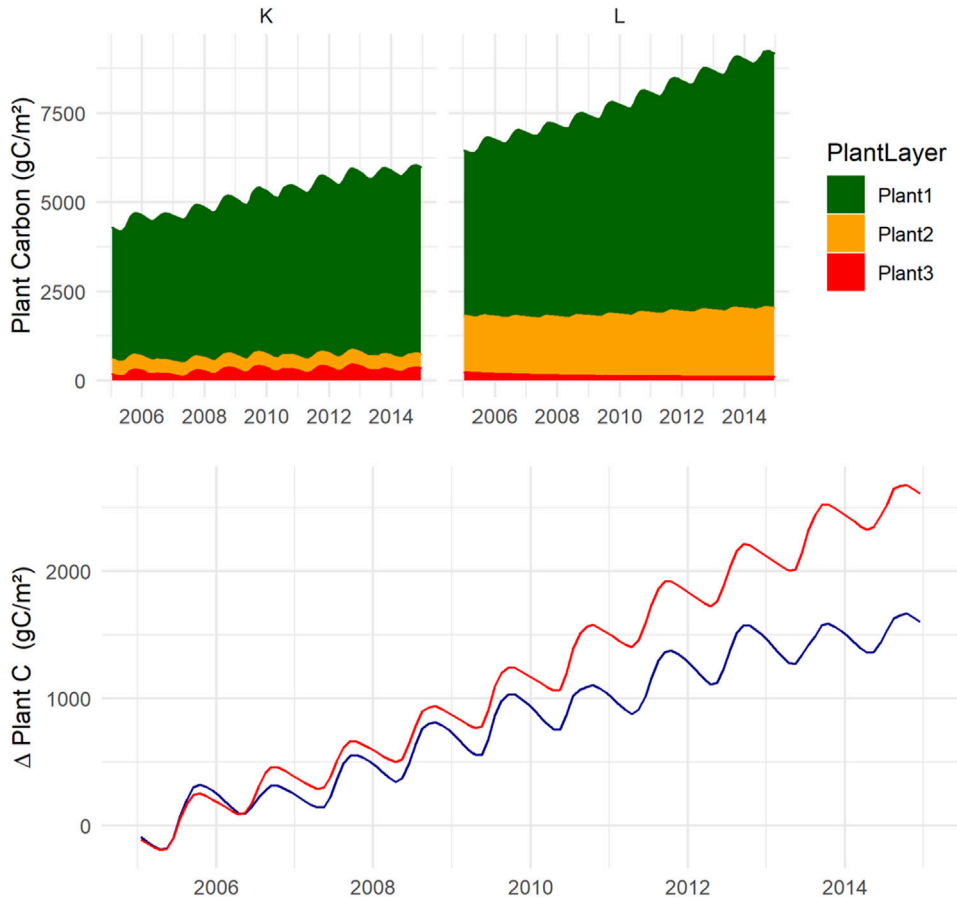

FIGURE 7 | Plant carbon accumulation (positive numbers) over 10 years, top panel shows C accumulated in vegetation and its change over the years. Vegetation1 (conifer trees) = dark green, Vegetation2 (deciduous trees and field layer vascular plants) = yellow and Vegetation3 (mosses) = red. Bottom panel shows total plant C accumulation of the two scenarios where K = blue and L = red. Mean of 100 accepted model runs.

on the carbon balance. High-resolution uncertainty was smoothed out but not disregarded within a daily resolution.

When forcing the long-term mean value to be without a bias, this increased performance indicator (RMSE) that emphasizes the short-term dynamics. Objective use of the Bayesian approach has been tested, with different error model assumptions, which displayed different problems, especially when high numbers of data were relatively close to zero compared to a few peaks with either high negative or positive values.

The final selection of using RMSE on yearly accumulated numbers was taken because of its simplicity and robustness. Normally this indicator displayed similarity with other indicators like the Nash-Sutcliffe efficiency. We also tested our calibration of the quality checked gap-filled data for the Kalevansuo site, however, this resulted in a less good performance based on our statistical indicator. Thus, we rejected the use of gap-filled data since it also added another model to the procedure.

To reduce the general uncertainty, we also considered using a multi-criteria approach considering different data: sensible heat flux, latent heat flux, and chamber-based gas flux measurement for various treatments of the areas. However, a multi-criteria approach would add even more subjectivity, especially for the representativity error of the measurements. Thus, the first choice was not to include other data than the NEE. However, we found it necessary to constrain the model by estimated total plant biomass accumulation (i.e., tree stand growth) of the two sites. Without this constraint, the partitioning between the soil and the plant was uncertain. Additional criteria may be added for future studies to further test the uncertainty and role of the different components of the ecosystem. It is possible to reduce the uncertainties in the simulated plant vegetation with good empirical data.

Parameter Results and Performance

In many aspects, K and L were similar since most parameters changed in the same direction. The parameter controlling photosynthesis, *N_PhotoFactor,* displayed the same importance since the range after calibration became narrower and lower than the prior range. Several differences between the sites can be seen in the parameter *TF SUM Start*, with a slower start of photosynthesis after the winter for K. Moreover, vascular

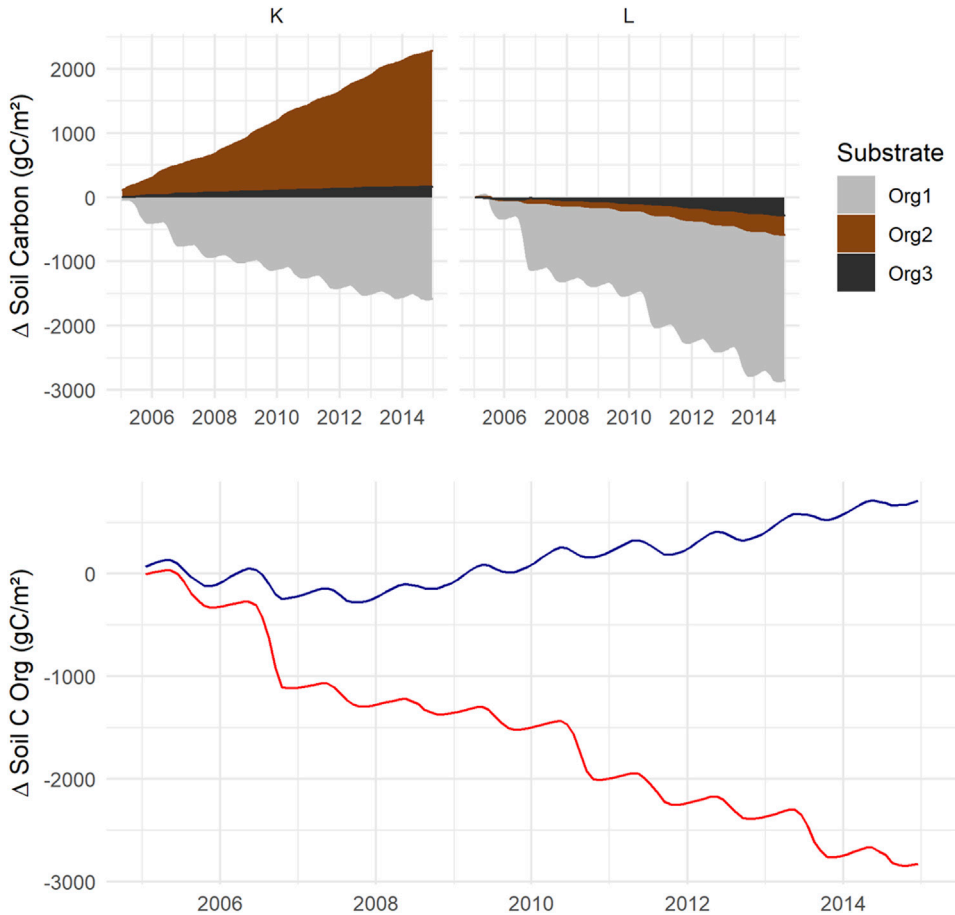

FIGURE 8 | Simulated change in soil C pools where positive numbers shows the accumulation. Top panel shows the change in SOC1 = grey, SOC2 = brown and SOC3 = black. Bottom panel shows the total soil C accumulation for scenario K = blue and L = red. Mean of 100 accepted model runs (**Supplementary Table S10-a**).

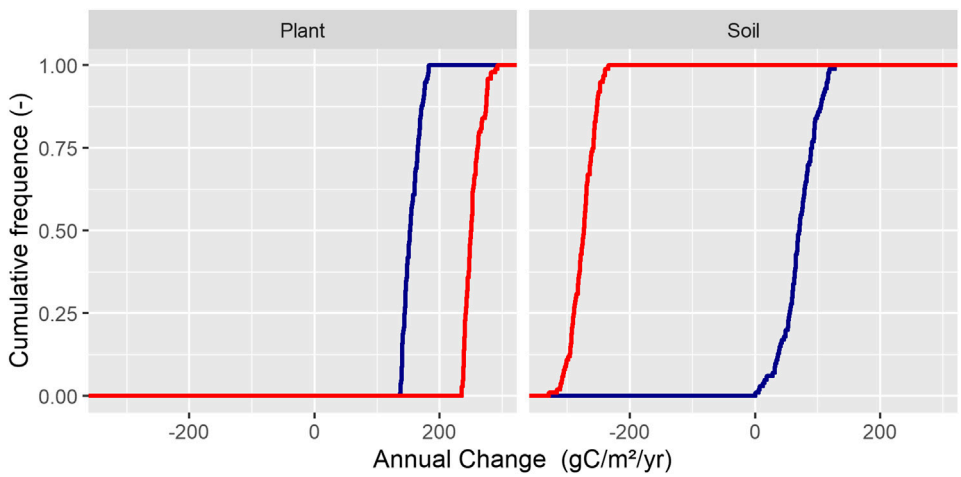

FIGURE 9 | Variation within the 100 accepted model runs is shown as the frequency distribution of annual carbon change in vegetation and soil, for K (blue) and L (red). A positive number here shows accumulation.

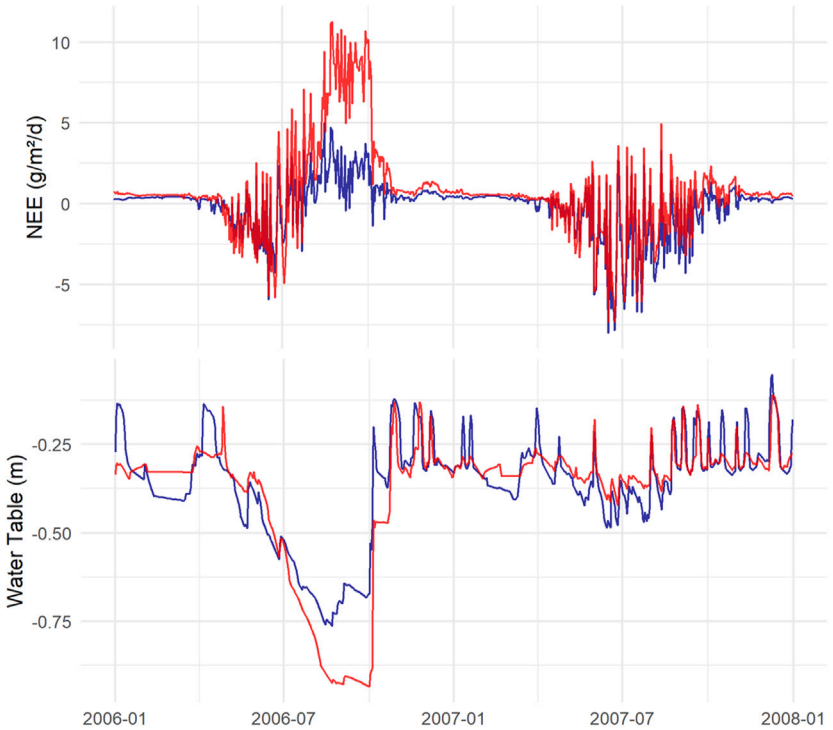

FIGURE 10 | Simulated NEE, where a negative number shows uptake, and WT fluctuations during the dry year 2006 and the following more normal year 2007, for K (blue) and L (red).

plants at K were revealed to be somewhat more sensitive to dry conditions than vascular plants at L, displayed by the parameter change of *CriticalThresholdDry*. For mosses, this parameter did not change. The central parameter, *RateCoeffSOC,* that described soil organic matter decomposition, was constructed to require small overall differences in soil decomposability between K and L. A prior proportionality of 1:5:50 (SOC1: SOC2: SOC3) for the minimum and 1:20:20 for the maximum values for the three SOC pools were used to meet this requirement (**Table 1**). After calibration, *RateCoeffSOC1, 2,* and *three* increased but were similar for both K and L as required. With this setting, we were able to describe with the model the measured NEE and biomass growth. However, it could be asked if our prior parameter setting was realistic since we had a large difference between decomposability of litter originating from vascular plants or mosses. Compared to experimental data compiled in Hobbie et al. (2000) we can see our SOC1 max value may have been a little high. However, the rate coefficient for SOC2 was similar to the measured values in Hobbie et al. (2000). By calibrating SOC1 and two independently but with the same prior range, the calibration resulted in different decomposability for the same litter quality at K and L, especially for the SOC2 (**Supplementary Table S11A,B**). The *RateCoeffSOC2* became lower after calibration, although not as low as in the main setting, and higher compared to data in Hobbie et al. (2000). In this setting, SOC3 was accumulating for both K and L, rather than the SOC2 pool, as was the result of the main approach. Since the three pools act in the model as communicating vessels, the model in the independent calibration showed that decomposed matter accumulated instead of litter. Thus, to fit data with overall soil loss at Lettosuo, the simulation in this alternative calibration displayed losses mostly from the SOC2 and the SOC1 pools. With rapid litter decomposition, the effect of the moss litter addition is more difficult to disentangle since C ends up in the decomposed pool, however, the same large moss litter addition occurred. We think our main setting where each of the SOC pools showed a similar rate coefficients for the same SOC quality for the two scenarios could explain more regarding the soil processes than rapid litter decomposition into a large soil C-pool. Since the experiments also displayed a difference in decomposability between leaf-litter from vascular plants compared with mosses, we find it more realistic to describe the soil and litter qualities with distinct different rate coefficients for these litters.

The EC-data of CO_2 exchange collected at Kalevansuo over 4 years used in this study was in an earlier study presented as gap-filled data resulting in a similar NEE, $-234\ g\ C\ m^{-2}\ yr^{-1}$ (Minkkinen et al., 2018). Using this gap-filled data in model calibration demonstrated less good performance which is why our choice was to use non-gap-filled NEE-data in our study. The modeled data reflected the measured NEE and biomass growth data quite well. Deviations between simulated and measured data were most pronounced during summer when gas exchange activities are high with large day-to-day fluctuations.

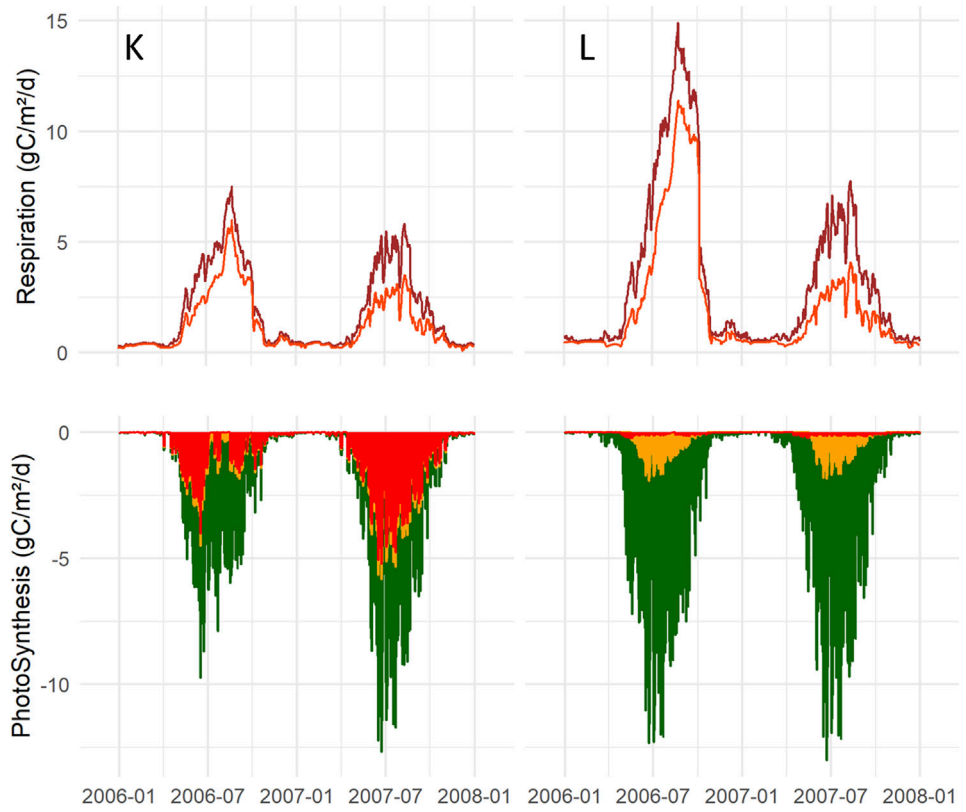

FIGURE 11 | Top panel shows total ecosystem respiration (Reco) brown line, and heterotrophic respiration delineated by the red line at K **(left)** and L **(right)** during the dry (2006) and normal year (2007). Bottom panel, stacked diagram of GPP including three vegetation layers, Vegetation1 = dark green, Vegetation2 = yellow and Vegetation3 = red.

Simulation Covering Wet and dry Years

Over the 10 simulated years, including both wet and dry years, the NEE was on average −232 g C m^{-2} yr^{-1} for K and +7 g C m^{-2} yr^{-1} for L. These numbers were close to the measured NEE on which the model was calibrated, −272 g C m^{-2} yr^{-1} and −61 g C m^{-2} yr^{-1} for Kalevansuo and Lettosuo, respectively, however, these numbers were measured in two different periods. The L system shifted from a small net sink in normal years into a source during the dry years. This variation between years is common, where some years are sources and other sinks, like for a pristine bog in Canada where NEE varied between +14 g C m^{-2} yr^{-1} and −89 g C m^{-2} yr^{-1} (Roulet et al., 2007).

The NEE was separated into photosynthesis and respiration, anchored on biomass accumulation data of trees. The overall photosynthesis was quite similar for K and L, with a somewhat lower overall annual GPP for K (−903 g C m^{-2} yr^{-1}) than L (−1,034 g C m^{-2} yr^{-1}). Interestingly, our model suggests that mosses contribute approximately 40% of the total GPP at K, while at L, the mosses were of minor importance, which is a crucial difference between the scenarios. Mosses have the same biomass each year, meaning that all production goes into the litter, which is decomposed at a much slower rate than vascular plant litter. With a high moss composition for K, and despite a lower overall GPP, the model simulated K to accumulate carbon into the soil. In earlier studies at Kalevansuo, using chamber data sampled during the summer of 2008 and 2009, the measured moss GPP contributed 19–27% of the ecosystem GPP (Badorek et al., 2011), and moss litter production was 20% of the total (Minkkinen et al., 2018), where the importance of mosses was somewhat smaller than modeled here. However, photosynthesis and biomass production can vary between years and results influenced by the methodology used. The aim of this modeling study was not to primarily fit all the model processes against measurements but to display possible influence of mosses and vascular plants on the ecosystem C-balance.

The model was conceptualized with three initial SOC components, quantities that did not change much over the 10 years in relation to each other. However, the overall stock increased for the K scenario and decreased for L. With the three components, it was possible to see that the SOC2 pool of K increased the most, defined as moss litter which was assumed to be added only in the second soil layer (no2), 5–15 cm soil depth, a layer which most times experienced aerobic conditions. In K, we also noticed a small increase in SOC3. In L, all the three SOC pools decreased over time. However, when we used the other concept for the *RateCoeffSOC* calibration, with a similar *RateCoeffSOC* independent of litter type, this demonstrated the SOC3 pool to accumulate for both K and L, whereas the SOC2 soil component decomposed the most for L. Thus, understanding how to conceptualize the ecosystem into a model may be of

importance for seeking answers on the function. However, by assuming similar decomposability of vascular plant and moss litter, more C ended up in the decomposed material. If one litter type (here mosses) decomposes slower, the only difference was that more undecomposed SOC2 accumulated in the soil. And it was the litter quantity per se that decided whether the soil accumulated C or not.

The WTs in K and L were generally relatively high, typically around 0.3-m depth, but the level fluctuated with seasons and weather conditions, with water saturation sometimes even close to the soil surface. In the dry summer of 2006, the WT was lower, reaching deeper than 0.9 m at L and 0.75 m at K. Despite K having wetter conditions in the dry summers the photosynthesis rate was affected more than for L. This we think can be explained by vegetation abundance differences, between the K and L, where the latter site with a higher relative abundance of vascular plants with roots can reach and access water at depths, thus able to continue photosynthesis. Thus, the L scenario with domination of vascular plants continued to deliver litter but this did not compensate for the soil losses. Where vascular plants can use the soil water for transpiration, mosses instead desiccate and survive the dry conditions waiting for the rain. It is known that mosses on the other hand are able to cope drought, becoming considerably dry and regain function when water becomes available (Proctor et al., 2007), with reduced growth during dry conditions (Norby et al., 2019). Thus where mosses dominates the ecosystem the photosynthesis is hampered by dry conditions, and the dry moss plants influence the soil water content less. The earlier added moss litter do also withstand oxygenated soil condition better than vascular plant litter, thus the model shows the K scenario SOC2 pool not to be as affected by the drought as the SOC1 pool. Thus the draught influence both photosynthesis and soil decomposition, where vascular plants increase the soil water withdrawal and an otherwise water-saturated soil became air-filled with increased soil decomposition. Besides draughts, warmer summers has also been demonstrated to affect the moss growth negatively (Gunnarsson et al., 2004); however, warmer conditions also induce desiccation, and it is difficult to separate a temperature effect from a water effect. In coming years dry conditions is expected to be more common why our understanding of the ecosystems on peatland soils is important for a management protecting the carbon.

Comparison With Other Studies

Ecosystem processes are influenced by many variables. It is a challenge to disentangle and explain the many ecosystem functions where carbon is simultaneously released and accumulated. In our simulation, the resulting GPP for the two scenarios were similar to GPP earlier estimated for forests in Finland and Sweden (Lagergren et al., 2008) as well as in Canada (Zha et al., 2013), at approximately −1,000 g C m^{-2} yr^{-1}. Similarly Minkkinen et al. (2018) in a study made at Kalevansuo found an average GPP of trees and ground vegetation of −1,037 g C m^{-2} yr^{-1} and Re of 807 g C m^{-2} yr^{-1}, where NEE was partitioned into photosynthesis based upon light, CO_2 in the air, and the water vapor deficit, and respiration upon air temperature. The authors here used an independent tree-growth model, Stand Photosynthesis Program (SPP), suggesting 70% of the overall GPP was produced by trees, leaving 30% for the ground vegetation. Another study at Kalevansuo, concluded share of mosses was 19–27% of measured total GPP (Badorek et al., 2011). In our modeling scenario for K, based on Kalevansuo, the GPP shares for the different vegetation layers 1, 2, and three were 56, 5, and 38%, respectively, which can explain different results.

The photosynthetic efficiency of mosses compared to vascular plants is uncertain. Several studies have demonstrated mosses to be less efficient compared to vascular plants (Whitehead and Gower, 2001; Yuan et al., 2014), while others have shown them to be similar when relating rates to chlorophyll content (Martin and Adamson, 2001). For simplicity, we assumed moss photosynthesis to have similar light use efficiency as vascular plants. In contrast to static models, the CoupModel estimates photosynthesis and respiration based on many influencing and interacting factors, like water and nitrogen limitation as well as the temperatures of both air and each of the soil layers, which change over time. Thus, detailed simulations can be made using the CoupModel based on each vegetation layer, simulated separately with many respiration components, with different temperature Q10 functions for the maintenance respiration for tissues above and below ground, and each soil layer which is influenced by the surroundings. There will always be certain discrepancies between how the system is described in the model and the reality. Both the model and measured data have uncertainties, where measured data are compiled during a short period with uncertainties in the methods.

Experimental data have demonstrated decomposability to be lowest in *Sphagnum* moss and woody litter, somewhat higher for forest moss litter, and being the highest in the leaf-litter of vascular plants (Hobbie et al., 2000; Strakova et al., 2011). For simplicity, in the model, we only assumed that leaf litter was added to the soil with no woody litter, and different decomposition rates were assumed only for the leaf litter of vascular plants and mosses. No differentiation was made between *Sphagnum* and forest mosses. As the field layer in Kalevansuo, besides mosses, also produces small shrubs which add woody litter among the growing mosses (Minkkinen et al., 2018), this could, together with moss litter addition, also explain the accumulation of C in the Kalevansuo peatland. However, the above suggestion of the importance of shrubs does not contradict the model results; namely, that mosses can contribute to C-accumulation since they are plants producing a litter with low decomposability and no living plant C-accumulation, where all the produce goes to litter.

Another explanation for the C-losses at Lettosuo could be a larger soil carbon content in the top 50 cm, where the L scenario lost more C than K during drought spells. Other studies have also, like our study, demonstrated increased soil respiration during dry conditions, which increased the most at spots with vascular plants in contrast to *Sphagnum* moss spots (Munir et al., 2017). In our study, we could explain soil decomposition size by 1) litter quality and quantity, 2) the soil aerobic volume, and 3) the soil carbon density, which are all connected with site fertility (Ojanen et al., 2013). The explicit inclusion and separation of mosses in this modeling study demonstrated the importance of these plants which contribute a relatively large part (38% in K) of the ecosystem GPP. Whereas trees direct their production to

growing biomass, the biomass of mosses remains the same, and all primary production is directed to litter with low decomposability.

In wet conditions, *Sphagnum* mosses are known as ecosystem engineers, forming peatlands (Van Breemen, 1995). In drained peatlands, mosses can still thrive at nutrient-poor sites, which remain relatively open compared to nutrient-rich sites, although species dominance may change from peat mosses to forest mosses, as is the case in Kalevansuo. In contrast to nutrient-poor sites, post-drainage change at nutrient-rich sites is rapid and often completely towards forest vegetation (Laine et al., 1995). A lowered WT favors trees at the expense of wetland-adapted plants, where a dominating tree layer takes hold on available light and nutrients out-competing field and ground plants (Laiho et al., 2003), which also affects soil C balance. In our study, mosses are suggested to be significant for soil C sequestration. This was also concluded in a literature review and modeling study, where more mosses facilitated soil C-accumulation owing to slow decomposition (Turetsky et al., 2012). Additionally, when moss vegetation was lost, C-accumulation in an ombrotrophic bog was reduced (Larmola et al., 2013).

Alongside the common suggestion of rewetting drained peat soils, to restore the C-accumulation, could be an attempt to keep a dense moss vegetation covering the soil. A WT as high as possible (30 cm) both decreased soil organic matter decomposition (Ojanen and Minkkinen, 2019) and favored moss plants. Although mosses are key for C sequestration in peatlands, changed silvicultural management could increase moss coverage. This could be reached by moving from even-aged rotation forestry with clear-cuts to continuous-cover forestry, where the tree stands are relatively open, allowing continuous regeneration of the trees. Our aim was here to discuss the role of vegetation and environment on C balances, to keep the carbon in the soil, but a continuous forestry management have also been suggested out of an aim to avoid ditch cleaning, as the remaining vegetation will still keep the site dry enough (Leppä et al., 2020). This shows that the trees need to be sparse enough to reduce evapotranspiration, to be able to raise the WT (Sarkkola et al., 2010). There is a large need to stop unsustainable land use and reduce global GHG emissions and thus the aim should be to raise the WT high enough, at least to a level of 30 cm but best would be 10 cm below the surface, for obtaining minimized GHG losses (Kasimir et al., 2018; Evans et al., 2021). Thus for protection of peat, both rewetting and more wetland-adapted plants are of need.

By using models, our shortfall of ecosystem understanding could be revealed and indicate where there is a need for better knowledge and numbers. Thus, the model results can be used to design new studies. Our modeling demonstrates a need to continue examining the impact of vegetation on the C-balance of ecosystems and soils; the impact by mosses needs to be especially highlighted. Additionally, the effect of tree types, conifers, and/or deciduous trees, alongside vegetation composition and tree density, should be examined. Moreover, we have not touched upon whether a dense leaf litter layer could hinder moss growth and peat accumulation or perhaps seal the soil surface (Laine and Vanhamajamaa, 1992), possibly reducing air exchange and causing anoxic soil conditions, which can be suggested for future investigations.

Using the model, we are confident that the set-up of the CoupModel made in this study may be used as a role-model for investigations of drained peat soils of slightly different use, as managed grasslands and forests. An advantage of the model is that it takes into account properties of different vegetation types and soil qualities and dynamically follows the processes of energy, water, carbon, and nutrients. However, it should be noted we only assumed water to enter the soil by precipitation, and care should be taken if vertical water addition is to be expected. In this study, we also used data from two sites close by and of relatively similar types. For model improvements and examination of processes, there is a need for long-term data from systems with distinctly different qualities and fluxes. Also, it is of high interest to further develop the uncertainty based calibration methods and to find common protocol designed for various purposes (Van Oijen et al., 2011; Wallach et al., 2021).

CONCLUSION

- In a dry spell, moss photosynthesis is reduced in contrast to trees and other vascular plants. For the latter, water access maintains photosynthesis and transpiration, causing the ground-water level to drop.
- Of moss net primary production, most goes into litter which, together with lower decomposability, results in carbon addition to the soil.
- Explicit consideration of differences between mosses and vascular plants is highly recommended for future studies.
- This study can be used as a base for continued studies on how C-balances in wetlands are influenced by hydrology and vegetation. However, there is still parameter uncertainty, and care should be taken before the model is applied for various peatlands.

DATA AVAILABILITY STATEMENT

The original contributions presented in the study are included in the article/**Supplementary Material**, further inquiries can be directed to the corresponding author.

AUTHORS CONTRIBUTIONS

ÅK led the work and wrote the text; HH made the initial set up on the Finnish data and made the initial calibrations; PEJ led the model design, calibrations, and made most figures; AL and KM contributed to the description of the sites and EC-data for calibration and commented on the manuscript.

FUNDING

We would like to acknowledge funding from FORMAS Research Council, grant nos 942-5015-1287 and 2019-01991; "Climate smart management practices on Norwegian organic soils" (MYR), funded by the Research Council of Norway, grant no

281109; the Swedish strategic research area "Biodiversity and Ecosystem Services in a Changing Climate" (BECC).

ACKNOWLEDGMENTS

We acknowledge Paavo Ojanen and Juha Heiskanen, Luke Finland, for help accessing data. The model and all the data used for this study is available by request from the corresponding authors and stored in an archive linked to the CoupModel home page (www.coupmodel.com).

SUPPLEMENTARY MATERIAL

The Supplementary Material for this article can be found online at: https://www.frontiersin.org/articles/10.3389/fenvs.2021.680430/full#supplementary-material

REFERENCES

Alm, J., Talanov, A., Saarnio, S., Silvola, J., Ikkonen, E., Aaltonen, H., et al. (1997). Reconstruction of the Carbon Balance for Microsites in a Boreal Oligotrophic Pine Fen, Finland. *Oecologia* 110, 423–431. doi:10.1007/s004420050177

Badorek, T., Tuittila, E.-S., Ojanen, P., and Minkkinen, K. (2011). Forest Floor Photosynthesis and Respiration in a Drained Peatland forest in Southern Finland. *Plant Ecol. Divers.* 4, 227–241. doi:10.1080/17550874.2011.644344

Bhuiyan, R., Minkkinen, K., Helmisaari, H.-S., Ojanen, P., Penttilä, T., and Laiho, R. (2017). Estimating Fine-Root Production by Tree Species and Understorey Functional Groups in Two Contrasting Peatland Forests. *Plant Soil* 412, 299–316. doi:10.1007/s11104-016-3070-3

Chadburn, S. E., Krinner, G., Porada, P., Bartsch, A., Beer, C., Belelli Marchesini, L., et al. (2017). Carbon Stocks and Fluxes in the High Latitudes: Using Site-Level Data to Evaluate Earth System Models. *Biogeosciences* 14, 5143–5169. doi:10.5194/bg-14-5143-2017

Dorrepaal, E., Cornelissen, J. H. C., Aerts, R., Wallén, B., and Van Logtestijn, R. S. P. (2005). Are Growth Forms Consistent Predictors of Leaf Litter Quality and Decomposability across Peatlands along a Latitudinal Gradient? *J. Ecol.* 93, 817–828. doi:10.1111/j.1365-2745.2005.01024.x

Evans, C. D., Peacock, M., Baird, A. J., Artz, R. R. E., Burden, A., Callaghan, N., et al. (2021). Overriding Water Table Control on Managed Peatland Greenhouse Gas Emissions. *Nature* 593 (7860), 548–552. doi:10.1038/s41586-021-03523-1

Frolking, S., Roulet, N. T., Moore, T. R., Richard, P. J. H., Lavoie, M., and Muller, S. D. (2001). Modeling Northern Peatland Decomposition and Peat Accumulation. *Ecosystems* 4, 479–498. doi:10.1007/s10021-001-0105-1

Gorham, E. (1991). Northern Peatlands: Role in the Carbon Cycle and Probable Responses to Climatic Warming. *Ecol. Appl.* 1, 182–195. doi:10.2307/1941811

Gunnarsson, U., Granberg, G., and Nilsson, M. (2004). Growth, Production and Interspecific Competition in Sphagnum : Effects of Temperature, Nitrogen and sulphur Treatments on a Boreal Mire. *New Phytol.* 163, 349–359. doi:10.1111/j.1469-8137.2004.01108.x

Günther, A., Barthelmes, A., Huth, V., Joosten, H., Jurasinski, G., Koebsch, F., et al. (2020). Prompt Rewetting of Drained Peatlands Reduces Climate Warming Despite Methane Emissions. *Nat. Commun.* 11, 1644. doi:10.1038/s41467-020-15499-z

He, H., Jansson, P.-E., and Gärdenäs, A. I. (2021). CoupModel (v6.0): An Ecosystem Model for Coupled Phosphorus, Nitrogen, and Carbon Dynamics - Evaluated against Empirical Data from a Climatic and Fertility Gradient in Sweden. *Geosci. Model. Dev.* 14, 735–761. doi:10.5194/gmd-14-735-2021

He, H., Jansson, P.-E., Svensson, M., Björklund, J., Tarvainen, L., Klemedtsson, L., et al. (2016b). Forests on Drained Agricultural Peatland Are Potentially Large Sources of Greenhouse Gases - Insights from a Full Rotation Period Simulation. *Biogeosciences* 13, 2305–2318. doi:10.5194/bg-13-2305-2016

He, H., Jansson, P.-E., Svensson, M., Meyer, A., Klemedtsson, L., and Kasimir, Å. (2016a). Factors Controlling Nitrous Oxide Emission from a Spruce Forest Ecosystem on Drained Organic Soil, Derived Using the CoupModel. *Ecol. Model.* 321, 46–63. doi:10.1016/j.ecolmodel.2015.10.030

Hobbie, S. E., Schimel, J. P., Trumbore, S. E., and Randerson, J. R. (2000). Controls over Carbon Storage and Turnover in High-Latitude Soils. *Glob. Change Biol.* 6, 196–210. doi:10.1046/j.1365-2486.2000.06021.x

Huang, Y. Y., Ciais, P., Luo, Y. Q., Zhu, D., Wang, Y. P., Qiu, C. J., et al. (2021). Tradeoff of CO2 and CH4 Emissions from Global Peatlands under Water-Table Drawdown. *Nat. Clim. Change* 11, 618–622. doi:10.1038/s41558-021-01059-w

Huth, V., Günther, A., Bartel, A., Gutekunst, C., Heinze, S., Hofer, B., et al. (2021). The Climate Benefits of Topsoil Removal and Sphagnum Introduction in Raised Bog Restoration. *Restoration Ecol.*, e13490. doi:10.1111/rec.13490

Jansson, P.-E., and Halldin, S. (1979). "Model for Annual Water and Energy Flow in a Layered Soil," in *Comparison of Forest and Energy Exchange*. Editor S. Halldin (Copenhagen: Society for Ecological Modelling), 145–163. doi:10.1016/b978-0-444-41844-9.50017-2

Jansson, P. E. (2012). Coupmodel: Model Use, Calibration, and Validation. *Trans. Asabe* 55, 1335–1344. doi:10.13031/2013.42245

Johnsson, H., Bergström, L., Jansson, P.-E., and Paustian, K. (1987). Simulated Nitrogen Dynamics and Losses in a Layered Agricultural Soil. *Agric. Ecosyst. Environ.* 18, 333–356. doi:10.1016/0167-8809(87)90099-5

Kasimir, Å., He, H., Coria, J., and Nordén, A. (2018). Land Use of Drained Peatlands: Greenhouse Gas Fluxes, Plant Production, and Economics. *Glob. Change Biol.* 24, 3302–3316. doi:10.1111/gcb.13931

Korkiakoski, M. (2020). *The Short-Term Effect of Partial Harvesting and Clearcutting on Greenhouse Gas Fluxes and Evapotranspiration in a Nutrient-Rich Peatland forest*. Helsinki: Helsingin yliopisto.

Kuhry, P., and Vitt, D. H. (1996). Fossil Carbon/Nitrogen Ratios as a Measure of Peat Decomposition. *Ecology* 77, 271–275. doi:10.2307/2265676

Lagergren, F., Lindroth, A., Dellwik, E., Ibrom, A., Lankreijer, H., Launiainen, S., et al. (2008). Biophysical Controls on CO2fluxes of Three Northern Forests Based on Long-Term Eddy Covariance Data. *Tellus B* 60, 143–152. doi:10.1111/j.1600-0889.2006.00324.x

Laiho, R., Vasander, H., Penttila, T., and Laine, J. (2003). Dynamics of Plant-Mediated Organic Matter and Nutrient Cycling Following Water-Level Drawdown in Boreal Peatlands. *Glob. Biogeochem. Cycles* 17, 11. doi:10.1029/2002gb002015

Laine, J., and Vanhamajamaa, I. (1992). Vegetation Ecology along a Trophic Gradient on Drained Pine Mires in Southern Finland. *Ann. Botanici Fennici* 29, 213–233.

Laine, J., Vasander, H., and Laiho, R. (1995). Long-Term Effects of Water Level Drawdown on the Vegetation of Drained pine Mires in Southern Finland. *J. Appl. Ecol.* 32, 785–802.

Lang, S. I., Cornelissen, J. H. C., Klahn, T., Van Logtestijn, R. S. P., Broekman, R., Schweikert, W., et al. (2009). An Experimental Comparison of Chemical Traits and Litter Decomposition Rates in a Diverse Range of Subarctic Bryophyte, Lichen and Vascular Plant Species. *J. Ecol.* 97, 886–900. doi:10.1111/j.1365-2745.2009.01538.x

Larmola, T., Bubier, J. L., Kobyljanec, C., Basiliko, N., Juutinen, S., Humphreys, E., et al. (2013). Vegetation Feedbacks of Nutrient Addition lead to a Weaker Carbon Sink in an Ombrotrophic Bog. *Glob. Change Biol.* 19, 3729–3739. doi:10.1111/gcb.12328

Leppä, K., Korkiakoski, M., Nieminen, M., Laiho, R., Hotanen, J.-P., Kieloaho, A.-J., et al. (2020). Vegetation Controls of Water and Energy Balance of a Drained Peatland forest: Responses to Alternative Harvesting Practices. *Agric. For. Meteorology* 295, 108198. doi:10.1016/j.agrformet.2020.108198

Lohila, A., Minkkinen, K., Aurela, M., Tuovinen, J.-P., Penttilä, T., Ojanen, P., et al. (2011). Greenhouse Gas Flux Measurements in a Forestry-Drained Peatland Indicate a Large Carbon Sink. *Biogeosciences* 8, 3203–3218. doi:10.5194/bg-8-3203-2011

Martin, C. E., and Adamson, V. J. (2001). Photosynthetic Capacity of Mosses Relative to Vascular Plants. *J. Bryology* 23, 319–323. doi:10.1179/jbr.2001.23.4.319

Mathijssen, P. J. H., Kähkölä, N., Tuovinen, J.-P., Lohila, A., Minkkinen, K., Laurila, T., et al. (2017). Lateral Expansion and Carbon Exchange of a Boreal Peatland in Finland Resulting in 7000 Years of Positive Radiative Forcing. *J. Geophys. Res. Biogeosci.* 122, 562–577. doi:10.1002/2016jg003749

Metzger, C., Jansson, P.-E., Lohila, A., Aurela, M., Eickenscheidt, T., Belelli-Marchesini, L., et al. (2015). CO2 Fluxes and Ecosystem Dynamics at Five European Treeless Peatlands - Merging Data and Process Oriented Modeling. *Biogeosciences* 12, 125–146. doi:10.5194/bg-12-125-2015

Metzger, C., Nilsson, M. B., Peichl, M., and Jansson, P.-E. (2016). Parameter Interactions and Sensitivity Analysis for Modelling Carbon Heat and Water Fluxes in a Natural Peatland, Using CoupModel V5. *Geosci. Model. Dev.* 9, 4313–4338. doi:10.5194/gmd-9-4313-2016

Meyer, A., Tarvainen, L., Nousratpour, A., Björk, R. G., Ernfors, M., Grelle, A., et al. (2013). A fertile Peatland forest Does Not Constitute a Major Greenhouse Gas Sink. *Biogeosciences* 10, 7739–7758. doi:10.5194/bg-10-7739-2013

Minkkinen, K., and Laine, J. (1998). Long-term Effect of forest Drainage on the Peat Carbon Stores of pine Mires in Finland. *Can. J. For. Res.* 28, 1267–1275. doi:10.1139/x98-104

Minkkinen, K., Ojanen, P., Penttilä, T., Aurela, M., Laurila, T., Tuovinen, J.-P., et al. (2018). Persistent Carbon Sink at a Boreal Drained Bog forest. *Biogeosciences* 15, 3603–3624. doi:10.5194/bg-15-3603-2018

Munir, T. M., Khadka, B., Xu, B., and Strack, M. (2017). Partitioning Forest-Floor Respiration into Source Based Emissions in a Boreal Forested Bog: Responses to Experimental Drought. *Forests* 8, 17. doi:10.3390/f8030075

Norby, R. J., Childs, J., Hanson, P. J., and Warren, J. M. (2019). Rapid Loss of an Ecosystem Engineer: Sphagnum Decline in an Experimentally Warmed Bog. *Ecol. Evol.* 9, 12571–12585. doi:10.1002/ece3.5722

Ojanen, P., Minkkinen, K., Lohila, A., Badorek, T., and Penttilä, T. (2012). Chamber Measured Soil Respiration: A Useful Tool for Estimating the Carbon Balance of Peatland forest Soils? *For. Ecol. Manage.* 277, 132–140. doi:10.1016/j.foreco.2012.04.027

Ojanen, P., Minkkinen, K., and Penttilä, T. (2013). The Current Greenhouse Gas Impact of Forestry-Drained Boreal Peatlands. *For. Ecol. Manage.* 289, 201–208. doi:10.1016/j.foreco.2012.10.008

Ojanen, P., and Minkkinen, K. (2019). The Dependence of Net Soil CO2 Emissions on Water Table Depth in Boreal Peatlands Drained for Forestry. *Mires and Peat* 24, 8. doi:10.19189/MaP.2019.OMB.StA.1751

Pedrotti, E., Rydin, H., Ingmar, T., Hytteborn, H., Turunen, P., and Granath, G. (2014). Fine-scale Dynamics and Community Stability in Boreal Peatlands: Revisiting a Fen and a Bog in Sweden after 50 Years. *Ecosphere* 5, 24. doi:10.1890/es14-00202.1

Proctor, M. C. F., Oliver, M. J., Wood, A. J., Alpert, P., Stark, L. R., Cleavitt, N. L., et al. (2007). Desiccation-tolerance in Bryophytes: a Review. *The Bryologist* 110, 595–621. doi:10.1639/0007-2745(2007)110[595:dibar]2.0.co;2

FAO (2014). "Towards Climate-Responsible Peatlands Management," in *Mitigation of Climate Change in Agriculture SERIES*. Editors R Biancalani and A. Avagyan (Rome: Food and Agriculture Organization of the United Nations (FAO)).

Roulet, N. T., Lafleur, P. M., Richard, P. J. H., Moore, T. R., Humphreys, E. R., and Bubier, J. (2007). Contemporary Carbon Balance and Late Holocene Carbon Accumulation in a Northern Peatland. *Glob. Change Biol.* 13, 397–411. doi:10.1111/j.1365-2486.2006.01292.x

Sarkkola, S., Hökkä, H., Koivusalo, H., Nieminen, M., Ahti, E., Päivänen, J., et al. (2010). Role of Tree Stand Evapotranspiration in Maintaining Satisfactory Drainage Conditions in Drained Peatlands. *Can. J. For. Res.* 40, 1485–1496. doi:10.1139/x10-084

St-Hilaire, F., Wu, J., Roulet, N. T., Frolking, S., Lafleur, P. M., Humphreys, E. R., et al. (2010). McGill Wetland Model: Evaluation of a Peatland Carbon Simulator Developed for Global Assessments. *Biogeosciences* 7, 3517–3530. doi:10.5194/bg-7-3517-2010

Straková, P., Niemi, R. M., Freeman, C., Peltoniemi, K., Toberman, H., Heiskanen, I., et al. (2011). Litter Type Affects the Activity of Aerobic Decomposers in a Boreal Peatland More Than Site Nutrient and Water Table Regimes. *Biogeosciences* 8, 2741–2755. doi:10.5194/bg-8-2741-2011

Svensson, M., Jansson, P.-E., and Berggren Kleja, D. (2008). Modelling Soil C Sequestration in spruce forest Ecosystems along a Swedish Transect Based on Current Conditions. *Biogeochemistry* 89, 95–119. doi:10.1007/s10533-007-9134-y

Turetsky, M. R., Bond-Lamberty, B., Euskirchen, E., Talbot, J., Frolking, S., Mcguire, A. D., et al. (2012). The Resilience and Functional Role of moss in Boreal and Arctic Ecosystems. *New Phytol.* 196, 49–67. doi:10.1111/j.1469-8137.2012.04254.x

Van Breemen, N. (1995). How Sphagnum Bogs Down Other Plants. *Trends Ecol. Evol.* 10, 270–275. doi:10.1016/0169-5347(95)90007-1

Van Oijen, M., Cameron, D. R., Butterbach-Bahl, K., Farahbakhshazad, N., Jansson, P.-E., Kiese, R., et al. (2011). A Bayesian Framework for Model Calibration, Comparison and Analysis: Application to Four Models for the Biogeochemistry of a Norway spruce forest. *Agric. For. Meteorology* 151, 1609–1621. doi:10.1016/j.agrformet.2011.06.017

Vesala, T., Kljun, N., Rannik, Ü., Rinne, J., Sogachev, A., Markkanen, T., et al. (2008). Flux and Concentration Footprint Modelling: State of the Art. *Environ. Pollut.* 152, 653–666. doi:10.1016/j.envpol.2007.06.070

Waddington, J. M., and Roulet, N. T. (1996). Atmosphere-Wetland Carbon Exchanges: Scale Dependency of CO2and CH4exchange on the Developmental Topography of a Peatland. *Glob. Biogeochem. Cycles* 10, 233–245. doi:10.1029/95gb03871

Wallach, D., Palosuo, T., Thorburn, P., Hochman, Z., Andrianasolo, F., Asseng, S., et al. (2021). Multi-Model Evaluation of Phenology Prediction for Wheat in Australia. *Agric. For. Meteorology* 298, 10. doi:10.1016/j.agrformet.2020.108289

Whitehead, D., and Gower, S. T. (2001). Photosynthesis and Light-Use Efficiency by Plants in a Canadian Boreal forest Ecosystem. *Tree Physiol.* 21, 925–929. doi:10.1093/treephys/21.12-13.925

Yu, Z. C. (2012). Northern Peatland Carbon Stocks and Dynamics: A Review. *Biogeosciences* 9, 4071–4085. doi:10.5194/bg-9-4071-2012

Yuan, W., Liu, S., Dong, W., Liang, S., Zhao, S., Chen, J., et al. (2014). Differentiating moss from Higher Plants Is Critical in Studying the Carbon Cycle of the Boreal Biome. *Nat. Commun.* 5, 4270. doi:10.1038/ncomms5270

Zha, T. S., Barr, A. G., Bernier, P.-Y., Lavigne, M. B., Trofymow, J. A., Amiro, B. D., et al. (2013). Gross and Aboveground Net Primary Production at Canadian forest Carbon Flux Sites. *Agric. For. Meteorology* 174-175, 54–64. doi:10.1016/j.agrformet.2013.02.004

Conflict of Interest: The authors declare that the research was conducted in the absence of any commercial or financial relationships that could be construed as a potential conflict of interest.

Publisher's Note: All claims expressed in this article are solely those of the authors and do not necessarily represent those of their affiliated organizations, or those of the publisher, the editors and the reviewers. Any product that may be evaluated in this article, or claim that may be made by its manufacturer, is not guaranteed or endorsed by the publisher.

frontiers in Earth Science

ORIGINAL RESEARCH
published: 05 November 2021
doi: 10.3389/feart.2021.676748

Advances in Amazonian Peatland Discrimination With Multi-Temporal PALSAR Refines Estimates of Peatland Distribution, C Stocks and Deforestation

Laura L. Bourgeau-Chavez[1], Sarah L. Grelik[1], Michael J. Battaglia[1], Dorthea J. Leisman[1], Rod A. Chimner[2], John A. Hribljan[2], Erik A. Lilleskov[3], Freddie C. Draper[4,5], Brian R. Zutta[6,7], Kristell Hergoualc'h[8], Rupesh K. Bhomia[9] and Outi Lähteenoja[10]*

[1]Michigan Tech Research Institute, Michigan Technological University, Ann Arbor, MI, United States, [2]College of Forest Resources and Environmental Science, Michigan Technological University, Houghton, MI, United States, [3]Climate, Fire, and Carbon Cycle Sciences Unit, USDA Forest Service Northern Research Station, Houghton, MI, United States, [4]School of Geography, University of Leeds, Leeds, United Kingdom, [5]Center for Global Conservation and Discovery Science, Arizona State University, Tempe, AZ, United States, [6]Spatial Informatics Group, LLC, Pleasanton, CA, United States, [7]SERVIR-Amazonia, Lima, Peru, [8]Center for International Forestry Research (CIFOR), Lima, Peru, [9]Center for International Forestry Research (CIFOR), Bogor, Indonesia, [10]School of Life Sciences, Arizona State University, Tempe, AZ, United States

OPEN ACCESS

Edited by:
Hanna Silvennoinen, Norwegian Institute of Bioeconomy Research (NIBIO), Norway

Reviewed by:
Flor Salvador, Natural History Museum, Peru
Tim Baker, University of Leeds, United Kingdom

***Correspondence:**
Laura L. Bourgeau-Chavez
lchavez@mtu.edu

Specialty section:
This article was submitted to Biogeoscience, a section of the journal Frontiers in Earth Science

Received: *05 March 2021*
Accepted: *14 October 2021*
Published: *05 November 2021*

Citation:
Bourgeau-Chavez LL, Grelik SL, Battaglia MJ, Leisman DJ, Chimner RA, Hribljan JA, Lilleskov EA, Draper FC, Zutta BR, Hergoualc'h K, Bhomia RK and Lähteenoja O (2021) Advances in Amazonian Peatland Discrimination With Multi-Temporal PALSAR Refines Estimates of Peatland Distribution, C Stocks and Deforestation. Front. Earth Sci. 9:676748. doi: 10.3389/feart.2021.676748

There is a data gap in our current knowledge of the geospatial distribution, type and extent of C rich peatlands across the globe. The Pastaza Marañón Foreland Basin (PMFB), within the Peruvian Amazon, is known to store large amounts of peat, but the remoteness of the region makes field data collection and mapping the distribution of peatland ecotypes challenging. Here we review methods for developing high accuracy peatland maps for the PMFB using a combination of multi-temporal synthetic aperture radar (SAR) and optical remote sensing in a machine learning classifier. The new map produced has 95% overall accuracy with low errors of commission (1–6%) and errors of omission (0–15%) for individual peatland classes. We attribute this improvement in map accuracy over previous maps of the region to the inclusion of high and low water season SAR images which provides information about seasonal hydrological dynamics. The new multi-date map showed an increase in area of more than 200% for pole forest peatland (6% error) compared to previous maps, which had high errors for that ecotype (20–36%). Likewise, estimates of C stocks were 35% greater than previously reported (3.238 Pg in Draper et al. (2014) to 4.360 Pg in our study). Most of the increase is attributed to pole forest peatland which contributed 58% (2.551 Pg) of total C, followed by palm swamp (34%, 1.476 Pg). In an assessment of deforestation from 2010 to 2018 in the PMFB, we found 89% of the deforestation was in seasonally flooded forest and 43% of deforestation was occurring within 1 km of a river or road. Peatlands were found the least affected by deforestation and there was not a noticeable trend over time. With development of improved transportation routes and population pressures, future land use change is likely to put South American tropical peatlands at risk, making continued monitoring a necessity. Accurate mapping of peatland ecotypes with high resolution (<30 m) sensors linked with field data are needed to

reduce uncertainties in estimates of the distribution of C stocks, and to aid in deforestation monitoring.

Keywords: peatland, tropical, Amazon, carbon, deforestation, PALSAR, L-band radar

INTRODUCTION

Despite covering a relatively small area of the Earth's terrestrial landscape (3–5% (Maltby and Proctor, 1996; Moomaw et al., 2018), peat-accumulating wetlands currently represent one of the largest carbon stores in the world with an estimated 25–30% of the global belowground soil organic C stock (Yu et al., 2010; Leifeld and Menichetti, 2018; Loisel et al., 2021). Although there have been many efforts to estimate the spatial distribution of peatlands and their C stocks, great uncertainties remain. One of the challenges with mapping the distribution of peatlands is in accurately distinguishing them from non-peat wetlands both in the field and from remotely sensed data. Efforts to map global wetlands from MODIS or other coarse resolution optical sources are ineffective in detecting and mapping peatlands. With coarse (250 m–1 km) resolution data, peatlands typically are grouped with a more general wetland class. Since peatlands are often small and interspersed with upland and other wetland types, it is essential to use finer resolution data (30 m or better) to distinguish peatland types. Further, hybrid remote sensing methods that use a combination of data sources and imagery from multiple seasons are necessary to capture the hydrologic and phenological variation that characterizes the diversity of peatlands that exist on the landscape (Bourgeau-Chavez et al., 2017; Bourgeau-Chavez et al., 2018).

Wetlands in general are difficult features to map due to their high variability in morphology and wetness conditions across the seasons. The utility of optical data alone is limited because peatland and non-peatland ecotypes can be floristically similar (Draper et al., 2014; Bourgeau-Chavez et al., 2017; Hribljan et al., 2017). Reliance on optical data is further challenged in regions like the tropics that are often laden with heavy cloud cover. In contrast, the long wavelength of L-band (~24 cm wavelength) synthetic aperture radar (SAR) allows for penetration of clouds and wetland canopies, and interacts with the wet or flooded soil differently than from dry soil, allowing discrimination of wetlands from non-wetlands. A better distinction between vegetation types (forested, shrubby, and herbaceous), peat- and non-peat wetlands, and peatland types (bog vs. fen) has been obtained through multi-date, multi-sensor SAR and optical approaches (Bourgeau-Chavez et al., 2015; Bourgeau-Chavez et al., 2017; Hribljan et al., 2017; Chimner et al., 2019). Using multiple date SAR images allows for monitoring of changes in hydrologic condition to help differentiate between mineral soil wetlands that are periodically inundated and organic soil peatlands that typically have saturated soils for longer portions of a year (e.g., Chimner et al., 2019). Similarly, multi-date Landsat allows the capture of phenological differences between dominant plant species and together the complementary sensors have been shown to improve wetland mapping in the coastal Great Lakes (Bourgeau-Chavez et al., 2015), boreal peatlands of Alberta and Northwest Territories Canada, Michigan's upper peninsula (Bourgeau-Chavez et al., 2017; Bourgeau-Chavez et al., 2019) and in tropical mountain peatlands (Hribljan et al., 2017; Chimner et al., 2019). However, these methods have not yet been applied to tropical lowland peatlands.

Compared to boreal peatlands, the distribution of tropical peatlands has only recently begun to be revealed. Although tropical Southeast Asian peatlands have been well-studied, recent efforts are discovering vast tropical peatland areas in both the Congo of Africa (Dargie et al., 2017) and the Amazon basin of South America (Lähteenoja et al., 2012; Gumbricht et al., 2017). Several groups have mapped tropical peatlands globally (Gumbricht et al., 2017; Xu et al., 2018), as well as for Indonesia (Margono et al., 2014; Warren et al., 2017; Crowson et al., 2019) and Peru (Lähteenoja et al., 2009a; Lähteenoja et al., 2012; Draper et al., 2014). These maps have relied on optical (Landsat) imagery from a single date (e.g., Lhteenoja et al., 2012) or more recently a hybrid of optical and SAR (e.g., PALSAR or Sentinel-1) also from a single date (Draper et al., 2014; Margono et al., 2014; Crowson et al., 2019). Improving peatland distribution maps and reducing uncertainties in estimates of C stocks requires additional field sampling and high resolution (<30 m) remote sensing analysis (Xu et al., 2018) that includes multi-date, multi-sensor imagery. Reducing errors in peatland map classifications will increase confidence in estimates of C stocks, and also allow for better understanding of threats to existing peatlands through monitoring of land cover and land use changes.

The main goal of our research was to determine if the application of a multi-date, multi-sensor SAR and optical approach can improve on previous mapping efforts employing a single date of SAR and optical data (Draper et al., 2014) for classification of tropical lowland peatlands of Peru. For this analysis, we focus on a similar study area to that of Draper et al. (2014) in the Pastaza Marañón Foreland Basin (PMFB) within the Peruvian Amazon. This region harbors extensive areas with deep peat reservoirs that sequester large C stocks (Lähteenoja et al., 2012; Draper et al., 2014; Bhomia et al., 2019). Tropical floodplain ecosystems such as these are defined by their seasonal cycles of inundation, lasting several months, alternating with seasonal drying (Hamilton et al., 1998). These periods of inundation vary across the landscape, leading to a complex mosaic of interspersed peatlands and seasonally flooded non-peat wetlands. Our objectives are to determine what improvements can be made over a single date of L-band radar and single date of Landsat in our mapping approach and also how helpful digital elevation model (DEM) derivatives may be in mapping this relatively flat region. We then compare

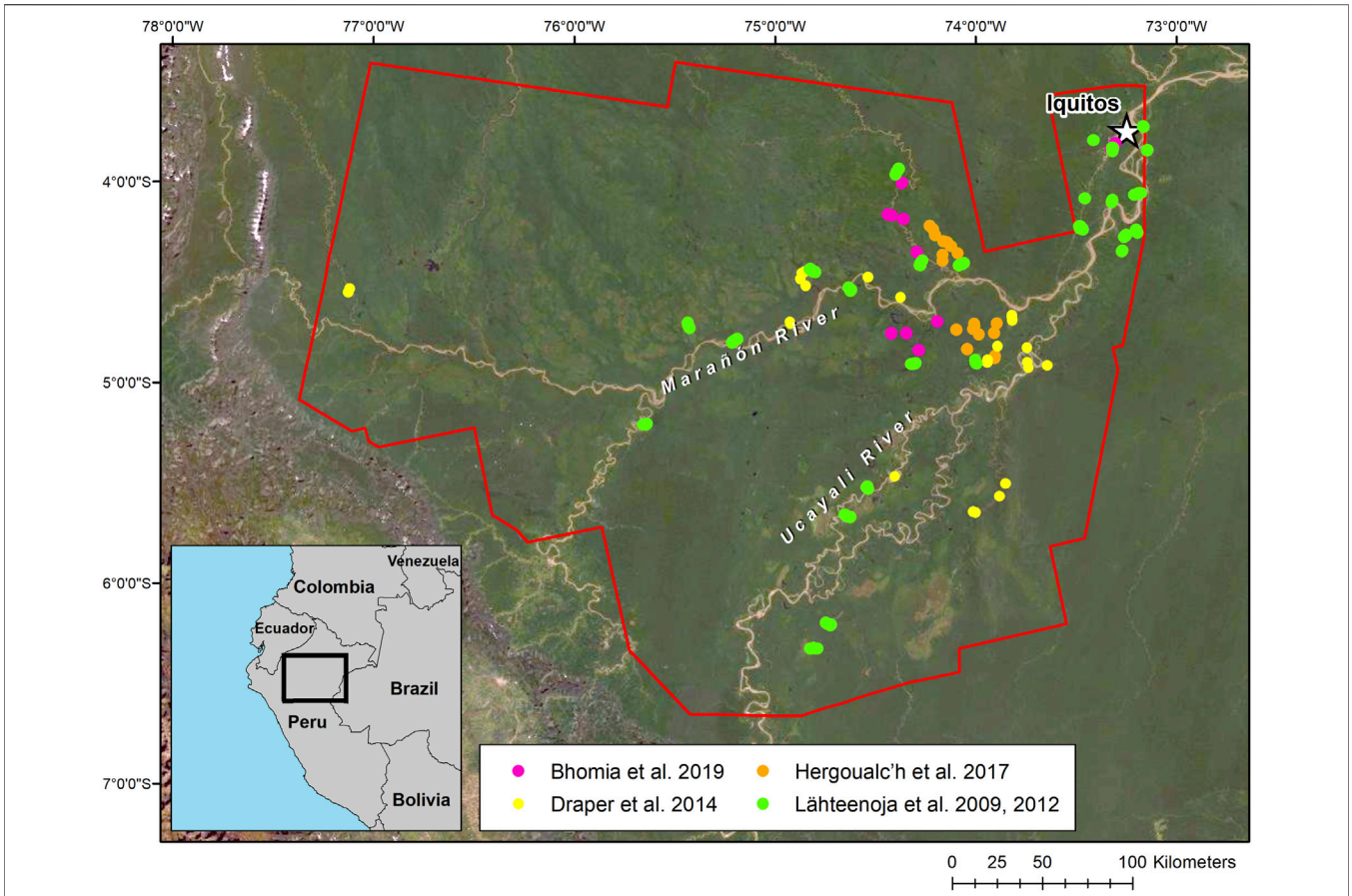

FIGURE 1 | Pastaza Marañón Foreland Basin (PMFB) study area location in northern Peru including the Ucayali and Marañón river watersheds. Mapped area is shown in red outline; field sites are color-coded by data source.

changes in estimates of carbon stocks based on these new maps using the field data and algorithms from Draper et al. (2014). Second, while it is imperative to improve accuracy in peatland mapping capability, it is also of great importance to recognize and quantify threats to these systems. Globally, from the arctic to the tropics, land use change (e.g., deforestation, oil, and gas exploration, grazing, agriculture, infrastructure development, hydrologic alterations, etc.) is one of the largest threats to peatlands. Until recently, human impacts on South American tropical peatlands were not widely studied. Most of the focus has been on Indonesia, where tropical peatlands have been rapidly deforested and converted to agricultural production such as palm oil and tree plantations (Miettinen et al., 2011; Miettinen et al., 2016). The Peruvian Amazon contrasts with Indonesia as it has not yet been heavily affected by widespread anthropogenic disturbance, but there is potential for more severe human impacts as economic and industrial development of the region increase (Roucoux et al., 2017; Lilleskov et al., 2019). Recent expansion of road networks in the Peruvian Amazon could directly affect these extensive peatland ecosystems. An accurate understanding and quantification of peatland extent, carbon storage, and human impacts is needed to inform policy and guide management. Thus, our second goal is to assess current deforestation rates in the PMFB peatlands, and patterns of deforestation in relation to proximity to river and road networks.

STUDY AREA

The 141,200 km^2 study area is a vast floodplain complex of the Pastaza-Marañón Foreland Basin (PMFB) in Amazonian Peru to the west and south of Iquitos (**Figure 1**). The region is dominated by palm swamps in the Marañón and Ucayali basins, which are remote and difficult to access. The larger landscape consists of a mosaic of uplands and wetlands, both peat forming and non-peat forming. Three peatland ecosystem types (palm swamp peatland, pole forest peatland, and open peatland) and two non-peatland ecosystem types (seasonally flooded forest, *Terra firme*/occasionally flooded forest) dominate the landscape (Lähteenoja and Page, 2011; Draper et al., 2014; Draper et al., 2018). Palm swamp peatlands (a portion of the ecosystems locally known as *aguajales* or *tahuampas*) are dominated by flood tolerant palms, especially *Mauritia flexuosa*, commonly known as *aguaje* (Draper et al., 2018), and are typically minerotrophic (i.e., fed by groundwater

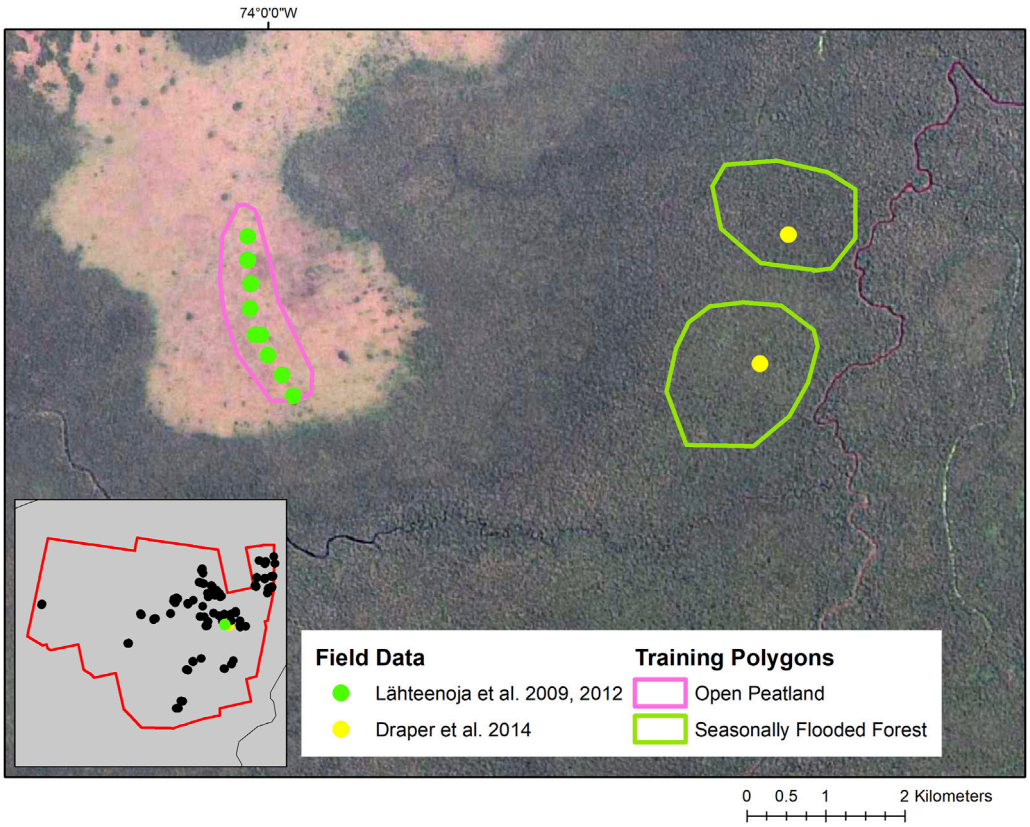

FIGURE 2 | Field transect data within the Pastaza Marañón Foreland Basin (PMFB) of the same ecosystem type, such as the Riñón open peatland transect displayed in green (Lähteenoja et al., 2009a; Lähteenoja et al., 2012), were clustered into single ecosystem training polygons. For individual field points, such as the two seasonally flooded forest points from Draper et al. (2014) depicted in yellow, unique training polygons were created.

and/or surface water). Seasonally flooded forests are annually inundated for a portion of the year, they represent a wide range of forest community types, but are predominately non-peat forming and are normally not dominated by palm species. Open peatlands are dominated by herbaceous vegetation, typically graminoids, ferns, and floating aquatic plants (Draper et al., 2014), and can be minerotrophic (Lähteenoja and Page, 2011) or ombrotrophic (i.e., rainwater fed) (Lähteenoja et al., 2009a; Lähteenoja et al., 2009b). Pole forest peatlands (*varillales hidromórfico*) are dominated by dense, thin, low-stature (<20 m) trees (Draper at al., 2014), and tend to be ombrotrophic (Lähteenoja and Page, 2011). The forests are morphologically similar to white-sand forests (*varillales* in Peru; Adeney et al., 2016) but have distinct vegetation (Draper et al., 2018). The pole forest peatlands tend to have the thickest, oldest and most ombrotrophic peat deposits, with peat domes that extend above the maximum flood level, while palm swamp peatlands are commonly minerotrophic with evidence of frequent flooding and locations typically close to large and geomorphically dynamic rivers (Lähteenoja and Page, 2011; Lähteenoja et al., 2012). Open peatlands were also found near large and dynamic rivers and it is suggested that they may be in the early succession of peatland development because they appear much younger than pole forests (Draper et al., 2014).

METHODS

Field Data

Due to the remoteness of the study area and availability of existing field data on ecosystem types from various previous studies (Lähteenoja et al., 2009a; Lähteenoja et al., 2012; Draper et al., 2014, Hergoualc'h et al., 2017; Bhomia et al., 2019), we chose to compile the existing data for training and testing the map classifier (**Figure 1**; **Supplemental Table S1**). A total of 350 field locations (most of which had peat cores sampled) were obtained from these multiple sources and grouped into the five classes as defined by Draper et al. (2014) (open peatland, palm swamp, pole forest, *Terra firme*/occasionally flooded forest, and seasonally flooded forest). The field data were clustered to the eastern side of the study area and a handful of locations north of the Marañón River in the west at accessible sites along roads and rivers (**Figure 1**). Ideally, field data would be collected in a random distribution across the entire study region, however in remote locations that is logistically infeasible. Field data for mapping purposes is also best collected at the scale of the

minimum mapping unit, which for our dataset is 0.4 ha (Bourgeau-Chavez et al., 2017). Thus, the point locations were used with image interpretation of sub-meter Worldview-2 or Google Earth imagery to create training and validation polygons of similar type, consisting of multiple pixels (minimum four pixels of 30 m size) in the Landsat-SAR imagery. For field data that consisted of multiple points along a transect in one wetland ecosystem type, we grouped the transect points into distinct training polygons using image interpretation of the sub-meter imagery as a guide (**Figure 2**). Thus, the actual number of training/validation polygons created for map classification was 85, much less than the 350 original field point locations, but areal coverage was much larger for each of the 85 polygons. This grouping was necessary to scale the field data to the remote sensing, thus maintaining field data at the scale of the minimum mapping unit (0.4 ha) or larger.

Remote Sensing Data

PALSAR Data

Advanced Land observing Satellite (ALOS) Phased Array type L-band Synthetic Aperture Radar (PALSAR) data (2007–2010) from fine beam single (FBS) and fine beam dual (FBD) modes were downloaded for the study area from the archive at the Alaska Satellite Facility (ASF) and radiometrically terrain corrected through ASF's MapReady software to sigma nought. FBS consists of 10 m resolution horizontal send and horizontal receive polarized data (L-HH). FBD consists of dual polarized L-HH and L-HV (horizontal send and vertical receive polarized data). For each PALSAR scene extent, this resulted in 10–15 images. Past mapping efforts using the multi-date, multi-sensor approach by the authors relied on field data within each PALSAR scene. Such an approach limited the need for normalizing between adjacent scenes of PALSAR or Landsat that is necessary when mosaicking images. However, due to the remoteness of the study area and the limited and isolated field data, the 44 PALSAR scenes making up the study area needed to be mosaicked and normalization methods had to be developed. Several options for normalization were considered, but because we had a time series of images (10–15 dates) for the whole area, we chose to employ Principal Component Analysis (PCA) and to also use weather data to help choose images to mosaic of similar environmental conditions from similar seasons (high- and low-water), to create three input PALSAR datasets (PCA1, High-Water, Low-Water).

The time series PCA was used based on input of all available temporal PALSAR data (~10–15 dates per scene area) in Erdas Imagine. PCA is a multivariate statistical technique that can be used to identify dominant spatial and temporal backscatter signatures (Jensen, 1996; Henebry, 1997; Bourgeau-Chavez et al., 2005). The first principal component (PCA1) captured dominant features across scenes, and reduced brightness/darkness inconsistencies between adjacent scenes, thus normalizing the data. This provided an image of stable scene elements, but changes in hydrological condition (high-vs. low-water seasons) also needed to be captured. A mosaic of low-water season PALSAR scenes as well as a mosaic of high-water season PALSAR scenes were needed. To do this, images from the same season/year and similar dates were chosen to build the mosaic. High-water season was defined as January–May and October–December, while the low-water season was defined as June–September. Next, images from other years from either the high- or low-water season were selected to fill in gaps. This was done by comparing precipitation data between scenes to capture similar environmental conditions and minimize variation in brightness across the mosaic. After each season (high- and low-water) of imagery was mosaicked it was filtered using a 3×3 median filter to reduce speckle. A total of 211 scenes were used for the high-water season and 156 for the low-water season (**Supplemental Tables S2, S3**). The PCA was not speckle filtered as the process already reduces speckle to higher order principal component (PC) images.

Landsat Data

Cloud free Landsat imagery was very limited in this area and similar dates were not available across the study area. Two sources of Landsat mosaics were available for the region which were composites of multiple Landsat images. The first was the circa 2,000 Landsat 5 cloud-free composite created by Hansen et al. (2013) for Peru. The 2,000 image composite included Landsat bands 3 (red), 4 (NIR), 5 (SWIR), and 7 (SWIR). The second source was a 2010 Landsat 5 mosaic created by Draper et al. (2014). The Draper mosaic had three Landsat bands: 4 (NIR), 5 (SWIR), and 7 (SWIR).

Digital Elevation Model and Derivative

Digital elevation model (DEM) data were downloaded from both the Earth Explorer [ASTER Global Digital Elevation Model (GDEM)] and the USGS Shuttle Radar Topography Mission (SRTM) DEM Directory. The 30 m SRTM DEM is based on interferometric SAR and was preferred but contained several data gaps which were filled with the ASTER GDEM. ASTER is an optical sensor and stereoscopic imaging was used to measure elevations and create the Global ASTER DEM product at 30 m horizontal resolution. Note that the work presented was created prior to the release of the SRTM Plus product that also has data gaps filled with ASTER and other sources.

Topographic Position Index

Topographic indices allow for improved identification of low-lying areas and depressions that are more likely to be wet, but also for domed areas, such as occur in pole forests. These indices are then combined with remote sensing data in the map classifier. We chose to use the topographic position index (TPI) which is a measure of a point's elevational position relative to the area immediately surrounding it (Weiss, 2001). To calculate TPI, each 30 m cell in the DEM was compared to the average value of cells in its surrounding neighborhood. In the resulting data set, negative values indicate a cell is relatively lower in elevation than the area around it, suggesting they are depressions, while positive values indicate the cell is relatively higher in elevation, such as peat domes. TPI is highly dependent on input parameters such as the shape and size of the neighborhood. For this project, a circular neighborhood with a 600 m (20-cell) radius was used. This 600 m radius tends

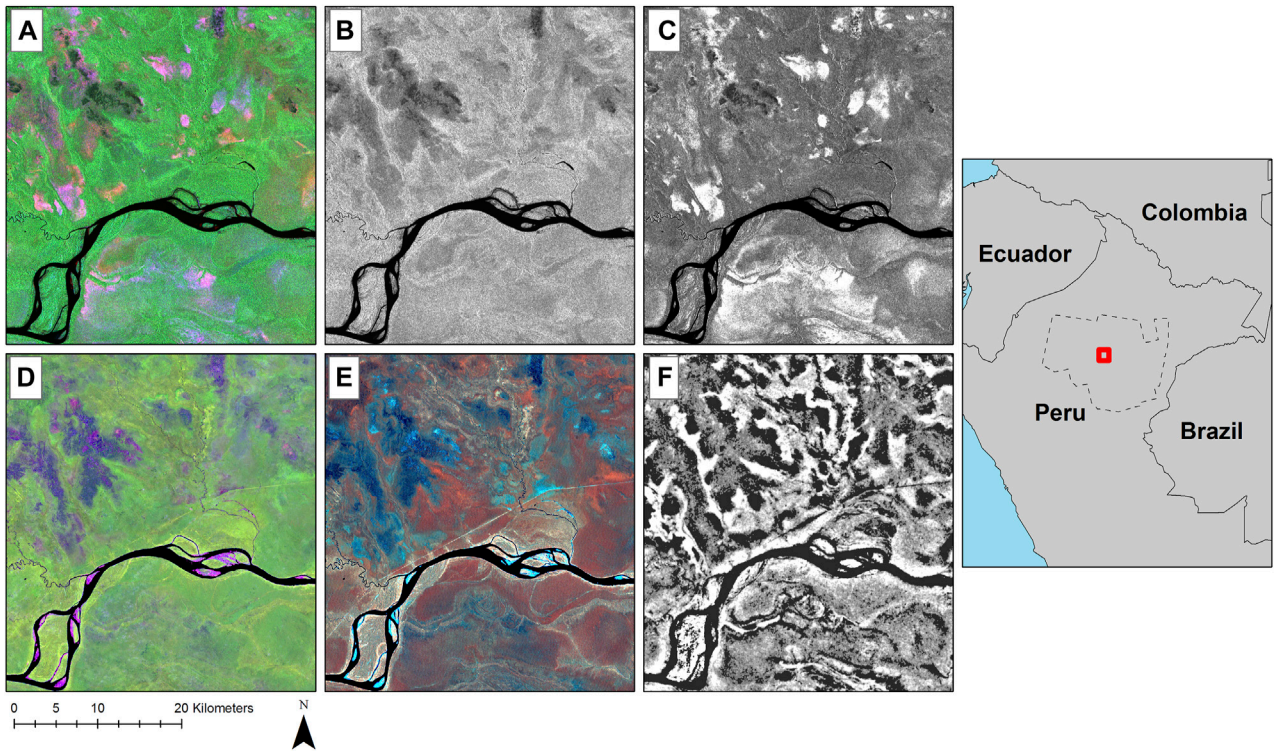

FIGURE 3 | Examples of the input Pastaza Marañón Foreland Basin (PMFB) SAR and Optical datasets from the red box of the location map: **(A)** PALSAR false color composite with high-water L-HH (red), low-water L-HV (green), and low-water L-HH (blue); **(B)** PALSAR low-water L-HV; **(C)** PALSAR PCA1; **(D)** Landsat 2001 bands 5 SWIR (red), 4 NIR (green), and 3 red (blue) (Hansen et al., 2013); **(E)** Landsat Draper et al. (2014) Mosaic circa 2010 bands 4 (red), 5 (green), 6 (blue), and **(F)** SRTM TPI with 20 cell radius resampled to 30 m.

to capture broad variability in landscapes without rugged topography.

Peatland Ecotype Mapping

The input datasets from PALSAR, Landsat, and either SRTM DEM or TPI (see examples in **Figure 3**) were used for classification to: 1) apply a single date of Landsat, PALSAR and SRTM DEM to mimic the Draper et al. (2014) approach; and 2) to test if there is improved accuracy of a multi-date approach. Models tested included all three data sources because it has already been demonstrated that adding PALSAR and SRTM DEM or derivatives improves peatland mapping accuracies over Landsat alone (Draper et al., 2014; Bourgeau-Chavez et al., 2017; Hribljan et al., 2017).

Interpretation of the various input images in combination can provide insight into land cover types and hydrologic variation (**Figure 3**). Dynamic hydrologic conditions are noticeable in **Figure 3A**, which is a false color composite of PALSAR high-water and low-water bands. The scattering occurring is a complex interaction of moisture content, vegetation structure and whether or not there is standing water. Areas appearing as shades of orange in **Figure 3A** represent vegetated areas that are exhibiting higher backscatter in the high-water L-HH image, likely due to flooding, while areas appearing pink exhibit high backscatter in both the high-water and the low-water L-HH image dates. We can infer that soil moisture or flooding was relatively higher in the pink areas than in green areas of the image in both seasons. In the low-water-HV image (**Figure 3B**), brighter areas correspond to higher biomass forests, while darker shades of grey correspond with open-canopied forbs and graminoid plants. Black areas, representing very low backscatter levels, show water features or saturated bare soils. Areas with high biomass (high L-HV) and wet conditions (high L-HH) likely represent forested wetlands, while similar areas with lower biomass are likely open wetlands. The machine learning classifier is trained for the various ecotypes and their respective backscatter signatures and reflectance based on field data.

The multi-date, multi-sensor map (hereafter referred to as multi-date map) was produced from 12 data layers including mosaics of the PALSAR PC1, PALSAR Low-water Season (L-HH and L-HV), PALSAR High-water Season (L-HH), SRTM TPI, and the 2000 (4 bands) and 2010 (3 bands) Landsat-5 mosaics. The map using the single date of Landsat and PALSAR imagery, similar to the Draper et al. (2014) map, had seven input layers including the PALSAR low-water season mosaic (L-HH and L-HV as well as a ratioed layer HH/HV), Landsat-5 2010 mosaic and SRTM DEM (not the TPI). Draper et al. (2014) used the 50 m PALSAR mosaic from JAXA, which is no longer available. Thus, we needed to reproduce that layer. From our reconnaissance of the image archive in comparison to the mosaic

shown in Draper et al. (2014), most of the images appeared to be from the low-water season, thus we chose that as input to the RF classifier. For direct comparison of the single date and multi-date products we used the Random Forest classifier for both. Note, that we are not trying to exactly reproduce the Draper map, but to test if adding multi-seasonal optical and SAR images and a TPI improves the map accuracy. Thus, we focus on using the same input training and testing data and single versus multiple season images and compare the results.

Random Forests (Breiman, 2001), a machine learning classifier, was used for both peatland ecotype map classifications. Random Forests is a robust method that can be applied to a large area with consistency. It comprises multiple decision trees generated from a random subset of input training data and bands. Once the forest of decision trees is created, an individual pixel's classification is determined by which class receives the most "votes" across all decision trees. One advantage of the algorithm is that it can easily handle missing attributes, such as cloud obscured pixels, as decision trees built without the missing attributes can be used to classify the compromised data.

Deforestation Data

Data products showing deforestation in the study region were available from Peru's Ministry of the Environment (MINAM) through the GeoBosques platform (http://geobosques.minam.gob.pe/). The deforestation product was created using Landsat data and a supervised decision tree classification approach to represent annual forest loss from 2001 to 2011 (Potapov et al., 2014). An updated version of the product from MINAM representing years from 2001 to 2018 was used for this analysis. Since our maps are based on imagery from circa 2000 to 2010, we focused on the deforestation occurring after 2010.

To determine if proximity to waterways or roads has an effect on deforestation of each forest class, buffers were calculated around each of the rivers and roads in 1-km increments, and area for each mapped class was calculated within those buffers.

To assess if post-2010 deforested areas within the PMFB that were near rivers were a result of natural causes due to river meandering or appeared to be human-caused (i.e., forest harvesting), we selected a random set of 100 deforestation locations and used image interpretation of high-resolution imagery in Google Earth and ArcMap to determine what percent appeared to be human versus natural caused. This assessment was conducted using the most recent imagery available first, and for instances where the cause of the change to the river and surrounding land was not immediately obvious or if the most recent imagery was cloudy or of poor quality, we used multi-year imagery from Google Earth.

Carbon Stocks

In order to better estimate the mean carbon stocks in the peatlands, we used a stratified estimator to calculate peatland cover area based on our error matrix (Olofsson et al., 2013). The mapped area of peatlands estimated from a pixel counting approach (counting pixels allocated to a map class and multiplying by the area of the pixel) may be quite different from the actual area on the ground due to weighted errors of omission and commission. While it is not possible to map where these errors are located, the actual area or adjusted area of each land cover class can be estimated using the error matrix and the percentage of area of each land cover class in the map (Olofsson et al., 2013). The assumptions for calculating adjusted area include having a random, systematic, or stratified random sample of ground truth points (Olofsson et al., 2013). Our ground truth samples were randomly selected from our training sites, which were sampled by several other researchers from accessible sites within a reasonable walking distance from a road or waterway (a necessary constraint due to remoteness of our study area). Peatland C storage across the mapping area was determined by summing the product of the total adjusted mapped peatland area for each peatland vegetation classification and the upper and lower limits of the C stock per area for each peatland vegetation type (palm swamp peatland, pole forest peatland, and open peatland) using the equation below from Draper et al. (2014) and Page et al. (2011):

$$\mathrm{CP} = \sum_{p=1}^{p_v} \frac{D_p \rho_p C_p A_p}{10^{12}} + \frac{AGC_p A_p}{10^{12}}$$

where CP is total peatland carbon pool (Pg), v represents total number of peatland ecosystems, D_p is peat thickness (m), ρ_p is dry bulk density (kg/m^3), C_p is carbon concentration (percentage mass of carbon in dry peat), AGC_p is above-ground carbon (kg/m^2), and A_p is area (m^2). Field-based estimates from Draper et al. (2014) were used for the peat thickness, dry bulk density, carbon concentrations, and AGC for each peatland type. We report the contribution of each peatland vegetation type to aboveground, belowground, and total peatland C storage. Errors were propagated along the computations.

Statistical Analyses

All statistical analyses were conducted in R statistical software version 1.3.1056.

Accuracy Assessment of Ecotype Maps

To assess the accuracy of each of the ecotype maps produced using Random Forests, twenty percent of training polygons were withheld from classification and used for validation. Whole polygons were randomly selected and reserved with priority to field-verified polygons.

This approach was used because the out-of-box validation of Random Forests does not represent an independent dataset for validation (Bourgeau-Chavez et al., 2015; Millard and Richardson, 2015).

Chi-Square Goodness of Fit Tests for Deforestation

To assess whether different ecotypes were being harvested preferentially in the deforestation analysis, a chi-square goodness of fit test was applied. This test allowed us to assess whether an ecotype was deforested more or less preferentially based on a null model of its availability on the landscape. Thus, we compared ratios of observed area deforested in each ecotype and expected values of area deforested in each type based on the full distribution of area deforested.

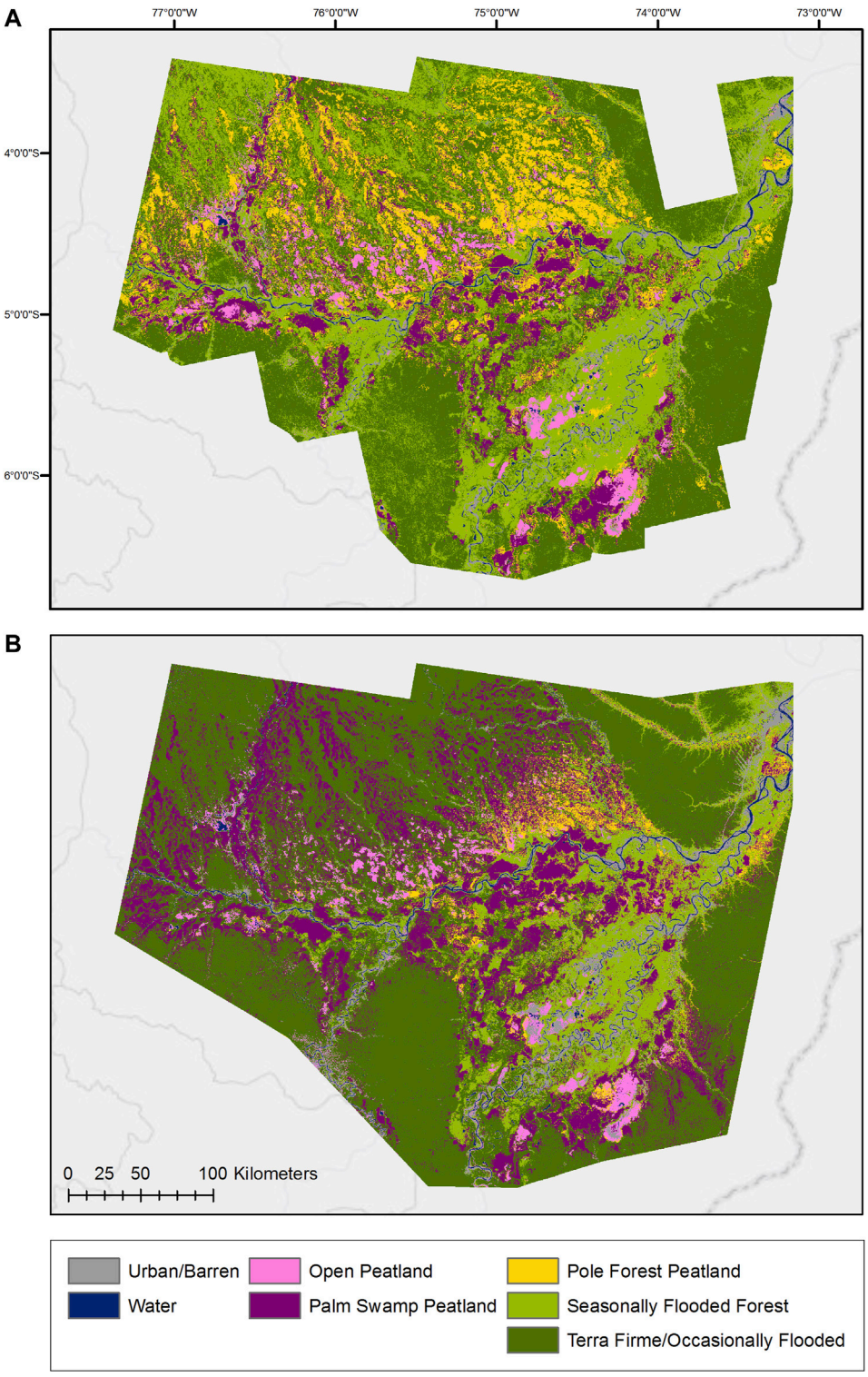

FIGURE 4 | Pastaza Marañón Foreland Basin (PMFB) multi-date, multi-sensor Random Forests map **(A)** produced from PALSAR high-water season HH, low-water season HH and HV, and PCA1, combined with Landsat-5 2000 (Hansen), Landsat-5 2010 (Draper), and SRTM TPI; compared to single date Draper et al. (2014) map **(B)** using PALSAR low-water season HH and HV, ratioed HH/HV, Landsat-5 2010, and SRTM DEM.

TABLE 1 | Error matrix for the multi-date, multi-sensor map. Numbers are pixel counts randomly sampled from the validation polygons in each ecosystem class.

Classified	Ground truth values									
	Urban/ barren	**Water**	**Open peatland**	**Palm swamp peatland**	**Pole forest peatland**	**Seasonally flooded forest**	***Terra firme*/ occasionally flooded forest**	**Sum**	**Commission (%)**	**User Acc. (%)**
Urban/barren	927	0	0	1	0	2	0	9,300	0.3	99.7
Water	11	1,006	0	0	0	0	0	1,017	1.0	99.0
Open peatland	7	0	997	0	0	0	0	1,004	1.0	99.0
Palm swamp peatland	0	0	0	868	13	0	0	881	1.5	98.5
Pole forest peatland	0	0	0	49	944	9	0	1,002	5.8	94.2
Seasonally flooded forest	47	0	0	73	0	798	57	975	18.2	81.8
Terra firme/Occasionally flooded forest	0	0	6	25	42	7	948	1,028	7.8	92.2
Sum	992	1,006	1,003	1,016	999	816	1,005			
Omission (%)	6.6	0.0	0.6	14.6	5.6	2.2	5.7			
Prod. Acc. (%)	93.4	100.0	99.4	85.4	94.4	97.8	94.3	Overall accuracy		94.9

TABLE 2 | Comparison of User's (UA) and producer's (PA) accuracies for the multi-date map vs. the single date map. Each are shown using the SRTM TPI or SRTM DEM in the RF classifier.

	Random forests 20–30 m data							
	Multi-date landsat, PALSAR, SRTM TPI		**Multi-date landsat, PALSAR, SRTM DEM**		**Single date landsat, PALSAR, SRTM TPI**		**Single date landsat, PALSAR, SRTM DEM**	
Class	**UA (%)**	**PA (%)**	**UA (%)**	**PA (%)**	**UA (%)**	**PA (%)**	**UA (%)**	**PA (%)**
Urban/barren	100	93	99	95	74	91	86	98
Water	99	100	100	100	100	100	98	100
Open peatland	99	99	98	99	89	78	99	88
Palm swamp peatland	99	85	79	66	68	57	77	69
Pole forest peatland	94	94.4	67	69	57	53	77	75
Seasonally flooded forest	82	98	78	92	79	77	88	81
Terra firme/occasionally flooded forest	92	94	80	77	63	71	87	100
Overall accuracy (%)	95		86		75		88	

RESULTS

Peatland Ecotype Mapping

The multi-date peatland map that included DEM-TPI (**Figure 4**) had an overall accuracy of 95% with individual peatland class producer's accuracies (PA) of 85–99% (error of omission 0–15%) and user's accuracies (UA) of 94–99% (errors of commission 1–6%, **Tables 1**, **2**). Accuracy is calculated from a random sample of pixels within reserved validation polygons. An example of reserved polygons from each peatland class in comparison to the classified map is shown in **Figure 5**. The Random Forests (RF) classified map using the single date imagery and the SRTM DEM (after Draper et al., 2014) had 88% overall map accuracy, with individual peatland class producer's accuracies of 69–88% (12–31% error of omission) and user's accuracies of 77–99% (1–23% error of commission). The lowest accuracies for the single date map were with palm swamp peatland (77% UA, 70% PA) and pole forest peatland (77% UA, 75% PA). Draper et al., 2014 also reported lower accuracies for pole forest peatland (64% UA, 80% PA) using the Support Vector Machine (SVM) classifier and for the producer's accuracy of palm swamp peatland (79% PA; 96% UA).

With any map product, it is important to also review the map to see if it appears correct based on knowledge of the landscape and comparison to other maps. **Figures 4**, **6** show a direct comparison between the actual Draper et al., 2014 map (recolored) and the new multi-date product. The single date Draper map (2014) has much less pole forest peatland and seasonally flooded forest than the multi-date map. The single date RF map we created is consistent with the SVM product published in Draper et al., 2014, but we show the Draper et al. (2014) map in **Figures 4**, **6** for direct comparison. The single date Draper et al. (2014) map shows large amounts of palm swamp peatland and *Terra firme* in place of pole forest peatland and seasonally flooded forest, respectively (**Figures 4**, **6**).

A comparison of SRTM DEM and TPI was conducted for each of the maps, single date and multi-date (**Table 2**). The accuracies were much lower for the multi-date map with the DEM rather than the TPI, while the single date map had reduced accuracy with the TPI. The peatland and non-peatland classes drop by

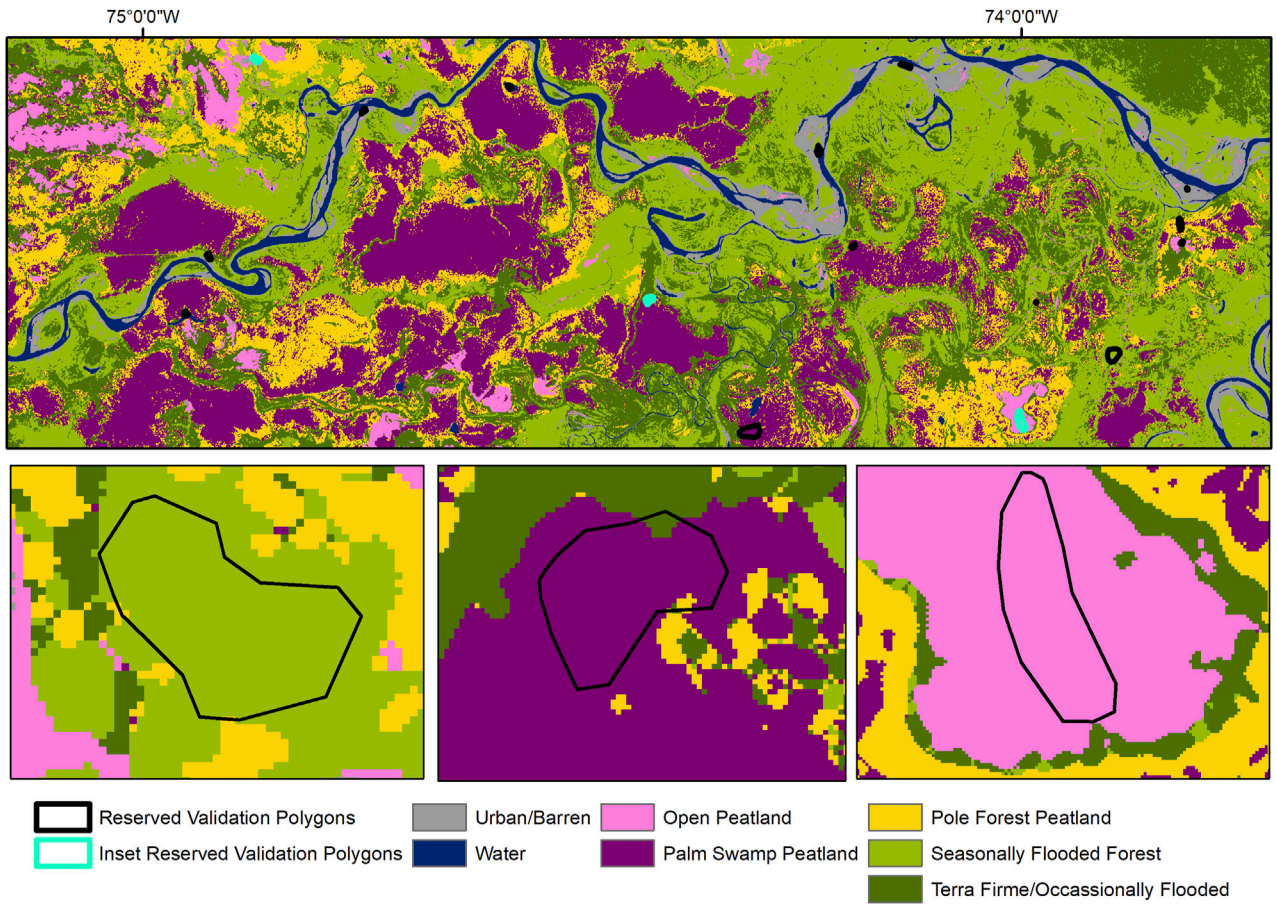

FIGURE 5 | Example of validation polygons in Pastaza Marañón Foreland Basin (PMFB) seasonally flooded forest (left), palm swamp peatland (center), and open peatland (right) compared to the multi-date map classification. Accuracy assessment was calculated from a random sample of pixels within each cover type's reserved validation polygons.

10–20 percentage points when using the TPI in the single date map. For the multi-date map, open peatland stays about the same with TPI or DEM in the model. However, the map is improved when including the TPI instead of the DEM for palm swamp peatland with an increase by 18–19 percentage points in accuracy with the TPI. Similarly, pole forest peatland increases by 27–28 percentage points and even *Terra firme*/occasionally flooded forest increases slightly in accuracy (**Table 2**) with the TPI in the multi-date map.

A review of band importance within RF was conducted by class for the single date (DEM) and multi-date (TPI) maps (**Figure 7**). In all cases the Landsat optical bands had high importance. For the single date map, out of seven input bands, the SRTM DEM was the most important variable for determining *Terre firme* and pole forest, it was second in importance for open peatland and fourth for palm swamp and seasonally flooded forest. Without the second date of PALSAR to help in distinguishing these peatland/non-peatland types, the classifier appears to have been reliant on the DEM to distinguish lowland from upland. For the single-date map, PALSAR low-water HV was third in importance for pole forest, but for the other classes it was fifth or sixth in importance. This contrasts with the multi-date map where PALSAR low-water HV was the most important variable for pole forest and TPI was last out of 12 input bands. For palm swamp, PALSAR PCA1 was third in importance and TPI is ninth of the 12 input bands. For *terre firme*, TPI is 12th. Only for open peatland does TPI seem to be of significant importance, where it is sixth, PALSAR low-water HV was fifth.

Estimating Carbon Storage

Using the multi-date map and adjusted area of each land cover class based on the error matrix and the percentage of area of each land cover class in the map (after Olofsson et al., 2013) resulted in 0.48 Pg of aboveground C, 3.88 Pg of belowground C, and a total C stock of 4.36 Pg (**Table 3**). These are higher contributions to aboveground, belowground and total peatland C across all peatland types than the Draper et al. (2014) map (**Table 3**). The total C stock increased by 35%, from 3.238 to 4.360 Pg. Based on the multi-date map, pole forest peatland contributed the most to the total C stock with 58% (2.551 Pg) of the total carbon, followed by palm swamp with 34% (1.476 Pg) and open peatlands with 8%

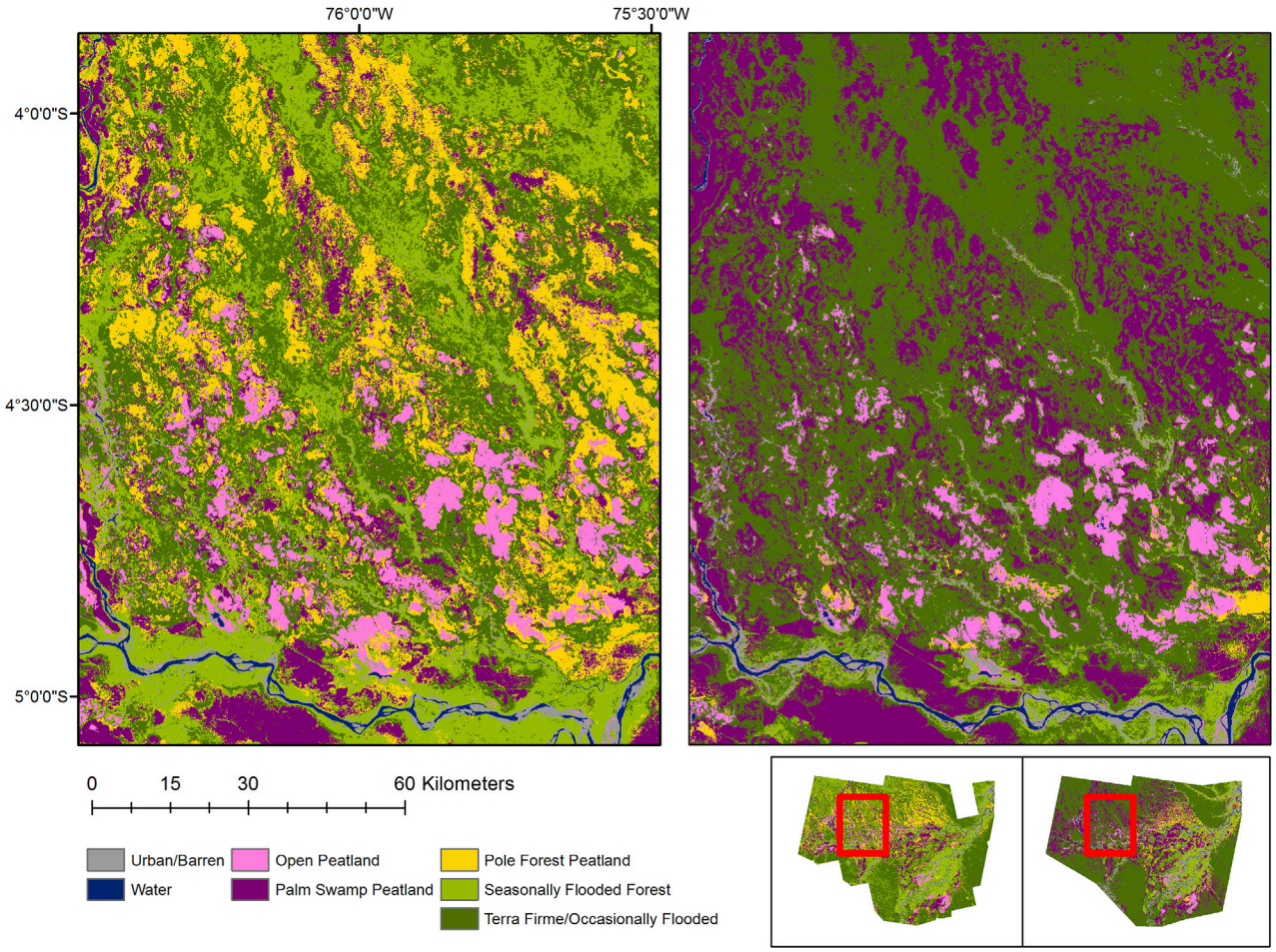

FIGURE 6 | Pastaza Marañón Foreland Basin (PMFB) zoomed-in comparison of multi-date SAR-optical-TPI map product (left) to Draper remote sensing layers single date SAR-optical-DEM (right) both in Random Forests. This map highlights differences in the distribution of Pole forest peatland, Palm swamp peatland and Seasonally flooded forest.

(0.33 Pg) of the total C. These proportions greatly differed from the Draper et al. (2014) map where the palm swamp contributed the most with 65% (2.116 Pg) of total C, followed by pole forest with 26% (0.831 Pg) and then open peatland with 9% (0.291 Pg) of the total C.

Much of the classified pole forest area in the multi-date map was classified as palm swamp and *Terra firme* in the Draper et al. (2014) map (**Figures 4**, **6**). This difference led to increased C storage in the multi-date map since pole forest peatlands are more carbon dense than palm peatlands (Draper et al., 2014). The classification of pole forest peatlands was greater than triple in area (from 534,100 to 1,687,000 ha) to that of the single date map, and this translated to a similar increase in contributions to C stocks (from 0.831 to 2.551 Pg of C), a 209% increase. Estimated palm swamp area decreased by 31% in the multi-date map from the Draper et a1. (2014) map (from 2,305,700 to 1,590,200 ha), resulting in a similar decrease in palm swamp carbon stocks (from 2.116 to 1.476 Pg). While less dramatic than the pole forest, the area, and C storage contributions of the open peatland also increased (15%) in the multi-date map (398,700 and 0.291 Pg of C to 462,000 and 0.333 Pg of C).

Deforestation/Degradation Analysis

The yearly deforestation product produced by MINAM shows 87,268 ha of forest lost between 2010 and 2018 within the PMFB study area. The multi-date, multi-sensor map was intersected with the deforestation product to calculate yearly forest loss by forest cover type (**Figure 8**). We found that primarily seasonally flooded forest is being harvested each year, followed by *terre firme* and pole forest peatland. Palm swamp peatland is the least affected by deforestation between 2010 and 2018.

An analysis of preferential harvesting given the availability of cover types on the landscape was assessed with a chi-square goodness of fit test. We found that seasonally flooded forest is deforested at a much higher than expected rate given its availability on the landscape (**Figure 9**). *Terra Firme*, palm swamp peatland and pole forest peatland are all observed to

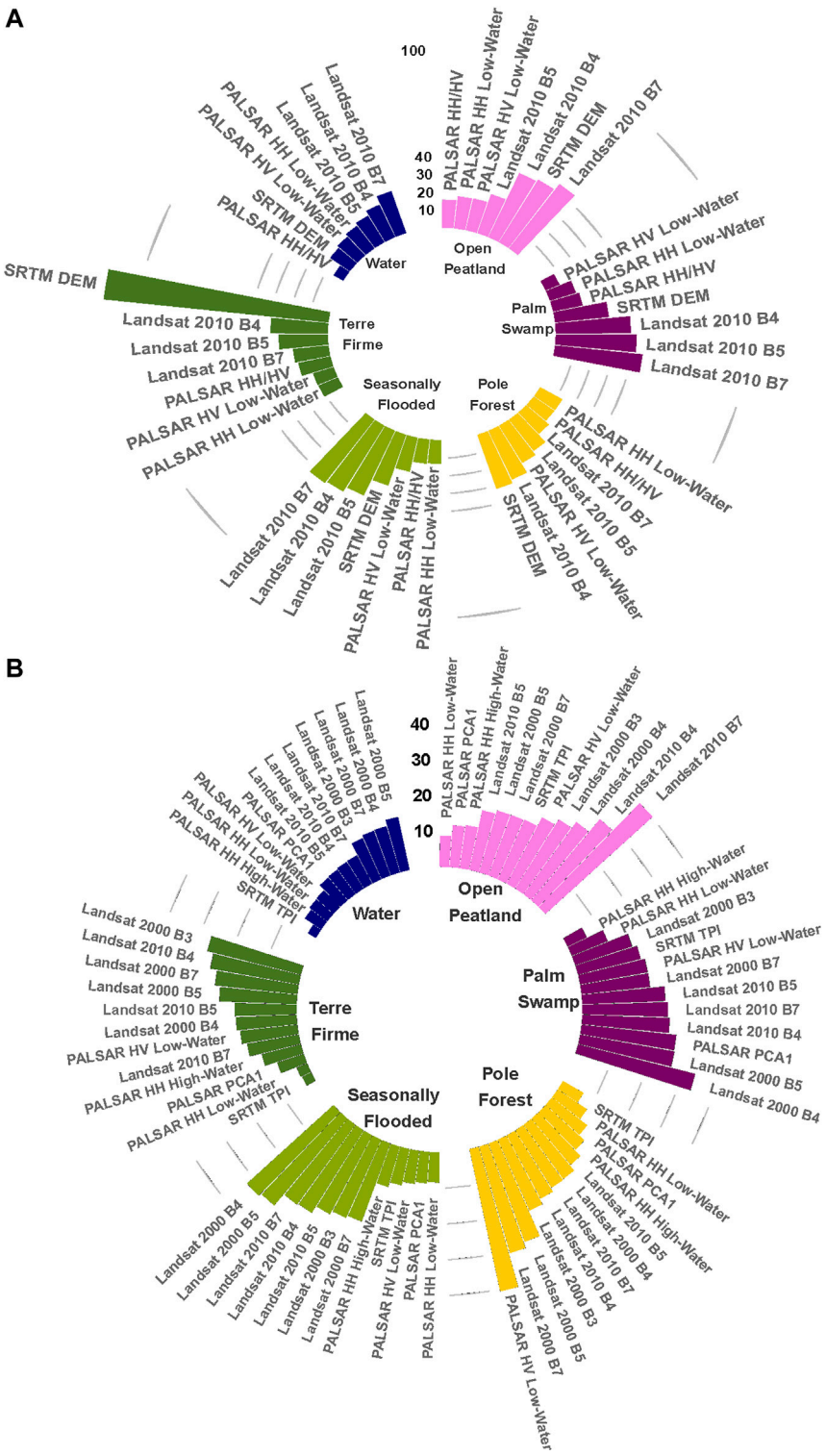

FIGURE 7 | Plots of mean decrease in accuracy from the random forests classifier for each Pastaza Marañón Foreland Basin (PMFB) land cover type: for the single date map **(A)** and multi-date map **(B)**. All classes are shown except urban/barren which had all the Landsat classes as most important.

TABLE 3 | Adjusted area of each land cover class estimated using the error matrix (**Table 1**) and the percentage of area of each land cover class in the map (after Olofsson et al., 2013), and C-stocks for above ground C (AGC), belowground C (BGC), and total C stock for the Draper et al. (2014) and the multi-date map. Note that we clipped the Draper et al. (2014) map (**Figure 3**) to match our area and thus the totals here are slightly lower than those reported in Draper et al. (2014).

		Draper area (ha)	Draper AGC (Pg)	Draper BGC (Pg)	Draper total C stock (Pg)	Multi-date area (ha)	Multi-date AGC (Pg)	Multi-date BGC (Pg)	Multi-date total C stock (Pg)
Pole forest	**mean ± 95% CI**	534,100 ± 78,500	0.087 ± 0.054	0.744 ± 0.250	0.831 ± 0.304	1,687,600 ± 66,700	0.250 ± 0.144	2.301 ± 0.543	2.551 ± 0.687
Palm swamp	**mean ± 95% CI**	2,305,700 ± 107,800	0.310 ± 0.207	1.806 ± 0.580	2.116 ± 0.787	1,590,200 ± 77,400	0.230 ± 0.143	1.246 ± 0.403	1.476 ± 0.546
Open peatland	**mean ± 95% CI**	398,700 ± 20,800	0.000	0.291 ± 0.146	0.291 ± 0.146	462,000 ± 23,900	0.000	0.333 ± 0.174	0.333 ± 0.174
Total	**mean ± 95% CI**	3,238,500 ± 207,200	0.397 ± 0.261	2.841 ± 0.976	3.238 ± 1.237	3,739,900 ± 168,100	0.480 ± 0.287	3.880 ± 1.120	4.360 ± 1.407

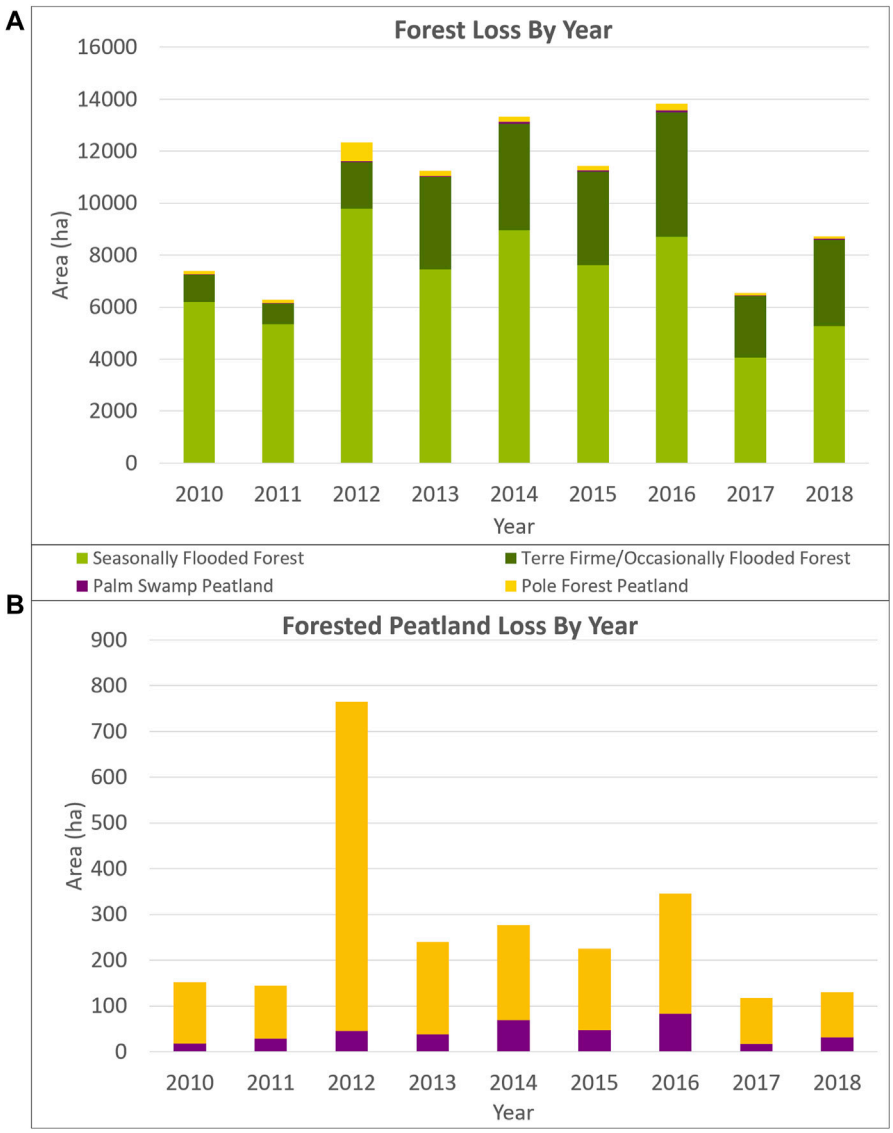

FIGURE 8 | For the Pastaza Marañón Foreland Basin (PMFB): **(A)** Forest loss by class for each year from 2010 to 2018. **(B)** Forest loss by peatland class for each year (2010–2018). Note the large *y*-axis change in area for peatland forest loss **(B)** in comparison to all forest loss **(A)**.

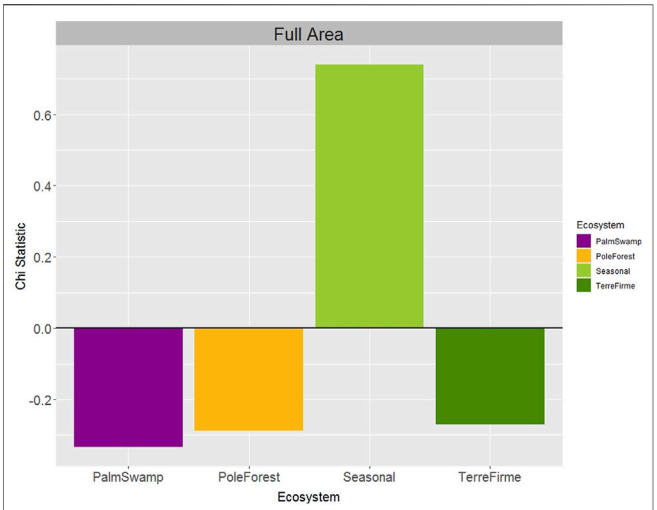

FIGURE 9 | Chi-gram showing residuals for the four Pastaza Marañón Foreland Basin (PMFB) forested classes.

be deforested less than expected based on their total distribution (**Figure 9**). Pole forest peatlands and palm swamp peatlands accounted for 12.3 and 11.9% of forested area in the classified map, respectively, while they accounted for only 2.2 and 0.4% of the deforested areas. Similarly, *Terra firme*/occasionally flooded forest accounted for 46.2% of the mapped area, yet only accounted for 27.8% of the deforested area. In contrast, seasonally flooded forest comprised 29.4% of the mapped area while accounting for 69.5% of the deforested area between 2010 and 2018.

The MINAM deforestation maps show that significant forest loss occurred along the road between the largest cities of Iquitos and Nauta as well as along roads near other towns, such as San Lorenzo and Yurimaguas. However, given the absence of roads in most of the area, most forest loss appears to occur along the river corridors (**Figure 10**). The Ucayali and Marañón have numerous large tributaries flowing into them, creating a vast network of streams and rivers throughout the region allowing navigation. Satellite imagery and MINAM products show that agricultural and timber harvest activity is clearly concentrated in these corridors (**Figure 10**).

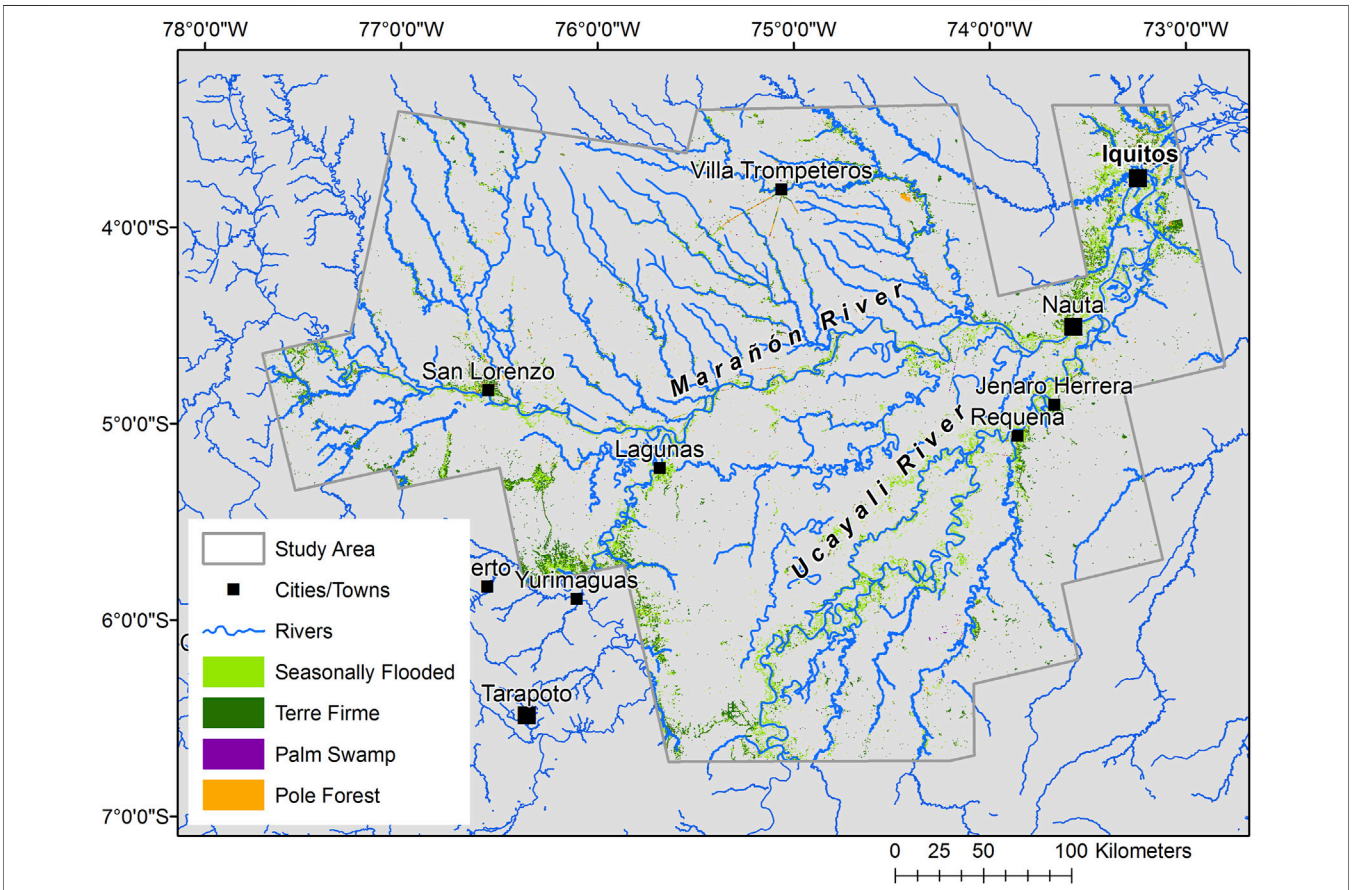

FIGURE 10 | Deforested areas in relation to rivers and large settlements in the Pastaza Marañón Foreland Basin (PMFB) study area, color coded by ecotype.

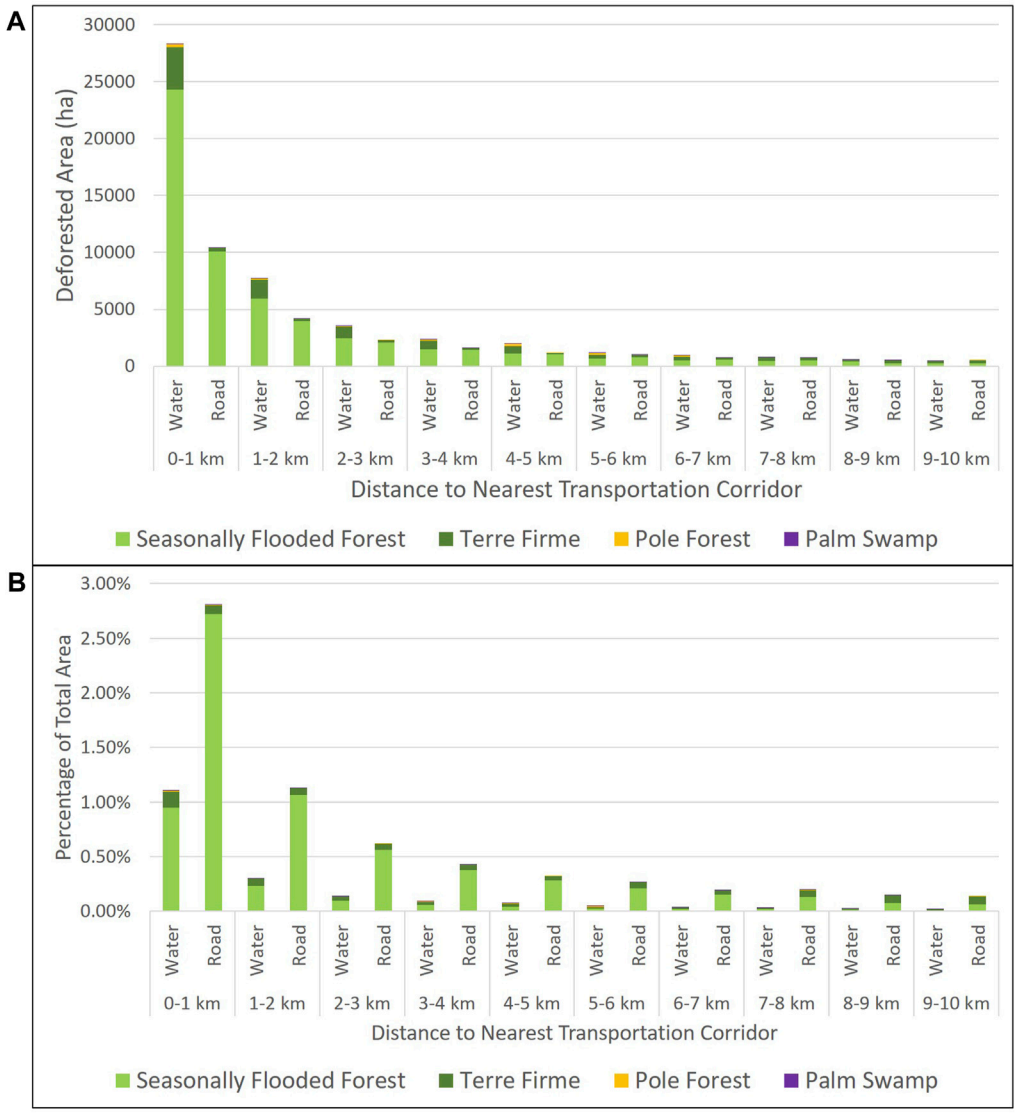

FIGURE 11 | (A) Actual area of PMFB deforestation with proximity to rivers (water) or roads in 1 km increments by ecotype; **(B)** percentage of deforested areas by ecotype relative to the total available area of that ecotype in 1 km increments.

An analysis of the distance of deforestation from roads and rivers (**Figure 11**) demonstrates that of the area classified as deforested between 2010 and 2018, 38,725 ha (42.5% of total deforested area) occurred less than 1 km from a river or a road (**Figures 11A,B**). Of these deforested areas within 1 km of rivers and roads, 88.8% was classified as seasonally flooded forest. Thus, it is not surprising that it is the cover type most affected. Since seasonally flooded forests occur along the meandering rivers which are dynamically changing, a visual inspection of the forest loss along rivers was conducted to determine if changes appeared to be due to harvest or natural changes. Potapov et al. (2014) reported that 6% of the gross forest loss mapped was due to flooding or river meander, but a majority of loss (92.2%) occurred as a result of clearing for agriculture. To assess this in the MINAM maps of 2010–2018 and within the PMFB, we chose 100 random deforested locations within 1 km of the waterways to determine probable causes of forest loss and found through image interpretation (**Figure 12**) that 32% were associated with flooding or river meander while the remainder were likely attributed to anthropogenic disturbance. Thus, the loss of seasonally flooded forests appears to be a combination of natural change due to dynamic hydrologic conditions and anthropogenic change due to timber harvesting (**Figure 12**), with a greater percentage due to the latter.

DISCUSSION AND CONCLUSION

The PMFB multi-date map showed improvement in statistical accuracy as compared to the single date map for all of the

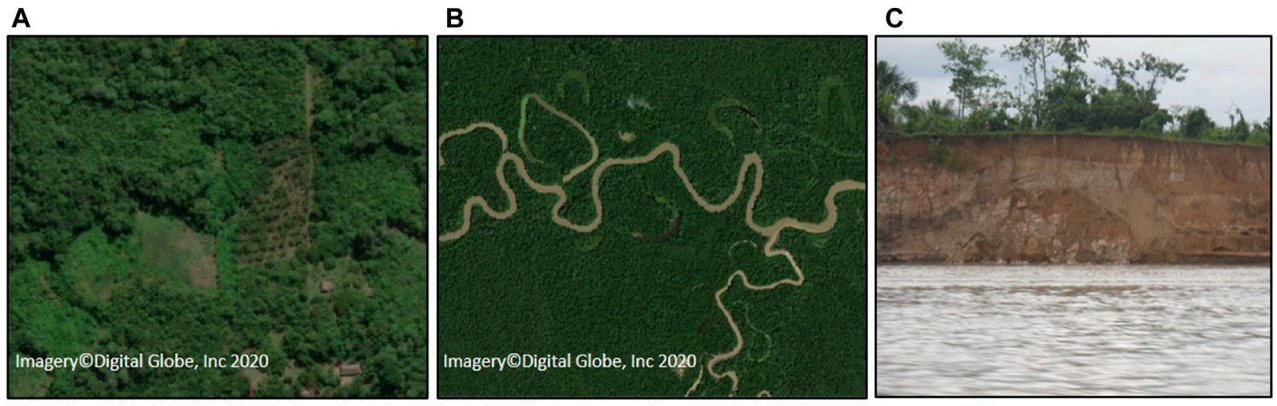

FIGURE 12 | Digital globe images of forest clearing with plantation **(A)**; meandering rivers **(B)**, and a field photo example of erosion/forest loss from a meandering river **(C)**; all in the Pastaza Marañón Foreland Basin (PMFB).

peatland and non-peatland ecotype classes. We attribute this to the inclusion of low- and high-water season SAR images in the multi-date map which provides information about seasonal hydrological dynamics, i.e., inter-seasonal changes in the extent of inundation and soil moisture. Similarly, use of multiple dates of SAR and Landsat imagery resulted in improved peatland map accuracies in boreal peatland ecotypes (Bourgeau-Chavez et al., 2017) and tropical mountain peatland systems (Hribljan et al., 2017). The results of the band importance (mean decrease in accuracy) plots (**Figure 7**) for the single-date vs. multi-date maps showed that the inclusion of two seasons of data reduced the importance of SRTM greatly across many of the classes. In particular, for pole forest, the SRTM DEM had the greatest importance for the single date map, and for the multi-date map PALSAR L-HV was of greatest importance and the SRTM TPI moved to 12th.

The multi-date map resulted in over 1.1 million ha greater area of pole forest peatland mapped than Draper et al. (2014). This increased area is particularly noticeable in the northern part of the study area where field data were sparse. Pole forest peatland was the class Draper et al. (2014) had the most difficulty mapping. It had the lowest accuracies in the SVM map (Draper et al., 2014), with Draper reporting 36% commission and 20% omission error estimated from their field data. Although this was slightly improved in the RF single date map of this study, using 20–30 m resolution data and an expanded field training dataset (23% commission and 25% omission error), the multi-date map made significant improvement in mapping this class (<6% commission and omission error). The increase in mapped area of pole forest peatland resulted in a correspondingly large decrease in the palm swamp peatland class. The multi-season map shows palm swamp peatland to be more closely associated with large and dynamic rivers which better matches how they were described in Draper et al. (2014). The open peatlands are geographically similar in both maps. The multi-date map also showed differences in areas mapped for the two forested non-peatland classes, seasonally flooded forest and *Terra firme*, in comparison to the single-date and Draper et al. (2014) maps.

Another class that has large changes in the multi-season map product is the seasonally flooded forest, which increased largely by mapping into areas previously mapped as *Terra firme* in Draper et al. (2014). With a single date of SAR data, it is difficult to distinguish the seasonally flooded forest from the *Terra firme* class, likely accounting for the large differences, particularly in the northern and western parts of the study area. Draper et al. (2014) reported a 20% omission error in their map for seasonally flooded forest. They found that their SAR-optical-SRTM mapping of seasonally flooded forest had lower user's accuracy than what was mapped with Landsat alone or Landsat and PALSAR. It was the only ecotype for which they did not have improvement by adding PALSAR and SRTM.

The estimates of PMFB C stocks, based on the higher accuracy multi-date map, increased by 35% from a total of 3.238 (Draper et al., 2014) to 4.26 Pg C. The major contributor to the total C stock was pole forest peatland with 58% (2.551 Pg), followed by palm swamp with 34% (1.476 Pg) and open peatlands with 8% (0.33 Pg). This increase in total C stocks from the previous estimates (Draper et al., 2014) is primarily attributed to the 1,153,500 ha increase in area of pole forest peatland mapped (216% increase in area) and the fact that pole forest peatlands are more carbon-dense than palm swamp peatlands (Draper et al., 2014). Although the area of palm swamp forest that was mapped decreased by 715,500 ha (31% decrease), this is more than offset by the 216% increase in mapped area of pole forest peatland. This large difference in C stock estimates between the two mapping approaches warrants additional field collection in the pole forest peatlands. Coincident research by Coronado et al. (2021), including field surveys of pole forest peatland, also expands the distribution of peatland pole forest in the PMFB, but mainly along the Tigre River. Understanding the vegetation structural differences in pole forest peatlands across the region, as well as the underlying ecohydrological processes resulting in their formation in low and high flow areas need further investigation, warranting additional field data collection in the upper PMFB, especially in the northwestern part of the basin associated with the geomorphologically distinct Pastaza fan. Our results exemplify the need for high resolution (<30 m), multi-season SAR and optical imagery for high accuracy maps, and complementary field data across all peatland types to produce more accurate and high confidence estimates of peatland carbon.

Our efforts to understand vulnerability of these peatlands to deforestation activities showed that between 2010 and 2018, 38.4% of

deforestation occurred less than 1 km from a river in predominantly (83%) seasonally flooded forest (**Figure 11C**). This ecotype is deforested more than expected given its availability on the landscape (chi-square goodness of fit, **Figure 9**). Seasonally flooded forest is primarily known as non-peat forming, although in a few cases extensive peat deposits have been found (Lahteenoja et al., 2009b; Draper et al., 2014). The field data have been too sparse to quantify what differentiates peat storing and non-peat storing seasonally flooded forests and their contributions to C stocks. We found overall low rates of deforestation in the peatlands of this region which is consistent with previous studies (e.g., Lilleskov et al., 2019). The extensive peatlands and other wetlands, and resulting absence of roads in most of the area, combined with the intensity of seasonal water table changes associated with the larger rivers, and the relatively low timber value of peatland tree species (Roucoux et al., 2017) has likely focused recent deforestation to the non-peatland river corridors.

Partitioning natural and human disturbance indicated that a majority of the disturbance was anthropogenic, although immediately along rivers natural disturbance was also an important contributor. The large rivers meander substantially, leading to erosion and forest loss (**Figure 12**). These riparian corridors are a focus of economic activity, including slash and burn agriculture, creating small clearings in the forest for temporary plantations (**Figure 12**). Although, as detected by the Potapov et al. (2014) method, deforestation within the peatlands is limited, these forests are also subject to economically unsustainable degradation caused by cutting of female *M. flexuosa* to harvest their fruits (Hergoualc'h et al., 2017; Bhomia et al., 2019; Hergoualc'h et al., 2020). We expect that as road networks at the margins of the peatland area expand, associated rates of deforestation will likely increase dramatically (Coronado et al., 2020). The extent to which this happens will depend on the type and enforcement of land protections put in place including those *via*: 1) Ramsar designation or as national reserves with associated ecological-economic zoning; 2) initiatives to provide alternative approaches for the harvest of palm fruits (Roucoux et al., 2017; Lilleskov et al., 2019); and 3) other national initiatives to protect the carbon in peatlands, such as those likely to arise from current efforts to establish nationally determined contributions (NDCs) to the Paris Agreement (Murdiyarso et al., 2019; López Gonzales et al., 2020; Wiese et al., 2021).

The huge reservoir of organic carbon currently harbored in tropical peatlands is particularly vulnerable to loss due to both climate and land use change (López Gonzales et al., 2020). Much of the literature on peatlands focuses on the need to accurately map their distribution, measure peat stores in the field and to monitor change for C accounting. While we demonstrate the gains in map accuracy through the use of multi-date L-band SAR and optical imagery, there remains a need for additional field sampling to improve estimates and reduce uncertainties in quantifying the distribution of peatlands and carbon stocks. In addition, there is a growing need to monitor effects of climate and land use change in peatlands. Land use change is predicted to play a key role in future shifts of peatlands from a net sink to a net source of C to the atmosphere (Loisel et al., 2021). As global populations continue to grow, pressures on peatlands for deforestation and farming will likely ensue, but the need to conserve peat may outweigh these pressures through policy and management decisions (Loisel et al., 2021). In the present study, the 216% increase in area of pole forest peatland mapped in the PMFB, taken together with our understanding of the greater vulnerability of pole forest peatland to drainage (because of their position above regional water tables—peat domes), raises concerns of an even larger scale on the potential impact of peatland drainage and land use change (e.g., to tree plantations) in the region. This fact is an important consideration for national efforts to incorporate peatlands into government policy.

DATA AVAILABILITY STATEMENT

The raw data and map products supporting the conclusion of this article will be made available by the authors upon request.

AUTHOR CONTRIBUTIONS

LB-C, EL, and RC contributed to conception and design of the study. LB-C led all aspects including the development of the peatland mapping approach, SG, FD, and JH organized the field database. FD, BZ, KH, RB, and OL provided field data. SG processed the imagery, produced the peatland type maps and conducted the statistical accuracy assessment and band importance. DL performed the statistical peatland area adjustment and calculated C stocks with equations from FD. MB produced the DEM TPI and intersected the peatland maps with the deforestation maps and conducted the analysis. LB-C, RC, and EL wrote the first draft of the manuscript. All authors contributed to manuscript revision, read, and approved the submitted version.

FUNDING

This research was supported by USAID Sustainable Landscapes Program funding to the Sustainable Wetlands Adaptation and Mitigation Program (SWAMP), a collaborative effort led by the USDA Forest Service and CIFOR.

ACKNOWLEDGMENTS

We would like to thank all those who contributed field data, including Jeffrey van Lent and Christopher Baraloto, as well as Eleanor Serocki for assisting with data processing, Mary Ellen Miller for assisting with adjusting the areas mapped using the accuracy and Jeremy Graham and Ryan Adkins for assisting with producing figures.

SUPPLEMENTARY MATERIAL

The Supplementary Material for this article can be found online at: https://www.frontiersin.org/articles/10.3389/feart.2021.676748/full#supplementary-material

REFERENCES

Adeney, J. M., Christensen, N. L., Vicentini, A., and Cohn-Haft, M. (2016). White-Sand Ecosystems in Amazonia. *Biotropica* 48 (1), 7–23. doi:10.1111/btp.12293

Bhomia, R. K., van Lent, J., Rios, J. M. G., Hergoualc'h, K., Coronado, E. N. H., and Murdiyarso, D. (2019). Impacts of Mauritia Flexuosa Degradation on the Carbon Stocks of Freshwater Peatlands in the Pastaza-Marañón River Basin of the Peruvian Amazon. *Mitig Adapt Strateg. Glob. Change* 24 (4), 645–668. doi:10.1007/s11027-018-9809-9

Bourgeau-Chavez, L. L., Smith, K. B., Brunzell, S. M., Kasischke, E. S., Romanowicz, E. A., and Richardson, C. J. (2005). Remote Monitoring of Regional Inundation Patterns and Hydroperiod in the Greater Everglades Using Synthetic Aperture Radar. *Wetlands* 25 (1), 176–191. doi:10.1672/0277-5212(2005)025[0176:rmorip]2.0.co;2

Bourgeau-Chavez, L., Endres, S., Battaglia, M., Miller, M., Banda, E., Laubach, Z., et al. (2015). Development of a Bi-National Great lakes Coastal Wetland and Land Use Map Using Three-Season PALSAR and Landsat Imagery. *Remote Sensing* 7 (7), 8655–8682. doi:10.3390/rs70708655

Bourgeau-Chavez, L. L., Endres, S., Powell, R., Battaglia, M. J., Benscoter, B., Turetsky, M., et al. (2017). Mapping Boreal Peatland Ecosystem Types from Multitemporal Radar and Optical Satellite Imagery. *Can. J. For. Res.* 47 (4), 545–559. doi:10.1139/cjfr-2016-0192

Bourgeau-Chavez, L. L., Endres, S. L., Graham, J. A., Hribljan, J. A., Chimner, R. A., Battaglia, M. J., et al. (2018). "Mapping Peatlands in Boreal and Tropical Ecoregions," in *Comprehensive Remote Sensing*. Editor S. Liang (Oxford: Elsevier), 6, 24–44. 9780128032206. doi:10.1016/b978-0-12-409548-9.10544-5

Bourgeau-Chavez, L. L., Graham, J. A., Endres, S., French, N. H. F., Battaglia, M., Hansen, D., et al. (2019). *ABoVE: Ecosystem Map, Great Slave Lake Area, Northwest Territories, Canada, 1997-2011*. Oak Ridge, Tennessee, USA: ORNL DAAC. doi:10.3334/ORNLDAAC/1695

Breiman, L. (2001). Random Forests. *Machine Learn.* 45 (1), 5–32. doi:10.1023/a:1010933404324

Chimner, R. A., Bourgeau-Chavez, L., Grelik, S., Hribljan, J. A., Clarke, A. M. P., Polk, M. H., et al. (2019). Mapping Mountain Peatlands and Wet Meadows Using Multi-Date, Multi-Sensor Remote Sensing in the Cordillera Blanca, Peru. *Wetlands* 39, 1057–1067. doi:10.1007/s13157-019-01134-1

Honorio Coronado, E., Mercado Torres, A., Del Castillo Torres, D., Dávila Cardoso, N., Martín Brañas, M., Ríos Torres, S., et al. (20202020). Impacto De La Construcción De La Carretera Iquitos-Saramiriza Sobre Los Bosques Y Turberas Del Río Tigre, Loreto, Perú. *Folia Amaz* 29 (1), 65–87. Available at: http://revistas.iiap.gob.pe/index.php/foliaamazonica/article/view/493/554. doi:10.24841/fa.v28i2.493

Honorio Coronado, E. N., Hastie, A., Reyna, J., Flores, G., Grández, J., Lähteenoja, O., et al. (2021). Intensive Field Sampling Increases the Known Extent of Carbon-Rich Amazonian Peatland Pole Forests. *Environ. Res. Lett.* 16 (7), 074048, 2021 . Available at: https://iopscience.iop.org/article/10.1088/1748-9326/ac0e65/meta. doi:10.1088/1748-9326/ac0e65

Crowson, M., Warren-Thomas, E., Hill, J. K., Hariyadi, B., Agus, F., Saad, A., et al. (2019). A Comparison of Satellite Remote Sensing Data Fusion Methods to Map Peat Swamp Forest Loss in Sumatra, Indonesia. *Remote Sens Ecol. Conserv* 5 (3), 247–258. doi:10.1002/rse2.102

Dargie, G. C., Lewis, S. L., Lawson, I. T., Mitchard, E. T. A., Page, S. E., Bocko, Y. E., et al. (2017). Age, Extent and Carbon Storage of the central Congo Basin Peatland Complex. *Nature* 542 (7639), 86–90. doi:10.1038/nature21048

Draper, F. C., Roucoux, K. H., Lawson, I. T., Mitchard, E. T. A., Honorio Coronado, E. N., Lähteenoja, O., et al. (2014). The Distribution and Amount of Carbon in the Largest Peatland Complex in Amazonia. *Environ. Res. Lett.* 9 (12), 124017. doi:10.1088/1748-9326/9/12/124017

Draper, F. C., Honorio Coronado, E. N., Roucoux, K. H., Lawson, I. T., Pitman, N. C. A., Phillips, O. L., et al. (2018). Peatland Forests Are the Least Diverse Tree Communities Documented in Amazonia, but Contribute to High Regional Beta-Diversity. *Ecography* 41 (8), 1256–1269. doi:10.1111/ecog.03126

Gumbricht, T., Roman-Cuesta, R. M., Verchot, L., Herold, M., Wittmann, F., Householder, E., et al. (2017). An Expert System Model for Mapping Tropical Wetlands and Peatlands Reveals South America as the Largest Contributor. *Glob. Change Biol.* 23 (9), 3581–3599. doi:10.1111/gcb.13689

Hamilton, S. K., de Souza, O. C., and Coutinho, M. E. (1998). Dynamics of Floodplain Inundation in the Alluvial Fan of the Taquari River (Pantanal, Brazil). *SIL Proc. 1922-2010* 26 (3), 916–922. doi:10.1080/03680770.1995.11900852

Hansen, M. C., Potapov, P. V., Moore, R., Hancher, M., Turubanova, S. A., Tyukavina, A., et al. (2013). High-Resolution Global Maps of 21st-Century Forest Cover Change. *Science* 342, 850–853. Data available on-line from: http://earthenginepartners.appspot.com/science-2013-global-forest. doi:10.1126/science.1244693

Henebry, G. M. (1997). "Advantages of Principal Components Analysis for Land Cover Segmentation from SAR Image Series," in Proceedings of Third ERS Symposium on space at the service of our environment, Noordwijk, The Netherlands, March 14–21, 1997 (SP-414, ESA), 175–178.

Hergoualc'h, K., Dezzeo, N., Verchot, L. V., Martius, C., van Lent, J., Aguila-Pasquel, J. D., et al. (2020). Spatial and Temporal Variability of Soil N_2O and CH_4 Fluxes along a Degradation Gradient in a Palm Swamp Peat forest in the Peruvian Amazon. *Glob. Change Biol.* 26, 7198–7216. doi:10.1111/gcb.15354

Hergoualc'h, K., Gutiérrez-Vélez, V. H., Menton, M., and Verchot, L. V. (2017). Characterizing Degradation of palm Swamp Peatlands from Space and on the Ground: An Exploratory Study in the Peruvian Amazon. *For. Ecol. Manage.* 393, 63–73. doi:10.1016/j.foreco.2017.03.016

Hribljan, J. A., Suarez, E., Bourgeau-Chavez, L., Endres, S., Lilleskov, E. A., Chimbolema, S., et al. (2017). Multidate, Multisensor Remote Sensing Reveals High Density of Carbon-Rich Mountain Peatlands in the Páramo of Ecuador. *Glob. Change Biol.* 23, 5412–5425. doi:10.1111/gcb.13807

Jensen, J. R. (1996). "Principal Component Analysis," in *Introductory Digital Image Processing; A Remote Sensing Perspective*. Editor K.C. Clarke (Upper Saddle River, NJ: Prentice-Hall), 172–179.

Lähteenoja, O., and Page, S. (2011). High Diversity of Tropical Peatland Ecosystem Types in the Pastaza-Marañón basin, Peruvian Amazonia. *J. Geophys. Res. Biogeosciences* 116 (G2), 15. doi:10.1029/2010jg001508

Lähteenoja, O., Ruokolainen, K., Schulman, L., and Oinonen, M. (2009a). Amazonian Peatlands: An Ignored C Sink and Potential Source. *Glob. Change Biol.* 15 (9), 2311–2320. doi:10.1111/j.1365-2486.2009.01920.x

Lähteenoja, O., Ruokolainen, K., Schulman, L., and Alvarez, J. (2009b). Amazonian Floodplains Harbour Minerotrophic and Ombrotrophic Peatlands. *Catena* 79, 140–145. doi:10.1016/j.catena.2009.06.006

Lähteenoja, O., Reátegui, Y. R., Räsänen, M., Torres, D. D. C., Oinonen, M., and Page, S. (2012). The Large Amazonian Peatland Carbon Sink in the Subsiding Pastaza-Marañón Foreland basin, Peru. *Glob. Change Biol.* 18 (1), 164–178. doi:10.1111/j.1365-2486.2011.02504.x

Leifeld, J., and Menichetti, L. (2018). The Underappreciated Potential of Peatlands in Global Climate Change Mitigation Strategies. *Nat. Commun.* 9 (1), 1071–1077. doi:10.1038/s41467-018-03406-6

Lilleskov, E., McCullough, K., Hergoualc'h, K., del Castillo Torres, D., Chimner, R., Murdiyarso, D., et al. (2019). Is Indonesian Peatland Loss a Cautionary Tale for Peru? A Two-Country Comparison of the Magnitude and Causes of Tropical Peatland Degradation. *Mitig Adapt Strateg. Glob. Change* 24, 591–623. doi:10.1007/s11027-018-9790-3

López Gonzales, M., Hergoualc'h, K., Angulo Núñez, Ó., Baker, T., Chimner, R., del Águila Pasquel, J., et al. (2020). *What Do We Know about Peruvian Peatlands? Occasional Paper 210*. Bogor, Indonesia: CIFOR.

Loisel, J., Gallego-Sala, A. V., Amesbury, M. J., Magnan, G., Anshari, G., Beilman, D. W., et al. (2021). Expert Assessment of Future Vulnerability of the Global Peatland Carbon Sink. *Nat. Clim. Chang.* 11, 70–77. doi:10.1038/s41558-020-00944-0

Maltby, E., and Proctor, M. C. F. (1996). "Peatlands: Their Nature and Role in the Biosphere," in *Global Peat Resources*. Editor E. Lappalainen (Jyska: International Peat Society and Geological Survey of Finland), 11–19.

Margono, B. A., Bwangoy, J.-R. B., Potapov, P. V., and Hansen, M. C. (2014). Mapping Wetlands in Indonesia Using Landsat and PALSAR Data-Sets and Derived Topographical Indices. *Geo-spatial Inf. Sci.* 17 (1), 60–71. doi:10.1080/10095020.2014.898560

Miettinen, J., Shi, C., and Liew, S. C. (2011). Deforestation Rates in Insular Southeast Asia between 2000 and 2010. *Glob. Change Biol.* 17 (7), 2261–2270. doi:10.1111/j.1365-2486.2011.02398.x

Miettinen, J., Shi, C., and Liew, S. C. (2016). Land Cover Distribution in the Peatlands of Peninsular Malaysia, Sumatra and Borneo in 2015 with Changes since 1990. *Glob. Ecol. Conservation* 6, 67–78. doi:10.1016/j.gecco.2016.02.004

Millard, K., and Richardson, M. (2015). On the Importance of Training Data Sample Selection in Random Forest Image Classification: A Case Study in Peatland Ecosystem Mapping. *Remote Sensing* 7 (7), 8489–8515. doi:10.3390/rs70708489

Moomaw, W. R., Chmura, G. L., Davies, G. T., Finlayson, C. M., Middleton, B. A., Natali, S. M., et al. (2018). Wetlands in a Changing Climate: Science, Policy and Management. *Wetlands* 38 (2), 183–205. doi:10.1007/s13157-018-1023-8

Murdiyarso, D., Lilleskov, E., and Kolka, R. (2019). Tropical Peatlands Under Siege: The Need for Evidence-Based Policies and Strategies. *Mitig Adapt Strateg. Glob. Change* 24 (4), 493–505. doi:10.1007/s11027-019-9844-1

Olofsson, P., Foody, G. M., Stehman, S. V., and Woodcock, C. E. (2013). Making Better Use of Accuracy Data in Land Change Studies: Estimating Accuracy and Area and Quantifying Uncertainty Using Stratified Estimation. *Remote Sensing Environ.* 129, 122–131. doi:10.1016/j.rse.2012.10.031

Page, S. E., Rieley, J. O., and Banks, C. J. (2011). Global and Regional Importance of the Tropical Peatland Carbon Pool. *Glob. Change Biol.* 17 (2), 798–818. doi:10.1111/j.1365-2486.2010.02279.x

Potapov, P. V., Dempewolf, J., Talero, Y., Hansen, M. C., Stehman, S. V., Vargas, C., et al. (2014). National Satellite-Based Humid Tropical forest Change Assessment in Peru in Support of REDD+ Implementation. *Environ. Res. Lett.* 9 (12), 124012. doi:10.1088/1748-9326/9/12/124012

Roucoux, K. H., Lawson, I. T., Baker, T. R., Del Castillo Torres, D., Draper, F. C., Lähteenoja, O., et al. (2017). Threats to Intact Tropical Peatlands and Opportunities for Their Conservation. *Conservation Biol.* 31 (6), 1283–1292. doi:10.1111/cobi.12925

Warren, M., Hergoualc'h, K., Kauffman, J. B., Murdiyarso, D., and Kolka, R. (2017). An Appraisal of Indonesia's Immense Peat Carbon Stock Using National Peatland Maps: Uncertainties and Potential Losses from Conversion. *Carbon Balance Manag.* 12 (1), 12. doi:10.1186/s13021-017-0080-2

Weiss, A. (2001). "Topographic Position and Landforms Analysis," in Poster presentation, ESRI user conference, San Diego, CA, July 9–13, 2001.

Wiese, L., Wollenberg, E., Alcántara-Shivapatham, V., Richards, M., Shelton, S., Hönle, S. E., et al. (2021). Countries' Commitments to Soil Organic Carbon in Nationally Determined Contributions. *Clim. Pol.* 21, 1005–1019. Available at: https://www.tandfonline.com/doi/full/10.1080/14693062.2021.1969883. doi:10.1080/14693062.2021.1969883

Xu, J., Morris, P. J., Liu, J., and Holden, J. (2018). PEATMAP: Refining Estimates of Global Peatland Distribution Based on a Meta-Analysis. *Catena* 160, 134–140. doi:10.1016/j.catena.2017.09.010

Yu, Z., Loisel, J., Brosseau, D. P., Beilman, D. W., and Hunt, S. J. (2010). Global Peatland Dynamics since the Last Glacial Maximum. *Geophys. Res. Lett.* 37 (13), L13402. doi:10.1029/2010gl043584

Conflict of Interest: BZ was employed by the company Spatial Informatics Group, LLC.

The remaining authors declare that the research was conducted in the absence of any commercial or financial relationships that could be construed as a potential conflict of interest.

The reviewer TB declared a past co-authorship with the authors / with several of the authors RD, EL, and KH to the handling editor.

Publisher's Note: All claims expressed in this article are solely those of the authors and do not necessarily represent those of their affiliated organizations, or those of the publisher, the editors and the reviewers. Any product that may be evaluated in this article, or claim that may be made by its manufacturer, is not guaranteed or endorsed by the publisher.

frontiers in Earth Science

SYSTEMATIC REVIEW
published: 17 February 2022
doi: 10.3389/feart.2022.670867

Biological Nitrogen Fixation and Nitrogen Accumulation in Peatlands

Tianya Yin[1], *Maoyuan Feng*[1], *Chunjing Qiu*[2] *and Shushi Peng*[1]*

[1]*Sino-French Institute for Earth System Science, College of Urban and Environmental Sciences, and Laboratory for Earth Surface Processes, Peking University, Beijing, China,* [2]*Laboratoire des Sciences du Climat et de l'Environnement, LSCE/IPSL, CEA-CNRS-UVSQ, Université Paris-Saclay, Gif-sur-Yvette, France*

Peatlands cover about 3% of the Earth's surface and are regarded as a vital carbon (C) pool and sink. The formation of peatland is supported by continuously supplied nitrogen (N) but the sources of this N remain unclear. Here, we first review N stocks and the rate they accumulate in peatlands, then we present the sources of N, especially through biological nitrogen fixation (BNF). We found that global peatlands store 5.9–25.9 Gt N. In the past millennia, northern peatlands have a lower N accumulated rate than tropical undisturbed peatlands. BNF rate is approximately 1.9 ± 2.7 g m^{-2} yr^{-1} in northern peatlands, higher than the rate of N deposition, 0.5 ± 0.4 g m^{-2} yr^{-1}. For tropical peatlands, BNF observation has hardly been reported yet and needs further investigation. This review provides a broad picture of peatland N cycling and suggests that there are large uncertainties, due to limited observations of BNF and N fluxes by inflow and outflow runoff. Therefore, we call for more efforts contributing to field observations and modelling of the N budget in peatlands.

Keywords: peatland, BNF, nitrogen fixation, nitrogen accumulation, nitrogen stock, nitrogen cycle

OPEN ACCESS

Edited by:
Annalea Lohila,
University of Helsinki, Finland

Reviewed by:
Zicheng Yu,
Lehigh University, United States
Pertti Juhani Martikainen,
University of Eastern Finland, Finland

***Correspondence:**
Shushi Peng
speng@pku.edu.cn

Specialty section:
This article was submitted to Biogeoscience, a section of the journal Frontiers in Earth Science

Received: *22 February 2021*
Accepted: *14 January 2022*
Published: *17 February 2022*

Citation:
Yin T, Feng M, Qiu C and Peng S (2022) Biological Nitrogen Fixation and Nitrogen Accumulation in Peatlands. Front. Earth Sci. 10:670867. doi: 10.3389/feart.2022.670867

INTRODUCTION

Peatland is a type of wetland ecosystem rich in peat, a type of soil that consists of partially decomposed organic material (Page and Baird, 2016). Although they cover only 3% of the global land surface (Yu et al., 2010), peatlands contain ~644 Gt C, which is 21% of the global total soil organic carbon (Leifeld and Menichetti, 2018). Moreover, this carbon (C) stock is increasing at a rate of 0.14 Pg C yr^{-1} (Gallego-Sala et al., 2018), making peatlands an important C sink and potential C source in the context of climate change. Peat formation requires nitrogen (N) supply according to the C/N stoichiometry (C/N ratio) in organic matter (Leifeld and Menichetti, 2018), and uncertainties surrounding N hampers accurate prediction of the land C sink into the future (Wieder et al., 2015). In the past 2 decades, although more and more works related to the N cycle in peatlands at the site/regional level were reported [e.g., León and Oliván (2014); Wang et al. (2015); van Bellen et al. (2020)], the global picture for the sources of N in peatlands remains still unclear.

There are three major ways of N input into a peatland ecosystem, i.e., atmospheric deposition, biological nitrogen fixation (BNF), and N inflow through upland runoff or discharge (Limpens et al., 2006). N deposition, which includes wet and dry deposition, varies across locations. For instance, total N deposition in peatlands ranges from less than 0.2 g N m^{-2} yr^{-1} in pristine bogs in Canada (Vile et al., 2014) to more than 4 g N m^{-2} yr^{-1} in polluted regions in Europe (Aerts, 1997; Tauchnitz et al., 2010). In many studies, only bulk deposition was reported (Fenn et al., 2003), which captures mainly wet deposition with a small amount of dry deposition (Limpens et al., 2006). Although the flux of dry deposition is comparable to wet deposition (Nadim et al., 2001; Godoy et al., 2003), the dry

deposition was often ignored, especially in sedge-dominated fens and wooded bogs, which may cause a large bias in peatland N budgets (Limpens et al., 2006).

BNF in peatlands can be found in free-living cyanobacteria (Granhall and Selander, 1973), quasi-symbiotic cyanobacteria associated with *Sphagnum* (Patova et al., 2020), methanotrophs (Larmola et al., 2014; Vile et al., 2014), actinorhizal (actinomycete-nodulated) plants (Schwintzer, 1983) and other heterotrophic bacteria (Kox et al., 2018). There are mainly two methods for measuring BNF: direct $^{15}N_2$ assimilation ($^{15}N_2$ method) (Saiz et al., 2019) and the indirect acetylene (C_2H_2) reduction assay (ARA) (Hardy et al., 1968). Both methods involve incubation of samples with a certain gas, $^{15}N_2$ or acetylene, respectively, followed by determination of the ^{15}N signature in the incubated samples through mass spectrometry ($^{15}N_2$ method) or amount of ethylene (C_2H_4) reduced from acetylene in the headspace through gas chromatography (ARA) (Rousk et al., 2018; van den Elzen et al., 2020). For ARA, a conversion factor is needed to convert the moles of ethylene produced by nitrogenase enzyme activity into moles of N_2 fixed. Since the high cost of the $^{15}N_2$ method prohibits its usage in widespread and repeated measurements, the indirect ARA is the most common method for measuring BNF (Saiz et al., 2019). BNF rates reported in peatlands range from less than 0.1 g N m^{-2} yr^{-1} (Waughman and Bellamy, 1980; Urban and Eisenreich, 1988) to more than 2.5 g N m^{-2} yr^{-1} (Larmola et al., 2014; Vile et al., 2014).

Nutrient supply through streamflow or groundwater flow may be important for net primary productivity and peat formation of minerotrophic peatlands and some bogs (Urban and Eisenreich, 1988; Limpens et al., 2006), but data are scarce. A watershed of Marcell Bog in Minnesota, United States, received approximately 0.2 g N m^{-2} yr^{-1} input through streamflow, 50% of which was retained in the bog (Verry and Timmons, 1982). A slope mire in Germany received 0.9 ± 0.2 g N m^{-2} yr^{-1} and discharged 1.9 ± 0.3 g N m^{-2} yr^{-1} through streamflow (Tauchnitz et al., 2010), which was much less than the atmospheric deposition (4.9 ± 0.4 g N m^{-2} yr^{-1}).

Thus, it is important to comb the knowns and unknowns of these three major sources into peatlands, and to understand the N cycle in peatlands. In this study, we first reviewed N stocks and N accumulation rates of global peatlands. Then we explored from literature the external sources of N in peatlands, especially via BNF. Overall, this meta-analysis provides information on N accumulation rates of peatlands and their sources, and summarizes current estimates of the N cycle in peatlands and knowledge gaps.

METHODS

N Stock

Hugelius et al. (2020) reported comprehensive estimates for the N stock of northern peatland (north of 30°N) as 10 ± 7 Gt N. Due to the lack of synthesis of N stocks in tropical and southern peatlands [mainly refer to Patagonian peatlands (Yu et al., 2010)], N stocks there were derived by dividing C stocks with the mean values of C/N mass ratio. **Table 1** and **Table 2** summarize area, C stocks, N stocks and C/N ratios of global peatlands from literature. The C stock of tropical peatlands from Ribeiro et al. (2020) was used here. For the C/N ratio of tropical peat, we compiled a dataset of 160 records (for details of all records, see **Supplementary Table S1**), which consists of two types of peatlands (defined by their degradation status): natural (labeled as "undisturbed"; $n = 71$ records), and disturbed (drained or logged, $n = 75$) peatlands. For undisturbed tropical peat, the oxic, above water-table active layer of peat is approximately 10–30 cm deep (Melling et al., 2005; Girkin et al., 2020). To avoid the overrepresentation of sampling from surface soil, we divided the C/N ratios into two depth groups: surface or near surface peat ("surface peat", $n = 78$) and deeper peat ("lower peat", $n = 51$). Here, we simply defined surface or near surface as sampling depth less than 25 cm, to match the availability of data (**Supplementary Table S1**). Furthermore, tropical peatlands could also be classified by two climate types: alpine or montane, and lowland. In southern peatlands, the C stock and C/N ratio (median, in order to eliminate the impact of outliers in surface peat) were estimated from Loisel and Yu (2013a) and Knorr et al. (2015), respectively.

Rates of N Accumulation

The long-term (apparent) rate of N accumulation (LORNA) was calculated as the cumulative N mass (g m^{-2}) of a peat core divided by the core's basal age (Tolonen and Turunen, 1996). In boreal peatlands, values of LORNA were collected from literature (Limpens et al., 2006; Loisel et al., 2014; Wang et al., 2015; Schillereff et al., 2016) as shown in **Table 2**. In tropical and southern peatlands, values of LORNA have seldom been reported, so we estimated them from the previously reported long-term carbon accumulated rate (LORCA) and C/N ratio (**Supplementary Table S1**). We compiled 26 records of LORCA of tropical peat, distributed in South America ($n = 19$), Southeast Asia ($n = 6$) and Africa ($n = 1$). Note that some records contain more than one peat core (For example, the Congo record in Africa is mean of 61 cores). Basal ages of these tropical peat cores range from >26,000 to 1,975 cal year BP.

Recent (apparent) rate of N accumulation (RERNA) was calculated as the cumulative N mass from the peat surface to a depth corresponding to a given date, divided by its age (Tolonen and Turunen, 1996; León and Oliván, 2014). In this paper, we defined "recent" as younger than 500 years since the oldest RERNA reported in literature was about 400 years old (León and Oliván, 2014). 75 records of northern peatlands were used to investigate the RERNA (**Table 3**). Specifically, records of RERNA in northern peatlands were divided into two groups: 1) Group A: RERNA calculated from peat core properties with the database provided by Loisel et al. (2014) (records are available via Pangaea). In this case, multiple cores taken from the same peatland were considered as independent records since these cores were not designed as replicates (Loisel et al., 2014). In total, group A consists of 19 records, distributed in Canada ($n = 14$), United States ($n = 1$), Sweden ($n = 1$), Scotland ($n = 2$) and Russia ($n = 1$). 2) Group B: data collected from literature other than Loisel et al. (2014) and Li et al. (2018), providing only RERNA but without information of properties of peat cores. Group B consisted of 56 records, distributed in Canada ($n = 45$), United States ($n = 6$) and Sweden ($n = 5$). The data from Li

TABLE 1 | Area, carbon pool and long-term (apparent) rate of carbon accumulation (LORCA) of global/regional peatlands.

Region/Location	Area (Mha)	Carbon pool (GtC)	LORCA (g C m^{-2} yr^{-1})	References
Northern/boreal				
Boreal and subarctic	342	455	—	Gorham (1991)
Northern	342	436	22.9 ± 0.2	Loisel et al. (2014)
Northern	400	547 (473–621)	18.6	Yu et al. (2010)
Boreal	360.9	427	—	Leifeld and Menichetti (2018)
Northern	320	545–1,055	33	Nichols and Peteet (2019)
Extratropical northern hemisphere (>23°N)	370 ± 50	415 ± 150	34	Hugelius et al. (2020)
Tropical				
Tropical	36.85	50	12.8	Yu et al. (2010)
Tropical	44	88.6 (81.7–91.9)	—	Page et al. (2011)
Tropical	—	104.7 (69.6–129.8)	—	Dargie et al. (2017)
Tropical	58.7	119.2	—	Leifeld and Menichetti (2018)
Tropical	90–170	152–288	24–300	Ribeiro et al. (2020)
Congo Basin	14.5	30.6 (6.3–46.8)	23.9 ± 5.8	Dargie et al. (2017)
Amazonian Peru	3.56 ± 0.21	3.14 (0.44–8.15)	52 ± 22	Draper et al. (2014)
Southern				
Patagonia	4.5	15 (13–18)	22	Yu et al. (2010)
Patagonia	4.5	7.6	—	Loisel and Yu (2013a)
West Tasmania	1	—	—	Pemberton (2005)
Eastern Australia	0.0085	0.0068	—	Cowley and Fryirs (2020)
Australian Alps	0.052	—	—	Grover et al. (2005)
Temperate (could overlap with Northern or Southern peatlands)				
Temperate	18.5	21.9	—	Leifeld and Menichetti (2018)
Hengduan Mountains	0.49	1.95	34.9	Liu et al. (2020)
Global				
Global	463.2	597.8	—	Leifeld and Menichetti (2018)
Global	423	—	—	Xu et al. (2018)
Global	—	530 ± 160	—	Hugelius et al. (2020)

TABLE 2 | Nitrogen pool, long-term (apparent) rate of nitrogen accumulation (LORNA) and the mass ratio of carbon/nitrogen of global peatlands.

Region	Area (Mha)	Nitrogen pool (Gt N)	LORNA (g N m^{-2} yr^{-1})	C/N mass ratio	References
Literature that provides estimated nitrogen pool					
Boreal	—	8–15	0.42(0.19–0.48)	30–55	Limpens et al. (2006)
Northern	342	9.7	0.5 ± 0.04	55 ± 33	Loisel et al. (2014)
Northern[a]	20.8	18.5	0.85	22.8 ± 6.1–33.0 ± 0.5	Wang et al. (2015)
Extratropical northern hemisphere	370 ± 50	10 ± 7	—	37 ± 14	Hugelius et al. (2020)
Tropical	58.7	4	—	29.7(median)±17.8	Leifeld and Menichetti (2018)
Literature that provides C/N ratio					
Patagonia	—	—	—	40–120	Broder et al. (2012)
Patagonia	—	—	—	36–175	Knorr et al. (2015)
Panama	—	—	—	19	Sjogersten et al. (2011)
Eastern Australia	0.0085	—	—	15–58	Cowley and Fryirs (2020)
Australian Alps	0.052	—		20.8–115	Grover et al. (2005)
Zoige, China	—	—	—	15.76–18.16	Li et al. (2011)
Minnesota, United States	—	—	—	35–74	Urban and Eisenreich (1988)
Britain	—	—	0.70 ± 0.09	41.2	Schillereff et al. (2016)

[a]*Northern peatlands are represented by sites in Ontario, Canada.*

TABLE 3 | Recent rate of nitrogen accumulation (RERNA) in peatlands.

Location	RERNA (g N m^{-2} yr^{-1})	Age (years)	Number of peatlands	References
Northern peatlands	0.6 ± 0.4	<500	19	Loisel et al. (2014)
Alberta, Canada	1.97 ± 0.12	25	15	Vile et al. (2014)
Alberta, Canada	0.94 ± 0.08	since 1850	7	van Bellen et al. (2020)
Eastern Canada	1.46 ± 0.67	150	23	Turunen et al. (2004); Moore et al. (2005)
Minnesota, United States	2.32	86	6	Urban and Eisenreich (1988)
Stordalen, northern Sweden	1.3	100	3	Malmer and Holm (1984)
Getamossen, southern Sweden	2.0	100	2	Malmer and Holm (1984)
Isla Grande de Chiloé, Chile	0.97 ± 0.68	<400	5	León and Oliván (2014)
Zoige Plateau, China	13.0 ± 7.4	<200	5	Li et al. (2018)

et al. (2018) were discussed in *Recent Rate of Nitrogen Accumulation*.

Biological Nitrogen Fixation

We collected information about BNF in peatlands from papers and books following the criteria as below:

Rate of BNF must have been measured in peatlands. Peatland was defined as where the surface soil layer (a minimum thickness of 30 cm) consists of at least 65% organic content (Page et al., 2011; Dargie et al., 2017). We believed in the authors' scientific judgement on the peatlands even without definite peat properties, i.e., once they claimed their study was carried out in peatlands (including statement as *mire, fen, bog or swamp*), the paper was included for our meta-analysis. However, if the studies were carried out in *wetland* when the author(s) did not indicate the existence of peat, they were not included in this analysis. In the case where a study contained multiple sites or types of peatlands, each site or type of peatland was considered as an independent record.

In total, we obtained 21 records that reported an annual N_2 fixation rate, and 8 records that reported short-term (i.e., daily or hourly) nitrogenase activities in peatlands (**Table 4**). Significance tests were performed with Student's *t*-test. Linear correlation analyses were performed on IBM® SPSS® Statistics 26.

In addition, climate data were derived from database CRU TS v4.04 (Harris et al., 2020). Mean temperature during the growing season and mean annual precipitation were obtained during the period of 1981–2010. The growing season was defined as early June to end of August (Vile et al., 2014; Rousk et al., 2015).

RESULTS AND DISCUSSION

C/N Ratio of Tropical Peatland and Nitrogen Stock

Of all the 160 records of C/N ratio in tropical peatlands, 78 records belong to surface peat, 51 records lower peat, and 31 records unknown. The C/N ratio ranges from 10 to 85.6, with a mean of 35.0 ± 18.4 (±standard deviation) for all records. For all the 129 records of known depth, 60 were from natural/undisturbed peatlands and 69 were from disturbed or degraded peatlands. For undisturbed peats, the C/N ratio is 25.9 ± 8.2 for surface peat (n = 31) and 33.0 ± 20.0 for lower peat (n = 29), however, the difference between surface and lower peat is not statistically significant ($p > 0.05$). For disturbed peats, the C/N ratio of lower peat (57.6 ± 21.6, n = 22) is significantly higher than that of surface peat (35.3 ± 16.0; n = 47) ($p < 0.01$). The disturbed peatlands tend to have a lower C/N ratio in the surface peat than in the lower peat. This suggests different loss rates of C and N in the disturbed surface layer, the C loss being faster than that of N under degradation of tropical peat. In addition, although the difference between C/N ratios of surface and lower peats in undisturbed tropical peatlands is nonsignificant, they show a contrary trend compared to northern peatlands. In non-permafrost northern peatlands, C/N ratios decline with increasing depth as a result of slow, but continuous, anaerobic decay remobilizing the carbon (Malmer and Holm, 1984; Kuhry and Vitt, 1996; Sannel and Kuhry, 2009; Wang et al., 2014).

For lower peats, C/N ratios show little dependence on the sampling depth (r = -0.21, p = 0.141). This indicates that the C/N ratio in deeper layers is more or less randomly distributed along the core depth despite that the C/N ratio in surface peat, or approximately active layer, is significantly lower than the deeper, less active layer. Thus, the C/N ratio for all tropical peat weighted by depth is 42.9 ± 24.5 (n = 114, including both disturbed and undisturbed peatlands), with the provision that the surface and lower peat have average sampling depths of 7.5 and 125 cm, respectively. The C/N ratio for undisturbed peatlands (32.6 ± 19.5) is slightly higher than the previous estimate of tropical peats of 29.7 ± 17.8 (Leifeld and Menichetti, 2018) since we included more records from lower peat that has higher C/N ratio. The C/N ratio for undisturbed tropical peatlands is in range of that of northern peatlands (30–55, Limpens et al., 2006).

We also noticed that C/N ratios of alpine or montane peatlands in tropical regions (19.9 ± 8.3, n = 23) and tropical lowland peatlands (37.2 ± 18.3, n = 125) show significant difference ($p < 0.001$). This is probably due to the lower C content in those alpine or montane peatlands in tropical regions ($p < 0.001$, compared with C% in tropical lowland peatland), suggesting the materials (leaf and root litters etc.) that formed peat are different from that in tropical lowland peatlands, or it is a bias caused by the small sampling set in alpine or montane peatlands.

By simply adopting the depth-weighted mean of C/N ratio of 43 (33 ± 20 for undisturbed and 56 ± 23 for disturbed peatlands) and C stock of 152–288 Gt C (Ribeiro et al., 2020), as C stocks for disturbed and undisturbed are not available yet, we estimated at

TABLE 4 | Rates of biological N_2 fixation (BNF) in peatlands. Conversion factor (CF) is the ratio between C_2H_4 produced using the ARA method and the N fixed using the $^{15}N_2$ method.

Location	Peatland type	BNF, annual (g N m^{-2} yr^{-1})	BNF, short-term	Major nitrogen-fixing organism	Assay method(s)	Incubation time	CF	Atmospheric deposition of nitrogen (g N m^{-2} yr^{-1})	References
Rates of BNF reported with annual value									
Stordalen, Swedish Lapland	Bog	0.03		Anaerobic bacteria in peat	ARA	2 h	1.5 (Hardy et al., 1971)	0.035 (precipitation)	Granhall and Selander (1973)
	Bog	0.15		Aerobic bacteria in peat					
	Fen	0.16		Mosses surrounded with free-living blue-green algae					
	Fen	9.4		Mosses with epiphytically and intracellularly associated blue-green algae					
	Fen	11.5		Free-living blue-green algae					
Stordalen, Swedish Lapland	Bog	1.0–6.4 (3.2 ± 2.4)		Cyanobacteria associated with *Sphagnum* and *Drepanocladus*	ARA	50–150 min	3 (Hardy et al., 1971)	0.35	Basilier et al. (1978)
Germany	Bog	0.07		Aerobic heterotrophs	—	—	—	—	Waughman and Bellamy (1980)
	Poor fen	0.53							
Massachusetts, United States	Bog	1.0		*Sphagnum* and peat	ARA, $^{15}N_2$ calibration	3 h	3.5	0.7 (bulk deposition)	Chapman and Hemond (1982)
Massachusetts, United States	Fen	3.6		Actinomycete symbiotic to *Myrica gale* nodules	ARA	22–30 h	4.0	0.65 (bulk deposition)	Schwintzer (1983)
Minnesota, United States	Bog	0.05–0.07		*Sphagnum* peat*	ARA	2–4 h	4.0 ± 0.5 (Basilier et al., 1978; Chapman and Hemond, 1982)	1.04 ± 0.1 (wet and dry deposition)	Urban and Eisenreich (1988)
Bothnian Bay, Finland	Mesotrophic fen	2.94	45 nmol N g^{-1} moss DW h^{-1}	Methanotrophs associated with *Sphagnum*	$^{15}N_2$, $^{13}CH_4$	45 h	—	0.3 (inorganic N)	Larmola et al. (2014)
	Oligotrophic fen	0.14	6 nmol N g^{-1} moss DW h^{-1}						
	Fen-bog	0.28	6 nmol N g^{-1} moss DW h^{-1}						
Alberta, Canada	Bog	2.58±0.24		Methanotrophs associated with *Sphagnum*, Beijerinckiaceae (Rhizobiales)	$^{15}N_2$, ARA	24 h	0.29±0.09 – 0.46±0.09	0.08-0.2 (wet and dry deposition)	Vile et al., 2014
Northern Sweden	Fen	0.26	13.7 μmol C_2H_2 m^{-2} h^{-1}	*Sphagnum* fuscum associated *Cyanobacteria*	ARA	2 h	2.48 (Sorensen et al., 2006)	<0.2	Rousk et al. (2015)

(Continued on following page)

TABLE 4 | (*Continued*) Rates of biological N_2 fixation (BNF) in peatlands. Conversion factor (CF) is the ratio between C_2H_4 produced using the ARA method and the N fixed using the $^{15}N_2$ method.

Location	Peatland type	BNF, annual (g N m^{-2} yr^{-1})	BNF, short-term	Major nitrogen-fixing organism	Assay method(s)	Incubation time	CF	Atmospheric deposition of nitrogen (g N m^{-2} yr^{-1})	References
Denmark	Bog	<0.4	4.2±1.4 μmol C_2H_2 m^{-2} h^{-1}	*Sphagnum* spp.	ARA	2 h	3	—	Rousk et al. (2018)
Russia	Bog	1.51-3.5	1.28-3.02 g C_2H_4 m^{-2} yr^{-1}	*Sphagnum*-associated *Cyanobacteria*: Nostoc paludosum, Microchaete tenera, Anabaena verrucose, Hapalosiphon pumilus	ARA	—	0.85 (Stewart et al., 2011)	0.27 (precipitation)	Patova et al. (2020)
Southern Sweden	Bog Rich fen Lagg fen	0.006 0.06 0.12		*Sphagnum* spp.	$^{15}N_2$	48 h	—	0.6 (wet and dry deposition)	van den Elzen et al. (2020)
Rates of BNF reported only with short-term value									
Minnesota, United States	Bog	—	0-163 μmol C_2H_4 m^{-2} h^{-1}	*Sphagnum fallax* and *S. angustifolium*	ARA, $^{15}N_2$	1 week	0.26	—	Warren et al. (2017)
Finland	Fen	—	1.4±0.2 μmol $^{15}N_2$ g^{-1} DW d^{-1}	*Sphagnum*-associated *Alphaproteobacteria*	$^{15}N_2$	48 h	—	0.40 (precipitation)	Kox et al. (2018)
Finland	Fen	—	0.07±0.07 μmol $^{15}N_2$ g^{-1} DW d^{-1}	sedges, *Carex, Sphagnum* spp.	$^{15}N_2$ + $^{13}CH_4$	48 h	—	—	Leppanen et al. (2015)
Minnesota, United States	Bog	—	15 (mean) nmol $^{15}N_2$ g^{-1} d^{-1}	*Sphagnum fallax*	ARA, $^{15}N_2$	1 week	—	—	Carrell et al. (2019)
Fochteloërveen, The Netherlands	Fen	—	6.5±0.9 μmol $^{15}N_2$ g^{-1} d^{-1}	*Molinia caerulea, S. palustre, S. fallax*	$^{15}N_2$	48 h	—	—	Kox et al. (2020)
Ilperveld, The Netherlands	Fen	—	4.4±0.2 μmol $^{15}N_2$ g^{-1} d^{-1}	*S. palustre*, *S. fallax*	$^{15}N_2$	48 h	—	—	Kox et al. (2020)
Site OBS, Patagonia	Bog	—	58±26 mmol N_2 m^{-2} d^{-1}	*Sphagnum magellanicum*	ARA, $^{15}N_2$	28 h, 72-80 h	0.4-0.5	—	Knorr et al. (2015)
Site SKY, Patagonia	Bog	—	32±13 mmol N_2 m^{-2} d^{-1}	Vascular *cushion* plants	ARA, $^{15}N_2$	28 h, 72-80 h	0.5-1.8	—	Korr et al. (2015)

nitrogen pool of 2.7–8.7 Gt N for tropical peatlands by taking the uncertainty of C/N ratio for disturbed and undisturbed peatlands. In southern peatlands, the N stock has not been reported yet. Since the peat formation condition in Patagonia is similar to that in boreal regions (Loisel and Yu, 2013a), we adopted a C stock of 7.6 Gt C (Loisel and Yu, 2013a) and a C/N ratio of 45 (Loisel et al., 2014), and estimated the N stock of Patagonia at 0.17 Gt N. With northern peatlands storing 10 ± 7 Gt N (Hugelius et al., 2020), summing up the peatland N stocks in the above three regions (i.e., 10 ± 7, 2.7–8.7 and 0.17 Gt N, respectively), the global peatland N stock was estimated at 5.9–25.9 Gt N, which is 4–19% of global total N stocks in the top 100 cm of soil layer [i.e., 133–140 Gt N (Vitousek et al., 1997)].

Generally, there are two approaches used to estimate nitrogen stock in peatlands. The first approach estimates the peatland N stock by dividing the C stock with a mean value of C/N ratio (Loisel et al., 2014; Wang et al., 2015; Leifeld and Menichetti, 2018). The second approach builds a linear relationship between peat depth and N stock with known data of peat cores, with which N stock could be predicted by peat depth (Hugelius et al., 2020). Through the first approach, Loisel et al. (2014) estimated the N stock of northern peatlands at 9.7 Gt N by assuming a mean C/N ratio of 45 based on N content data of 40 peat cores. Through the same approach, Wang et al. (2015) analyzed more than 400 peat cores from Ontario, Canada, and showed that C/N ratio ranged from 22.8 ± 6.1 to 33.0 ± 0.5 (n = ~1,600), thus they estimated northern peatlands had accumulated 18.5 Gt N since deglaciation. There were two key differences between the above two studies: Wang et al. (2015) collected information on more peat cores while the cores were distributed in a much more

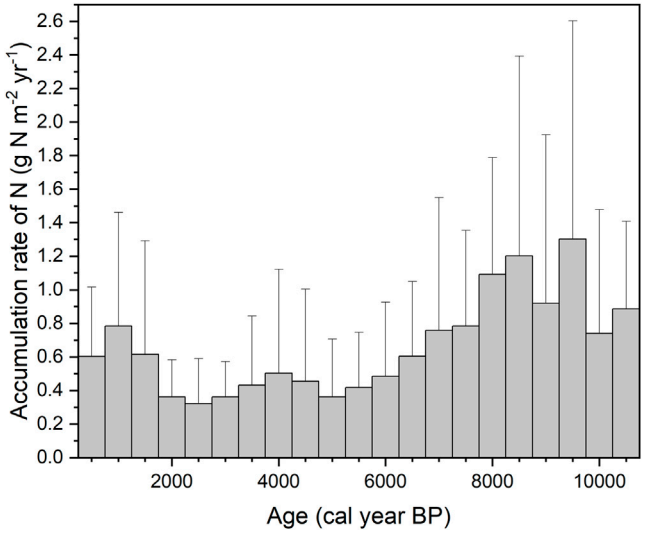

FIGURE 1 | Accumulation rate of N in each 500-year bins from 10,500 to 500 cal year BP. Error bars show the standard deviations. Data are from database at https://peatlands.lehigh.edu (n = 19).

extended area in Loisel et al. (2014). For tropical peatlands, Leifeld and Menichetti (2018) estimated the N stock at 4 Gt N based on a median C/N ratio of 29.7 and a C stock of 119.2 Gt C.

Through the second approach, the N stock of northern peatlands was estimated at 10 ± 7 Gt N, and the large uncertainty came from the high variability of depth and total N content (Hugelius et al., 2020). There are several factors that may have large effects on N content and C/N ratio. Vegetation types that form peat are different, with *Sphagnum* peat having significantly lower N content and higher C/N ratio than woody and herbaceous peat (Loisel et al., 2014). Histories of peatland formation and the evolution of N content and the C/N ratio could be largely driven by climate change in Holocene (Yu, 2011; Zhao et al., 2014).

Decomposition and degradation history also affect N stock of a peatland (Anshari et al., 2010; Yu, 2012). Overall, the estimated regional N stocks still have large uncertainty because of the large spatial heterogeneity of peat C/N ratio and N stock as well as the quite limited data in both of above two approaches.

Long-Term Rate of Nitrogen Accumulation

As summarized in **Table 2**, the estimation of LORNA of northern peatlands ranges from 0.42 to 0.85 g N m^{-2} yr^{-1} (Limpens et al., 2006; Loisel et al., 2014; Wang et al., 2015; Schillereff et al., 2016). In tropical peatlands, the average LORCA was 41.0 ± 20.9 g C m^{-2} yr^{-1} (n = 26; Supplementary Data). By applying a depth-weighted mean of the C/N ratio as 33 for undisturbed tropical peatlands (see *C/N Ratio of Tropical Peatland and Nitrogen Stock*), the average LORNA of tropical undisturbed peatlands was estimated at 1.24 ± 0.63 g N m^{-2} yr^{-1}. The LORNA in tropical peatlands is faster than that in northern peatlands, which could be mainly explained by the higher LORCA in tropical peatlands than northern peatlands (34 g C m^{-2} yr^{-1}, Hugelius et al., 2020). In southern peatlands, the LORNA in Patagonia was estimated at 0.49 g N m^{-2} yr^{-1} by adopting a LORCA of 22 g C m^{-2} yr^{-1} (Yu et al., 2010) and an average C/N ratio of 45.

A more representative dataset of peat properties would help improve the estimation of LORNAs. For example, by estimating the time-weighted C/N ratio (55 ± 33) from 40 peat cores across North America and northern Eurasia, Loisel et al. (2014) indicated that northern peatlands had accumulated N at a rate of 0.5 ± 0.04 g N m^{-2} yr^{-1} during the Holocene. Moreover, based on the data of more than 400 peat cores from Ontario, Canada, Wang et al. (2015) obtained the mean of C/N ratio as 27, and estimated LORNA of northern peatlands at 0.85 g N m^{-2} yr^{-1} by adopting the LORCA of 23 g C m^{-2} yr^{-1} from Loisel et al. (2014). However, it is unknown whether the C/N ratio of 27 or 55 ± 33 is more representative for northern peatlands. Thus, more peat cores containing C and N content are needed to help improve both spatial and temporal resolution for the estimation of N accumulation.

Since LORNA is the average accumulation rate during the whole life-time of a peat-core, it is difficult to reflect the transient or short-term behaviors of N accumulation as well as its change with time. **Figure 1** illustrates the changes of a 500-year N accumulation rate from 11,000 years ago to present, which was derived from the dataset of Loisel et al. (2014) that contains 19 peat core profiles with a high-resolution of age and N content data. Although the LORNA was estimated at 0.59 g N m^{-2} yr^{-1}, the highest N accumulation rate was observed to be between 9.5 and 8 kyr BP, equivalent to 1.3 (mean) g N m^{-2} yr^{-1}, and the lowest was observed to be between 3 and 2 kyr BP, equivalent to 0.32 g N m^{-2} yr^{-1}. The variation of the N accumulation rate in peat cores reflected the possible peatlands' development history—in the early stage of peatland development, peatlands were covered by more herbaceous vegetation characterized by low C/N ratio and high N content, but in the latest stage, they were shifted into *Sphagnum*-dominated bog characterized by high C/N ratio and low N content (Larmola et al., 2014; Loisel et al., 2014). By calculating the apparent rate of N accumulation from surface to bottom horizon of a peat profile, it was shown that, across the 19 peat cores, the apparent rate had a much higher variability in the most recent period but a lower variability during the Holocene. This pattern is possibly related to large spatial variation of N deposition and/or other N inputs across the peat cores for the most recent period.

Recent Rate of Nitrogen Accumulation

Most of the RERNA data were reported in northern peatlands, only one data of RERNA was reported in southern peatlands (0.97 ± 0.68 g N m^{-2} yr^{-1} in Isla Grande de Chiloé, Chile, León and Oliván, 2014) and no data had yet been reported in tropical peatlands. Therefore, the analysis of RERNA mainly focused on that in northern peatlands, as summarized in **Table 3**.

In northern peatlands, RERNA of Group A was estimated at 0.6 ± 0.4 g N m^{-2} yr^{-1} (n = 19), which was 1.2 times that of LORNA (i.e., 0.5 ± 0.04 g N m^{-2} yr^{-1}). In Group B, RERNA ranged from 0.94 to 2.32 g N m^{-2} yr^{-1}, with a mean of 1.63 ±

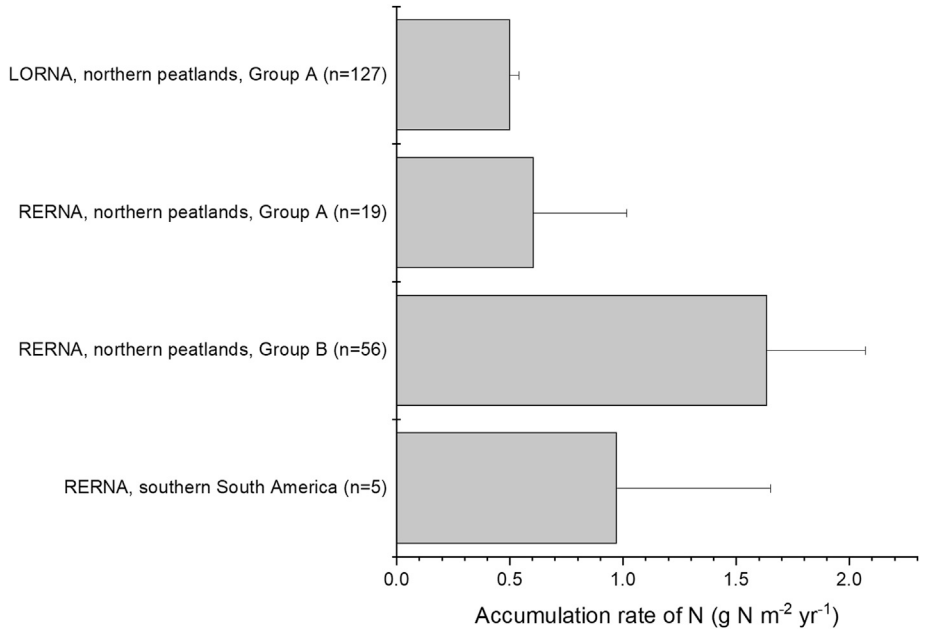

FIGURE 2 | Comparison of LORNA and RERNA in peatlands. Group A (n = 127 for LORNA and n = 19 for RERNA) includes data from the database of peat cores provided by Loisel et al. (2014) and Group B (n = 56, total number of cores) includes data from other literature that did not provide properties of peat cores but only provide calculated RERNA. Error bar of LORNA of Group A shows 1 SE, while other error bars show one SD.

0.43 g N m^{-2} yr^{-1} (n = 56) (Malmer and Holm, 1984; Urban and Eisenreich, 1988; Turunen et al., 2004; Moore et al., 2005; Vile et al., 2014; van Bellen et al., 2020). The mean of all records from Group A and Group B was 1.35 ± 0.56 g N m^{-2} yr^{-1}, which was ~2.7 times of LORNA. The largest RERNA was reported in the Zoige Plateau, China, as 13.0 ± 7.4 g N m^{-2} yr^{-1}, corresponding to a rapid recent rate of C accumulation (RERCA) of 259 ± 137 g C m^{-2} yr^{-1} (Li et al., 2018). This rapid RERCA was much larger compared to other northern peatlands where RERCAs varied between 40 and 120 g C m^{-2} yr^{-1} in the recent 200 years (Turunen et al., 2004; Loisel and Yu, 2013b; van Bellen et al., 2020). Peat cores from other parts of China also showed rapid RERCAs e.g., 184~376 g C m^{-2} yr^{-1} in the recent 100 years in Greater Khingan Range and Sanjiang Plain (Liu et al., 2019) and 124~293 g C m^{-2} yr^{-1} in the recent 200 years in Changbai Mountains (Bao et al., 2010). Moreover, it is still unclear whether all peatlands in China accumulate C (and N as well) at such rapid rates in recent centuries, and an explanation remains to be found. Thus, as the area of Chinese peatlands accounts only a small part for northern peatlands (~5%, Xu et al., 2018), we did not take this abnormal rate in our global upscaling of RERNA in the following discussion.

The apparent accumulation rate of N shows both high spatial and temporal variations (**Figure 1**, **Figure 2**). For example, in Group A, three out of the 19 profiles show the largest apparent accumulation rate in the most recent 500 years, six profiles in the most recent 2,000 years, and the other 10 profiles show the highest accumulation rate between 11 and 7 kyr BP (Loisel et al., 2014). This suggests that accumulated rate of N could depend on the developing periods and the locations with different input and output rates of N.

BNF and N Balance in Peatlands

Most of the BNF studies were performed in northern peatlands, and these available data on peatland BNF are quite limited and with large uncertainty (**Table 3**). Annual BNF rates were between 0.006–11.5 g N m^{-2} yr^{-1} in northern peatlands, with an arithmetic mean of 1.9 ± 2.7 g N m^{-2} yr^{-1} (n = 21, **Table 3**). In different types of peatland, the mean rates of BNF were 2.7 ± 3.9 g N m^{-2} yr^{-1} in fens and 0.8 ± 1.1 g N m^{-2} yr^{-1} in bogs, but the difference was non-significant (p = 0.13). Previous studies suggested that added phosphorus (P) could stimulate N fixing to meet increased N demand from plant (Larmola et al., 2014; Kox et al., 2016), and molybdenum (Mo) availability limited nitrogenase activity (Rousk and Michelsen, 2017; Warren et al., 2017). Both elements (P and Mo) should be better supplied in fens than in bogs and, indeed, a mesotrophic fen had more BNF than any other stage of peatland development of the same succession in Finland (Larmola et al., 2014). However, our results reflect large uncertainty in peatland BNF.

Despite that BNF rate was reported to be positively correlated with temperature in previous studies (Basilier et al., 1978; Schwintzer, 1983; Urban and Eisenreich, 1988), we found a weak correlation between annual BNF rate and the mean growing season temperature in northern peatlands (**Figure 3A**, r = −0.26, p = 0.276). Moreover, we also observed a weak and non-significant correlation between annual BNF rate and mean annual precipitation (**Figure 3B**, r = −0.20, p = 0.423). Our results are consistent with a recent review which found that the correlations between BNF and annual temperature as well as precipitation were weak across the globe (Davies-Barnard and Friedlingstein, 2020). But it should

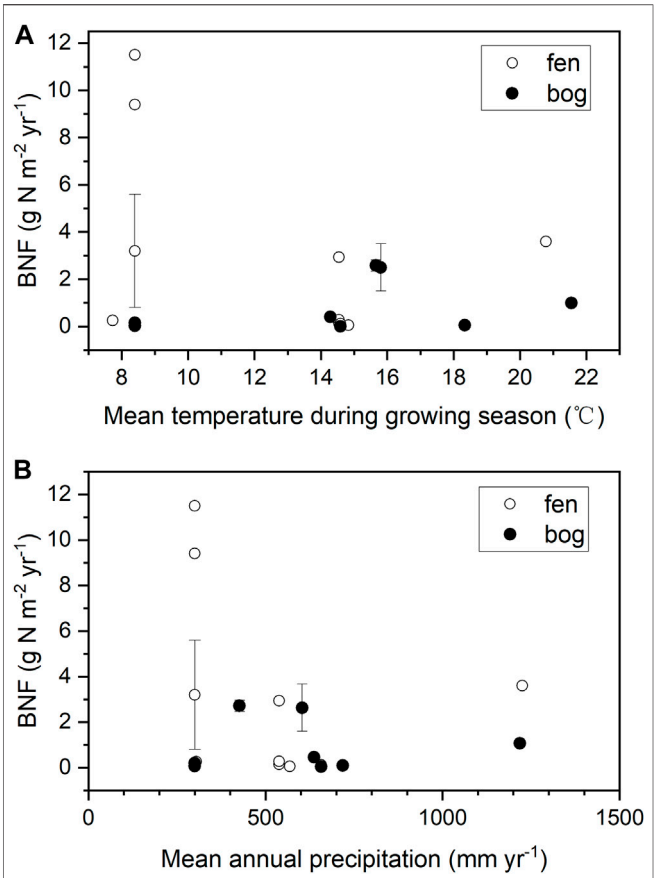

FIGURE 3 | BNF plotted against **(A)** mean temperature during growing season (June-August, °C), and **(B)** annual precipitation (mm yr^{-1}). Climate data are mean between years of 1981–2010. Error bars show one SD.

be noticed that our result did not take tropical peatlands into account due to the lack of data. In *Long-Term Rate of Nitrogen Accumulation*, the LORNA in tropical peatlands was approximately 2 times that in northern peatlands; thus, we suggest that the BNF in tropical peatlands might be much higher than that in northern peatlands, and more observations are needed to determine this point.

The method used to determine the BNF rate might introduce large uncertainty (Flett et al., 1975; Knorr et al., 2015; Saiz et al., 2019). The most common method, ARA, is based on the versatility of the nitrogenase enzyme: its preference for performing a reaction of reducing C_2H_2 to C_2H_4 is higher than that of reducing N_2 (Schollhorn and Burris, 1967). Based on electron transfer equivalents, a theoretical conversion factor (CF) of 4:1 (moles of C_2H_4 produced per mole of N_2 fixed) was considered *in vitro* and 3:1 *in vivo* (Hardy et al., 1971). These theoretical CFs were used in many studies (Basilier et al., 1978; Markham, 2009; Rousk et al., 2018). However, ARA could either underestimate or overestimate nitrogenase activity (Flett et al., 1975; Witty, 1979; Vile et al., 2014). For example, C_2H_2 inhibits the nitrogenase activity of N_2-fixing methanotrophs, by inhibiting methane oxidation (King, 1996) which provides ATP needed in the reduction of C_2H_2 (Hardy et al., 1968). N_2-fixing methanotrophs also transform C_2H_2 into compounds undetectable for ARA, thus making ARA unreliable (Flett et al., 1975). Overestimation happens when the amount of endogenously produced ethylene is comparable to the ethylene produced by nitrogenase where BNF rates are less than 1 g N ha^{-1} d^{-1} (Witty, 1979). Early studies indicated the bias of CF from theoretical values and suggested site-specific calibration of the CF (Granhall and Selander, 1973; Schwintzer, 1983). Recent studies obtained CF ranging from 0.26 to 1.8 by calibration with the $^{15}N_2$ method (Vile et al., 2014; Knorr et al., 2015; Warren et al., 2017).

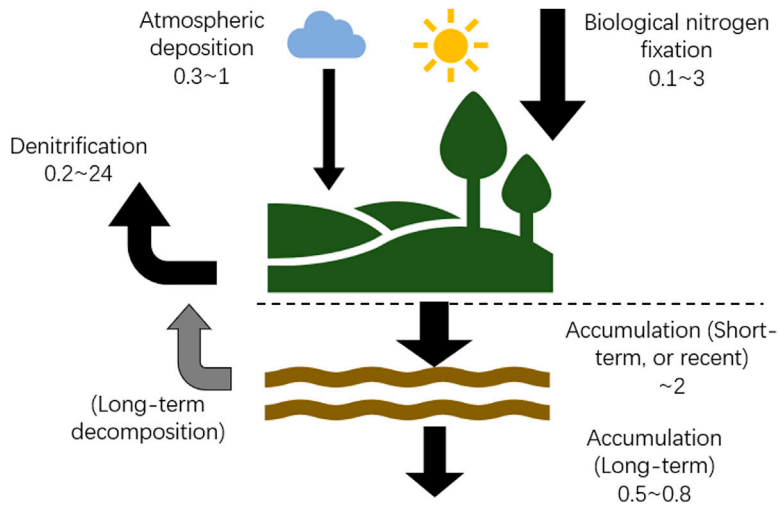

FIGURE 4 | Schematic diagram of N inputs and outputs in a boreal bog. Rates are summarized from literature. Unit of rates is g N m^{-2} yr^{-1}.

However, an elaborate study found that CF was highly variable—from 0.001 to 5.363—across different *Sphagnum* species, site scales and over time, indicating accurate calibration may not be practical in peatlands (Saiz et al., 2019).

Generally, BNF is performed by microbes, mainly rhizobium in many ecosystems (Cleveland et al., 1999). However, legumes are usually rare in peatland ecosystems (Schwintzer, 1983; Vitt, 2006; Borken et al., 2016; Laine et al., 2021) and the main N_2-fixers in peatlands remain controversial. Early studies reported that the nitrogen-fixing organisms in peatlands were cyanobacteria for *Sphagnum* and actinomycete symbionts for dwarf shrubs (Basilier et al., 1978; Schwintzer, 1983). However, recent studies suggested that methanotrophs introduced most BNF in early stage of peatland development (Larmola et al., 2014; Vile et al., 2014; Rousk et al., 2015). By quantifying the genetic expression of 16S rRNA and nitrogenase-encoding *nif*H, Vile et al. (2014) showed that BNF rates were mainly originated from methanotrophs rather than cyanobacteria in pristine bogs in boreal Alberta, Canada. Leppanen et al. (2015) confirmed that most of *nif*H sequences were assigned to the class Alphaproteobacteria (82%), and only a few were assigned to Cyanobacteria (5%). However, elevated CH_4 concentration did not enhance BNF (Leppanen et al., 2015), indicating that BNF may not be solely controlled by methanotroph activity. Kox et al. (2018) had similar conclusion that most of the 16S rRNA genes were assigned to Alphaproteobacteria, and only 0.1% were *bona fide* methane-oxidizing taxa and addition of methane did not simulate incorporation of ^{15}N-nitrogen into biomass whereas oxygen depletion increased the activity of the nitrogen-fixing community. Another candidate of N-fixing organisms is *Azospirillum*, which co-exists with methanotrophic bacteria (Doroshenko et al., 2007) and symbiotic bacteria (i.e., *Frankia* (Actinomycetaceae) and Beijerinckiaceae (Rhizobiales)) (HussDanell, 1997; Huguet et al., 2001; Vile et al., 2014; Borken et al., 2016). Nevertheless, the activity of N_2-fixing organisms could be limited by other nutrients, especially phosphorus, despite sufficient C supply (Limpens et al., 2004; Larmola et al., 2014; Ho and Bodelier, 2015). Therefore, more efforts are needed to understand the mechanisms and contributions of different N-fixing organisms on BNF in peatlands.

Since BNF rates in boreal peatlands are weakly correlated with temperature, precipitation and nutrient condition (ombrotrophic bog or minerotrophic fen), the BNF could not be predicted from these factors. The method of BNF measurement and the knowledge of N_2-fixing microbes also decrease the accuracy of determination of BNF rates. Based on what we know, we simply assessed the BNF rate of global peatlands. The annual BNF of northern peatlands was estimated at 6.5 Tg N yr^{-1}, by adopting a mean rate of 1.9 g N m^{-2} yr^{-1} from measurements in boreal peatlands, and an area of 342 Mha of northern peatlands (Hugelius et al., 2020). The BNF of global peatlands was estimated at 8.0 Tg N yr^{-1} by adopting the same rate as that in northern peatlands, and applying a global peatland area of 423 Mha (Xu et al., 2018). This number accounts for ~14% of the pre-industrial BNF rate of global terrestrial ecosystems (58 Tg N yr^{-1}) (Vitousek et al., 2013), and is at the same order of reactive N produced by lightning (5 ± 3 Tg N yr^{-1}) (Schumann and Huntrieser, 2007).

In addition to N inputs as discussed above, the N budget of peatlands also includes several major N outputs such as denitrification and runoff/discharge (Limpens et al., 2006). Denitrification involves a series of complicated biochemical processes where microbes convert nitrate (NO_3^-) and nitrite (NO_2^-) to nitric oxide (NO), nitrous oxide (N_2O) and dinitrogen (N_2) in gas form (Seitzinger et al., 2006; Groffman and Peter, 2012). Denitrification is difficult to quantify because of the challenge of distinguishing its end product N_2 from ambient atmospheric N_2, and the lack of a suitable method for upscaling the site scale measurements to regional scale due to high spatial and temporal variability (van Groenigen et al., 2015). Limpens et al. (2006) suggested a denitrification (in the form of emission of N_2O) rate of 0.2 g N m^{-2} yr^{-1} by reviewing previous studies. Hill et al. (2016) reported a denitrification rate of <0.1 g N m^{-2} yr^{-1} in central peats in a bog and a fen in Minnesota, United States, and a denitrification rate of 0.36 g N m^{-2} yr^{-1} in the lag/transition part of the bog. However, Wray and Bayley (2007) reported much larger denitrification rates of 11 g N m^{-2} yr^{-1} in marshes and 24 g N m^{-2} yr^{-1} in fens in Alberta, Canada. N outflow through runoff was estimated at 0.3 (0.15–0.63) g N m^{-2} yr^{-1} (Limpens et al., 2006), but this flux is highly site-dependent, ranging from 0.01 g N m^{-2} yr^{-1} in boreal oligotrophic bogs (Hill et al., 2016) to 1.9 ± 0.3 g N m^{-2} yr^{-1} in a slope mire in Germany (Tauchnitz et al., 2010). Overall, the outputs of N are highly variant and uncertain, and limited observations critically limit global estimation.

For peatlands with measured annual BNF rates (**Table 4**), the mean of atmospheric N deposition was 0.5 ± 0.4 g N m^{-2} yr^{-1} (n = 11), the mean of BNF was 1.9 ± 2.7 g N m^{-2} yr^{-1} (n = 21), and average RERNA of northern peatlands was 1.35 ± 0.56 g N m^{-2} yr^{-1} (n = 80; *Recent Rate of Nitrogen Accumulation*). Assuming inflow and outflow of boreal oligotrophic bogs are negligible (Moore and Bubier, 2020), BNF and atmospheric deposition are the largest and second largest sources of N, which account for ~75 and 25%, respectively, of the total input. Denitrification, the only N output to balance the N budget, is 1.0 g N m^{-2} yr^{-1}. A conceptual diagram (**Figure 4**) shows the N cycle with large uncertainties based on literature reports of peatland N budget.

CONCLUSION

Peatlands have accumulated large amount of nitrogen in the past thousands of years. The large uncertainty of estimates of N stock and its accumulation rate in global peatlands is due to the large spatial and temporal variation of the C/N ratio and C accumulation rate in peats. For the sources of the large N stock in peatlands, our synthesis suggests that BNF may have the largest contribution to N input of peatlands, at least larger than atmospheric N deposition at the millennial timescale.

In this study, our findings are based on limited observations. There are still many unknowns in the N cycle of peatlands. The most pressing issue is that the great difference between the LORNA and RERNA indicates that most of N retained in peatland in a short-term timescale would not enter the long-term N stock. It is known that decomposition continues for a very long time in the C accumulation dynamics of peatlands (Young et al., 2019). However, we do not know in which form, how much and through which biogeochemical processes this N is released. It also remains unclear how N, if released, might affect adjacent ecosystems. Applying the $^{15}N_2$ assimilation method instead of ARA would help improve the accuracy of BNF rate measurements. Nutrient supply through groundwater has long been ignored, but this absent part, along with streamflow, may help explain the "missing N" in peatlands. More field and modeling studies are both needed to improve our understanding of the N cycle in peatlands.

DATA AVAILABILITY STATEMENT

The original contributions presented in the study are included in the article/**Supplementary Material**, further inquiries can be directed to the corresponding author.

AUTHOR CONTRIBUTIONS

SP designed the study. TY performed the analysis and created all the tables and figures. All authors contributed the writing of the manuscript.

FUNDING

This study was supported by the National Natural Science Foundation of China (Grant Number 41830643).

ACKNOWLEDGMENTS

We acknowledge the community shared the data of peat cores (https://peatlands.lehigh.edu/).

SUPPLEMENTARY MATERIAL

The Supplementary Material for this article can be found online at: https://www.frontiersin.org/articles/10.3389/feart.2022.670867/full#supplementary-material

REFERENCES

Aerts, R. (1997). Atmospheric Nitrogen Deposition Affects Potential Denitrification and N2O Emission from Peat Soils in the Netherlands. *Soil Biol. Biochem.* 29 (7), 1153–1156. doi:10.1016/s0038-0717(96)00308-2

Anshari, G. Z., Afifudin, M., Nuriman, M., Gusmayanti, E., Arianie, L., Susana, R., et al. (2010). Drainage and Land Use Impacts on Changes in Selected Peat Properties and Peat Degradation in West Kalimantan Province, Indonesia. *Biogeosciences* 7 (11), 3403–3419. doi:10.5194/bg-7-3403-2010

Bao, K., Yu, X., Jia, L., and Wang, G. (2010). Recent Carbon Accumulation in Changbai Mountain Peatlands, Northeast China. *Mountain Res. Dev.* 30 (1), 33–41. doi:10.1659/mrd-journal-d-09-00054.1

Basilier, K., Granhall, U., Stenström, T.-A., and Stenstrom, T.-A. (1978). Nitrogen Fixation in Wet Minerotrophic Moss Communities of a Subarctic Mire. *Oikos* 31 (2), 236–246. doi:10.2307/3543568

Borken, W., Horn, M. A., Geimer, S., Aguilar, N. A. B., and Knorr, K.-H. (2016). Associative Nitrogen Fixation in Nodules of the conifer Lepidothamnus Fonkii (Podocarpaceae) Inhabiting Ombrotrophic Bogs in Southern Patagonia. *Sci. Rep.* 6, 8. doi:10.1038/srep39072

Broder, T., Blodau, C., Biester, H., and Knorr, K. H. (2012). Peat Decomposition Records in Three Pristine Ombrotrophic Bogs in Southern Patagonia. *Biogeosciences* 9 (4), 1479–1491. doi:10.5194/bg-9-1479-2012

Carrell, A. A., Kolton, M., Glass, J. B., Pelletier, D. A., Warren, M. J., Kostka, J. E., et al. (2019). Experimental Warming Alters the Community Composition, Diversity, and N 2 Fixation Activity of Peat moss (Sphagnum Fallax) Microbiomes. *Glob. Change Biol.* 25 (9), 2993–3004. doi:10.1111/gcb.14715

Chapman, R. R., and Hemond, H. F. (1982). Dinitrogen Fixation by Surface Peat and Sphagnum in an Ombrotrophic Bog. *Can. J. Bot.* 60 (5), 538–543. doi:10.1139/b82-072

Cleveland, C. C., Townsend, A. R., Schimel, D. S., Fisher, H., Howarth, R. W., Hedin, L. O., et al. (1999). Global Patterns of Terrestrial Biological Nitrogen (N2) Fixation in Natural Ecosystems. *Glob. Biogeochem. Cycles* 13 (2), 623–645. doi:10.1029/1999gb900014

Cowley, K. L., and Fryirs, K. A. (2020). Forgotten Peatlands of Eastern Australia: An Unaccounted Carbon Capture and Storage System. *Science of the Total Environment* 720, 8. doi:10.1016/j.scitotenv.2020.139067

Dargie, G. C., Lewis, S. L., Lawson, I. T., Mitchard, E. T. A., Page, S. E., Bocko, Y. E., et al. (2017). Age, Extent and Carbon Storage of the central Congo Basin Peatland Complex. *Nature* 542(7639), 86, 90. doi:10.1038/nature21048

Davies-Barnard, T., and Friedlingstein, P. (2020). The Global Distribution of Biological Nitrogen Fixation in Terrestrial Natural Ecosystems. *Glob. Biogeochem. Cycles* 34 (3), 17. doi:10.1029/2019gb006387

Doroshenko, E. V., Boulygina, E. S., Spiridonova, E. M., Tourova, T. P., and Kravchenko, I. K. (2007). Isolation and Characterization of Nitrogen-Fixing Bacteria of the Genus Azospirillum from the Soil of a Sphagnum Peat Bog. *Microbiology* 76 (1), 93–101. doi:10.1134/s0026261707010134

Draper, F. C., Roucoux, K. H., Lawson, I. T., Mitchard, E. T. A., Coronado, E. N. H., Lahteenoja, O., et al. (2014). The Distribution and Amount of Carbon in the Largest Peatland Complex in Amazonia. *Environmental Research Letters* 9 (12), 12. doi:10.1088/1748-9326/9/12/124017

Fenn, M. E., Haeuber, R., Tonnesen, G. S., Baron, J. S., Grossman-Clarke, S., Hope, D., et al. (2003). Nitrogen Emissions, Deposition, and Monitoring in the Western United States. *Bioscience* 53 (4), 391–403. doi:10.1641/0006-3568(2003)053[0391:nedami]2.0.co;2

Flett, R. J., Rudd, J. W. M., and Hamilton, R. D. (1975). Acetylene Reduction Assays for Nitrogen Fixation Freshwaters: a Note of Caution. *Appl.environ.microbiol.* 29, 580–583. doi:10.1128/am.29.5.580-583.1975

Gallego-Sala, A. V., Charman, D. J., Brewer, S., Page, S. E., Prentice, I. C., Friedlingstein, P., et al. (2018). Latitudinal Limits to the Predicted Increase of the Peatland Carbon Sink with Warming. *Nat. Clim. Change* 8 (10), 907. doi:10.1038/s41558-018-0271-1

Girkin, N. T., Lopes dos Santos, R. A., Vane, C. H., Ostle, N., Turner, B. L., and Sjögersten, S. (2020). Peat Properties, Dominant Vegetation Type and Microbial Community Structure in a Tropical Peatland. *Wetlands* 40 (5), 1367–1377. doi:10.1007/s13157-020-01287-4

Godoy, R., Paulino, L., Oyarzún, C., and Boeckx, P. (2003). ATMOSPHERIC N DEPOSITION IN CENTRAL AND SOUTHERN CHILE: AN OVERVIEW. *Gayana Bot.* 60 (1), 47–53. doi:10.4067/s0717-66432003000100008

Gorham, E. (1991). Northern Peatlands - Role in the Carbon-Cycle and Probable Responses to Climatic Warming. *Ecological Applications* 1 (2), 182–195. doi:10.2307/1941811

Granhall, U., and Selander, H. (1973). Nitrogen Fixation in a Subarctic Mire. *Oikos* 24 (1), 8–15. doi:10.2307/3543247

Groffman, P. M., and Peter, M. (2012). Terrestrial Denitrification: Challenges and Opportunities. *Ecol. Process.* 1 (1), 1. doi:10.1186/2192-1709-1-11

Grover, S. P. P., McKenzie, B. M., Baldock, J. A., and Papst, W. A. (2005). Chemical Characterisation of Bog Peat and Dried Peat of the Australian Alps. *Australian Journal of Soil Research* 43 (8), 963–971. doi:10.1071/sr04014

Hardy, R. W. F., Holsten, R. D., Jackson, E. K., and Burns, R. C. (1968). The Acetylene-Ethylene Assay for N2 Fixation: Laboratory and Field Evaluation. *Plant Physiol.* 43 (8), 1185–1207. doi:10.1104/pp.43.8.1185

Hardy, R. W. F., Burns, R. C., Holsten, R. D., Hebert, R. R., and Jackson, E. K. (1971). BIOLOGICAL NITROGEN FIXATION - KEY TO WORLD PROTEIN. *Plant and Soil* 35, 561–590. doi:10.1007/bf02661879

Harris, I., Osborn, T. J., Jones, P., and Lister, D. (2020). Version 4 of the CRU TS Monthly High-Resolution Gridded Multivariate Climate Dataset. *Sci. Data* 7 (1), 109. doi:10.1038/s41597-020-0453-3

Hill, B. H., Jicha, T. M., Lehto, L. L. P., Elonen, C. M., Sebestyen, S. D., and Kolka, R. K. (2016). Comparisons of Soil Nitrogen Mass Balances for an Ombrotrophic Bog and a Minerotrophic Fen in Northern Minnesota. *Sci. Total Environ.* 550, 880–892. doi:10.1016/j.scitotenv.2016.01.178

Ho, A., and Bodelier, P. L. (2015). Diazotrophic Methanotrophs in Peatlands: the Missing Link. *Plant Soil* 389 (1-2), 419–423. doi:10.1007/s11104-015-2393-9

Hugelius, G., Loisel, J., Chadburn, S., Jackson, R. B., Jones, M., MacDonald, G., et al. (2020). Large Stocks of Peatland Carbon and Nitrogen Are Vulnerable to Permafrost Thaw. *Proc. Natl. Acad. Sci. USA* 117 (34), 20438–20446. doi:10.1073/pnas.1916387117

Huguet, V., Batzli, J. M., Zimpfer, J. F., Normand, P., Dawson, J. O., and Fernandez, M. P. (2001). Diversity and Specificity of Frankia Strains in Nodules of Sympatric Myrica Gale, Alnus Incana , and Shepherdia canadensis Determined by Rrs Gene Polymorphism. *Appl. Environ. Microbiol.* 67 (5), 2116–2122. doi:10.1128/aem.67.5.2116-2122.2001

Huss-danell, K. (1997). Actinorhizal Symbioses and Their N 2 Fixation. *New Phytol.* 136 (3), 375–405. doi:10.1046/j.1469-8137.1997.00755.x

King, G. M. (1996). *In Situ* analyses of Methane Oxidation Associated with the Roots and Rhizomes of a Bur Reed, Sparganium Eurycarpum, in a Maine Wetland. *Appl. Environ. Microbiol.* 62 (12), 4548–4555. doi:10.1128/aem.62.12.4548-4555.1996

Knorr, K.-H., Horn, M. A., and Borken, W. (2015). Significant Nonsymbiotic Nitrogen Fixation in Patagonian Ombrotrophic Bogs. *Glob. Change Biol.* 21 (6), 2357–2365. doi:10.1111/gcb.12849

Kox, M. A. R., Lüke, C., Fritz, C., van den Elzen, E., van Alen, T., Op den Camp, H. J. M., et al. (2016). Effects of Nitrogen Fertilization on Diazotrophic Activity of Microorganisms Associated with Sphagnum Magellanicum. *Plant Soil* 406 (1-2), 83–100. doi:10.1007/s11104-016-2851-z

Kox, M. A. R., Aalto, S. L., Penttilä, T., Ettwig, K. F., Jetten, M. S. M., and van Kessel, M. A. H. J. (2018). The Influence of Oxygen and Methane on Nitrogen Fixation in Subarctic Sphagnum Mosses. *AMB Express* 8, 9. doi:10.1186/s13568-018-0607-2

Kox, M. A. R., Kop, L. F. M., van den Elzen, E., van Alen, T. A., Lamers, L. P. M., van Kessel, M., et al. (2020). Functional Redundancy of the Methane-Oxidising and Nitrogen-Fixing Microbial Community Associated with Sphagnum Fallax and Sphagnum Palustre in Two Dutch Fens. *Mires and Peat* 26, 15. doi:10.19189/MaP.2019.SNPG.StA.1885

Kuhry, P., and Vitt, D. H. (1996). Fossil Carbon/nitrogen Ratios as a Measure of Peat Decomposition. *Ecology* 77 (1), 271–275. doi:10.2307/2265676

Laine, A. M., Lindholm, T., Nilsson, M., Kutznetsov, O., Jassey, V. E. J., and Tuittila, E. S. (2021). Functional Diversity and Trait Composition of Vascular Plant and Sphagnum moss Communities during Peatland Succession across Land Uplift Regions. *J. Ecol.* 109 (4), 1774–1789. doi:10.1111/1365-2745.13601

Larmola, T., Leppanen, S. M., Tuittila, E.-S., Aarva, M., Merila, P., Fritze, H., et al. (2014). Methanotrophy Induces Nitrogen Fixation during Peatland Development. *Proc. Natl. Acad. Sci.* 111 (2), 734–739. doi:10.1073/pnas.1314284111

Leifeld, J., and Menichetti, L. (2018). The Underappreciated Potential of Peatlands in Global Climate Change Mitigation Strategies. *Nat. Commun.* 9, 7. doi:10.1038/s41467-018-03406-6

León, C. A., and Oliván, G. (2014). Recent rates of carbon and nitrogen accumulation in peatlands of Isla Grande de Chiloé-Chile. *Rev. Chil. de Hist. Nat.* 87. doi:10.1186/s40693-014-0026-y

Leppänen, S. M., Rissanen, A. J., and Tiirola, M. (2015). Nitrogen Fixation in Sphagnum Mosses Is Affected by moss Species and Water Table Level. *Plant Soil* 389 (1-2), 185–196. doi:10.1007/s11104-014-2356-6

Li, C., Huang, Y., Guo, H., Cui, L., and Li, W. (2018). Draining Effects on Recent Accumulation Rates of C and N in Zoige Alpine Peatland in the Tibetan Plateau. *Water* 10 (5), 576. doi:10.3390/w10050576

Li, L., Gao, J.-Q., Lei, G.-C., Lu, c., Suo, L.-E., et al. (2011). Distribution Patterns of Soil Organic Carbon and Total Nitrogen in Zoige Peat Land With Different Ground Water Table. *Shengtaixue Zazhi* 30 (11), 2449–2455.

Limpens, J., Berendse, F., and Klees, H. (2004). How Phosphorus Availability Affects the Impact of Nitrogen Deposition on Sphagnum and Vascular Plants in Bogs. *Ecosystems* 7 (8), 793–804. doi:10.1007/s10021-004-0274-9

Limpens, J., Heijmans, M. M. P. D., and Berendse, F. (2006). "The Nitrogen Cycle in Boreal Peatlands," in *Boreal Peatland Ecosystems*. Editors R. K. Wieder and D. H. Vitt, 195–230.

Liu, H., Yu, Z., Han, D., Gao, C., Yu, X., and Wang, G. (2019). Temperature Influence on Peatland Carbon Accumulation over the Last century in Northeast China. *Clim. Dyn.* 53 (3-4), 2161–2173. doi:10.1007/s00382-019-04813-1

Liu, L. J., Chen, H., Yu, Z. C., Zhu, D., He, Y. X., Liu, J. L., et al. (2020). Peatland Development and Carbon Dynamics Since the Last Glacial Maximum in the Hengduan Mountains Region. *Catena* 190, 9. doi:10.1016/j.catena.2020.104525

Loisel, J., Yu, Z., Beilman, D. W., Camill, P., Alm, J., Amesbury, M. J., et al. (2014). A Database and Synthesis of Northern Peatland Soil Properties and Holocene Carbon and Nitrogen Accumulation. *The Holocene* 24 (9), 1028–1042. doi:10.1177/0959683614538073

Loisel, J., and Yu, Z. (2013a). Holocene Peatland Carbon Dynamics in Patagonia. *Quat. Sci. Rev.* 69, 125–141. doi:10.1016/j.quascirev.2013.02.023

Loisel, J., and Yu, Z. (2013b). Recent Acceleration of Carbon Accumulation in a Boreal Peatland, South central Alaska. *J. Geophys. Res. Biogeosci.* 118 (1), 41–53. doi:10.1029/2012jg001978

Malmer, N., and Holm, E. (1984). Variation in the C/N-Quotient of Peat in Relation to Decomposition Rate and Age Determination with 210 Pb. *Oikos* 43 (2), 171–182. doi:10.2307/3544766

Markham, J. H. (2009). Variation in moss-associated Nitrogen Fixation in Boreal forest Stands. *Oecologia* 161 (2), 353–359. doi:10.1007/s00442-009-1391-0

Melling, L., Hatano, R., and Goh, K. J. (2005). Soil CO2 Flux from Three Ecosystems in Tropical Peatland of Sarawak, Malaysia. *Tellus B: Chem. Phys. Meteorology* 57 (1), 1–11. doi:10.3402/tellusb.v57i1.16772

Moore, T., Blodau, C., Turunen, J., Roulet, N., and Richard, P. J. H. (2005). Patterns of Nitrogen and Sulfur Accumulation and Retention in Ombrotrophic Bogs, Eastern Canada. *Glob. Change Biol* 11 (2), 356–367. doi:10.1111/j.1365-2486.2004.00882.x

Moore, T. R., and Bubier, J. L. (2020). Plant and Soil Nitrogen in an Ombrotrophic Peatland, Southern Canada. *Ecosystems* 23 (1), 98–110. doi:10.1007/s10021-019-00390-w

Nadim, F., Trahiotis, M. M., Stapcinskaite, S., Perkins, C., Carley, R. J., Hoag, G. E., et al. (2001). Estimation of Wet, Dry and Bulk Deposition of Atmospheric Nitrogen in Connecticut. *J. Environ. Monitor.* 3 (6), 671–680. doi:10.1039/b107008h

Nichols, J. E., and Peteet, D. M. (2019). Rapid Expansion of Northern Peatlands and Doubled Estimate of Carbon Storage. *Nature Geoscience* 12 (11), 917. doi:10.1038/s41561-019-0454-z

Page, S. E., and Baird, A. J. (2016). "Peatlands and Global Change: Response and Resilience,". *Annual Review of Environment and Resources*. Editors A. Gadgil and T. P. Gadgil (Palo Alto: Annual Reviews), 41, 35–57. doi:10.1146/annurev-environ-110615-085520

Page, S. E., Rieley, J. O., and Banks, C. J. (2011). Global and Regional Importance of the Tropical Peatland Carbon Pool. *Glob. Change Biol.* 17 (2), 798–818. doi:10.1111/j.1365-2486.2010.02279.x

Patova, E. N., Sivkov, M. D., Goncharova, N. N., and Shubina, T. P. (2020). Associations between Nitrogen-Fixing Cyanobacteria and Sphagnum Mosses in Floodplain Bogs of the Middle Taiga (European Northeast). *Theor. Appl. Ecol.* (1), 117–123. doi:10.25750/1995-4301-2020-1-117-123

Pemberton, M. (2005). Australian Peatlands: a Brief Consideration of Their Origin, Distribution, Natural Values and Threats. *Journal of the Royal Society of Western Australia* 88, 81–89.

Ribeiro, K., Pacheco, F. S., Ferreira, J. W., Sousa-Neto, E. R., Hastie, A., Krieger Filho, G. C., et al. (2020). Tropical Peatlands and Their Contribution to the Global Carbon Cycle and Climate Change. *Glob. Change Biol.* 27, 489–505. doi:10.1111/gcb.15408

Rousk, K., Sorensen, P. L., Lett, S., and Michelsen, A. (2015). Across-Habitat Comparison of Diazotroph Activity in the Subarctic. *Microb. Ecol.* 69 (4), 778–787. doi:10.1007/s00248-014-0534-y

Rousk, K., Vestergård, M., and Christensen, S. (2018). Are Nitrous Oxide Emissions and Nitrogen Fixation Linked in Temperate Bogs? *Soil Biol. Biochem.* 123, 74–79. doi:10.1016/j.soilbio.2018.05.002

Rousk, K., and Michelsen, A. (2017). Ecosystem Nitrogen Fixation throughout the Snow-free Period in Subarctic Tundra: Effects of Willow and Birch Litter Addition and Warming. *Glob. Change Biol.* 23 (4), 1552–1563. doi:10.1111/gcb.13418

Saiz, E., Sgouridis, F., Drijfhout, F. P., and Ullah, S. (2019). Biological Nitrogen Fixation in Peatlands: Comparison between Acetylene Reduction Assay and 15N2 Assimilation Methods. *Soil Biol. Biochem.* 131, 157–165. doi:10.1016/j.soilbio.2019.01.011

Sannel, A. B. K., and Kuhry, P. (2009). Holocene Peat Growth and Decay Dynamics in Sub-arctic Peat Plateaus, West-central Canada. *Boreas* 38 (1), 13–24. doi:10.1111/j.1502-3885.2008.00048.x

Schillereff, D. N., Boyle, J. F., Toberman, H., Adams, J. L., Bryant, C. L., Chiverrell, R. C., et al. (2016). Long-term Macronutrient Stoichiometry of UK Ombrotrophic Peatlands. *Sci. Total Environ.* 572, 1561–1572. doi:10.1016/j.scitotenv.2016.03.180

Schollhorn, R., and Burris, R. H. (1967). Acetylene as a Competitive Inhibitor of N-2 Fixation. *Proc. Natl. Acad. Sci.* 58(1), 213, 216. doi:10.1073/pnas.58.1.213

Schumann, U., and Huntrieser, H. (2007). The Global Lightning-Induced Nitrogen Oxides Source. *Atmos. Chem. Phys.* 7 (14), 3823–3907. doi:10.5194/acp-7-3823-2007

Schwintzer, C. R. (1983). Nonsymbiotic and Symbiotic Nitrogen Fixation in a Weakly Minerotrophic Peatland. *Am. J. Bot.* 70 (7), 1071–1078. doi:10.1002/j.1537-2197.1983.tb07908.x

Seitzinger, S., Harrison, J. A., Böhlke, J. K., Bouwman, A. F., Lowrance, R., Peterson, B., et al. (2006). Denitrification across Landscapes and Waterscapes: A Synthesis. *Ecol. Appl.* 16 (6), 2064–2090. doi:10.1890/1051-0761(2006)016[2064:dalawa]2.0.co;2

Sjogersten, S., Cheesman, A. W., Lopez, O., and Turner, B. L. (2011). Biogeochemical Processes Along a Nutrient Gradient in a Tropical Ombrotrophic Peatland. *Biogeochemistry* 104, 147–163.

Sorensen, P. L., Jonasson, S., and Michelsen, A. (2006). Nitrogen Fixation, Denitrification, and Ecosystem Nitrogen Pools in Relation to Vegetation Development in the Subarctic. *Arctic, Antarctic, Alpine Res.* 38 (2), 263–272. doi:10.1657/1523-0430(2006)38[263:nfdaen]2.0.co;2

Stewart, K. J., Coxson, D., and Grogan, P. (2011). Nitrogen Inputs by Associative Cyanobacteria across a Low Arctic Tundra Landscape. *Arctic, Antarctic, Alpine Res.* 43 (2), 267–278. doi:10.1657/1938-4246-43.2.267

Tauchnitz, N., Meissner, R., Bernsdorf, S., and Wegener, U. (2010). Nitrogen Fluxes of a Slope Mire in the German Harz Mountains. *Water Air Soil Pollut.* 205 (1-4), 107–112. doi:10.1007/s11270-009-0059-z

Tolonen, T., and Turunen, J. (1996). Accumulation of Carbon in Mires of Finland and Implications for Climatic Change. *Holocene* 6, 171–178. doi:10.1177/095968369600600204

Turunen, J., Roulet, N. T., Moore, T. R., and Richard, P. J. H. (2004). Nitrogen Deposition and Increased Carbon Accumulation in Ombrotrophic Peatlands in Eastern Canada. *Glob. Biogeochem. Cycles* 18 (3), a–n. doi:10.1029/2003gb002154

Urban, N. R., and Eisenreich, S. J. (1988). NITROGEN CYCLING IN A FORESTED MINNESOTA BOG. *Can. J. Bot.* 66 (3), 435–449. doi:10.1139/b88-069

van Bellen, S., Shotyk, W., Magnan, G., Davies, L., Nason, T., Mullan-Boudreau, G., et al. (2020). Carbon and Nitrogen Accumulation Rates in Ombrotrophic Peatlands of central and Northern Alberta, Canada, during the Last Millennium. *Biogeochemistry* 151 (2-3), 251–272. doi:10.1007/s10533-020-00724-0

van den Elzen, E., Bengtsson, F., Fritz, C., Rydin, H., and Lamers, L. P. M. (2020). Variation in Symbiotic N2 Fixation Rates Among Sphagnum Mosses. *Plos One* 15 (2), e0228383. doi:10.1371/journal.pone.0228383

van Groenigen, J. W., Huygens, D., Boeckx, P., Kuyper, T. W., Lubbers, I. M., Rütting, T., et al. (2015). The Soil N Cycle: New Insights and Key Challenges. *Soil* 1 (1), 235–256. doi:10.5194/soil-1-235-2015

Verry, E. S., and Timmons, D. R. (1982). Waterborne Nutrient Flow through an Upland-Peatland Watershed in Minnesota. *Ecology* 63 (5), 1456–1467. doi:10.2307/1938872

Vile, M. A., Kelman Wieder, R., Živković, T., Scott, K. D., Vitt, D. H., Hartsock, J. A., et al. (2014). N2-fixation by Methanotrophs Sustains Carbon and Nitrogen Accumulation in Pristine Peatlands. *Biogeochemistry* 121 (2), 317–328. doi:10.1007/s10533-014-0019-6

Vitousek, P. M., Aber, J. D., Howarth, R. W., Likens, G. E., Matson, P. A., Schindler, D. W., et al. (1997). Human Alteration of the Global Nitrogen Cycle: Sources and Consequences. *Ecol. Appl.* 7 (3), 737–750. doi:10.1890/1051-0761(1997)007[0737:haotgn]2.0.co;2

Vitousek, P. M., Menge, D. N. L., Reed, S. C., and Cleveland, C. C. (2013). Biological Nitrogen Fixation: Rates, Patterns and Ecological Controls in Terrestrial Ecosystems. *Phil. Trans. R. Soc. B* 368 (1621), 20130119. doi:10.1098/rstb.2013.0119

Vitt, D. H. (2006). "Functional Characteristics and Indicators of Boreal Peatlands," in *Ecological Studies*. Editors R. K. Wieder and D. H. Vitt, 9–24.

Wang, M., Moore, T. R., Talbot, J., and Richard, P. J. H. (2014). The cascade of C:N:P Stoichiometry in an Ombrotrophic Peatland: from Plants to Peat. *Environ. Res. Lett.* 9 (2), 024003. doi:10.1088/1748-9326/9/2/024003

Wang, M., Moore, T. R., Talbot, J., and Riley, J. L. (2015). The Stoichiometry of Carbon and Nutrients in Peat Formation. *Glob. Biogeochem. Cycles* 29 (2), 113–121. doi:10.1002/2014gb005000

Warren, M. J., Lin, X., Gaby, J. C., Kretz, C. B., Kolton, M., Morton, P. L., et al. (2017). Molybdenum-Based Diazotrophy in a Sphagnum Peatland in Northern Minnesota. *Appl. Environ. Microbiol.* 83 (17), 14. doi:10.1128/aem.01174-17

Waughman, G. J., and Bellamy, D. J. (1980). Nitrogen Fixation and the Nitrogen Balance in Peatland Ecosystems. *Ecology* 61 (5), 1185–1198. doi:10.2307/1936837

Wieder, W. R., Cleveland, C. C., Smith, W. K., and Todd-Brown, K. (2015). Future Productivity and Carbon Storage Limited by Terrestrial Nutrient Availability. *Nat. Geosci* 8 (6), 441–444. doi:10.1038/ngeo2413

Witty, J. F. (1979). Acetylene Reduction Assay Can Overestimate Nitrogen-Fixation in Soil. *Soil Biol. Biochem.* 11 (2), 209–210. doi:10.1016/0038-0717(79)90103-2

Wray, H. E., and Bayley, S. E. (2007). Denitrification Rates in Marsh Fringes and Fens in Two Boreal Peatlands in Alberta, Canada. *Wetlands* 27 (4), 1036–1045. doi:10.1672/0277-5212(2007)27[1036:drimfa]2.0.co;2

Xu, J., Morris, P. J., Liu, J., and Holden, J. (2018). PEATMAP: Refining Estimates of Global Peatland Distribution Based on a Meta-Analysis. *Catena* 160, 134–140. doi:10.1016/j.catena.2017.09.010

Young, D. M., Baird, A. J., Charman, D. J., Evans, C. D., Gallego-Sala, A. V., Gill, P. J., et al. (2019). Misinterpreting Carbon Accumulation Rates in Records from Near-Surface Peat. *Sci. Rep.* 9, 8. doi:10.1038/s41598-019-53879-8

Yu, Z. (2011). Holocene Carbon Flux Histories of the World's Peatlands. *The Holocene* 21 (5), 761–774. doi:10.1177/0959683610386982

Yu, Z. C. (2012). Northern Peatland Carbon Stocks and Dynamics: a Review. *Biogeosciences* 9 (10), 4071–4085. doi:10.5194/bg-9-4071-2012

Yu, Z., Loisel, J., Brosseau, D. P., Beilman, D. W., and Hunt, S. J. (2010). Global Peatland Dynamics since the Last Glacial Maximum. *Geophys. Res. Lett.* 37, a–n. doi:10.1029/2010gl043584

Zhao, Y., Tang, Y., Yu, Z., Li, H., Yang, B., Zhao, W., et al. (2014). Holocene Peatland Initiation, Lateral Expansion, and Carbon Dynamics in the Zoige Basin of the Eastern Tibetan Plateau. *The Holocene* 24 (9), 1137–1145. doi:10.1177/0959683614538077

Conflict of Interest: The authors declare that the research was conducted in the absence of any commercial or financial relationships that could be construed as a potential conflict of interest.

Publisher's Note: All claims expressed in this article are solely those of the authors and do not necessarily represent those of their affiliated organizations, or those of the publisher, the editors and the reviewers. Any product that may be evaluated in this article, or claim that may be made by its manufacturer, is not guaranteed or endorsed by the publisher.

Advantages of publishing in Frontiers

OPEN ACCESS
Articles are free to read for greatest visibility and readership

FAST PUBLICATION
Around 90 days from submission to decision

HIGH QUALITY PEER-REVIEW
Rigorous, collaborative, and constructive peer-review

TRANSPARENT PEER-REVIEW
Editors and reviewers acknowledged by name on published articles

Frontiers
Avenue du Tribunal-Fédéral 34
1005 Lausanne | Switzerland

Visit us: www.frontiersin.org
Contact us: frontiersin.org/about/contact

REPRODUCIBILITY OF RESEARCH
Support open data and methods to enhance research reproducibility

DIGITAL PUBLISHING
Articles designed for optimal readership across devices

FOLLOW US
@frontiersin

IMPACT METRICS
Advanced article metrics track visibility across digital media

EXTENSIVE PROMOTION
Marketing and promotion of impactful research

LOOP RESEARCH NETWORK
Our network increases your article's readership